

**Development of Selective and Deeply Reducing Systems with Electrochemistry and
Photoredox Catalysis**

By

Colleen P. Chernowsky

A dissertation submitted in partial fulfillment of

the requirements for the degree of

Doctor of Philosophy

(Chemistry)

At the

UNIVERSITY OF WISCONSIN-MADISON

2023

Date of final oral examination: 03/24/2023

The dissertation is approved by the following members of the Final Oral Committee:

Zachary K. Wickens, Assistant Professor of Chemistry

Shannon S. Stahl, Professor of Chemistry

Jeffery D. Martell, Assistant Professor of Chemistry

Tehshik P. Yoon, Professor of Chemistry

Development of Selective and Deeply Reducing Systems with Electrochemistry and Photoredox Catalysis

By

Colleen P. Chernowsky

Under the supervision of Professor Zachary K. Wickens

At the University of Wisconsin-Madison

Abstract

Reductive single electron transfer is one of the most fundamental elementary steps in the synthesis of organic molecules and because of its importance, there are a myriad of strategies to induce this reactivity. Despite the development of chemical, electrochemical, and photochemical platforms for reductive SET, a significant discrepancy remains between the reductive potency of a system and its chemoselectivity. The work in this dissertation details the development of a new catalytic platform for reductive SET that addresses the challenge of promoting deeply reducing reactions with tolerance for sensitive functional groups and selectivity for radical reactivity. Leveraging the underexplored reductive potency of excited state radical anion catalysts enabled the reduction of various arene and alkyne substrates that are inert under traditional photoredox catalysis. Notably, this work revealed that both electrochemistry and photoreduction with a formate terminal reductant could promote this powerful reactivity, demonstrating the versatility of electron-primed photoredox catalysis as a reductive platform. The development of this platform is expected to enable mild and selective SET reductions across a broad range of synthetic applications as well as inform future studies in expanding and improving electron-primed photoredox catalysis as a reductive strategy.

Acknowledgements

First, I would like to thank my Ph.D. advisor, Zach Wickens. Zach has been an incredible and supportive mentor throughout my Ph.D. and all the challenges of the last five years. I feel lucky have been a part of his group and to have benefitted from his seemingly endless knowledge and experience. I would also like to thank the all the amazing members of the Wickens research group that I have had the privilege to get to know and work with during my time at UW-Madison. This talented and incredible group of people have been an essential support system for me that not only made completion of my Ph.D. possible but also made it a joy to do. I would especially like to thank my cohort members, Dylan and Diana, as well as senior group member Oliver for undertaking the start of a new research group with me and sharing in all the challenges and excitement that comes with it.

I would also like to acknowledge all the people that make up the amazing instrument and workshop staff and UW-Madison. The work that I have done in my Ph.D. would not have been possible without Tracy Drier, who fabricated all the electrochemical glassware that I used in my experiments and Dr. Blaise Thompson, who not only designed and constructed the electrical equipment that made all my projects possible but also had the patience to teach me how to construct the circuit boards myself. I would like to thank the instrumentation staff of UW-Madison including Heike Hofstetter, Charly Fry, Cathy Clewett, and Martha Vestling who are endlessly patient and supportive of the researchers and who went above and beyond during COVID restrictions and building shutdowns to keep our samples running.

I thank the incredible chemistry community of UW-Madison who have created a supportive environment where equipment, resources and knowledge are freely shared. I would like to especially thank the members of the Stahl group who were always available to answer my questions about organic electrochemistry, members of the Yoon group who shared their knowledge of photoredox, and members of the Weix group for teaching me about the metal

catalysis. I also thank the Martell group for generously allowing me to share lab space with them for three months while the building holding the Wickens lab space was shut down for construction.

Finally, I would like to thank my parents for being my loudest cheerleaders since day one, having them to encourage me has been an important part of my life. I thank my sisters Claire and Ellen for always being on my side while also being constant reminders to not take myself too seriously in the way that only siblings can. Completing my Ph.D. would not have been possible without the enthusiasm and encouragement of my whole family and I thank them for all the support they have given me over the years.

Table of Contents

Abstract	i
Acknowledgements	ii
Chapter 1: Introduction to Reductive Single Electron Transfer Strategies.....	1
1.1 Introduction.....	2
1.1.1 Introduction to Reductive SET.....	2
1.1.2 The Scope of this Overview	3
1.2 Classic Reductive SET	3
1.2.1 Metal Reductants	3
1.2.2 Dissolving Metal Conditions	4
1.3 Reductive SET via Electrochemistry	7
1.3.1 Introduction to electrochemical Reduction.....	7
1.3.2 Direct Electrolysis	8
1.3.3 Mediated Electrolysis	10
1.4 Visible-Light Photoredox Catalysis	13
1.4.1 Introduction to Photoreduction	13
1.4.2 Classic Visible-Light Photoredox Reactions	15
1.4.3 Improving Photocatalysis Through Catalyst Design	17
1.5 Electron-Primed Photoredox Catalysis	19
1.5.1 Photoactivity of Radical Anion Structures.....	19
1.5.2 Reductive SET via Photoexcited Radical Anions.....	20
1.6 References	25
Chapter 2: Potent Photoreductants via Electron-Primed Photoredox Catalysis: Unlocking Aryl Chlorides for Radical Coupling	35
2.1 Abstract.....	36
2.2 Introduction	36
2.3 Results and Discussion	38
2.4 Conclusions.....	45
2.5 Acknowledgements	46
2.6 References.....	46
2.7 Supplemental Information.....	52
2.7.1 General Methods and Materials	52
2.7.2 Electrochemical Equipment and Experimental Set-Up	52
2.7.3 Electrochemical Characterization.....	55
2.7.4 Synthesis of Non-Commercial Substrates	59

2.7.5	Preparation of Imide Catalysts	60
2.7.6	General Procedures for Electron-Primed Photocatalysis.....	61
2.7.7	Radical Clock Experiment and Competition Experiment.....	62
2.7.8	Comparison of Methods for Reductive Activation	69
2.7.9	Constant Current Control Experiments.....	71
2.7.10	Product Isolation and Characterization.....	74
2.7.11	NMR Spectra	80
Chapter 3: Electrochemical Activation of Diverse Conventional Photoredox Catalysts Induces Potent Photoreductant Activity		96
3.1	Abstract.....	97
3.2	Introduction	97
3.3	Results and Discussion	100
3.4	Conclusions.....	109
3.5	Acknowledgements	110
3.6	References.....	110
3.7	Supplemental Information.....	118
3.7.1	General Methods and Materials	118
3.7.2	Electrochemical Equipment and Experimental Set-Up	118
3.7.3	Catalyst Exploration	120
3.7.4	Characterization of 4DPAIPN Radical Anion	130
3.7.5	Synthesis of Non-Commercial Substrates	134
3.7.6	Defunctionalization Reactions	138
3.7.7	Gas Chromatography Calibrations	143
3.7.8	Reaction Progress Kinetics Analysis.....	144
3.7.9	Syntheses Using Phenol as a Traceless Directing Group	153
3.7.10	Synthesis of a Tricyclic Resorcinol Derivative	156
3.7.11	Redox Neutral Coupling Reactions	157
3.7.12	NMR Spectra	160
Chapter 4: Non-Innocent Radical Ion Intermediates in Photoredox Catalysis: Parallel Reduction Modes Enable Coupling of Diverse Aryl Chlorides		200
4.1	Abstract.....	201

4.2	Introduction	201
4.3	Results and Discussion	204
4.4	Conclusions.....	212
4.5	Acknowledgements	213
4.6	References.....	213
4.7	Supplemental Information.....	219
4.7.1	General Methods and Materials	219
4.7.2	Experimental Set-Up.....	219
4.7.3	Preparation of Catalysts and Starting Materials	220
4.7.4	General Experimental Procedures for Photoredox Reduction	221
4.7.5	Reaction Optimization	224
4.7.6	Photocatalyst and Reductant Evaluation.....	228
4.7.7	Evaluation of Leaving Groups not Susceptible to XAT	229
4.7.8	Reductants Evaluated with 4DPAIPN	229
4.7.9	Control Experiments	230
4.7.10	Radical Clock Experiment	230
4.7.11	High Throughput Experimentation with Aryl Halide Informer Plate	231
4.7.12	Cyclic Voltammetry	232
4.7.13	Gas Chromatography Calibration Curves.....	233
4.7.14	Stern Volmer and UV-Vis Data.....	236
4.7.15	NMR Experiment for 4DPAIPN •– Generation	239
4.7.16	Plausible Mechanism for CO ₂ •– Generation from Thiyl Radical	240
4.7.17	Probing Substrate Reduction by CO ₂ •–.....	240
4.7.18	Product Characterization.....	241
4.7.19	NMR Spectra	250
Chapter 5: E-Selective Semi-Hydrogenation of Alkynes via Electron-Primed Photoredox Catalysis		278
5.1	Abstract.....	279
5.2	Introduction	279
5.3	Results and Discussion	281

5.4	Conclusions.....	286
5.5	Acknowledgements	286
5.6	References.....	287
5.7	Supplemental Information.....	292
5.7.1	General Methods and Materials	292
5.7.2	Electrochemical Equipment and Experimental Set-Up	292
5.7.3	Catalyst Synthesis	294
5.7.4	Cyclic Voltammetry	294
5.7.5	Synthesis of Non-Commercial Substrates.....	296
5.7.6	Screening Engines for Electron-Primed Photoredox Catalysis	299
5.7.7	Controlling the Degree of Hydrogenation	302
5.7.8	Semi-Hydrogenation of Aliphatic Alkynes.....	303
5.7.9	Preliminary Scope Investigations	305
5.7.10	Investigation of Isomerization Mechanism.....	307
5.7.11	UV-Vis of 4DPAIPN	310
5.7.12	NMR Spectra	312
Chapter 6: An Electrochemical Copper Strategy for Mild and Selective Nitrile Reduction		
	319
6.1	Abstract.....	320
6.2	Introduction	320
6.3	Results and Discussion	322
6.4	Conclusions.....	326
6.5	Acknowledgements	326
6.6	References.....	327
6.7	Supplemental Information.....	330
6.7.1	General Methods and Materials	330
6.7.2	Electrochemical Equipment and Experimental Set-Up	330
6.7.3	Reaction Optimization	331
6.7.4	Glorius Screen	337
6.7.5	Control Experiments	343

Chapter 1: Introduction to Reductive Single Electron Transfer Strategies

1.1 Introduction

1.1.1 Introduction to Reductive SET

Organic radicals are important intermediates in synthesis due to their unique reactivity patterns that enable a wide range of transformations^{1–3} complementary to those carried out under polar reaction manifolds. Precise control over the formation of these radical intermediates is crucial to engaging them in organic synthesis to their fullest potential.⁴ One of the most extensively explored strategies for initiating radical reactivity is reductive single electron transfer (SET)^{5–7} where a donor species transfers an electron to an organic acceptor (**Figure 1.1**). The

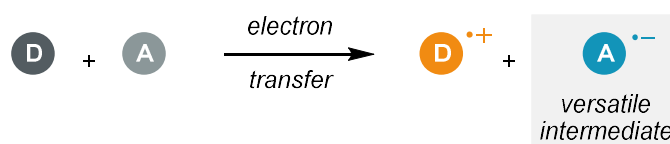


Figure 1.1. Basic single electron transfer between a donor species (D) and an acceptor (A).

resulting radical anion of the acceptor can be engaged in a myriad of downstream transformations and bond forming reactions.⁸ There are several mechanistic challenges associated with reductive SET that are directly correlated to the identity of the electron donor. One such challenge is balancing the potency of the reductant with selectivity in the electron transfer. There are a wide range of challenging electron rich substrates that are desirable to engage in reductive SET reactions but require very negative reduction potentials for activation⁹

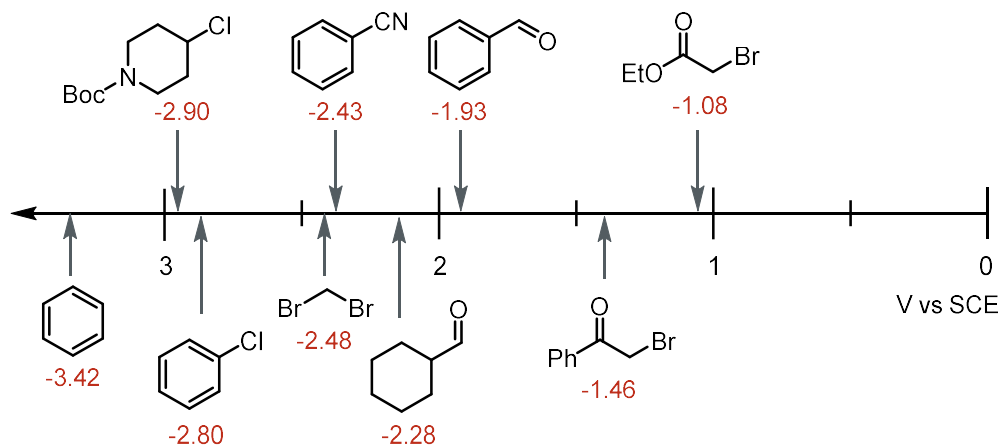


Figure 1.2. Reduction potentials of a select range of organic substrates

(**Figure 1.2**). Unfortunately, powerful reductants capable of activating these substrates tend to have poor chemoselectivity and functional group tolerance which limits their use in synthesis (**Figure 1.3**). Additionally, radical intermediates can easily be over reduced to an anion^{10–12} preventing radical reactivity in the presence of strong reductants. Developing systems with reductive potency to activate challenging substrates while retaining selectivity for functional groups as well as radical intermediates has been a focus in reductive SET research in recent years.

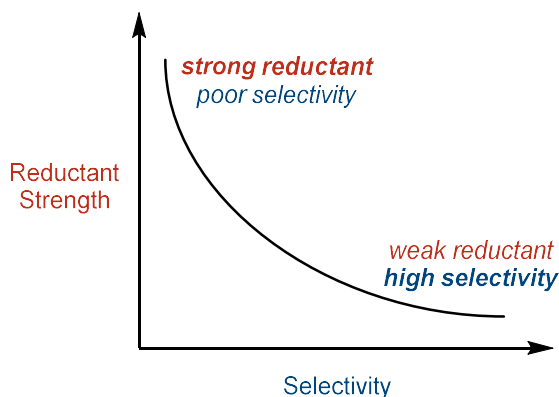


Figure 1.3. Opposing reductive potency versus selectivity trends.

1.1.2. The Scope of this Overview

The identity of an electron donor is a key factor in designing reductive SET systems and is directly tied to the advantages and limitations of the platforms that will be discussed in this overview. The scope of this overview will include a discussion of classic reductive SET reactions and systems as well as their fundamental challenges and limitations. Additionally, alternative platforms that have been developed for reductive SET will be presented with a critical evaluation of their effectiveness at addressing the reductive potency versus selectivity challenge.

1.2 Classic Reductive SET

1.2.1 Metal Reductants

Metals are classic single electron reductants for activation of organic molecules. There are several metals used for reductive SET with discreet redox potentials (**Figure 1.4**) such as zinc^{13,14} or manganese^{15,16} for more mild transformations, magnesium^{17–19} and samarium^{20,21} for

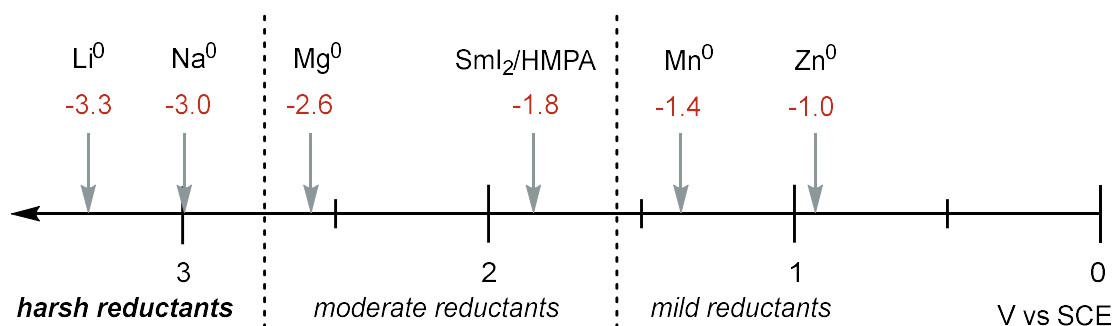


Figure 1.4. Metal reductants and their reduction potentials

more challenging single electron reductions, and the most aggressive metals, sodium and lithium,^{22–24} for activation of electron rich substrates requiring very negative reduction potentials. While these metals together offer a range of redox potentials, the variety is still limited, and the potential is inherent to the identity of the metal offering very little tunability in the reductive potency of a system. In addition to a limited range of redox potentials, metal reductants are used in stoichiometric or super stoichiometric quantities. This often leads to poor tolerance for radical intermediates due to the facile nature of over reduction of radicals to anions. For example, an arene radical generated through reductive SET followed by mesolytic cleavage, possesses a reduction potential of +0.05 V vs SCE¹⁰ leading to rapid over reduction in the presence of a stoichiometric reductant and preventing radical reactivity. The aggressive nature of the reductants coupled with stoichiometric quantities results in this strategy having poor functional group tolerance and being limited to mostly hydrogenation reactions.

1.2.2 Dissolving Metal Conditions

The most regularly used metal reductants are sodium and lithium due to their negative potentials capable of reducing a wide range of functional groups. These reactions proceed via a solvated electron mechanism in liquid ammonia¹⁹ under reaction parameters referred to as “dissolving metal conditions”. These aggressive dissolving metal conditions were first disclosed as early as 1903 by Bouveault and Blanc²⁵ where sodium was leveraged in absolute ethanol to hydrogenate esters to primary alcohols (**Figure 1.5**). Since then, these metals have received

Bouveault and Blanc, 1903

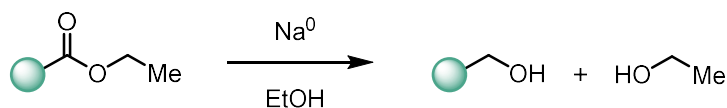


Figure 1.5. First example of dissolving metal conditions

widespread application in challenging reduction reactions. A well-known reaction involving dissolving metal conditions is the Birch reduction²² first disclosed in 1944 (**Figure 1.6**). This reaction dearomatizes arene substrates via hydrogenation and has been extensively studied and applied to synthesis in the last eighty years.^{26,27} The Birch reduction proceeds via a sequential electron transfer, proton transfer (ETPT) mechanism and since this reaction is heavily dependent on protonation of radical anion intermediates, the Birch reduction has rarely been extended beyond hydrogen bond forming transformations. Additionally, the difficulty

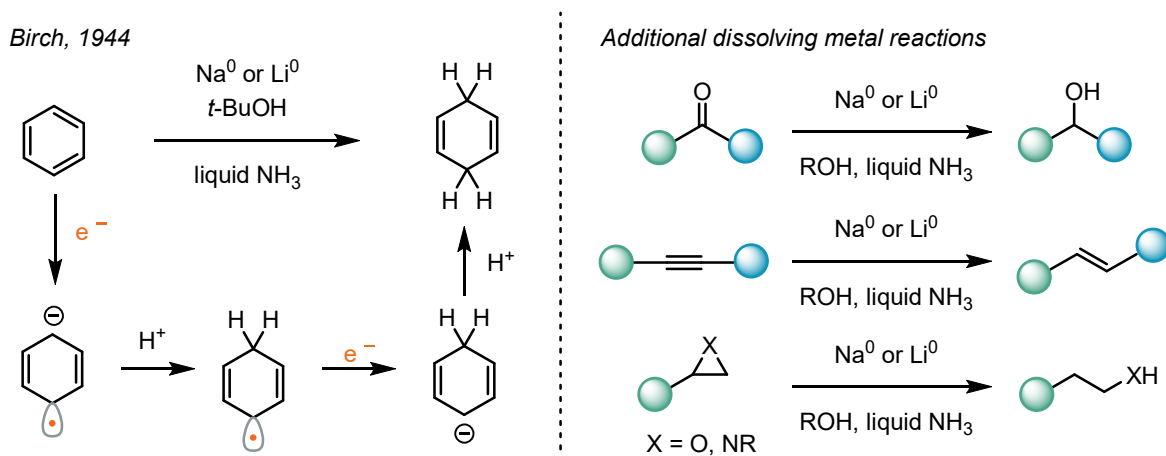


Figure 1.6. Reactions promoted using dissolving metal conditions

involved in dearomatizing arenes and the unselective nature of lithium and sodium metal reductants has led to a very poor scope for the Birch reduction, limited to substrates with reductively robust functional groups. Additional reactions that use dissolving metal conditions (**Figure 1.6**) include transformations like *E*-selective semi-hydrogenation of alkynes,^{28,29} reduction of ketones³⁰ to alcohols, as well as aziridine³¹ and epoxide³² ring openings. Like the Birch reduction, there are very few examples of these reactions being engaged in transformations beyond hydrogenation.

Dissolving metal conditions represent some of the most powerfully reducing conditions available in the literature capable of promoting SET reduction of most functional groups. However, the highly reactive nature of sodium and lithium metals makes them very poorly selective and indiscriminate in reducing functional groups and radical intermediates. These harsh reaction conditions typically require dissolving metal reductions to either be carried out early in a synthetic sequence²⁸ or after extensive protection of installed functional groups.³³ Furthermore, super stoichiometric quantities of the metal reductant make over reduction of radical intermediates a significant challenge and prevents meaningful development of radical transformations under dissolving metal conditions.

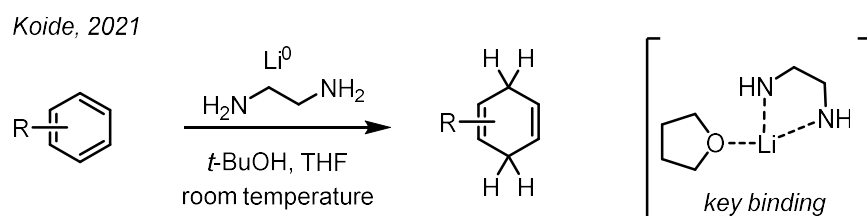


Figure 1.7. Improved conditions for the Birch reduction.

In addition to the difficulty of controlling the reactivity of dissolving metal conditions, there are also practical challenges associated with handling sodium and lithium metals. Their pyrophoric nature introduces significant hazards to the reaction setup and most dissolving metal reactions leverage liquid ammonia as the solvent,³⁴ requiring cryogenic temperatures. Koide and coworkers³⁵ recently disclosed improved conditions for the Birch reduction (**Figure 1.7**) via the addition of ethylenediamine as a promoter which allowed arene reductions to be conducted in tetrahydrofuran at room temperature. While these improvements negate the need for cryogenic temperatures and enables the Birch reduction to be conducted on scale, lithium metal remains a hazardous reductant with a poor selectivity profile. Despite the limitations in selectivity and the hazards associated with pyrophoric metals, dissolving metal conditions continue to be leveraged in both academic^{28,33} and industrial³⁴ contexts (**Figure 1.8**) as reductive SET on electron rich substrates is a valuable synthetic strategy. Developing alternative engines for reductive SET that

negate the use of harsh stoichiometric reductants has been an area of interest and extensive research in the last several decades.

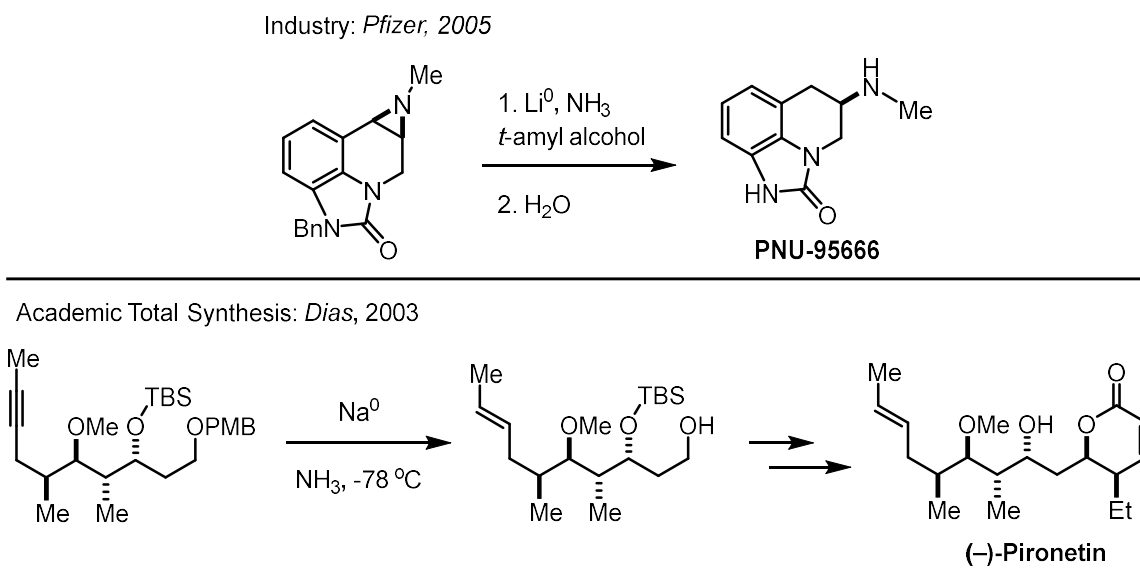


Figure 1.8. Examples of dissolving metal conditions in industry and academic synthetic routes.

1.3 Reductive SET via Electrochemistry

1.3.1 Introduction to Electrochemical Reduction

Electrochemistry as a tool to promote single electron reduction offers a flexible and greener alternative to classic chemical reductants and has been used to promote numerous valuable organic transformation.^{36–38} This flexibility originates in the tunability of the applied potential at the cathode offering a wide range of values with a high degree of precision.³⁹ Another significant advantage of electrochemistry is the ability to decouple the cathodic potential from the identity and potential of the terminal reductant enabling the use of electron sources like $\text{Zn}(0)$ or tertiary amines that are too weak to activate the substrate alone.⁴⁰ Furthermore, the use of a divided cell prevents detrimental interactions between chemical reductants and key substrates, intermediates or catalysts.⁴¹ A significant consequence of the presence of terminal reductants is back electron transfer between reduced radical intermediates generated after SET reduction and oxidation radical cation byproducts (**Figure 1.9(a)**).⁴² Removing these radical cation byproducts with a divided cell prevents back electron transfer and increases the concentration of key reduced

intermediates. Another common side reaction is associated with terminal reductants such as stoichiometric trialkylamines with weak and labile C-H bonds.⁴³ When exposed to carbon centered radical intermediates, these amines can easily undergo hydrogen atom transfer (HAT) resulting in overreduction of the intermediate to a C-H bond (**Figure 1.9(b)**).^{44,45} Separating the anode and cathode chambers removes these amine reductants from the reaction solution which avoids overreduction pathways via HAT and enables radical transformations.

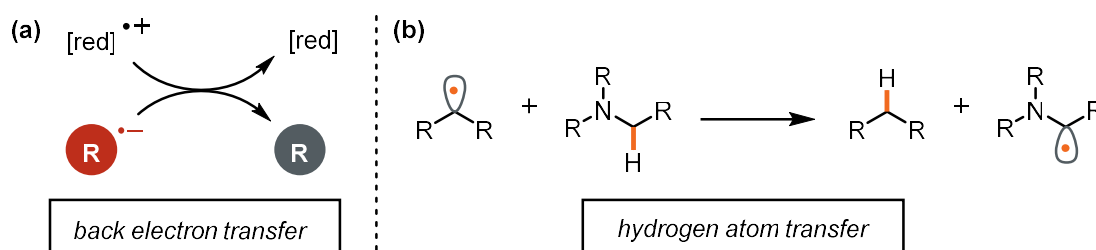


Figure 1.9. Detrimental side reactions from the presence of a terminal reductant in a reaction solution. (a) Back electron transfer between key radical anion intermediates and terminal reductant oxidized byproducts. (b) Hydrogen atom transfer to alkyl radical intermediates when the terminal reductant is a trialkylamine.

1.3.2 Direct Electrolysis

The simplest way to use electrochemical reduction to activate molecules is through direct electrolysis. In this reaction regime, electron transfer to substrates occurs directly at the electrode surface (**Figure 1.10(a)**) and can either be driven at a constant current or through a constant applied potential.^{41,46} While this strategy retains all the general benefits of electrochemistry, there are still significant synthetic drawbacks with respect to selectivity. Firstly, challenging substrates that require negative potentials will require applied potentials either as equally negative or with a significant overpotential when electron transfer kinetics are poor (**Figure 1.10(b)**).^{47,48} This requirement leads to having a very reducing surface in the reaction solution that is unable to differentiate electron transfer to different functional groups. As a result, direct electrolysis often has poor functional group tolerance akin to dissolving metal conditions despite being more tunable and a much less hazardous approach to reductions. Additionally,

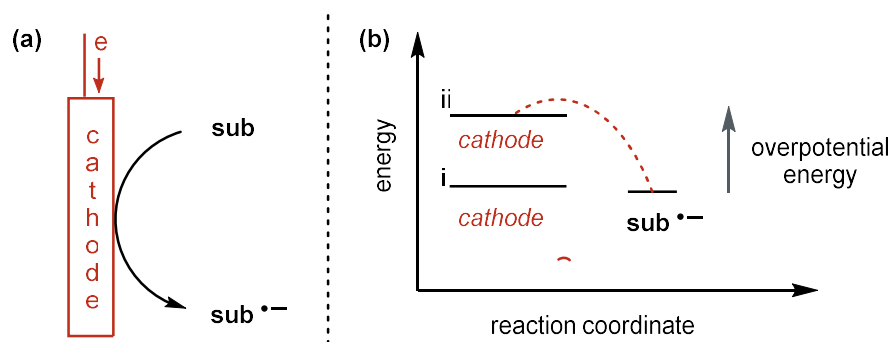


Figure 1.10. (a) Direct electrolysis where substrate reduction occurs on the surface of the electrode. (b) *i.* Applied potential of the cathode is the same as the potential of the substrate - efficient electron transfer kinetics. *ii.* An overpotential is necessary - inefficient electron transfer kinetics.

the hydrogen evolution reaction (HER) becomes increasingly competitive at more negative potentials,⁴⁹ not only consuming proton sources often required for net reductive reactions but also preventing necessary substrate SET. Negative electrode potentials can also lead to corrosion of the electrode surface^{50,51} or degradation of the supporting electrolyte.⁵² Baran and Minter⁵³ report a significant advance in designing direct electrolysis systems to avoid undesired electrode passivation and electrolyte reduction in reactions similar to classic dissolving metal reductions (**Figure 1.11**). Inspired by lithium-ion battery chemistry,⁵⁴ tris(pyrrolidino)phosphoramidate was added as an overcharge protection reagent to prevent undesired corrosion and enabled a set of general, safe and scalable conditions for direct

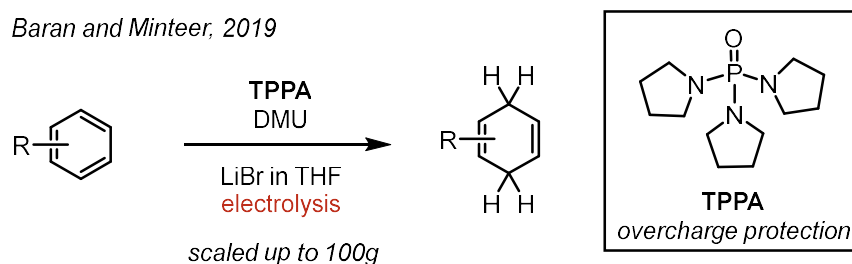


Figure 1.11. A direct electrolysis method under constant current for classic deeply reducing reactions

electrolysis reductions. Despite advances, direct electrolysis is still an unselective method for promoting radical reactivity. The highly reducing environment at the electrode surface coupled with the ease of radical overreduction results in rapid anion formation that outcompetes the rate of diffusion away from the electrode surface.⁵⁵ Work from Shono and coworkers¹¹ (**Figure 1.12**)

shows this behavior in the formation of an anionic ring opened product resulting from overreduction of an alkyl radical intermediate formed in close proximity to the cathode. Additional work from Pinson and Andrieux¹⁰ (**Figure 1.12**) studied the potentials of aryl radical intermediates formed via SET reduction followed by mesolytic cleavage of aryl diazonium salts and found the radical/anion redox couple to be a facile +0.05 V vs SCE. The selectivity challenges inherent to highly reducing cathodic reduction with respect to functional group tolerance and radical overreduction make direct electrolysis a poor strategy to promote chemoselective radical transformations.

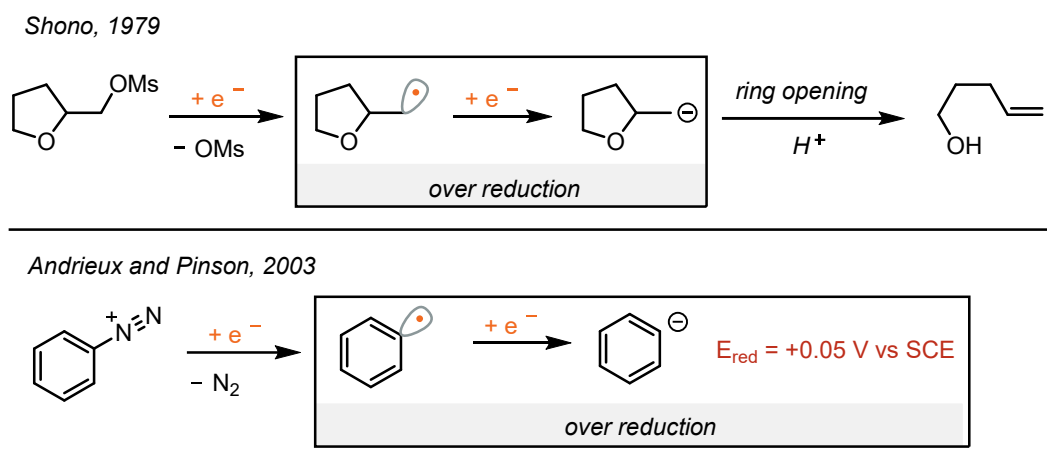


Figure 1.12. Over reduction of alkyl and aromatic radicals to anions.

1.3.3 Mediated Electrolysis

An alternative method for electrochemical reduction that circumvents many of the challenges associated with direct electrolysis is achieved by the addition of a catalytic or stoichiometric homogeneous redox mediator.^{56–59} Mediated electrolysis enables overall lower cathode potentials and promotes substrate reduction in the bulk reaction solution away from the cathode surface (**Figure 1.13(a)**).⁴⁶ This spatial separation of SET generated radical intermediates and the cathode surface facilitates a wider range of radical transformations by dramatically decreasing undesired overreduction to anionic intermediates.⁵⁶ To serve as an effective redox mediator, a structure must fulfill a restrictive set of requirements.^{56,60} The most notable and challenging requirement demands that the mediator be stable upon cathodic

reduction so as not to decompose yet also reactive enough to undergo SET with the substrate (**Figure 1.13(b)**).^{59,61} This results in a limit in the potential difference between what is applied at the cathode and the potential of the substrate. The most facile mediations will be exergonic from

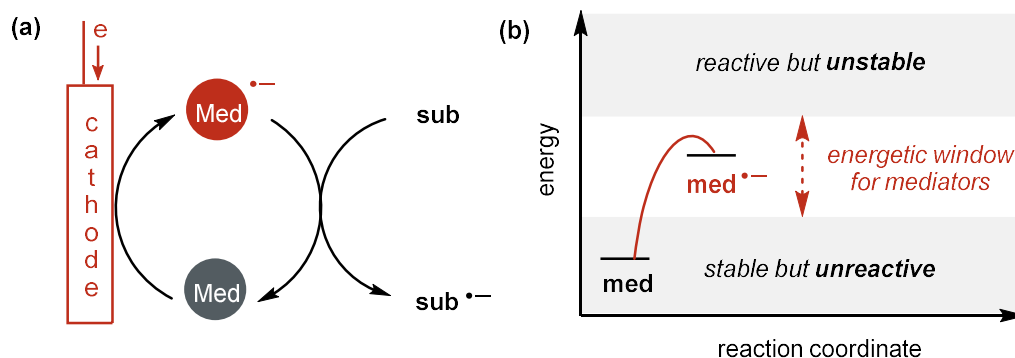


Figure 1.13. (a) Generic mechanism for SET reduction via mediated electrolysis. (b) The energetic requirements for a mediator's radical anion to be used for SET reduction.

the cathode to the substrate but mediators are also capable of driving mildly endergonic electron transfers.^{58,59,62} Some of the most common metal-based mediators to initiate radical reactivity via SET are titanium or chromium metal salts that are electrochemically reduced to reactive low valent redox states.^{56,58,59} Nickel or cobalt salen based structures^{56,59,63} are another common class of metal-based mediators, however, these catalysts more commonly use electrochemical reduction of the metal to promote elementary steps such as oxidative addition rather than SET reduction of

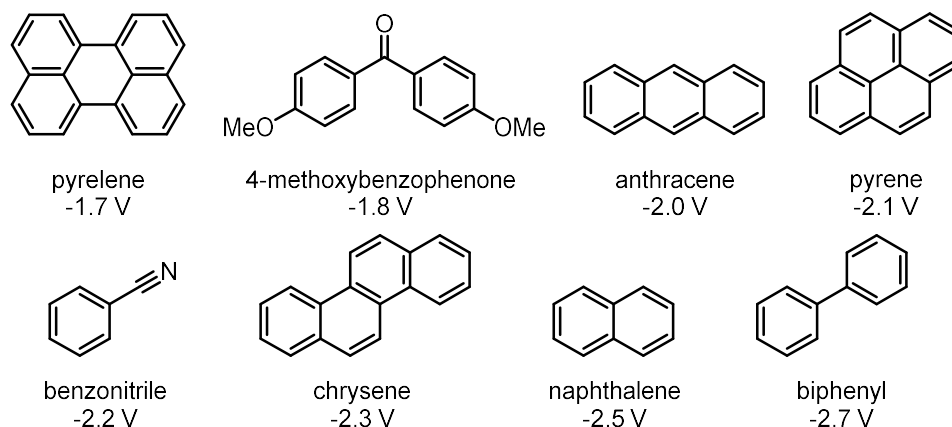


Figure 1.14. Common organic aromatic compounds used as electrochemical mediators for SET reductions. (Potentials are $E_{1/2}$ values versus SCE)

the substrate. Aromatic organic compounds^{59,64–67} are by far the most extensively explored and effective class of mediators to promote SET reductions. Delocalization of the radical anion over an extended aromatic surface provides the stabilization required for these structures to act as effective mediators between the cathode and the substrate. **Figure 1.14** summarizes several common organic mediators that have been explored for SET reduction.⁵⁶ Unfortunately, despite a range of reported structures, highly reducing mediations are challenging because the more negative the potential required for SET, the more unstable and prone to decomposition the reduced mediator becomes. For example, Lund and Simonet⁶⁸ observe alkylation byproducts (Figure 1.15) of a deeply reducing naphthalene mediator (-2.5 V vs SCE) from coupling between alkyl radical intermediates (generated from

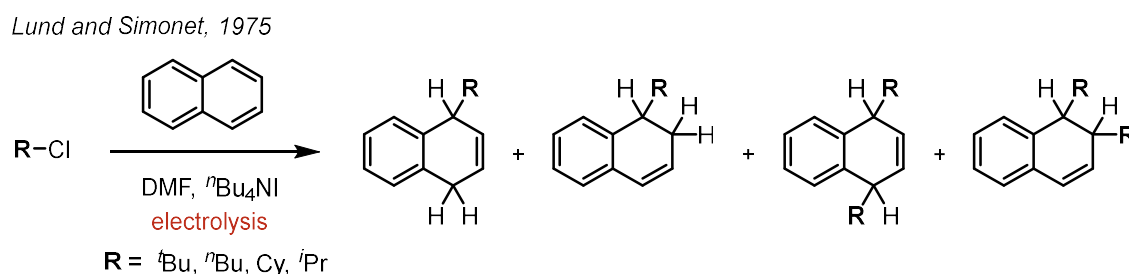


Figure 1.15. Alkylation byproducts of a naphthalene mediator from functionalization of the naphthalene radical anion.

reduction of alkyl halides) and the reactive naphthalene radical anion. In addition to there being a very limited number of mediators suitable for deeply reducing reactions, chemoselectivity also becomes increasingly poor with more negative potentials as the cathode still presents a highly reducing surface that can degrade reductively sensitive functional groups. An example of a mediated system for a deeply reducing reaction was reported by Kariv-Miller⁶⁹ (**Figure 1.16**) where aliphatic ketones were reduced and the subsequent ketyl radical intermediates were engaged in radical cyclization reactions. This system relied on the use of dimethylpyrrolidinium salts as mediators which allowed the applied cathodic potential to be lowered from -3.0 V under direct electrolysis to -2.7 V (vs SCE) and improved selectivity for radical cyclization products. Unfortunately, precise control over the applied potential was still required to prevent overreduction

pathways via competitive direct electrolysis and the negative applied potentials led to very poor functional group tolerance. While mediated electrolysis enables radical transformations by promoting SET reductions away from the electrode surface, it also remains constrained in driving more reducing reactions because of the inherent limitations in mediator stability and the negative cathodic potentials that are still required.

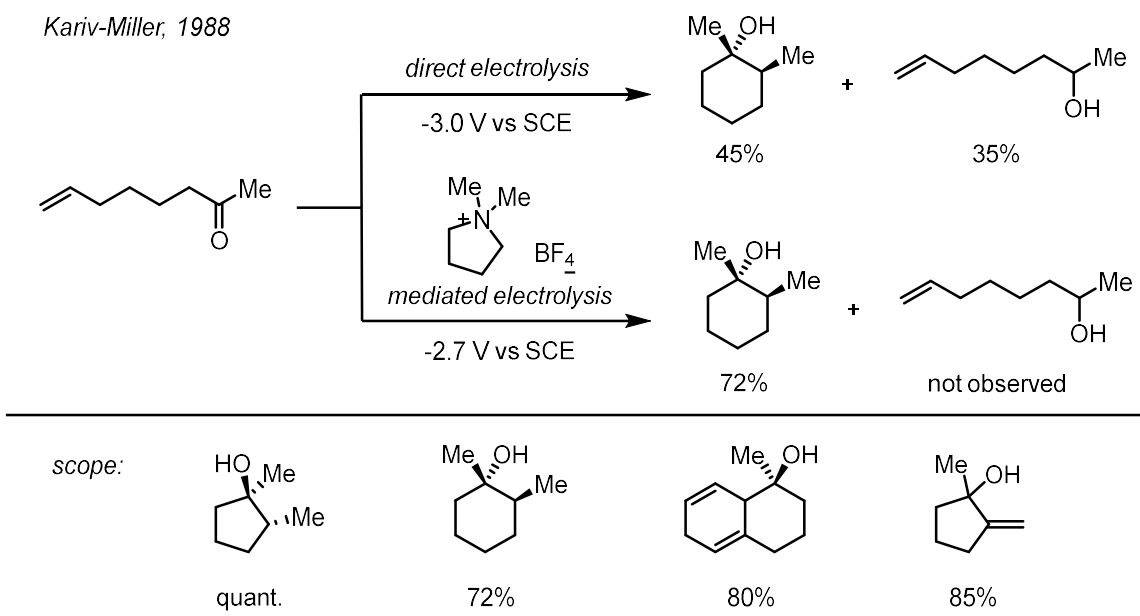


Figure 1.16. Mediated electrolysis at negative applied potentials with selectivity for radical cyclization.

1.4 Visible-Light Photoredox Catalysis

1.4.1 Introduction to Photoreduction

The use of light as an energy source to drive SET has been widely explored and developed in the last fifteen years.^{70–75} One of the primary advantages of reductions via visible-light photoredox catalysis is the excellent selectivity profile that arises from generating a low concentration of active reductant in solution.⁷⁶ These low concentrations attenuate overreduction pathways of radical intermediates and have enabled extensive development of radical based transformations in organic synthesis. Two mechanisms are generally proposed for SET substrate reductions, both of which rely on photon absorption by a photoactive catalytic species followed by either oxidative or reductive quenching.^{72,76–78} The first mechanism proceeds via oxidative

quenching between the photocatalyst excited state and the substrate of interest generating both the desired substrate radical anion and a one electron oxidized catalyst intermediate which undergoes turnover by SET with a terminal reductant. Photocatalysts that are best suited to

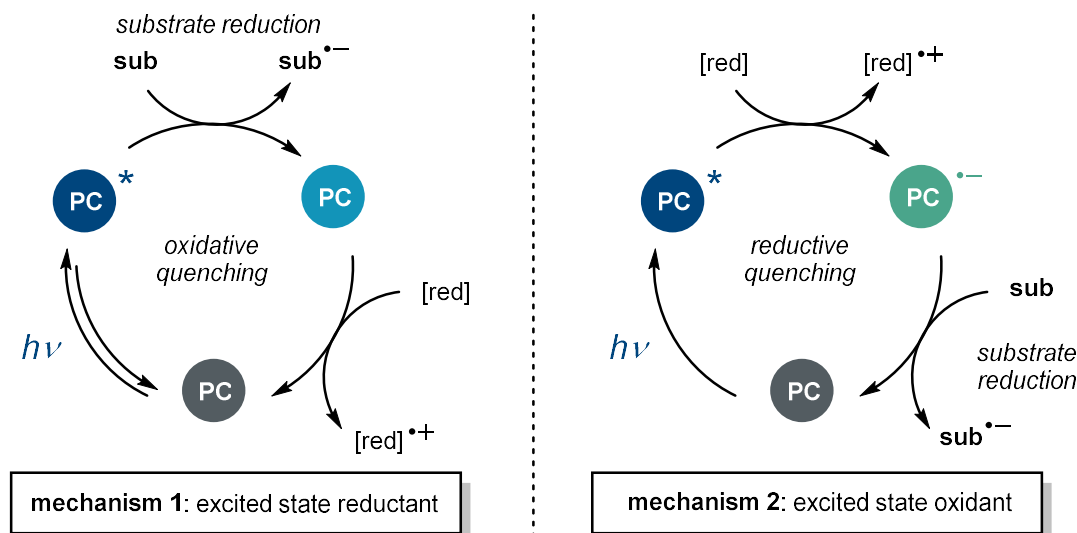


Figure 1.17. General mechanisms for substrate SET reduction by photoredox catalysis.

promote this mechanism typically possess strongly reducing excited states^{79–81} or are capable of pre-associating with the substrate prior to excitation. In contrast, the second mechanism commonly proposed for SET reductions proceeds via reductive quenching of the photocatalyst excited state by a terminal reductant. The resulting one electron reduced catalyst intermediate is the active reductant that engages the substrate in SET reduction leading to both formation of the desired substrate radical anion and catalyst turnover. The photocatalysts that are most effective for this mechanism have both an oxidizing excited states as well as a stable and highly reducing ground state radical anion.^{80,82} Regardless of the mechanism used to drive SET reduction, either by oxidative or reductive quenching, the ultimate source of the energy for these radical initiations comes from visible light. While blue light has a significant amount of energy (440 nm provides 2.8 eV of energy)⁸⁰ that could theoretically promote SET reduction to substrates with very negative redox potentials, these challenging substrates are inactive under classic photoredox catalysis conditions.⁹ This is due to the significant amount of energy that is lost photophysical processes

such as intersystem crossing or vibrational relaxations in the photocatalyst excited state (**Figure 1.18**).^{80,83–86} These energetic losses have severely limited the substrates that can be engaged under visible-light photoredox catalysis to those that are activated for SET reduction.

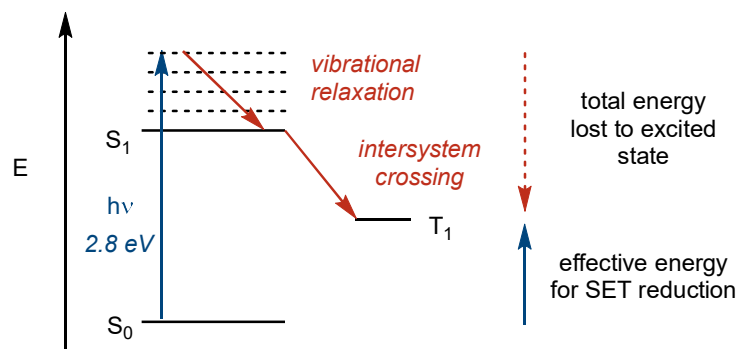


Figure 1.18. Pathways for energy loss in the excited state through vibrational relaxation and intersystem crossing

1.4.2 Classic Visible-Light Photoredox Reactions

The earliest work in activating organic molecules with reductive photoredox catalysis comes from Kellogg's seminal report⁸⁷ in 1978 where a known photoactive ruthenium tris-bipyridine salt was used to reduce alpha-keto sulfonium salts. This report was soon followed by

Kellogg 1978

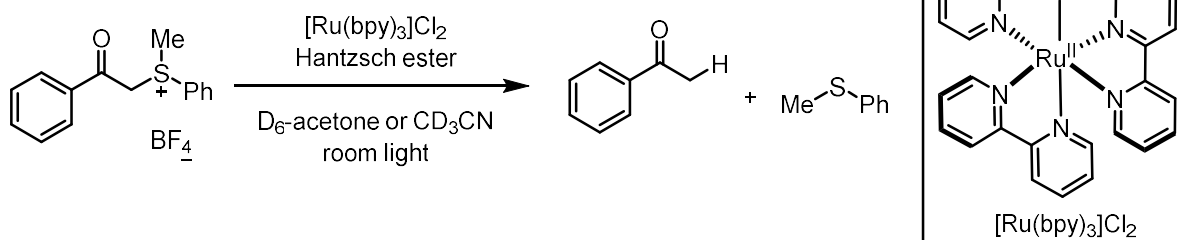


Figure 1.19. Early report of SET reduction of an organic substrate promoted by visible-light photoredox catalysis

a myriad of studies investigating various photoactive molecules as single electron reductants to generate open-shell organic compounds throughout the 1980s and 1990s.^{88–93} However, it wasn't until the late 2000s that the generality of photoredox catalysis was fully explored and applied to synthetic organic transformations. A new era of developing reductive photoredox catalysis began with three seminal reports from MacMillan,⁹⁴ Yoon,⁹⁵ and Stephenson⁹⁶ (**Figure 1.20**) where carbon centered radicals were effectively generated via photoreduction and then engaged in an

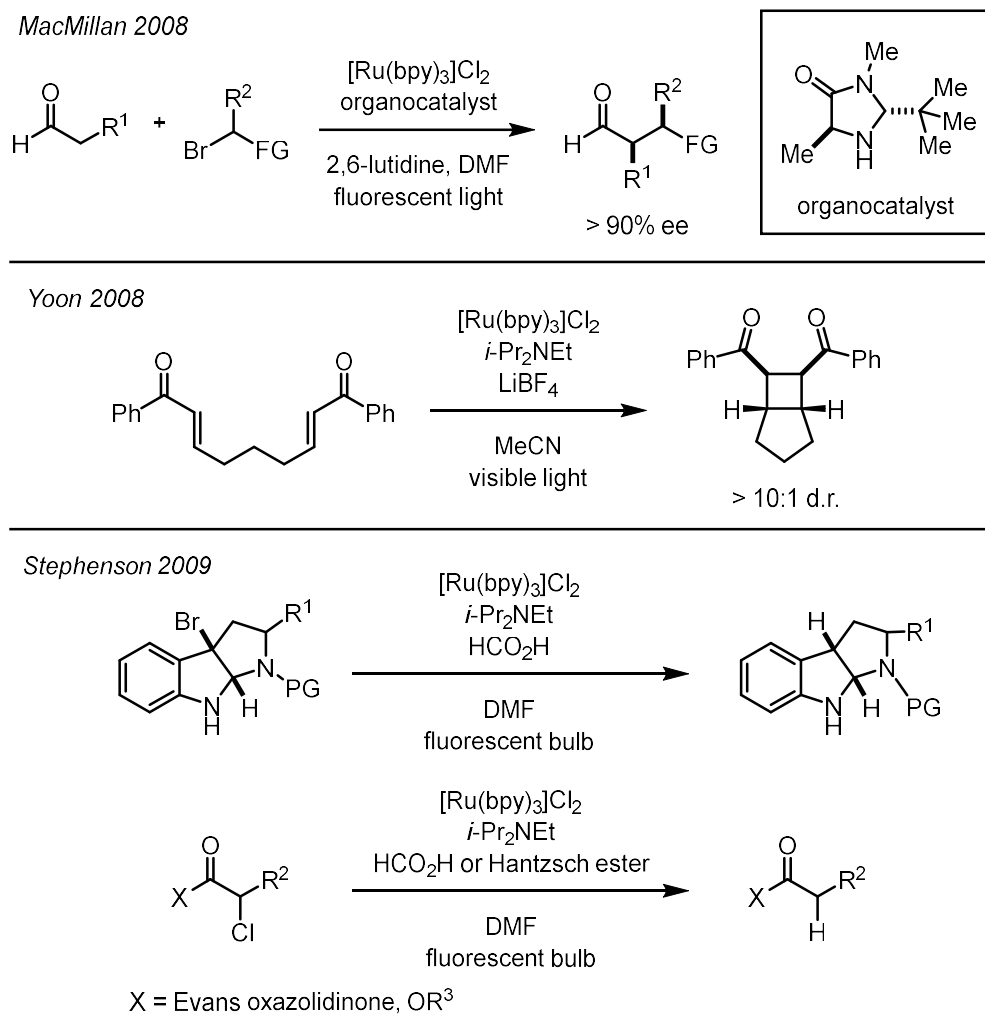


Figure 1.20. Early examples of visible light photoredox catalysis for radical organic transformations

array of bond forming reactions. These reports demonstrate the power of photoredox catalysis to initiate radical coupling reactions across a range of diverse substrate structures as well as its compatibility with highly diastereoselective and enantioselective transformations. In the last fifteen years, extensive progress has been made in expanding visible light photoredox catalysis as a synthetic tool for radical initiation as well as redox neutral and net reductive transformations, however, photoredox catalysis remains limited to substrates that are activated for SET reduction. This is a fundamental limitation that arises from both the finite energy of a single blue photon and the significant loss of that energy in photocatalyst excited states.

1.4.3. Improving Photocatalysis Through Catalyst Design

One of the primary strategies leveraged to minimize energetic losses has been the extensive investigation and design of catalyst structures to better conserve energy upon excitation and to prolong the lifetime of the excited state.^{81,82,97–102} While much of the early literature for synthetic photochemistry relies on a $\text{Ru}(\text{bpy})_3$ catalyst,^{87,88,90–93} this work was quickly followed by development of a series of additional photoactive ruthenium and iridium complexes (**Figure 1.21(a)**) with a variety of excited state and ground state redox potentials.^{80,103,104} Computation and photophysical studies revealed that these families of structures are effective photocatalysts due to metal to ligand charge transfer (MLCT) character where an electron is excited from a metal bound d orbital to a ligand π^* orbital (**Figure 1.21(b)**).^{105–110} The spatial separation of the ground state orbital and the excited state orbital is proposed to be responsible for prolonging the excited state lifetimes and increasing the potency of ruthenium and iridium complexes as

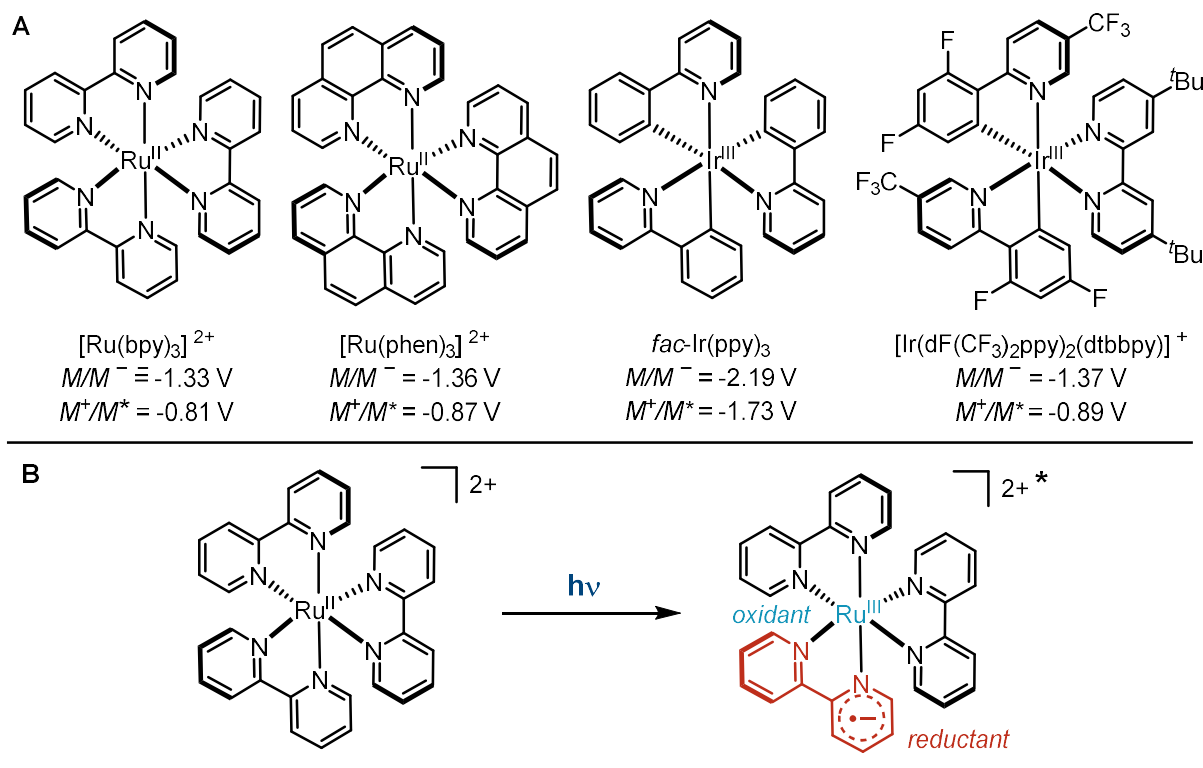


Figure 1.21. (a) Common ruthenium and iridium based photocatalysts used in synthesis and their reductive redox potentials. (b) Electron localization during metal to ligand charge transfer (MLCT).

photoreductants. A complementary direction of catalyst development has centered on designing photoactive organic molecules for reductive SET. Many of the most powerful and versatile structures possess a spatial separation between the ground state and excited state orbitals mimicking the MLCT character of metal based photocatalysts.¹¹¹ This property is referred to as donor-acceptor character^{112–114} and is most commonly achieved with a twisted catalyst core structure. This twisted property can be seen in the myriad of xanthene structures^{72,115,116} available for reductive transformations as well as in the widely used acridinium based catalysts developed and derivatized by Fukuzumi¹¹⁷ as well as Nicewicz.⁹⁸ Another powerful class of organic photocatalysts are substituted cyanoarene structures^{82,111,116,118} that were developed to optimize donor-acceptor character for OLED applications and have recently been leveraged in a variety of organic transformations.^{119,120} One of the most powerfully reducing organic photocatalyst scaffolds are the N-aryl phenothiazine structures^{121–124} first applied to radical polymerization and other organic transformations by Hawker and de Alaniz.¹²⁵ Despite being one of the strongest reducing organic photocatalyst families, N-aryl phenothiazines are ineffective for reduction events more negative than -2.5 V vs SCE which highlights the practical energetic limitations of visible light photochemical reduction. While photoredox catalysis offers one of the most radical selective

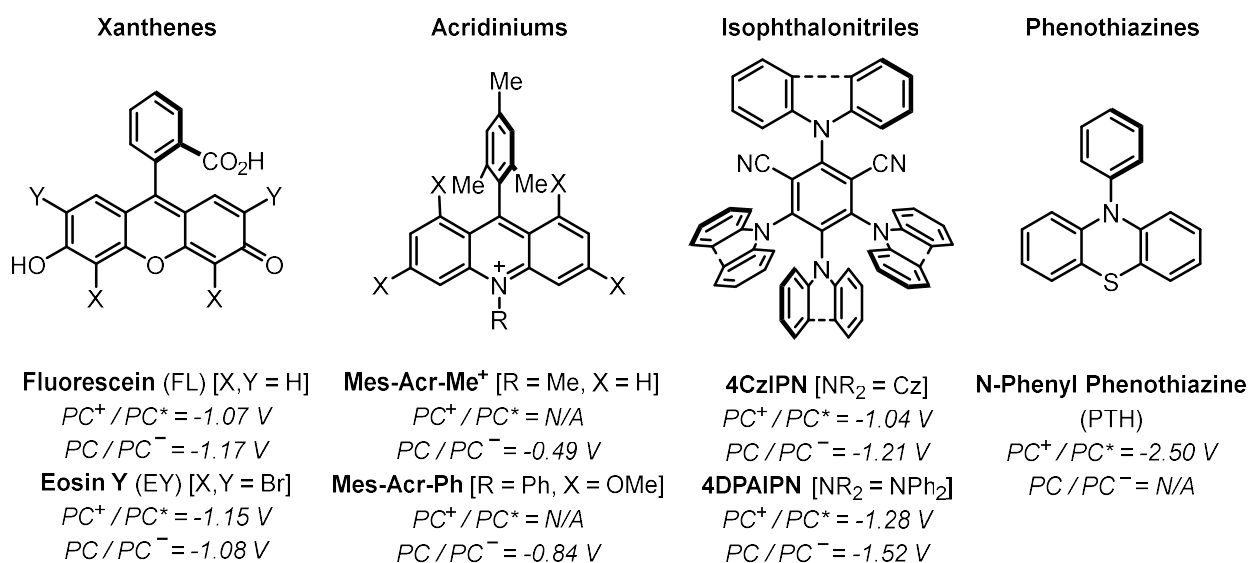


Figure 1.22. Some classic organic photoredox catalyst structures that have donor-acceptor character and their redox potentials as both ground state and excited state reductants.

and functional group tolerant strategies for promoting single electron reduction, it remains limited in reductive potency and many desirable substrates are inert to visible light photoreduction.⁹ Despite the advances in catalyst design to improve the redox potentials accessible with photocatalysis, it still falls significantly short in energetic potential when compared to dissolving metal conditions or electrochemical reductions.

1.5. Electron-Primed Photoredox Catalysis

1.5.1. Photoactivity of Radical Anion Structures

Designing a system for reductive SET that addresses the discrepancy between reductive potency and selectivity has been an area of interest and innovation in recent years. The most successful systems have relied on supplementing the energy harnessed from photoredox catalysis with a secondary energy source in the form of an SET reduction event to generate photoactive radical anions (**Figure 1.23**).^{126–128} The use of radical anions as photoreductants

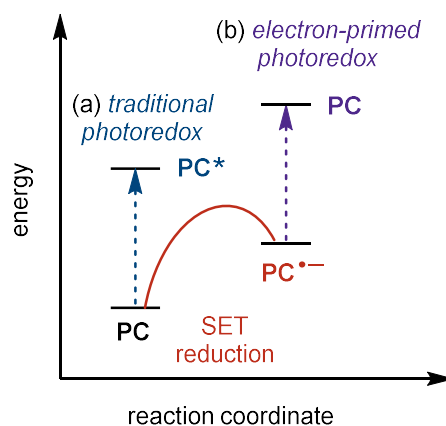


Figure 1.23. (a) The energy pathway and active excited state for traditional photoredox catalysis where energy is harnessed from light alone. (b) The energy pathway for electron-primed photoredox catalysis where energy is harnessed from both reduction and excitation

would effectively combine the energy inputs of the SET reduction event and the excitation to overall achieve more negative redox potentials while maintaining the selectivity profile characteristic of photoredox catalysis. Photophysical studies from the 1970s through the 1990s reveal that some radical anions generated via SET reduction are photoactive and can potentially be used to promote reduction of organic substrates (**Figure 1.24**). For example, Lund and

Carlsson¹²⁹ demonstrated via cyclic voltammetry that pyrene was photoactive upon SET reduction and could promote catalytic reduction of *m*-chlorotoluene. Work from Eriksen and Lund¹³⁰ as well as Eggins¹³¹ showed that additional radical anions of small molecules such as dicyanoanthracene or various quinones¹³¹ undergo fluorescence quenching by a range of unactivated arene substrates. Importantly, Wasielewski's¹³² investigation of various diimide catalyst structures revealed that electrochemical reduction followed by excitation results in powerfully reducing excited state radical anions. These studies taken together not only support the proposal that visible light excitation of radical anions can produce highly reducing excited state catalysts but also suggest that these catalysts can be leveraged to promote SET reduction of organic substrates.

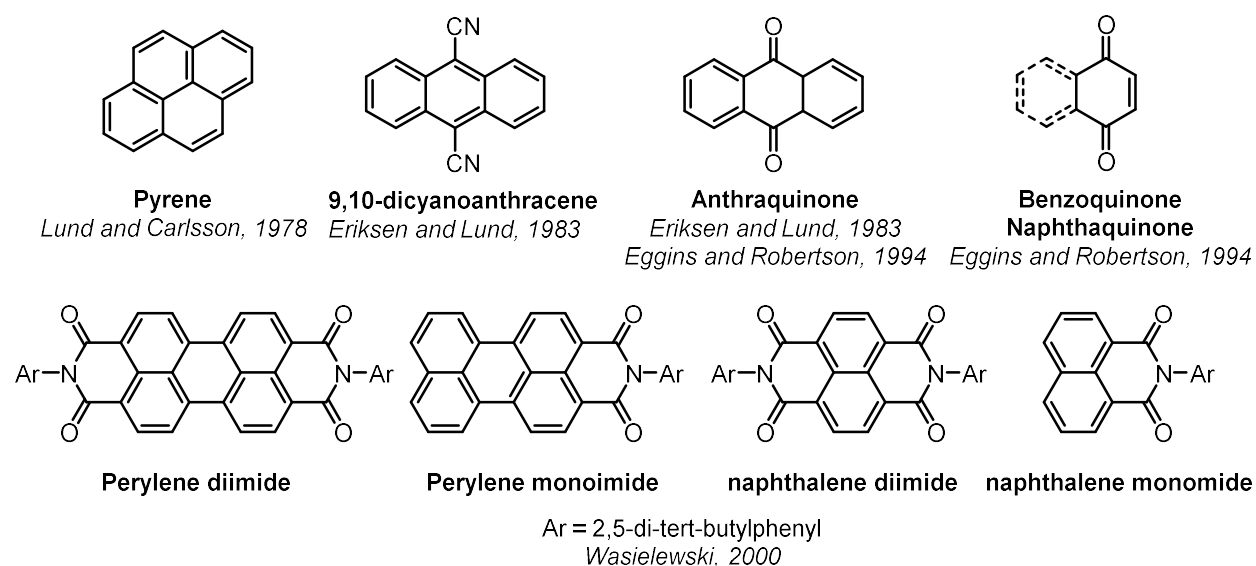


Figure 1.24. Organic catalyst structures that have been shown to be photoactive radical anions through CV studies or fluorescence quenching studies.

1.5.2. Reductive SET via Photoexcited Radical Anions

While it has been established that numerous radical anion structures are active as photoreductants, they have rarely been applied to synthetic organic transformations. Seminal work from König in 2014¹³³ reported the use of perylene diimide as a radical anion photoreductant (**Figure 1.26**) to promote SET reduction of aryl. This transformation was achieved via a consecutive photoinduced electron transfer (conPET) mechanism (**Figure 1.25**) where the active

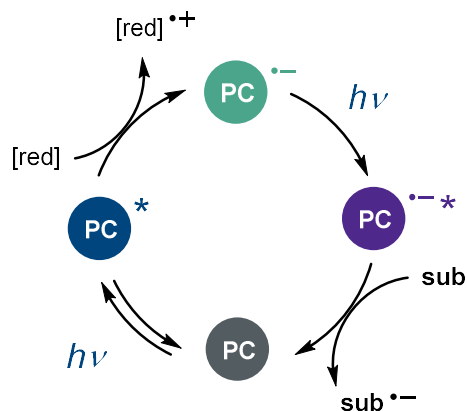
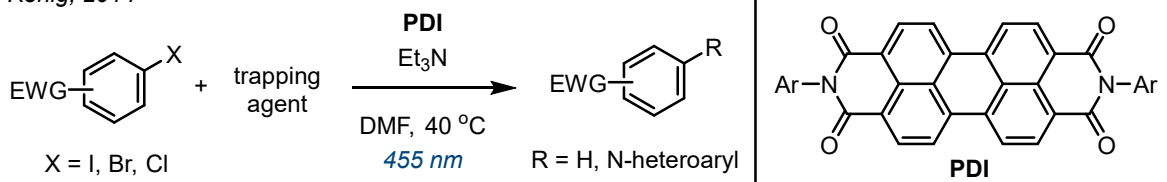


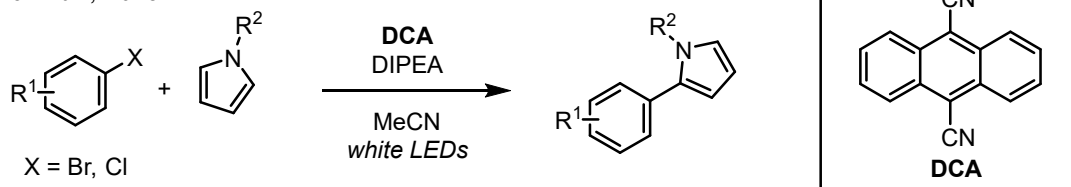
Figure 1.25. Mechanism for consecutive photoinduced electron transfer (conPET)

photoreductant is generated by a photoreduction event with a terminal reductant to provide the catalyst radical anion ground state. The radical anion then undergoes a second excitation event which produces a highly reducing excited state to promote SET with aryl halide substrates generating aryl radicals via mesolytic cleavage. Following this work, a conPET mechanism was leveraged by numerous groups¹³⁴ including Pérez-Ruiz,¹³⁵ Wickens,¹³⁶ and Nicewicz¹³⁷ (**Figure 1.26**) to promote challenging reductions of aryl halides with a variety of structurally diverse photocatalysts. ConPET systems have also been applied to substrates beyond aryl halides such as the reduction and cleavage of aliphatic tosyl amines from Nicewicz¹³⁷ (**Figure 1.26**), as well as Birch reduction of unactivated arenes from Miyake¹³⁸ (**Figure 1.26**). In these reports, the substrates engaged in reductive SET possess difficult reduction potentials that are well outside the range of traditional photoredox catalysis. Despite this, overreduction of radical intermediates is not an observed competitive pathway and radical couplings are carried out with good functional group tolerance suggesting that conPET reduction could be a broad and powerful platform for reductive chemistry. Unfortunately, this platform presents challenges in designing new catalyst structures or applications to new organic reactions. A conPET strategy requires that both oxidation states of a catalyst be photoactive and able to engage in SET events under a single set of reaction conditions. Additionally, both catalyst ground states as well as any reactive substrate derived intermediates must be compatible with a terminal reductant and any of its oxidation

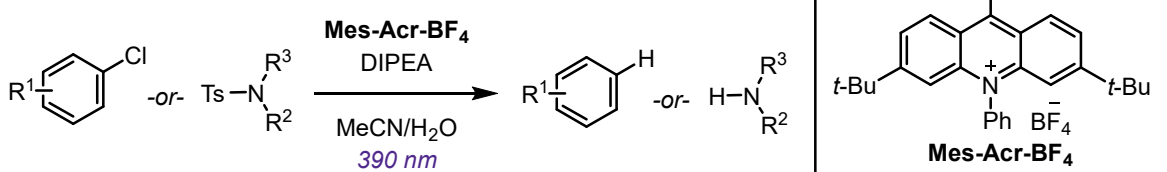
König, 2014



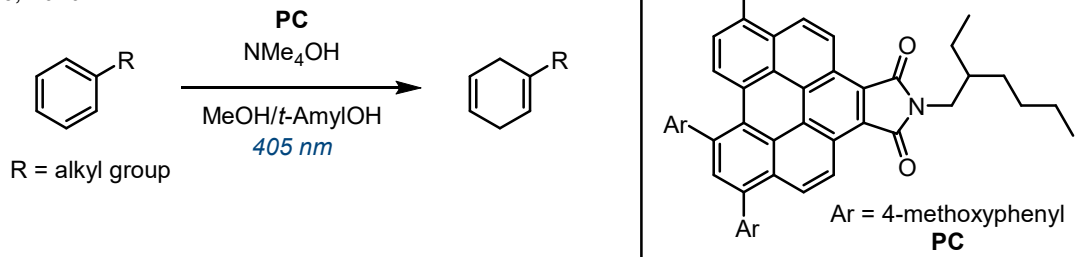
Pérez-Ruiz, 2018



Nicewicz, 2020



Miyake, 2020



Wickens, 2021

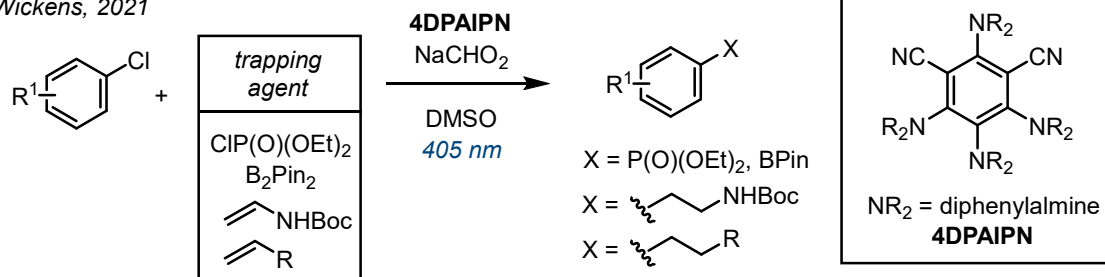


Figure 1.26. Reports of electron-primed photoredox catalysis reactions promoted by conPET mechanisms. Ar = 2,6-diisopropylphenyl.

byproducts. These requirements introduce significant restrictions and complexity to developing new conPET reactions. Using electrochemistry to access photoactive radical anions offers an attractive alternative to photoreduction as it removes many of the restrictions required for a

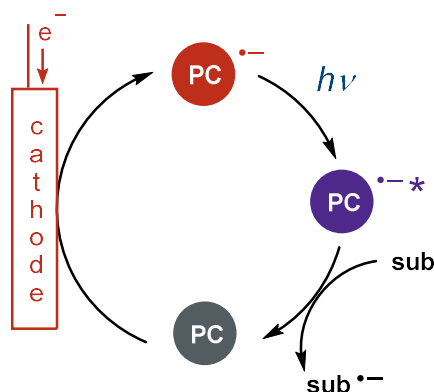
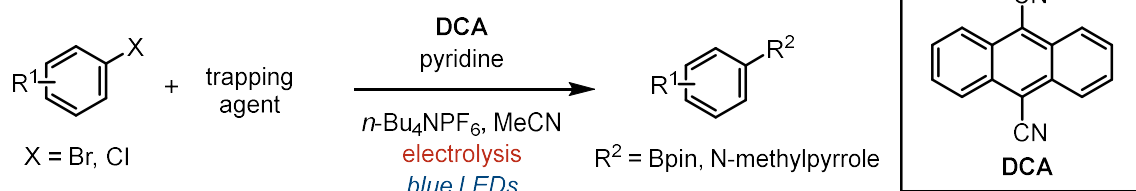


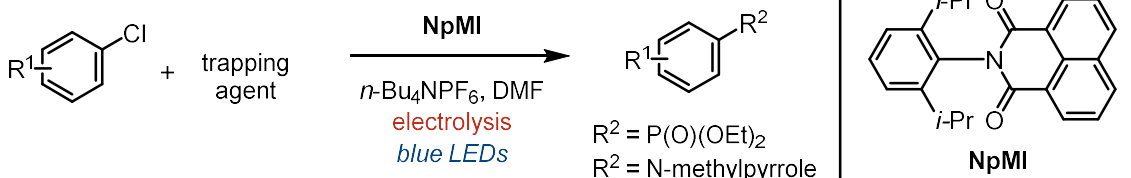
Figure 1.27. Mechanism for electrochemically driven radical anion photocatalysis.

conPET mechanism.¹²⁶ Electrochemical catalyst reduction (**Figure 1.27**) not only offers versatility in the applied potential to study numerous catalytic structures under the same reaction conditions, but also requires only a single excitation event to generate the active excited radical anion reductant. Furthermore, use of a divided cell negates the compatibility requirement between terminal reductants or byproducts and the catalytic cycle. The fewer design requirements for the catalytic cycle makes electrochemistry an ideal exploratory tool for expanding the field of radical anion photocatalysis. Indeed, several studies in the last five years have shown electrochemistry to be valuable for rapidly studying numerous catalytic structures as potent photoreductants. Lambert and Lin¹³⁹ (**Figure 1.28**) revealed improved reactivity for a 9,10-dicyanoanthracene catalyst in promoting aryl halide reductions compared to a conPET system¹³⁵ by forming the radical anion via electrochemistry rather than photoreduction. Concurrent work from Wickens¹⁴⁰ (**Figure 1.28**) also showed that electrochemical reduction enabled potent photoreductant activity of a naphthalene monoimide radical anion catalyst that had previously been known to be photoactive¹³² but had not been applied to reductive SET on challenging substrates. Additional work from Wickens¹⁴¹ (**Figure 1.28**) leveraged electrochemistry to expand electron-primed photoredox catalysis and revealed that many known catalytic structures have radical anion states with unreported potent photoreductant activity. A particularly effective catalyst, 4DPAIPN,¹²⁰ was discovered to promote SET reduction of previously inert trialkylarylammonium salts^{142,143} as well

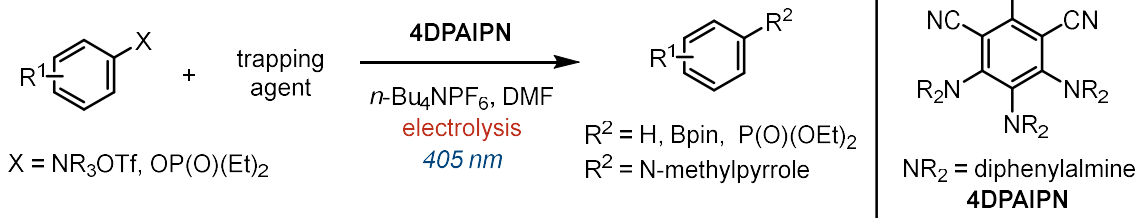
Lambert and Lin, 2020



Wickens, 2020



Wickens, 2021



Barham and König, 2021

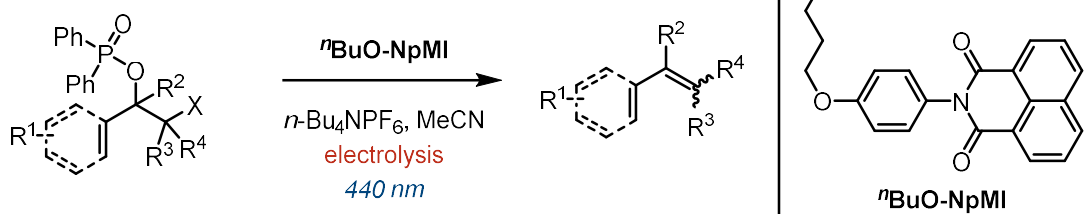


Figure 1.28. Reports of electron-primed photoredox catalysis reactions promoted by electrochemical reduction.

as aryl phosphate esters¹⁴⁴ and engage them in radical coupling reactions. Barham and König¹⁴⁵ (**Figure 1.28**) expanded the application of an electrochemical catalytic platform beyond arene substrate reduction by showing that a naphthyl imide catalyst can be used to activate conjugated phosphinates for mesolytic cleavage under electrophotochemical conditions. Taken together, these reports demonstrate the value of electrochemistry as a versatile tool for catalyst discovery and reaction development. Despite the challenging reduction potentials of the substrates reduced

in these electrochemical studies, excellent functional group tolerance was observed as well as a preference for radical pathways.

The work that has been done to develop the field of electron-primed photoredox catalysis, both by conPET or electrochemical reduction mechanisms, has proven this system to be both powerful for reductive SET but also selective toward radical transformations and sensitive functional groups.¹²⁶ While this field is still being developed, it is already showing great promise as a solution to reconciling deeply reducing conditions with reaction selectivity which is a significant obstacle in dissolving metal conditions, electrolysis, and classic photoredox catalysis.

1.6 References

- (1) Yan, M.; Lo, J. C.; Edwards, J. T.; Baran, P. S. Radicals: Reactive Intermediates with Translational Potential. *J. Am. Chem. Soc.* **2016**, *138* (39), 12692–12714. <https://doi.org/10.1021/jacs.6b08856>.
- (2) Houmam, A. Electron Transfer Initiated Reactions: Bond Formation and Bond Dissociation. *Chem. Rev.* **2008**, *108* (7), 2180–2237. <https://doi.org/10.1021/cr068070x>.
- (3) Ebersson, L. Electron-Transfer Reactions in Organic Chemistry. In *Advances in Physical Organic Chemistry*; Gold, V., Bethell, D., Eds.; Academic Press, 1982; Vol. 18, pp 79–185. [https://doi.org/10.1016/S0065-3160\(08\)60139-2](https://doi.org/10.1016/S0065-3160(08)60139-2).
- (4) Studer, A.; Curran, D. P. Catalysis of Radical Reactions: A Radical Chemistry Perspective. *Angew. Chem. Int. Ed.* **2016**, *55* (1), 58–102. <https://doi.org/10.1002/anie.201505090>.
- (5) Ashby, E. C. Single-Electron Transfer, a Major Reaction Pathway in Organic Chemistry. An Answer to Recent Criticisms. *Acc. Chem. Res.* **1988**, *21* (11), 414–421. <https://doi.org/10.1021/ar00155a005>.
- (6) Zhang, N.; Samanta, S. R.; Rosen, B. M.; Percec, V. Single Electron Transfer in Radical Ion and Radical-Mediated Organic, Materials and Polymer Synthesis. *Chem. Rev.* **2014**, *114* (11), 5848–5958. <https://doi.org/10.1021/cr400689s>.
- (7) Broggi, J.; Terme, T.; Vanelle, P. Organic Electron Donors as Powerful Single-Electron Reducing Agents in Organic Synthesis. *Angew. Chem. Int. Ed.* **2014**, *53* (2), 384–413. <https://doi.org/10.1002/anie.201209060>.
- (8) W. Friese, F.; Studer, A. New Avenues for C–B Bond Formation via Radical Intermediates. *Chem. Sci.* **2019**, *10* (37), 8503–8518. <https://doi.org/10.1039/C9SC03765A>.
- (9) Nicewicz, D. Experimental and Calculated Electrochemical Potentials of Common Organic Molecules for Applications to Single-Electron Redox Chemistry. *Synlett* **2016**, *27*, 714–723.
- (10) Andrieux, C. P.; Pinson, J. The Standard Redox Potential of the Phenyl Radical/Anion Couple. *J. Am. Chem. Soc.* **2003**, *125* (48), 14801–14806. <https://doi.org/10.1021/ja0374574>.
- (11) Shono, T.; Matsumura, Y.; Tsubata, K.; Yoshihiro, S. Selective Transformation of Aliphatic Alcohols to Alkanes by Electroreductive Method. *Tetrahedron Lett.* **1979**, *20* (23), 2157–2160. [https://doi.org/10.1016/S0040-4039\(01\)86289-4](https://doi.org/10.1016/S0040-4039(01)86289-4).
- (12) Wardman, P. Reduction Potentials of One-Electron Couples Involving Free Radicals in Aqueous Solution. *J. Phys. Chem. Ref. Data* **1989**, *18* (4), 1637–1755. <https://doi.org/10.1063/1.555843>.

- (13) Peng, D.; Fan, W.; Zhao, X.; Chen, W.; Wen, Y.; Zhang, L.; Li, S. Zinc–Brønsted Acid Mediated Practical Hydrotrifluoromethylation of Alkenes with CF₃Br. *Org. Chem. Front.* **2021**, 8 (22), 6356–6363. <https://doi.org/10.1039/D1QO01073E>.
- (14) Kroemer, J.; Kirkpatrick, C.; Maricle, B.; Gawrych, R.; Mosher, M. D.; Kaufman, D. Rieke Zinc as a Reducing Agent for Common Organic Functional Groups. *Tetrahedron Lett.* **2006**, 47 (36), 6339–6341. <https://doi.org/10.1016/j.tetlet.2006.07.003>.
- (15) Li, Z.; Wang, K.-F.; Zhao, X.; Ti, H.; Liu, X.-G.; Wang, H. Manganese-Mediated Reductive Functionalization of Activated Aliphatic Acids and Primary Amines. *Nat. Commun.* **2020**, 11 (1), 5036. <https://doi.org/10.1038/s41467-020-18834-6>.
- (16) Knappke, C. E. I.; Grupe, S.; Gärtner, D.; Corpet, M.; Gosmini, C.; Jacobi von Wangelin, A. Reductive Cross-Coupling Reactions between Two Electrophiles. *Chem. – Eur. J.* **2014**, 20 (23), 6828–6842. <https://doi.org/10.1002/chem.201402302>.
- (17) Dai, P.; Dussault, P. H.; Trullinger, T. K. Magnesium/Methanol: An Effective Reducing Agent for Peroxides. *J. Org. Chem.* **2004**, 69 (8), 2851–2852. <https://doi.org/10.1021/jo035191d>.
- (18) Ohno, T.; Sakai, M.; Ishino, Y.; Shibata, T.; Maekawa, H.; Nishiguchi, I. Mg-Promoted Regio- and Stereoselective C-Acylation of Aromatic α,β -Unsaturated Carbonyl Compounds. *Org. Lett.* **2001**, 3 (22), 3439–3442. <https://doi.org/10.1021/ol016376e>.
- (19) Combellas, C.; Kanoufi, F.; Thiébault, A. Solutions of Solvated Electrons in Liquid Ammonia: Part 1. Chemical Properties of Magnesium Solutions. *J. Electroanal. Chem.* **2001**, 499 (1), 144–151. [https://doi.org/10.1016/S0022-0728\(00\)00504-0](https://doi.org/10.1016/S0022-0728(00)00504-0).
- (20) Hoz, S. Samarium Iodide Showcase: Unraveling the Mechanistic Puzzle. *Acc. Chem. Res.* **2020**, 53 (11), 2680–2691. <https://doi.org/10.1021/acs.accounts.0c00497>.
- (21) Nicolaou, K. C.; Ellery, S. P.; Chen, J. S. Samarium Diodide Mediated Reactions in Total Synthesis. *Angew. Chem. Int. Ed.* **2009**, 48 (39), 7140–7165. <https://doi.org/10.1002/anie.200902151>.
- (22) Birch, A. J. 117. Reduction by Dissolving Metals. Part I. *J. Chem. Soc. Resumed* **1944**, No. 0, 430–436. <https://doi.org/10.1039/JR9440000430>.
- (23) Rabideau, P. W. The Metal-Ammonia Reduction of Aromatic Compounds. *Tetrahedron* **1989**, 45 (6), 1579–1603. [https://doi.org/10.1016/S0040-4020\(01\)80022-3](https://doi.org/10.1016/S0040-4020(01)80022-3).
- (24) Zimmerman, H. E. Orientation in Metal Ammonia Reductions. *Tetrahedron* **1961**, 16 (1), 169–176. [https://doi.org/10.1016/0040-4020\(61\)80067-7](https://doi.org/10.1016/0040-4020(61)80067-7).
- (25) Bouveault, L.; Blanc, G. Préparation Des Alcools Primaires Au Moyen Des Acides Correspondants. *Compt Rend* **1903**, 136, 1676–1678.
- (26) Heravi, M. M.; Fard, M. V.; Faghihi, Z. Recent Applications of Birch Reduction in Total Synthesis of Natural Products. *Curr. Org. Chem.* **19** (15), 1491–1525.
- (27) Zimmerman, H. E. A Mechanistic Analysis of the Birch Reduction. *Acc. Chem. Res.* **2012**, 45 (2), 164–170. <https://doi.org/10.1021/ar2000698>.
- (28) Dias, L. C.; de Oliveira, L. G.; de Sousa, M. A. Total Synthesis of (–)-Pironetin. *Org. Lett.* **2003**, 5 (3), 265–268. <https://doi.org/10.1021/ol027211o>.
- (29) Han, M.; Ding, Y.; Yan, Y.; Li, H.; Luo, S.; Adijiang, A.; Ling, Y.; An, J. Transition-Metal-Free, Selective Reductive Deuteration of Terminal Alkynes with Sodium Dispersions and EtOD-D₁. *Org. Lett.* **2018**, 20 (10), 3010–3013. <https://doi.org/10.1021/acs.orglett.8b01036>.
- (30) Huffman, J. W.; McWhorter, W. W. Dissolving Metal Reduction of Cyclic Ketones. *J. Org. Chem.* **1979**, 44 (4), 594–599. <https://doi.org/10.1021/jo01318a023>.
- (31) Kaiser, E. M.; Edmonds, C. G.; Grubb, S. D.; Smith, J. W.; Tramp, D. Alkali Metal Reductions of Epoxides, Ketals, and Related Heterocycles. Intermediacy of Carbanions. *J. Org. Chem.* **1971**, 36 (2), 330–335. <https://doi.org/10.1021/jo00801a019>.
- (32) Paquette, L. A.; Fuhr, K. H. Intramolecular Epoxide Cleavage by Dissolving Metal Reduction of Proximal Cyclopropane Rings. *J. Am. Chem. Soc.* **1972**, 94 (26), 9221–9222. <https://doi.org/10.1021/ja00781a040>.

- (33) Chuang, K. V.; Xu, C.; Reisman, S. E. A 15-Step Synthesis of (+)-Ryanodol. *Science* **2016**, 353 (6302), 912–915. <https://doi.org/10.1126/science.aag1028>.
- (34) Joshi, D. K.; Sutton, J. W.; Carver, S.; Blanchard, J. P. Experiences with Commercial Production Scale Operation of Dissolving Metal Reduction Using Lithium Metal and Liquid Ammonia. *Org. Process Res. Dev.* **2005**, 9 (6), 997–1002. <https://doi.org/10.1021/op050155x>.
- (35) Burrows, J.; Kamo, S.; Koide, K. Scalable Birch Reduction with Lithium and Ethylenediamine in Tetrahydrofuran. *Science* **2021**, 374 (6568), 741–746. <https://doi.org/10.1126/science.abk3099>.
- (36) Yan, M.; Kawamata, Y.; Baran, P. S. Synthetic Organic Electrochemical Methods Since 2000: On the Verge of a Renaissance. *Chem. Rev.* **2017**, 117 (21), 13230–13319. <https://doi.org/10.1021/acs.chemrev.7b00397>.
- (37) Yoshida, J.; Kataoka, K.; Horcajada, R.; Nagaki, A. Modern Strategies in Electroorganic Synthesis. *Chem. Rev.* **2008**, 108 (7), 2265–2299. <https://doi.org/10.1021/cr0680843>.
- (38) Wiebe, A.; Gieshoff, T.; Möhle, S.; Rodrigo, E.; Zirbes, M.; Waldvogel, S. R. Electrifying Organic Synthesis. *Angew. Chem. Int. Ed.* **2018**, 57 (20), 5594–5619. <https://doi.org/10.1002/anie.201711060>.
- (39) Brett, C. Fundamentals of Electrochemistry. In *Piezoelectric Transducers and Applications*; Arnau Vives, A., Ed.; Springer: Berlin, Heidelberg, 2004; pp 185–194. https://doi.org/10.1007/978-3-662-05361-4_11.
- (40) Moeller, K. D. Using Physical Organic Chemistry To Shape the Course of Electrochemical Reactions. *Chem. Rev.* **2018**, 118 (9), 4817–4833. <https://doi.org/10.1021/acs.chemrev.7b00656>.
- (41) Kingston, C.; Palkowitz, M. D.; Takahira, Y.; Vantourout, J. C.; Peters, B. K.; Kawamata, Y.; Baran, P. S. A Survival Guide for the “Electro-Curious.” *Acc. Chem. Res.* **2020**, 53 (1), 72–83. <https://doi.org/10.1021/acs.accounts.9b00539>.
- (42) Narra, S.; Nishimura, Y.; Witek, H. A.; Shigeto, S. Mechanism of Back Electron Transfer in an Intermolecular Photoinduced Electron Transfer Reaction: Solvent as a Charge Mediator. *ChemPhysChem* **2014**, 15 (14), 2945–2950. <https://doi.org/10.1002/cphc.201402411>.
- (43) Lalevée, J.; Allonas, X.; Fouassier, J.-P. N–H and α (C–H) Bond Dissociation Enthalpies of Aliphatic Amines. *J. Am. Chem. Soc.* **2002**, 124 (32), 9613–9621. <https://doi.org/10.1021/ja0204168>.
- (44) Shen, Y.; Funez-Ardoiz, I.; Schoenebeck, F.; Rovis, T. Site-Selective α -C–H Functionalization of Trialkylamines via Reversible Hydrogen Atom Transfer Catalysis. *J. Am. Chem. Soc.* **2021**, 143 (45), 18952–18959. <https://doi.org/10.1021/jacs.1c07144>.
- (45) Le, C.; Liang, Y.; Evans, R. W.; Li, X.; MacMillan, D. W. C. Selective Sp³ C–H Alkylation via Polarity-Match-Based Cross-Coupling. *Nature* **2017**, 547 (7661), 79–83. <https://doi.org/10.1038/nature22813>.
- (46) Hilt, G. Basic Strategies and Types of Applications in Organic Electrochemistry. *ChemElectroChem* **2020**, 7 (2), 395–405. <https://doi.org/10.1002/celec.201901799>.
- (47) Appel, A. M.; Helm, M. L. Determining the Overpotential for a Molecular Electrocatalyst. *ACS Catal.* **2014**, 4 (2), 630–633. <https://doi.org/10.1021/cs401013v>.
- (48) Stahl, S. S.; Gerken, J.; Nutting, J. “How Should I Think about Voltage? What Is Overpotential?": Establishing an Organic Chemistry Intuition for Electrochemistry. *J. Org. Chem.* **2021**, 86 (22), 15875–15885.
- (49) Ren, Y.; Yu, C.; Tan, X.; Huang, H.; Wei, Q.; Qiu, J. Strategies to Suppress Hydrogen Evolution for Highly Selective Electrocatalytic Nitrogen Reduction: Challenges and Perspectives. *Energy Environ. Sci.* **2021**, 14 (3), 1176–1193. <https://doi.org/10.1039/D0EE03596C>.

- (50) Edinger, C.; Waldvogel, S. R. Electrochemical Deoxygenation of Aromatic Amides and Sulfoxides. *Eur. J. Org. Chem.* **2014**, 2014 (24), 5144–5148. <https://doi.org/10.1002/ejoc.201402714>.
- (51) Edinger, C.; Grimaudo, V.; Broekmann, P.; Waldvogel, S. R. Stabilizing Lead Cathodes with Diammonium Salt Additives in the Deoxygenation of Aromatic Amides. *ChemElectroChem* **2014**, 1 (6), 1018–1022. <https://doi.org/10.1002/celec.201402050>.
- (52) Fang, C.; Tran, T.-N.; Zhao, Y.; Liu, G. Electrolyte Decomposition and Solid Electrolyte Interphase Revealed by Mass Spectrometry. *Electrochimica Acta* **2021**, 399, 139362. <https://doi.org/10.1016/j.electacta.2021.139362>.
- (53) Peters, B. K.; Rodriguez, K. X.; Reisberg, S. H.; Beil, S. B.; Hickey, D. P.; Kawamata, Y.; Collins, M.; Starr, J.; Chen, L.; Udyavara, S.; Klunder, K.; Gorey, T. J.; Anderson, S. L.; Neurock, M.; Minter, S. D.; Baran, P. S. Scalable and Safe Synthetic Organic Electroreduction Inspired by Li-Ion Battery Chemistry. *Science* **2019**, 363 (6429), 838–845. <https://doi.org/10.1126/science.aav5606>.
- (54) Mizushima, K.; Jones, P. C.; Wiseman, P. J.; Goodenough, J. B. LiCoO₂ (0. *Mater. Res. Bull.* **1980**, 15 (6), 783–789. [https://doi.org/10.1016/0025-5408\(80\)90012-4](https://doi.org/10.1016/0025-5408(80)90012-4).
- (55) Koch, D. A.; Henne, B. J.; Bartak, D. E. Carbanion and Radical Intermediacy in the Electrochemical Reduction of Benzyl Halides in Acetonitrile. *J. Electrochem. Soc.* **1987**, 134 (12), 3062–3067. <https://doi.org/10.1149/1.2100340>.
- (56) Francke, R.; Little, R. D. Redox Catalysis in Organic Electrosynthesis: Basic Principles and Recent Developments. *Chem. Soc. Rev.* **2014**, 43 (8), 2492–2521. <https://doi.org/10.1039/C3CS60464K>.
- (57) Meyer, T. H.; Finger, L. H.; Gandeepan, P.; Ackermann, L. Resource Economy by Metallalectrocatalysis: Merging Electrochemistry and CH Activation. *Trends Chem.* **2019**, 1 (1), 63–76. <https://doi.org/10.1016/j.trechm.2019.01.011>.
- (58) Steckhan, E. Indirect Electroorganic Syntheses—A Modern Chapter of Organic Electrochemistry [New Synthetic Methods (59)]. *Angew. Chem. Int. Ed. Engl.* **1986**, 25 (8), 683–701. <https://doi.org/10.1002/anie.198606831>.
- (59) Steckhan, E. Organic Syntheses with Electrochemically Regenerable Redox Systems. In *Electrochemistry I*; Steckhan, E., Ed.; Topics in Current Chemistry; Springer: Berlin, Heidelberg, 1987; pp 1–69. https://doi.org/10.1007/3-540-17871-6_11.
- (60) Hammerich, O.; Speiser, B. *Organic Electrochemistry: Revised and Expanded*; CRC Press, 2015.
- (61) Francke, R.; Little, R. D. Optimizing Electron Transfer Mediators Based on Arylimidazoles by Ring Fusion: Synthesis, Electrochemistry, and Computational Analysis of 2-Aryl-1-Methylphenanthro[9,10-d]imidazoles. *J. Am. Chem. Soc.* **2014**, 136 (1), 427–435. <https://doi.org/10.1021/ja410865z>.
- (62) Little, R. D. A Perspective on Organic Electrochemistry. *J. Org. Chem.* **2020**, 85 (21), 13375–13390. <https://doi.org/10.1021/acs.joc.0c01408>.
- (63) Folest, J.-C.; Duprilot, J.-M.; Perichon, J.; Robin, Y.; Devynck, J. Electrocatalyzed Carboxylation of Organic Halides by a Cobalt-Salen Complex. *Tetrahedron Lett.* **1985**, 26 (22), 2633–2636. [https://doi.org/10.1016/S0040-4039\(00\)98122-X](https://doi.org/10.1016/S0040-4039(00)98122-X).
- (64) Boujlél, K.; Simonet, J. Cathodic Cleavage of Carbon-Oxygen Bonds (V). Direct and Indirect Electrochemical Reduction of Epoxides. *Electrochimica Acta* **1979**, 24 (5), 481–487. [https://doi.org/10.1016/0013-4686\(79\)85020-3](https://doi.org/10.1016/0013-4686(79)85020-3).
- (65) Boujlél, K.; Simonet, J.; Barnier, J.-P.; Girard, C.; Conia, J.-M. Electrochemically Induced Opening of Three-Membered Rings: Direct and Indirect Reduction of Methylene cyclopropanes. *J. Electroanal. Chem. Interfacial Electrochem.* **1981**, 117 (1), 161–166. [https://doi.org/10.1016/S0022-0728\(81\)80460-3](https://doi.org/10.1016/S0022-0728(81)80460-3).

- (66) Hosoi, K.; Inagi, S.; Kubo, T.; Fuchigami, T. O-Carborane as an Electron-Transfer Mediator in Electrocatalytic Reduction. *Chem. Commun.* **2011**, 47 (30), 8632–8634. <https://doi.org/10.1039/C1CC12912K>.
- (67) Fuchigami, T.; Kasuga, M.; Konno, A. Electro-Organic Chemistry of Fullerenes. Part 1. Indirect Cathodic Reduction of Vic-Dihalides and Perfluoroalkyl Halides Using C60 as Mediator. Cyclic Voltammetric Study and Preparative-Scale Electrolysis. *J. Electroanal. Chem.* **1996**, 411 (1), 115–119. [https://doi.org/10.1016/0022-0728\(96\)04583-4](https://doi.org/10.1016/0022-0728(96)04583-4).
- (68) Simonet, J.; Michel, M.-A.; Lund, H.; Nimmich, W.; Servin, R.; Sternerup, H. Indirect Electrolysis. Reaction between Alkyl Halides and Electrolytically Generated Anion Radicals. *Acta Chem. Scand.* **1975**, 29b, 489–498. <https://doi.org/10.3891/acta.chem.scand.29b-0489>.
- (69) Swartz, J. E.; Mahachi, T. J.; Kariv-Miller, Essie. Electrochemical Reduction of Ketones Mediated by (Dimethylpyrrolidino)Mercury. Reductive Cyclization of Unsaturated Ketones and Redox Catalysis Studies. *J. Am. Chem. Soc.* **1988**, 110 (11), 3622–3628. <https://doi.org/10.1021/ja00219a042>.
- (70) Prier, C. K.; Rankic, D. A.; MacMillan, D. W. C. Visible Light Photoredox Catalysis with Transition Metal Complexes: Applications in Organic Synthesis. *Chem. Rev.* **2013**, 113 (7), 5322–5363. <https://doi.org/10.1021/cr300503r>.
- (71) Shaw, M. H.; Twilton, J.; MacMillan, D. W. C. Photoredox Catalysis in Organic Chemistry. *J. Org. Chem.* **2016**, 81 (16), 6898–6926. <https://doi.org/10.1021/acs.joc.6b01449>.
- (72) Romero, N. A.; Nicewicz, D. A. Organic Photoredox Catalysis. *Chem. Rev.* **2016**, 116 (17), 10075–10166. <https://doi.org/10.1021/acs.chemrev.6b00057>.
- (73) Skubi, K. L.; Blum, T. R.; Yoon, T. P. Dual Catalysis Strategies in Photochemical Synthesis. *Chem. Rev.* **2016**, 116 (17), 10035–10074. <https://doi.org/10.1021/acs.chemrev.6b00018>.
- (74) DiRocco, D. A.; Dykstra, K.; Krska, S.; Vachal, P.; Conway, D. V.; Tudge, M. Late-Stage Functionalization of Biologically Active Heterocycles Through Photoredox Catalysis. *Angew. Chem. Int. Ed.* **2014**, 53 (19), 4802–4806. <https://doi.org/10.1002/anie.201402023>.
- (75) Narayanam, J. M. R.; Stephenson, C. R. J. Visible Light Photoredox Catalysis: Applications in Organic Synthesis. *Chem. Soc. Rev.* **2010**, 40 (1), 102–113. <https://doi.org/10.1039/B913880N>.
- (76) D. Bell, J.; A. Murphy, J. Recent Advances in Visible Light-Activated Radical Coupling Reactions Triggered by (i) Ruthenium, (ii) Iridium and (iii) Organic Photoredox Agents. *Chem. Soc. Rev.* **2021**, 50 (17), 9540–9685. <https://doi.org/10.1039/D1CS00311A>.
- (77) Medina, E.; Sandoval-Pauker, C.; Salvador, P.; Pinter, B. Mechanistic Insights into the Oxidative and Reductive Quenching Cycles of Transition Metal Photoredox Catalysts through Effective Oxidation State Analysis. *Inorg. Chem.* **2022**, 61 (47), 18923–18933. <https://doi.org/10.1021/acs.inorgchem.2c02945>.
- (78) Reckenthäler, M.; Griesbeck, A. G. Photoredox Catalysis for Organic Syntheses. *Adv. Synth. Catal.* **2013**, 355 (14–15), 2727–2744. <https://doi.org/10.1002/adsc.201300751>.
- (79) Kim, D.; Teets, T. S. Strategies for Accessing Photosensitizers with Extreme Redox Potentials. *Chem. Phys. Rev.* **2022**, 3 (2), 021302. <https://doi.org/10.1063/5.0084554>.
- (80) Arias-Rotondo, D. M.; McCusker, J. K. The Photophysics of Photoredox Catalysis: A Roadmap for Catalyst Design. *Chem. Soc. Rev.* **2016**, 45 (21), 5803–5820. <https://doi.org/10.1039/C6CS00526H>.
- (81) Herr, P.; Glaser, F.; Büldt, L. A.; Larsen, C. B.; Wenger, O. S. Long-Lived, Strongly Emissive, and Highly Reducing Excited States in Mo(0) Complexes with Chelating Isocyanides. *J. Am. Chem. Soc.* **2019**, 141 (36), 14394–14402. <https://doi.org/10.1021/jacs.9b07373>.

- (82) Speckmeier, E.; Fischer, T. G.; Zeitler, K. A Toolbox Approach To Construct Broadly Applicable Metal-Free Catalysts for Photoredox Chemistry: Deliberate Tuning of Redox Potentials and Importance of Halogens in Donor–Acceptor Cyanoarenes. *J. Am. Chem. Soc.* **2018**, *140* (45), 15353–15365. <https://doi.org/10.1021/jacs.8b08933>.
- (83) Roundhill, D. M. *Photochemistry and Photophysics of Metal Complexes*; Springer US: Boston, MA, 1994. <https://doi.org/10.1007/978-1-4899-1495-8>.
- (84) Sartor, S. M.; Lattke, Y. M.; McCarthy, B. G.; Miyake, G. M.; Damrauer, N. H. Effects of Naphthyl Connectivity on the Photophysics of Compact Organic Charge-Transfer Photoredox Catalysts. *J. Phys. Chem. A* **2019**, *123* (22), 4727–4736. <https://doi.org/10.1021/acs.jpca.9b03286>.
- (85) Fischer, C.; Kerzig, C.; Zilate, B.; Wenger, O. S.; Sparr, C. Modulation of Acridinium Organophotoredox Catalysts Guided by Photophysical Studies. *ACS Catal.* **2020**, *10* (1), 210–215. <https://doi.org/10.1021/acscatal.9b03606>.
- (86) Dick, B. 2. Photophysics of Photocatalysts. In *2. Photophysics of photocatalysts*; De Gruyter, 2020; pp 17–44. <https://doi.org/10.1515/9783110576764-002>.
- (87) Hedstrand, D. M.; Kruizinga, W. H.; Kellogg, R. M. Light Induced and Dye Accelerated Reductions of Phenacyl Onium Salts by 1,4-Dihydropyridines. *Tetrahedron Lett.* **1978**, *19* (14), 1255–1258. [https://doi.org/10.1016/S0040-4039\(01\)94515-0](https://doi.org/10.1016/S0040-4039(01)94515-0).
- (88) Mashraqui, S. H.; Kellogg, R. M. 3-Methyl-2,3-Dihydrobenzothiazoles as Reducing Agent. Dye Enhanced Photoreactions. *Tetrahedron Lett.* **1985**, *26* (11), 1453–1456. [https://doi.org/10.1016/S0040-4039\(00\)99069-5](https://doi.org/10.1016/S0040-4039(00)99069-5).
- (89) Maidan, R.; Goren, Z.; Becker, J. Y.; Willner, I. Application of Multielectron Charge Relays in Chemical and Photochemical Debromination Processes. The Role of Induced Disproportionation of N,N'-Dioctyl-4,4'-Bipyridinium Radical Cation in Two-Phase Systems. *J. Am. Chem. Soc.* **1984**, *106* (21), 6217–6222. <https://doi.org/10.1021/ja00333a017>.
- (90) Cano-Yelo, H.; Deronzier, A. Photocatalysis of the Pschorr Reaction by Tris-(2,2'-Bipyridyl)Ruthenium(II) in the Phenanthrene Series. *J. Chem. Soc. Perkin Trans. 2* **1984**, No. 6, 1093–1098. <https://doi.org/10.1039/P29840001093>.
- (91) Fukuzumi, Shunichi.; Mochizuki, Seiji.; Tanaka, Toshio. Photocatalytic Reduction of Phenacyl Halides by 9,10-Dihydro-10-Methylacridine: Control between the Reductive and Oxidative Quenching Pathways of Tris(Bipyridine)Ruthenium Complex Utilizing an Acid Catalysis. *J. Phys. Chem.* **1990**, *94* (2), 722–726. <https://doi.org/10.1021/j100365a039>.
- (92) Pac, C.; Ihama, M.; Yasuda, M.; Miyauchi, Y.; Sakurai, H. Tris(2,2'-Bipyridine)Ruthenium(2+)-Mediated Photoreduction of Olefins with 1-Benzyl-1,4-Dihydronicotinamide: A Mechanistic Probe for Electron-Transfer Reactions of NAD(P)H-Model Compounds. *J. Am. Chem. Soc.* **1981**, *103* (21), 6495–6497. <https://doi.org/10.1021/ja00411a040>.
- (93) Hironaka, K.; Fukuzumi, S.; Tanaka, T. Tris(Bipyridyl)Ruthenium(II)-Photosensitized Reaction of 1-Benzyl-1,4-Dihydronicotinamide with Benzyl Bromide. *J. Chem. Soc. Perkin Trans. 2* **1984**, No. 10, 1705–1709. <https://doi.org/10.1039/P29840001705>.
- (94) Nicewicz, D. A.; MacMillan, D. W. C. Merging Photoredox Catalysis with Organocatalysis: The Direct Asymmetric Alkylation of Aldehydes. *Science* **2008**, *322* (5898), 77–80. <https://doi.org/10.1126/science.1161976>.
- (95) Ischay, M. A.; Anzovino, M. E.; Du, J.; Yoon, T. P. Efficient Visible Light Photocatalysis of [2+2] Enone Cycloadditions. *J. Am. Chem. Soc.* **2008**, *130* (39), 12886–12887. <https://doi.org/10.1021/ja805387f>.
- (96) Narayanam, J. M. R.; Tucker, J. W.; Stephenson, C. R. J. Electron-Transfer Photoredox Catalysis: Development of a Tin-Free Reductive Dehalogenation Reaction. *J. Am. Chem. Soc.* **2009**, *131* (25), 8756–8757. <https://doi.org/10.1021/ja9033582>.

- (97) Theriot, J. C.; Lim, C.-H.; Yang, H.; Ryan, M. D.; Musgrave, C. B.; Miyake, G. M. Organocatalyzed Atom Transfer Radical Polymerization Driven by Visible Light. *Science* **2016**, 352 (6289), 1082–1086. <https://doi.org/10.1126/science.aaf3935>.
- (98) Joshi-Pangu, A.; Lévesque, F.; Roth, H. G.; Oliver, S. F.; Campeau, L.-C.; Nicewicz, D.; DiRocco, D. A. Acridinium-Based Photocatalysts: A Sustainable Option in Photoredox Catalysis. *J. Org. Chem.* **2016**, 81 (16), 7244–7249. <https://doi.org/10.1021/acs.joc.6b01240>.
- (99) Hockin, B. M.; Li, C.; Robertson, N.; Zysman-Colman, E. Photoredox Catalysts Based on Earth-Abundant Metal Complexes. *Catal. Sci. Technol.* **2019**, 9 (4), 889–915. <https://doi.org/10.1039/C8CY02336K>.
- (100) Larsen, C. B.; Wenger, O. S. Photoredox Catalysis with Metal Complexes Made from Earth-Abundant Elements. *Chem. – Eur. J.* **2018**, 24 (9), 2039–2058. <https://doi.org/10.1002/chem.201703602>.
- (101) Stevenson, S. M.; Shores, M. P.; Ferreira, E. M. Photooxidizing Chromium Catalysts for Promoting Radical Cation Cycloadditions. *Angew. Chem. Int. Ed.* **2015**, 54 (22), 6506–6510. <https://doi.org/10.1002/anie.201501220>.
- (102) Ahn, J. M.; Peters, J. C.; Fu, G. C. Design of a Photoredox Catalyst That Enables the Direct Synthesis of Carbamate-Protected Primary Amines via Photoinduced, Copper-Catalyzed *N*-Alkylation Reactions of Unactivated Secondary Halides. *J. Am. Chem. Soc.* **2017**, 139 (49), 18101–18106. <https://doi.org/10.1021/jacs.7b10907>.
- (103) Baranoff, E.; Collin, J.-P.; Flamigni, L.; Sauvage, J.-P. From Ruthenium(II) to Iridium(III): 15 Years of Triads Based on Bis-Terpyridine Complexes. *Chem. Soc. Rev.* **2004**, 33 (3), 147–155. <https://doi.org/10.1039/B308983E>.
- (104) Koike, T.; Akita, M. Visible-Light Radical Reaction Designed by Ru- and Ir-Based Photoredox Catalysis. *Inorg Chem Front* **2014**, 1 (8), 562–576. <https://doi.org/10.1039/C4QI00053F>.
- (105) Seneviratne, D. S.; Uddin, Md. J.; Swayambunathan, V.; Schlegel, H. B.; Endicott, J. F. Characteristics and Properties of Metal-to-Ligand Charge-Transfer Excited States in 2,3-Bis(2-Pyridyl)Pyrazine and 2,2'-Bypyridine Ruthenium Complexes. Perturbation-Theory-Based Correlations of Optical Absorption and Emission Parameters with Electrochemistry and Thermal Kinetics and Related Ab Initio Calculations. *Inorg. Chem.* **2002**, 41 (6), 1502–1517. <https://doi.org/10.1021/ic010172c>.
- (106) Gao, C.; Wang, J.; Xu, H.; Xiong, Y. Coordination Chemistry in the Design of Heterogeneous Photocatalysts. *Chem. Soc. Rev.* **2017**, 46 (10), 2799–2823. <https://doi.org/10.1039/C6CS00727A>.
- (107) Zhou, J.-Y.; Luo, T.; She, W.-L.; Huang, X.-G.; Peng, W.-J.; Wu, J.-Z.; Ji, L.-N. Metal-to-Ligand Charge Transfer Spectra for Transition Metal Complexes of Chelated Aromatic Ligands: Theory and Experiment. In *Laser in Forschung und Technik / Laser in Research and Engineering*; Waidelich, W., Hügel, H., Opower, H., Tiziani, H., Wallenstein, R., Zinth, W., Eds.; Springer: Berlin, Heidelberg, 1996; pp 168–170. https://doi.org/10.1007/978-3-642-80263-8_38.
- (108) Ogawa, T.; Sinha, N.; Pfund, B.; Prescimone, A.; Wenger, O. S. Molecular Design Principles to Elongate the Metal-to-Ligand Charge Transfer Excited-State Lifetimes of Square-Planar Nickel(II) Complexes. *J. Am. Chem. Soc.* **2022**, 144 (48), 21948–21960. <https://doi.org/10.1021/jacs.2c08838>.
- (109) Sýkora, J.; Šima, J. Photochemistry of Coordination Compounds. *Coord. Chem. Rev.* **1990**, 107, 1–212. [https://doi.org/10.1016/0010-8545\(90\)80055-X](https://doi.org/10.1016/0010-8545(90)80055-X).
- (110) Vogler, A.; Kunkely, H. Photoreactivity of Metal-to-Ligand Charge Transfer Excited States. *Coord. Chem. Rev.* **1998**, 177 (1), 81–96. [https://doi.org/10.1016/S0010-8545\(98\)00131-3](https://doi.org/10.1016/S0010-8545(98)00131-3).

- (111) Jeong, D. Y.; You, Y. Organic Photoredox Catalysts Exhibiting Long Excited-State Lifetimes. *Synlett* **2022**, 33 (12), 1142–1153. <https://doi.org/10.1055/a-1608-5633>.
- (112) Nakanotani, H.; Furukawa, T.; Morimoto, K.; Adachi, C. Long-Range Coupling of Electron-Hole Pairs in Spatially Separated Organic Donor-Acceptor Layers. *Sci. Adv.* **2016**, 2 (2), e1501470. <https://doi.org/10.1126/sciadv.1501470>.
- (113) Zhang, J.; Xu, W.; Sheng, P.; Zhao, G.; Zhu, D. Organic Donor–Acceptor Complexes as Novel Organic Semiconductors. *Acc. Chem. Res.* **2017**, 50 (7), 1654–1662. <https://doi.org/10.1021/acs.accounts.7b00124>.
- (114) Goetz, K. P.; Iqbal, H. F.; Bittle, E. G.; Hacker, C. A.; Pookpanratana, S.; Jurchescu, O. D. Organic Single Crystals of Charge-Transfer Complexes: Model Systems for the Study of Donor/Acceptor Interactions. *Mater. Horiz.* **2022**, 9 (1), 271–280. <https://doi.org/10.1039/D1MH01214B>.
- (115) Wu, C.; Corrigan, N.; Lim, C.-H.; Jung, K.; Zhu, J.; Miyake, G.; Xu, J.; Boyer, C. Guiding the Design of Organic Photocatalyst for PET-RAFT Polymerization: Halogenated Xanthene Dyes. *Macromolecules* **2019**, 52 (1), 236–248. <https://doi.org/10.1021/acs.macromol.8b02517>.
- (116) Amy Bryden, M.; Zysman-Colman, E. Organic Thermally Activated Delayed Fluorescence (TADF) Compounds Used in Photocatalysis. *Chem. Soc. Rev.* **2021**, 50 (13), 7587–7680. <https://doi.org/10.1039/D1CS00198A>.
- (117) Fukuzumi, S.; Kotani, H.; Ohkubo, K.; Ogo, S.; Tkachenko, N. V.; Lemmetyinen, H. Electron-Transfer State of 9-Mesityl-10-Methylacridinium Ion with a Much Longer Lifetime and Higher Energy Than That of the Natural Photosynthetic Reaction Center. *J. Am. Chem. Soc.* **2004**, 126 (6), 1600–1601. <https://doi.org/10.1021/ja038656q>.
- (118) Tlili, A.; Lakhdar, S. Acridinium Salts and Cyanoarenes as Powerful Photocatalysts: Opportunities in Organic Synthesis. *Angew. Chem. Int. Ed.* **2021**, 60 (36), 19526–19549. <https://doi.org/10.1002/anie.202102262>.
- (119) Shang, T.-Y.; Lu, L.-H.; Cao, Z.; Liu, Y.; He, W.-M.; Yu, B. Recent Advances of 1,2,3,5-Tetrakis(Carbazol-9-Yl)-4,6-Dicyanobenzene (4CzIPN) in Photocatalytic Transformations. *Chem. Commun.* **2019**, 55 (38), 5408–5419. <https://doi.org/10.1039/C9CC01047E>.
- (120) Singh, P. P.; Srivastava, V. Recent Advances in Using 4DPAIPN in Photocatalytic Transformations. *Org. Biomol. Chem.* **2021**, 19 (2), 313–321. <https://doi.org/10.1039/D0OB01884H>.
- (121) Discekici, E. H.; Treat, N. J.; Poelma, S. O.; Mattson, K. M.; Hudson, Z. M.; Luo, Y.; Hawker, C. J.; Alaniz, J. R. de. A Highly Reducing Metal-Free Photoredox Catalyst: Design and Application in Radical Dehalogenations. *Chem. Commun.* **2015**, 51 (58), 11705–11708. <https://doi.org/10.1039/C5CC04677G>.
- (122) Speck, F.; Rombach, D.; Wagenknecht, H.-A. N-Arylphenothiazines as Strong Donors for Photoredox Catalysis – Pushing the Frontiers of Nucleophilic Addition of Alcohols to Alkenes. *Beilstein J. Org. Chem.* **2019**, 15 (1), 52–59. <https://doi.org/10.3762/bjoc.15.5>.
- (123) Yang, C.; Kärkäs, M. D.; Magallanes, G.; Chan, K.; Stephenson, C. R. J. Organocatalytic Approach to Photochemical Lignin Fragmentation. *Org. Lett.* **2020**, 22 (20), 8082–8085. <https://doi.org/10.1021/acs.orglett.0c03029>.
- (124) Shibutani, S.; Kodo, T.; Takeda, M.; Nagao, K.; Tokunaga, N.; Sasaki, Y.; Ohmiya, H. Organophotoredox-Catalyzed Decarboxylative C(Sp³)–O Bond Formation. *J. Am. Chem. Soc.* **2020**, 142 (3), 1211–1216. <https://doi.org/10.1021/jacs.9b12335>.
- (125) Treat, N. J.; Sprafke, H.; Kramer, J. W.; Clark, P. G.; Barton, B. E.; Read de Alaniz, J.; Fors, B. P.; Hawker, C. J. Metal-Free Atom Transfer Radical Polymerization. *J. Am. Chem. Soc.* **2014**, 136 (45), 16096–16101. <https://doi.org/10.1021/ja510389m>.
- (126) Wu, S.; Kaur, J.; Karl, T. A.; Tian, X.; Barham, J. P. Synthetic Molecular Photoelectrochemistry: New Frontiers in Synthetic Applications, Mechanistic Insights and

- Scalability. *Angew. Chem. Int. Ed.* **2022**, *61* (12), e202107811. <https://doi.org/10.1002/anie.202107811>.
- (127) Schmalzbauer, M.; Marcon, M.; König, B. Excited State Anions in Organic Transformations. *Angew. Chem. Int. Ed.* **2021**, *60* (12), 6270–6292. <https://doi.org/10.1002/anie.202009288>.
- (128) La Porte, N. T.; Martinez, J. F.; Chaudhuri, S.; Hedström, S.; Batista, V. S.; Wasielewski, M. R. Photoexcited Radical Anion Super-Reductants for Solar Fuels Catalysis. *Coord. Chem. Rev.* **2018**, *361*, 98–119. <https://doi.org/10.1016/j.ccr.2018.01.018>.
- (129) Lund, H.; Carlsson, H. S.; Nishida, T.; Enzell, C. R.; Matsuno, T. Photochemistry of Radical Ions. *Acta Chem. Scand.* **1978**, *32b*, 505–509. <https://doi.org/10.3891/acta.chem.scand.32b-0505>.
- (130) Eriksen, J.; Lund, H.; Nyvad, A. I.; Yamato, T.; Mitchell, R. H.; Dingle, T. W.; Williams, R. V.; Mahedevan, R. Electron-Transfer Fluorescence Quenching of Radical Ions. *Acta Chem. Scand.* **1983**, *37b*, 459–466. <https://doi.org/10.3891/acta.chem.scand.37b-0459>.
- (131) Eggins, B. R.; Robertson, P. K. J. Photoelectrochemistry Using Quinone Radical Anions. *J. Chem. Soc. Faraday Trans.* **1994**, *90* (15), 2249–2256. <https://doi.org/10.1039/FT9949002249>.
- (132) Gosztola, D.; Niemczyk, M. P.; Svec, W.; Lukas, A. S.; Wasielewski, M. R. Excited Doublet States of Electrochemically Generated Aromatic Imide and Diimide Radical Anions. *J. Phys. Chem. A* **2000**, *104* (28), 6545–6551. <https://doi.org/10.1021/jp000706f>.
- (133) König, B.; Ghosh, I.; Ghosh, T.; Bardagi, J. I. Reduction of Aryl Halides by Consecutive Visible Light-Induced Electron Transfer Processes. *Science* **2014**, *346* (6210), 725–728. <https://doi.org/10.1126/science.1258232>.
- (134) Caby, S.; Bouchet, L. M.; Argüello, J. E.; Rossi, R. A.; Bardagi, J. I. Excitation of Radical Anions of Naphthalene Diimides in Consecutive- and Electro-Photocatalysis**. *ChemCatChem* **2021**, *13* (13), 3001–3009. <https://doi.org/10.1002/cctc.202100359>.
- (135) Neumeier, M.; Sampedro, D.; Májek, M.; de la Peña O'Shea, V. A.; Jacobi von Wangelin, A.; Pérez-Ruiz, R. Dichromatic Photocatalytic Substitutions of Aryl Halides with a Small Organic Dye. *Chem. – Eur. J.* **2018**, *24* (1), 105–108. <https://doi.org/10.1002/chem.201705326>.
- (136) Chmiel, A. F.; Williams, O. P.; Chernowsky, C. P.; Yeung, C. S.; Wickens, Z. K. Non-Innocent Radical Ion Intermediates in Photoredox Catalysis: Parallel Reduction Modes Enable Coupling of Diverse Aryl Chlorides. *J. Am. Chem. Soc.* **2021**, *143* (29), 10882–10889. <https://doi.org/10.1021/jacs.1c05988>.
- (137) MacKenzie, I. A.; Wang, L.; Onuska, N. P. R.; Williams, O. F.; Begam, K.; Moran, A. M.; Dunietz, B. D.; Nicewicz, D. A. Discovery and Characterization of an Acridine Radical Photoreductant. *Nature* **2020**, *580* (7801), 76–80. <https://doi.org/10.1038/s41586-020-2131-1>.
- (138) Cole, J. P.; Chen, D.-F.; Kudisch, M.; Pearson, R. M.; Lim, C.-H.; Miyake, G. M. Organocatalyzed Birch Reduction Driven by Visible Light. *J. Am. Chem. Soc.* **2020**, *142* (31), 13573–13581. <https://doi.org/10.1021/jacs.0c05899>.
- (139) Kim, H.; Kim, H.; Lambert, T.; Lin, S. *Reductive Electrophotocatalysis: Merging Electricity and Light to Achieve Extreme Reduction Potentials*; preprint; 2019. <https://doi.org/10.26434/chemrxiv.9936623.v2>.
- (140) Cowper, N. G. W.; Chernowsky, C. P.; Williams, O. P.; Wickens, Z. K. Potent Reductants via Electron-Primed Photoredox Catalysis: Unlocking Aryl Chlorides for Radical Coupling. *J. Am. Chem. Soc.* **2020**, *142* (5), 2093–2099. <https://doi.org/10.1021/jacs.9b12328>.
- (141) Chernowsky, C. P.; Chmiel, A. F.; Wickens, Z. K. Electrochemical Activation of Diverse Conventional Photoredox Catalysts Induces Potent Photoreductant Activity**. *Angew. Chem. Int. Ed.* **2021**, *60* (39), 21418–21425. <https://doi.org/10.1002/anie.202107169>.

- (142) Washington, J. B. Trialkylammonium Salt Degradation: Implications for Methylation and Cross-Coupling. *Chem Sci* **2021**, 15.
- (143) Chakma, P.; Digby, Z. A.; Shulman, M. P.; Kuhn, L. R.; Morley, C. N.; Sparks, J. L.; Konkolewicz, D. Anilinium Salts in Polymer Networks for Materials with Mechanical Stability and Mild Thermally Induced Dynamic Properties. *ACS Macro Lett.* **2019**, 8 (2), 95–100. <https://doi.org/10.1021/acsmacrolett.8b00819>.
- (144) Xu, H.; Yu, B.; Zhang, H.; Zhao, Y.; Yang, Z.; Xu, J.; Han, B.; Liu, Z. Reductive Cleavage of Inert Aryl C–O Bonds to Produce Arenes. *Chem. Commun.* **2015**, 51 (61), 12212–12215. <https://doi.org/10.1039/C5CC03563E>.
- (145) Tian, X.; Karl, T. A.; Reiter, S.; Yakubov, S.; de Vivie-Riedle, R.; König, B.; Barham, J. P. Electro-Mediated PhotoRedox Catalysis for Selective C(Sp³)–O Cleavages of Phosphinated Alcohols to Carbanions. *Angew. Chem. Int. Ed.* **2021**, 60 (38), 20817–20825. <https://doi.org/10.1002/anie.202105895>.

Chapter 2: Potent Reductants via Electron-Primed Photoredox Catalysis: Unlocking Aryl Chlorides for Radical Coupling

This work is published: Cowper, N.G.W.*; Chernowsky, C.P.*; Williams, O.P.; Wickens, Z.K.; *J.Am.Chem.Soc.*, **2020**, 142, 2093-2099

* denotes equal contribution

2.1. Abstract

We describe a new catalytic strategy to transcend the energetic limitations of visible light by electrochemically priming a photocatalyst prior to excitation. This new catalytic system is able to productively engage aryl chlorides with reduction potentials hundreds of millivolts beyond the potential of Na^0 in productive radical coupling reactions. The aryl radicals produced via this strategy can be leveraged for both carbon–carbon and carbon–heteroatom bond-forming reactions. Through direct comparison, we illustrate the reactivity and selectivity advantages of this approach relative to electrolysis and photoredox catalysis.

2.2. Introduction

Activation of organic molecules through single electron transfer (SET) is a pillar of preparative chemistry. New strategies to induce redox events have the potential to significantly impact organic synthesis.^{1–5} In the past decade, visible-light photoredox catalysis has enabled a tremendous array of carbon–carbon and carbon–heteroatom bond forming reactions.^{6–11} Unfortunately, blue light (440 nm) possesses sufficient energy for a maximum driving force of only 2.8 eV, and the available energy is further diminished by nonradiative pathways and intersystem crossing.¹² Thus, despite catalyst design improvements,^{13–20} many desirable substrates remain inert to visible-light photoredox catalysis.²¹ As a result of this limitation, dissolving metal conditions,^{22,23} which employ reactive alkali metals in condensed ammonia, remain uniquely potent reductants in the synthetic arsenal^{24,25} and are still commonly used despite significant hazards and poor chemoselectivity.^{26–29} Aiming to provide safer and more scalable conditions for challenging reductions, recent efforts have exploited overcharge protection to unlock deeply reducing cathodic potentials for electroorganic synthesis.³⁰ However, the requisite electrode overpotentials intrinsically limit the functional group tolerance. Furthermore, radical intermediates generated at a cathode are prone to reduction to anions.^{31,32} Overall, a new catalytic paradigm to access extremely reducing potentials under mild conditions and without reduction of radical intermediates would address a long-standing challenge in organic synthesis (**Figure 2.1**).

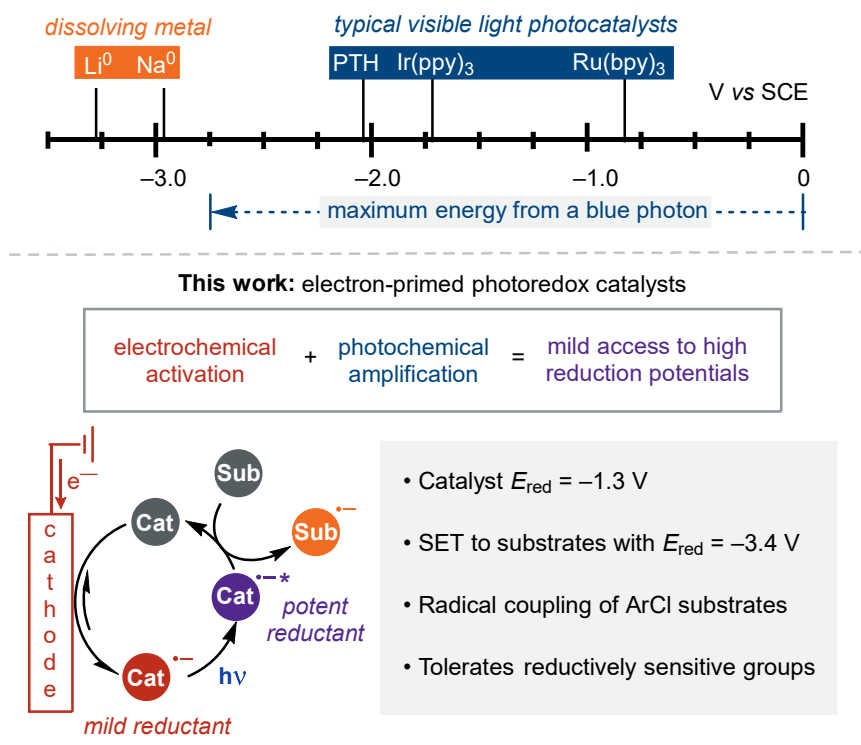


Figure 2.1. Strategies to induce SET reduction: All potentials provided relative to SCE. PTH = 10-phenylphenothiazine.

To overcome the energetic limitations of blue photons, König and co-workers recently introduced an appealing approach designed to drive challenging SET events using the energy of two photons rather than one.^{33–36} This strategy relies on the light-mediated generation and subsequent photochemical excitation of catalytic radical anion intermediates. Although these systems push the limits of photoredox catalysis, they remain many orders of magnitude less reducing than alkali metals. Inspired by photophysical studies suggesting that other organic radical ions can serve as potent photoreductants,^{37–41} we questioned whether an alternative means of priming a photoredox catalyst with an electron prior to excitation could provide a general catalyst design platform to transcend the energetic limitations of visible light.

We hypothesized that electrochemistry^{42–47} could offer a more flexible approach than photoreduction to generate electron-primed photoredox catalysts. In addition to providing access to new catalysts, this approach eliminates the complications⁴⁸ that can arise from the terminal reductants commonly used in photoredox catalysis, such as Et_3N . This strategy builds on both

long-standing^{49–53} and recent^{54–57} pioneering efforts combining electrochemistry with photochemistry.⁵⁸ The majority of these examples take advantage of the desirable features of electrochemistry to generate known photochemically active intermediates or catalysts. However, electrochemical generation of new families of photocatalysts for organic synthesis remains largely unexplored. Recently, Lambert and co-workers reported a new and highly oxidizing photocatalyst (with a calculated potential of +3.3 V vs SCE) that is electrochemically accessible under a mildly oxidizing potential.⁵⁷ Concurrently, we were exploring the use of electrochemistry to access new, electronically destabilized photocatalysts for challenging reductions. Herein we demonstrate that electrochemistry is a viable strategy to generate highly reducing electron-primed photoredox catalysts (**Figure 2.1**). We exploit this approach to identify an aryl imide photocatalyst capable of engaging substrates with reduction potentials on par with alkali metals in SET-initiated radical coupling reactions under otherwise mild conditions. To explore this idea, we targeted the reductive generation of aryl radicals from unactivated precursors. These reactive intermediates are known to participate in a range of synthetically useful carbon–carbon and carbon–heteroatom bond-forming reactions; however, they are typically generated from diazonium salts or aryl iodides using modern photoredox catalysts.^{59,60} With the most reducing visible-light photoredox catalysts, aryl bromides are suitable radical precursors.^{61–64} Unfortunately, aryl chlorides comprise over half of the commercially available aryl halides⁶⁵ yet are inert under conventional visible-light photoredox catalysis unless they bear electron-withdrawing groups.^{33,59,66–69} This limitation is a result of the combination of thermodynamically challenging SET and the low fragmentation rate due to the relatively strong C(sp²)–Cl bond.³²

2.3. Results and Discussion

To assess the viability of the proposed electrophotocatalytic approach, we investigated the dehalogenation of 4-bromobiphenyl (**1**) because of its reduction potential beyond the standard range of photoredox catalysts (–2.4 V vs SCE) and rapid fragmentation after reduction, as this provides a high fidelity readout for successful SET.³² Using this model reaction, we assessed a

series of aryl imides for activity under visible-light irradiation and an appropriate electrochemical potential to reductively activate the imide (**Table 2.1**). The radical anion derived from perylene diimide (**PDI**) can act as an electron-primed photoredox catalyst under two-photon conditions³³ and is also well-behaved electrochemically.⁷⁰ Unfortunately, **PDI** proved ineffective in the dehalogenation of under these conditions. Photophysical studies have indicated that naphthlene-based analogues (**NpDI** and **NpMI**) are more potent photoreductants after they are primed with an electron,⁴¹ but they have yet to be leveraged in synthesis. Excitingly, under electrophotocatalytic conditions both **NpDI** and **NpMI** promoted the dehalogenation of **1**, despite significant electrochemical underpotentials in each case (1.6 and 1.1 V vs SCE respectively). While both **NpMI** and **NpDI** are sufficiently potent photoreductants to reduce **1**, **NpMI** promoted dehalogenation significantly more efficiently. However, further stripping down the aromatic core to a phthalimide derivative, **PhMI**, resulted in a less effective photocatalyst than **NpMI**. On the basis of these data, we selected **NpMI** for further study after verifying that no significant conversion was observed in the absence of an applied voltage, light, or the catalyst.

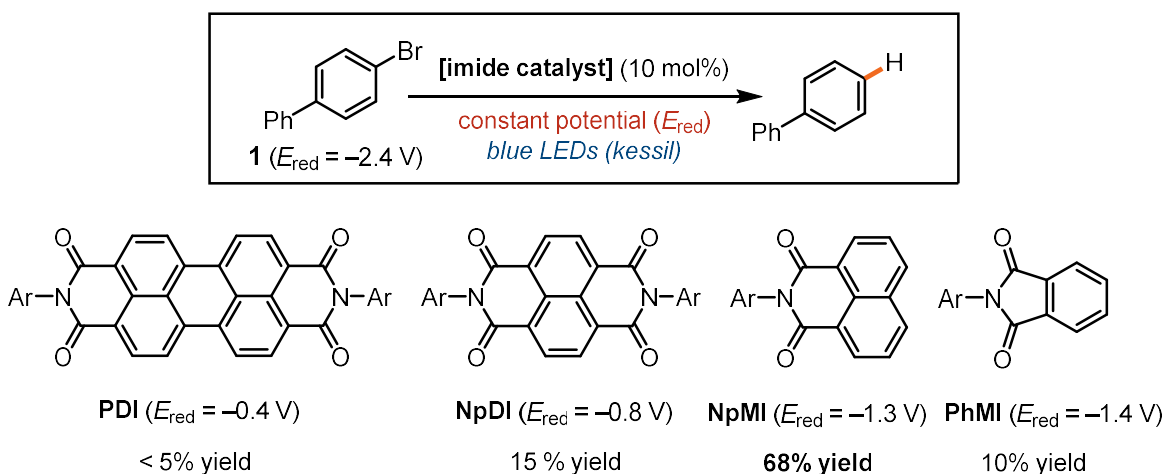
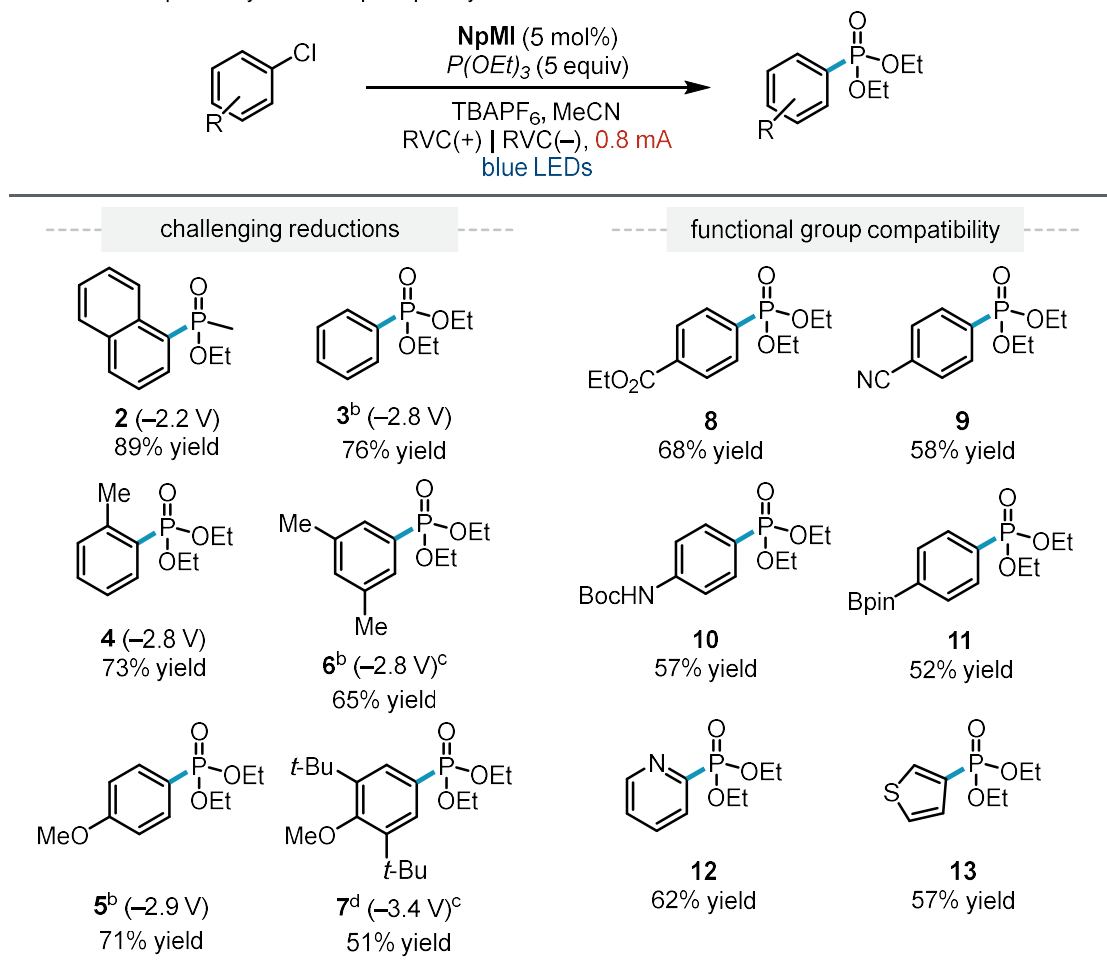


Table 2.1. Catalyst evaluation. All redox potentials are vs. SCE. Ar = 2,2-diisopropylphenyl. Reactions were run on a 0.4 mmol scale in DMF (0.1 M Bu₄NPF₆) with 2,4,6-tri-*tert*-butylphenol (10 mol%) and 2-propanol (1 equiv). See the SI for more details.

Having identified a promising electrochemically accessible photocatalyst, we explored whether this system could engage abundant but much more challenging aryl chlorides in radical coupling reactions. We first probed the viability of a photo-Arbuzov process,⁷¹ a classic carbon–heteroatom bond-forming reaction that proceeds through an aryl radical intermediate (**Table 2.2**). For these studies, we employed more convenient constant-current conditions (see SI for details). We found that under simultaneous electrolysis and irradiation, **NpMI** induced the high-yielding coupling of aryl chlorides with reduction potentials at and beyond the limits of conventional visible-light photoredox catalysis (**2–3**). To identify the limits of this catalytic system, we next evaluated increasingly electron-rich aryl chloride substrates. Excitingly, aryl

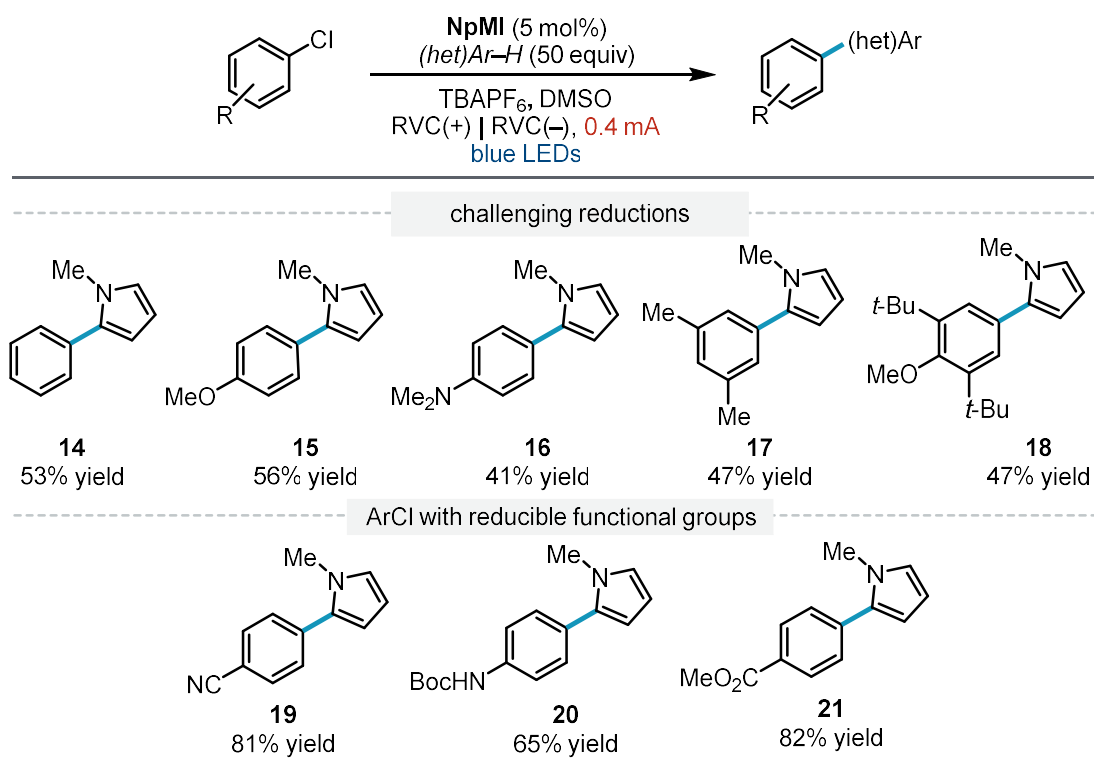
Table 2.2. Scope of aryl chloride phosphonylation



All potentials versus SCE. ^aReactions conducted on 0.4 mmol scale and run for 8 h. Et₃N (2 equiv) in the anode was the counter See SI for further experimental details. ^breaction run 14 h. ^c*E*_{red} determined by differential pulse voltammetry ^d0.4 mA current.

chloride substrates bearing electron-donating groups still underwent efficient SET induced phosphorylation (**4–7**) even though they possess reduction potentials comparable to that of Na^0 (-2.9 V vs SCE). Notably, an exceptionally electron-rich aryl chloride (-3.4 V vs SCE) (see SI for details) was successfully reduced to produce **7**. This result indicates that these conditions provide potency comparable to that of Li^0 (-3.3 V vs SCE). To our delight, despite the presence of such a potent reductant, aryl chloride substrates bearing potentially sensitive functional groups,²¹ such as esters (**8**), nitriles (**9**), carbamates (**10**), organoboron reagents (**11**), and heterocycles (**12** and **13**) all underwent productive SET-induced radical phosphorylation, and the corresponding products were isolated in good to excellent yields. Having established the viability of carbon–heteroatom bond-forming reactions from diverse aryl chlorides, we next aimed to intercept the aryl radical intermediate with a heterocycle to form a new carbon–carbon bond (**Table 2.3**). We found that the aryl radical intermediates generated under these conditions

Table 2.3. Scope of aryl chloride (hetero)arylation



^aReactions conducted on 0.4 mmol scale and run for 27h. Et_3N (2 equiv) was employed in the anode as the counter reaction. See the SI for further experimental details.

from neutral to electron-rich aryl chlorides (**14–18**) could be effectively coupled to N-methylpyrrole, a classic radical trap.⁷² Again, reductively sensitive functional groups were well-tolerated despite the potency of the photoreductant employed (**19–21**). With a new catalytic strategy in hand, we next compared its efficacy to those of traditional photochemical and electrochemical approaches for the reductive activation of aryl chlorides (**Figure 2.2**). To this end, we investigated the relative yields of N-methylpyrrole coupling and dehalogenation within a subset of aryl chloride substrates ranging from electron deficient to electron-rich. When the electron-primed photoredox system was used, each substrate delivered the desired product with excellent selectivity for radical coupling over dehalogenation. In contrast, 10-phenylphenothiazine (**PTH**), an exceptionally reducing photoredox catalyst (-2.1 V vs SCE),⁶² could only induce the coupling of the electron deficient aryl chloride. The neutral and electron-rich substrates were unconverted by **PTH**, consistent with the energetic limitations of visible-light photoredox. Direct electrolysis,

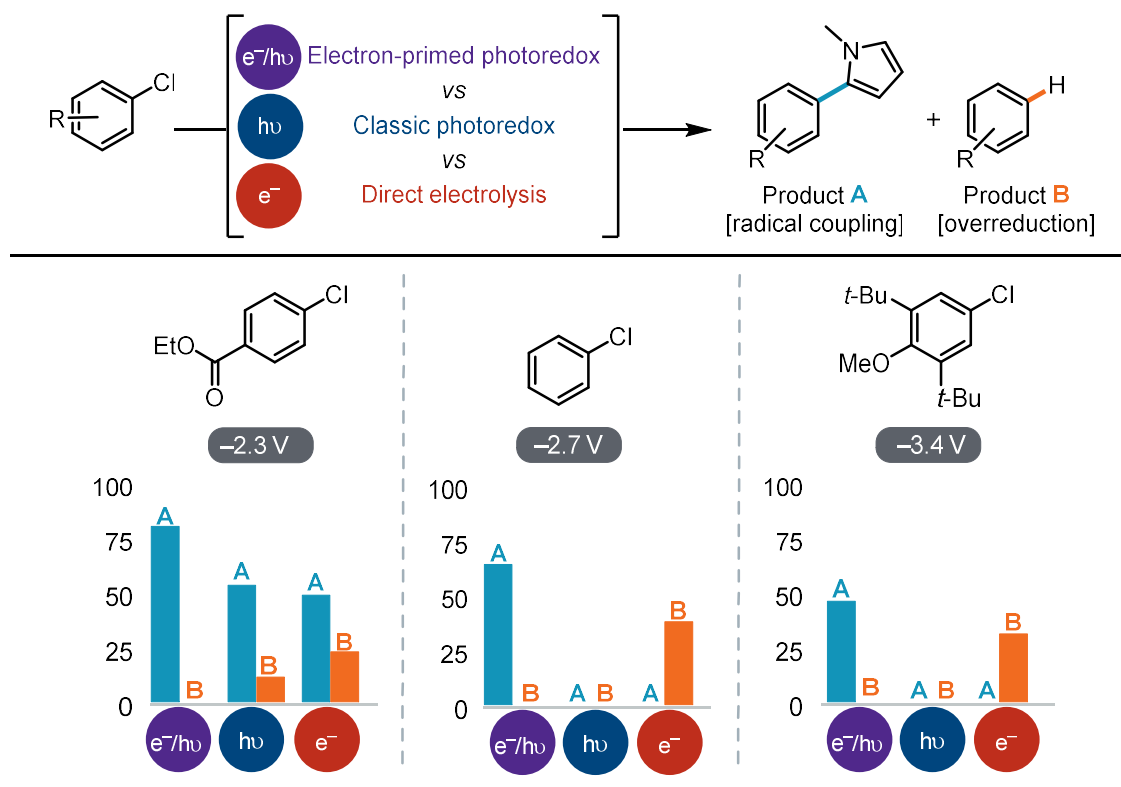
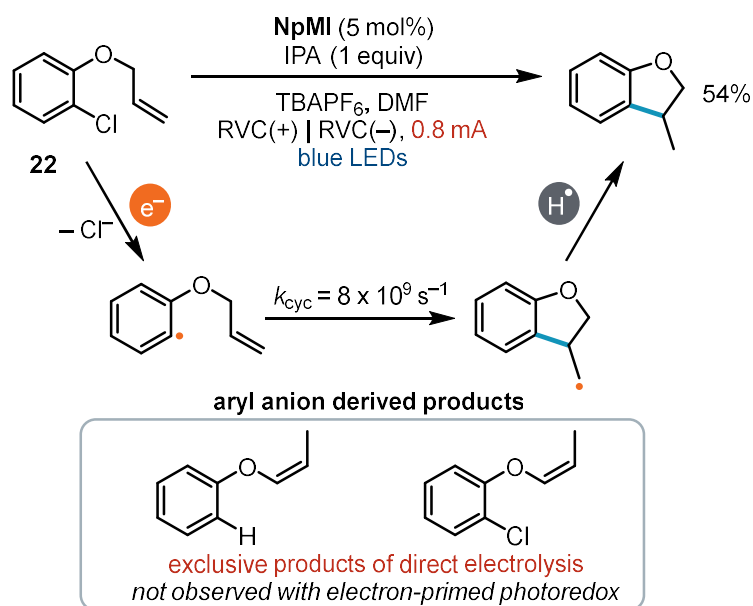


Figure 2.2. Comparison of reduction methods. Yields of coupling and dehalogenation measured relative to an internal standard. Electron-primed photoredox conditions from Table 2.3. Photoredox conditions employ PTH as a photocatalyst. Several direct electrolysis conditions were attempted and reported conditions provided highest yield of A. For further details see the SI.

on the other hand, provided significantly diminished selectivity for coupling of the electron-deficient substrate (2:1) and the other two substrates yielded in exclusively dehalogenation. These results are consistent with over-reduction at the electrode surface that precludes radical coupling reactions at the requisite potentials for aryl chloride reduction. We next subjected radical clock **22** to both electron-primed photoredox and direct electrolysis conditions to probe the presence of an aryl radical intermediate and benchmark the rate of its over-reduction (**Scheme 1**). The aryl radical derived from **22** undergoes radical cyclization with a rate of $8 \times 10^9 \text{ s}^{-1}$.⁷³ As anticipated, **NpMI** under blue-light irradiation and constant-current electrolysis delivered selective cyclization (54% yield, $\geq 20:1$ selectivity for cyclization over dehalogenation and aryl anion-derived⁷⁴ isomerization products). This result is fully consistent with the proposed intermediacy of



Scheme 2.1. Comparison of radical clock outcomes. reactions conducted on 0.4 mmol scale for 20h.

an aryl radical intermediate and high selectivity for radical chemistry instead of over-reduction. Direct electrolysis, however, provided no observable cyclization and generated only dehalogenation and isomerization products consistent with anionic intermediates. This indicates that under the direct electrolysis conditions investigated, any radical reactions with rate constants lower than 10^9 s^{-1} will not be viable because of competitive electrochemical reduction of the

radical. This is consistent with the facile reduction of aryl radical intermediates at electrode surfaces (phenyl radical $E_{\text{red}} = +0.05 \text{ V vs SCE}$).⁷⁵ Finally, we aimed to gain preliminary insight into the promising chemoselectivity observed with this potent catalytic reductant. Notably, classic photoredox approaches are sensitive to not only the reduction potential of the substrate but also the fragmentation rate of the radical anion formed via SET.⁵⁹ This is likely due to competition between back electron transfer and the productive fragmentation and coupling. Although back electron transfer can be a hindrance,⁷⁶ we suspect that this feature also contributes to the excellent chemoselectivity profiles observed in photoredox catalysis. Thus, we wanted to ascertain whether the exceptionally potent photoreductant explored herein exhibited analogous reactivity or whether SET was irreversible.

To this end, we conducted a series of one-pot intermolecular competition experiments between bromo- and chlorobiphenyl (**Figure 2.3**). These halogen congeners possess the same reduction potential (-2.4 V vs SCE), but their radical anions exhibit significantly different fragmentation rates.^{32,77} We subjected a 1:1 mixture of the two aryl halides to **NpMI** under

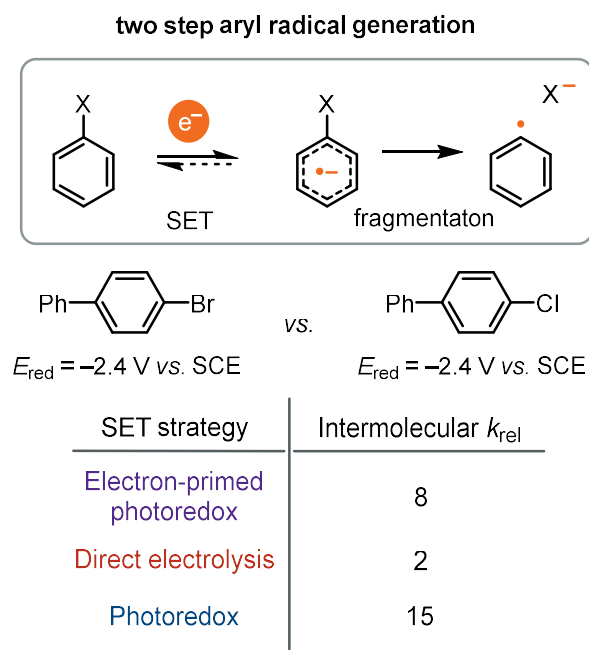


Figure 2.3. Comparison of one pot competition experiments. k_{rel} is given as $k_{\text{Br}}/k_{\text{Cl}}$ and was measured by gas chromatography based on reactions run to low conversion (<20%). See the SI for experimental details.

simultaneous irradiation and a working potential of -1.3 V vs SCE. We found that the initial rate of $\text{C}(\text{sp}^2)\text{-Br}$ cleavage was significantly higher than that of $\text{C}(\text{sp}^2)\text{-Cl}$ cleavage ($k_{\text{rel}} = 8$) despite the fact the two aryl halides possess identical reduction potentials. This observation excludes that conversion is based exclusively on the reduction potential. In stark contrast, the two substrates are converted at similar rates under direct electrolysis conditions ($k_{\text{rel}} = 2$).⁷⁸ Consistent with prior work in photoredox catalysis, **PTH** promoted the dehalogenation of bromobiphenyl more rapidly than that of the chloride ($k_{\text{rel}} = 15$). Taken together, these data indicate that productive conversion is not governed exclusively by the reduction potential under either electron-primed or conventional photoredox catalysis. This observation provides a plausible rationale for the promising chemoselectivity observed under the conditions reported herein relative to deeply reducing direct electrolysis, which predominantly commits to product formation on the basis of the substrate reduction potential.

2.4 Conclusions

Overall, we have demonstrated that electrochemical stimulation is a viable strategy to generate catalytic photoreductants capable of transcending the limits of modern photoredox catalysis. We report effective radical couplings of substrates hundreds of millivolts more challenging to reduce than previous photoredox strategies, including substrates with reduction potentials well beyond that of Na^0 and more negative than that of Li^0 . Crucially, despite accessing such negative potentials, the reactions possess functional group tolerance profiles more consistent with traditional photoredox catalysis than direct electrolysis and result in high selectivity for radical coupling over dehalogenation. Beyond unlocking electronically diverse aryl chlorides as aryl radical precursors, these data lay the foundation for a new catalyst design paradigm. We anticipate that electrochemically priming photocatalysts prior to excitation will allow much more challenging reductions than are feasible with blue light alone and will result in a myriad of transformations inspired by what is feasible under dissolving metal conditions and beyond.

2.5 Acknowledgments

We thank Prof. Alison Wendlandt, Prof. Tehshik Yoon, Prof. Daniel Weix, Prof. Bill Morandi, and Sara Alektiar for helpful suggestions and manuscript proofreading. Additionally, we thank the entire Weix group for allowing us to use their GC and the Stahl, Weix, Yoon, and Schomaker groups for sharing their chemical inventory. Dr. Blaise J. Thompson is acknowledged for his assistance with galvanostat design and fabrication. Tracy Drier is acknowledged for electrochemical glassware fabrication. We also acknowledge the invaluable support and helpful suggestions from group members Dylan Holst and Diana Wang throughout this project. This work was financially supported by the Office of the Vice Chancellor for Research and Graduate Education at the University of WisconsinMadison with funding from the Wisconsin Alumni Research Foundation. Spectroscopic instrumentation was supported by a generous gift from Paul. J. and Margaret M. Bender, NSF (CHE-1048642), and NIH (1S10 OD020022-1).

2.6 References

- (1) Ashby, E. C. Single-Electron Transfer, a Major Reaction Pathway in Organic Chemistry. An Answer to Recent Criticisms. *Acc. Chem. Res.* **1988**, *21* (11), 414–421. <https://doi.org/10.1021/ar00155a005>.
- (2) Zhang, N.; Samanta, S. R.; Rosen, B. M.; Percec, V. Single Electron Transfer in Radical Ion and Radical-Mediated Organic, Materials and Polymer Synthesis. *Chem. Rev.* **2014**, *114* (11), 5848–5958. <https://doi.org/10.1021/cr400689s>.
- (3) Broggi, J.; Terme, T.; Vanelle, P. Organic Electron Donors as Powerful Single-Electron Reducing Agents in Organic Synthesis. *Angew. Chem., Int. Ed.* **2014**, *53* (2), 384–413. <https://doi.org/10.1002/anie.201209060>.
- (4) Girard, P.; Namy, J. L.; Kagan, H. B. Divalent Lanthanide Derivatives in Organic Synthesis. 1. Mild Preparation of Samarium Iodide and Ytterbium Iodide and Their Use as Reducing or Coupling Agents. *J. Am. Chem. Soc.* **1980**, *102* (8), 2693–2698. <https://doi.org/10.1021/ja00528a029>.
- (5) Ebersson, L. Electron-Transfer Reactions in Organic Chemistry. In *Advances in Physical Organic Chemistry*; Gold, V., Bethell, D., Eds.; Academic Press, 1982; Vol. 18, pp 79–185. [https://doi.org/10.1016/S0065-3160\(08\)60139-2](https://doi.org/10.1016/S0065-3160(08)60139-2).
- (6) Prier, C. K.; Rankic, D. A.; MacMillan, D. W. C. Visible Light Photoredox Catalysis with Transition Metal Complexes: Applications in Organic Synthesis. *Chem. Rev.* **2013**, *113* (7), 5322–5363. <https://doi.org/10.1021/cr300503r>.
- (7) Shaw, M. H.; Twilton, J.; MacMillan, D. W. C. Photoredox Catalysis in Organic Chemistry. *J. Org. Chem.* **2016**, *81* (16), 6898–6926. <https://doi.org/10.1021/acs.joc.6b01449>.
- (8) Romero, N. A.; Nicewicz, D. A. Organic Photoredox Catalysis. *Chem. Rev.* **2016**, *116* (17), 10075–10166. <https://doi.org/10.1021/acs.chemrev.6b00057>.
- (9) Skubi, K. L.; Blum, T. R.; Yoon, T. P. Dual Catalysis Strategies in Photochemical Synthesis. *Chem. Rev.* **2016**, *116* (17), 10035–10074. <https://doi.org/10.1021/acs.chemrev.6b00018>.

- (10) DiRocco, D. A.; Dykstra, K.; Krska, S.; Vachal, P.; Conway, D. V.; Tudge, M. Late-Stage Functionalization of Biologically Active Heterocycles Through Photoredox Catalysis. *Angewandte Chemie International Edition* **2014**, *53* (19), 4802–4806. <https://doi.org/10.1002/anie.201402023>.
- (11) Narayanam, J. M. R.; Stephenson, C. R. J. Visible Light Photoredox Catalysis: Applications in Organic Synthesis. *Chem. Soc. Rev.* **2010**, *40* (1), 102–113. <https://doi.org/10.1039/B913880N>.
- (12) Arias-Rotondo, D. M.; McCusker, J. K. The Photophysics of Photoredox Catalysis: A Roadmap for Catalyst Design. *Chem. Soc. Rev.* **2016**, *45* (21), 5803–5820. <https://doi.org/10.1039/C6CS00526H>.
- (13) Theriot, J. C.; Lim, C.-H.; Yang, H.; Ryan, M. D.; Musgrave, C. B.; Miyake, G. M. Organocatalyzed Atom Transfer Radical Polymerization Driven by Visible Light. *Science* **2016**, *352* (6289), 1082–1086. <https://doi.org/10.1126/science.aaf3935>.
- (14) Speckmeier, E.; Fischer, T. G.; Zeitler, K. A Toolbox Approach To Construct Broadly Applicable Metal-Free Catalysts for Photoredox Chemistry: Deliberate Tuning of Redox Potentials and Importance of Halogens in Donor–Acceptor Cyanoarenes. *J. Am. Chem. Soc.* **2018**, *140* (45), 15353–15365. <https://doi.org/10.1021/jacs.8b08933>.
- (15) Joshi-Pangu, A.; Lévesque, F.; Roth, H. G.; Oliver, S. F.; Campeau, L.-C.; Nicewicz, D.; DiRocco, D. A. Acridinium-Based Photocatalysts: A Sustainable Option in Photoredox Catalysis. *J. Org. Chem.* **2016**, *81* (16), 7244–7249. <https://doi.org/10.1021/acs.joc.6b01240>.
- (16) Hockin, B. M.; Li, C.; Robertson, N.; Zysman-Colman, E. Photoredox Catalysts Based on Earth-Abundant Metal Complexes. *Catal. Sci. Technol.* **2019**, *9* (4), 889–915. <https://doi.org/10.1039/C8CY02336K>.
- (17) Larsen, C. B.; Wenger, O. S. Photoredox Catalysis with Metal Complexes Made from Earth-Abundant Elements. *Chemistry – A European Journal* **2018**, *24* (9), 2039–2058. <https://doi.org/10.1002/chem.201703602>.
- (18) Herr, P.; Glaser, F.; Büldt, L. A.; Larsen, C. B.; Wenger, O. S. Long-Lived, Strongly Emissive, and Highly Reducing Excited States in Mo(0) Complexes with Chelating Isocyanides. *J. Am. Chem. Soc.* **2019**, *141* (36), 14394–14402. <https://doi.org/10.1021/jacs.9b07373>.
- (19) Stevenson, S. M.; Shores, M. P.; Ferreira, E. M. Photooxidizing Chromium Catalysts for Promoting Radical Cation Cycloadditions. *Angewandte Chemie International Edition* **2015**, *54* (22), 6506–6510. <https://doi.org/10.1002/anie.201501220>.
- (20) Ahn, J. M.; Peters, J. C.; Fu, G. C. Design of a Photoredox Catalyst That Enables the Direct Synthesis of Carbamate-Protected Primary Amines via Photoinduced, Copper-Catalyzed N-Alkylation Reactions of Unactivated Secondary Halides. *J. Am. Chem. Soc.* **2017**, *139* (49), 18101–18106. <https://doi.org/10.1021/jacs.7b10907>.
- (21) Roth, H. G.; Romero, N. A.; Nicewicz, D. A. Experimental and Calculated Electrochemical Potentials of Common Organic Molecules for Applications to Single-Electron Redox Chemistry. *Synlett* **2016**, *27* (05), 714–723. <https://doi.org/10.1055/s-0035-1561297>.
- (22) Bouveault, L.; Blanc, G. Préparation Des Alcools Primaires Au Moyen Des Acides Correspondants. *Compt. Rend.* **1903**, *136*, 1676–1678.
- (23) Birch, A. J. 117. Reduction by Dissolving Metals. Part I. *J. Chem. Soc.* **1944**, No. 0, 430–436. <https://doi.org/10.1039/JR9440000430>.
- (24) Edmonds, D. J.; Johnston, D.; Procter, D. J. Samarium(II)-Iodide-Mediated Cyclizations in Natural Product Synthesis. *Chem. Rev.* **2004**, *104* (7), 3371–3404. <https://doi.org/10.1021/cr030017a>.

- (25) Nicolaou, K. C.; Ellery, S. P.; Chen, J. S. Samarium Diiodide Mediated Reactions in Total Synthesis. *Angewandte Chemie International Edition* **2009**, *48* (39), 7140–7165. <https://doi.org/10.1002/anie.200902151>.
- (26) Chuang, K. V.; Xu, C.; Reisman, S. E. A 15-Step Synthesis of (+)-Ryanodol. *Science* **2016**, *353* (6302), 912–915. <https://doi.org/10.1126/science.aag1028>.
- (27) Liu, Y.-T.; Li, L.-P.; Xie, J.-H.; Zhou, Q.-L. Divergent Asymmetric Total Synthesis of Mulinane Diterpenoids. *Angewandte Chemie International Edition* **2017**, *56* (41), 12708–12711. <https://doi.org/10.1002/anie.201706994>.
- (28) He, C.; Stratton, T. P.; Baran, P. S. Concise Total Synthesis of Herquelines B and C. *J. Am. Chem. Soc.* **2019**, *141* (1), 29–32. <https://doi.org/10.1021/jacs.8b13029>.
- (29) Joshi, D. K.; Sutton, J. W.; Carver, S.; Blanchard, J. P. Experiences with Commercial Production Scale Operation of Dissolving Metal Reduction Using Lithium Metal and Liquid Ammonia. *Org. Process Res. Dev.* **2005**, *9* (6), 997–1002. <https://doi.org/10.1021/op050155x>.
- (30) Peters, B. K.; Rodriguez, K. X.; Reisberg, S. H.; Beil, S. B.; Hickey, D. P.; Kawamata, Y.; Collins, M.; Starr, J.; Chen, L.; Udyavara, S.; Klunder, K.; Gorey, T. J.; Anderson, S. L.; Neurock, M.; Minter, S. D.; Baran, P. S. Scalable and Safe Synthetic Organic Electroreduction Inspired by Li-Ion Battery Chemistry. *Science* **2019**, *363* (6429), 838–845. <https://doi.org/10.1126/science.aav5606>.
- (31) Nelleborg, P.; Lund, H.; Eriksen, J. Photochemical vs. Electrochemical Electron-Transfer Reactions. One-Electron Reduction of Aryl Halides by Photoexcited Anion Radicals. *Tetrahedron Letters* **1985**, *26* (14), 1773–1776. [https://doi.org/10.1016/S0040-4039\(00\)98335-7](https://doi.org/10.1016/S0040-4039(00)98335-7).
- (32) Costentin, C.; Robert, M.; Savéant, J.-M. Fragmentation of Aryl Halide π Anion Radicals. Bending of the Cleaving Bond and Activation vs Driving Force Relationships. *J. Am. Chem. Soc.* **2004**, *126* (49), 16051–16057. <https://doi.org/10.1021/ja045989u>.
- (33) Ghosh, I.; Ghosh, T.; Bardagi, J. I.; König, B. Reduction of Aryl Halides by Consecutive Visible Light-Induced Electron Transfer Processes. *Science* **2014**, *346* (6210), 725–728. <https://doi.org/10.1126/science.1258232>.
- (34) Ghosh, I.; König, B. Chromoselective Photocatalysis: Controlled Bond Activation through Light-Color Regulation of Redox Potentials. *Angewandte Chemie International Edition* **2016**, *55* (27), 7676–7679. <https://doi.org/10.1002/anie.201602349>.
- (35) Neumeier, M.; Sampedro, D.; Májek, M.; de la Peña O'Shea, V. A.; Jacobi von Wangelin, A.; Pérez-Ruiz, R. Dichromatic Photocatalytic Substitutions of Aryl Halides with a Small Organic Dye. *Chem. Eur. J.* **2018**, *24* (1), 105–108. <https://doi.org/10.1002/chem.201705326>.
- (36) Kerzig, C.; Guo, X.; Wenger, O. S. Unexpected Hydrated Electron Source for Preparative Visible-Light Driven Photoredox Catalysis. *J. Am. Chem. Soc.* **2019**, *141* (5), 2122–2127. <https://doi.org/10.1021/jacs.8b12223>.
- (37) La Porte, N. T.; Martinez, J. F.; Chaudhuri, S.; Hedström, S.; Batista, V. S.; Wasielewski, M. R. Photoexcited Radical Anion Super-Reductants for Solar Fuels Catalysis. *Coordination Chemistry Reviews* **2018**, *361*, 98–119. <https://doi.org/10.1016/j.ccr.2018.01.018>.
- (38) Fox, M. Anne. The Photoexcited States of Organic Anions. *Chem. Rev.* **1979**, *79* (3), 253–273. <https://doi.org/10.1021/cr60319a002>.
- (39) Fukuzumi, S.; Ohkubo, K.; Chen, Y.; Pandey, R. K.; Zhan, R.; Shao, J.; Kadish, K. M. Photophysical and Electrochemical Properties of New Bacteriochlorins and Characterization of Radical Cation and Radical Anion Species. *J. Phys. Chem. A* **2002**, *106* (20), 5105–5113. <https://doi.org/10.1021/jp025665x>.
- (40) Fujitsuka, M.; Kim, S. S.; Lu, C.; Tojo, S.; Majima, T. Intermolecular and Intramolecular Electron Transfer Processes from Excited Naphthalene Diimide Radical Anions. *J. Phys. Chem. B* **2015**, *119* (24), 7275–7282. <https://doi.org/10.1021/jp510850z>.

- (41) Gosztola, D.; Niemczyk, M. P.; Svec, W.; Lukas, A. S.; Wasielewski, M. R. Excited Doublet States of Electrochemically Generated Aromatic Imide and Diimide Radical Anions. *J. Phys. Chem. A* **2000**, *104* (28), 6545–6551. <https://doi.org/10.1021/jp000706f>.
- (42) Yan, M.; Kawamata, Y.; Baran, P. S. Synthetic Organic Electrochemical Methods Since 2000: On the Verge of a Renaissance. *Chem. Rev.* **2017**, *117* (21), 13230–13319. <https://doi.org/10.1021/acs.chemrev.7b00397>.
- (43) Yoshida, J.; Kataoka, K.; Horcajada, R.; Nagaki, A. Modern Strategies in Electroorganic Synthesis. *Chem. Rev.* **2008**, *108* (7), 2265–2299. <https://doi.org/10.1021/cr0680843>.
- (44) Wiebe, A.; Gieshoff, T.; Möhle, S.; Rodrigo, E.; Zirbes, M.; Waldvogel, S. R. Electrifying Organic Synthesis. *Angewandte Chemie International Edition* **2018**, *57* (20), 5594–5619. <https://doi.org/10.1002/anie.201711060>.
- (45) Moeller, K. D. Using Physical Organic Chemistry To Shape the Course of Electrochemical Reactions. *Chem. Rev.* **2018**, *118* (9), 4817–4833. <https://doi.org/10.1021/acs.chemrev.7b00656>.
- (46) Francke, R.; Little, R. D. Redox Catalysis in Organic Electrosynthesis: Basic Principles and Recent Developments. *Chem. Soc. Rev.* **2014**, *43* (8), 2492–2521. <https://doi.org/10.1039/C3CS60464K>.
- (47) Meyer, T. H.; Finger, L. H.; Gandeepan, P.; Ackermann, L. Resource Economy by Metallalectrocatalysis: Merging Electrochemistry and CH Activation. *Trends in Chemistry* **2019**, *1* (1), 63–76. <https://doi.org/10.1016/j.trechm.2019.01.011>.
- (48) Et₃N can promote premature radical quenching through hydrogen atom transfer and back electron transfer to Et₃N^{•+} For details see ref [7]. *Et₃N can promote premature radical quenching through hydrogen atom transfer and back electron transfer to Et₃N^{•+} For details see ref [7]*.
- (49) Lund, H.; Simonet, J. Anion Radicals and Dianions as Electron Transfer Reagents. *Journal of Electroanalytical Chemistry and Interfacial Electrochemistry* **1975**, *65* (1), 205–218. [https://doi.org/10.1016/0368-1874\(75\)85118-5](https://doi.org/10.1016/0368-1874(75)85118-5).
- (50) Shukla, S. S.; Rusling, J. F. Photoelectrocatalytic Reduction of 4-Chlorobiphenyl Using Anion Radicals and Visible Light. *J. Phys. Chem.* **1985**, *89* (15), 3353–3358. <https://doi.org/10.1021/j100261a039>.
- (51) Lund, H.; Carlsson, H. S.; Nishida, T.; Enzell, C. R.; Matsuno, T. Photochemistry of Radical Ions. *Acta Chem. Scand.* **1978**, *32b*, 505–509. <https://doi.org/10.3891/acta.chem.scand.32b-0505>.
- (52) Eriksen, J.; Lund, H.; Nyvad, A. I.; Yamato, T.; Mitchell, R. H.; Dingle, T. W.; Williams, R. V.; Mahedevan, R. Electron-Transfer Fluorescence Quenching of Radical Ions. *Acta Chem. Scand.* **1983**, *37b*, 459–466. <https://doi.org/10.3891/acta.chem.scand.37b-0459>.
- (53) Scheffold, R.; Orlinski, R. Synthesis and Reactions of Porphine-Type Metal Complexes. 15. Carbon-Carbon Bond Formation by Light Assisted B12-Catalysis. Nucleophilic Acylation of Michael Olefins. *J. Am. Chem. Soc.* **1983**, *105* (24), 7200–7202. <https://doi.org/10.1021/ja00362a047>.
- (54) Li, T.; Kasahara, T.; He, J.; Dettelbach, K. E.; Sammis, G. M.; Berlinguette, C. P. Photoelectrochemical Oxidation of Organic Substrates in Organic Media. *Nature Communications* **2017**, *8* (1), 390. <https://doi.org/10.1038/s41467-017-00420-y>.
- (55) Yan, H.; Hou, Z.-W.; Xu, H.-C. Photoelectrochemical C–H Alkylation of Heteroarenes with Organotrifluoroborates. *Angewandte Chemie International Edition* **2019**, *58* (14), 4592–4595. <https://doi.org/10.1002/anie.201814488>.
- (56) Wang, F.; Stahl, S. S. Merging Photochemistry with Electrochemistry: Functional-Group Tolerant Electrochemical Amination of C(Sp³)–H Bonds. *Angewandte Chemie International Edition* **2019**, *58* (19), 6385–6390. <https://doi.org/10.1002/anie.201813960>.
- (57) Huang, H.; Strater, Z. M.; Rauch, M.; Shee, J.; Sisto, T. J.; Nuckolls, C.; Lambert, T. H. Electrophotocatalysis with a Trisaminocyclopropenium Radical Dication. *Angewandte*

- Chemie International Edition* **2019**, *58* (38), 13318–13322.
<https://doi.org/10.1002/anie.201906381>.
- (58) Capaldo, L.; Quadri, L. L.; Ravelli, D. Merging Photocatalysis with Electrochemistry: The Dawn of a New Alliance in Organic Synthesis. *Angew. Chem., Int. Ed.* **2019**, *58* (49), 17508–17510. <https://doi.org/10.1002/anie.201910348>.
- (59) Ghosh, I.; Marzo, L.; Das, A.; Shaikh, R.; König, B. Visible Light Mediated Photoredox Catalytic Arylation Reactions. *Acc. Chem. Res.* **2016**, *49* (8), 1566–1577.
<https://doi.org/10.1021/acs.accounts.6b00229>.
- (60) Wang, C.-S.; Dixneuf, P. H.; Soulé, J.-F. Photoredox Catalysis for Building C–C Bonds from C(Sp²)–H Bonds. *Chem. Rev.* **2018**, *118* (16), 7532–7585.
<https://doi.org/10.1021/acs.chemrev.8b00077>.
- (61) Devery, J. J.; Nguyen, J. D.; Dai, C.; Stephenson, C. R. J. Light-Mediated Reductive Debromination of Unactivated Alkyl and Aryl Bromides. *ACS Catal.* **2016**, *6* (9), 5962–5967.
<https://doi.org/10.1021/acscatal.6b01914>.
- (62) Discekici, E. H.; Treat, N. J.; Poelma, S. O.; Mattson, K. M.; Hudson, Z. M.; Luo, Y.; Hawker, C. J.; Alaniz, J. R. de. A Highly Reducing Metal-Free Photoredox Catalyst: Design and Application in Radical Dehalogenations. *Chem. Commun.* **2015**, *51* (58), 11705–11708.
<https://doi.org/10.1039/C5CC04677G>.
- (63) Boyington, A. J.; Riu, M.-L. Y.; Jui, N. T. Anti-Markovnikov Hydroarylation of Unactivated Olefins via Pyridyl Radical Intermediates. *J. Am. Chem. Soc.* **2017**, *139* (19), 6582–6585.
<https://doi.org/10.1021/jacs.7b03262>.
- (64) Cheng, Y.; Gu, X.; Li, P. Visible-Light Photoredox in Homolytic Aromatic Substitution: Direct Arylation of Arenes with Aryl Halides. *Org. Lett.* **2013**, *15* (11), 2664–2667.
<https://doi.org/10.1021/ol400946k>.
- (65) Huang, L.; Ackerman, L. K. G.; Kang, K.; Parsons, A. M.; Weix, D. J. LiCl-Accelerated Multimetallic Cross-Coupling of Aryl Chlorides with Aryl Triflates. *J. Am. Chem. Soc.* **2019**, *141* (28), 10978–10983. <https://doi.org/10.1021/jacs.9b05461>.
- (66) Ghosh, I.; Shaikh, R. S.; König, B. Sensitization-Initiated Electron Transfer for Photoredox Catalysis. *Angew. Chem., Int. Ed.* **2017**, *56* (29), 8544–8549.
<https://doi.org/10.1002/anie.201703004>.
- (67) Meyer, A. U.; Slanina, T.; Heckel, A.; König, B. Lanthanide Ions Coupled with Photoinduced Electron Transfer Generate Strong Reduction Potentials from Visible Light. *Chemistry – A European Journal* **2017**, *23* (33), 7900–7904.
<https://doi.org/10.1002/chem.201701665>.
- (68) Yin, H.; Jin, Y.; Hertzog, J. E.; Mullane, K. C.; Carroll, P. J.; Manor, B. C.; Anna, J. M.; Schelter, E. J. The Hexachlorocerate(III) Anion: A Potent, Benchtop Stable, and Readily Available Ultraviolet A Photosensitizer for Aryl Chlorides. *J. Am. Chem. Soc.* **2016**, *138* (50), 16266–16273. <https://doi.org/10.1021/jacs.6b05712>.
- (69) Matsubara, R.; Yabuta, T.; Md Idros, U.; Hayashi, M.; Ema, F.; Kobori, Y.; Sakata, K. UVA- and Visible-Light-Mediated Generation of Carbon Radicals from Organochlorides Using Nonmetal Photocatalyst. *J. Org. Chem.* **2018**, *83* (16), 9381–9390.
<https://doi.org/10.1021/acs.joc.8b01306>.
- (70) Sun, G.; Ren, S.; Zhu, X.; Huang, M.; Wan, Y. Direct Arylation of Pyrroles via Indirect Electroreductive C–H Functionalization Using Perylene Bisimide as an Electron-Transfer Mediator. *Org. Lett.* **2016**, *18* (3), 544–547. <https://doi.org/10.1021/acs.orglett.5b03581>.
- (71) Plumb, J. B.; Obrycki, R.; Griffin, C. E. Phosphonic Acids and Esters. XVI. Formation of Dialkyl Phenylphosphonates by the Photoinitiated Phenylation of Trialkyl Phosphites^{1,2}. *J. Org. Chem.* **1966**, *31* (8), 2455–2458. <https://doi.org/10.1021/jo01346a006>.
- (72) Beveridge, S.; Huppatz, J. L. The Pschorr Cyclization. A Novel Pschorr Reaction with a Pyrrole Derivative: Synthesis of a Pyrrolo[1,2-c]Quinazoline and a New Route to Arylpyrroles. *Aust. J. Chem.* **1970**, *23* (4), 781–789. <https://doi.org/10.1071/ch9700781>.

- (73) Newcomb, M. Radical Kinetics and Clocks. In *Encyclopedia of Radicals in Chemistry, Biology and Materials*; American Cancer Society, 2012. <https://doi.org/10.1002/9781119953678.rad007>.
- (74) Kimura, M.; Miyahara, H.; Moritani, N.; Sawaki, Y. Electroreductive Dehalogenation of Chlorinated Aromatic Ethers. Unexpected Electrogenenerated Base-Catalyzed Reactions. *J. Org. Chem.* **1990**, *55* (12), 3897–3902. <https://doi.org/10.1021/jo00299a037>.
- (75) Andrieux, C. P.; Pinson, J. The Standard Redox Potential of the Phenyl Radical/Anion Couple. *J. Am. Chem. Soc.* **2003**, *125* (48), 14801–14806. <https://doi.org/10.1021/ja0374574>.
- (76) Ruccolo, S.; Qin, Y.; Schnedermann, C.; Nocera, D. G. General Strategy for Improving the Quantum Efficiency of Photoredox Hydroamidation Catalysis. *J. Am. Chem. Soc.* **2018**, *140* (44), 14926–14937. <https://doi.org/10.1021/jacs.8b09109>.
- (77) Takeda, N.; Poliakov, P. V.; Cook, A. R.; Miller, J. R. Faster Dissociation: Measured Rates and Computed Effects on Barriers in Aryl Halide Radical Anions. *J. Am. Chem. Soc.* **2004**, *126* (13), 4301–4309. <https://doi.org/10.1021/ja0389671>.
- (78) Ke, J.; Wang, H.; Zhou, L.; Mou, C.; Zhang, J.; Pan, L.; Chi, Y. R. Hydrodehalogenation of Aryl Halides through Direct Electrolysis. *Chemistry – A European Journal* **2019**, *25* (28), 6911–6914. <https://doi.org/10.1002/chem.201901082>.

2.7. Supplemental Information

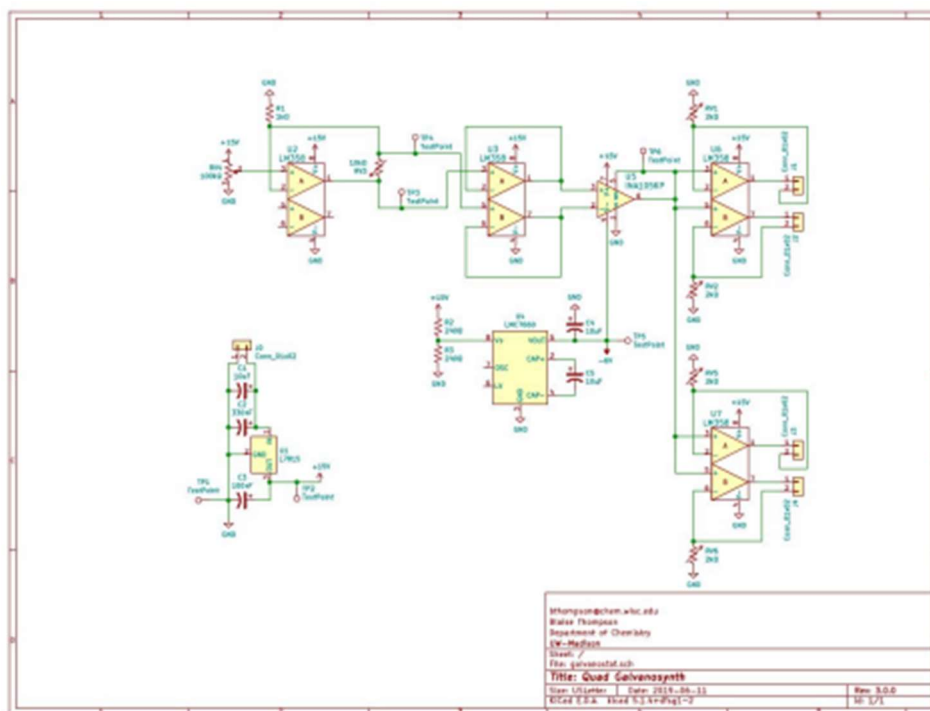
2.7.1 General Methods and Materials

Unless otherwise noted, reactions were performed under an inert N₂ atmosphere in an anhydrous solvent thoroughly degassed by freeze-pump-thaw. MeCN and DMF were dried by passing through activated alumina columns. Anhydrous DMSO was purchased from Sigma-Aldrich and stored under N₂. All tetra-butylammonium electrolyte salts were recrystallized from hot ethyl acetate prior to use. Triethylphosphite was distilled from NaO under vacuum. All heterocycles and amines were distilled from NaO or CaH₂ prior to use. Unless otherwise noted, other commercially-available reagents were used as received. Crude mixtures were evaluated by thin-layer chromatography using EMD/Merck silica gel 60 F254 pre-coated plates (0.25 mm) and were visualized by UV, CAM, p-anisaldehyde, or KMnO₄ staining. Flash chromatography was performed with a Biotage Isolera One automated chromatography system with re-packed silica columns (technical grade silica, pore size 60 Å, 230-400 mesh particle size, 40-63 particle size). Purified materials were dried in vacuo (0.050 Torr) to remove trace solvent. ¹H, ¹³C, ³¹P Spectra were taken using a Bruker Avance-400 with a BBFO Probe or a Bruker Avance-500 with a DCH Cryoprobe. NMR data are reported relative to residual CHCl₃ (¹H, δ = 7.26 ppm), CDCl₃ (¹³C, δ = 77.16 ppm). Data for ¹H NMR spectra are reported as follows: chemical shift (δ ppm) (multiplicity, coupling constant (Hz), integration). Multiplicity and qualifier abbreviations are as follows: s = singlet, d = doublet, t = triplet, q = quartet, m = multiplet, br = broad. GC traces were taken on an Agilent 7890A GC with dual DB-5 columns (20 m × 180 μ m × 0.18 μ m), dual FID detectors, and hydrogen as the carrier gas. A sample volume of 1 μ L was injected at a temperature of 300 °C and a 100:1 split ratio. The initial inlet pressure was 20.3 psi but varied as the column flow was held constant at 1.8 mL/min for the duration of the run, FID temperature was 325 °C.

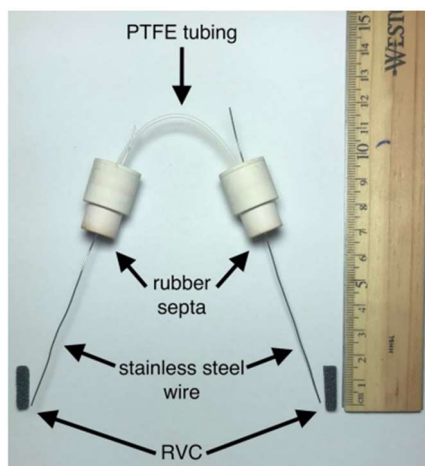
2.7.2 Electrochemical Equipment and Experimental Set-Up

All cyclic voltammetric, chronoamperometric and chronopotentiometric measurements were performed at room temperature using a Pine WaveNowXV. The CV experiments were carried out in a three-electrode cell configuration with a glassy carbon (GC) working electrode (3 mm diameter, unless otherwise stated) and a platinum wire counter electrode. Chronoamperometric and chronopotentiometric measurements were carried out in divided cells with RVC (15 × 3 × 5mm) as working and counter electrodes affixed to stainless steel wire. The potentials were measured versus an Ag/AgNO₃ (0.01 M in MeCN with 0.1M Bu₄N•PF₆) reference electrode (all electrodes from Pine Research). Bulk constant current electrolysis experiments were performed in divided H cells with RVC (15×3×5mm) as working and counter electrodes affixed to stainless steel wire and driven with a custom-made low current power supply (see Scheme below) which was externally calibrated with a multimeter using a 10 or 1–Ohm resistor.

Low-current Power Supply: Original design and fabrication by Dr. Blaise J. Thompson. Provides an operational range of ±0.01–9.99 mA, tunable by analog input, delivering power to multiple banana socket pairs. The power supply is limited to ±15 V for bulk electrolyses and is powered by an 18 V wall wart. Circuitry is housed within an aluminum enclosure.



H-cells and electrode assembly fabrication:



Polytetrafluoroethylene (PTFE) tubing purchased from Cole-Parmer; 1/32" ID, 1/16" OD, item number EW-06407-41. 14/20 Rubber septa purchased from VWR, item number 89064-940.

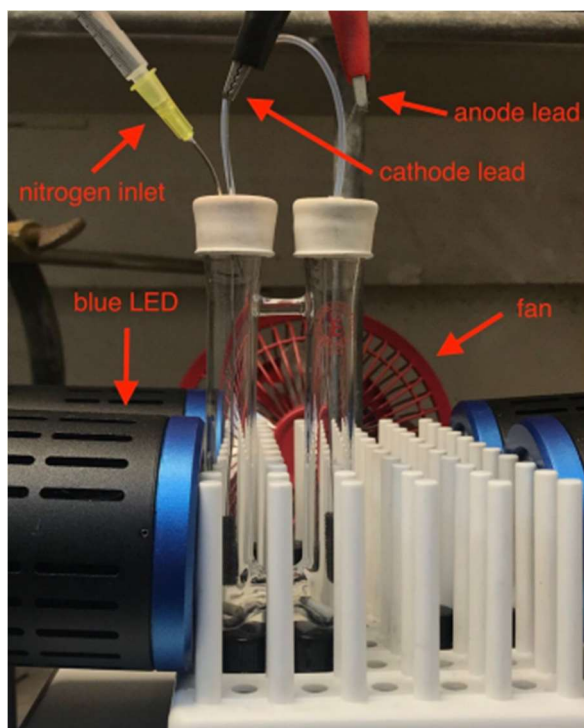
Stainless steel wire purchased from Grainger; stainless steel lockwire, 0.025" diameter, item number 16Y043. Reticulated vitreous carbon (RVC) purchased from SELEE Corporation; 80 ppi, 04-07 g/cc, cut into 15×3×5 mm pieces.



Divided cell fabricated in-house. Porosity E glass filter disc purchased from Ace Glass; 8 mm diameter, part number 7176-21



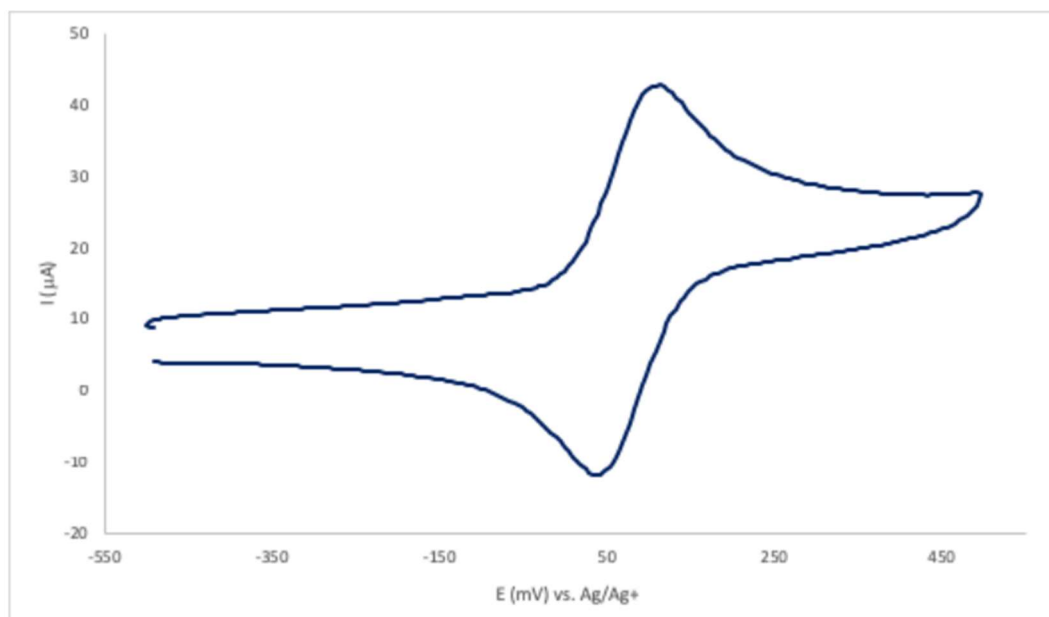
Assembled cell. RVC attached by piercing with stainless steel wire.



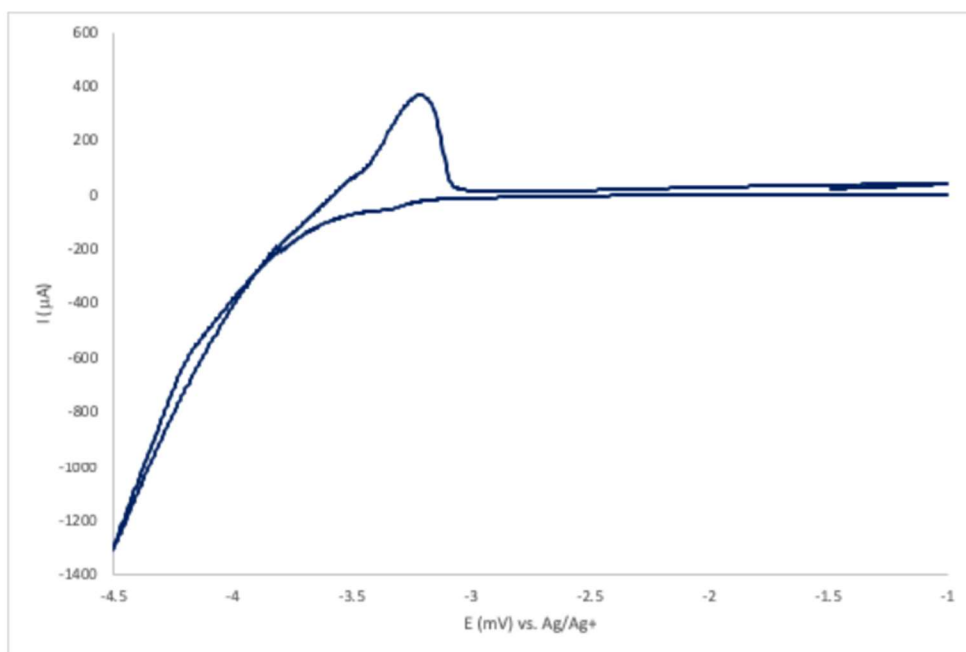
Anode and cathode leads connected to low-current power supply. Kessil lamps; A160WE Tuna Blue.

2.7.3 Electrochemical Characterization

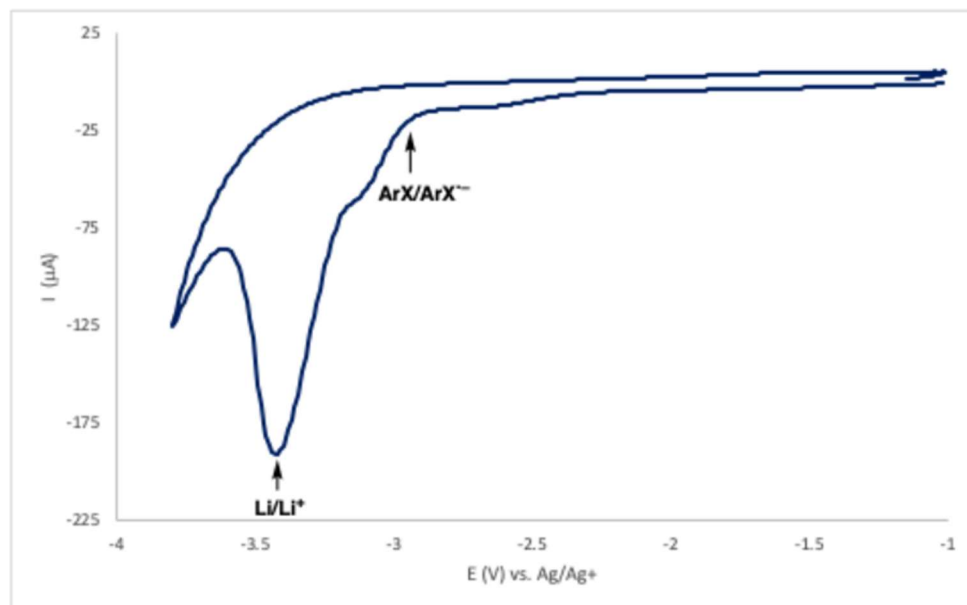
External Standard—ferrocene in DMSO vs Ag/AgNO₃ in MeCN(0.1 M LiClO₄)



Cyclic Voltammetry— DMSO (0.1 M LiClO₄)

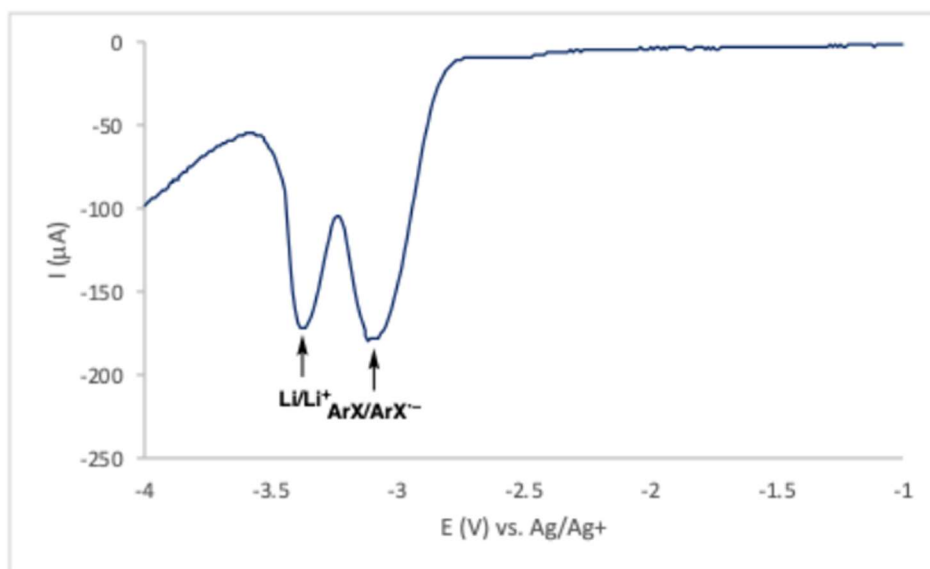


Cyclic Voltammetry—5-chloro-m-xylene in DMSO (0.1 M LiClO₄)



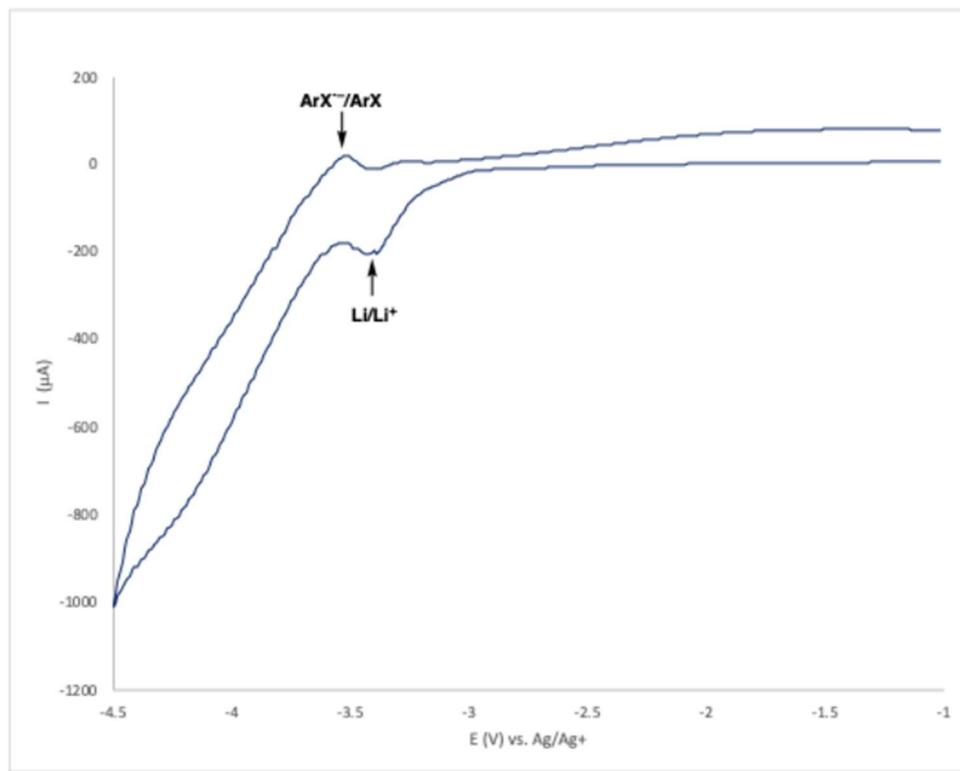
$$E_{\text{onset}} \approx -2.6 \text{ V } (-2.9 \text{ V vs. Ag/Ag}^+)$$

Differential Pulse Voltammetry—5-chloro-m-xylene in DMSO (0.1 M LiClO₄)



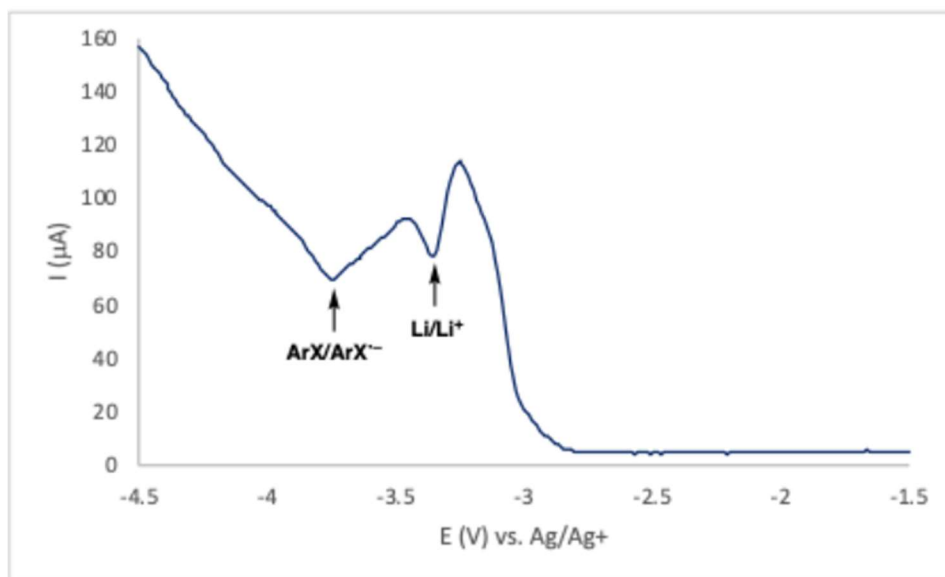
$$E_{1/2} = -2.76 \text{ V vs SCE } (-3.11 \text{ V vs Ag/Ag+})$$

Cyclic Voltammetry—4-chloro-2,6-di-tert-butylanisole (S1)



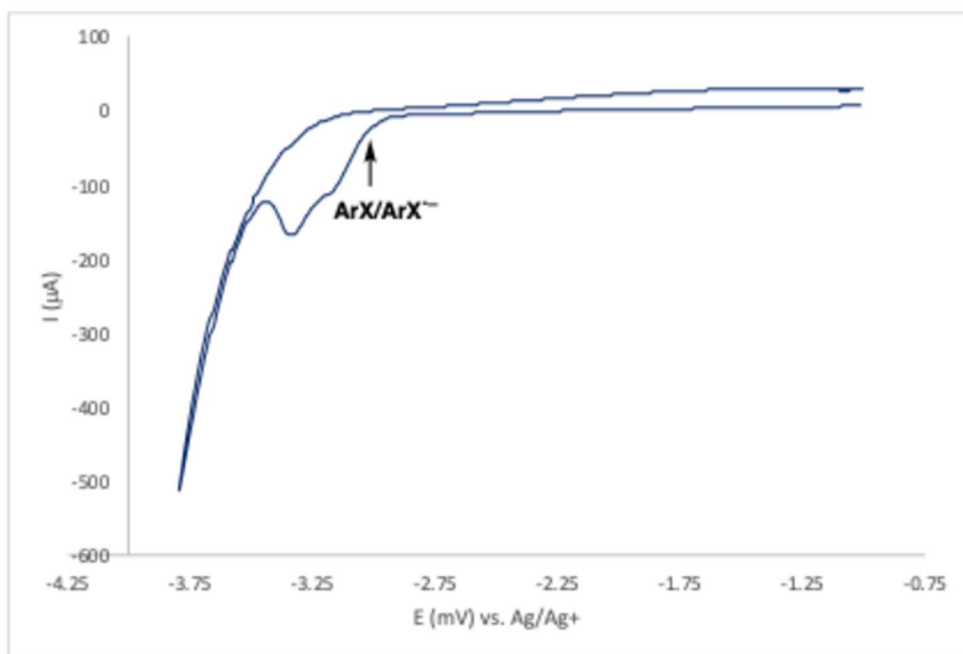
$$E_{\text{onset}} \approx -3.3 \text{ V } (-3.6 \text{ V vs Ag/Ag+})$$

Differential Pulse Voltammetry—4-chloro-2,6-di-tert-butylanisole (S1)

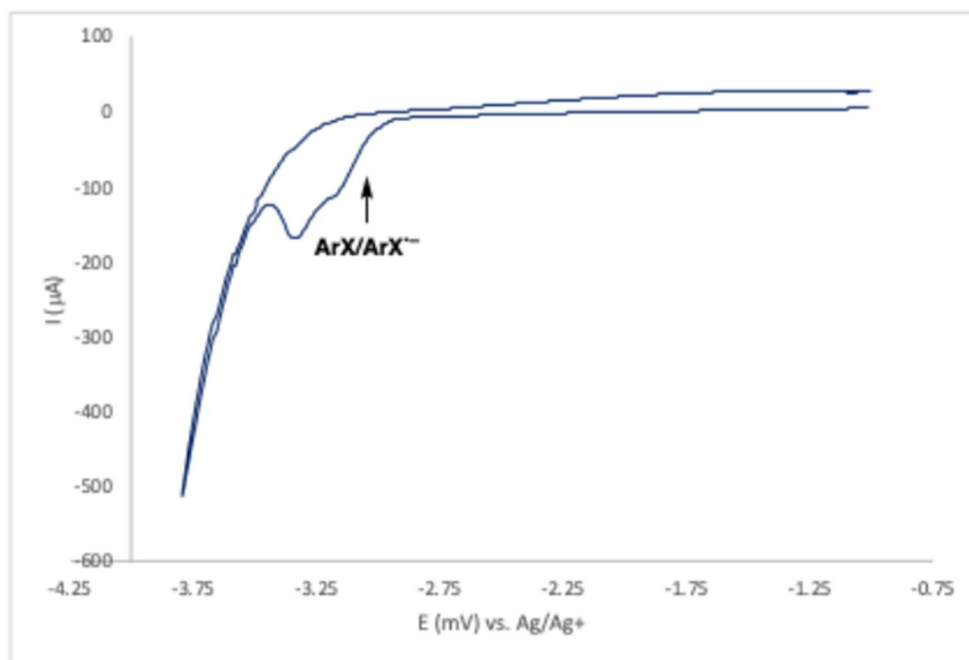


$$E_{1/2} = -3.40 \text{ V vs SCE } (-3.75 \text{ V vs Ag/Ag}^+)$$

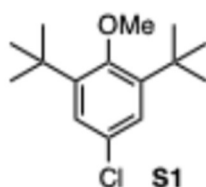
Cyclic Voltammetry—4-chloro-N,N-dimethylaniline



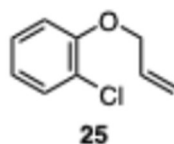
Cyclic Voltammetry—4-Chlorophenylboronic acid pinacol ester



2.7.4 Synthesis of Non-Commercial Substrates

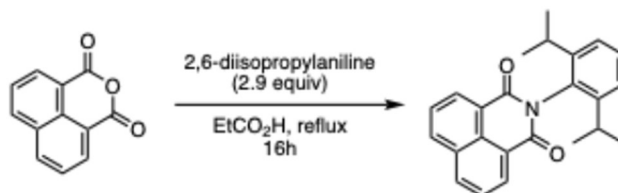


4-chloro-2,6-di-tert-butylanisole or “super anisole” (S1) was donated by the Weix group at UW-Madison as material from their previous methodological studies (JACS 2019, 141, 28, 10978). Prior to use, the material was recrystallized from MeCN/H₂O.

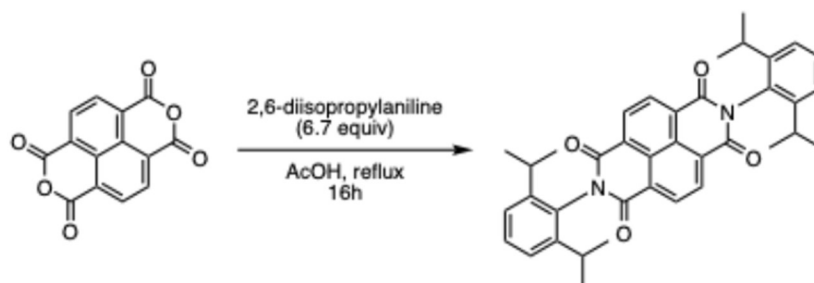


Allyl (2-chlorophenyl) ether (25) was prepared by literature procedure. (Tetrahedron, 2003, 59, 43, 8525). ¹H NMR (500 MHz, CDCl₃) δ 7.37 (dd, J = 7.8, 1.6 Hz, 1H), 7.20 (ddd, J = 8.2, 7.5, 1.6 Hz, 1H), 6.93 (dd, J = 8.3, 1.4 Hz, 1H), 6.90 (td, J = 7.6, 1.4 Hz, 1H), 6.08 (ddt, J = 17.3, 10.4, 5.1 Hz, 1H), 5.47 (dq, J = 17.3, 1.6 Hz, 1H), 5.31 (dq, J = 10.5, 1.5 Hz, 1H), 4.62 (dt, J = 5.1, 1.6 Hz, 2H) consistent with reported spectra.

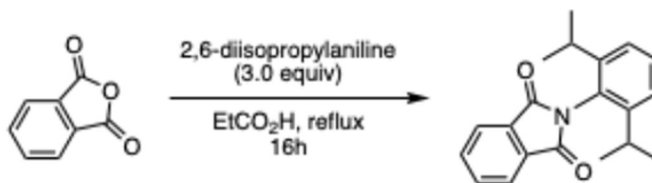
2.7.5 Preparation of Imide Catalysts



NpMI—Suspend 1,8-naphthalic anhydride (6.73 g, 34.0 mmol, 1.00 equiv) in propanoic acid (100 mL). Add 2,6-diisopropylaniline (19.0 mL, 17.9 g, 100 mmol, 2.9 equiv). Reflux mixture for 16h. Cool to ambient temperature. Dilute with DI H₂O (100 mL) and collect precipitate by filtration. Wash precipitate with DI H₂O (2×25 mL) followed by Hexanes(3×25 mL). Dry precipitate in vacuo. Recrystallize crude material from hot CHCl₃ (150 mL)/Hexanes (175 mL) slowly cooled to -20 °C overnight to yield an off-white crystalline product, pure by NMR (11.21 g, 92% yield). For best results, a second recrystallization of the aryl imide was performed. Recrystallization from CHCl₃ (100 mL) and Hexanes (200 mL) by layer diffusion at -20 °C provided pure product (8.28 g, 23.2 mmol, 68% yield). **¹H NMR** (500 MHz, CDCl₃) δ 8.67 (dd, J = 7.2, 1.1 Hz, 2H), 8.30 (dd, J = 8.3, 1.1 Hz, 2H), 7.81 (dd, J = 8.2, 7.2 Hz, 2H), 7.47 (t, J = 7.8 Hz, 1H), 7.33 (d, J = 7.8 Hz, 2H), 2.75 (p, J = 6.8 Hz, 2H), 1.16 (d, J = 6.8 Hz, 12H). **¹³C NMR** S13 (126 MHz, CDCl₃) δ 164.35, 145.82, 134.31, 131.99, 131.88, 131.00, 129.63, 128.98, 127.18, 124.16, 122.94, 29.27, 24.13. HRMS (ESI⁺) Calc: [M+H]⁺ (C₂₄H₂₃NO₂) 358.1802; measured: 358.1802 = 2.0 ppm difference.



NpDI—Suspend 1,4,5,8-naphthalene-tetracarboxylic dianhydride (1.34 g, 5.0 mmol, 1.00 equiv) in acetic acid (70 mL). Add 2,6-diisopropylaniline (6.32 mL, 5.94 g, 33.5 mmol, 6.7 equiv). Reflux mixture for 16h. Cool to ambient temperature. Dilute with DI H₂O (70 mL) and collect precipitate by filtration. Wash precipitate with DI H₂O (2×20 mL) followed by Hexanes(3×20 mL). Dry precipitate in vacuo. Recrystallize crude material from CHCl₃/Hexanes to yield an off-white solid (2.59 g, 4.41 mmol, 88% yield). **¹H NMR** (500 MHz, CDCl₃) δ 8.89 (s, 4H), 7.52 (t, J = 7.8 Hz, 2H), 7.36 (d, J = 7.8 Hz, 4H), 2.71 (p, J = 6.8 Hz, 4H), 1.17 (d, J = 6.9 Hz, 24H), consistent with reported spectra (Org. Lett., 2010, 12, 15, 3460).



PhMI—Suspend phthalic anhydride (741 mg, 5.0 mmol, 1.00 equiv) in propanoic acid (15 mL). Add 2,6-diisopropylaniline (2.83 mL, 2.66 g, 15 mmol, 3.0 equiv). Reflux mixture for 16h. Cool to ambient temperature. Dilute with DI H₂O (70 mL) and collect precipitate by filtration. Wash precipitate with DI H₂O (2×20 mL) followed by Hexanes(3×20 mL). Dry precipitate in vacuo. Recrystallize crude material from CHCl₃/Hexanes to yield an off-white solid (1.10 g, 3.58 mmol, 72% yield). ¹ H NMR (500 MHz, CDCl₃) δ 7.98 (dd, J = 5.5, 3.0 Hz, 2H), 7.82 (dd, J = 5.5, 3.1 Hz, 2H), 7.46 (t, J = 7.8 Hz, 1H), 7.29 (d, J = 7.8 Hz, 3H), 2.72 (p, J = 6.8 Hz, 2H), 1.17 (d, J = 6.9 Hz, 13H), consistent with reported spectra (J. Org. Chem., 2018, 83, 1, 104).

N,N'-Bis(2,6-diisopropylphenyl)-3,4,9,10-perylenetetracarboxylic diimide is commercially available, purchased from TCI chemicals, and used as received.

2.7.6 General Procedures for Electron-Primed Photocatalysis

General Procedure A— Dehalogenation

Add imide catalyst (0.040 mmol, 10 mol %), tri-tert-butylphenol (10.2 mg, 0.040 mmol, 10 mol %), and 4-bromobiphenyl (93.2 mg, 0.40 mmol, 1.0 equiv) to the cathodic chamber of the divided cell. Add Bu₄N•PF₆ (195 mg, 0.50 mmol) to both the anodic and cathodic chambers. Add a stir bar to each chamber. Wrap reference cell with teflon tape, affix a three electrode assembly, and seal the cell. Purge cells with nitrogen for 10 minutes; inlet needle into cathodic chamber, outlet needle into anodic chamber. Add isopropanol (30 μL, 0.40 mmol, 1 equiv), and DMF (5.0 mL) to the cathode. Add triethylamine (110 μL, 0.8 mmol, 2 equiv), and DMF (5.0 mL) to the anode. Connect electrodes to potentiostat. With fan cooling, electrolyze at −1.3 V vs SCE and irradiate with a blue Kessil lamp for 16h.

For GC analyses: Add mesitylene (28 μL, 0.20 mmol, 0.50 equiv) to crude reaction and remove a 0.2 mL aliquot. Dilute with diethyl ether (4.0 mL), filter off precipitated electrolyte, and further dilute the filtrate (0.2 mL) with diethyl ether (1.0 mL).

General Procedure B— Phosphorylation

Add NpMI (7.1 mg, 0.020 mmol, 5 mol %) to the cathodic chamber of the divided cell. If a solid, add the aryl chloride (0.40 mmol, 1.0 equiv) to the cathodic chamber. Add Bu₄N•PF₆ (155 mg, 0.40 mmol) to both the anodic and cathodic chambers. Add a stir bar to each chamber. Affix the electrode assembly and seal the cell (see H-cells and electrode assembly fabrication). Purge cells with nitrogen for 10 minutes; inlet needle into cathodic chamber, outlet needle into anodic chamber. If a liquid, add aryl chloride (0.40 mmol, 1.0 equiv) to the cathodic chamber. Add triethylphosphite (340 μL, 2.0 mmol, 5.0 equiv), and MeCN (4.0 mL) to the cathode. Add triethylamine (110 μL, 0.80 mmol, 2.0 equiv), and MeCN (4.0 mL) to the anode. Connect steel electrodes to a low-current power supply. With fan cooling, electrolyze at 0.8 mA and irradiate with a blue Kessil lamp for 14h (1 F/mol) or 8h (0.6 F/mol).

Crude cathode and anode solution extracted from NaHCO₃ (50 mL) with EtOAc (3×25mL). Organic layer washed with brine (50 mL) and dried over MgSO₄. Concentrate crude material and dilute with 1:1 EtOAc/Hexanes (10 mL) to precipitate excess electrolyte, filter off solid and wash precipitate with 1:1 EtOAc/Hexanes. Concentrate crude product and purify by flash chromatography with silica.

General Procedure C— Heteroarylation

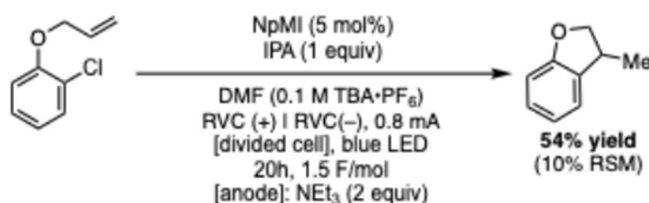
Add NpMI (7.1 mg, 0.020 mmol, 5 mol %) to the cathodic chamber of the divided cell. If a solid, add the aryl chloride (0.40 mmol, 1.0 equiv) to the cathodic chamber. Add Bu₄N•PF₆ (155 mg, 0.40 mmol) to both the anodic and cathodic chambers. Add a stir bar to each chamber. Affix the electrode assembly and seal the cell (see H-cells and electrode assembly fabrication). Purge cells with nitrogen for 10 minutes; inlet needle into cathodic chamber, outlet needle into anodic chamber. If a liquid, add aryl chloride (0.40 mmol, 1.0 equiv) to the cathodic chamber. Add N-methylpyrrole (1.77 mL, 20.0 mmol, 50 equiv) and DMSO (0.3 mL) to the cathodic chamber. Add triethylamine (110 μ L, 0.8 mmol, 2 equiv) and DMSO (2.0 mL) to the anodic chamber. Place cells so that the cathodic chamber is touching the Kessil lamp. Connect the cell to the a low-current power supply via the stainless steel leads. Irradiate and cool with a fan while electrolyzing at 0.4 mA for 24h (0.9 F/mol).

Combine the contents of the cathodic and anodic chambers and extracted from NaHCO₃ (50 mL) with EtOAc (3 \times 25mL). Wash combined organic layers with brine (2 \times 50mL) and dry over MgSO₄. Filter and concentrate crude product for purification by flash chromatography with silica.

2.7.7 Radical Clock Experiment and Competition Experiment

Radical Clock Experiment

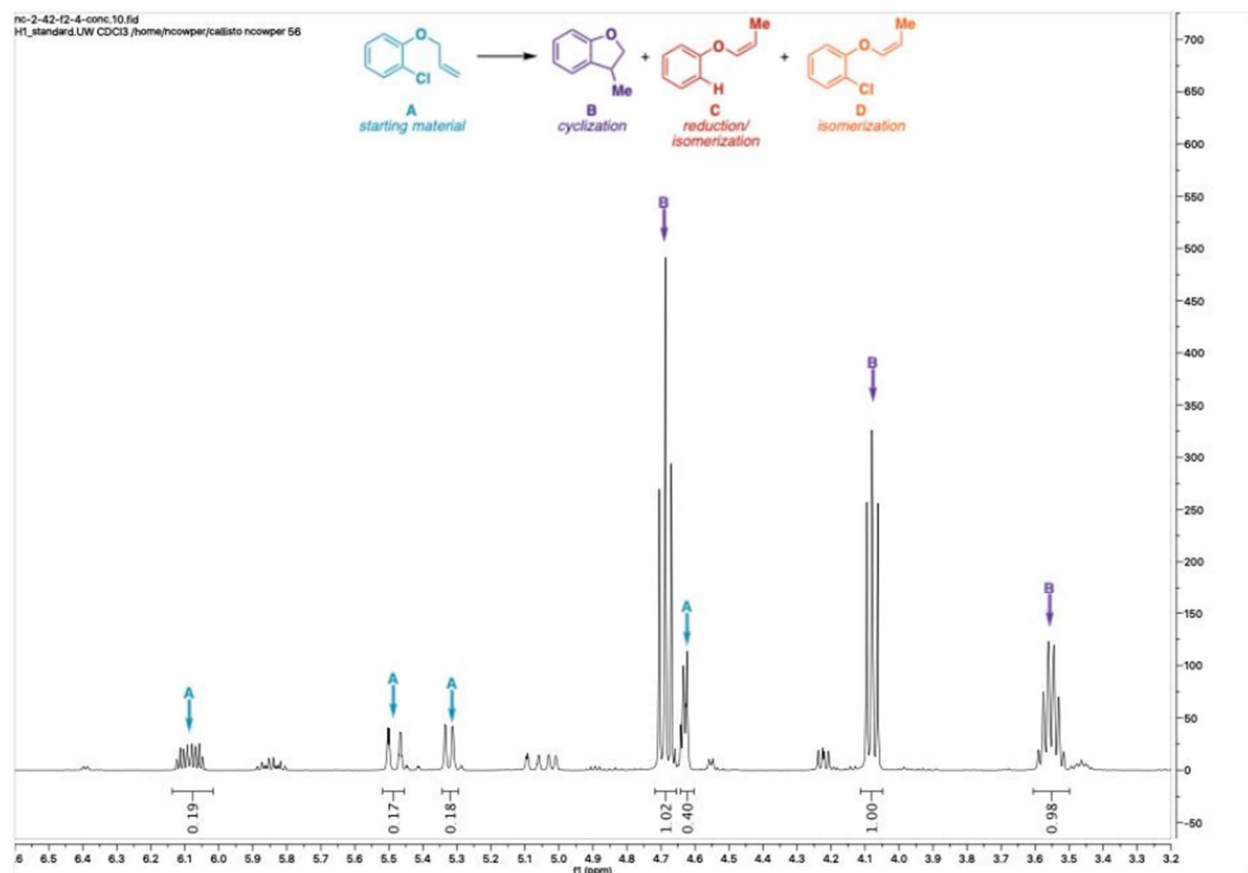
Electron-Primed Photocatalysis—Intramolecular Radical Cyclization



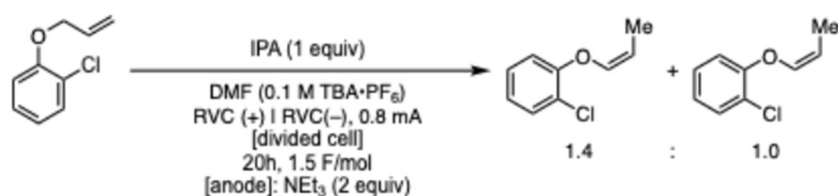
Add NpMI (7.1 mg, 0.020 mmol, 5 mol %) to the cathodic chamber of the divided cell. Add Bu₄N•PF₆ (155 mg, 0.40 mmol) to both the anodic and cathodic chambers. Add a stir bar to each chamber. Affix the two electrode assembly and seal the cell. Purge cells with nitrogen for 10 minutes; inlet needle into cathodic chamber, outlet needle into anodic chamber. Add allyl 2-chlorophenyl ether (67.4 mg, 0.40 mmol, 1.0 equiv) to the cathodic chamber via tared 100 μ L microsyringe. Add isopropanol (30 μ L, 0.40 mmol, 1 equiv), and DMF (5.0 mL) to the cathode. Add triethylamine (110 μ L, 0.8 mmol, 2 equiv), and DMF (5.0 mL) to the anode. Connect steel electrode leads to a low-current power supply. With fan cooling, electrolyze at 0.8 mA and irradiate with a blue Kessil lamp for 20h (1.5 F/mol).

Crude cathode and anode solution extracted from NaHCO₃ (50 mL) with EtOAc (3 \times 25 mL). Organic layer washed with brine (50 mL). Dry combined organics over MgSO₄, concentrate. 1:1 EtOAc/Hexanes (10 mL) to precipitate excess electrolyte, filter off solid, and wash precipitate with 1:1 EtOAc/Hexanes. Concentrate crude material and remove base-line impurities on silica a mixture of cyclized product and starting material (38.1 mg, 76 wt% ptd, 0.21 mmol, 54% yield) see annotated 1 H NMR below.

Radical Clock —Electron-Primed Photocatalysis



Direct Electrolysis—Isomerization of Radical Clock Substrate

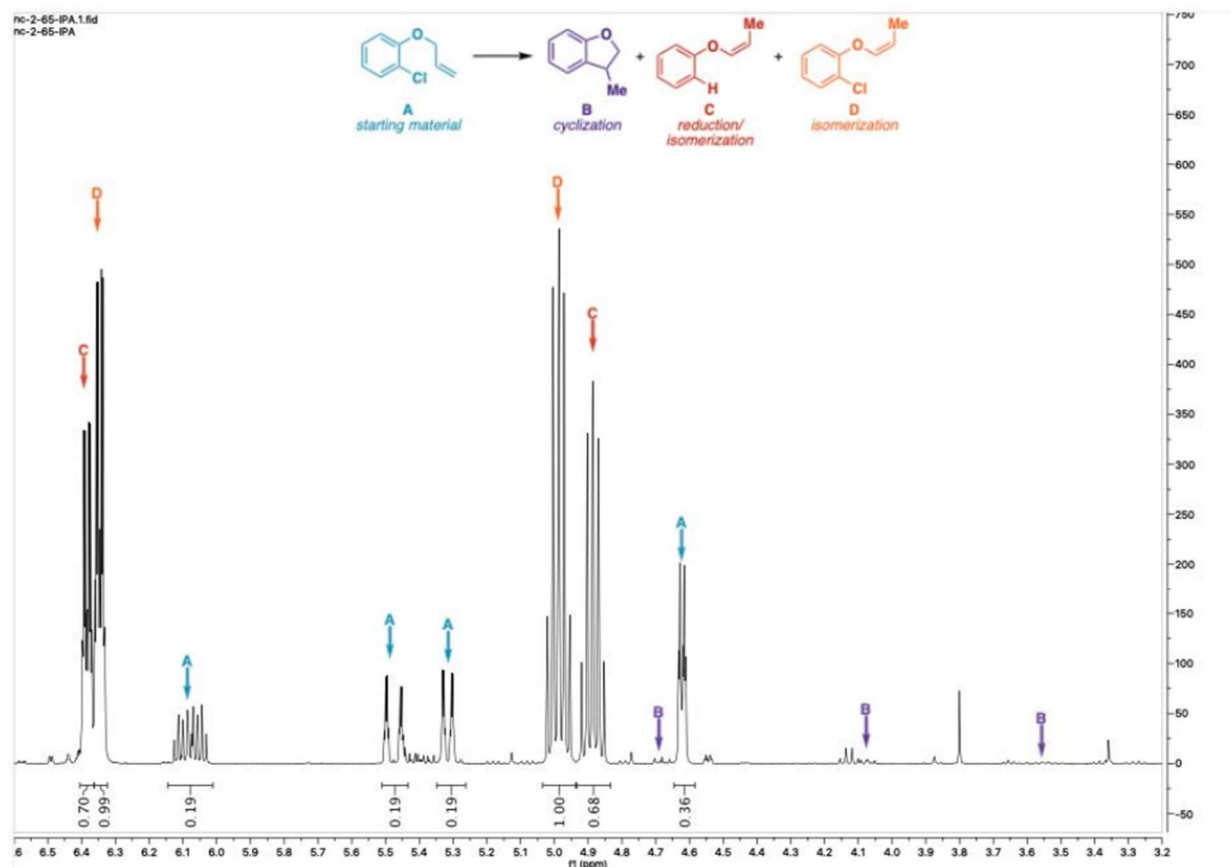


The direct electrolysis of the radical clock was performed analogously, excluding the addition of NpMI and direct irradiation with blue light. Add tri-tert-butylphenol (10.2 mg, 0.040 mmol, 10 mol %) to the cathodic chamber of the divided cell. Add Bu₄N•PF₆ (155 mg, 0.40 mmol) to both the anodic and cathodic chambers. Add a stir bar to each chamber. Affix the electrode assembly and seal the cell. Purge cells with nitrogen for 10 minutes; inlet needle into cathodic chamber, outlet needle into anodic chamber. Add allyl 2-chlorophenyl ether (67.4 mg, 0.40 mmol, 1.0 equiv) to the cathodic chamber via tared 100 μ L microsyringe. Add isopropanol (30 μ L, 0.40 mmol, 1.0 equiv), and DMF (5.0 mL) to the cathode. Add triethylamine (110 μ L, 0.8 mmol, 2 equiv), and DMF (5.0 mL) to the anode. Connect steel electrode leads to a low-current power supply. With fan cooling, electrolyze at 0.8 mA, excluding light, for 16h (1.1 F/mol).

Crude cathode and anode solution extracted from NaHCO₃ (50 mL) with EtOAc (3 \times 25 mL). Organic layer washed with brine (50 mL). Partially concentrate combined organics to 25 mL and

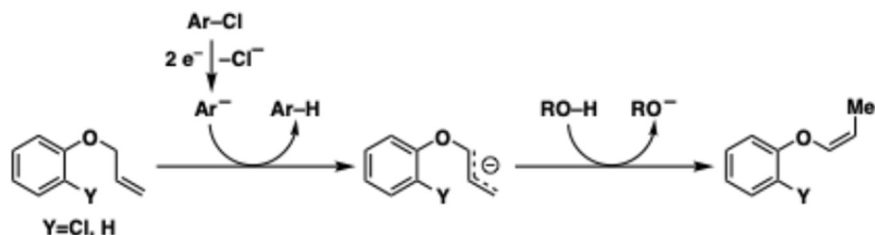
dry over MgSO_4 . Dilute organic layer with hexanes (75 mL) filter through silica plug, rinsing thoroughly with 25% EtOAc in Hexanes. ^1H NMR analysis shows a 1.4:1 mixture of chlorinated (D) and dehalogenated (C) olefin isomer products.

Radical Clock — Direct Electrolysis

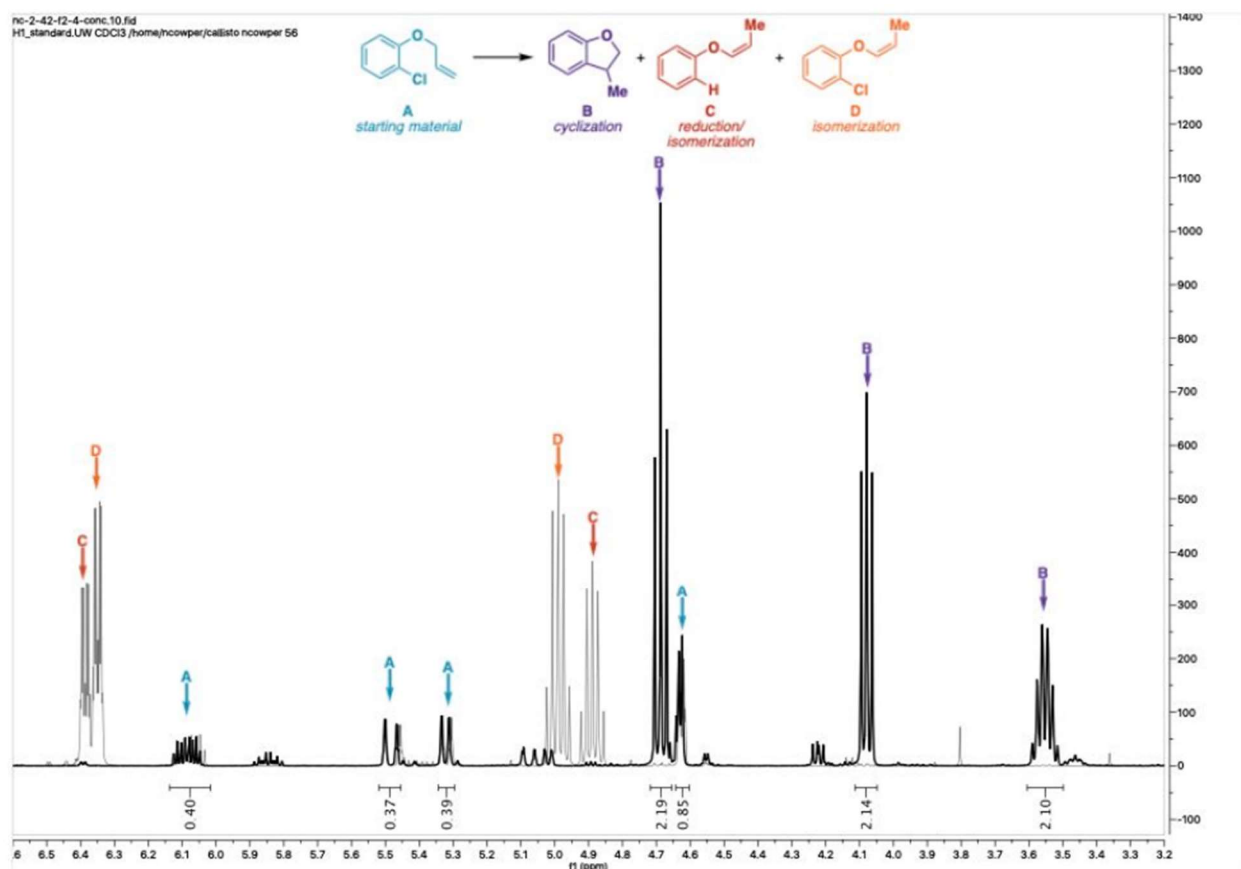


No cyclized product is observed under direct electrolysis, consistent with the rapid reduction of the putative aryl radical at the electrode surface. Isomerization of allyl 2-chlorophenyl ether during reductive electrolysis is consistent with a previous report by Kimura et al. (J. Org. Chem., 1990, 55, 3897), proposed to proceed by aryl anion-mediated deprotonation at the allylic site.

Proposed Mechanism of Olefin Isomerization under Direct Reductive Electrolysis



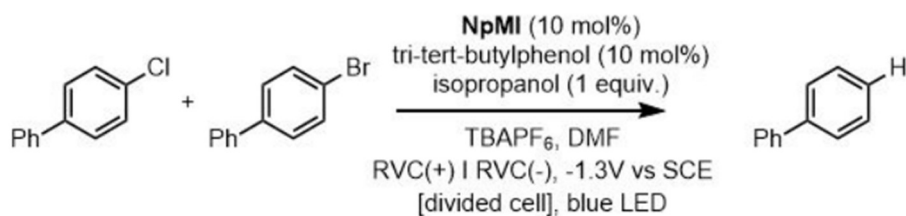
Radical Clock —Electron-Primed Photocatalysis vs Direct Electrolysis



Overlay of the reactions profiles highlights the distinct selectivity between reductive electron-primed photoredox catalysis and direct electrolysis.

Competition Experiments

Starting and ending mmol quantities for each reaction component were ascertained by GC relative to internal mesitylene standard. Each sample was analyzed by GC in triplicate to minimize instrumental error. Both conversion of each substrate and overall yield of biphenyl was determined to ensure



run	Starting chlorobiphenyl (mmol)	Starting bromobiphenyl (mmol)	Ending bromobiphenyl (mmol)	Ending chlorobiphenyl (mmol)	Relative rate
1	0.05	0.05	0.03343	0.04769	8.6
2	0.05	0.05	0.03286	0.04736	7.7
3	0.05	0.05	0.03339	0.04754	8.0

These data provide an average k_{rel} of 8.

Direct electrolysis was conducted using two procedures:

Procedure 1: Omit catalyst and light from General Procedure A and apply a constant current of 0.20 mA for 3 hours (0.23 F/mol).

run	Starting chlorobiphenyl (mmol)	Starting bromobiphenyl (mmol)	Ending bromobiphenyl (mmol)	Ending chlorobiphenyl (mmol)	Relative rate
1	0.05	0.05	0.03818	0.03890	1.07
2	0.05	0.05	0.03902	0.03971	1.07
3	0.05	0.05	0.03750	0.03828	1.06

These data provide an average k_{rel} of 1.

Procedure 2: Procedure followed from a recent dehalogenation report in the literature. Electrolysis at 5 mA stopped after 8 minutes (0.25 F/mol) (Chem. Eur. J., 2019, 25, 6911).

run	Starting chlorobiphenyl (mmol)	Starting bromobiphenyl (mmol)	Ending bromobiphenyl (mmol)	Ending chlorobiphenyl (mmol)	Relative rate
1	0.05	0.05	0.03375	0.04056	1.9
2	0.05	0.05	0.03388	0.04002	1.7
3	0.05	0.05	0.03366	0.04030	1.8

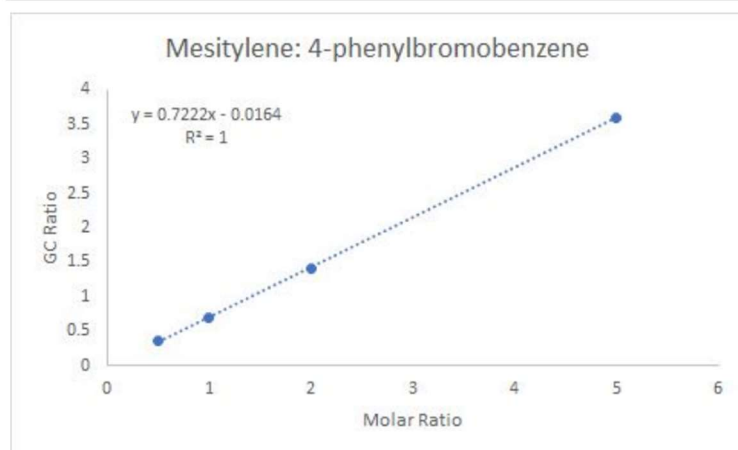
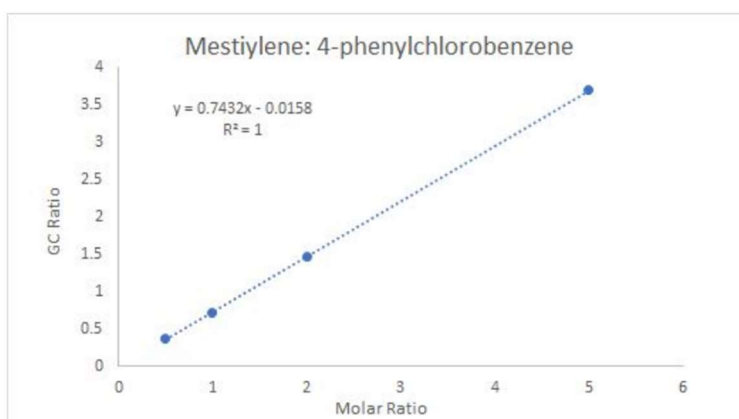
These data provide an average k_{rel} of 2.

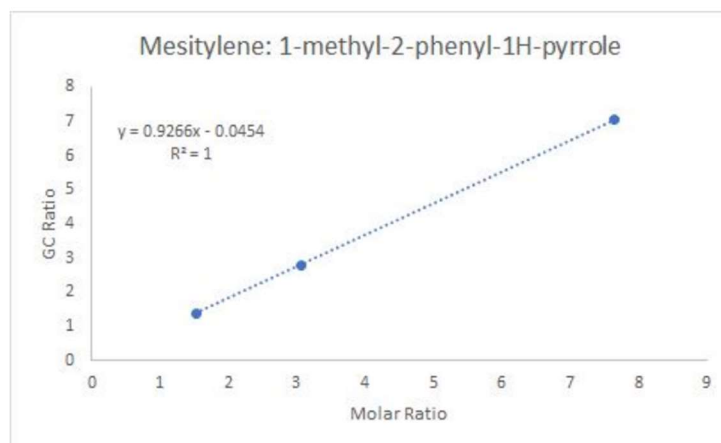
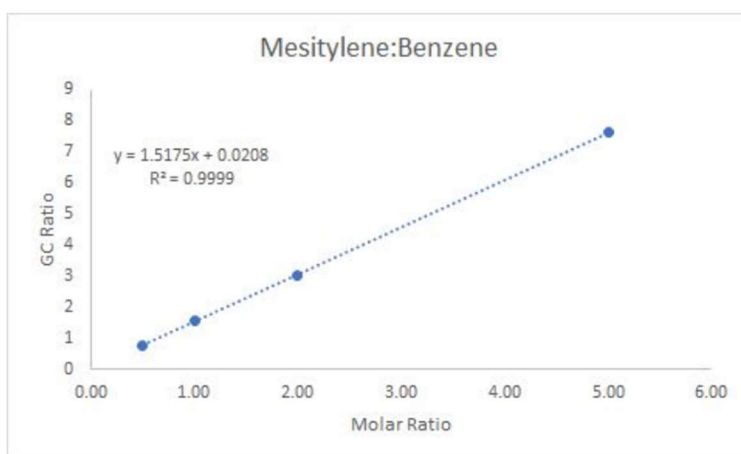
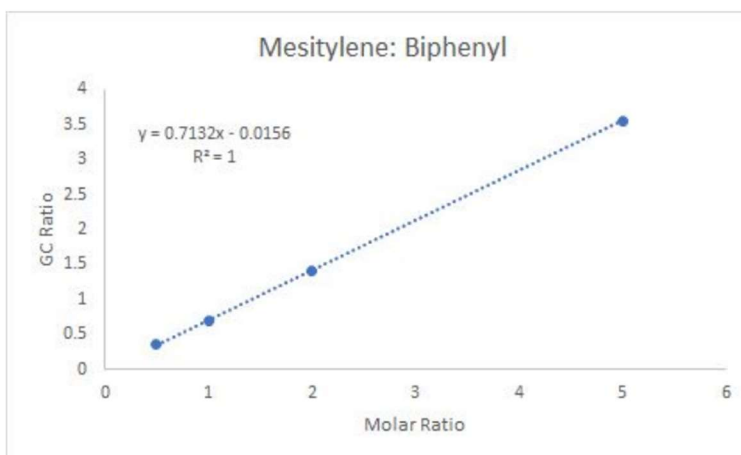
Procedure 3: Photoredox procedure followed from a recent literature report. (J. Org. Chem. 2016, 81, 7155).

run	Starting chlorobiphenyl (mmol)	Starting bromobiphenyl (mmol)	Ending bromobiphenyl (mmol)	Ending chlorobiphenyl (mmol)	Relative rate
1	0.05	0.05	0.04149	0.04941	15.8
2	0.05	0.05	0.04184	0.04942	15.3
3	0.05	0.05	0.04192	0.04940	14.6

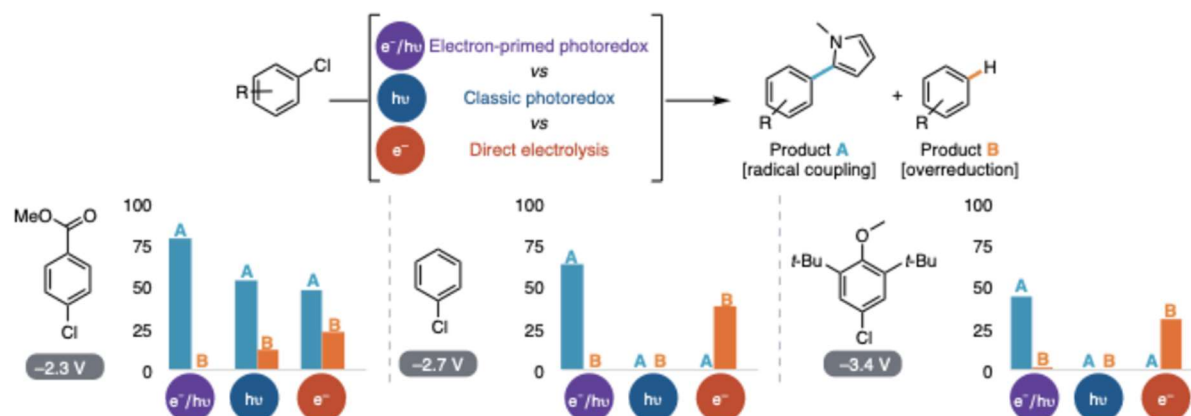
These data provide an average k_{rel} of 15.

GC Calibration Curves



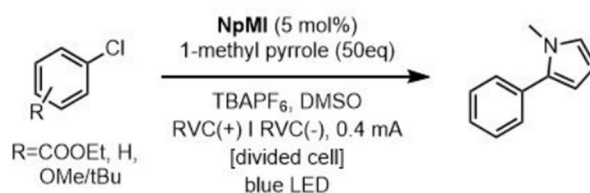


2.7.8 Comparison of Methods for Reductive Activation



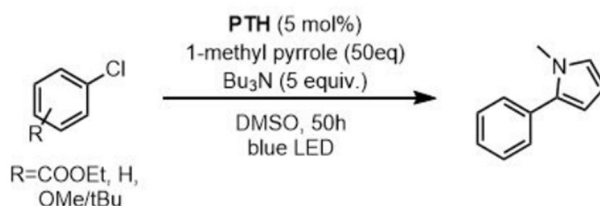
^aYields of coupling and dehalogenation measured relative to an internal standard. Electron-primed photoredox conditions from as Table 3. Photoredox conditions followed pyrrole coupling procedures from the literature employing PTH as a photocatalyst. Several direct electrolysis conditions were attempted. Reported conditions provided highest yield of A and were standard reaction conditions from Table 3 without catalyst. For further details see SI.

Electron-primed photoredox results obtained from General Procedure C. Reaction results were determined by NMR relative to an internal mesitylene standard for 4-chloro-methylbenzoate and 3,5-ditertbutyl-4-chloroanisole. Reaction products of chlorobenzene were analyzed by GC relative to an internal mesitylene standard.

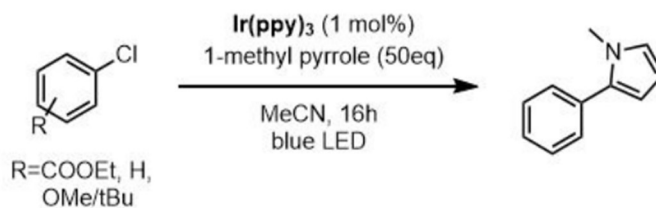


Classic photoredox results were obtained using two procedures:

Procedure 1: The reaction was conducted following a procedure from a recent literature report for coupling aryl radicals employing a 10-phenylphenothiazine photocatalyst (*J. Org. Chem.* 2016, 81, 7155–7160) and an Ir(ppy)₃ photocatalyst (*Chem. Lett.* 2013, 42, 1203–1205).

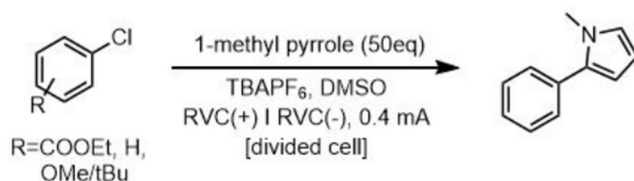


Procedure 2: The reaction was conducted following a procedure from a recent literature report for coupling aryl radicals employing an Ir(ppy)₃ photocatalyst (*Chem. Lett.* 2013, 42, 1203–1205).

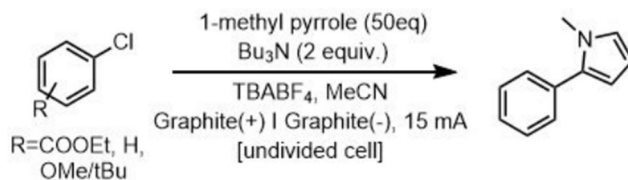


Direct electrolysis results were obtained using two procedures:

Procedure 1: The reaction was conducted following General Procedure C except catalyst and light were omitted.



Procedure 2: The reaction was conducted following a procedure from a recent literature report for generation of aryl radicals (*Chem. Eur. J.* **2019**, 25, 6911 – 6914).



Yields under the above described conditions are described below:

Electron-Primed Photoredox

<i>Substrate</i>	<i>% pdt</i>	<i>% Dehalogenation</i>	<i>% RSM</i>
Cl methyl benzoate	79	0	4
Chlorobenzene	63	0	6
Cl Superanisole	44	<2	45

Direct electrolysis-procedure 1

<i>Substrate</i>	<i>% pdt</i>	<i>% Dehalogenation</i>	<i>% RSM</i>
Cl methyl benzoate	48	23	0
Chlorobenzene	0	38	47
Cl Superanisole	0	30	45

Direct electrolysis-procedure 2

<i>Substrate</i>	<i>% pdt</i>	<i>% Dehalogenation</i>	<i>% RSM</i>
Cl methyl benzoate	0	13	1
Chlorobenzene	0	39	13
Cl Superanisole	0	75	20

Photoredox-procedure 1

<i>Substrate</i>	<i>% pdt</i>	<i>% Dehalogenation</i>	<i>% RSM</i>
Cl methyl benzoate	54	12	0
Chlorobenzene	0	0	100
Cl Superanisole	0	0	91

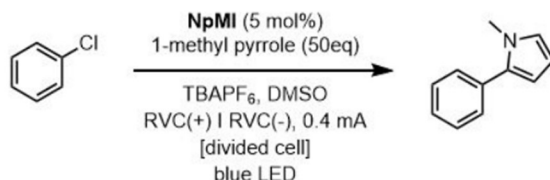
Photoredox-procedure 2

<i>Substrate</i>	<i>% pdt</i>	<i>% Dehalogenation</i>	<i>% RSM</i>
Cl methyl benzoate	0	0	97
Chlorobenzene	0	0	100
Cl Superanisole	0	0	100

2.7.9 Constant Current Control Experiments

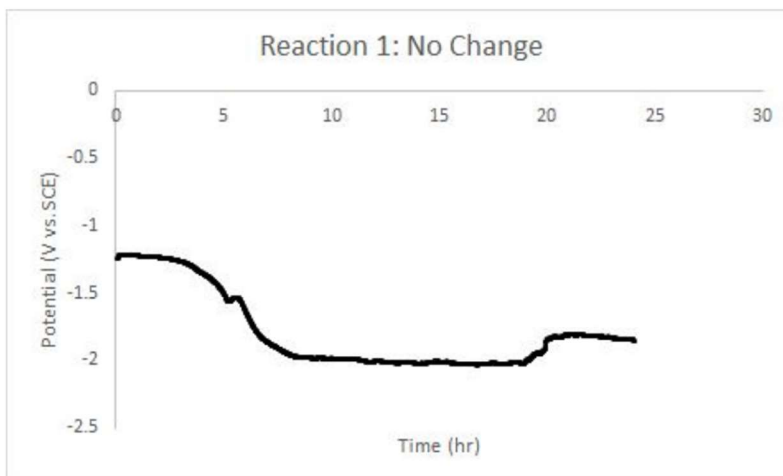
Over the course of our experimentation, we found that to maintain a constant current part way through an experiment, the voltage of the working electrode become more reducing. We suspect that this is due to catalyst decomposition but further investigation is necessary.

Although our data are inconsistent with direct electrolysis, we conducted a series of experiments to demonstrate that the reaction still requires both electrolysis and blue light irradiation and that product is formed before the working potential decreases.

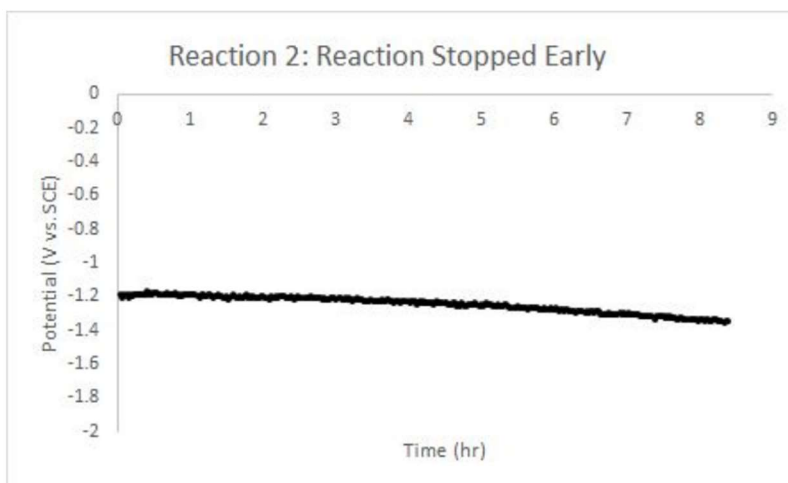


Reaction 1 (no changes):

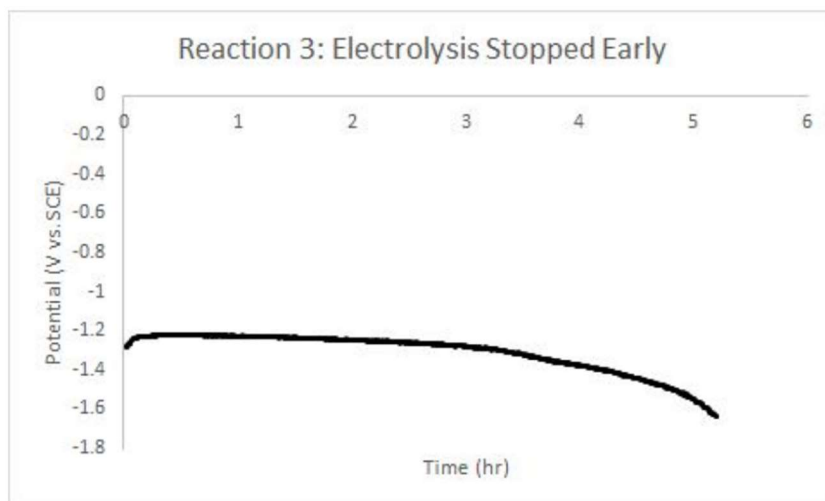
General Procedure C was followed except a WavenowXV Potentiostat was employed. No other changes. This delivered 53% yield, 6% proteo-dehalogenation and recovered 27% starting material (determined by GC relative to mesitylene internal standard).

*Reaction 2 (reaction stopped early):*

General Procedure C was followed except a WavenowXV Potentiostat was employed and the reaction was stopped upon a lowering of the potential (more reducing) after 8.4 hours. This delivered 16% yield, 4% proteo-dehalogenation and recovered 73% starting material (determined by GC relative to mesitylene internal standard).

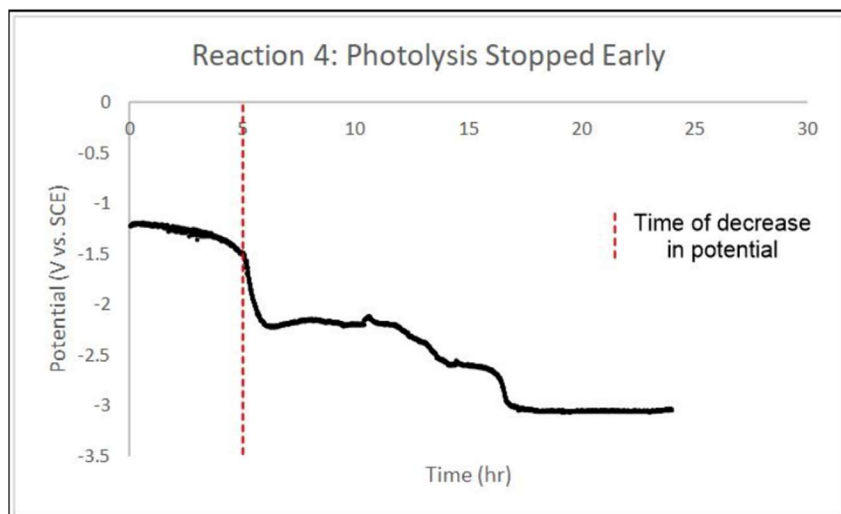
*Reaction 3 (electrolysis stopped early):*

General Procedure C was followed except a WavenowXV Potentiostat was employed and the electrolysis was stopped upon a lowering of the potential (more reducing) after 5.19 hours but the reaction was stirred for the full time under visible light irradiation. This delivered 10% yield, 2% proteo-dehalogenation, and recovered 70% starting material (determined by GC relative to mesitylene internal standard).

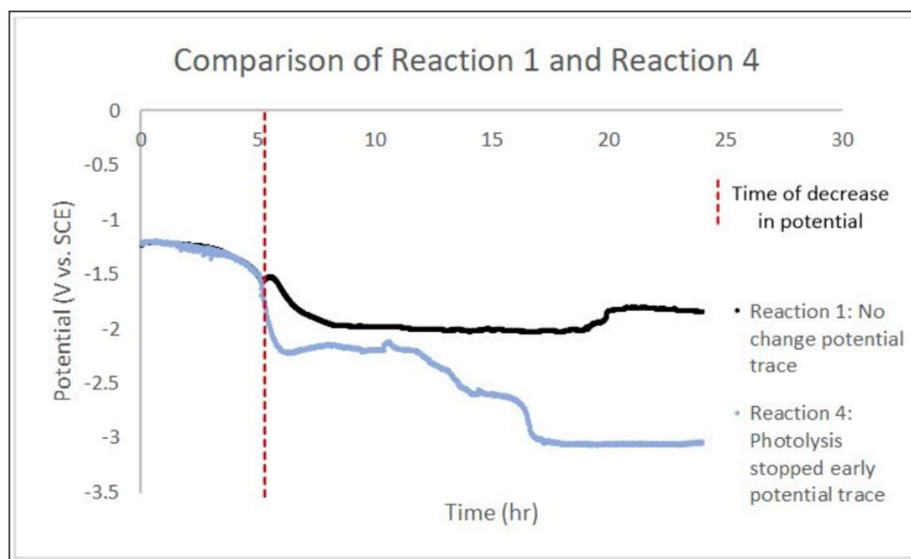


Reaction 4 (photolysis stopped early):

General Procedure C was followed except a WavenowXV Potentiostat was employed and blue light irradiation was stopped upon a lowering of the potential (more reducing) after 5.15 hours but the reaction was stirred for the full time under constant current electrolysis. This delivered 5% yield, 12% proteo-dehalogenation and recovered 30% starting material (determined by GC relative to mesitylene internal standard).



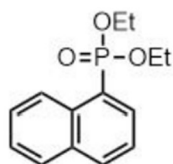
A direct comparison of reaction 1 and reaction 4 show that upon stopping photolysis and entering into a direct electrolysis regime, the working potential becomes increasingly reducing conditions to maintain a constant current.



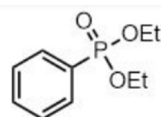
The product yields of reaction 4 compared to reaction 1 indicate that the catalytic system, despite lowering of the applied potential, does not behave only as an electrochemical mediator and that light is still necessary for productive chemistry.

All four of these experiments taken together show that product can be formed under the initial, low potential regime and that both light and electrochemistry are required to maintain productive chemistry.

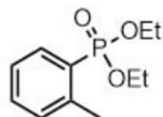
2.7.10 Product Isolation and Characterization



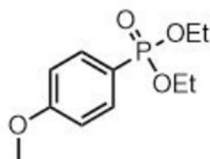
Diethyl (naphthalen-1-yl)phosphonate (2): 99.5 mg obtained following General Procedure B as an intractable mixture with triethylphosphate (8 mol% triethylphosphate). This corresponds to 94.3 mg (89% yield) of product **1** **H NMR** (400MHz, CDCl₃) δ 8.54 (d, J = 8.5 Hz, 1H), 8.27 (dd, J = 16.3, 7.1 Hz, 1H), 8.1 (d, J = 8.4 Hz, 1H), 7.91 (d, J = 8.1 Hz, 1H), 7.63 (ddd, J = 8.5, 6.8, 1.5 Hz, 1H), 7.57 (m, 2H), 4.22 (m, 2H), 4.10 (m, 2H), 1.33 (t, J = 7.0 Hz, 6H); **¹³C NMR** and **³¹P NMR** consistent with reported spectra (Org. Lett., 2015, 17, 23, 5906-5909).



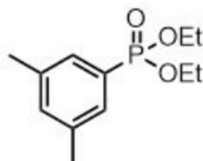
Diethyl phenylphosphonate (3): 73.5 mg obtained following General Procedure B as an intractable mixture with triethylphosphate (16 mol% triethylphosphate). This corresponds to 64.7 mg (76% yield) of product **1** **H NMR** (400MHz, CDCl₃) δ 7.74 (dd, J = 13.3, 6.9 Hz, 2H), 7.48 (t, J = 7.3 Hz, 1H), 7.39 (td, J = 7.6, 4.2 Hz, 2H), 4.05 (m, 4H), 1.25 (t, J = 7.1 Hz, 6H); **¹³C NMR** and **³¹P NMR** consistent with reported spectra (Org. Lett., 2013, 15, 20, 5362-5365).



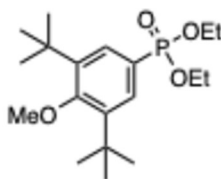
Diethyl (2-methylphenyl)phosphonate (4): 73.2 mg obtained following General Procedure B as an intractable mixture with triethylphosphate (12 mol% triethylphosphate). This corresponds to 66.6 mg (73% yield) of product **1** **H NMR** (400MHz, CDCl₃) δ 7.89 (dd, J = 14.4, 8.0 Hz, 1H), 7.40 (t, J = 7.4 Hz, 1H), 7.23 (m, 2H), 4.09 (m, 4H), 2.56 (s, 3H), 1.31 (t, J = 7.1 Hz, 6H); **13 C NMR** and **31 P NMR** consistent with reported spectra (Chem. Comm., **2017**, 53, 5, 956-958).



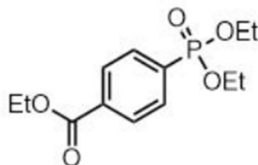
Diethyl 4-methoxyphenylphosphonate (5): 69.0 mg (71% yield) obtained as a brown oil following General Procedure B. **1 H NMR** (400MHz, CDCl₃) δ 7.67 (dd, J = 12.8, 8.7 Hz, 2H), 6.89 (dd, J = 8.6, 3.3 Hz, 2H), 4.01 (m, 4H), 3.77 (s, 3H), 1.24 (t, J = 7.1 Hz, 6H); **13 C NMR** and **31 P NMR** consistent with reported spectra (Org. Lett., **2018**, 20, 14, 4164-4167).



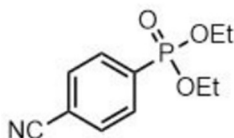
Diethyl (3',5'-dimethyl)phenylphosphonate (6): 63.2 mg (65% yield) obtained following general procedure B. **1 H NMR** (400MHz, CDCl₃) δ 7.34 (d, J = 13.6 Hz, 2H), 7.10 (s, 1H), 4.02 (m, 4H), 2.27 (s, 6H), 1.25 (t, J = 7.1 Hz, 6H); **13 C NMR** and **31 P NMR** consistent with reported spectra (Org. Lett., **2018**, 20, 14, 4164-4167).



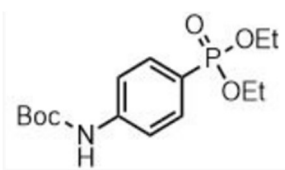
Diethyl (4-methoxy-3,5-di-tert-butylphenyl)phosphonate (7): 73.3 mg (51% yield) obtained as a colorless oil following a modified procedure B with a 0.4 mA constant current. **1 H NMR** (500 MHz, CDCl₃) δ 7.66 (d, J = 14.2 Hz, 2H), 4.20 – 4.03 (m, 4H), 3.70 (s, 3H), 1.43 (s, 18H), 1.33 (t, J = 7.1 Hz, 6H). **13 C NMR** (126 MHz, CDCl₃) δ 163.40 (d, J = 3.9 Hz), 144.38 (d, J = 15.1 Hz), 130.47 (d, J = 11.6 Hz), 122.06 (d, J = 191.4 Hz), 64.53 (d, J = 1.2 Hz), 62.08 (d, J = 5.4 Hz), 36.06, 32.06, 16.52 (d, J = 6.4 Hz). **31 P NMR** (162 MHz, CDCl₃) δ 20.65. HRMS (ESI+) Calc: [M+H]⁺ (C₁₉H₃₄O₄P) 357.2189; measured: 357.2184 = 1.4 ppm difference.



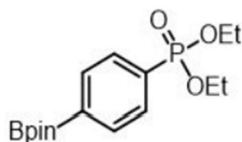
Diethyl (4-ethoxycarbonylphenyl)phosphonate (8): 78.0 mg (68% yield) obtained as a colorless following procedure B. **¹H NMR** (400MHz, CDCl₃) δ 8.06 (dd, J = 8.3, 3.9 Hz, 2H), 7.82 (dd, J = 13.0, 8.3 Hz, 2H), 4.34 (q, J = 7.1 Hz, 2H), 4.06 (m, 4H), 1.34 (t, J = 7.1 Hz, 3H), 1.26 (t, J = 7.0 Hz, 6H); **¹³C NMR** and **³¹P NMR** consistent with reported spectra (Org. Lett. 2019, 21, 17, 6835-6838).



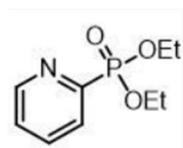
Diethyl (4-cyanophenyl)phosphonate (9): 55.1 (58% yield) obtained as a yellow oil following procedure B. **¹H NMR** (400MHz, CDCl₃) δ 7.85 (dd, J = 13.1, 8.4 Hz, 2H), 7.69 (dd, J = 8.5, 3.6 Hz, 2H), 4.08 (m, 4H), 1.77 (t, J = 7.0 Hz, 6H); **¹³C NMR** and **³¹P NMR** consistent with reported spectra (Angew. Chem., 2017, 129, 12892 - 12896).



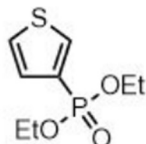
Tert-butyl (4-(diethoxyphosphoryl)phenyl)carbamate (10): 74.7 mg (57% yield) obtained as an off white solid following procedure B. **¹H NMR** (500MHz, CDCl₃) δ 7.75 (dd, J = 12.8, 8.6 Hz, 2H), 7.49 (dd, J = 8.5, 3.5 Hz, 2H), 6.67 (s, 1H), 4.10 (m, 4H), 1.55 (s, 9H), 1.33 (t, J = 7.1 Hz, 6H); **¹³C NMR** (500MHz, CDCl₃) δ 152.2, 142.3, 133.1 (d, J = 10.8 Hz), 122.0 (d, J = 193.2 Hz), 117.7 (d, J = 15.4 Hz), 81.3, 62.0, 28.3, 16.3 (d, J = 6.6 Hz); **³¹P NMR** (400MHz, CDCl₃) δ 19.11 ppm; HRMS (ESI+) Calc: [M+H]⁺ (C₁₅H₂₅NO₅P) 330.1465; measured: 330.1460 = 1.5 ppm difference.



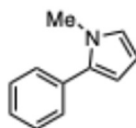
Diethyl [4-(4,4,5,5-tetramethyl-1,3,2-dioxaborolan-2-yl)phenyl]phosphonate (11): 70.1 mg (52% yield) obtained as a colorless crystalline solid following procedure B. **¹H NMR** (400MHz, CDCl₃) δ 7.89 (dd, J = 7.9, 4.5 Hz, 2H), 7.70 (dd, J = 13.2, 8.1 Hz, 2H), 4.09 (m, 4H), 1.35 (s, 12H), 1.30 (t, J = 7.0 Hz, 6H); **¹³C NMR** and **³¹P NMR** consistent with reported spectra (J. Am. Chem. Soc. 2017, 139, 23, 7745 - 7748).



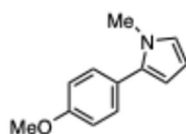
Diethyl 2-pyridylphosphonate (12): 53.2 mg (62% yield) obtained as a yellow oil following procedure B. **¹H NMR** (400MHz, CDCl₃) δ 8.82 (d, J = 4.0 Hz, 1H), 8.00 (t, J = 6.0 Hz, 1H), 7.82 (tdd, J = 7.6, 5.7, 1.7 Hz, 1H), 7.44 (dddd, J = 7.8, 4.8, 2.3, 1.3 Hz, 1H), 4.25 (m, 4H), 1.37 (t, J = 7.0 Hz, 6H); **¹³C NMR** and **³¹P NMR** consistent with reported spectra (Org. Lett. 2019, 21, 5, 1301-1305).



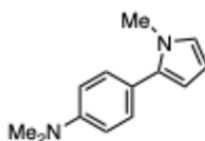
Diethyl (thiophen-3-yl)phosphonate (13): 50.0 mg (57% yield) obtained as a pale yellow oil following procedure B. **¹H NMR** (400MHz, CDCl₃) δ 7.96 (ddd, J = 8.2, 2.9, 1.1 Hz, 1H), 7.40 (dt, J = 5.1, 3.1 Hz, 1H), 7.31 (ddd, J = 5.0, 4.0, 1.1 Hz, 1H), 4.09 (m, 4H), 1.30 (t, J = 7.0 Hz, 6H); **¹³C NMR** and **³¹P NMR** consistent with reported spectra (Chem. Comm., 2014, 50, 66, 9343-9345).



1-methyl-2-phenyl-1H-pyrrole (14): 33.3 mg (53% yield) obtained following procedure C. **¹H NMR** (500 MHz, CDCl₃) δ 7.42 – 7.37 (m, 4H), 7.32 – 7.28 (m, 1H), 6.72 (dd, J = 2.6, 1.9 Hz, 1H), 6.23 (dd, J = 3.5, 1.8 Hz, 1H), 6.21 (dd, J = 3.6, 2.7 Hz, 1H), 3.67 (s, 3H); consistent with reported spectra (Chem. Eur. J., 2017, 23, 7900).

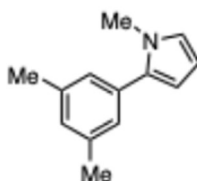


1-methyl-2-(4-methoxyphenyl)-1H-pyrrole (15): 41.8 mg (56% yield) obtained as an off-white solid following procedure C. **¹H NMR** (500 MHz, CDCl₃) δ 7.32 (d, J = 8.8 Hz, 1H), 6.94 (d, J = 8.7 Hz, 2H), 6.69 (dd, J = 2.7, 1.9 Hz, 1H), 6.18 (dd, J = 3.6, 2.7 Hz, 1H), 6.15 (dd, J = 3.5, 1.8 Hz, 1H), 3.84 (s, 3H), 3.63 (s, 3H); consistent with reported spectra (J. Org. Chem., 2019, 84, 16, 9946-9956)

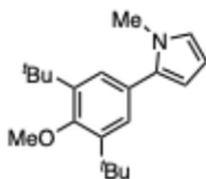


1-methyl-2-(4-dimethylaminophenyl)-1H-pyrrole (16): 32.8 mg (41% yield) obtained as an off-white solid following procedure C. **¹H NMR** (500 MHz, CDCl₃) δ 7.28 (d, J = 8.8 Hz, 2H),

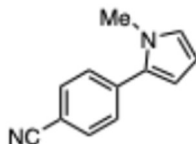
6.76 (d, $J = 8.8$ Hz, 2H), 6.67 (m, 1H), 6.18 (t, $J = 3.1$ Hz, 1H), 6.12 (dd, $J = 3.5, 1.8$ Hz, 1H), 3.63 (s, 3H), 2.98 (s, 6H). consistent with reported spectra (Tetrahedron, 2008, 64, 46, 10605-10618)



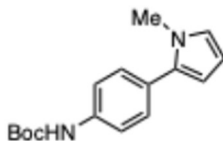
1-methyl-2-(3,5-dimethylphenyl)-1H-pyrrole (17): 35.1 mg (47% yield) obtained following procedure C. **¹H NMR** (500 MHz, CDCl₃) δ 7.05 (d, $J = 1.6$ Hz, 2H), 6.98 (s, 1H), 6.72 (t, $J = 2.2$ Hz, 1H), 6.25 – 6.19 (m, 2H), 3.68 (s, 3H), 2.38 (s, 6H); consistent with reported spectra (J. Org. Chem., 2019, 84, 16, 9946-9956).



1-methyl-2-(4-methoxy-3,5-di-tert-butylphenyl)-1H-pyrrole (18): 55.7 mg (47% yield) obtained following procedure C. **¹H NMR** (500 MHz, CDCl₃) δ 7.26 (s, 2H), 6.70 (t, $J = 2.3$ Hz, 1H), 6.20 (t, $J = 3.1$ Hz, 1H), 6.18 (dd, $J = 3.6, 1.8$ Hz, 1H), 3.73 (s, 3H), 3.65 (s, 3H), 1.46 (s, 18H); **¹³C NMR** (126 MHz, CDCl₃) δ 158.70, 143.53, 135.52, 127.75, 127.41, 123.10, 108.02, 107.69, 64.34, 35.96, 35.13, 32.28; HRMS (ESI⁺) Calc: [M+H]⁺ (C₂₀H₃₀NO) 300.2322; measured: 300.2321 = 0.3 ppm difference.

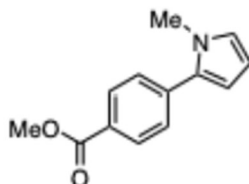


4-(1-methyl-1H-pyrrol-2-yl)benzonitrile (19): 58.9 mg (81% yield) obtained following procedure C. **¹H NMR** (500 MHz, CDCl₃) δ 7.67 (d, $J = 8.4$ Hz, 2H), 7.50 (d, $J = 8.4$ Hz, 2H), 6.83 – 6.73 (m, 1H), 6.35 (dd, $J = 3.7, 1.8$ Hz, 1H), 6.23 (dd, $J = 3.7, 2.6$ Hz, 1H), 3.72 (s, 3H); consistent with reported spectra (Org. Lett. 2016, 18, 3, 544-547).



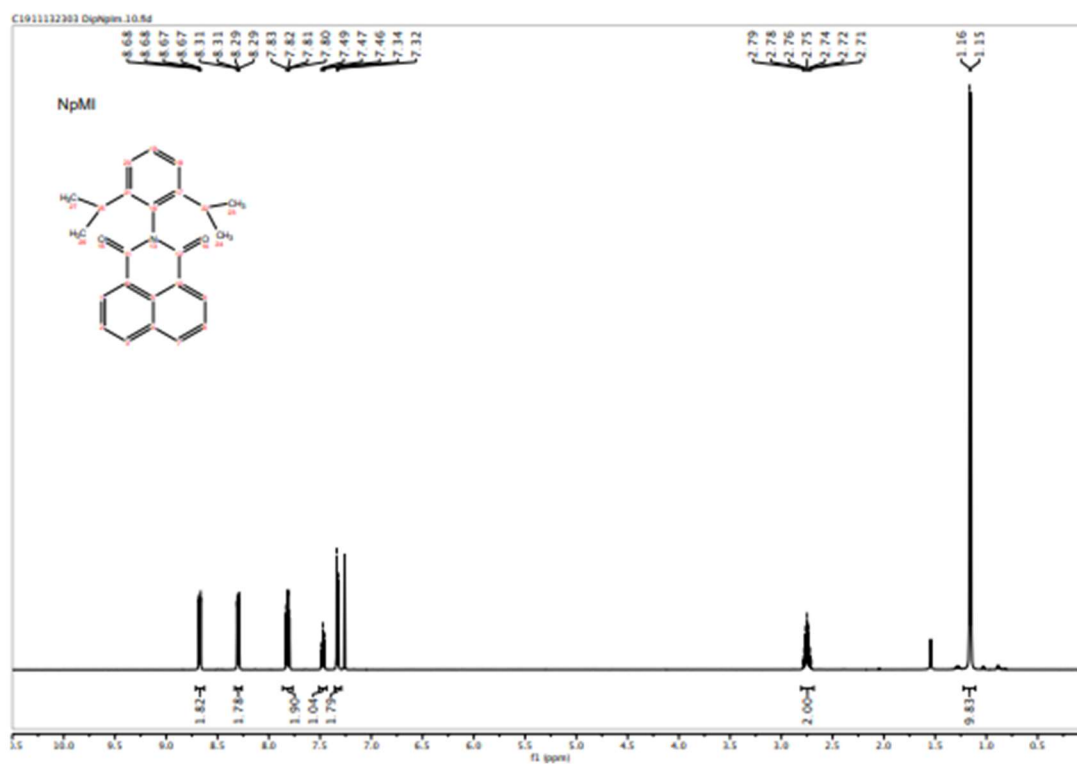
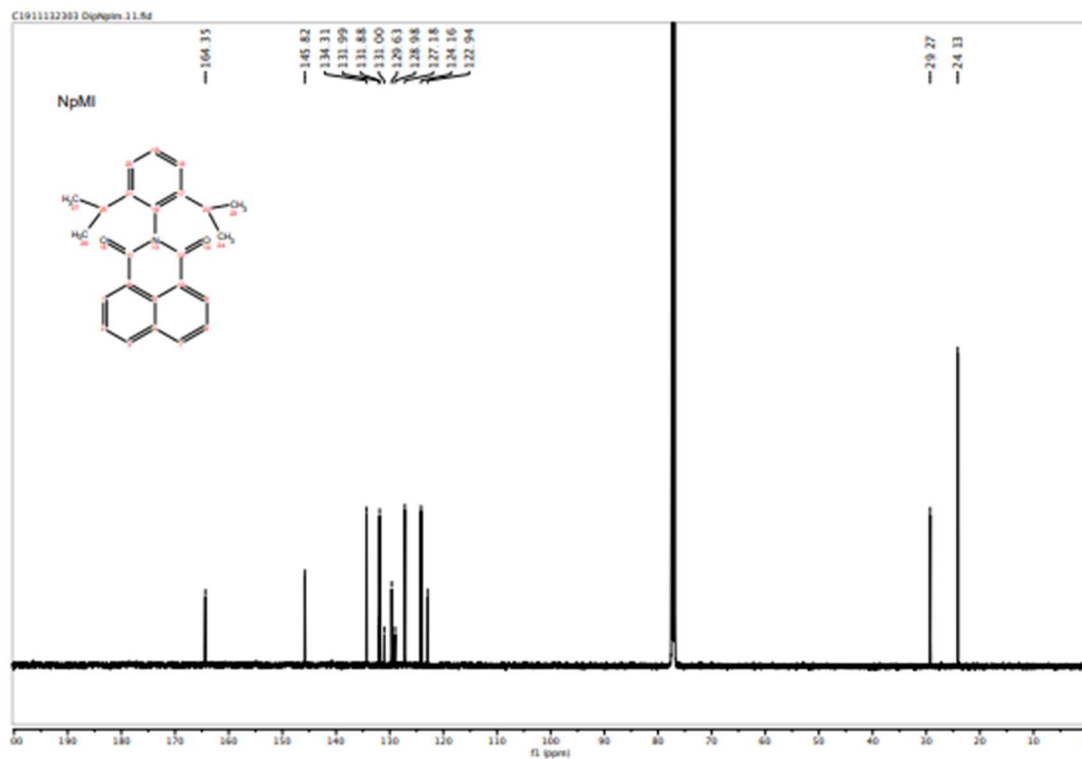
Tert-butyl (4-(1-methyl-1H-pyrrol-2-yl)phenyl)carbamate (20): 71.2 mg (65% yield) obtained following procedure C. **¹H NMR** (500 MHz, CDCl₃) δ 7.39 (d, $J = 8.3$ Hz, 2H), 7.35 – 7.29 (m, 2H), 6.69 (t, $J = 2.3$ Hz, 1H), 6.52 (s, 1H), 6.25 – 6.12 (m, 2H), 3.63 (s, 3H), 1.54 (s, 9H); **¹³C NMR** (126 MHz, CDCl₃) δ 152.89, 137.24, 134.37, 129.46, 128.36, 123.45, 118.63, 108.39,

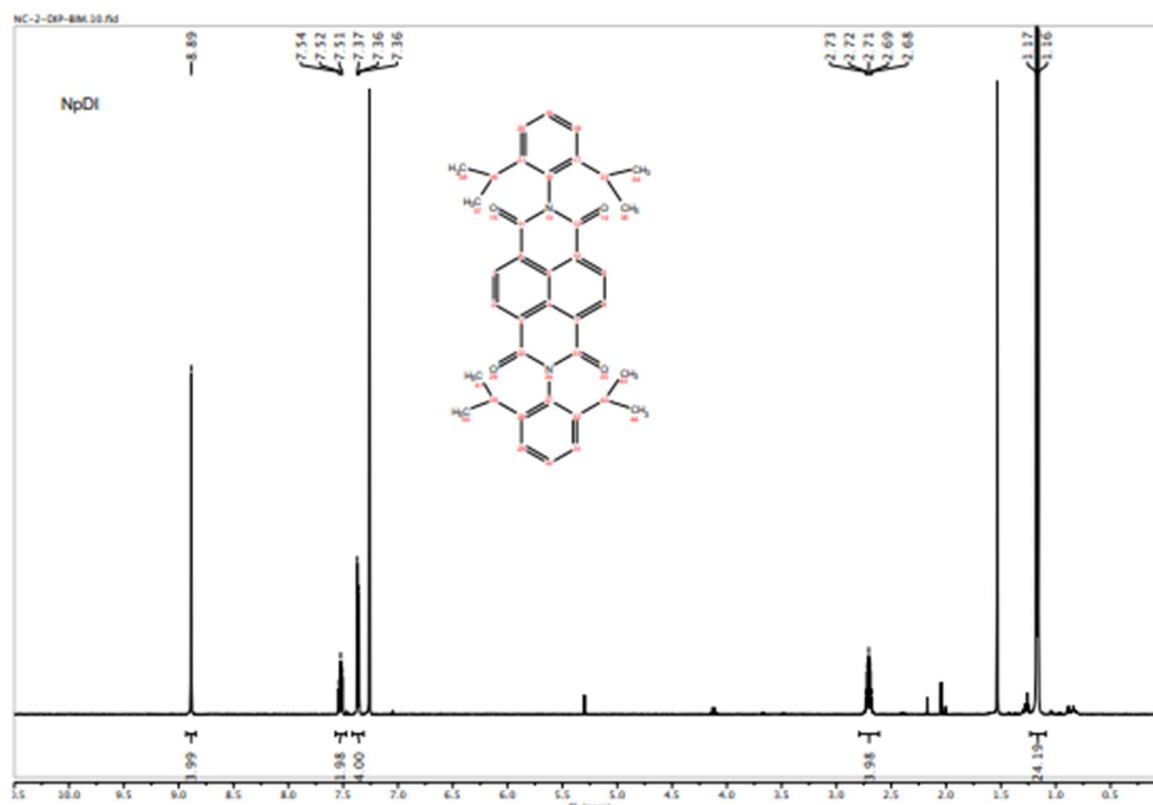
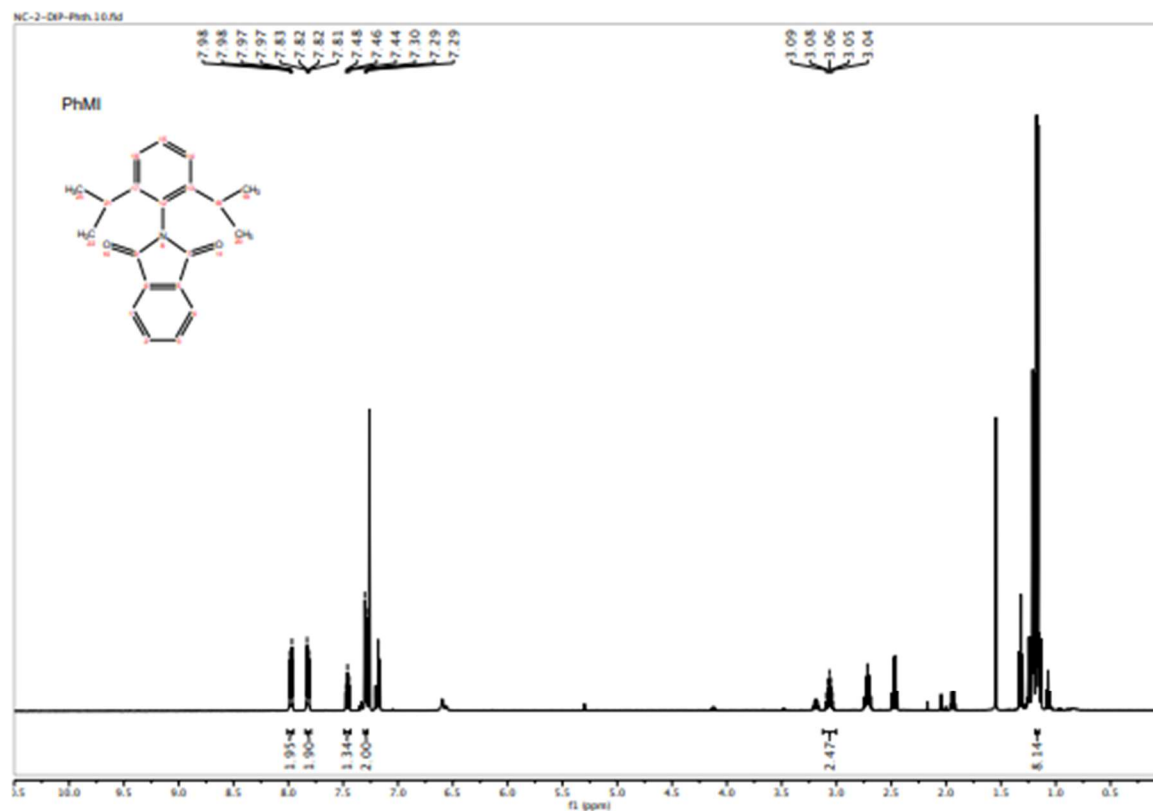
107.80, 80.79, 35.10, 28.49; HRMS (ESI+) Calc: $[M+H]^+$ (C₁₆H₂₁N₂O₂) 273.1598; measured: 273.1593 = 1.8 ppm difference.

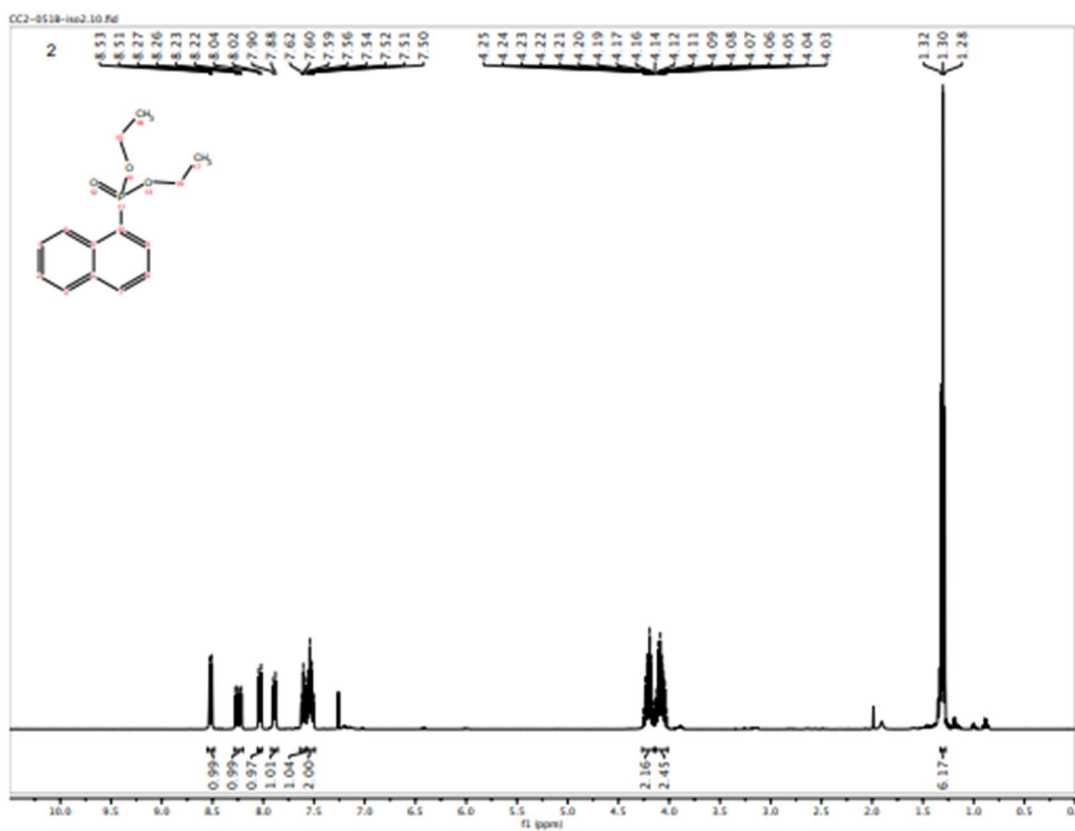
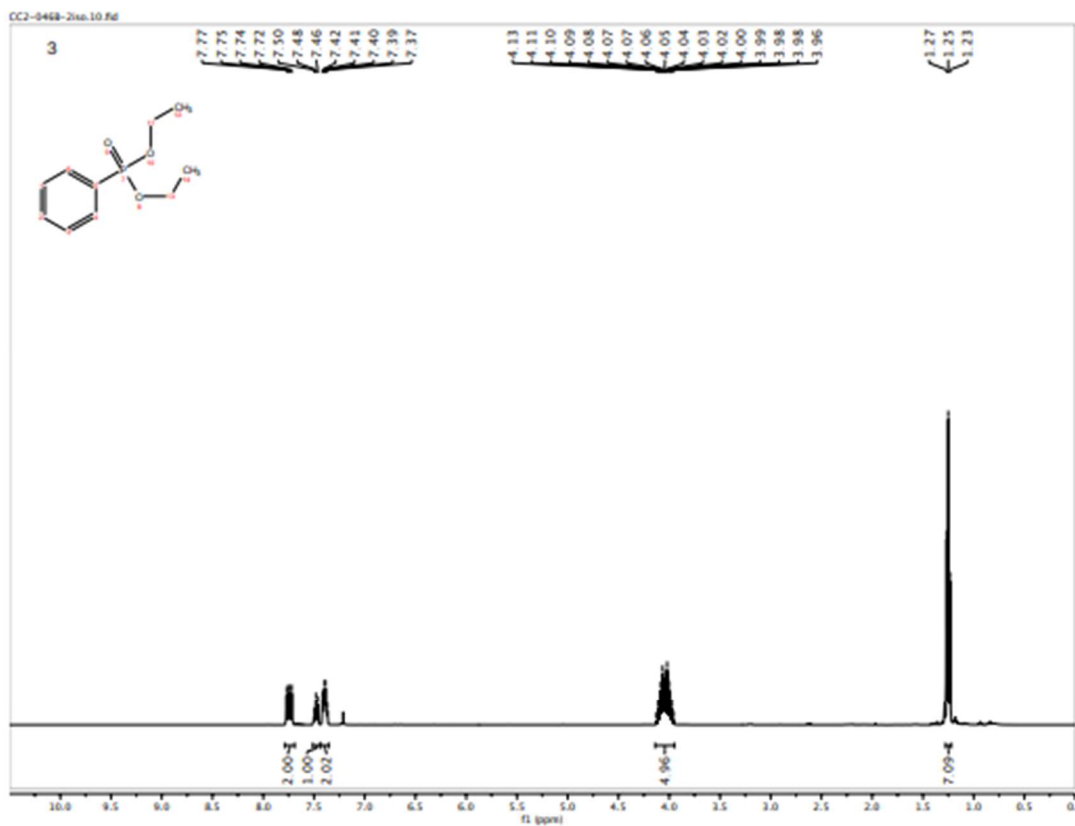


1-methyl-2-(4-(methoxycarbonyl)phenyl)-1H-pyrrole (21): 70.6 mg (82% yield) obtained following procedure C. **¹H NMR** (500 MHz, CDCl₃) δ 8.06 (d, J = 8.4 Hz, 2H), 7.48 (d, J = 8.4 Hz, 2H), 6.76 (dd, J = 2.7, 1.8 Hz, 1H), 6.34 (dd, J = 3.7, 1.8 Hz, 1H), 6.23 (dd, J = 3.6, 2.7 Hz, 1H), 3.94 (s, 3H), 3.72 (s, 3H); consistent with reported spectra (Synlett, 2013, 24(4), 507-513).

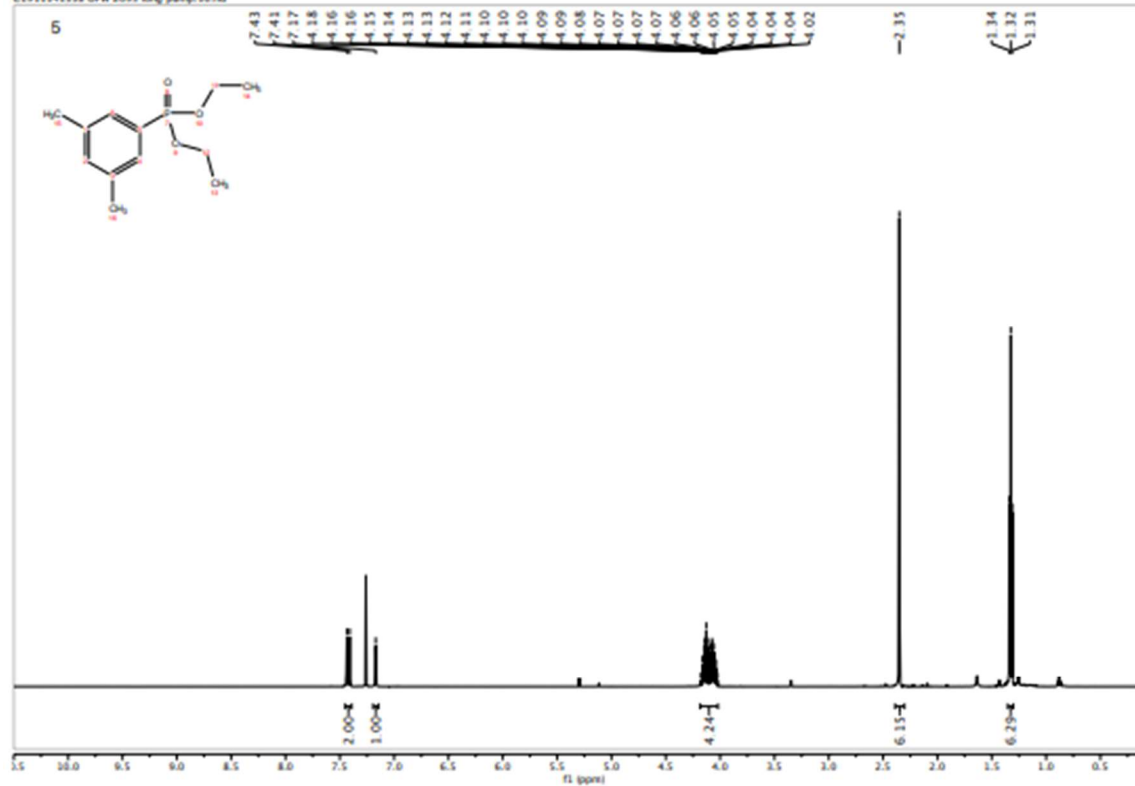
2.7.11 NMR Spectra



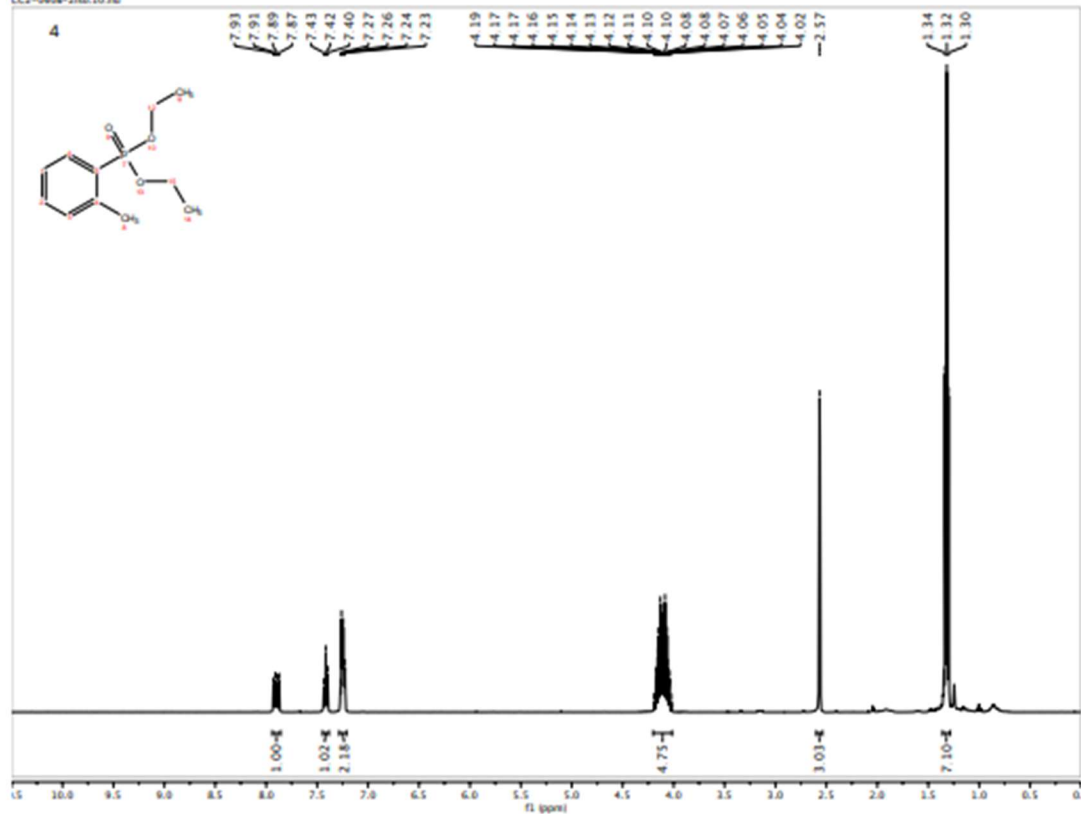




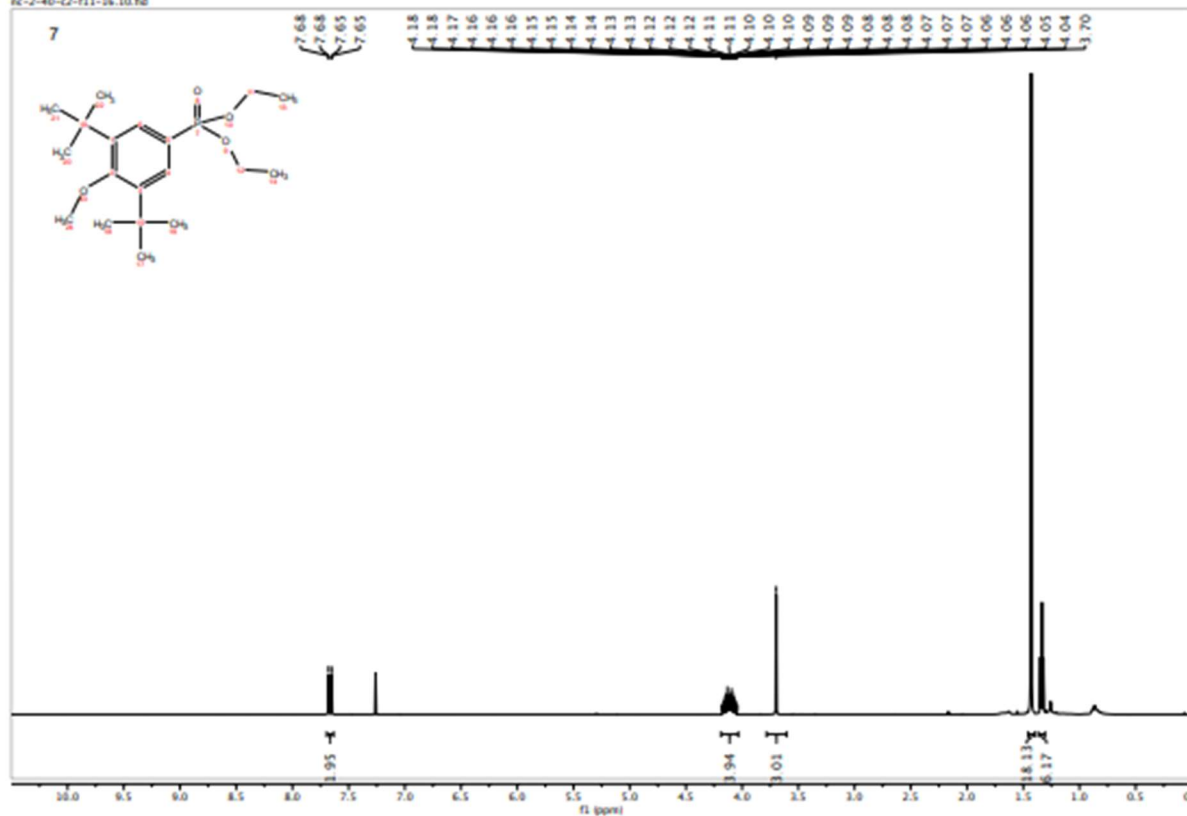
C1911141258 OPW 2095 long pump.10.fid



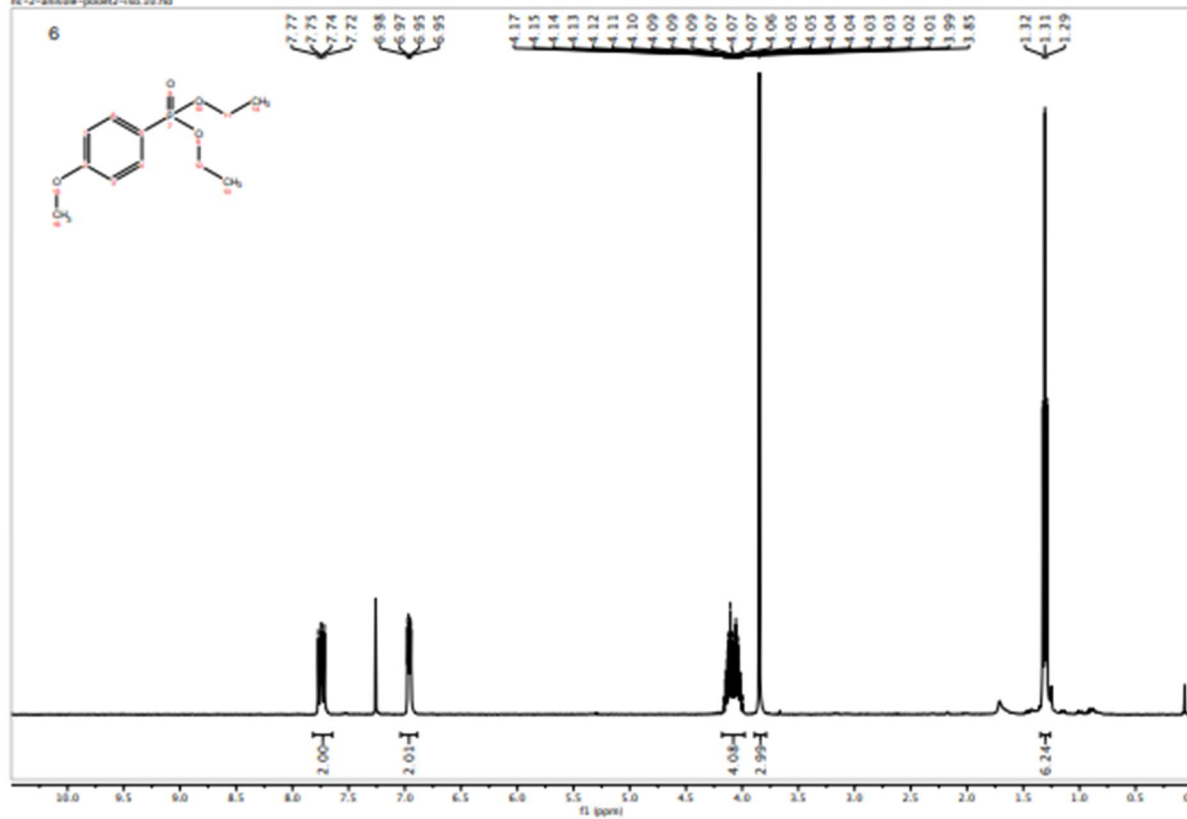
CC2-0608-21ex.10.fid



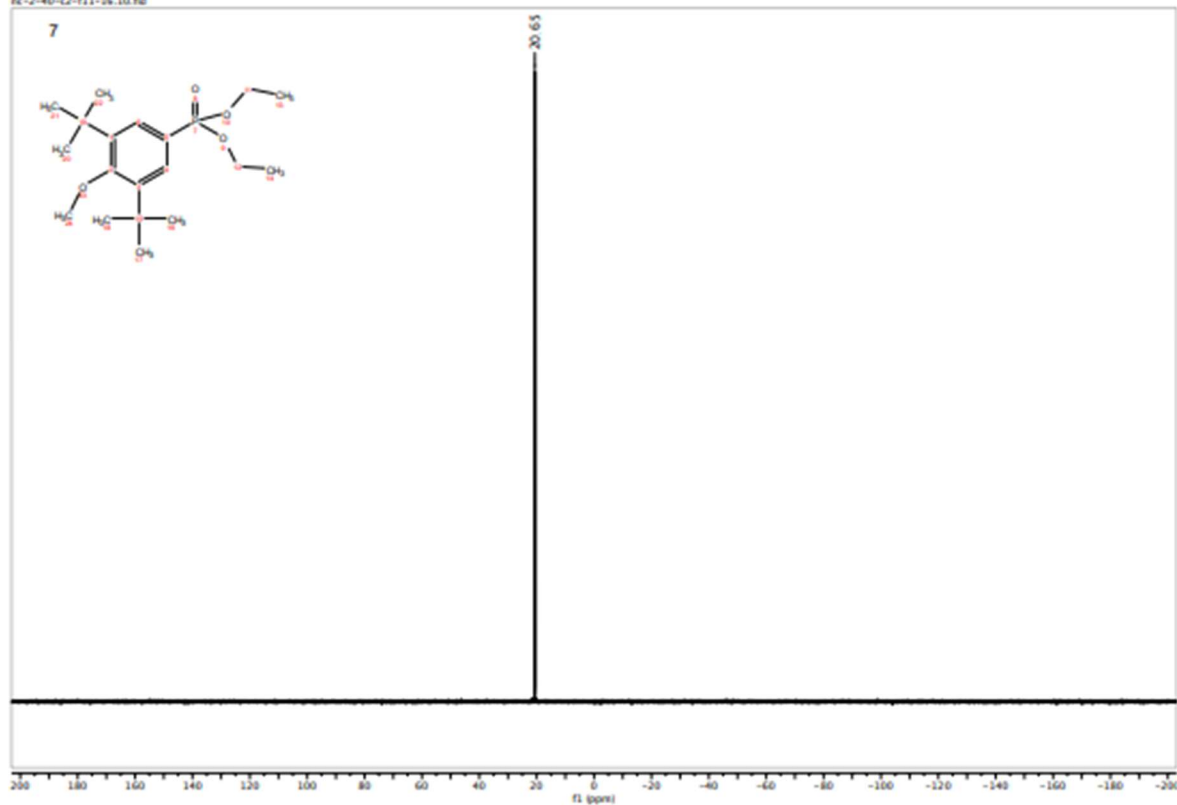
pc-2-40-c2-f11-16.10.fid



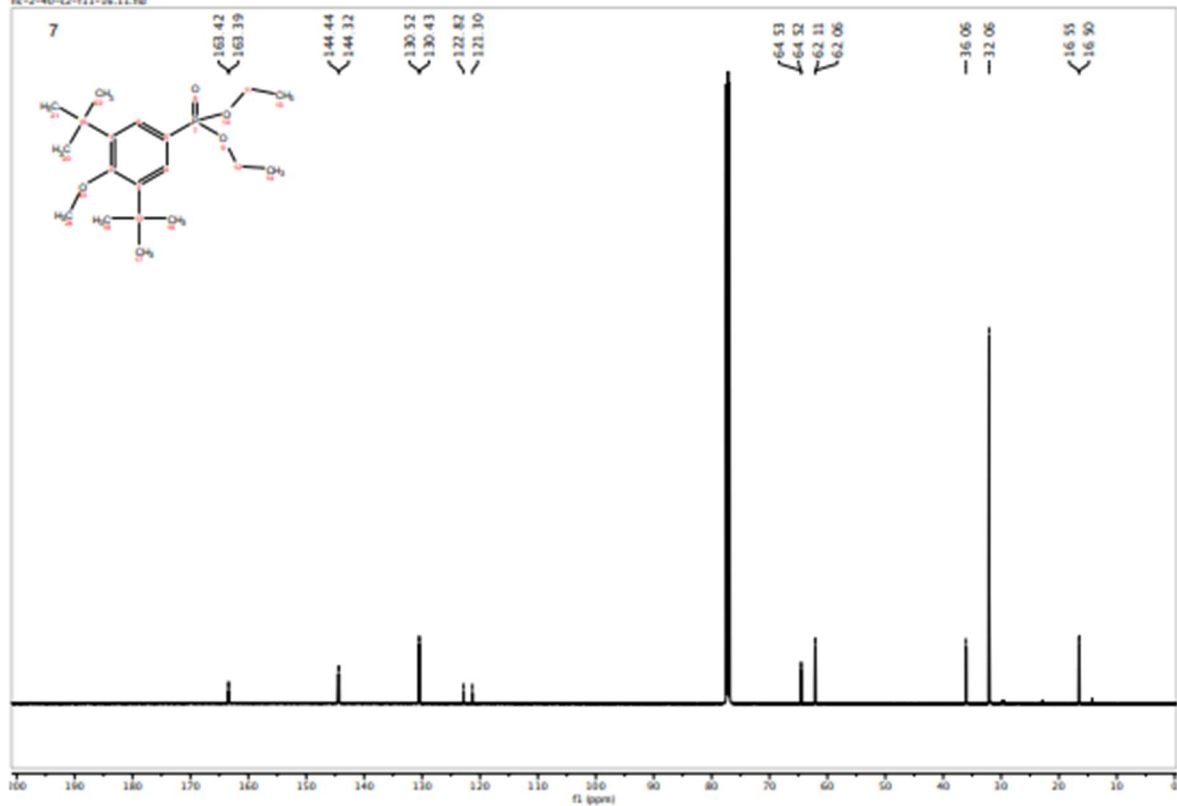
pc-2-antile-poor2-10.10.fid

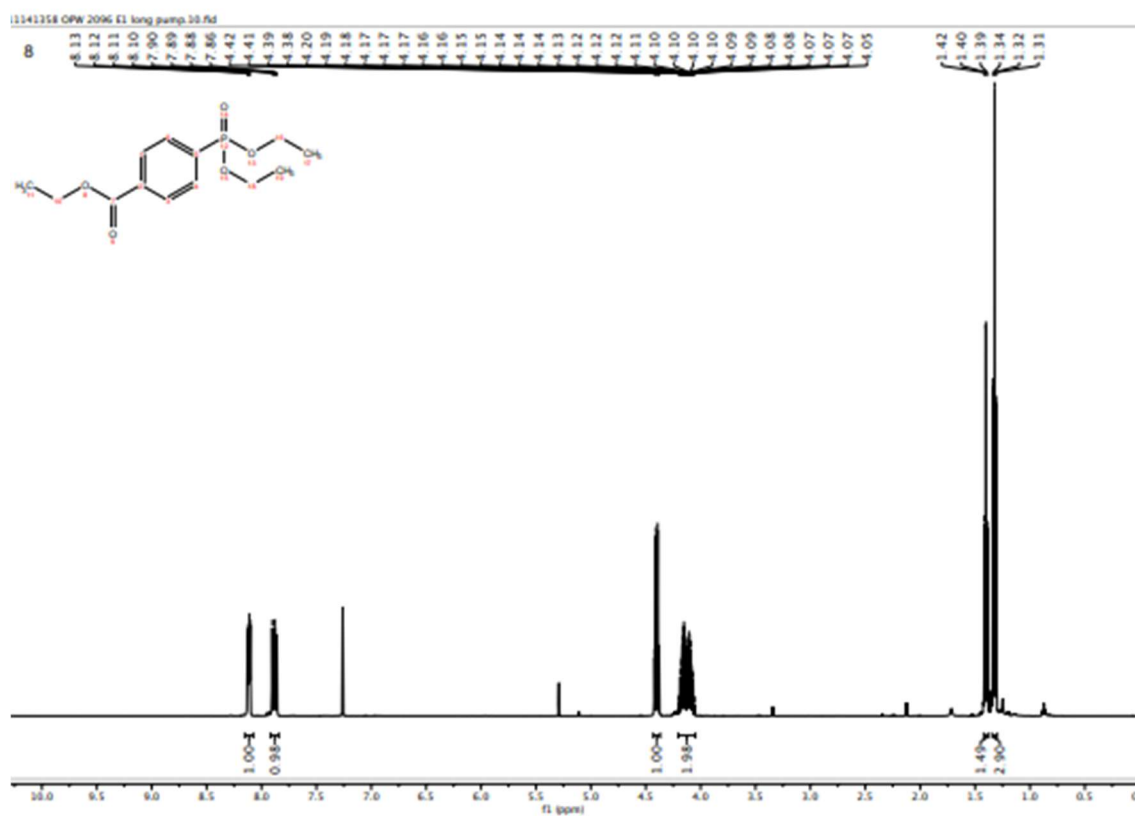
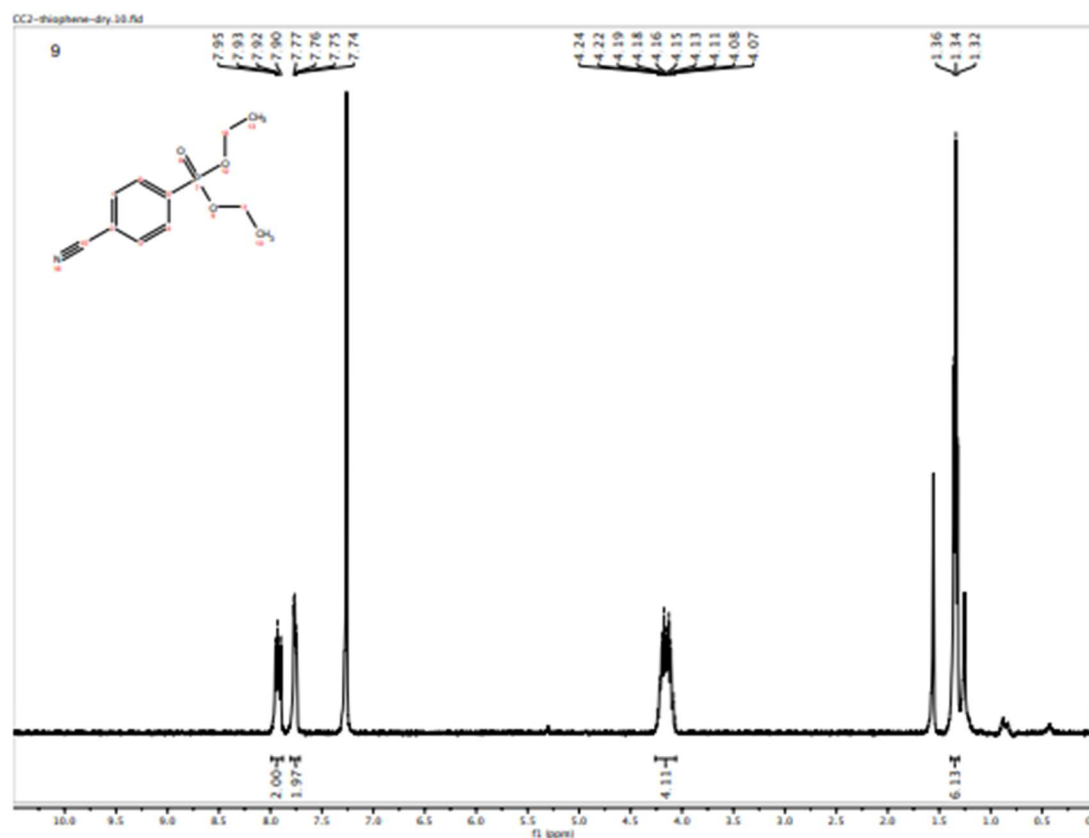


nc-2-40-c2-f11-16.10.fid

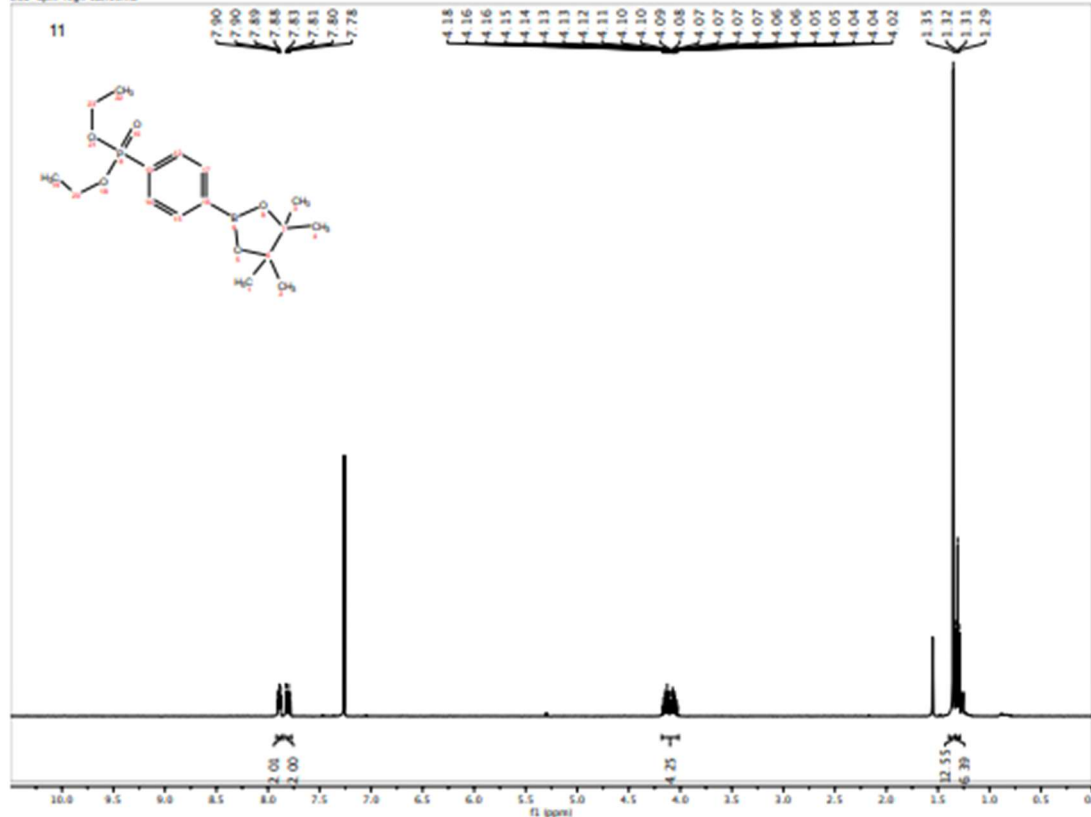


nc-2-40-c2-f11-16.11.fid

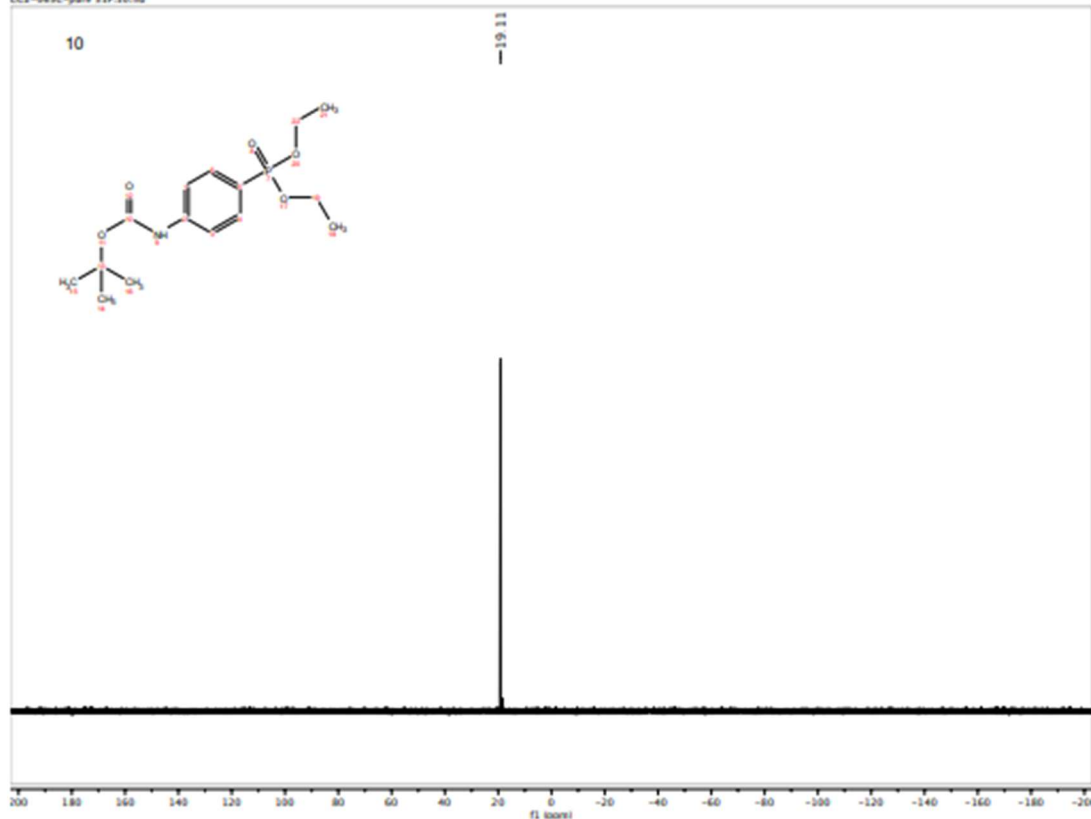




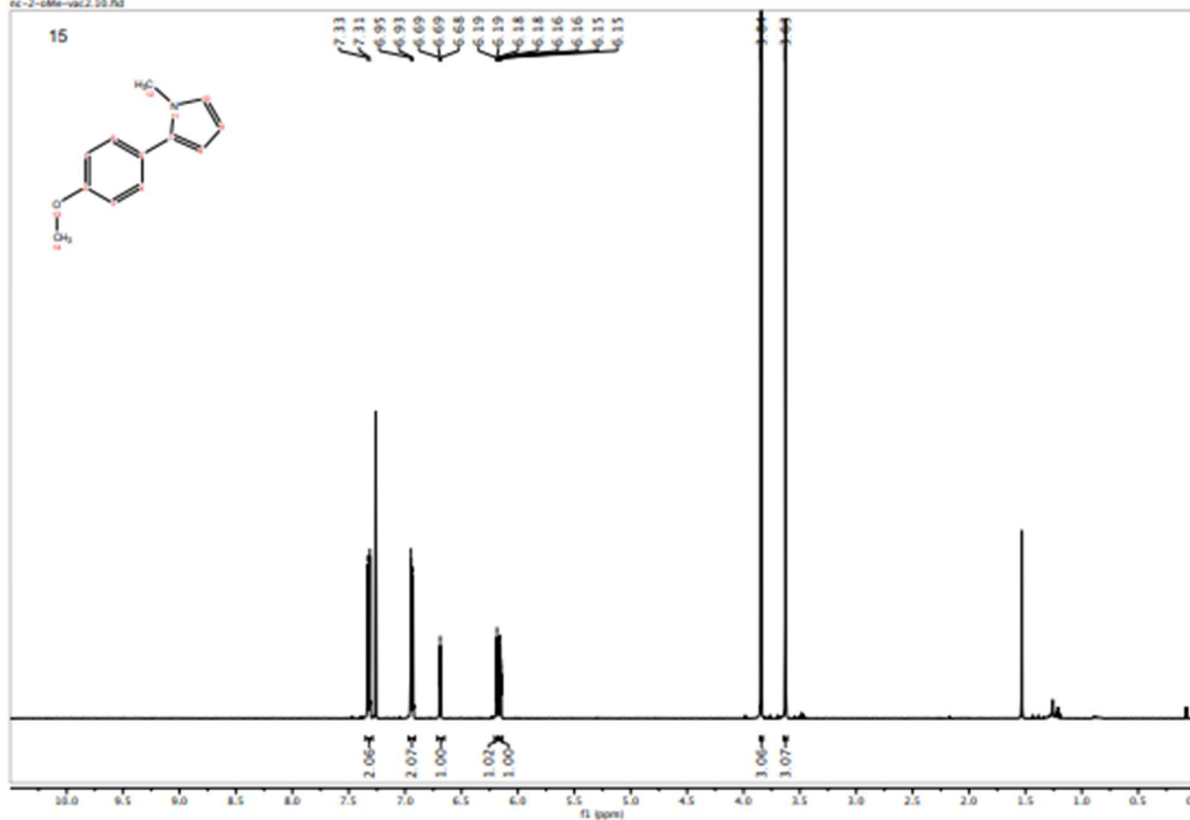
CC2-Bpin-high vac.10.fid



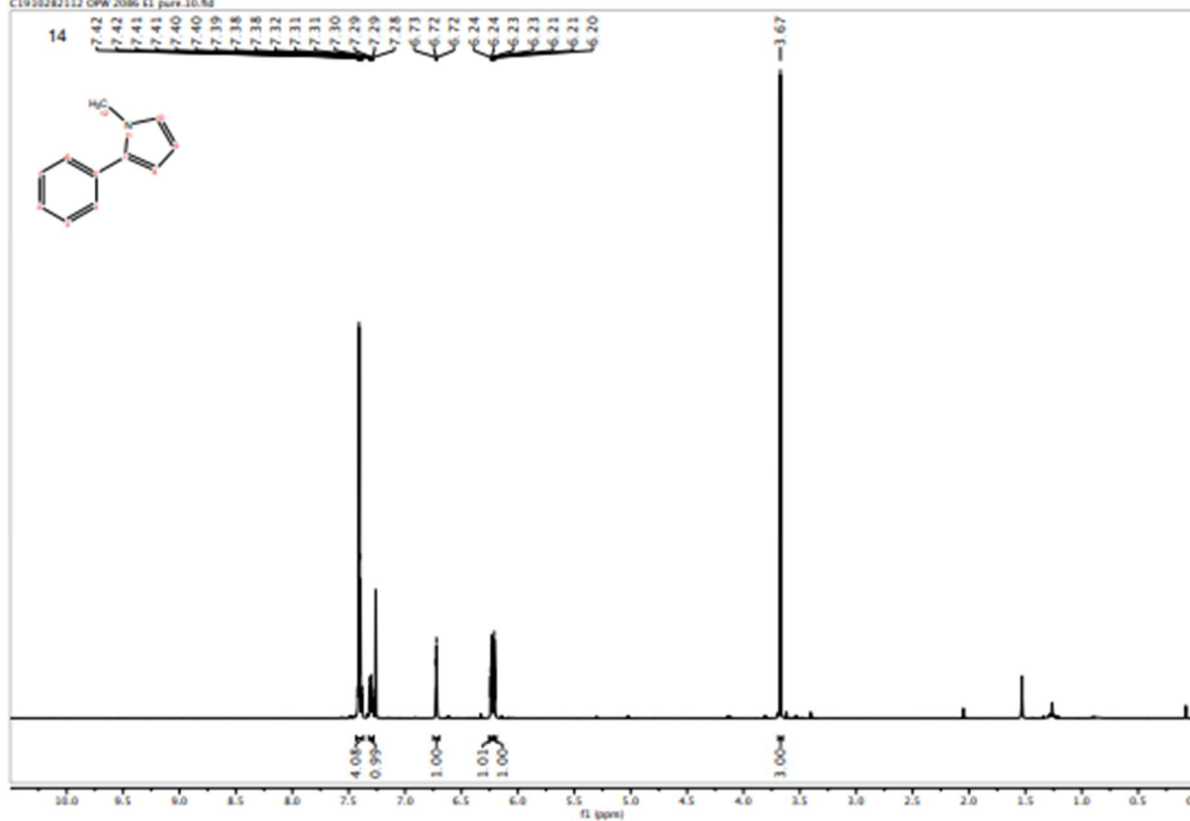
CC2-063C-pure 11P.10.fid



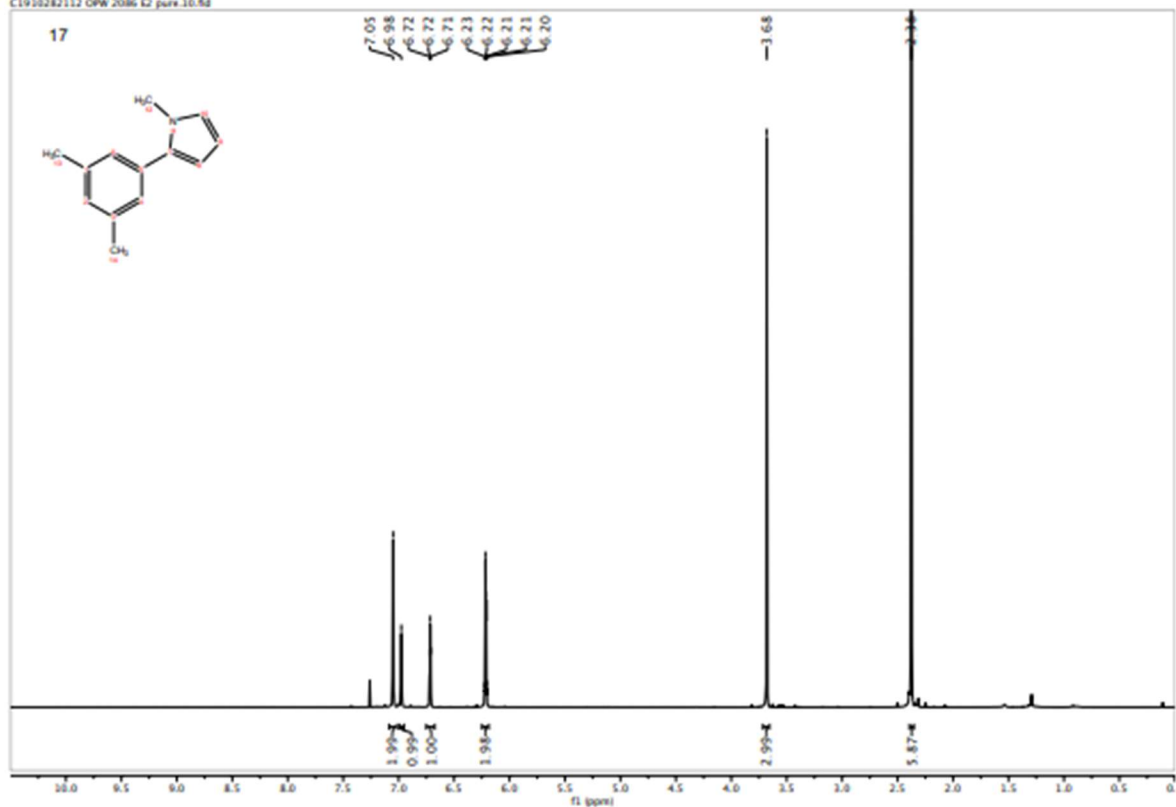
nc-2-cMe-vac2.10.fid



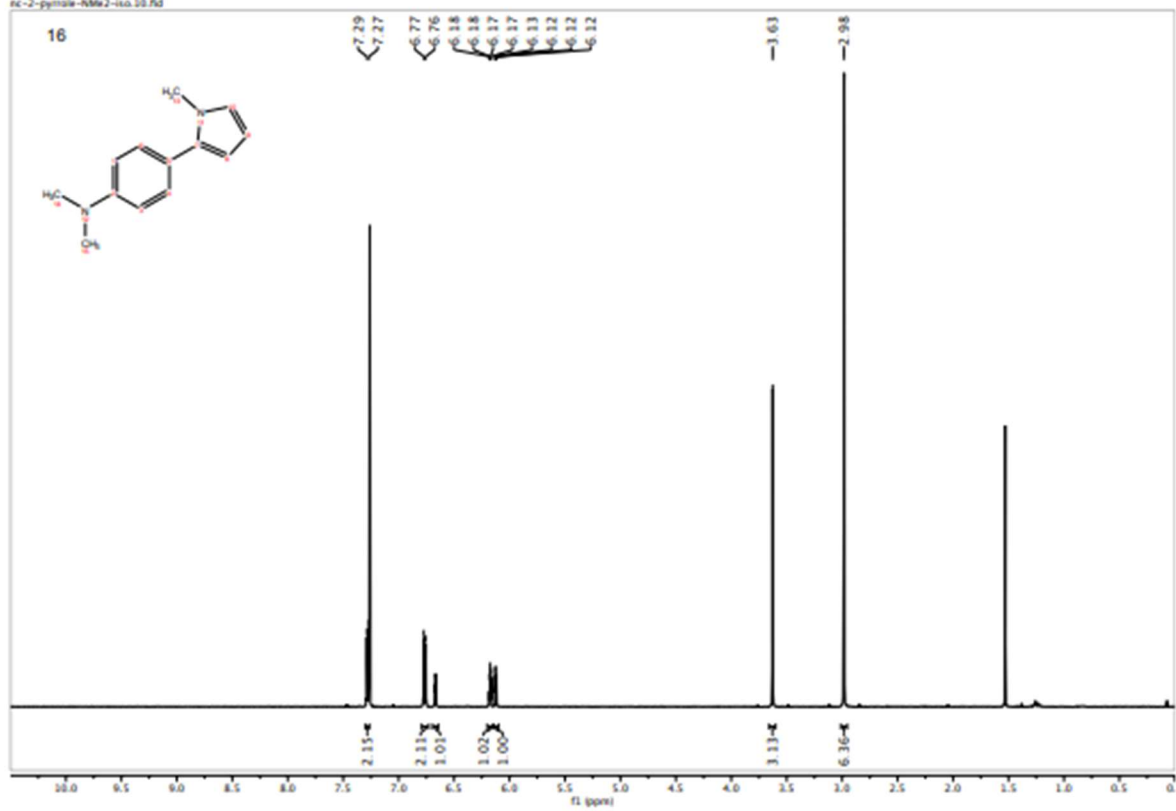
C1910282112 OPW 2086 F1 pure 10.fid



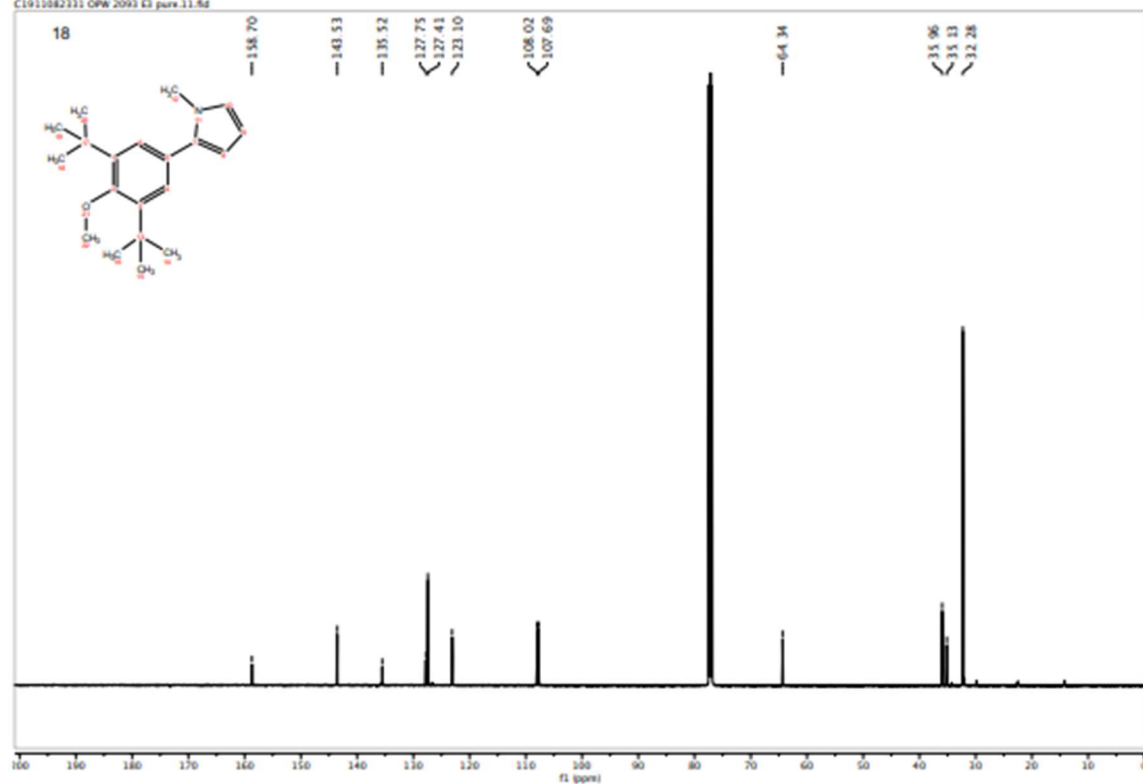
C1910282112 OPW 2086 E2 pure 10.6d



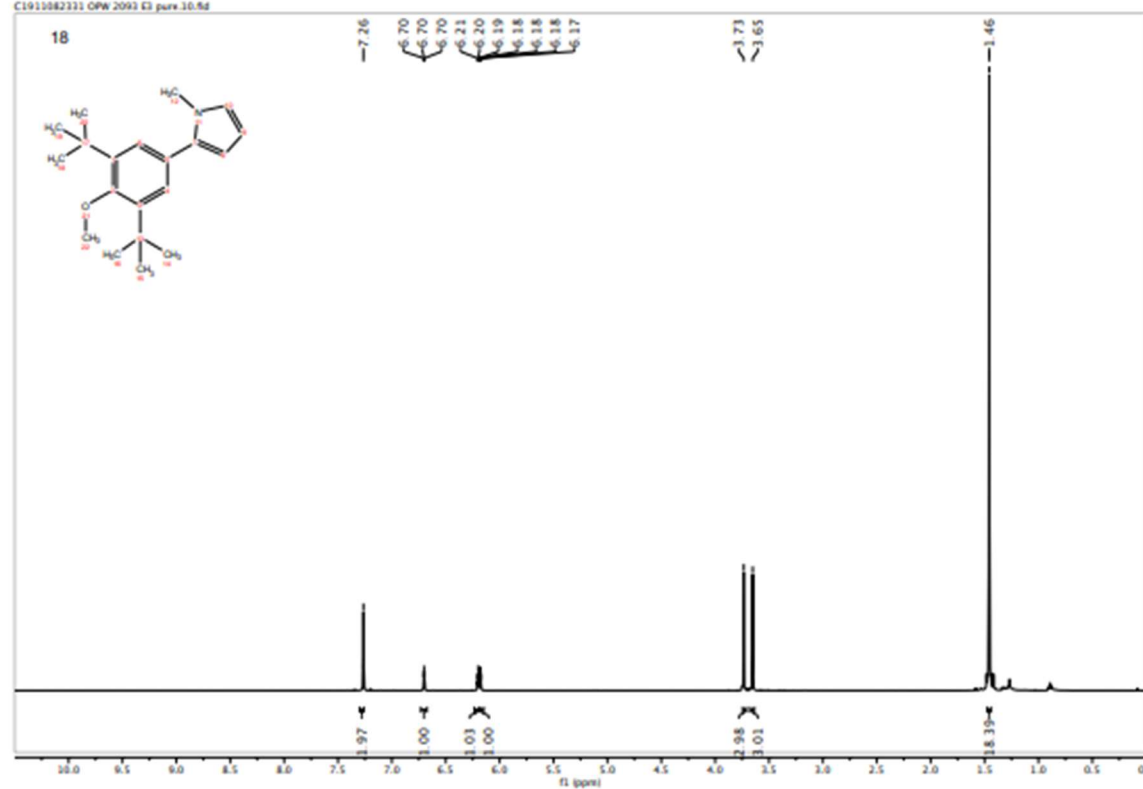
nc-2-pyrrole-4Me2-iso 10.6d



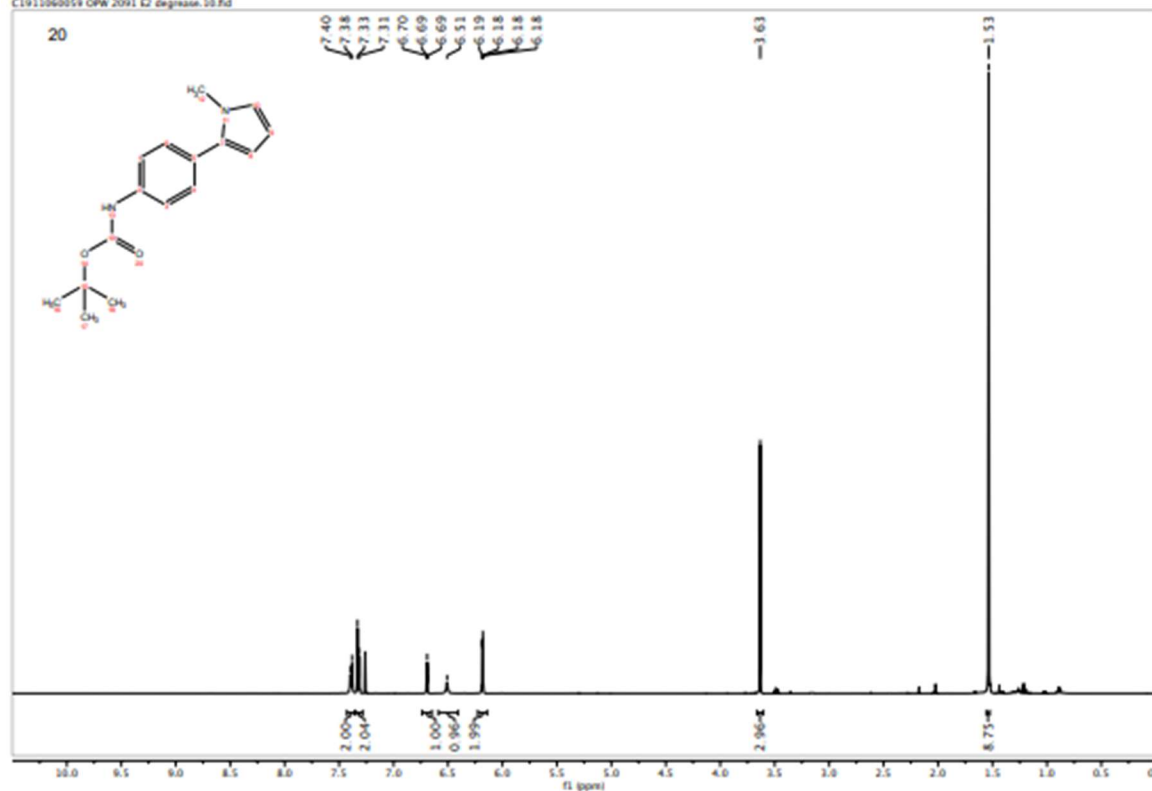
C1911082331 OPW 2093 E3 pure 11.fid



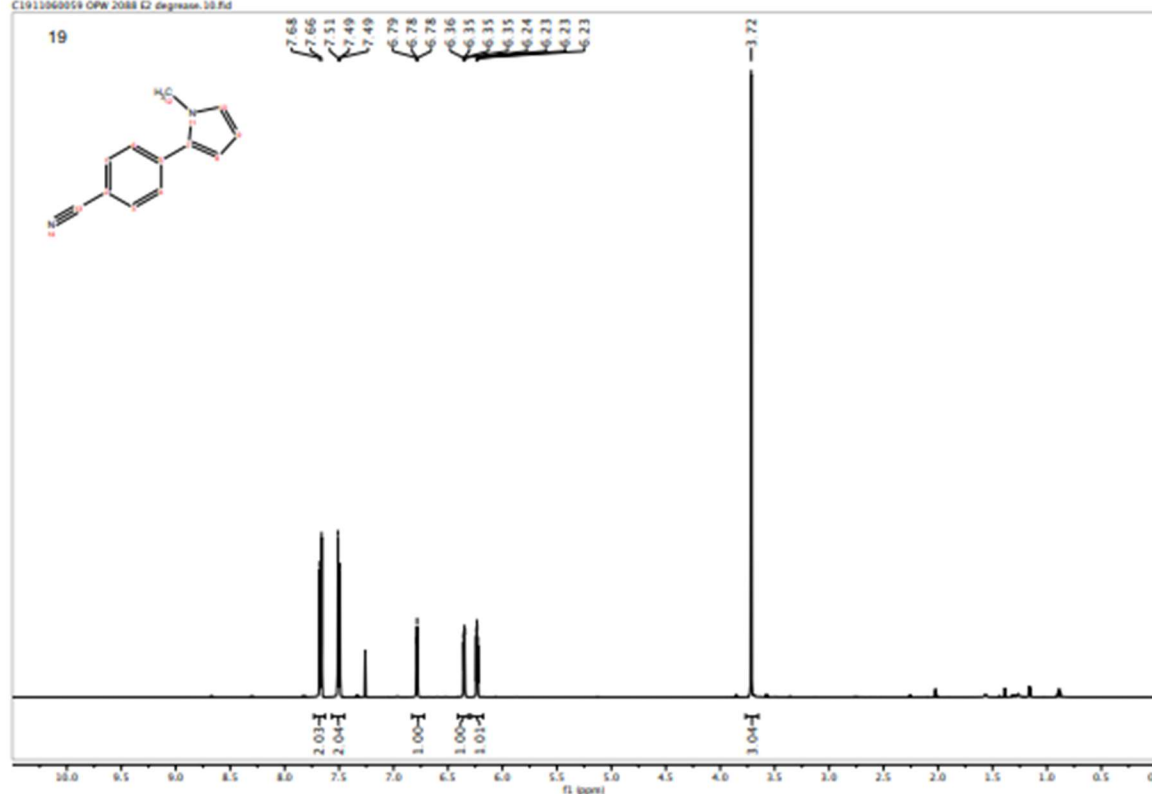
C1911082331 OPW 2093 E3 pure 10.fid



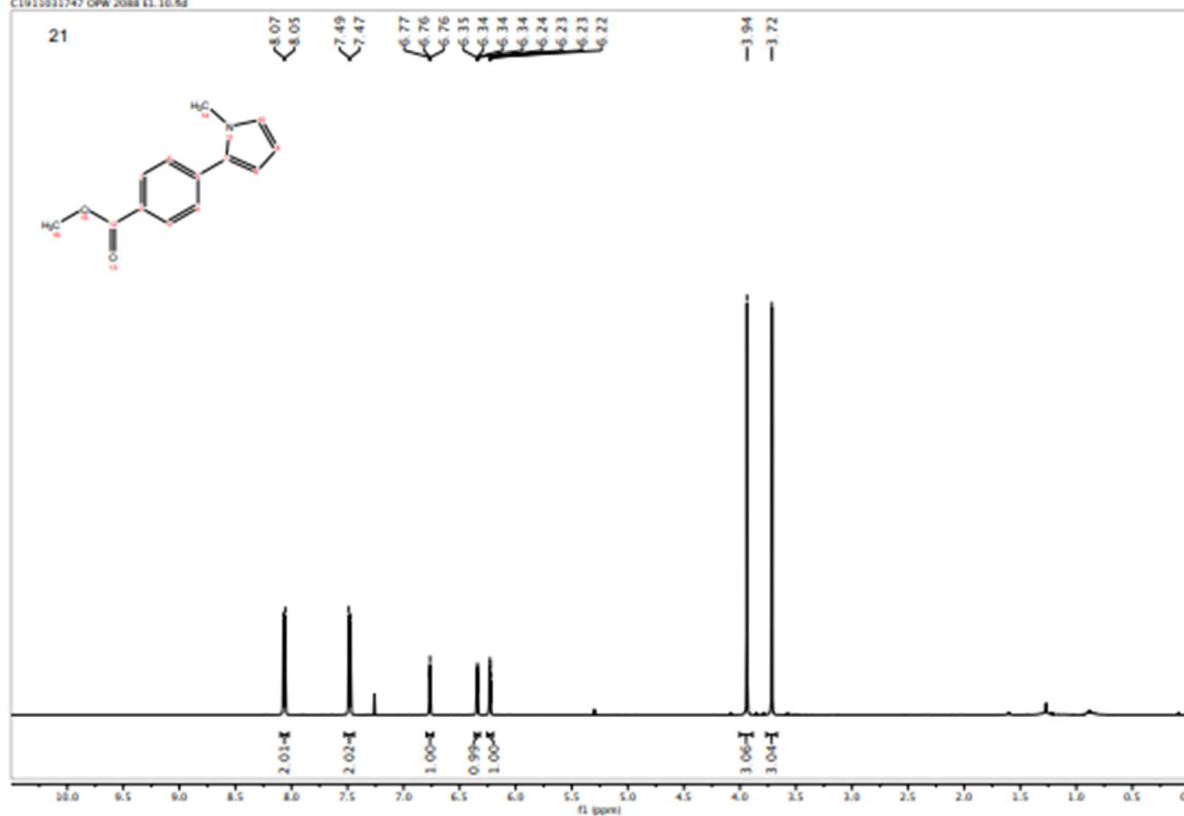
C1911060059 OPW 2091 K2 degrease.10.fid



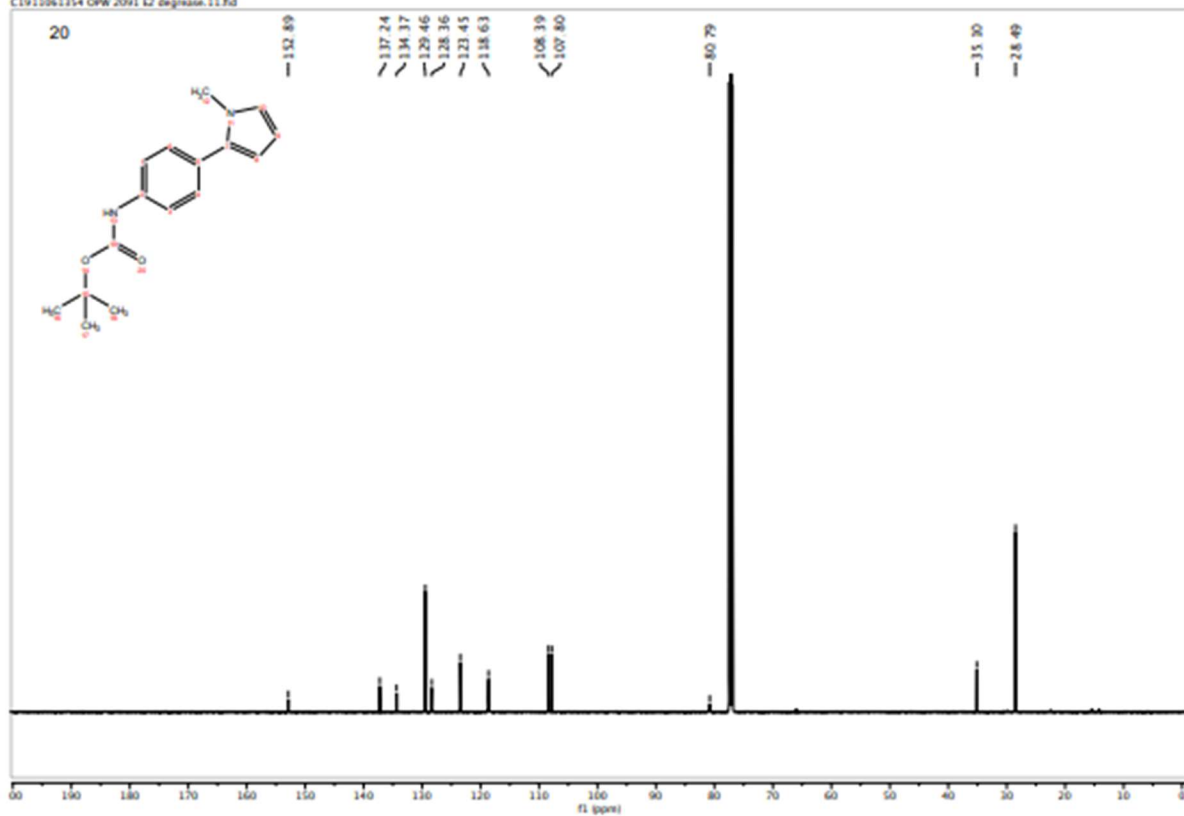
C1911060059 OPW 2088 K2 degrease.10.fid

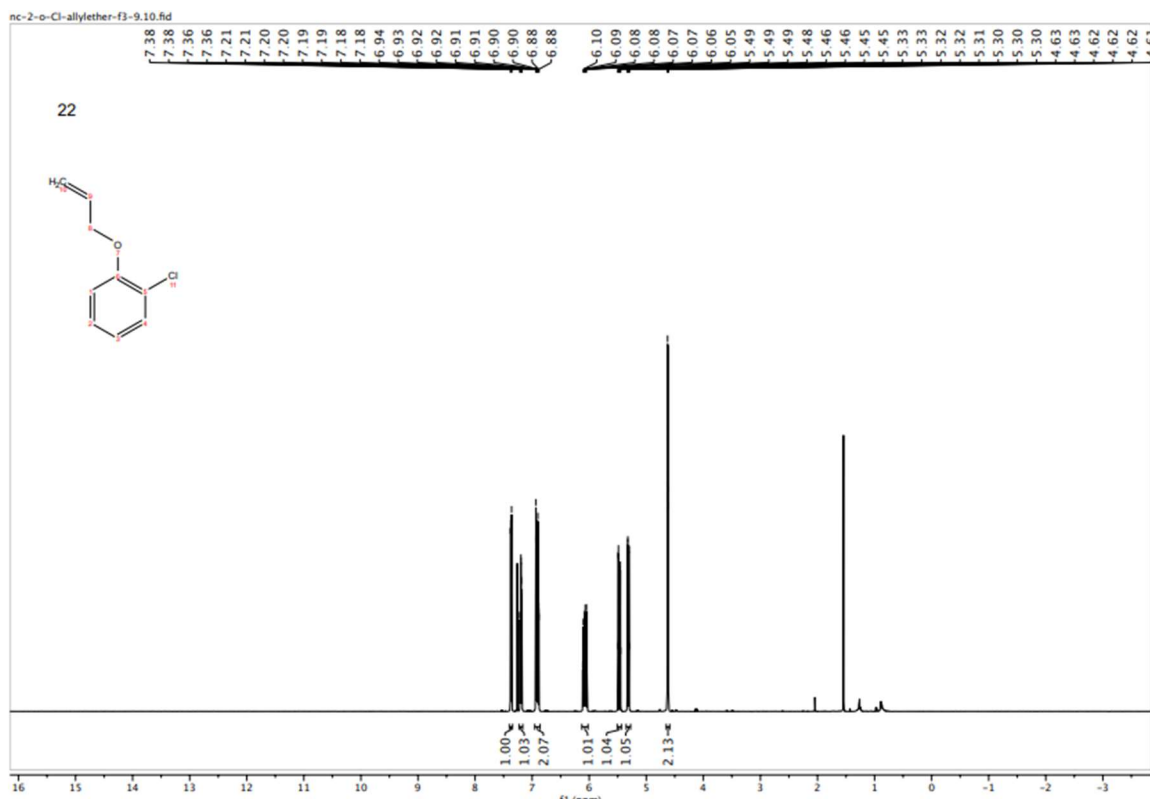


C1911011747 OPW 2088 f1.10.fid



C1911061354 OPW 2091 f2 deproton.11.fid





**Chapter 3: Electrochemical Activation of Diverse Conventional Photoredox Catalysts
Induces Potent Photoreductant Activity**

This work is published: Chernowsky, C.P.; Chmiel, A.F.; Wickens, Z.K.; *Angew. Chem. Int. Ed.*
2021, *60*, 21418 – 21425

3.1. Abstract

Herein, we disclose that electrochemical stimulation induces new photocatalytic activity from a range of structurally diverse conventional photocatalysts. These studies uncover a new electron-primed photoredox catalyst capable of promoting the reductive cleavage of strong C(sp²)–N and C(sp²)–O bonds even when reduction potentials hundreds of mV more negative than Li⁰ are required. We illustrate several examples of the synthetic utility of these deeply reducing but otherwise safe and mild catalytic conditions. Finally, we employ electrochemical current measurements to perform a reaction progress kinetic analysis. This technique reveals that the improved activity of this new system is a consequence of an enhanced catalyst stability profile.

3.2. Introduction

Reductive activation of organic molecules through single electron transfer (SET) is a fundamental elementary step at the heart of a myriad of synthetically useful transformations.^{1–4} In recent years, photoredox catalysis has emerged as a mild and chemoselective method to induce redox events.^{5–10} Unfortunately, while 400 nm light possesses sufficient energy for a maximum driving force of 3.1 eV, this energy is diminished by 25–50% through vibrational relaxation, internal conversion, and intersystem crossing.¹¹ As a consequence, many abundant but thermodynamically stable molecules remain inert to photoredox activation.^{12,13} Indeed, in the context of reductions, alkali metals have remained reductants of unparalleled potency for over a century. These reagents continue to be used in both academic^{14,15} and industrial¹⁶ settings despite their implicit hazards, poor chemoselectivity, and inextricable chemical waste. To address this, the development of new strategies to deliver extreme reduction potentials (significantly more negative than –2 V vs. SCE) with the safety and chemoselectivity profile of photoredox catalysis is an emerging area of considerable contemporary interest.^{11,17–22}

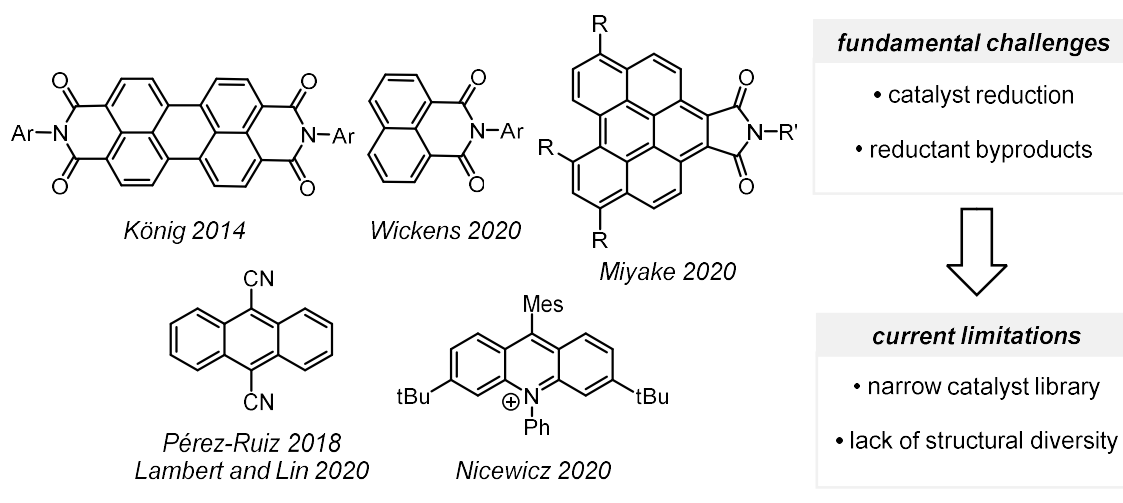


Figure 3.1. Established catalysts known to promote reductive SET events through electron-primed photoredox catalysis. Ar = 2,6-diisopropylphenyl. R = *p*-OMePh. R' = 2-ethylhexyl.

Over the past several years, numerous groups,^{23–28} including ours,²⁶ have examined catalytic systems designed to leverage mildly reducing radical species as a new family of photocatalysts (**Figure 3.1**). We have dubbed these reductively activated species electron-primed photoredox catalysts to distinguish them from more conventional photocatalytic reductants. Pioneering work from König used a consecutive photoinduced electron transfer (conPET) approach to photochemically generate an electron-primed photocatalyst, albeit one that did not possess an excited state reduction potentials more negative than -2 V vs. SCE.²⁹ The conPET strategy requires a carefully balanced system; both catalyst oxidation states must engage in excited state intermolecular SET under a single set of reaction conditions.¹⁹ Additionally, the byproducts of catalyst activation, which are typically reactive amine radical cations and easily reduced iminium ions, must not deactivate the catalyst or interfere in subsequent steps.³⁰ These fundamental challenges associated with catalyst generation and turnover have resulted in only a small collection of electron-primed photocatalytic systems being identified in the subsequent years^{29,31} despite photophysical studies establishing that numerous persistent radical anions absorb visible light.^{32–36}

We envisioned that electrochemistry would offer a flexible approach to generate electron-primed photoredox catalysts as cathodic reduction is highly tunable and divided cell electrolysis excludes interfering oxidized byproducts.^{37–39} Indeed, we previously used this approach to introduce a novel electron-primed photocatalyst capable of reducing aryl chloride substrates with E_{red} on par with Li^0 .²⁶ Contemporaneous efforts by Lambert and Lin disclosed that 9,10-dicyanoanthracene, an electron-primed photoredox catalyst previously accessed via conPET,³¹ exhibits enhanced reactivity towards aryl chloride substrates when driven electrochemically.²⁵ However, while these two discoveries validated the use of electrochemistry to generate potent photoreductants, both of these electrophotocatalysts remained structurally analogous to established conPET-based photocatalysts. While rapid progress has been made in net-oxidative electrophotocatalytic transformations,^{40–48} electrophotocatalytic reductions remain comparatively underdeveloped.^{49,50} Herein, we employ cathodic reduction to elicit new photocatalytic activity from numerous organic and inorganic structures (**Figure 3.2**). These studies reveal a new electron-primed photoredox catalyst that enables cleavage of strong $\text{C}(\text{sp}^2)\text{--N}$ and $\text{C}(\text{sp}^2)\text{--O}$ bonds.

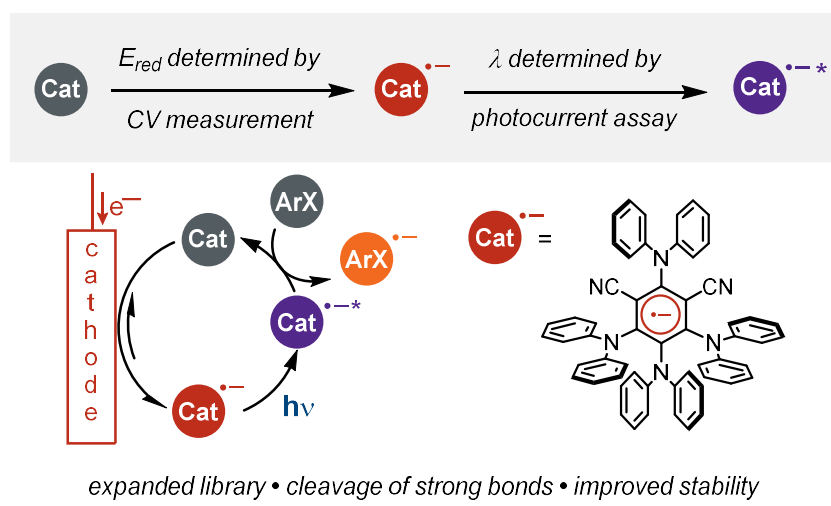


Figure 3.2. Electrochemistry-enabled discovery of new photoreductant **4DPAIPN**.

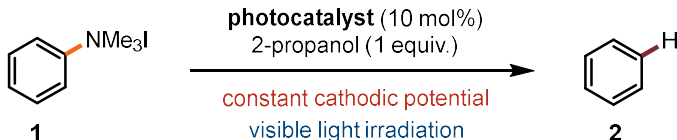
3.3. Results and Discussion

The generation of aryl radical intermediates is a well-established arena to benchmark new photoreductants. Bench-stable^{51–54} trialkylanilinium salts and activated phenols are readily accessible and can be reductively cleaved to aryl radical intermediates through deeply reducing direct electrolysis or alkali metal reductants, however, they remain difficult to activate under photocatalytic conditions.^{55,56} Within the past year, Larionov and König illustrated that anilide and thiolate photocatalysts are capable of promoting the borylation of anilinium salts and activated phenols via photoreduction.^{57,58} However, boron plays a non-innocent role in these processes and photochemical net-reductive transformations of these substrates remains limited. Reductive defunctionalization is a powerful synthetic tactic to leverage aniline and phenol activating groups in a traceless manner.^{59–62} Current methods to remove these directing groups rely on harsh dissolving metal conditions^{63,64} or palladium catalysis.^{65,66} We envisioned that cleavage of these strong bonds was a perfect arena to explore new potent reductants given recently reported halogen-atom transfer strategies, which in some cases can circumvent deeply reducing potentials,⁶⁷ are unlikely to be amenable to the cleavage of these less polarizable heteroatoms.^{68,69}

We initiated our studies with the reductive cleavage of an N,N,N-trimethyl anilinium salt, **1** (**Table 3.1**). We anticipated that the thermodynamic and kinetic challenges presented by aryl C(sp²)–N bond cleavage would expose the limitations of current electron-primed photocatalysts. We found that **NpMI**, the electron-primed photoredox catalyst we recently reported,²⁶ could cleave the C(sp²)–N bond in 42% yield under a constant cathodic potential and visible light irradiation. This result validated that an electron-primed photoredox system is capable of engaging this substrate but also highlighted the need for improved catalysts. We next evaluated a collection of structures related to the **NpMI** core. Electrochemistry facilitated rapid catalyst evaluation in two primary ways: (1) cyclic voltammetry studies established the minimum cathodic potential to

generate the radical anion photocatalyst and (2) evaluation of wavelength dependent photocurrent established the optimal irradiation wavelength (see SI for details).⁷⁰ These studies revealed that various derivatives of **NpMI** including **NpDI**, **PMI**, and **Nplmz** each provided the defunctionalized product, albeit in reduced yield relative to **NpMI**. Given these data, we concluded that a fundamentally different catalyst scaffold was likely necessary to efficiently promote these challenging reductions.

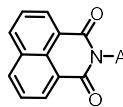
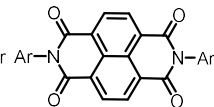
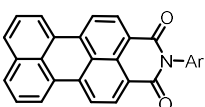
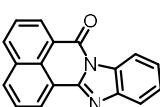
Table 3.1. Evaluation of Electrochemically-Generated Persistent Radical Anions for Photocatalytic Activity



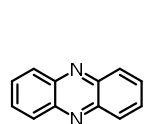
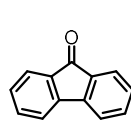
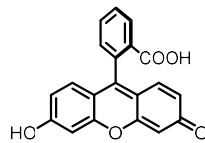
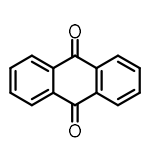
1

2

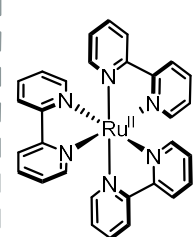
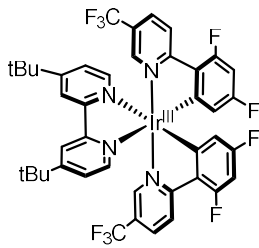
imide-based persistent radical anions

			
NpMI^a	NpDI^a	PMI^a	Nplmz
$E_{\text{red}} = -1.3 \text{ V}$	$E_{\text{red}} = -0.4 \text{ V}$	$E_{\text{red}} = -0.8 \text{ V}$	$E_{\text{red}} = -1.2 \text{ V}$
405 nm	390 nm	405 nm	405 nm
42% yield	11% yield	16% yield	41% yield

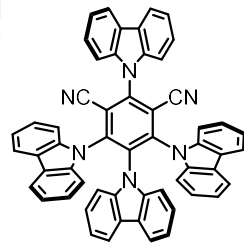
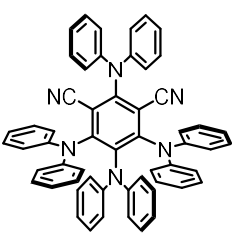
persistent organic radical anions

			
PZ	FL	FC	AQ
$E_{\text{red}} = -1.2 \text{ V}$	$E_{\text{red}} = -1.3 \text{ V}$	$E_{\text{red}} = -1.2 \text{ V}$	$E_{\text{red}} = -0.9 \text{ V}$
440 nm	405 nm	405 nm	405 nm
36% yield	45% yield	34% yield	10% yield

metal-based scaffolds

	
(Ru-1)	(Ir-1)
$E_{\text{red}} = -1.3 \text{ V}$, 427 nm	$E_{\text{red}} = -1.4 \text{ V}$, 427 nm
9% yield	25% yield

isophthalonitrile scaffolds

	
4-CzIPN	4-DPAIPN
$E_{\text{red}} = -1.3 \text{ V}$, 390 nm	$E_{\text{red}} = -1.6 \text{ V}$, 405 nm
65% yield	98% yield

Yields provided are of **2**, determined by GC analysis. All redox potentials reported vs SCE. ^a Ar = 2,6-diisopropylphenyl. See the SI for further details.

We next targeted more structurally diverse persistent radical anion precursors that have not been explored as electron-primed photocatalysts.^{36,71–74} We found that phenazine, fluorenone, and fluorescein each promote reduction of **1** in comparable yields to **NpMI** under appropriate

electrophotocatalytic conditions. Control reactions revealed that no conversion is observed in the absence of electrolysis indicating that the photoactivity of the neutral structures is insufficient to drive defunctionalization of **1**. These data suggest that electrochemical reduction can coax potent photocatalytic activity out of a much broader range of molecules than previously appreciated. Next, we recognized that nearly all photoredox catalysts, by design, undergo reversible redox events and many possess persistent radical anion congeners.^{6,7,10} We questioned whether the structural features that render molecules effective as conventional photoredox catalysts would translate to the electron-primed photoredox manifold.^{23,75,76} Intriguingly, we found that electrolysis at the E_{red} of several commonly employed photoredox catalysts **Ru(bpy)₃**,⁷⁷ **Ir(dF-CF₃-ppy)₂(dtbpy)**,⁷⁷ and **4CzIPN**⁷⁸ turned on photocatalytic activity in this challenging reduction.⁷⁹ While there is a sole report proposing photochemical activity of the reduced congener of an Ir-based photoredox catalyst,⁸⁰ these are the first data consistent with either Ru-based or isophthalonitrile structures acting as electron-primed photoredox catalysts. Given that cathodic reduction of **4CzIPN** resulted in a meaningful improvement in photochemical deamination yield, we examined other isophthalonitrile catalysts. This investigation revealed that **4DPAIPN**⁸¹ promotes the reduction of model substrate **1** in nearly quantitative yield under electrophotocatalytic conditions. Overall, the structural diversity of the potent photocatalysts identified through these studies suggest that reductively induced photoactivity is a general phenomenon and provides a clear link between catalyst structure and reaction outcome.

We next evaluated whether **4DPAIPN** was promoting this reaction through excitation of a cathodically generated species. Under electrochemical stimulation **4DPAIPN** acts as a far more potent photoreductant than anticipated by its established redox potentials ($E_{1/2} \text{ PC}^+/\text{PC}^* = -1.3$ V and $E_{1/2} (\text{PC}/\text{PC}^{\bullet-}) = -1.5$ V vs. SCE)⁸¹ (**Figure 3.3**). First, we conducted a series of control experiments and found that catalyst, electrolysis, and light were all required for product formation. Next, we examined whether electrochemical reduction of **4DPAIPN** was necessary to promote

the defunctionalization reaction. Inspired by an elegant experiment conducted by Lambert and Lin,²⁵ we measured the defunctionalization yield at varied cathodic potentials. Overlaying these data with the cyclic voltammogram of **4DPAIPN** illustrates that reactivity is observed only when a sufficient potential to reduce **4DPAIPN** is applied. These data are fully consistent with cathodic catalyst reduction and subsequent excitation as necessary steps for this difficult reductive transformation.⁸²

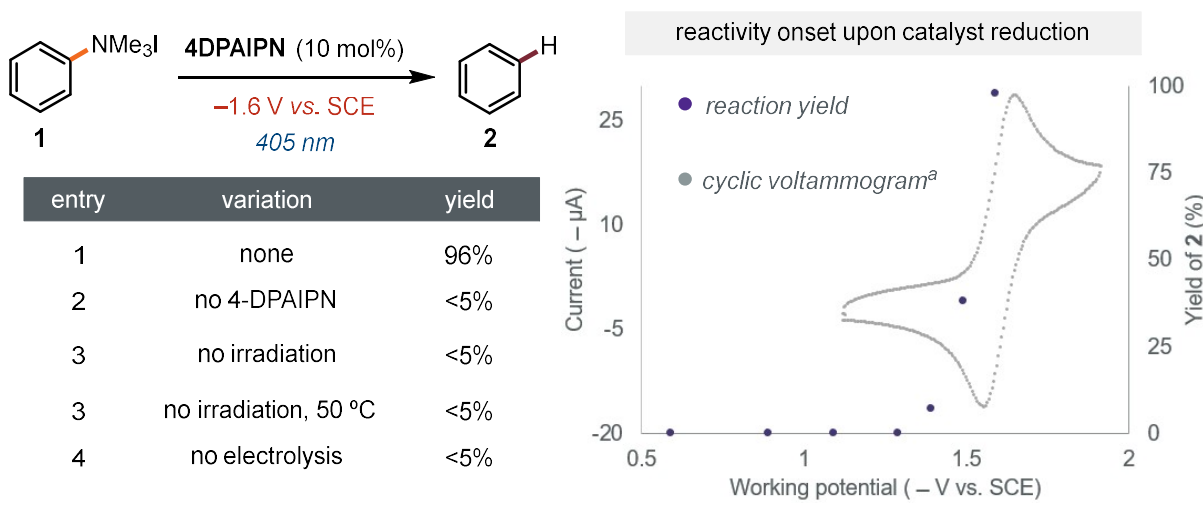
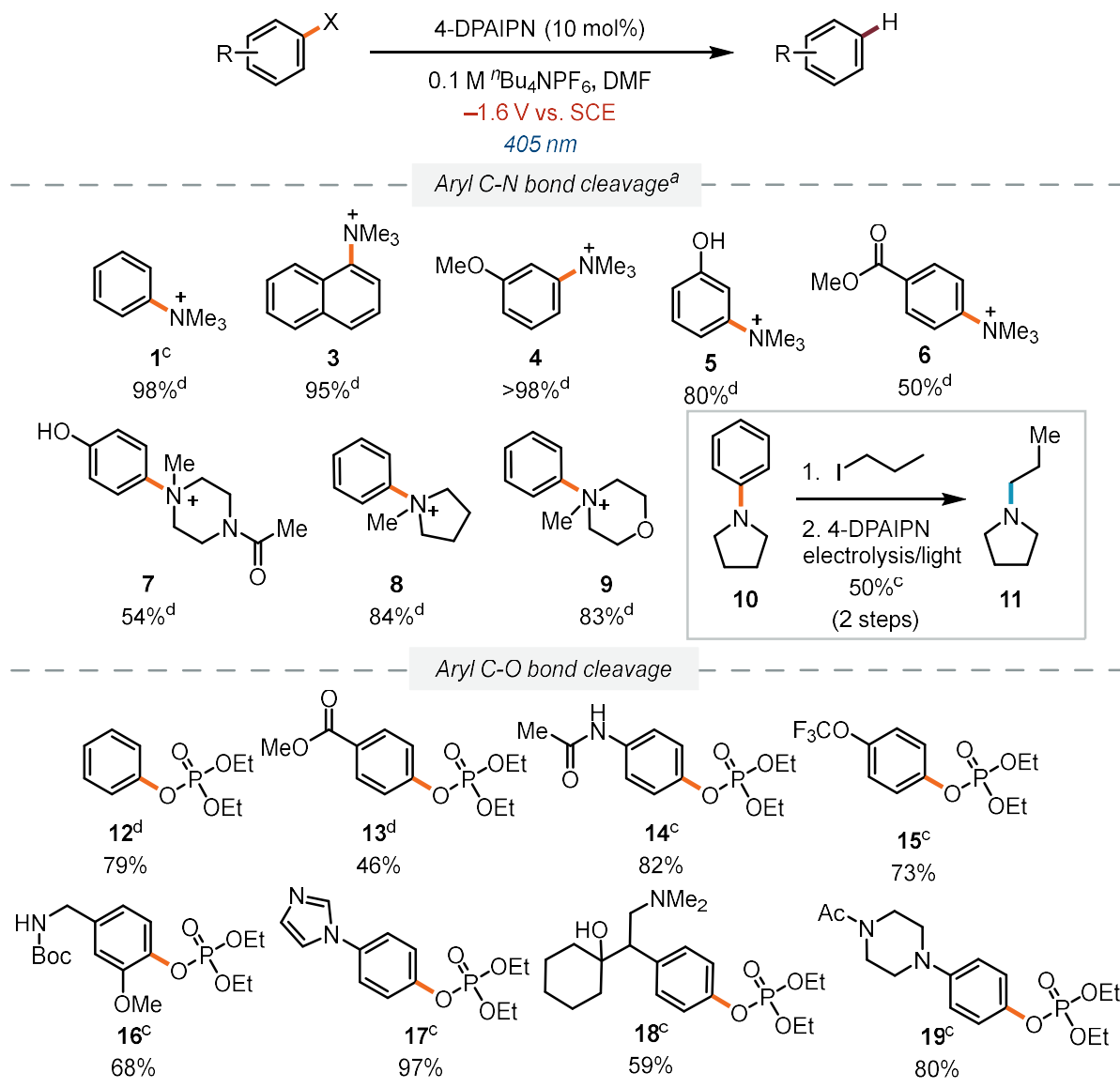


Figure 3.3. Control experiments to probe the mode of reactivity of the catalyst. ^aCV is of 4-DPAIPN. See the SI for experimental details.

We next probed the scope of this catalytic C(sp²)–N cleavage process (**Table 3.2**). We found ethers (**4**), free alcohols (**5**), esters (**6**), and amides (**7**) as well as heterocycles such as piperazine (**7**), pyrrolidine (**8**), and morpholine (**9**) were all well-tolerated. Notably, this reaction enables a molecular editing strategy wherein an N-aryl ring can be replaced by an alkyl group through an alkylation/reductive cleavage sequence as both aryl and amine fragments can be recovered after C(sp²)–N reduction. Given the promising activity of this catalytic system in the cleavage of anilinium salts, we turned our attention to more difficult to reduce C(sp²)–O bonds. Phenol derivatives (e.g. triflates and phosphates) possess deep reduction potentials (typically <–2.7 V vs. SCE).^{83–85} Despite the energetic demands of C(sp²)–O cleavage, phosphate ester substrates bearing a range of functional groups such as esters (**13**), amides (**14**), ethers (**15**),

benzylic amines (**16**), unprotected alcohols and tertiary amines (**18**) as well as heterocycles such as imidazole (**17**) and piperazine (**19**) each underwent productive C(sp²)-O cleavage. While each of these reactions are conducted far below the cathodic potential required to reduce the substrate, we questioned whether deeply reducing electrolysis could recapitulate this electrophotocatalytic activity. To probe this, we carried out direct electrolysis reactions on two substrates bearing functional groups to investigate the role of the catalyst in preserving chemoselectivity. Under

Table 3.2. Scope of Aryl C(sp²)-N and C(sp²)-O Bond Cleavage



^a The counter ion is OTf unless otherwise noted. ^b **1** used as the iodide salt. ^c NMR yield. ^d GC yield. See the SI for experimental details.

constant current conditions in the absence of catalyst, **16** and **19** showed significant conversion to an intractable mixture containing <20% product. By promoting reduction through a photocatalytic mediator under mild electrochemical potentials, chemoselectivity and functional group tolerance can be vastly improved compared to direct electrolysis conditions.

Phenols are electron-donating groups that enable a wide range of reactions at the arene core.^{86–90} We envisioned that the scope of products accessible using these processes could be expanded through a chemoselective excision of the phenolic activating group via an electrophotocatalytic system (**Figure 3.4**). For example, this strategy allows selective formation of meta-substituted products inaccessible via direct Friedel–Crafts reactions.⁹¹ To illustrate this strategy, we prepared a suite of meta-substituted arene products from simple precursors using a phenol-directed alkylation-defunctionalization sequence (**20–23**). As a direct comparison, we subjected **23** to constant current conditions in the absence of catalyst and observed high conversion with substantially diminished yield. To demonstrate the value of a phenol-directed alkylation-defunctionalization approach, we targeted the synthesis of a tricyclic resorcinol derivative that was developed as a conformationally restricted cannabinoid agonist. The route, devised by Makriyannis,⁹² hinged on phenol-enabled Friedel–Crafts alkylation followed by a Li⁰-promoted excision of the phenol activating group. In our hands, the Friedel–Crafts process and subsequent phosphorylation proceeded smoothly to deliver tricyclic intermediate **24**. Gratifyingly, electron-primed photoredox C(sp²)–O cleavage furnished intermediate **25** despite a nearly 2 V underpotential supplied at the cathode. Global demethylation furnished **26** in 18% yield over 4 steps. These data demonstrate how this new catalytic platform can directly fit into synthetic sequences and circumvent the need for more hazardous chemical reductants in the preparation of complex biologically active molecules.

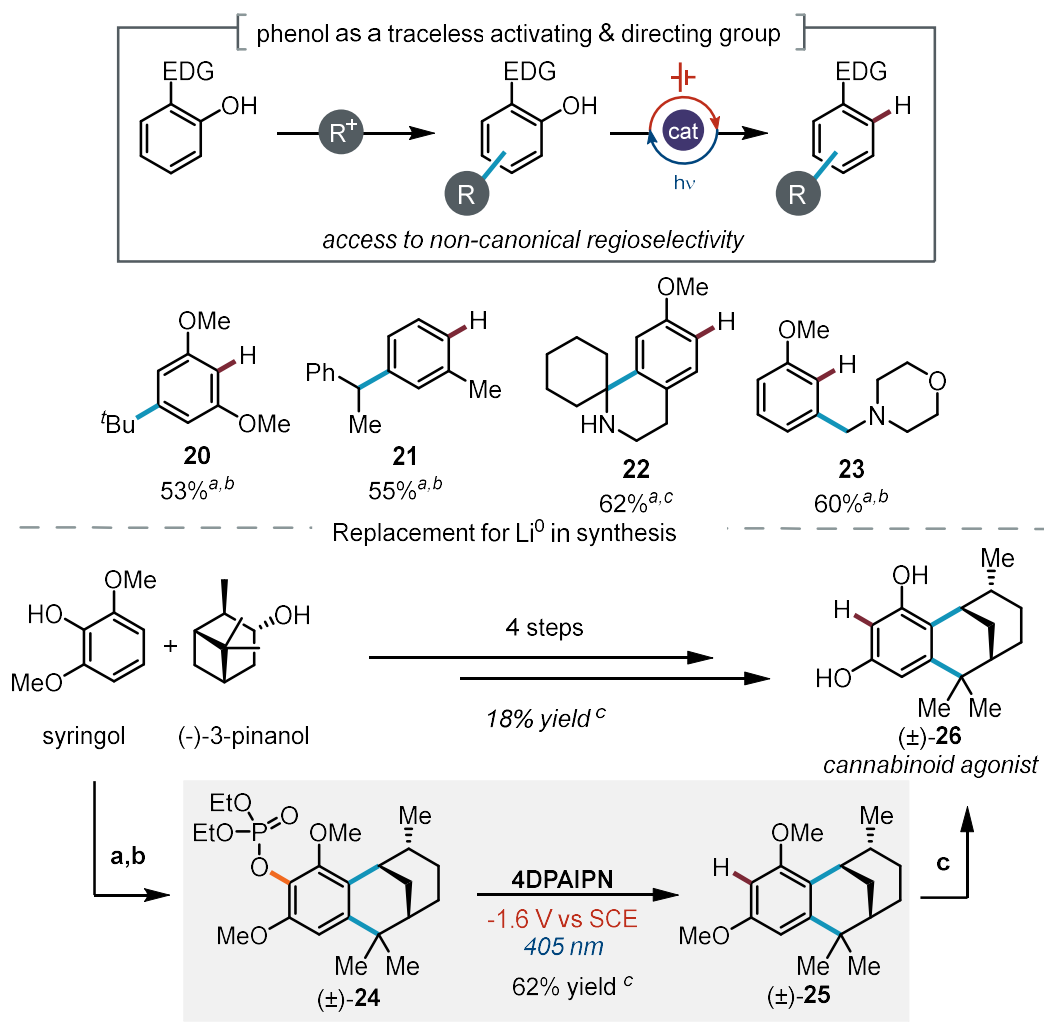


Figure 3.4. Phenol as a traceless directing group enabled by electron-primed photoredox catalysis. ^a Yields reported are for the phosphate defunctionalization step. ^b NMR yield. ^c Isolated yield. (a) 70% aq MeSO₃H, 70 °C, 12 h (45% yield). (b) CIP(O)(OEt)₂, DABCO, MeCN, 18 h (70% yield). (c) BBr₃, DCM, -78 °C, 12 h, (91% yield). Conversion of **24** to **25** was accomplished under conditions analogous to those in Table 2. See the SI for experimental details.

We next questioned whether the aryl radical intermediates generated upon reductive cleavage of anilinium salts and phosphate esters could be intercepted by classic aryl radical traps. We investigated several aryl radical coupling reactions: phosphonylation, borylation, and heteroarylation (**27-29**). We found that both C(sp²)-N and C(sp²)-O radical precursors were amenable to each of these radical coupling reactions (**Figure 3.5**).

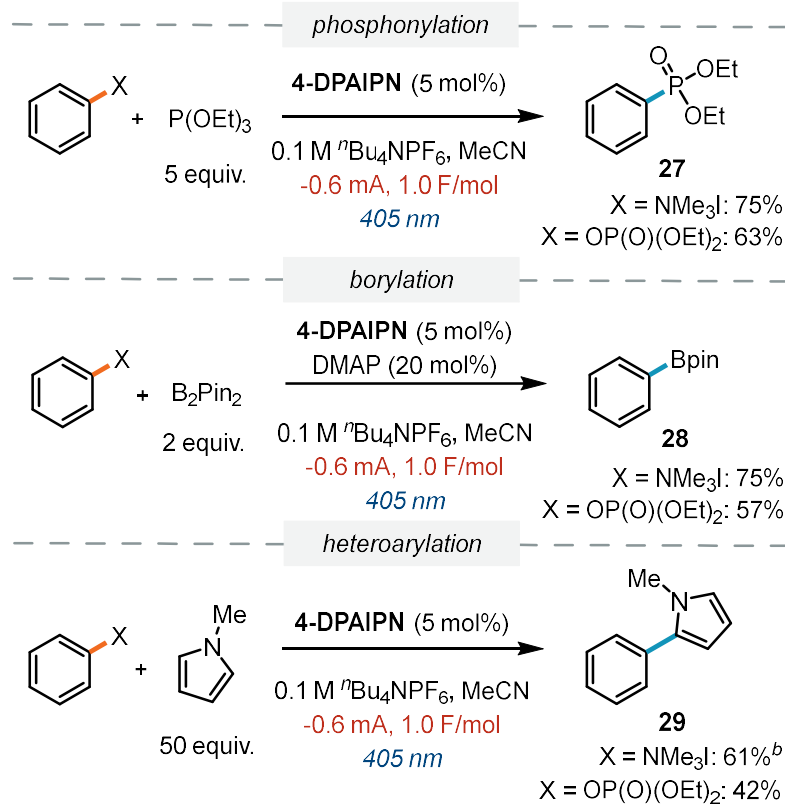


Figure 3.5. Redox neutral coupling reactions from aryl $\text{C}(\text{sp}^2)\text{-N}$ and $\text{C}(\text{sp}^2)\text{-O}$ bonds. All reactions conducted on a 0.2 mmol scale and reported as NMR yields. ^aNMR yield. ^bCatalyst loading was 2.5 mol%. See the SI for details.

Having established that **4DPAIPN** is a broadly effective electron-primed photoredox catalyst with immediate synthetic utility, we next aimed to understand the origin of the improved performance of **4DPAIPN** relative to prior electron-primed photoredox catalysts. Specifically, we questioned whether **4DPAIPN** possessed enhanced reactivity, superior catalyst stability,⁹³ or both. To address this question, we envisioned that electrochemical current could be employed as a non-invasive in situ rate monitoring technique to unlock tools from reaction progress kinetic analysis (RPKA).⁹⁴ This method can reveal phenomena such as catalyst decomposition and product inhibition typically invisible to classic initial rate kinetics because the analysis is conducted under typical preparative conditions. We conducted a "same excess" experiment with both our previously reported electron-primed photocatalyst, **NpMI**, and **4DPAIPN** to compare the extent of catalyst deactivation in each case (**Figure 3.6**). We selected aryl chloride **30** as the model

substrate because both catalysts can engage this substrate under constant potential conditions and preliminary investigations indicated it exhibited a well-behaved kinetic profile.^{95,96} We carried out two separate constant potential experiments for **NpMI** at different initial concentrations of **30** (traces a and b). When the conversion rate of **30** is plotted as a function of, the two curves do not overlay. This indicates either catalyst death or product inhibition.⁹⁷ Inhibition by the arene product was excluded by addition of **31**, which did not restore overlay between the curves. Furthermore,

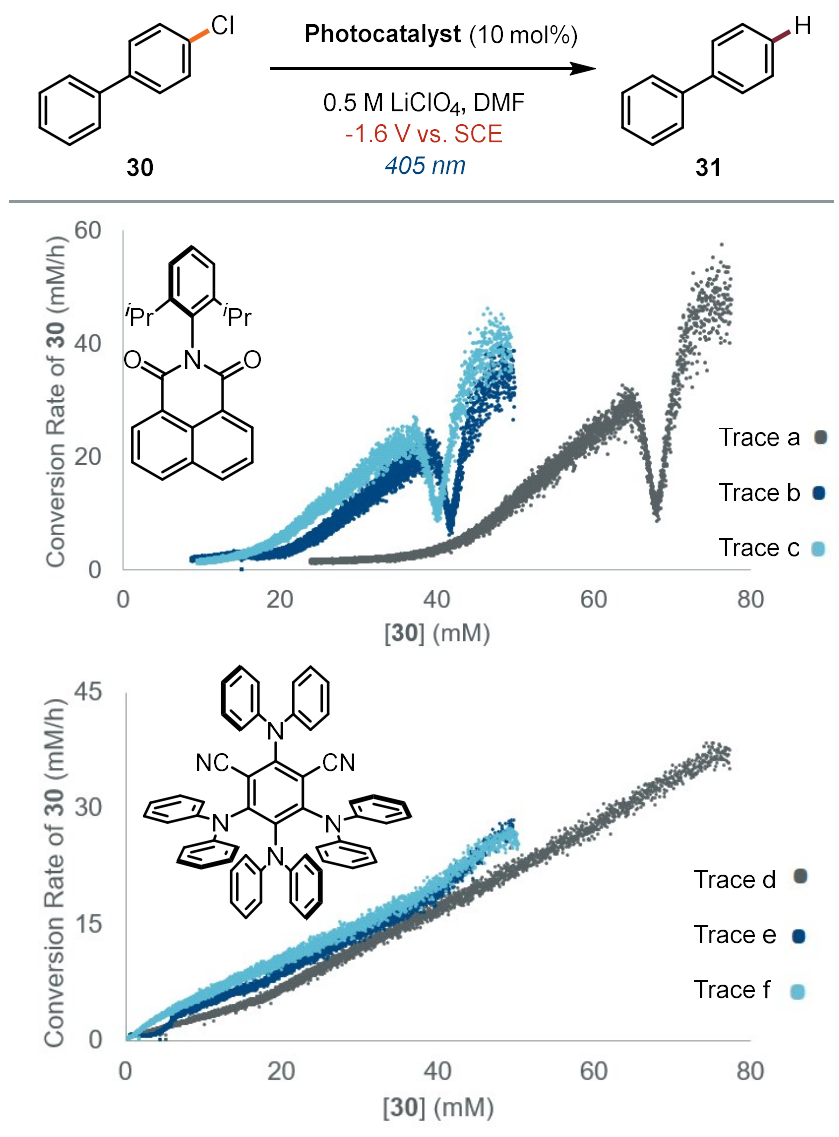


Figure 3.6. Reaction progress kinetics analysis to study catalyst decomposition. Trace a and d: [ArCl]₀ = 0.08 M (standard reaction concentration), Trace b and e: [ArCl]₀ = 0.052 M, Trace c and f: [ArCl]₀ = 0.052 M, [ArH]₀ = 0.028 M. See the SI for details.

NpMI exhibited an unusual kinetic profile consistent with decomposition into a new catalytically active species that subsequently decomposes. These data implicate rapid deactivation of **NpMI** under these conditions. In stark contrast, an analogous “same excess” experiment with **4DPAIPN** resulted in clean first order reaction profiles that nearly overlay. These data are consistent with turnover limiting photoreduction of **30** and minimal catalyst decomposition or product inhibition (see SI for details). As with **NpMI**, addition of **31** excluded product inhibition and suggests **4DPAIPN** decomposition occurs^{98–101} but is attenuated relative to **NpMI**. These data indicate that the improved performance of **4DPAIPN** can be attributed to it forming a more robust electron-primed photoredox catalyst. Indeed, the initial rate of dehalogenation promoted by **NpMI** is faster than **4DPAIPN** but rapid decomposition of this catalyst renders it ineffective for more challenging substrates that are slower to fragment following reduction.

3.4. Conclusion

Overall, we have demonstrated that electrochemistry is an effective tool to explore structurally diverse electron-primed photoredox catalysts. These investigations revealed electrochemical reduction can induce potent photoreductant behavior from structurally diverse catalyst precursors. Among these, a common photoredox catalyst, **4DPAIPN**, is an exceptionally reducing electron-primed photoredox catalyst. This discovery enabled a new catalytic system to promote the reductive cleavage of diverse C(sp²)-N and C(sp²)-O bonds, which we anticipate will enable an array of synthetic sequences that previously would have mandated alkali metal reductants. Finally, we illustrated how principles from RPKA could be directly employed in electrophotocatalysis, using electrochemical current to monitor reaction rate in situ throughout a reaction. We anticipate radical anions will serve as a structurally diverse family of photoredox catalysts for challenging reductive processes and that these studies will provide a roadmap for the use of electrochemistry to both drive and interrogate such systems.

3.5. Acknowledgements

We thank Prof. Alison Wendlandt for helpful suggestions. We thank the Stahl lab for their assistance in use of spectroelectrochemical equipment. Additionally, we thank the Stahl, Weix, Yoon, and Schomaker groups for sharing their chemical inventory. Tracy Drier is acknowledged for electrochemical glassware fabrication. This work was financially supported by the Office of the Vice Chancellor for Research and Graduate Education at the University of Wisconsin–Madison with funding from the Wisconsin Alumni Research Foundation. This material is based upon work supported by the National Science Foundation under Grant No. (2047108). Acknowledgment is made to the Donors of the American Chemical Society Petroleum Research Fund for partial funding of this research (60677-DNI1). Spectroscopic instrumentation was supported by a generous gift from Paul. J. and Margaret M. Bender, NSF (CHE-1048642), and NIH (1S10 OD020022-1).

3.6. References

- (1) Ashby, E. C. Single-Electron Transfer, a Major Reaction Pathway in Organic Chemistry. An Answer to Recent Criticisms. *Acc. Chem. Res.* **1988**, *21* (11), 414–421. <https://doi.org/10.1021/ar00155a005>.
- (2) Zhang, N.; Samanta, S. R.; Rosen, B. M.; Percec, V. Single Electron Transfer in Radical Ion and Radical-Mediated Organic, Materials and Polymer Synthesis. *Chem. Rev.* **2014**, *114* (11), 5848–5958. <https://doi.org/10.1021/cr400689s>.
- (3) Broggi, J.; Terme, T.; Vanelle, P. Organic Electron Donors as Powerful Single-Electron Reducing Agents in Organic Synthesis. *Angew. Chem. Int. Ed.* **2014**, *53* (2), 384–413. <https://doi.org/10.1002/anie.201209060>.
- (4) Ebersson, L. Electron-Transfer Reactions in Organic Chemistry. In *Advances in Physical Organic Chemistry*; Gold, V., Bethell, D., Eds.; Academic Press, 1982; Vol. 18, pp 79–185. [https://doi.org/10.1016/S0065-3160\(08\)60139-2](https://doi.org/10.1016/S0065-3160(08)60139-2).
- (5) Prier, C. K.; Rankic, D. A.; MacMillan, D. W. C. Visible Light Photoredox Catalysis with Transition Metal Complexes: Applications in Organic Synthesis. *Chem. Rev.* **2013**, *113* (7), 5322–5363. <https://doi.org/10.1021/cr300503r>.
- (6) Shaw, M. H.; Twilton, J.; MacMillan, D. W. C. Photoredox Catalysis in Organic Chemistry. *J. Org. Chem.* **2016**, *81* (16), 6898–6926. <https://doi.org/10.1021/acs.joc.6b01449>.
- (7) Romero, N. A.; Nicewicz, D. A. Organic Photoredox Catalysis. *Chem. Rev.* **2016**, *116* (17), 10075–10166. <https://doi.org/10.1021/acs.chemrev.6b00057>.
- (8) Skubi, K. L.; Blum, T. R.; Yoon, T. P. Dual Catalysis Strategies in Photochemical Synthesis. *Chem. Rev.* **2016**, *116* (17), 10035–10074. <https://doi.org/10.1021/acs.chemrev.6b00018>.

- (9) DiRocco, D. A.; Dykstra, K.; Krska, S.; Vachal, P.; Conway, D. V.; Tudge, M. Late-Stage Functionalization of Biologically Active Heterocycles Through Photoredox Catalysis. *Angew. Chem. Int. Ed.* **2014**, *53* (19), 4802–4806. <https://doi.org/10.1002/anie.201402023>.
- (10) Narayanam, J. M. R.; Stephenson, C. R. J. Visible Light Photoredox Catalysis: Applications in Organic Synthesis. *Chem. Soc. Rev.* **2010**, *40* (1), 102–113. <https://doi.org/10.1039/B913880N>.
- (11) Arias-Rotondo, D. M.; McCusker, J. K. The Photophysics of Photoredox Catalysis: A Roadmap for Catalyst Design. *Chem. Soc. Rev.* **2016**, *45* (21), 5803–5820. <https://doi.org/10.1039/C6CS00526H>.
- (12) Kundu, K. K.; Rakshit, A. K.; Das, M. N. Standard Potentials of Li/Li⁺, Na/Na⁺ and K/K⁺ Electrodes in Ethylene Glycol and Its Aqueous Mixtures at 25°C and the Related Thermodynamic Behaviour of the Alkali Halides. *Electrochimica Acta* **1972**, *17* (10), 1921–1937. [https://doi.org/10.1016/0013-4686\(72\)85084-9](https://doi.org/10.1016/0013-4686(72)85084-9).
- (13) Roth, H. G.; Romero, N. A.; Nicewicz, D. A. Experimental and Calculated Electrochemical Potentials of Common Organic Molecules for Applications to Single-Electron Redox Chemistry. *Synlett* **2016**, *27* (05), 714–723. <https://doi.org/10.1055/s-0035-1561297>.
- (14) Chuang, K. V.; Xu, C.; Reisman, S. E. A 15-Step Synthesis of (+)-Ryanodol. *Science* **2016**, *353* (6302), 912–915. <https://doi.org/10.1126/science.aag1028>.
- (15) He, C.; Stratton, T. P.; Baran, P. S. Concise Total Synthesis of Herquelines B and C. *J. Am. Chem. Soc.* **2019**, *141* (1), 29–32. <https://doi.org/10.1021/jacs.8b13029>.
- (16) Joshi, D. K.; Sutton, J. W.; Carver, S.; Blanchard, J. P. Experiences with Commercial Production Scale Operation of Dissolving Metal Reduction Using Lithium Metal and Liquid Ammonia. *Org. Process Res. Dev.* **2005**, *9* (6), 997–1002. <https://doi.org/10.1021/op050155x>.
- (17) Speckmeier, E.; Fischer, T. G.; Zeitler, K. A Toolbox Approach To Construct Broadly Applicable Metal-Free Catalysts for Photoredox Chemistry: Deliberate Tuning of Redox Potentials and Importance of Halogens in Donor–Acceptor Cyanoarenes. *J. Am. Chem. Soc.* **2018**, *140* (45), 15353–15365. <https://doi.org/10.1021/jacs.8b08933>.
- (18) Peters, B. K.; Rodriguez, K. X.; Reisberg, S. H.; Beil, S. B.; Hickey, D. P.; Kawamata, Y.; Collins, M.; Starr, J.; Chen, L.; Udyavara, S.; Klunder, K.; Gorey, T. J.; Anderson, S. L.; Neurock, M.; Minter, S. D.; Baran, P. S. Scalable and Safe Synthetic Organic Electroreduction Inspired by Li-Ion Battery Chemistry. *Science* **2019**, *363* (6429), 838–845. <https://doi.org/10.1126/science.aav5606>.
- (19) Glaser, F.; Larsen, C. B.; Kerzig, C.; Wenger, O. S. Aryl Dechlorination and Defluorination with an Organic Super-Photoreductant. *Photochem. Photobiol. Sci.* **2020**, *19* (8), 1035–1041. <https://doi.org/10.1039/D0PP00127A>.
- (20) Connell, T. U.; Fraser, C. L.; Czyz, M. L.; Smith, Z. M.; Hayne, D. J.; Doeven, E. H.; Agugiaro, J.; Wilson, D. J. D.; Adcock, J. L.; Scully, A. D.; Gómez, D. E.; Barnett, N. W.; Polyzos, A.; Francis, P. S. The Tandem Photoredox Catalysis Mechanism of [Ir(Ppy)₂(Dtb-Bpy)]⁺ Enabling Access to Energy Demanding Organic Substrates. *J Am Chem Soc* **2019**, *141*, 13.
- (21) Shon, J.-H.; Kim, D.; Rathnayake, M. D.; Sittel, S.; Weaver, J.; Teets, T. S. Photoredox Catalysis on Unactivated Substrates with Strongly Reducing Iridium Photosensitizers. *Chem. Sci.* **2021**, *12* (11), 4069–4078. <https://doi.org/10.1039/D0SC06306A>.
- (22) Kerzig, C.; Guo, X.; Wenger, O. S. Unexpected Hydrated Electron Source for Preparative Visible-Light Driven Photoredox Catalysis. *J. Am. Chem. Soc.* **2019**, *141* (5), 2122–2127. <https://doi.org/10.1021/jacs.8b12223>.
- (23) MacKenzie, I. A.; Wang, L.; Onuska, N. P. R.; Williams, O. F.; Begam, K.; Moran, A. M.; Dunietz, B. D.; Nicewicz, D. A. Discovery and Characterization of an Acridine Radical

- Photoreductant. *Nature* **2020**, *580* (7801), 76–80. <https://doi.org/10.1038/s41586-020-2131-1>.
- (24) Cole, J. P.; Chen, D.-F.; Kudisch, M.; Pearson, R. M.; Lim, C.-H.; Miyake, G. M. Organocatalyzed Birch Reduction Driven by Visible Light. *J. Am. Chem. Soc.* **2020**, *142* (31), 13573–13581. <https://doi.org/10.1021/jacs.0c05899>.
 - (25) Kim, H.; Kim, H.; Lambert, T. H.; Lin, S. Reductive Electrophotocatalysis: Merging Electricity and Light To Achieve Extreme Reduction Potentials. *J. Am. Chem. Soc.* **2020**, *142* (5), 2087–2092. <https://doi.org/10.1021/jacs.9b10678>.
 - (26) Cowper, N. G. W.; Chernowsky, C. P.; Williams, O. P.; Wickens, Z. K. Potent Reductants via Electron-Primed Photoredox Catalysis: Unlocking Aryl Chlorides for Radical Coupling. *J. Am. Chem. Soc.* **2020**. <https://doi.org/10.1021/jacs.9b12328>.
 - (27) Cabby, S.; Bouchet, L. M.; Argüello, J. E.; Rossi, R. A.; Bardagi, J. I. Excitation of Radical Anions of Naphthalene Diimides in Consecutive- and Electro-Photocatalysis**. *ChemCatChem* **2021**, *13* (13), 3001–3009. <https://doi.org/10.1002/cctc.202100359>.
 - (28) Chen, Y.-J.; Lei, T.; Hu, H.-L.; Wu, H.-L.; Zhou, S.; Li, X.-B.; Chen, B.; Tung, C.-H.; Wu, L.-Z. Tandem Photoelectrochemical and Photoredox Catalysis for Efficient and Selective Aryl Halides Functionalization by Solar Energy. *Matter* **2021**. <https://doi.org/10.1016/j.matt.2021.05.004>.
 - (29) Ghosh, I.; Ghosh, T.; Bardagi, J. I.; König, B. Reduction of Aryl Halides by Consecutive Visible Light-Induced Electron Transfer Processes. *Science* **2014**, *346* (6210), 725–728. <https://doi.org/10.1126/science.1258232>.
 - (30) Et₃N can promote premature radical quenching through hydrogen atom transfer and back electron transfer to Et₃N^{•+} For details see ref [7]. *Et₃N can promote premature radical quenching through hydrogen atom transfer and back electron transfer to Et₃N^{•+} For details see ref [7]*.
 - (31) Neumeier, M.; Sampedro, D.; Májek, M.; de la Peña O'Shea, V. A.; Jacobi von Wangelin, A.; Pérez-Ruiz, R. Dichromatic Photocatalytic Substitutions of Aryl Halides with a Small Organic Dye. *Chem. – Eur. J.* **2018**, *24* (1), 105–108. <https://doi.org/10.1002/chem.201705326>.
 - (32) Gosztola, D.; Niemczyk, M. P.; Svec, W.; Lukas, A. S.; Wasielewski, M. R. Excited Doublet States of Electrochemically Generated Aromatic Imide and Diimide Radical Anions. *J. Phys. Chem. A* **2000**, *104* (28), 6545–6551. <https://doi.org/10.1021/jp000706f>.
 - (33) Fujitsuka, M.; Kim, S. S.; Lu, C.; Tojo, S.; Majima, T. Intermolecular and Intramolecular Electron Transfer Processes from Excited Naphthalene Diimide Radical Anions. *J. Phys. Chem. B* **2015**, *119* (24), 7275–7282. <https://doi.org/10.1021/jp510850z>.
 - (34) Nakashima, H.; Honda, Y.; Shida, T.; Nakatsuji, H. Electronic Excitation Spectra of Doublet Anion Radicals of Cyanobenzene and Nitrobenzene Derivatives: SAC-CI Theoretical Studies. *Mol. Phys.* **2015**, *113* (13–14), 1728–1739. <https://doi.org/10.1080/00268976.2015.1008064>.
 - (35) La Porte, N. T.; Martinez, J. F.; Chaudhuri, S.; Hedström, S.; Batista, V. S.; Wasielewski, M. R. Photoexcited Radical Anion Super-Reductants for Solar Fuels Catalysis. *Coord. Chem. Rev.* **2018**, *361*, 98–119. <https://doi.org/10.1016/j.ccr.2018.01.018>.
 - (36) Fox, M. Anne. The Photoexcited States of Organic Anions. *Chem. Rev.* **1979**, *79* (3), 253–273. <https://doi.org/10.1021/cr60319a002>.
 - (37) Yu, Y.; Guo, P.; Zhong, J.-S.; Yuan, Y.; Ye, K.-Y. Merging Photochemistry with Electrochemistry in Organic Synthesis. *Org. Chem. Front.* **2019**, *7* (1), 131–135. <https://doi.org/10.1039/C9QO01193E>.
 - (38) Barham, J. P.; König, B. Synthetic Photoelectrochemistry. *Angew. Chem. Int. Ed.* **2020**, *59* (29), 11732–11747. <https://doi.org/10.1002/anie.201913767>.

- (39) Liu, J.; Lu, L.; Wood, D.; Lin, S. New Redox Strategies in Organic Synthesis by Means of Electrochemistry and Photochemistry. *ACS Cent. Sci.* **2020**, 6 (8), 1317–1340. <https://doi.org/10.1021/acscentsci.0c00549>.
- (40) Huang, H.; Lambert, T. H. Electrophotocatalytic SNAr Reactions of Unactivated Aryl Fluorides at Ambient Temperature and Without Base. *Angew. Chem. Int. Ed.* **2020**, 59 (2), 658–662. <https://doi.org/10.1002/anie.201909983>.
- (41) Huang, H.; Strater, Z. M.; Rauch, M.; Shee, J.; Sisto, T. J.; Nuckolls, C.; Lambert, T. H. Electrophotocatalysis with a Trisaminocyclopropenium Radical Dication. *Angew. Chem. Int. Ed.* **2019**, 58 (38), 13318–13322. <https://doi.org/10.1002/anie.201906381>.
- (42) Huang, H.; Strater, Z. M.; Lambert, T. H. Electrophotocatalytic C–H Functionalization of Ethers with High Regioselectivity. *J. Am. Chem. Soc.* **2020**, 142 (4), 1698–1703. <https://doi.org/10.1021/jacs.9b11472>.
- (43) Chen, C.; Wang, M.; Lu, H.; Zhao, B.; Shi, Z. Enabling the Use of Alkyl Thianthrenium Salts in Cross-Coupling Reactions by Copper Catalysis. *Angew. Chem. Int. Ed.* **2021**, 60 (40), 21756–21760. <https://doi.org/10.1002/anie.202109723>.
- (44) Capaldo, L.; Quadri, L. L.; Ravelli, D. Merging Photocatalysis with Electrochemistry: The Dawn of a New Alliance in Organic Synthesis. *Angew. Chem. Int. Ed.* **2019**, 58 (49), 17508–17510. <https://doi.org/10.1002/anie.201910348>.
- (45) Yan, H.; Hou, Z.-W.; Xu, H.-C. Photoelectrochemical C–H Alkylation of Heteroarenes with Organotrifluoroborates. *Angew. Chem. Int. Ed.* **2019**, 58 (14), 4592–4595. <https://doi.org/10.1002/anie.201814488>.
- (46) Wu, S.; Žurauskas, J.; Domański, M.; Hitzfeld, P. S.; Butera, V.; Scott, D. J.; Rehbein, J.; Kumar, A.; Thyrhaug, E.; Hauer, J.; Barham, J. P. Hole-Mediated Photoredox Catalysis: Tris(*p*-Substituted)Biarylammonium Radical Cations as Tunable, Precomplexing and Potent Photooxidants. *Org. Chem. Front.* **2021**, 8 (6), 1132–1142. <https://doi.org/10.1039/D0QO01609H>.
- (47) barham oxidation note. *barham oxidation note*.
- (48) Qiu, Y.; Scheremetjew, A.; Finger, L. H.; Ackermann, L. Electrophotocatalytic Undirected C–H Trifluoromethylations of (Het)Arenes. *Chem. – Eur. J.* *n/a* (n/a). <https://doi.org/10.1002/chem.201905774>.
- (49) Far fewer examples exist of electrophotochemical reductions compared to oxidative electrophotochemistry—the existing reports exclusively activating aryl chloride substrates. For details see refs: [25], [26], [27], [28]. *Far fewer examples exist of electrophotochemical reductions compared to oxidative electrophotochemistry—the existing reports exclusively activating aryl chloride substrates. For details see refs: [25], [26], [27], [28].*
- (50) While this manuscript was under review, an electrophotocatalytic reductive olefination system was reported. This new system relied on careful tuning of a naphthene imide core structure, see: *Angew. Chem. Int. Ed.* 10.1002/anie.202105895. *While this manuscript was under review, an electrophotocatalytic reductive olefination system was reported. This new system relied on careful tuning of a naphthene imide core structure, see: Angew. Chem. Int. Ed. 10.1002/anie.202105895.*
- (51) *Aniline substrates can be converted into diazonium salts, which readily undergo reductive fragmentation to aryl radical intermediates. However, these salts are explosive and the conditions to generate them are highly oxidizing. For more information, see: [52], [53], [54].*
- (52) Oger, N.; Grogne, E. L.; Felpin, F.-X. Handling Diazonium Salts in Flow for Organic and Material Chemistry. *Org. Chem. Front.* **2015**, 2 (5), 590–614. <https://doi.org/10.1039/C5QO00037H>.
- (53) Chakma, P.; Digby, Z. A.; Shulman, M. P.; Kuhn, L. R.; Morley, C. N.; Sparks, J. L.; Konkolewicz, D. Anilinium Salts in Polymer Networks for Materials with Mechanical Stability

- and Mild Thermally Induced Dynamic Properties. *ACS Macro Lett.* **2019**, 8 (2), 95–100. <https://doi.org/10.1021/acsmacrolett.8b00819>.
- (54) Washington, J. B. Trialkylammonium Salt Degradation: Implications for Methylation and Cross-Coupling. *Chem Sci* **2021**, 15.
- (55) Azzena, U.; Denurra, T.; Melloni, G.; Fenude, E.; Rassu, G. Electron-Transfer-Induced Reductive Demethoxylation of Anisole: Evidence for Cleavage of a Radical Anion. *J. Org. Chem.* **1992**, 57 (5), 1444–1448. <https://doi.org/10.1021/jo00031a022>.
- (56) Xu, H.; Yu, B.; Zhang, H.; Zhao, Y.; Yang, Z.; Xu, J.; Han, B.; Liu, Z. Reductive Cleavage of Inert Aryl C–O Bonds to Produce Arenes. *Chem. Commun.* **2015**, 51 (61), 12212–12215. <https://doi.org/10.1039/C5CC03563E>.
- (57) Jin, S.; Dang, Hang. T.; Haug, G. C.; He, R.; Nguyen, V. D.; Nguyen, V. T.; Arman, H. D.; Schanze, K. S.; Larionov, O. V. Visible Light-Induced Borylation of C–O, C–N, and C–X Bonds. *J. Am. Chem. Soc.* **2020**, 142 (3), 1603–1613. <https://doi.org/10.1021/jacs.9b12519>.
- (58) Wang, S.; Wang, H.; König, B. Photo-Induced Thiolate Catalytic Activation of Inert Caryl-Hetero Bonds for Radical Borylation. *Chem* **2021**. <https://doi.org/10.1016/j.chempr.2021.04.016>.
- (59) Kalvet, I.; Deckers, K.; Funes-Ardoiz, I.; Magnin, G.; Sperger, T.; Kremer, M.; Schoenebeck, F. Selective Ortho-Functionalization of Adamantylarenes Enabled by Dispersion and an Air-Stable Palladium(I) Dimer. *Angew. Chem. Int. Ed.* **2020**, 59 (20), 7721–7725. <https://doi.org/10.1002/anie.202001326>.
- (60) Duclos, R. I.; Lu, D.; Guo, J.; Makriyannis, A. Synthesis and Characterization of 2-Substituted Bornane Pharmacophores for Novel Cannabinergic Ligands. *Tetrahedron Lett.* **2008**, 49 (39), 5587–5589. <https://doi.org/10.1016/j.tetlet.2008.07.029>.
- (61) Manmade, A.; Marshall, J. L.; Minns, R. A.; Dalzell, H.; Razdan, R. K. Total Synthesis of (+,–)-3-Deoxy-7,8-Dihydromorphinone. *J. Org. Chem.* **1982**, 47 (9), 1717–1721. <https://doi.org/10.1021/jo00348a022>.
- (62) Paras, N. A.; MacMillan, D. W. C. The Enantioselective Organocatalytic 1,4-Addition of Electron-Rich Benzenes to α,β -Unsaturated Aldehydes. *J. Am. Chem. Soc.* **2002**, 124 (27), 7894–7895. <https://doi.org/10.1021/ja025981p>.
- (63) Aviv, H.; Bar, R.; Schickler, M.; Amselem, S. United States Patent Application: 0040110827 - High Enantiomeric Purity Dexanabinol for Pharmaceutical Compositions. 20040110827, A1. <https://appft1.uspto.gov/netacgi/nph-Parser?Sect1=PTO1&Sect2=HITOFF&d=PG01&p=1&u=%2Fnetacgi%2FPTO%2Fsrchnu.html&r=1&f=G&l=50&s1=%2220040110827%22.PGNR.&OS=DN/20040110827&RS=DN/20040110827> (accessed 2021-05-28).
- (64) Paras, N. A.; Simmons, B.; MacMillan, D. W. C. A Process for the Rapid Removal of Dialkylamino-Substituents from Aromatic Rings. Application to the Expedient Synthesis of (R)-Tolterodine. *Tetrahedron* **2009**, 65 (16), 3232–3238. <https://doi.org/10.1016/j.tet.2008.12.054>.
- (65) Burgett, A. W. G.; Li, Q.; Wei, Q.; Harran, P. G. A Concise and Flexible Total Synthesis of (–)-Diazonamide A. *Angew. Chem. Int. Ed.* **2003**, 42 (40), 4961–4966. <https://doi.org/10.1002/anie.200352577>.
- (66) Kodama, S.; Hamashima, Y.; Nishide, K.; Node, M. Total Synthesis of (–)-Galanthamine by Remote Asymmetric Induction. *Angew. Chem. Int. Ed.* **2004**, 43 (20), 2659–2661. <https://doi.org/10.1002/anie.200353636>.
- (67) Since halogen atom transfer relies on bond strength and polarizability, the vast majority of examples involve organoiodide or organobromide substrates. *Since halogen atom transfer relies on bond strength and polarizability, the vast majority of examples involve organoiodide or organobromide substrates.*

- (68) Constantin, T.; Zanini, M.; Regni, A.; Sheikh, N. S.; Juliá, F.; Leonori, D. Aminoalkyl Radicals as Halogen-Atom Transfer Agents for Activation of Alkyl and Aryl Halides. *Science* **2020**, 367 (6481), 1021–1026. <https://doi.org/10.1126/science.aba2419>.
- (69) Constantin, T.; Juliá, F.; Sheikh, N. S.; Leonori, D. A Case of Chain Propagation: α -Aminoalkyl Radicals as Initiators for Aryl Radical Chemistry. *Chem. Sci.* **2020**, 11 (47), 12822–12828. <https://doi.org/10.1039/D0SC04387G>.
- (70) Costentin, C.; Fortage, J.; Collomb, M.-N. Electrophotocatalysis: Cyclic Voltammetry as an Analytical Tool. *J. Phys. Chem. Lett.* **2020**, 11 (15), 6097–6104. <https://doi.org/10.1021/acs.jpclett.0c01662>.
- (71) Fujita, M.; Ishida, A.; Majima, T.; Takamuku, S. Lifetimes of Radical Anions of Dicyanoanthracene, Phenazine, and Anthraquinone in the Excited State from the Selective Electron-Transfer Quenching. *J. Phys. Chem.* **1996**, 100 (13), 5382–5387. <https://doi.org/10.1021/jp953203w>.
- (72) Eggins, B. R.; Robertson, P. K. J. Photoelectrochemistry Using Quinone Radical Anions. *J. Chem. Soc. Faraday Trans.* **1994**, 90 (15), 2249–2256. <https://doi.org/10.1039/FT9949002249>.
- (73) Fujitsuka, M.; Majima, T. Reaction Dynamics of Excited Radical Ions Revealed by Femtosecond Laser Flash Photolysis. *J. Photochem. Photobiol. C Photochem. Rev.* **2018**, 35, 25–37. <https://doi.org/10.1016/j.jphotochemrev.2017.12.003>.
- (74) Compton, R. G.; Coles, B. A.; Pilkington, M. B. G. Photoelectrochemical Electron Spin Resonance. Part 3.—The Reduction of Fluorescein: A 'Photo-DISP2' Reaction. *J. Chem. Soc. Faraday Trans. 1 Phys. Chem. Condens. Phases* **1988**, 84 (12), 4347. <https://doi.org/10.1039/f19888404347>.
- (75) Targos, K.; Williams, O. P.; Wickens, Z. K. Unveiling Potent Photooxidation Behavior of Catalytic Photoreductants. *J. Am. Chem. Soc.* **2021**, 143 (11), 4125–4132. <https://doi.org/10.1021/jacs.1c00399>.
- (76) *Given recent work from Nicewicz [23] and our group [77] that suggested that the odd electron congener of two common photoredox catalysts was photocatalytically active, we hypothesized that photochemical activity of oxidized and reduced photocatalysts might be a more general phenomenon.*
- (77) Koike, T.; Akita, M. Visible-Light Radical Reaction Designed by Ru- and Ir-Based Photoredox Catalysis. *Inorg Chem Front* **2014**, 1 (8), 562–576. <https://doi.org/10.1039/C4QI00053F>.
- (78) Shang, T.-Y.; Lu, L.-H.; Cao, Z.; Liu, Y.; He, W.-M.; Yu, B. Recent Advances of 1,2,3,5-Tetrakis(Carbazol-9-Yl)-4,6-Dicyanobenzene (4CzIPN) in Photocatalytic Transformations. *Chem. Commun.* **2019**, 55 (38), 5408–5419. <https://doi.org/10.1039/C9CC01047E>.
- (79) *We also questioned whether these catalysts could act either directly as photoreductants or electrochemically mediate the transformation (without input of light). Given that the PC/PC•– couple is more negative in each case than the PC*/PC•+ couple, we conducted control experiments with each catalyst in the dark and found none furnished defunctionalized product without irradiation.*
- (80) Giedyk, M.; Narobe, R.; Weiß, S.; Touraud, D.; Kunz, W.; König, B. Photocatalytic Activation of Alkyl Chlorides by Assembly-Promoted Single Electron Transfer in Microheterogeneous Solutions. *Nat. Catal.* **2020**, 3 (1), 40–47. <https://doi.org/10.1038/s41929-019-0369-5>.
- (81) Singh, P. P.; Srivastava, V. Recent Advances in Using 4DPAIPN in Photocatalytic Transformations. *Org. Biomol. Chem.* **2021**, 19 (2), 313–321. <https://doi.org/10.1039/D0OB01884H>.
- (82) *While these data suggest reductive generation of the radical anion of 4-DPAIPN is necessary for reaction success, at this stage, we cannot exclude subsequent*

functionalization of the radical anion to form a secondary photoactive species, which could be either closed or open shell.

- (83) *While direct electrolysis at deeply reducing potentials or C(sp²)-O homolysis via high energy UV light can rupture these bonds, these approaches remain limited. For examples, see: ref [56], [84] and [85].*
- (84) Mfuh, A. M.; Doyle, J. D.; Chhetri, B.; Arman, H. D.; Larionov, O. V. Scalable, Metal- and Additive-Free, Photoinduced Borylation of Haloarenes and Quaternary Arylammonium Salts. *J. Am. Chem. Soc.* **2016**, 138 (9), 2985–2988. <https://doi.org/10.1021/jacs.6b01376>.
- (85) Liu, W.; Yang, X.; Gao, Y.; Li, C.-J. Simple and Efficient Generation of Aryl Radicals from Aryl Triflates: Synthesis of Aryl Boronates and Aryl Iodides at Room Temperature. *J. Am. Chem. Soc.* **2017**, 139 (25), 8621–8627. <https://doi.org/10.1021/jacs.7b03538>.
- (86) Calloway, N. O. The Friedel-Crafts Syntheses. *Chem. Rev.* **1935**, 17 (3), 327–392. <https://doi.org/10.1021/cr60058a002>.
- (87) BLICKE, F. F.; McCARTY, F. J. The Use of Substituted Phenols in the Mannich Reaction and the Dehalogenation of Aminomethylhalophenols. *J. Org. Chem.* **1959**, 24 (8), 1061–1069. <https://doi.org/10.1021/jo01090a008>.
- (88) Omura, Y.; Taruno, Y.; Irisa, Y.; Morimoto, M.; Saimoto, H.; Shigemasa, Y. Regioselective Mannich Reaction of Phenolic Compounds and Its Application to the Synthesis of New Chitosan Derivatives. *Tetrahedron Lett.* **2001**, 42 (41), 7273–7275. [https://doi.org/10.1016/S0040-4039\(01\)01491-5](https://doi.org/10.1016/S0040-4039(01)01491-5).
- (89) Cuny, G. D. Synthesis of (±)-Aporphine Utilizing Pictet–Spengler and Intramolecular Phenol Ortho-Arylation Reactions. *Tetrahedron Lett.* **2004**, 45 (26), 5167–5170. <https://doi.org/10.1016/j.tetlet.2004.04.194>.
- (90) Huang, Z.; Lumb, J.-P. Phenol-Directed C–H Functionalization. *ACS Catal* **2019**, 35.
- (91) Roberts, R. M. *Friedel-Crafts Alkylation Chemistry: A Century of Discovery*; M. Dekker, [1984] ©1984: New York, 1984.
- (92) Lu, D.; Nikas, S. P.; Han, X.-W.; Parrish, D. A.; Makriyannis, A. Synthesis and Characterization of a Compact Tricyclic Resorcinol from (+)- and (À)-3-Pinanol. *Tetrahedron Lett.* **2012**, 3.
- (93) Hong, S. H.; Day, M. W.; Grubbs, R. H. Decomposition of a Key Intermediate in Ruthenium-Catalyzed Olefin Metathesis Reactions. *J. Am. Chem. Soc.* **2004**, 126 (24), 7414–7415. <https://doi.org/10.1021/ja0488380>.
- (94) Blackmond, D. G. Reaction Progress Kinetic Analysis: A Powerful Methodology for Mechanistic Studies of Complex Catalytic Reactions. *Angew. Chem. Int. Ed.* **2005**, 44 (28), 4302–4320. <https://doi.org/10.1002/anie.200462544>.
- (95) *Altering electrolyte identity to lithium perchlorate as well as increasing electrolyte concentration significantly improved reproducibility of current traces of both 4-DPAIPN and NpMI with little to no impact on substrate conversion or product yield. Altering electrolyte identity to lithium perchlorate as well as increasing electrolyte concentration.*
- (96) *We validated that current correlated to reaction rate by comparing the reaction profiles obtained via aliquot-based GC measurements to the current readout. These data indicated that current was directly proportional to reaction rate but required a minor scalar correction factor for faradaic efficiency. See SI for details.*
- (97) *If catalyst is not decomposing, the rate of substrate conversion should be independent of previous catalyst turnovers. Therefore, for a well-behaved system, rate of conversion should be identical across multiple reactions at each substrate concentration. Accordingly, plotting rate vs. [substrate] for reactions with different initial substrate concentration should overlay. Lack of overlay indicates that different amounts of catalyst are active, which could be explained by either catalyst death or product inhibition. For a detailed discussion of RPKA, see ref [94].*

- (98) *Previous studies have found that 4-CzIPN can decompose via attack by carbon-centered radical intermediates. It is possible that 4-DPAIPN could undergo analogous decomposition mechanisms with radical intermediates. For examples, see: refs [99], [100], [101].*
- (99) Grotjahn, S.; König, B. Photosubstitution in Dicyanobenzene-Based Photocatalysts. *Org. Lett.* **2021**, 23 (8), 3146–3150. <https://doi.org/10.1021/acs.orglett.1c00836>.
- (100) Donabauer, K.; Maity, M.; Berger, A. L.; Huff, G. S.; Crespi, S.; König, B. Photocatalytic Carbanion Generation – Benzylolation of Aliphatic Aldehydes to Secondary Alcohols. *Chem. Sci.* **2019**, 10 (19), 5162–5166. <https://doi.org/10.1039/C9SC01356C>.
- (101) Kong, D.; Munch, M.; Qiqige, Q.; Cooze, C. J. C.; Rotstein, B. H.; Lundgren, R. J. Fast Carbon Isotope Exchange of Carboxylic Acids Enabled by Organic Photoredox Catalysis. *J. Am. Chem. Soc.* **2021**, 143 (5), 2200–2206. <https://doi.org/10.1021/jacs.0c12819>.

3.7. Supplemental Information

3.7.1 General Methods and Materials

Unless otherwise noted, reactions were performed under an inert N₂ atmosphere in an anhydrous solvent thoroughly degassed by freeze-pump-thaw. DMF was dried by passing through activated alumina columns. All tetra-butylammonium electrolyte salts and lithium perchlorate electrolyte salts were recrystallized from hot ethyl acetate prior to use. Unless otherwise noted, other commercially-available reagents were used as received. Crude mixtures were evaluated by thin-layer chromatography using EMD/Merck silica gel 60 F254 pre-coated plates (0.25 mm) and were visualized by UV, CAM, p-anisaldehyde, or KMnO₄ staining. Flash chromatography was performed with a Biotage Isolera One automated chromatography system with re-packed silica columns (technical grade silica, pore size 40 Å, 230-400 mesh particle size, 40-63 particle size). Purified materials were dried in vacuo (0.050 Torr) to remove trace solvent. ¹H, ¹³C, ³¹P Spectra were taken using a Bruker Avance-400 with a BBFO Probe or a Bruker Avance-500 with a DCH Cryoprobe. NMR data are reported relative to residual CHCl₃ (¹H, δ = 7.26 ppm), CDCl₃ (¹³C, δ = 77.16 ppm). Data for ¹H NMR spectra are reported as follows: chemical shift (δ ppm) (multiplicity, coupling constant (Hz), integration). Multiplicity and qualifier abbreviations are as follows: s = singlet, d = doublet, t = triplet, q = quartet, m = multiplet, br = broad. EPR spectra were taken using a Bruker EleXsys E500 instrument with the following parameters:

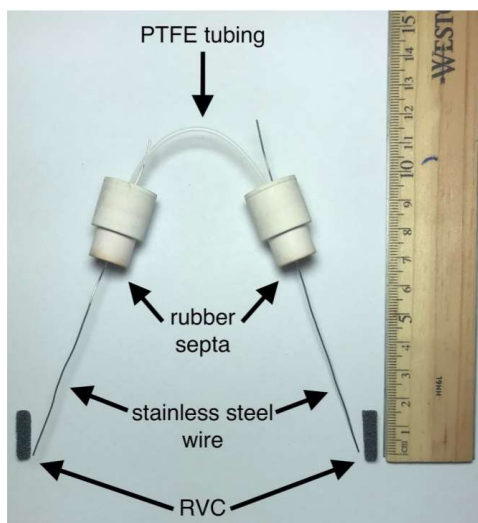
Microwave power = 0.6325 mW
 Center Field = 3497.8 G
 Sweep Width = 100.0 G
 Receiver Gain = 40.0 dB
 Modulation frequency = 100.0 kHz
 Modulation amplitude = 1.000 G
 Time Constant = 1.28 ms
 Conversion Time = 5.12 s
 Resolution = 1024 points

GC traces were taken on an Agilent 7890A GC with dual DB-5 columns (20 m × 180 μ m × 0.18 μ m), dual FID detectors, and hydrogen as the carrier gas.

3.7.2 Electrochemical Equipment and Experimental Set-Up

All cyclic voltametric and controlled potential measurements were performed at room temperature using a Pine WaveNowXV. The CV experiments were carried out in a three-electrode cell configuration with a glassy carbon (GC) working electrode (3 mm diameter, unless otherwise stated) and a platinum wire counter electrode. CV experiments were carried out with a 0.1 M ⁿBu₄NPF₆ in DMF solution. Bulk constant potential experiments were carried out in divided H cells with RVC (10 × 5 × 5mm) as working and counter electrodes affixed to stainless steel wire. The potentials were measured versus an Ag/AgNO₃ (0.01 M in MeCN with 0.01M ⁿBu₄NPF₆) reference electrode (all electrodes from Pine Research). LEDs (PAR20-18W LG 405 nm) used in this study were purchased from HepatoChem (PAR20-18W LG 405 nm) and Kessil (KSPR160L-390, KSPR160L-427, KSPR160L-440).

Electrode Assembly and Fabrication:



Polytetrafluoroethylene (PTFE) tubing purchased from Cole-Parmer; 1/32" ID, 1/16" OD, item number EW-06407-41. 14/20 Rubber septa purchased from VWR, item number 89064-940. Stainless steel wire purchased from Grainger; stainless steel lockwire, 0.025" diameter, item number 16Y043. Reticulated vitreous carbon (RVC) purchased from SELEE Corporation; 80 ppi, 04-07 g/cc, cut into 15×3×5 mm pieces.

H-Type Cell Fabrication:



Divided cell fabricated in-house (*FUSION, Journal of the ASGS*, **2020**, 67, 4, 19-26). Porosity E glass filter disc purchased from Ace Glass; 8 mm diameter, part number 7176-21.

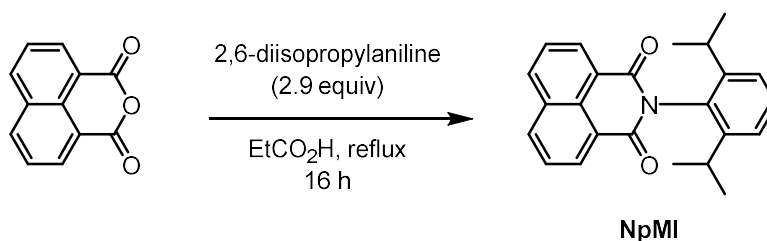
Standard reaction setup:



3.7.3 Catalyst Exploration

Synthesis of Non-Commercial Catalysts

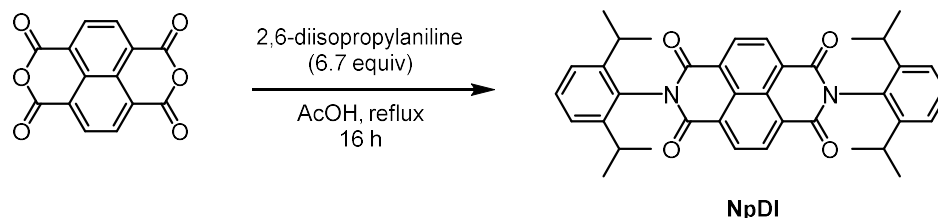
2-(2,6-diisopropylphenyl)-1H-benzo[de]isoquinoline-1,3(2H)-dione (**NpMI**)



A flame dried RBF was charged with 1,8-naphthalic anhydride (6.73 g, 34.0 mmol, 1 equiv) and propanoic acid (100 mL) under nitrogen atmosphere. The solution was stirred at room temperature and 2,6-diisopropylaniline (19.0 mL, 17.9 g, 100 mmol, 2.9 equiv) was added. Solution was stirred at reflux for 16 hours and then cooled to room temperature. Mixture was diluted with water (100 mL) and the precipitate was collected by vacuum filtration and washed with water (2x25 mL) and hexanes (3x25 mL). Precipitate was dried *in vacuo* and the crude product was recrystallized from hot CHCl₃ (150 mL)/hexanes (175 mL) mixture, slowly cooled to -20°C overnight to yield an off-white crystalline product pure by NMR (11.21 g, 92% yield). *For best results*, the aryl imide product was recrystallized a second time from CHCl₃ (100 mL) and hexanes (200 mL) by later diffusion at -20 °C to provide pure product as a white crystalline solid (8.28 g, 23.2 mmol, 68% yield). **¹H NMR** (500 MHz, CDCl₃) δ 8.67 (dd, J = 7.2, 1.1 Hz, 2H), 8.30 (dd, J = 8.3, 1.1 Hz, 2H), 7.81 (dd, J = 8.2, 7.2 Hz, 2H), 7.47 (t, J = 7.8 Hz, 1H), 7.33 (d, J = 7.8 Hz, 2H), 2.75 (p, J = 6.8 Hz, 2H), 1.16 (d, J = 6.8 Hz, 12H). **¹³C NMR** (126 MHz, CDCl₃) δ 164.35, 145.82, 134.31, 131.99, 131.88, 131.00, 129.63, 128.98, 127.18, 124.16, 122.94, 29.27,

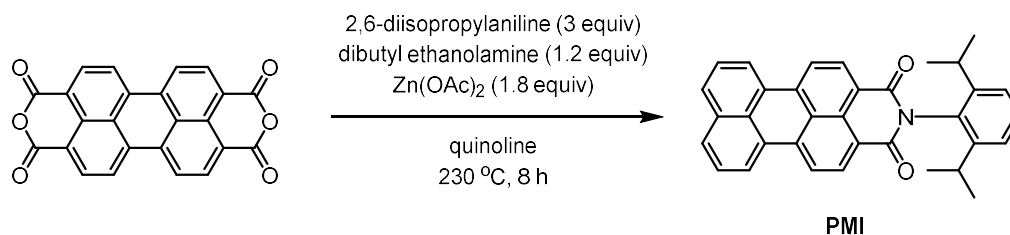
24.13. **HRMS** (ESI+) Calc: $[M+H]^+$ ($C_{24}H_{23}NO_2$) 358.1802; measured: 358.1802 = 2.0 ppm difference.

2,7-bis(2,6-diisopropylphenyl)benzo[*lmn*][3,8]phenanthroline-1,3,6,8(2*H*,7*H*)-tetraone (NpDI)



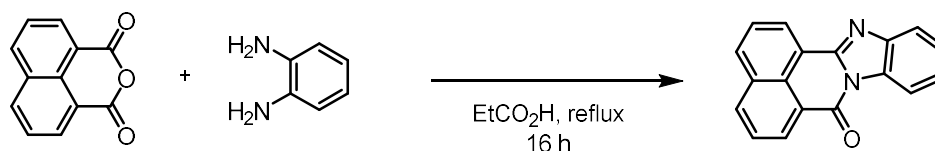
A flame dried RBF was charged with 1,4,5,8-naphthalene-tetracarboxylic dianhydride (1.34 g, 5.0 mmol, 1 equiv) and acetic acid (70 mL) under nitrogen atmosphere. The solution was stirred at room temperature and 2,6-diisopropylaniline (6.32 mL, 5.94 g, 33.5 mmol, 6.7 equiv) was added. Solution was stirred at reflux for 16 hours and then cooled to room temperature. Mixture was diluted with water (70 mL) and the precipitate was collected by vacuum filtration and washed with water (2x25 mL) and hexanes (3x25 mL). Precipitate was dried *in vacuo* and the crude product was recrystallized from hot $CHCl_3$ (150 mL)/hexanes (175 mL) mixture, slowly cooled to $-20^\circ C$ overnight to yield an off-white crystalline solid (2.59 g, 4.41 mmol, 88% yield). **1H NMR** (500 MHz, $CDCl_3$) δ 8.89 (s, 4H), 7.52 (t, $J = 7.8$ Hz, 2H), 7.36 (d, $J = 7.8$ Hz, 4H), 2.71 (p, $J = 6.8$ Hz, 4H), 1.17 (d, $J = 6.9$ Hz, 24H), consistent with reported spectra (*Org. Lett.*, **2010**, 12, 15, 3460).

2-(2,6-diisopropylphenyl)-1*H*-benzo[10,5]anthra[2,1,9-*def*]isoquinoline-1,3(2*H*)-dione (PMI)



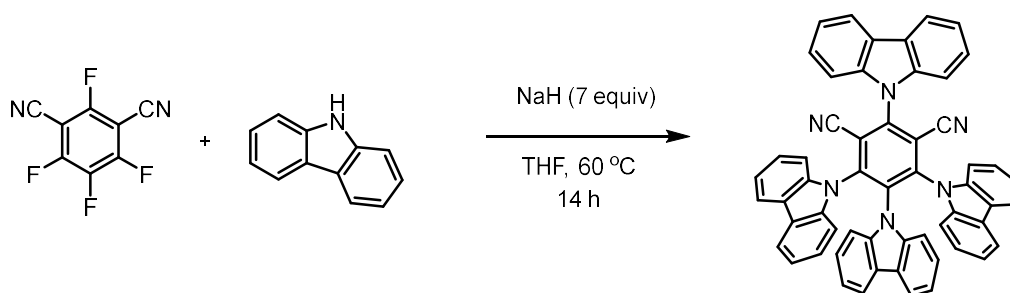
To a flame dried round bottom flask was added perylene anhydride (4.0 g, 10.0 mmol, 1 equiv.) and zinc acetate (3.4 g, 19.0 mmol, 1.8 equiv). Quinoline (15 mL, distilled) was added to the mixture under a nitrogen atmosphere followed by dibutyl ethanolamine (2.4 mL, 12.0 mmol, 1.2 equiv) and diisopropylaniline (5.7 mL, 30.0 mmol, 3.0 equiv). The solution was heated to $230^\circ C$ and stirred under nitrogen for 8 hours. The reaction mixture was then poured into ethanol (500 mL) and the precipitate was collected. The solid crude mixture was then dispersed in a mixture of ethanol (20 mL) and 20% sulfuric acid (4 mL) and filtered again. The crude solid was dried before dissolving in chloroform and washing with 1 M HCl followed by brine. The organic layer was dried over $MgSO_4$, filtered and concentrated. The crude reaction mixture was then further purified by column chromatography to yield a red solid (2.9 g, 60%). **1H NMR** (500 MHz, $CDCl_3$) δ 8.68 (d, $J = 8.0$ Hz, 2H), 8.50 (t, $J = 7.5$ Hz, 4H), 7.94 (d, $J = 8.1$ Hz, 2H), 7.67 (t, $J = 7.8$ Hz, 2H), 7.51 – 7.44 (m, 1H), 7.34 (d, $J = 7.7$ Hz, 2H), 2.77 (p, $J = 6.9$ Hz, 2H), 1.18 (d, $J = 6.8$ Hz, 12H), consistent with reported spectra (*J. Org. Chem.* 2018, 83, 10, 5339–5346).

7H-benzo[de]benzo[4,5]imidazo[2,1-a]isoquinolin-7-one (Nplmz)



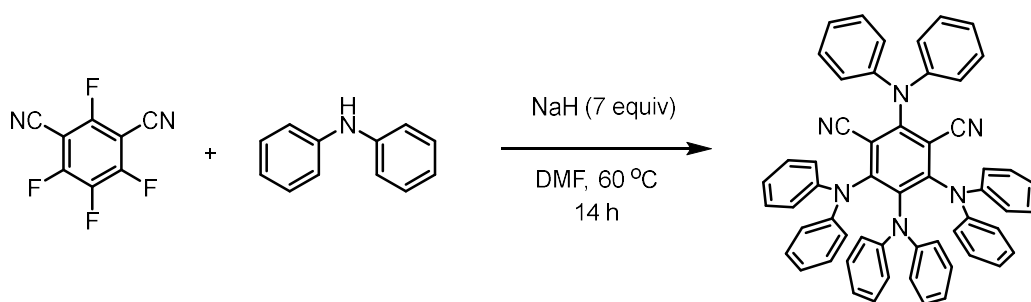
A flame dried RBF was charged with 2-aminoaniline (2.5 g, 23 mmol, 1 equiv) and propanoic acid (70 mL) under nitrogen atmosphere. The solution was stirred at room temperature and 1,8-naphthalic anhydride (9.2 g, 46 mmol, 2 equiv) was added. Solution was stirred at reflux for 16 hours and then cooled to room temperature. Mixture was diluted with water (70 mL) and the precipitate was collected by vacuum filtration and washed with hexanes (3x25 mL). Precipitate was diluted in CHCl₃ and remaining water was separated. Crude product was purified by column chromatography on silica gel (EtOAc:10%hexanes/CHCl₃). Product was collected and an orange impurity was oiled out by adding hexanes and EtOAc/CHCl₃. Enriched product solution was decanted off and concentrated to yield a bright yellow solid (5.1 g, 18.9 mmol, 82%). ¹H NMR (500 MHz, CDCl₃) δ 8.96 (d, J = 7.5 Hz, 1H), 8.85 (dd, J = 7.3, 1.2 Hz, 1H), 8.61 (dd, J = 6.5, 2.9 Hz, 1H), 8.21 (d, J = 8.2 Hz, 1H), 7.97 – 7.91 (m, 1H), 7.57 – 7.50 (m, 2H), 7.15 (dd, J = 8.1, 1.5 Hz, 1H), 7.00 – 6.93 (m, 2H). consistent with reported spectra (*J. Org. Chem.* **2019**, 84, 12, 8337-8343).

2,4,5,6-tetra(9H-carbazol-9-yl)isophthalonitrile (4-CzIPN)



A flame dried RBF was charged with NaH (60% dispersion, 3.0 g, 75 mmol, 7 equiv) and placed under nitrogen atmosphere and THF (100 mL) was added to the flask. In a separate flask, 1-H-carbazole (8.4 g, 50 mmol, 5 equiv) was dissolved in THF (25 mL) and the solution was added dropwise to the reaction flask and the solution was heated to 60 °C and stirred for 1 hour. In a separate flask, 2,4,5,6-tetrafluoroisophthalonitrile (2.0 g, 10 mmol, 1 equiv) was dissolved in THF (25 mL) and the solution was added dropwise to the reaction vessel and the solution was cooled and stirred at 40 °C overnight. Reaction was cooled to room temperature and excess NaH was quenched by adding isopropanol dropwise. Water (200 mL) was added to precipitate crude product. Precipitate was collected by filtration and washed with water and dried *in vacuo*. Crude product was purified by dissolving in DCM passing through a silica plug and recrystallized from DCM/hexanes to provide pure product as a bright yellow solid (6.5 g, 8.2 mmol, 82 %). ¹H NMR (500 MHz, CDCl₃) δ 8.24 (d, J = 7.8 Hz, 2H), 7.73 (m, 8H), 7.51 (ddd, J = 8.0, 6.7, 1.5 Hz, 2H), 7.35 (m, 2H), 7.25 (dd, J = 7.8, 1.4 Hz, 4H), 7.11 (tt, J = 7.4, 5.8 Hz, 8H), 6.85 (m, 4H), 6.65 (td, J = 7.7, 1.2 Hz, 2H), consistent with reported spectra (*Chem. Eur. J.* **2016**, 22, 4889-4898).

2,4,5,6-tetrakis(diphenylamino)isophthalonitrile (4-DPAIPN)

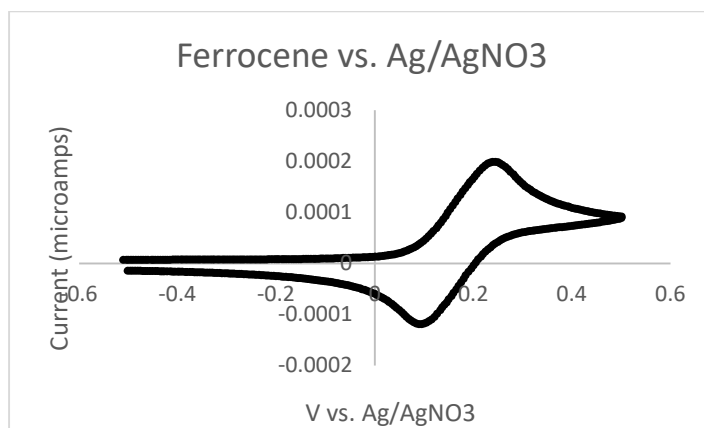


A flame dried RBF was charged with NaH (60% dispersion, 3.0 g, 75 mmol, 7 equiv) and placed under nitrogen atmosphere and DMF (100 mL) was added to the flask. In a separate flask, diphenylamine (8.5 g, 50 mmol, 5 equiv) was dissolved in DMF (25 mL) and the solution was added dropwise to the reaction flask and the solution was heated to 60 °C and stirred for 1 hour. In a separate flask, 2,4,5,6-tetrafluoroisophthalonitrile (2.0 g, 10 mmol, 1 equiv) was dissolved in DMF (25 mL) and the solution was added dropwise to the reaction vessel and the solution was cooled and stirred at 40 °C overnight. Reaction was cooled to room temperature and excess NaH was quenched by adding isopropanol dropwise. Water (200 mL) was added to precipitate crude product. Precipitate was collected by filtration and washed with water and dried *in vacuo*. Crude product was purified by dissolving in DCM passing through a silica plug and recrystallized from DCM/hexanes to provide pure product as a yellow solid (5.2 g, 6.6 mmol, 66%). **¹H NMR** (500 MHz, CDCl₃) δ 7.35 – 7.24 (m, 4H), 7.15 – 7.07 (m, 12H), 7.07 – 7.01 (m, 2H), 6.97 – 6.86 (m, 8H), 6.75 – 6.69 (m, 10H), 6.58 (d, J = 7.5 Hz, 4H). Consistent with reported spectra (*Angew. Chem. Int. Ed.* **2019**, 131, 8266-8270).

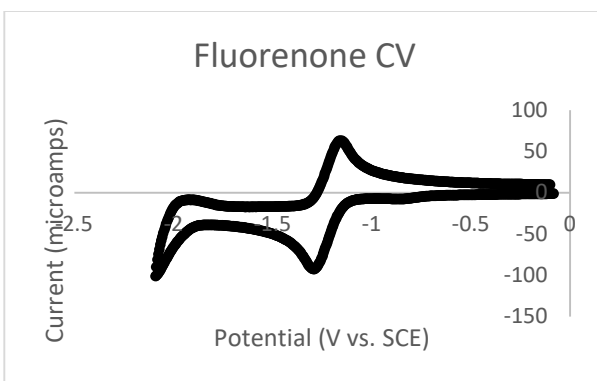
Cyclic Voltammograms

All CV measurements were conducted in DMF against Ag/AgNO₃ (0.01 M in MeCN) reference cell and 0.1 M ⁿBu₄NPF₆ supporting electrolyte. Analyte was measured in 10 mM concentration.

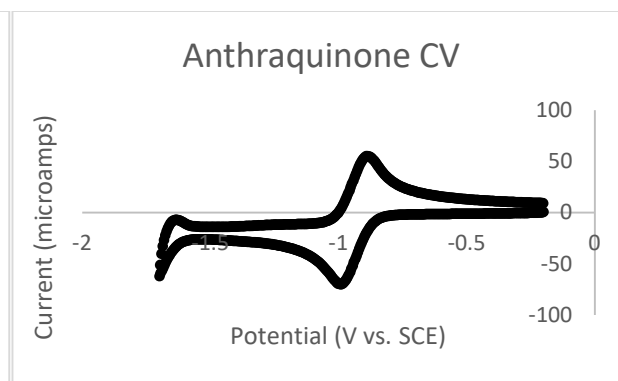
Conversion from the Ag/AgNO₃ reference used for measurements to standard SCE reference was obtained by measuring the ferrocene redox couple and using standard conversion values between ferrocene and SCE.



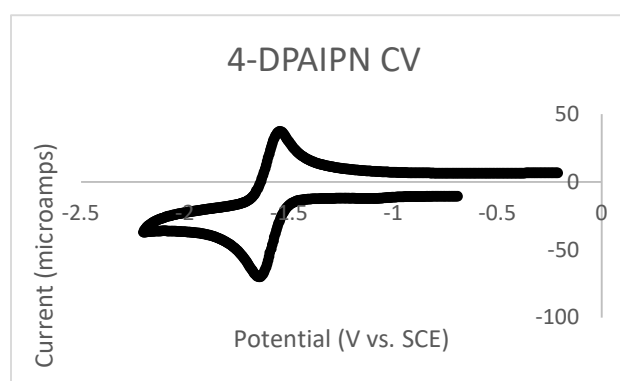
Fc/Fc⁺ E_{1/2} = 0.17 V vs. Ag/AgNO₃ (Ag/AgNO₃ to SCE conversion = 300 mV)



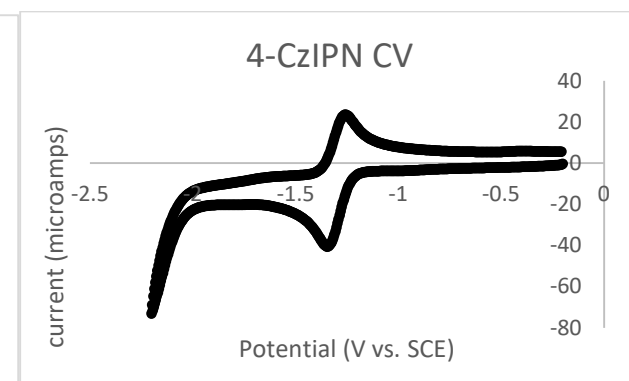
FL $E_{\text{red}} = -1.28 \text{ V vs. SCE}$



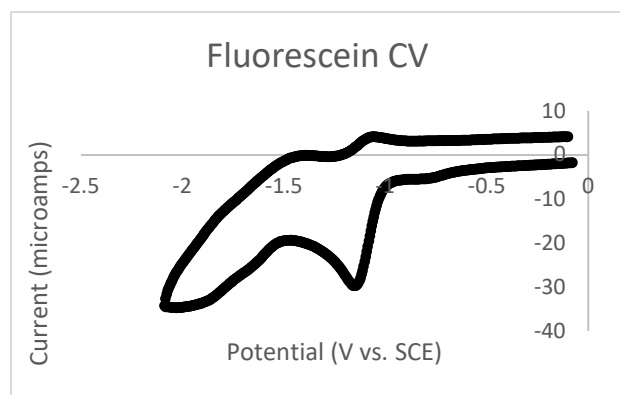
AQ $E_{\text{red}} = -0.99 \text{ V vs. SCE}$



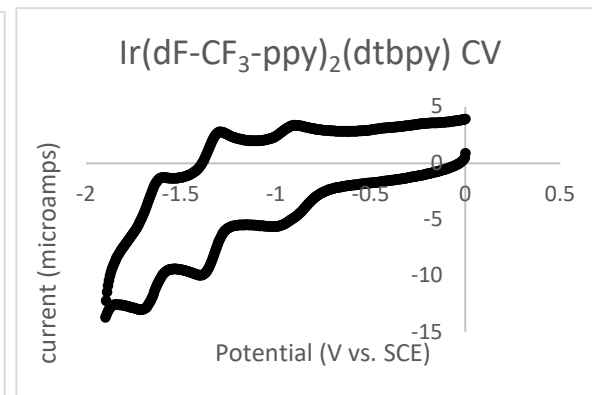
4-DPAIPN $E_{\text{red}} = -1.64 \text{ V vs. SCE}$



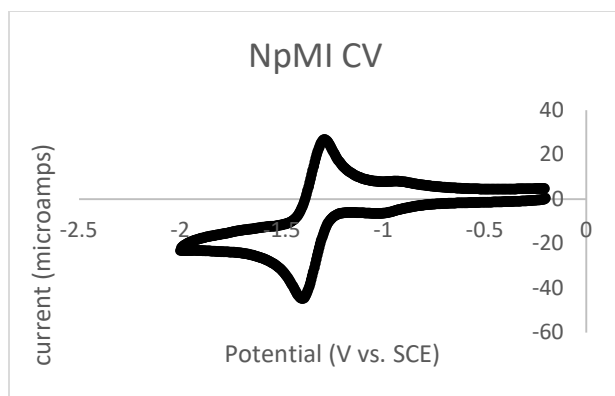
4-CzIPN $E_{\text{red}} = -1.35 \text{ V vs. SCE}$



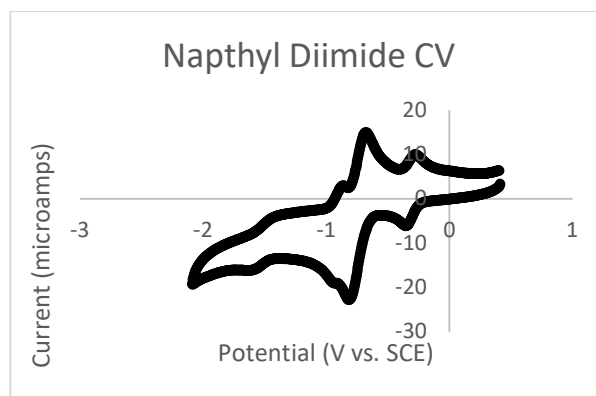
FC $E_{\text{red}} = -1.16 \text{ V vs. SCE}$



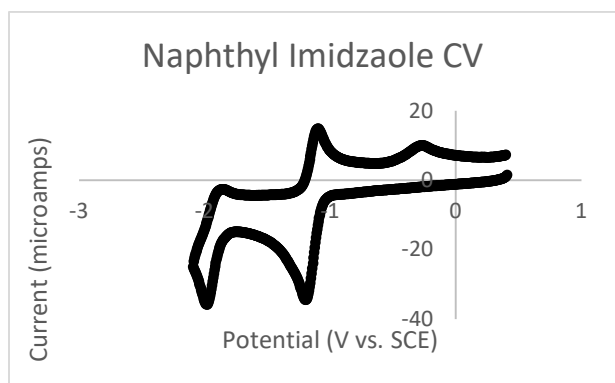
$\text{Ir}(\text{dF-CF}_3\text{-ppy})_2(\text{dtbbpy}) \text{ } E_{\text{red}} = -1.38 \text{ V vs. SCE}$



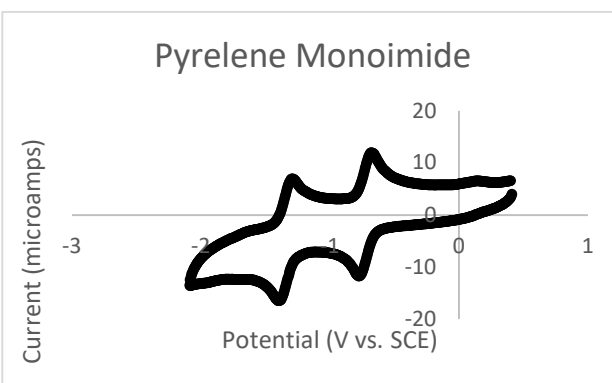
FC $E_{\text{red}} = -1.39 \text{ V vs. SCE}$



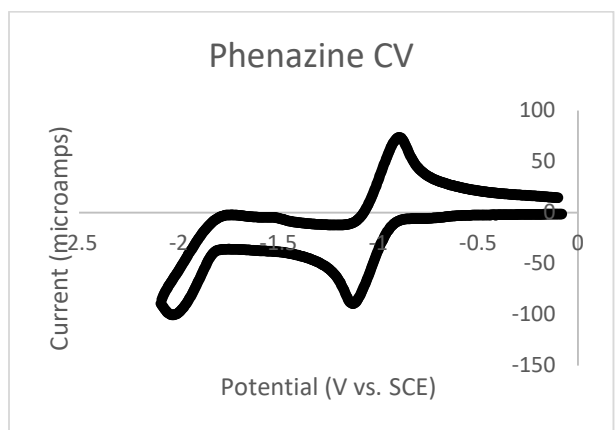
NpDI $E_{\text{red}} = -0.35 \text{ V vs. SCE}$



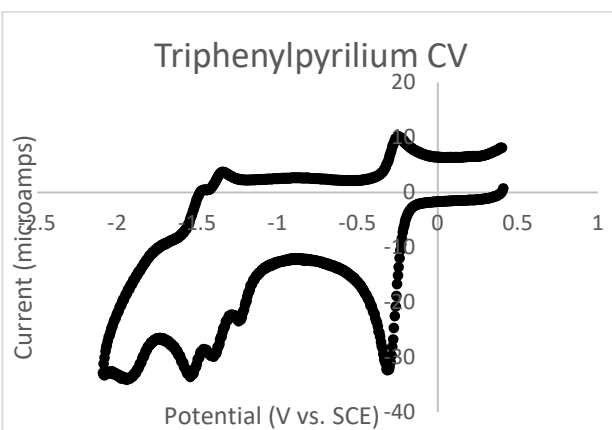
NpImz $E_{\text{red}} = -1.19 \text{ V vs. SCE}$



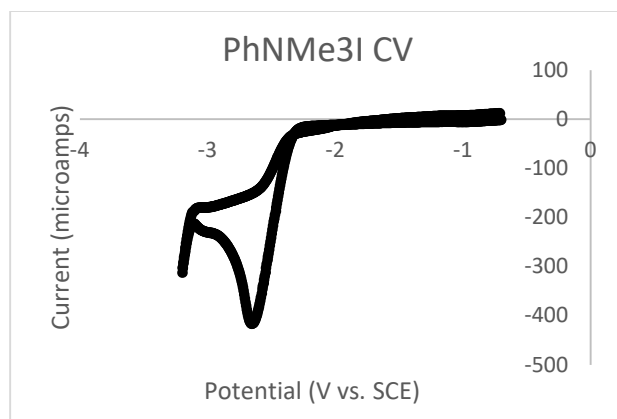
PMI $E_{\text{red}} = -0.77 \text{ V vs. SCE}$



PZ $E_{\text{red}} = -1.13 \text{ V vs. SCE}$

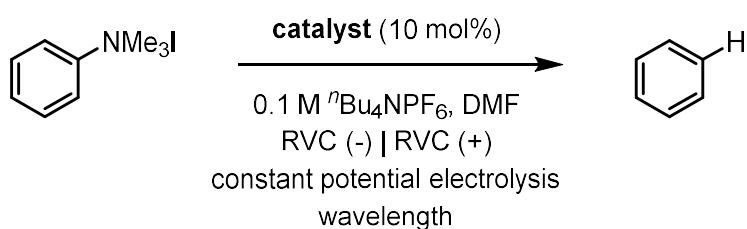


TPP $E_{\text{red}} = -0.32 \text{ V vs. SCE}$



PhNMe3I $E_{\text{red}} = -2.64$ V vs. SCE

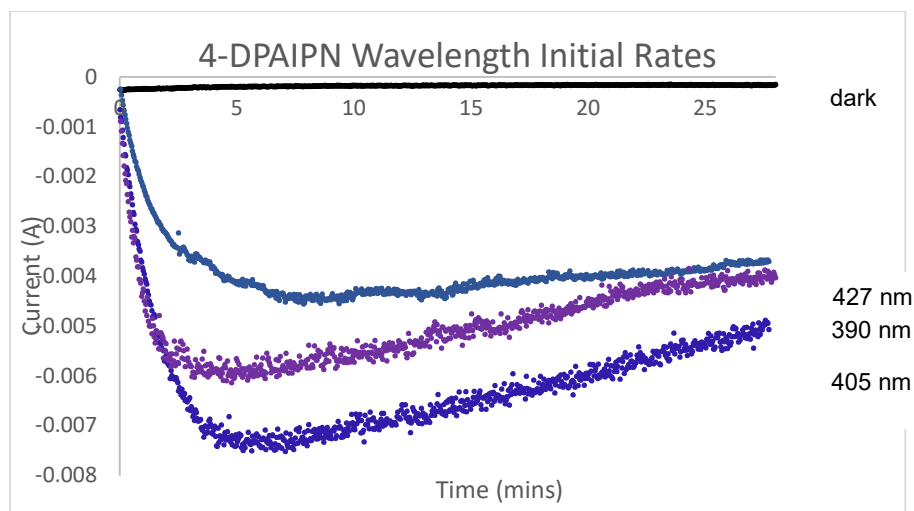
Catalyst defunctionalization screening



Each catalyst was studied under a constant applied potential equal to that of the E_{red} found via cyclic voltammetry.

The optimal wavelength was found for each catalyst studied by observing the current response on the potentiostat computer when subjected to different wavelengths of light. Since current is a measure of rate of electrons being passed and proportional to the rate of catalysis, the wavelength that resulted in the highest magnitude current readout was selected as the irradiation wavelength for each catalyst.

Example: three separate reaction mixtures with **4-DPAIPN** catalyst were prepared and each was subjected to a different wavelength of light and the current magnitude provided by the potentiostat computer was observed. The three trials under 427 nm, 405 nm, and 390 nm revealed a local maximum in rate at 405 nm and this wavelength was selected as the optimal wavelength for all reactions using **4-DPAIPN** as the catalyst.



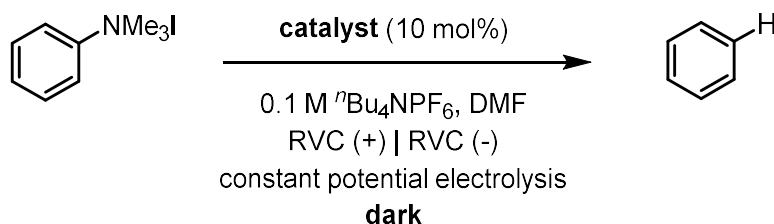
The results for each catalyst tested at their peak reduction potential and under optimal wavelength irradiation are summarized below:

Catalyst	E _{red} (V vs. SCE)	Optimal Wavelength (nm)	Yield (%)
<i>NpMI</i>	-1.3	405	42
<i>NpDI</i>	-0.4	390	11
<i>PMI</i>	-0.8	405	16
<i>Nplmz</i>	-1.2	405	41
<i>FL</i>	-1.2	440	36
<i>FC</i>	-1.3	405	45
<i>PZ</i>	-1.2	405	34
<i>AQ</i>	-0.9	405	10
<i>TPP</i>	-0.4	No photocurrent observed	0
<i>Ru(bpy)₃</i>	-1.3	427	25
<i>Ir(dF-CF₃-ppy)₂(dtbpy)(PF₆)*</i>	-1.4	427	9
<i>4-CzIPN</i>	-1.3	390	65
<i>4-DPAIPN</i>	-1.6	405	98

*Iridium photocatalyst run at 1 mol % catalyst loading

B.3.4 Control Reactions

We recognized that several of the catalysts tested herein possessed reduction potentials negative enough to potentially drive reactivity through electrochemical mediation. These catalysts were tested under standard reaction conditions according to general procedure C but in the absence of irradiation. The results are summarized below:

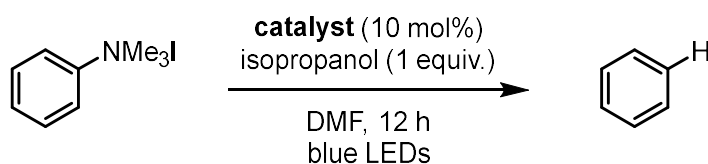


Catalyst	Ered (V vs. SCE)	Yield (%)
4-DPAIPN	-1.6	0
4-CzIPN	-1.3	0
Ru(bpy) ₃	-1.3	0
Ir(dF-CF ₃ -ppy) ₂ (dtbpy)(PF ₆)*	-1.4	0

*Iridium photocatalyst run at 1 mol % catalyst loading

We further recognized that numerous photocatalysts tested are competent singlet/triplet manifold photocatalysts that could potentially drive reactivity without an initial reduction event. These catalysts were tested under the following reaction conditions:

To a 10 mL Schlenk flask was added a stir bar, N,N,N-trimethyl phenyl ammonium salt (52.6 mg, 0.2 mmol, 1 equiv.), and catalyst (0.02 mmol, 10 mol%). The flask was placed under vacuum and backfilled with nitrogen 3 times before isopropanol (15.3 μ L, 0.2 mmol, 1 equiv) and DMF (2.5 mL) was added under a positive N₂ pressure. The flask was sealed under N₂ and irradiated at the optimal wavelength for each catalyst for 12 hours. The reaction was analyzed by GC analysis with a mesitylene standard. The results are summarized below:

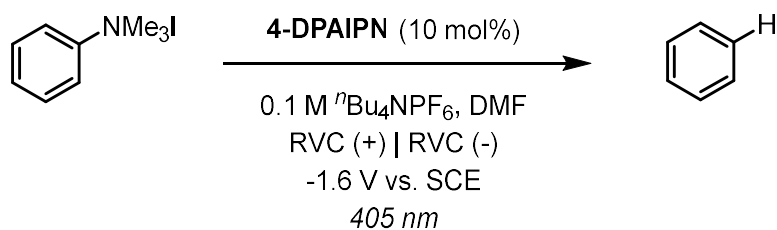


Catalyst	Wavelength (nm)	Yield (%)
PZ	405	0
FL	405	0
FC	405	0
AQ	405	0
Ru(bpy) ₃	427	0
Ir(dF-CF ₃ -ppy) ₂ (dtbpy)(PF ₆)*	427	0
4-CzIPN	390	0

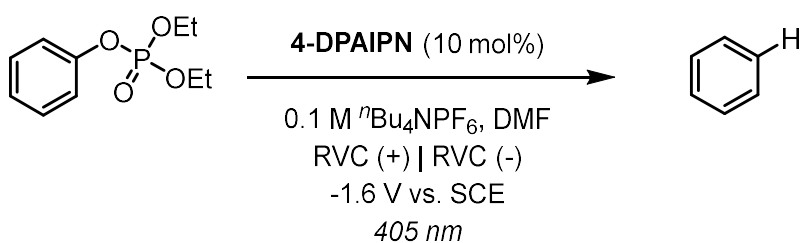
* Iridium photocatalyst run at 1 mol % catalyst loading

The lack of reactivity observed under just irradiation confirms that reduction of all of these catalysts to their radical anion congeners is necessary to generate a reductant potent enough to activate phenyl trimethylammonium iodide.

To confirm that both light and electricity are necessary for obtaining product with **4-DPAIPN** both substrate classes studied in this report were subjected to general procedure C but with systematic exclusion of reaction components. The results are summarized below:

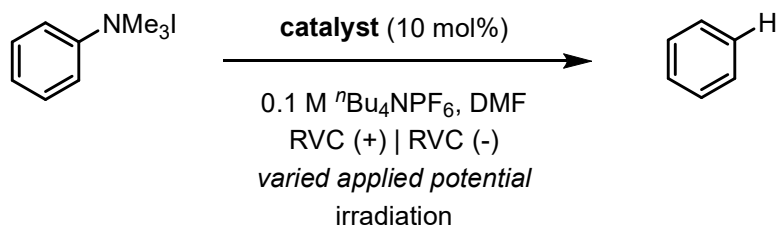


Variation	Yield (%)
none	96
no 4-DPAIPN	<5
no irradiation	<5
no irradiation, 50 °C	<5
no electrolysis	<5



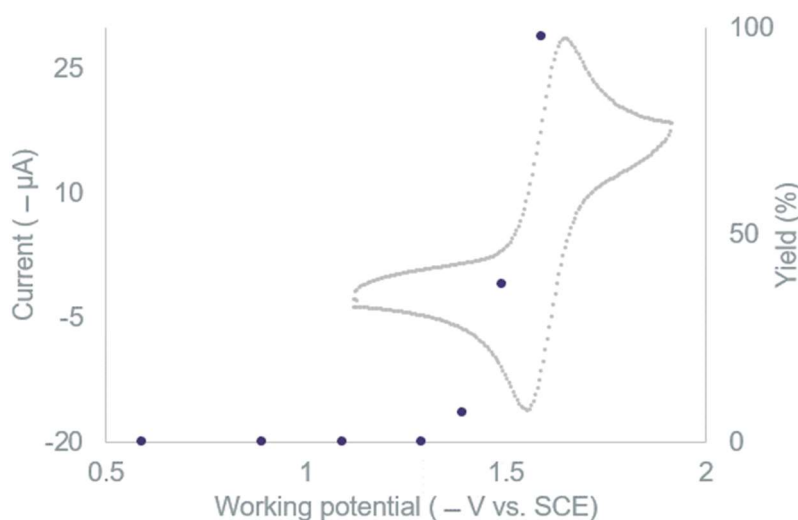
Variation	Yield (%)
none	79
no 4-DPAIPN	<5
no irradiation	<5
no irradiation, 50 °C	<5
no electrolysis	<5

To confirm that reactivity observed with **4-DPAIPN** was a result of the radical anion, the applied potential was varied and the yield of the reaction measured under the same reaction conditions according to procedure C. Under standard conditions with an applied potential of -1.6 V vs. SCE, the reaction showed completion after 4 h. All subsequent reactions at lower potentials were also carried out for 4 h. The results are summarized below:



Applied (V vs. SCE)	Yield (%)
-0.64	0
-0.94	0
-1.14	0
-1.34	0
-1.44	7
-1.54	38
-1.64	98

The potential vs. yield data collected was plotted with a cyclic voltammogram of 4-DPAIPN to compare the potential where reactivity turns on with the onset of current on the reduction wave:



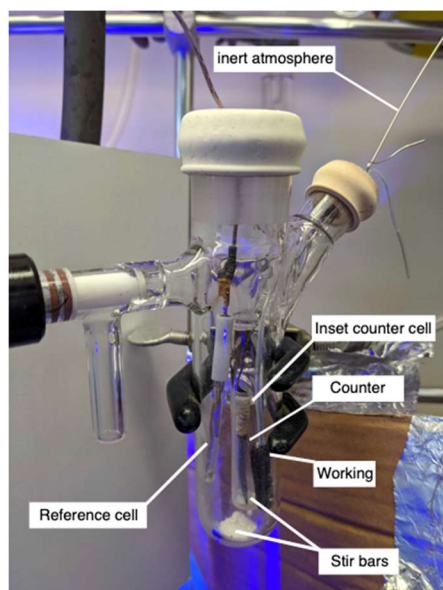
Plotting these data together reveal that conversion of starting material to product only occurs once a potential that is reducing enough to convert 4-DPAIPN to the radical anion is applied.

All the control data taken together are consistent with the reactivity observed for defunctionalization of trimethylanilinium resulting from excited state DPAIPN radical anion reducing substrate.

3.7.4 Characterization of 4DPAIPN radical anion

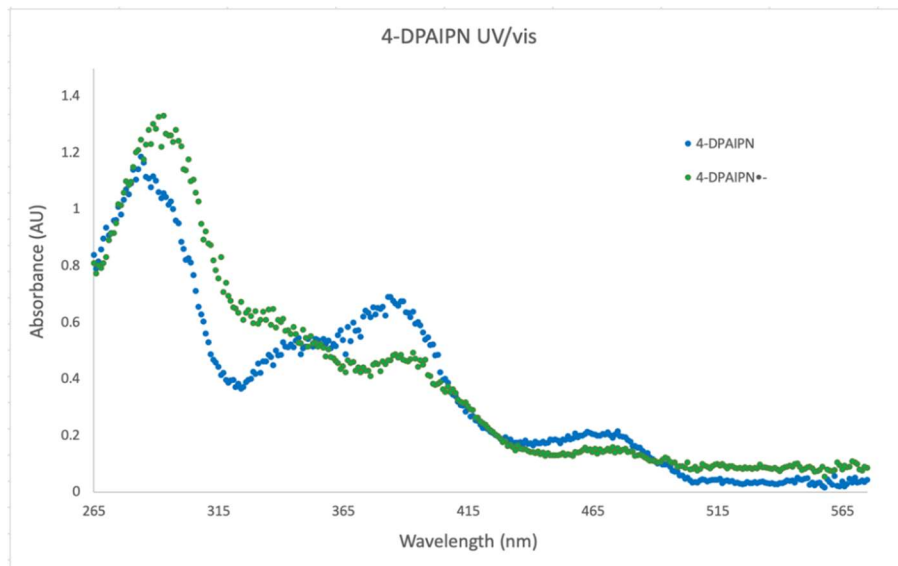
Electro-UV-Vis Sample preparation

To the oven-dried electrochemical cell with stir bars was added $n\text{Bu}_4\text{PF}_6$ (200 mg, 0.05 M) to each the anode and cathode. A three-electrode setup was assembled with a RVC cathode, a platinum sacrificial anode, and a reference cell wrapped in Teflon. The divided cell was equipped with the electrode assembly, sealed with septa and purged with a flow of Ar for 10 minutes. While under Ar, degassed DMF (8 mL, 0.05 M) was added to the cell. In a separate flame-dried vial, 4-DPAIPN (16 mg, 20 μmol) was added then flushed vial with Ar for 5 minutes. DMF (1 mL) was added to the vial of catalyst.

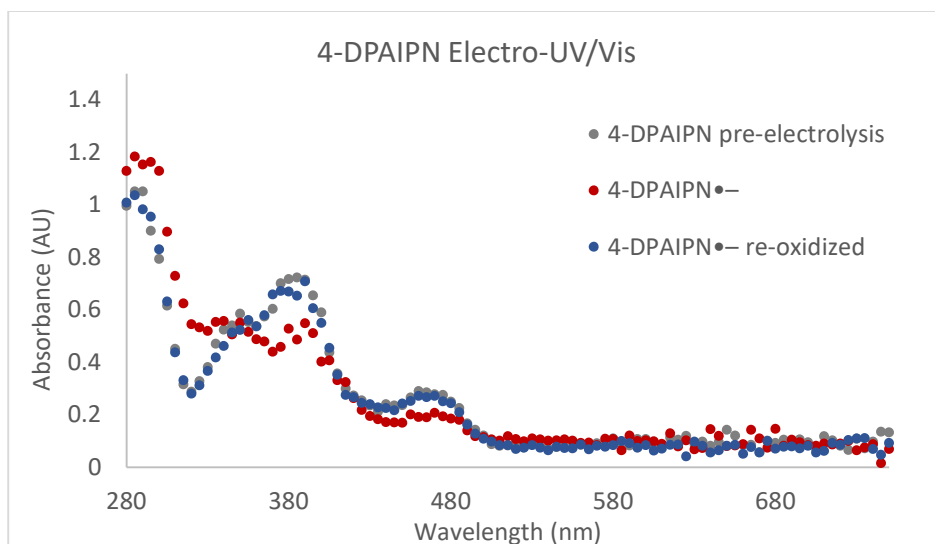


Electrochemical reduction and UV/Vis measurements

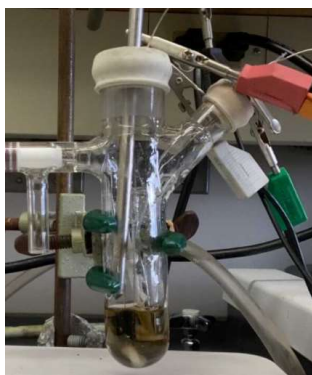
A fiberoptic dip-probe was inserted through the septum and into the electrolyte solution. After measuring a blank UV/Vis of the electrolyte solution, 4-DPAIPN stock solution (25 μL , 0.5 μmol) was added to the cell. A UV/Vis measurement was taken of neutral 4-DPAIPN. Finally, the solution was electrolyzed at -1.6 V vs. SCE until the yellow solution turned black. A measurement was taken of the solution to reveal the UV/Vis spectrum of 4-DPAIPN \bullet^- .



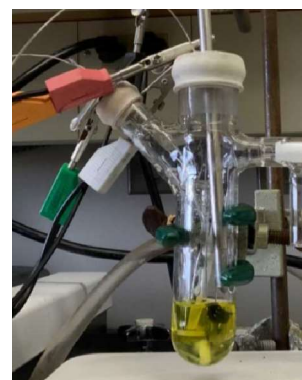
To confirm that the change in spectrum features was a result of formation of 4-DPAIPN \bullet^- rather than decomposition, the above experiment was repeated followed by re-oxidation of the solution at +0.50 V vs. SCE until current fell below 100 microamps. An additional UV-Vis spectrum was then taken and showed complete recovery of the features present in the initial spectrum of neutral 4-DPAIPN. The return of the spectrum features to neutral 4-DPAIPN confirms that the changes in the spectrum observed upon electrochemical reduction are a result of reversible formation of 4-DPAIPN \bullet^- .



Prior to reduction

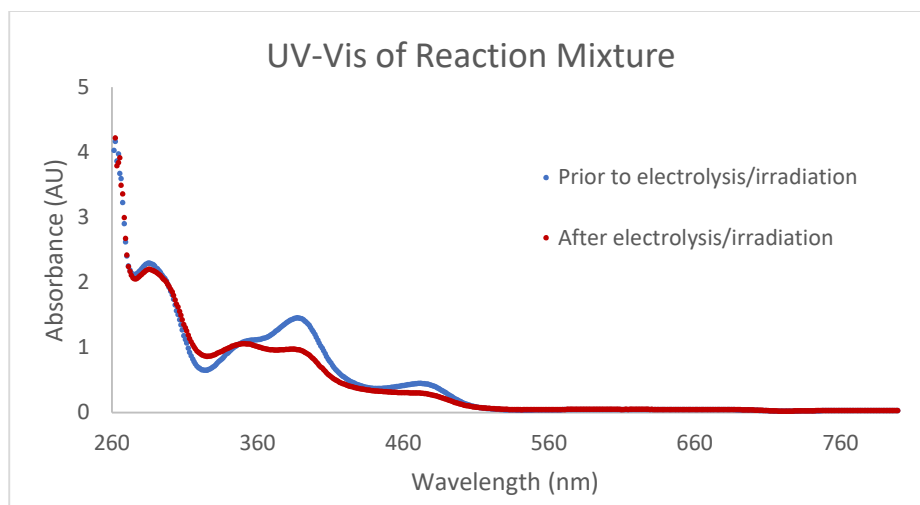


After reduction



After re-oxidation

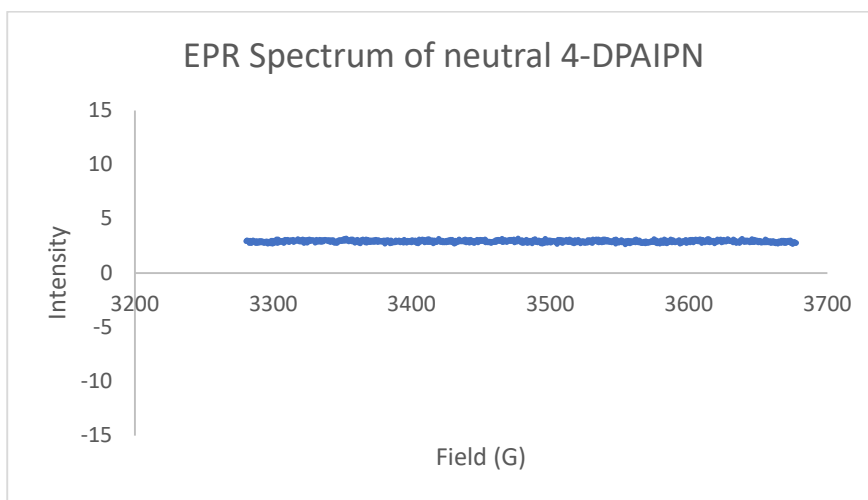
Additionally, UV-Vis spectra were collected on a reaction mixture to confirm that the same 4-DPAIPN radical anion features are present during the course of a reaction with an arene substrate. A standard reaction was prepared according to procedure C with phenyl trimethylammonium iodide in the glovebox. A UV-Vis spectrum was collected of the reaction mixture prior to electrolysis by removing a 20 microliter aliquot into an air free cuvette and dilution to 0.5 mM. Electrolysis and irradiation were carried out on the reaction solution to 25% conversion of substrate and an additional UV-Vis spectrum was collected with an additional 20 microliter aliquot.



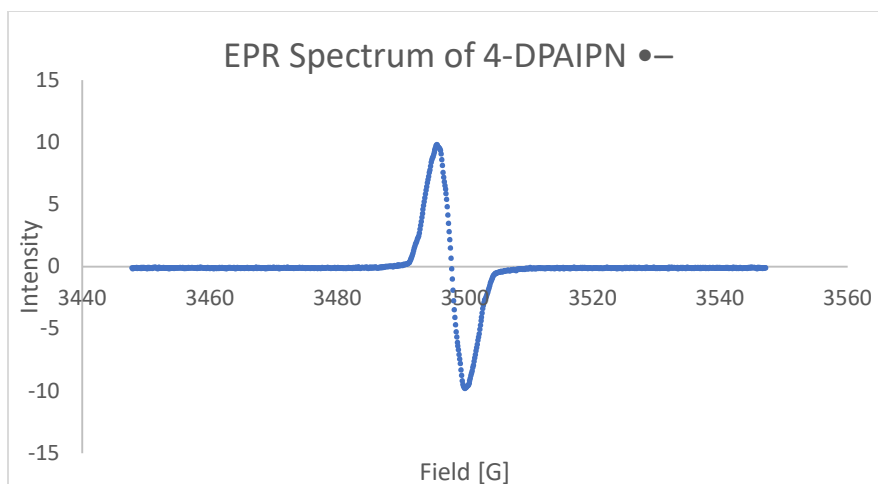
The spectra collected revealed the presence of neutral 4-DPAIPN prior to electrolysis and irradiation and after the solution had been electrolyzed and irradiated changes occurred in features consistent with 4-DPAIPN radical anion. This is consistent with formation of 4-DPAIPN radical anion during the course of the reaction to defunctionalize phenyl trimethylammonium iodide.

EPR Measurement of 4-DPAIPN:

To the cathode of an H-type divided cell in the glovebox was added ${}^n\text{Bu}_4\text{NPF}_6$ (96 mg, 0.25 mmol) and 4-DPAIPN (8 mg, 0.01 mmol). To the anode was added ${}^n\text{Bu}_4\text{NPF}_6$ (96 mg, 0.25 mmol). To the cathode and anode was added DMF (2.5 mL) and the solution was mixed until homogeneous. A 15 microliter aliquot was removed in a capillary tube and sealed on either end. An EPR spectrum was collected and showed no peak consistent with no unpaired electrons.

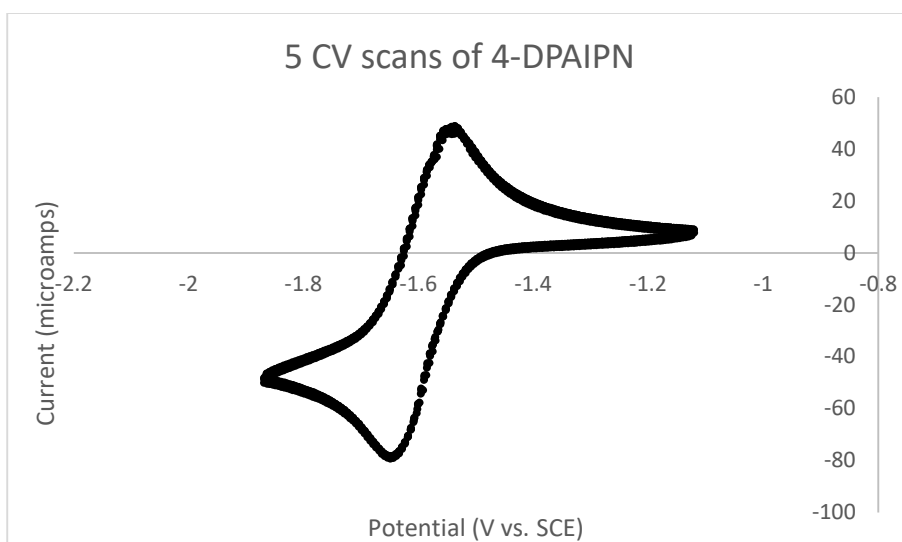


The remaining solution was electrolyzed at -1.6 V vs. SCE until current dropped below 100 microamps. Another 15 microliter aliquot was collected and sealed in a capillary tube. An EPR spectrum was collected and showed the presence of a single unpaired electron peak. This reveals that electrochemical reduction at the E_{red} of 4-DPAIPN produces a radical species, consistent with one electron reduction of the catalyst to the radical anion.



Stability of 4-DPAIPN Radical Anion:

To probe the stability of the 4-DPAIPN radical anion on the timescale of a CV, five cycles of measurements were taken in succession. The results are shown below:

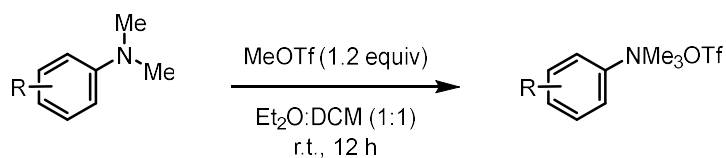


The lack of variation with each voltammogram cycle measured is consistent with a radical anion structure that is not decomposing under the reaction conditions on the timescale of a CV measurement.

3.7.5 Synthesis of non-commercial substrates

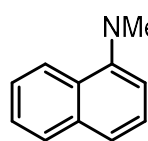
B.5.1 Aryl ammonium salts

General Procedure A – aryl quaternary ammonium salt synthesis



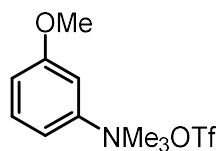
To a flask was added aryl amine (2.0 mmol, 1 equiv) and 50:50 Et₂O:DCM (5 mL). The solution was cooled to 0 °C and methyl trifluoromethanesulfonate (2.4 mmol, 1.2 equiv) was added dropwise. After stirring for 1 hour, the reaction mixture was warmed to room temperature and stirred overnight. If precipitate formed, the precipitate was collected and washed with diethyl ether to provide pure product. If no precipitate formed, the solution was concentrated and then washed with diethyl ether to yield pure product.

N,N,N-trimethylnaphthalen-1-aminium triflate (3)



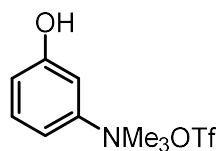
3 was prepared according to general procedure A (2.0 mmol) to give a white solid (584 mg, 87%). ¹H NMR (400 MHz, DMSO) δ 8.63 (d, *J* = 8.8 Hz, 1H), 8.27 – 8.19 (m, 2H), 8.12 (d, *J* = 8.0 Hz, 1H), 7.81 (ddd, *J* = 8.7, 6.9, 1.6 Hz, 1H), 7.75 (ddd, *J* = 7.9, 6.8, 1.0 Hz, 1H), 7.70 (t, *J* = 8.1 Hz, 1H), 3.92 (s, 9H). consistent with reported spectra (*Chem. Comm.*, **2016**, 52, 10894-10897)

3-methoxy-N,N,N-trimethylbenzenaminium triflate (4)



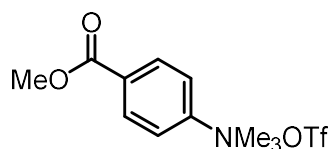
4 was prepared according to general procedure A (2.0 mmol) to give a white solid (630 mg, 99%). ¹H NMR (400 MHz, DMSO) δ 7.56 (t, *J* = 8.2 Hz, 1H), 7.53 – 7.47 (m, 2H), 7.21 – 7.14 (m, 1H), 3.86 (s, 3H), 3.59 (s, 9H); ¹³C NMR (126 MHz, DMSO) δ 165.32, 153.52, 136.15, 120.35, 117.31, 112.57, 61.62, 61.16. ; HRMS (ESI+) Calc: [M+H]⁺ (C₁₁H₁₆NO) 166.2; measured: 166.1.

53-hydroxy-N,N,N-trimethylbenzenaminium triflate (5)



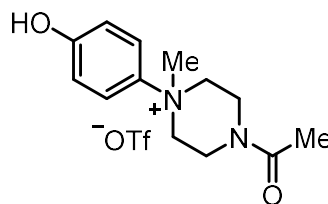
5 was prepared according to general procedure A (2.0 mmol) to give a purple solid (183 mg, 30%). ¹H NMR (400 MHz, DMSO) δ 10.26 (s, 1H), 7.42 (t, *J* = 8.2 Hz, 1H), 7.35 (dd, *J* = 8.4, 2.6 Hz, 1H), 7.28 (t, *J* = 2.4 Hz, 1H), 6.97 (dd, *J* = 8.0, 2.1 Hz, 1H), 3.55 (s, 9H). ¹³C NMR (126 MHz, DMSO) δ 163.64, 136.06, 121.91, 115.71, 112.98, 61.52. HRMS (ESI+) Calc: [M+H]⁺ (C₁₀H₁₄NO) 152.2; measured: 152.1.

4-(methoxycarbonyl)-N,N,N-trimethylbenzenaminium triflate (6)



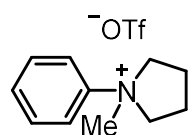
6 was prepared according to general procedure A (2.0 mmol) to give a white solid (645 mg, 94%). ¹H NMR (400 MHz, DMSO) δ 8.16 (q, *J* = 8.6 Hz, 4H), 3.91 (s, 3H), 3.64 (s, 9H); ¹³C NMR (126 MHz, DMSO) δ 170.12, 155.72, 136.29, 135.99, 126.58, 61.61, 57.92; HRMS (ESI+) Calc: [M+H]⁺ (C₁₂H₁₆NO₂) 194.3; measured: 194.1.

4-acetyl-1-(4-hydroxyphenyl)-1-methylpiperazin-1-ium triflate (7)

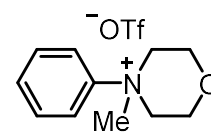


7 was prepared according to general procedure A (2.0 mmol) to give a light pink solid (440 mg, 57%). ¹H NMR (400 MHz, DMSO) δ 10.26 (s, 1H), 7.73 (d, *J* = 9.2 Hz, 2H), 6.96 (d, *J* = 9.1 Hz, 2H), 4.29 (t, *J* = 15.3 Hz, 2H), 4.09 (d, *J* = 15.5 Hz, 1H), 3.89 (dt, *J* = 37.5, 14.1 Hz, 3H), 3.51 (d, *J* = 17.4 Hz, 1H), 3.44 (s, 3H), 3.31 (d, *J* = 11.3 Hz, 1H), 2.05 (s, 3H).; ¹³C NMR (126 MHz, DMSO) δ 174.02, 163.56, 139.65, 128.07, 121.69, 66.00, 65.72, 61.55, 41.11, 26.15; HRMS (ESI+) Calc: [M+H]⁺ (C₁₃H₁₉N₂O₂) 235.3; measured: 235.1.

1-methyl-1-phenylpyrrolidin-1-ium triflate (8)

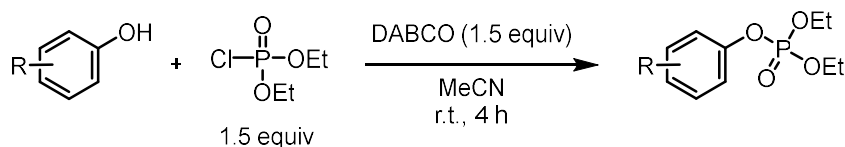
 **8** was prepared according to general procedure A (2.0 mmol) to give an off-white solid (620 mg, 99%). **¹H NMR** (400 MHz, DMSO) δ 7.88 (dd, J = 7.7, 1.9 Hz, 2H), 7.64 (td, J = 7.2, 6.3, 1.5 Hz, 2H), 7.61 – 7.55 (m, 1H), 4.29 (ddd, J = 9.9, 7.4, 4.4 Hz, 2H), 3.93 (qd, J = 8.7, 8.0, 3.1 Hz, 2H), 3.38 (s, 3H), 2.33 – 2.12 (m, 4H). Consistent with reported spectra (*J. Am. Chem. Soc.*, **2020**, 142, 3, 1603-1613).

4-methyl-4-phenylmorpholin-4-ium triflate (**9**)

 **9** was prepared according to general procedure A (2.0 mmol) to give a white solid (539 mg, 82%). **¹H NMR** (400 MHz, DMSO) δ 7.94 (d, J = 8.1 Hz, 2H), 7.69 (t, J = 7.8 Hz, 2H), 7.62 (t, J = 7.1 Hz, 1H), 4.42 – 4.29 (m, 2H), 4.07 (t, J = 12.3 Hz, 4H), 3.71 (dd, J = 13.7, 8.2 Hz, 2H), 3.52 (s, 3H). Consistent with reported spectra (*J. Org. Chem.* **2018**, 83, 8417-8425).

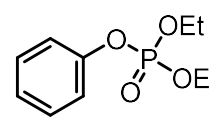
B.5.2 Aryl Phosphate Substrates

General Procedure B – aryl phosphate synthesis

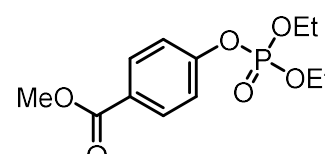


To a flame dried flask was added phenol substrate (1 equiv) and 1,4-diazabicyclo[2.2.2]octane (1.5 equiv) and the flask was placed under a nitrogen atmosphere. Acetonitrile (0.3 M) was added to the flask and stirred for 5 minutes. Chlorodiethylphosphate (1.5 equiv) was added to the solution dropwise and a white precipitate formed. The solution was stirred at room temperature for 12 hours after which the solution was diluted with DCM (25 mL) and water (50 mL). The organic layer was extracted and the aqueous layer was washed with additional DCM (2x25). The organic layers were combined and washed with brine, dried over MgSO_4 and concentrated to yield a crude oil. The crude product was purified by column chromatography on silica gel (EtOAc:Hexanes). (procedure adapted from the literature *Synlett*, **2012**, 23, 18, 2667-2671).

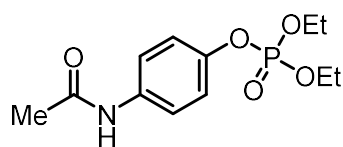
Diethyl phenyl phosphate (**12**)

 **12** was prepared according to general procedure B (6.00 mmol) to give a colorless oil (1.1 g, 78%). **¹H NMR** (400 MHz, CDCl_3) δ 7.33 (dd, J = 8.6, 7.2 Hz, 2H), 7.24 – 7.19 (m, 2H), 7.16 (t, J = 7.2 Hz, 1H), 4.29 – 4.14 (m, 4H), 1.34 (td, J = 7.1, 1.1 Hz, 6H). Consistent with reported spectra (*Synlett*, **2012**, 23, 2667-2671).

methyl 4-((diethoxyphosphoryl)oxy)benzoate (**13**)

 **13** was prepared according to general procedure B (5.00 mmol) to give a colorless oil (1.27 g, 88%). **¹H NMR** (400 MHz, CDCl_3) δ 7.96 (d, J = 8.2 Hz, 2H), 7.21 (d, J = 8.3 Hz, 2H), 4.16 (h, J = 8.1, 7.7 Hz, 4H), 3.83 (d, J = 3.3 Hz, 3H), 1.28 (t, J = 7.1 Hz, 6H); **¹³C NMR** (126 MHz, CDCl_3) δ 166.25, 154.38, 131.56, 126.87, 119.83, 64.87, 52.16, 16.10; **³¹P NMR** (400 MHz, CDCl_3) δ -6.9 ppm; **HRMS** (ESI+) Calc: $[\text{M}+\text{H}]^+$ ($\text{C}_{12}\text{H}_{17}\text{O}_6\text{P}$) 289.24; measured: 289.1.

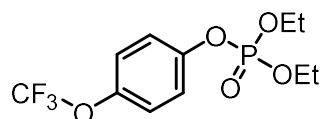
4-acetamidophenyl diethyl phosphate (**14**)



14 was prepared according to general procedure B (5.00 mmol) to give a colorless oil (431 mg, 30%). **¹H NMR** (400 MHz, CDCl₃) δ 9.02 (s, 1H), 7.42 (d, *J* = 8.9 Hz, 2H), 7.04 – 6.97 (m, 2H), 4.16 (ddd, *J* = 8.4, 7.2, 1.5 Hz, 4H), 2.06 (s, 3H), 1.34 – 1.27 (m, 7H). Consistent with reported spectra (*J. Org. Chem.* **1996**, 61, 7633–

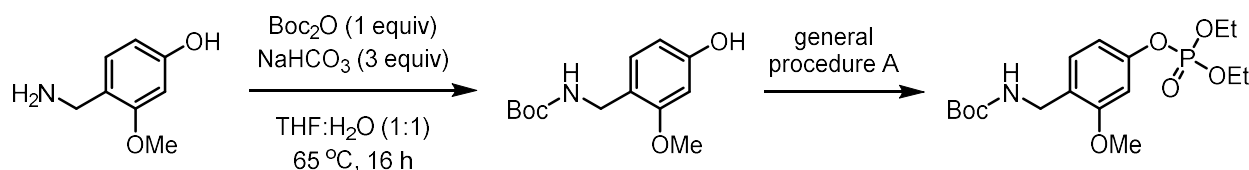
7636).

diethyl (4-(trifluoromethoxy)phenyl) phosphate (**15**)



15 was prepared according to general procedure B (10.0 mmol) to give a colorless oil (3.8 g, 98%). **¹H NMR** (400 MHz, CDCl₃) δ 7.27 (dd, *J* = 9.3, 1.1 Hz, 2H), 7.21 (d, *J* = 8.8 Hz, 2H), 4.29 – 4.19 (m, 4H), 1.38 (td, *J* = 7.1, 1.1 Hz, 6H); **¹³C NMR** (126 MHz, CDCl₃) δ 149.10, 145.92, 122.42, 121.27, 64.78, 16.04.; **¹⁹F NMR** (400 MHz, CDCl₃) δ -58.3 ppm; **HRMS** (ESI+) Calc: [M+H]⁺ (C₁₁H₁₄F₃O₅P) 315.20; measured: 315.0.

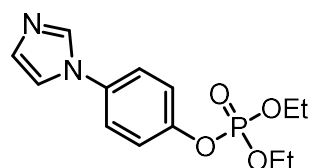
tert-butyl (4-((diethoxyphosphoryl)oxy)-2-methoxybenzyl)carbamate (**16**)



To a flask was added 4-(aminomethyl)-3-methoxyphenol (1.53 g, 10 mmol, 1 equiv) and sodium bicarbonate (2.52 g, 30 mmol, 3 equiv) and the mixture was placed under a nitrogen atmosphere. A mixture of THF:H₂O (1:1 v:v) was added to the flask and the solution was cooled to 0 °C. To the solution was added di-tert-butyl dicarbonate (2.3 mL, 2.18 g, 10 mmol, 1 equiv) dropwise via syringe. After stirring at 0 °C for 10 minutes the solution was warmed to room temperature and then heated to 65 °C and stirred for 16 hours. Ethyl acetate (50 mL) and water (50 mL) was added to the mixture and the organic layer was extracted. The aqueous layer was washed with additional EtOAc (3x20 mL). Crude product was obtained upon concentration and used without further purification.

16 was prepared according to general procedure B (7 mmol) to give a colorless, viscous oil that crystallized upon standing and cooling (1.39g, 37% total yield over two steps). **¹H NMR** (400 MHz, CDCl₃) δ 7.10 (d, *J* = 8.1 Hz, 1H), 6.80 (s, 1H), 6.69 (dd, *J* = 8.1, 2.1 Hz, 1H), 5.32 (s, 1H), 4.19 – 4.07 (m, 6H), 3.73 (s, 3H), 1.35 (s, 9H), 1.25 (t, *J* = 7.1 Hz, 6H); **¹³C NMR** (126 MHz, CDCl₃) δ 155.89, 150.77, 139.17, 136.77, 121.31, 119.59, 112.02, 64.55, 55.96, 44.46, 28.40, 16.05; **³¹P NMR** (400 MHz, CDCl₃) δ -6.02 ppm; **HRMS** (ESI+) Calc: [M+H]⁺ (C₁₇H₂₈NO₇P) 390.38; measured: 390.2

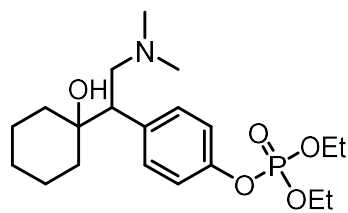
4-(1H-imidazol-1-yl)phenyl diethyl phosphate (**17**)



17 was prepared according to general procedure B (5.0 mmol) to give a yellow oil (1.04 g, 70%). **¹H NMR** (400 MHz, CDCl₃) δ 7.87 (s, 1H), 7.42 – 7.33 (m, 4H), 7.27 – 7.20 (m, 2H), 4.26 (dq, *J* = 10.3, 7.1, 2.0 Hz, 4H), 1.39 (td, *J* = 7.1, 1.1 Hz, 6H); **¹³C NMR** δ 149.85, 135.69,

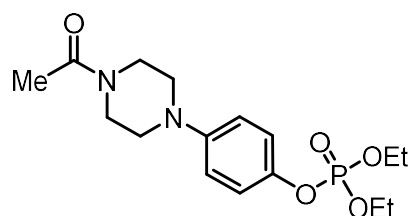
134.32, 130.56, 122.98, 121.46, 118.44, 64.85, 16.08; ^{31}P NMR (400 MHz, CDCl_3) δ -6.3 ppm; **HRMS** (ESI+) Calc: $[\text{M}+\text{H}]^+$ ($\text{C}_{13}\text{H}_{17}\text{NO}_4\text{P}$) 297.26; measured: 297.1

4-(2-(dimethylamino)-1-(1-hydroxycyclohexyl)ethyl)phenyl diethyl phosphate (18)



18 was prepared according to general procedure B (1.9 mmol) to give a colorless, viscous oil (194 mg, 64%). ^1H NMR (400 MHz, CDCl_3) δ 7.10 – 6.99 (m, 4H), 4.15 (p, J = 7.3 Hz, 4H), 3.29 (s, 1H), 2.96 (d, J = 11.5 Hz, 1H), 2.30 (s, 6H), 1.71 – 1.55 (m, 3H), 1.48 (m, 3H), 1.29 (t, J = 7.0 Hz, 6H), 1.18 (q, J = 9.2, 8.3 Hz, 2H), 0.96 – 0.71 (m, 3H); ^{13}C NMR (126 MHz, CDCl_3) δ 149.44, 137.41, 130.38, 119.40, 74.11, 64.54, 61.03, 51.89, 45.48, 38.11, 31.17, 25.97, 21.58, 21.30, 16.12; ^{31}P NMR (400 MHz, CDCl_3) δ -6.2 ppm; **HRMS** (ESI+) Calc: $[\text{M}+\text{H}]^+$ ($\text{C}_{20}\text{H}_{34}\text{NO}_5\text{P}$) 400.47; measured: 400.2

4-(4-acetylpiperazin-1-yl)phenyl diethyl phosphate (19)



19 was prepared according to general procedure B (3.1 mmol) to give a pink oil (720 mg, 65%). ^1H NMR (400 MHz, CDCl_3) δ 7.07 (d, J = 9.1 Hz, 2H), 6.82 (d, J = 8.6 Hz, 2H), 4.13 (dq, J = 8.0, 7.1, 2.7 Hz, 4H), 3.74 – 3.67 (m, 2H), 3.55 (t, J = 5.0 Hz, 2H), 3.04 (dt, J = 13.3, 5.1 Hz, 4H), 2.07 (s, 3H), 1.28 (t, J = 7.1 Hz, 6H). ^{13}C NMR (126 MHz, CDCl_3) δ 169.01, 148.34, 144.60, 120.71, 117.99, 64.48, 50.32, 49.94, 46.24, 41.35, 21.33, 16.09; ^{31}P NMR (400 MHz, CDCl_3) δ -5.78 ppm; **HRMS** (ESI+) Calc: $[\text{M}+\text{H}]^+$ ($\text{C}_{16}\text{H}_{25}\text{N}_2\text{O}_5\text{P}$) 357.36; measured: 357.1.

3.7.6 Defunctionalization Reactions

General Procedure C – Defunctionalization

An oven dried, H-type divided cell with a glass frit was equipped with stir bars and arene substrate (0.2 mmol), 4-DPAIPN (0.02 mmol, 0.1 equiv., 15.9 mg), and $^n\text{Bu}_4\text{PF}_6$ (0.25 mmol, 97 mg) were added to the cathodic chamber while $^n\text{Bu}_4\text{PF}_6$ (0.25 mmol, 97 mg) was added to the anodic chamber. A three-electrode setup was assembled with a RVC cathode and anode and a reference cell wrapped in Teflon. The divided cell was equipped with the electrode assembly, sealed with septa and purged with a flow of N_2 for 10 minutes (inlet needle in the anode, outlet needle in the cathode). To the anode and then cathode was added DMF (2.5 mL) and triethylamine (220 μL , 1.6 mmol, 4 equiv) was added to the anode. Electrodes were connected to a WaveNow potentiostat and electrolyzed at -1.6 V vs. SCE and irradiated with HepatoChem 405 nm LEDs for 12 hours. Temperature was maintained by electric fans cooling.

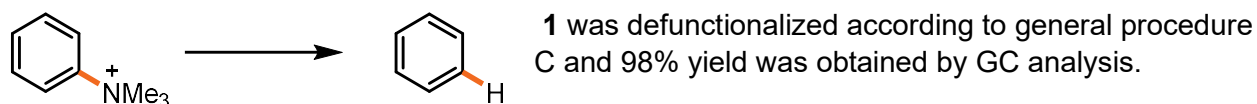
For GC analyses: Mesitylene (18 μL , 0.13 mmol) was added to crude reaction mixture and a 0.2 mL aliquot was removed. The aliquot was diluted with diethyl ether (2 mL) and electrolyte was filtered off through a silica pipette plug and the plug was rinsed with additional diethyl ether (1.0 mL). This ether solution (1 μL) was injected on a GC for analysis.

For NMR analyses: The crude reaction mixture was poured into 10% LiCl aqueous solution (100 mL) and extracted with EtOAc (3x75mL). The organic layers were combined, washed with brine and dried over MgSO_4 . The crude reaction mixture was concentrated and

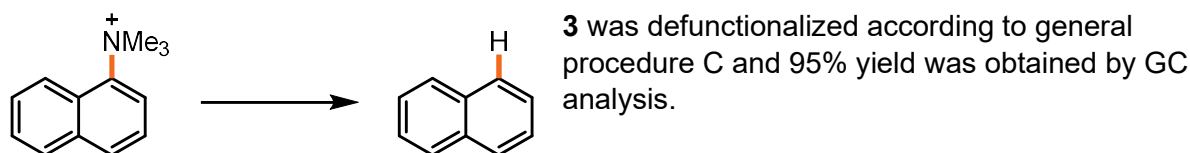
dibromomethane (7 μ L, 0.1 mmol) was added. An NMR spectrum in CDCl_3 was obtained of the mixture to gain an analytic yield.

Aryl ammonium defunctionalization:

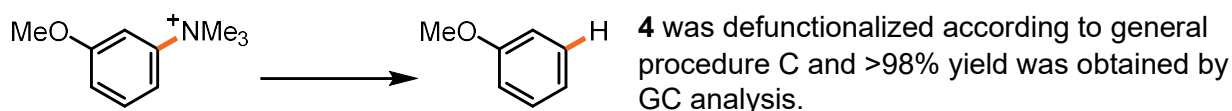
N,N,N-trimethylbenzenaminium (**1**)



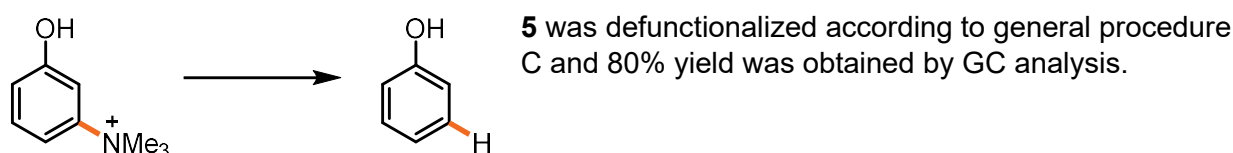
N,N,N-trimethylnaphthalen-1-aminium (**3**)



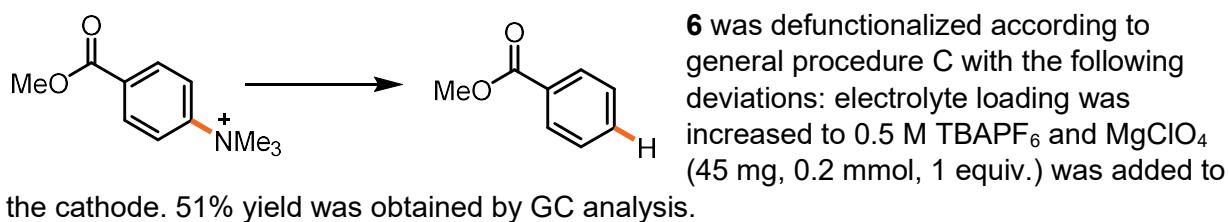
3-methoxy-*N,N,N*-trimethylbenzenaminium (**4**)



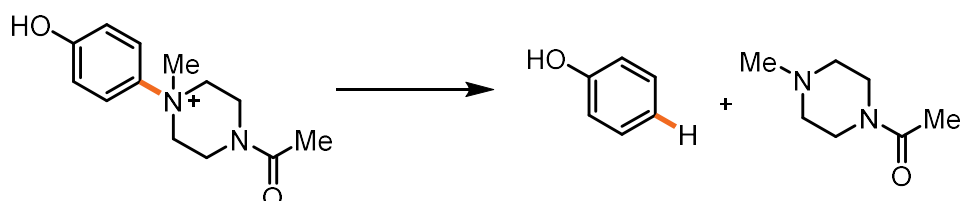
3-hydroxy-*N,N,N*-trimethylbenzenaminium (**5**)



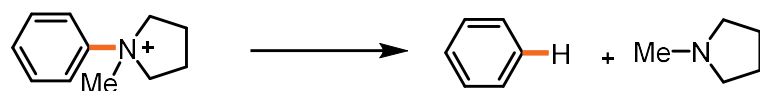
4-(methoxycarbonyl)-*N,N,N*-trimethylbenzenaminium (**6**)



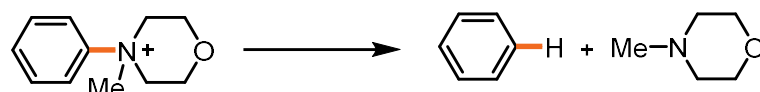
4-acetyl-1-(4-hydroxyphenyl)-1-methylpiperazin-1-ium (**7**)



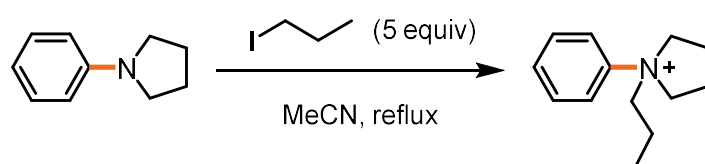
7 was defunctionalized according to general procedure C with the following deviations: electrolysis was halted once 28 coulombs of charge had been passed through the system (< 12 h). 54% yield was obtained by GC analysis of the phenol product.

1-methyl-1-phenylpyrrolidin-1-ium (8)

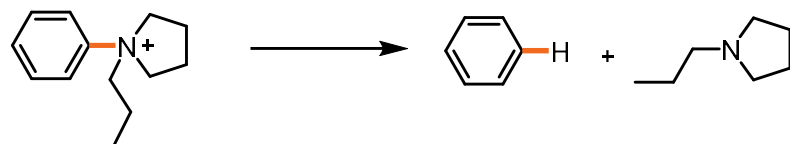
8 was defunctionalized according to general procedure C and 84% yield was obtained by GC analysis of the benzene product.

4-methyl-4-phenylmorpholin-4-ium (9)

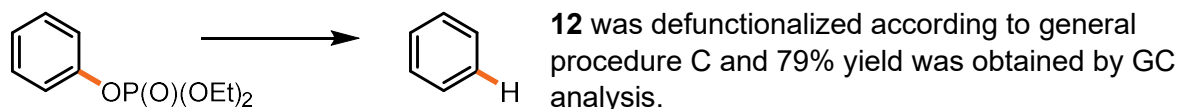
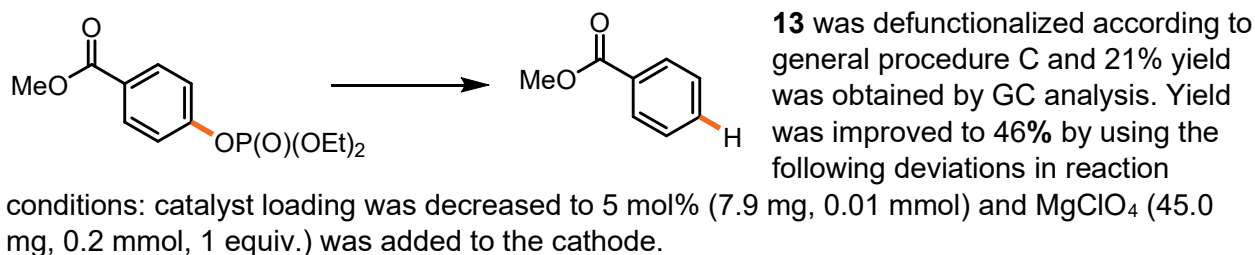
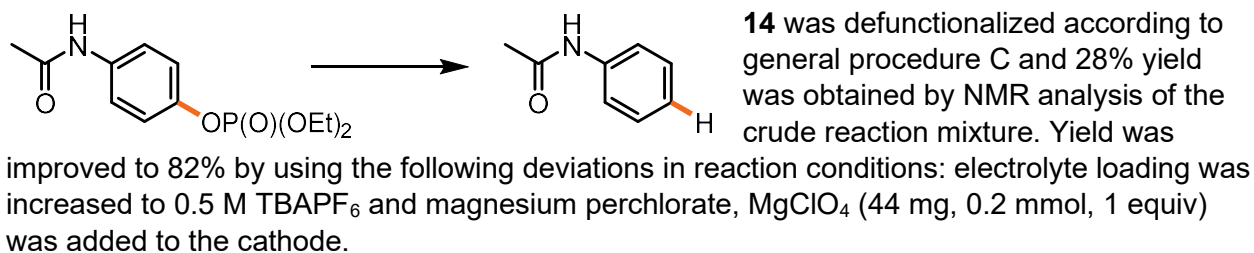
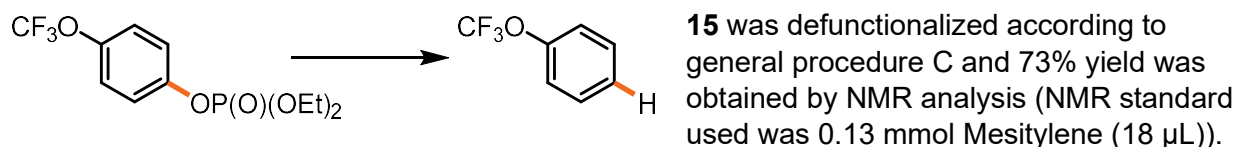
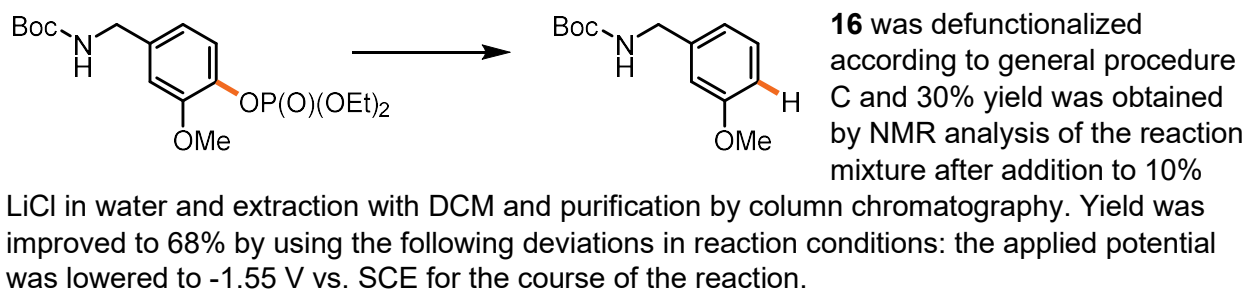
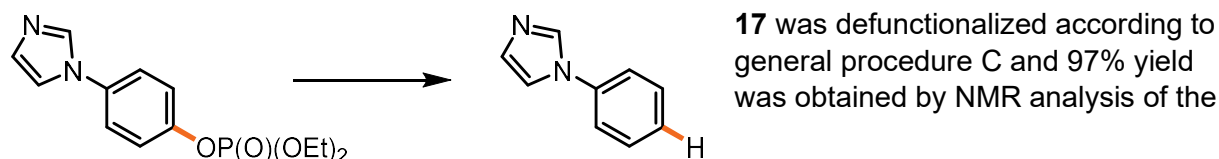
9 was defunctionalized according to general procedure C and 83% yield was obtained by GC analysis of the benzene product.

1-phenyl-1-propylpyrrolidin-1-ium (10)

1-phenyl-1-propylpyrrolidin-1-ium was prepared according to the following procedure adapted from the literature (*Med. Chem.* **2015**, 11, 1, 21-29). To a dried round bottom flask was added N-methyl pyrrolidine (552 μ L, 3.0 mmol, 1 equiv) and 1-iodopropane (1.47 mL, 15.0 mmol, 5 equiv) in acetonitrile (5 mL) and heated at reflux for 24 hours. The solution was cooled to room temperature and diethyl ether (20 mL) was added to the solution and precipitate was filtered, washed with ether and dried to yield pure product as an off white solid (714 mg, 75%). **¹H NMR** (400 MHz, DMSO) δ 7.88 – 7.82 (m, 2H), 7.67 – 7.56 (m, 3H), 4.26 – 4.16 (m, 2H), 4.03 (q, J = 5.7 Hz, 2H), 3.69 – 3.59 (m, 2H), 2.23 (d, J = 7.4 Hz, 2H), 2.05 (s, 2H), 1.33 – 1.19 (m, 2H), 0.77 (t, J = 7.3 Hz, 3H). **¹³C NMR** (126 MHz, DMSO) δ 143.71, 130.58, 122.66, 65.92, 64.00, 20.59, 17.26, 10.68; **HRMS** (ESI+) Calc: $[M+H]^+$ ($C_{13}H_{20}N$) 190.3; measured: 190.1

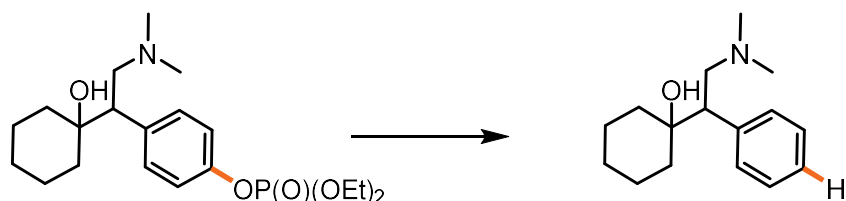


10 was defunctionalized according to general procedure C with the following deviations: electrolyte was changed from 0.1 M TBAPF₆ to 0.1 M LiClO₄ to improve visualization of the product by NMR and electrolysis was halted after 25 C had been passed through the system (3 hours). 67% yield was obtained by NMR analysis of the crude reaction mixture. Signals were consistent with reported spectra (*J. Am. Chem. Soc.* **2015**, 137, 40, 12796-12799).

Aryl phosphate defunctionalizations:**diethyl phenyl phosphate (12)****methyl 4-((diethoxyphosphoryl)oxy)benzoate (13)****4-acetamidophenyl diethyl phosphate (14)****diethyl (4-(trifluoromethoxy)phenyl) phosphate (15)****tert-butyl (4-((diethoxyphosphoryl)oxy)-3-methoxybenzyl)carbamate (16)****4-(1H-imidazol-1-yl)phenyl diethyl phosphate (17)**

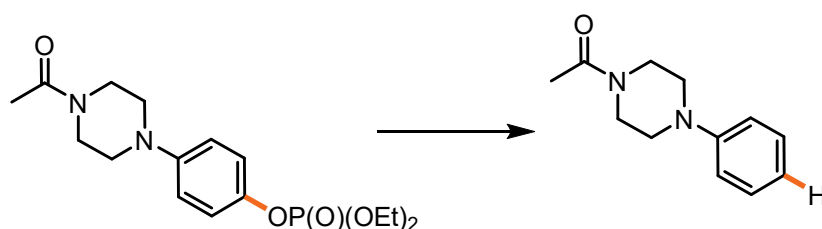
crude reaction mixture after addition to 10% LiCl in water and extraction with diethyl ether.

*diethyl (4-(1-(1-hydroxycyclohexyl)-2-(trimethyl-1*l*-azaneyl)ethyl)phenyl) phosphate (18)*



18 was defunctionalized according to general procedure C and 59% yield was obtained by NMR analysis of the crude reaction mixture.

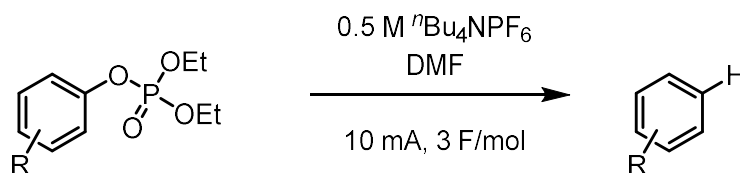
4-(4-acetypiperazin-1-yl)phenyl diethyl phosphate (19)



19 was defunctionalized according to general procedure C except with 81.0 mg (0.227 mmol) of **19** and 80% yield was obtained by NMR analysis of the crude reaction mixture.

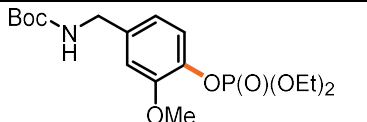
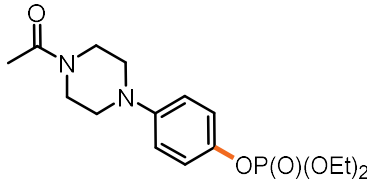
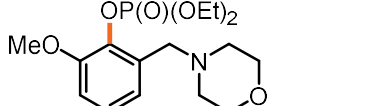
Direct Electrolysis Comparisons:

We recognized that direct electrolysis is a viable method for reductively defunctionalizing molecules. We hypothesized that under the extreme potentials required to activate many of the substrates studied herein, functional group tolerance and molecule integrity would be compromised. To investigate this hypothesis and gain insight into the chemoselectivity gained through using electron-primed photoredox catalysis, we carried out direct electrolysis reactions on several substrates bearing more sensitive functional groups under the following conditions:



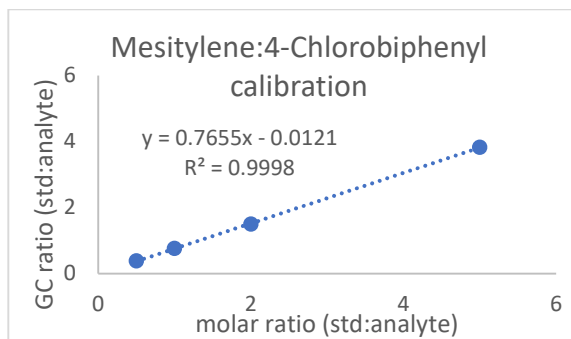
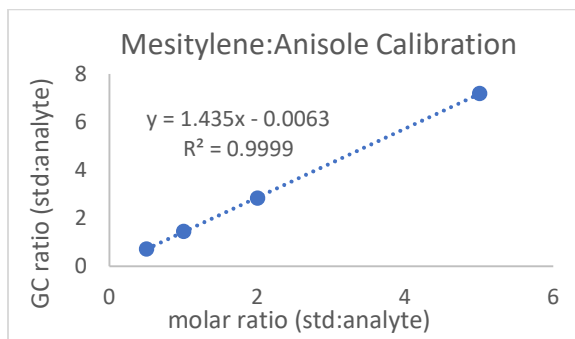
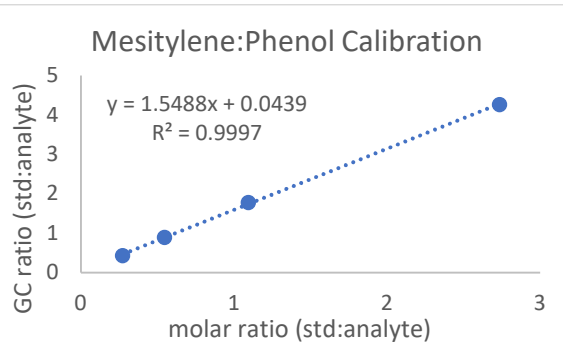
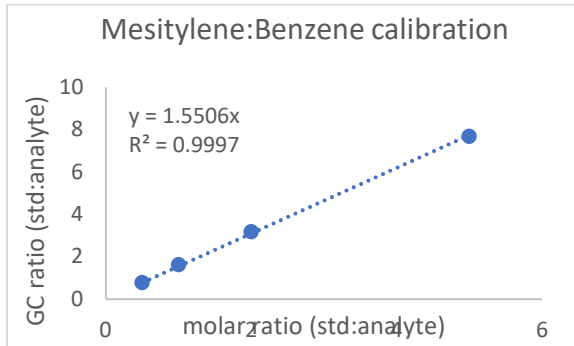
An oven dried, H-type divided cell with a glass frit was equipped with stir bars and arene substrate (0.2 mmol) and $n\text{Bu}_4\text{PF}_6$ (1.25 mmol, 484 mg) were added into the cathodic chamber while $n\text{Bu}_4\text{PF}_6$ (1.25 mmol, 484 mg) was added to the anodic chamber. An electrode setup was assembled with RVC on stainless steel cathode and anode. The divided cell was equipped with the electrode assembly, sealed with septa and purged with a flow of N_2 for 10 minutes (inlet needle in the anode, outlet needle in the cathode). DMF (2.5 mL) was added to the cathode and triethylamine (220 μL , 1.6 mmol, 4 equiv.) and DMF (2.5 mL) was added to the anode. Electrodes were connected to a Doctor Meter and electrolyzed at a constant current of 10 mA for 1.6 hours for a total of 3 F/mol. The cathode solution was added to 10% LiCl (aq) solution (100 mL) and extracted with Et_2O (3x60mL) and EtOAc (50 mL). The ether layers were combined, dried with brine and MgSO_4 , and filtered. The EtOAc was also dried and added to the ether layers after filtration. Product mixtures were analyzed by crude reaction mixture and identifiable products were isolated by column chromatography.

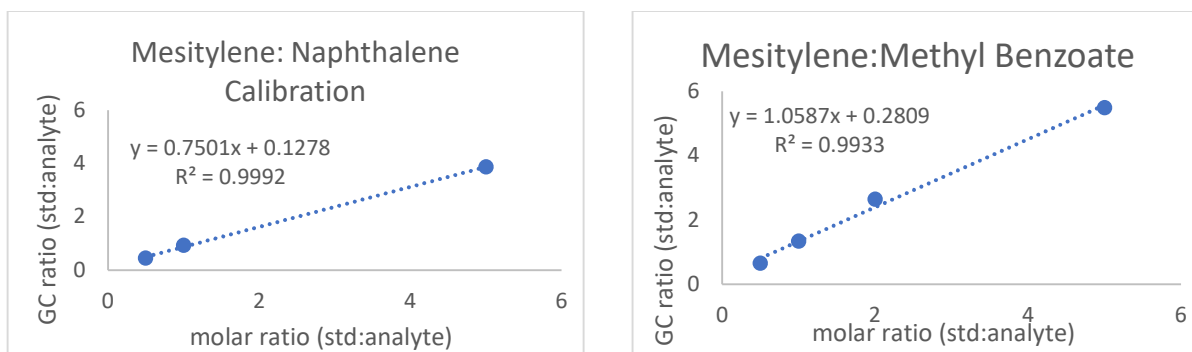
The results are summarized below:

Substrate	Yield (%)	RSM (%)
	8	16
	20	31
	36	10

While these experiments revealed that product could be obtained via direct electrolysis, the yield is significantly reduced compared to the yield obtained through electron-primed photoredox catalysis. Furthermore, high conversion of the starting material was observed leading to a product mixture of unidentifiable byproducts and poor mass balance. We concluded that direct electrolysis can achieve the reduction potentials required to defunctionalize difficult substrates, however, chemoselectivity and functional group tolerance is drastically diminished compared to defunctionalization by electron-primed photoredox catalysis.

3.7.7 Gas Chromatography Calibrations

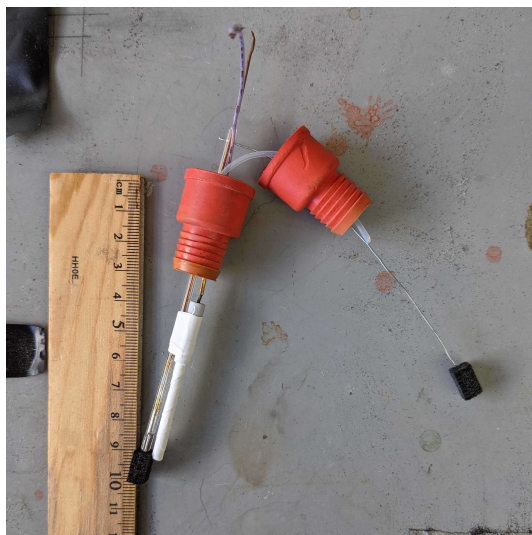




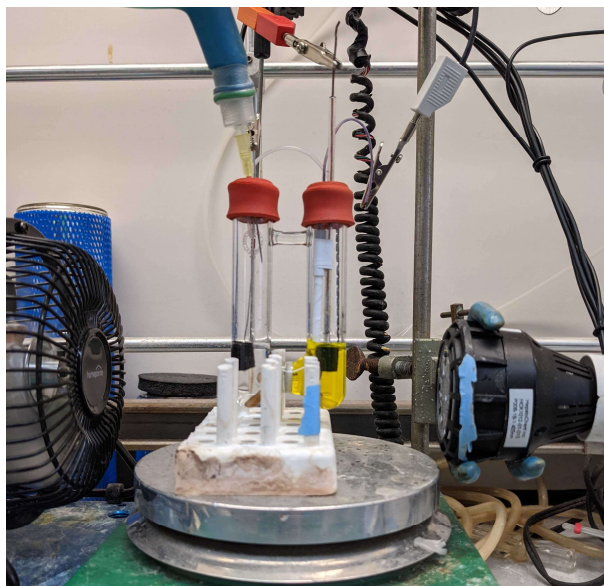
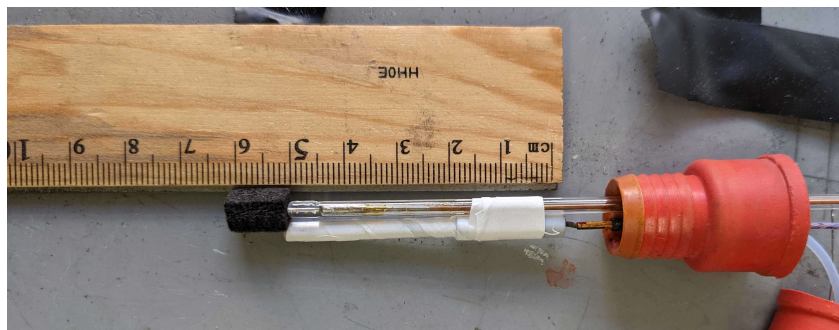
3.7.8 Reaction Progress Kinetics Analysis

Starting and ending mmol quantities for 4-chlorobiphenyl were obtained by GC analysis relative to internal mesitylene standard.

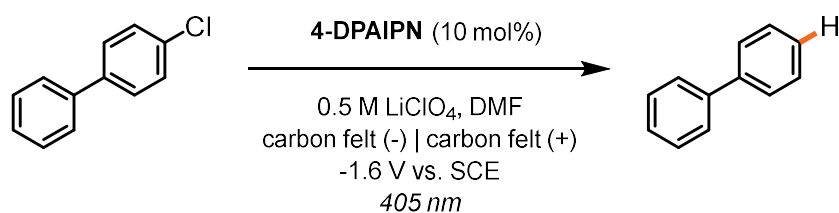
Reaction equipment included a 10 mL H-type cell with septa and carbon felt (1 mm x 7 mm x 6 mm) cathode supported by a platinum spike secured into a glass rod through the cathodic septum to create a rigid setup with reproducible electrode placement. Anodic electrode was constructed of carbon felt (1 cm x 1 cm x 6 mm) supported by a steel wire through the anodic septum.



A standard reference cell was used wrapped in Teflon tape and then Teflon taped to the cathode glass rod such that the frit of the reference electrode was level with the top of the cathode carbon felt electrode. A rigid placement and regular spatial setup between the working electrode and reference electrode was found to be crucial for obtaining reproducible rate data.



Data transformation process:



Current vs. time data for the above reaction was exported from the potentiostat computer as an excel file. The following data transformations were done to the data set:

1. Current values were transformed into mol/s by dividing by Faraday's constant (96485.33 C/mol)
2. Mol/s rate data was transformed into positive values via the absolute value function and then converted to Molarity/s by dividing by the reaction volume
3. Moles of ArCl consumed at a given time point was found by using a trapezoid integration method between two consecutive data points according to the equation:

$$((t_{n+1} - t_n) * R_{n+1}) + \left(\frac{(t_{n+1} - t_n) * (R_n + R_{n+1})}{2} \right)$$

where t = time (s) and R = rate (mol/s).

4. Moles of ArCl remaining in the reaction solution at time t was found by subtracting the instantaneous ArCl moles consumed at time t (divided by a scalar correction factor to account for imperfect faradaic efficiency) from the moles of ArCl remaining at the preceding time point according to the equation:

$$(\text{ArCl}_{\text{mmol}} \text{ at } t_{n+1}) = \left[\frac{((t_{n+1} - t_n) * R_{n+1}) + \left(\frac{(t_{n+1} - t_n) * (R_n + R_{n+1})}{2} \right)}{\text{Correction factor } x} \right]$$

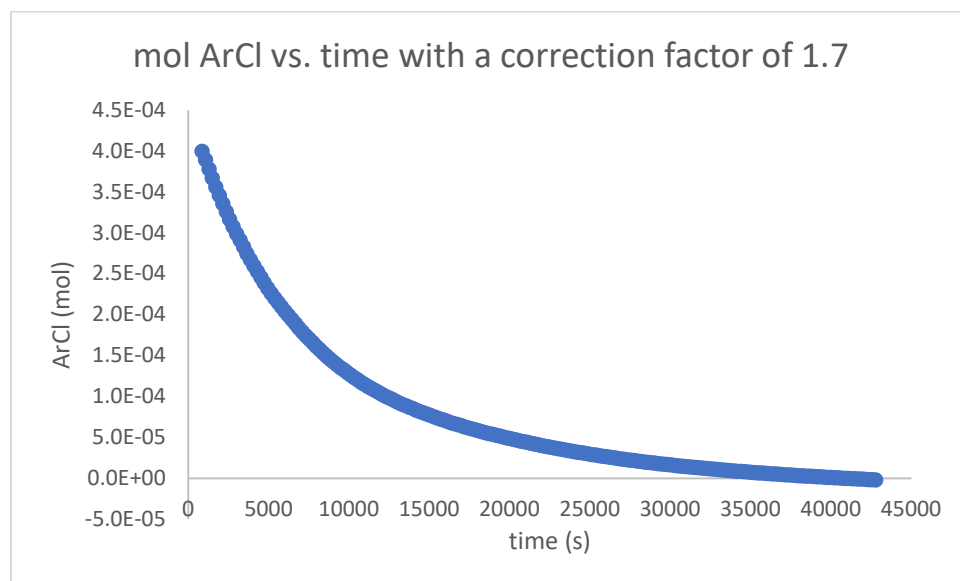
where t = time (s) and R = rate (mol/s).

5. Moles of ArCl at time t was converted to $[\text{ArCl}]$ (M) at time t by divided by the reaction volume.
6. Rate (M/s) values were corrected to account for imperfect faradaic efficiency by dividing by a correction factor.
7. Corrected $[\text{ArCl}]$ (M) was plotted against corrected Rate (M/s) to observe and compare kinetic rate data

Finding Scalar Correction Factor:

A scalar correction factor for each data set was applied to *ArCl (mol) at time t* and *Rate (M/s)* data points to account for imperfect faradaic efficiency.

The raw data was transformed as stated above and ArCl (mol) at time t [column G, below] was plotted against time (s) [column A, below] and the correction factor was found by adjusting the scalar value until the terminal data point on the ArCl (mol) vs. time (s) matched the remaining ArCl mol measured by GC at the end of the reaction.



Mol of ArCl
measured at the
end of the reaction
= 0 mol.

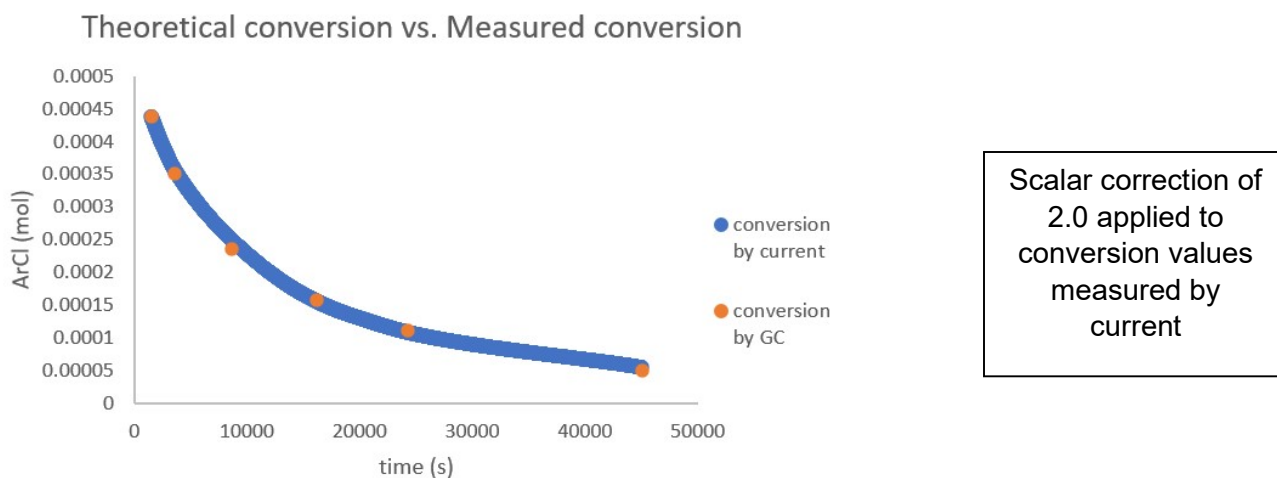
Representative data set transformation:

A	B	C	D	E	F	G	H	I
time (s)	current (A)	Conversion Rate (mol/s) [B2/96485.33]	Absolute value of Rate (mol/s) [Abs(C2)]	Rate (M/s) [D2/0.005]	ArCl (mol) consumed at time t $(((A3-A2)*D30)+(((A3-A2)*(D2-D3))/2))$	ArCl at t (mol) $[G2-(F3/(\text{faradaic efficiency correction factor}))]$	[ArCl] (M) at t [G2/0.005]	M/s corrected $[E2/\text{faradaic efficiency correction factor}]$
859.57	-0.0002	-2.5E-09	2.5E-09	5.1E-07	8.9E-06	4.0E-04	8.0E-02	3.0E-07
1074.57	-0.0077	-8.0E-08	8.0E-08	1.6E-05	1.8E-05	3.9E-04	7.8E-02	9.4E-06
1289.57	-0.0086	-9.0E-08	9.0E-08	1.8E-05	1.9E-05	3.8E-04	7.6E-02	1.1E-05
1504.57	-0.0084	-8.7E-08	8.7E-08	1.7E-05	1.9E-05	3.7E-04	7.3E-02	1.0E-05
1719.57	-0.0085	-8.8E-08	8.8E-08	1.8E-05	1.8E-05	3.6E-04	7.1E-02	1.0E-05
1934.57	-0.008	-8.3E-08	8.3E-08	1.7E-05	1.8E-05	3.5E-04	6.9E-02	9.8E-06
2149.57	-0.0078	-8.1E-08	8.1E-08	1.6E-05	1.7E-05	3.4E-04	6.7E-02	9.5E-06
2364.57	-0.0075	-7.8E-08	7.8E-08	1.6E-05	1.7E-05	3.3E-04	6.5E-02	9.2E-06
2579.57	-0.0073	-7.6E-08	7.6E-08	1.5E-05	1.6E-05	3.2E-04	6.3E-02	8.9E-06
2794.57	-0.007	-7.2E-08	7.2E-08	1.4E-05	1.5E-05	3.1E-04	6.2E-02	8.5E-06
3009.57	-0.0067	-7.0E-08	7.0E-08	1.4E-05	1.4E-05	3.0E-04	6.0E-02	8.2E-06
3224.57	-0.0063	-6.5E-08	6.5E-08	1.3E-05	1.4E-05	2.9E-04	5.8E-02	7.6E-06
3439.57	-0.0061	-6.3E-08	6.3E-08	1.3E-05	1.4E-05	2.8E-04	5.7E-02	7.4E-06
3654.57	-0.0064	-6.7E-08	6.7E-08	1.3E-05	1.4E-05	2.7E-04	5.5E-02	7.8E-06
3869.57	-0.0059	-6.1E-08	6.1E-08	1.2E-05	1.3E-05	2.7E-04	5.3E-02	7.2E-06
4084.57	-0.0057	-6.0E-08	6.0E-08	1.2E-05	1.3E-05	2.6E-04	5.2E-02	7.0E-06
4299.57	-0.0055	-5.7E-08	5.7E-08	1.1E-05	1.2E-05	2.5E-04	5.1E-02	6.7E-06
4514.57	-0.0054	-5.6E-08	5.6E-08	1.1E-05	1.2E-05	2.5E-04	4.9E-02	6.6E-06
4729.57	-0.0052	-5.4E-08	5.4E-08	1.1E-05	1.1E-05	2.4E-04	4.8E-02	6.4E-06
4944.57	-0.005	-5.1E-08	5.1E-08	1.0E-05	1.1E-05	2.3E-04	4.7E-02	6.1E-06
5159.57	-0.0048	-5.0E-08	5.0E-08	1.0E-05	1.1E-05	2.3E-04	4.5E-02	5.9E-06
5374.57	-0.0047	-4.8E-08	4.8E-08	9.7E-06	1.0E-05	2.2E-04	4.4E-02	5.7E-06
5589.57	-0.0043	-4.4E-08	4.4E-08	8.8E-06	9.4E-06	2.2E-04	4.3E-02	5.2E-06
5804.57	-0.0042	-4.3E-08	4.3E-08	8.7E-06	9.1E-06	2.1E-04	4.2E-02	5.1E-06
6019.57	-0.004	-4.1E-08	4.1E-08	8.3E-06	9.0E-06	2.0E-04	4.1E-02	4.9E-06
6234.57	-0.0041	-4.2E-08	4.2E-08	8.4E-06	8.9E-06	2.0E-04	4.0E-02	5.0E-06
6449.57	-0.0039	-4.1E-08	4.1E-08	8.1E-06	8.6E-06	1.9E-04	3.9E-02	4.8E-06
6664.57	-0.0038	-3.9E-08	3.9E-08	7.9E-06	8.5E-06	1.9E-04	3.8E-02	4.6E-06
6879.57	-0.0038	-4.0E-08	4.0E-08	8.0E-06	8.5E-06	1.8E-04	3.7E-02	4.7E-06
7094.57	-0.0038	-3.9E-08	3.9E-08	7.9E-06	8.0E-06	1.8E-04	3.6E-02	4.6E-06
7309.57	-0.0034	-3.5E-08	3.5E-08	7.1E-06	7.9E-06	1.7E-04	3.5E-02	4.2E-06
7524.57	-0.0036	-3.8E-08	3.8E-08	7.5E-06	7.7E-06	1.7E-04	3.4E-02	4.4E-06
7739.57	-0.0033	-3.4E-08	3.4E-08	6.8E-06	7.3E-06	1.7E-04	3.3E-02	4.0E-06
7954.57	-0.0032	-3.4E-08	3.4E-08	6.7E-06	7.2E-06	1.6E-04	3.2E-02	3.9E-06
8169.57	-0.0032	-3.3E-08	3.3E-08	6.6E-06	7.0E-06	1.6E-04	3.2E-02	3.9E-06
8384.57	-0.0031	-3.2E-08	3.2E-08	6.3E-06	6.8E-06	1.5E-04	3.1E-02	3.7E-06

Calibrating *in situ* current monitoring by GC aliquots (validating scalar correction method)

A flame dried large H-cell was equipped with stir bars and lithium perchlorate (266 mg, 2.5 mmol) was added to the anode and cathode chambers. 4-chlorobiphenyl (75.5 mg, 0.40 mmol), 4-DPAIPN (31.9 mg, 0.04 mmol) and mesitylene (18 μ L, 0.13 mmol) were added to the cathode. The cell was equipped with a three electrode setup and purged with a balloon of argon. Freeze/pump/thawed DMF (5.0 mL) was added to the cathode chamber with a reusable glass syringe at the same time as DMF (5.0 mL) was added to the anode under an argon atmosphere. Triethylamine (300 μ L) was added to the anode. The reaction was electrolyzed at -1.6 V vs. SCE in the dark and with an aluminum foil shield until current magnitude decreased $> -200 \mu$ A after which the aluminum foil shield was removed and the reaction was irradiated at 405 nm for 12 hours. Aliquots (20 μ L) were removed for GC analysis at $t = 0$ min, 25 min, 60 min, 143 min, 268 min, 404 min, and after the reaction was terminated.

The current data was transformed as described above and ArCl (mol) at time t was plotted against time (s). The conversion measured at various timepoints by GC was plotted over the theoretical conversion data. By applying a scalar correction factor of 2.0 to each data point of ArCl (mol) at time t as determined by current passed, the two data sets overlaid. This confirmed that faradaic efficiency was imperfect but constant throughout the reaction course and that by applying a correction factor to each data set gathered via potentiostat, current could be used as a proportional measurement of conversion over time.



This also confirmed that a unique correction factor could be found for each reaction profile without needing timepoints throughout by measuring ArCl by GC after the reaction was terminated and applying a value that made the ending ArCl (mol) according to current passed overlap with ArCl (mol) measured by GC.

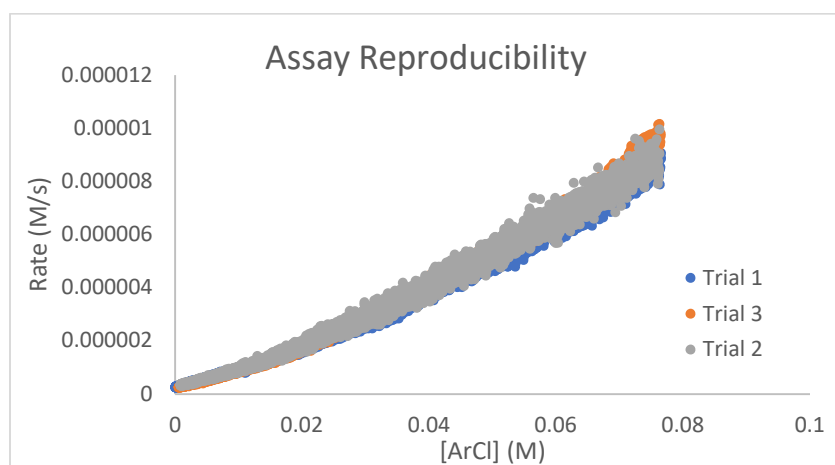
Reproducibility of the assay:

A flame dried large H-cell was equipped with stir bars and lithium perchlorate (266 mg, 2.5 mmol) was added to the anode and cathode chambers. 4-chlorobiphenyl (75.5 mg, 0.40 mmol), 4-DPAIPN (31.9 mg, 0.04 mmol) and mesitylene (18 μ L, 0.13 mmol) was added to the cathode. The cell was equipped with a three electrode setup and purged with a balloon of argon. Freeze/pump/thawed DMF (5.0 mL) was added to the cathode chamber with a reusable glass syringe at the same time as DMF (5.0 mL) was added to the anode under an argon atmosphere.

Triethylamine (300 μL) was added to the anode. The reaction was electrolyzed at -1.6 V vs. SCE in the dark and with an aluminum foil shield until current magnitude decreased $> -200\ \mu\text{A}$ after which the aluminum foil shield was removed and the reaction was irradiated at 405 nm for 12 hours. After 12 hours GC analysis showed complete conversion of 4-chlorobiphenyl.

Altering electrolyte identity to lithium perchlorate as well as increasing electrolyte concentration significantly improved reproducibility of current traces of both **4-DPAIPN** and **NpMI** with little to no impact on substrate conversion or product yield.

Two additional trials of this reaction were carried out and the rate data for all three trials were transformed as stated above and compared to assess reproducibility of the developed assay:



Reaction assay was found to be suitably reproducible.

*Same Excess Experiment for **4DPAIPN***

Stock solution A – A 4.0 M solution of 4-Chlorobiphenyl in DMF was prepared in a 1 mL volumetric flask

Stock solution B – 0.008 M **4DPAIPN**, 0.5 M LiClO_4 in DMF was prepared in a 25 mL volumetric flask and transferred to a schlenk tube and degassed by 3 freeze/pump/thaw cycles and stored wrapped in tin foil.

General Procedure D: A flame dried large H-cell was equipped with stir bars and lithium perchlorate (266 mg, 2.5 mmol) was added to the anode chamber and an appropriate stock solution (see experiment details below) was added to the cathode. The cell was equipped with a three electrode setup and purged with a balloon of argon. Stock solution B (5.0 mL) was added to the cathode chamber with a reusable glass syringe at the same time as DMF (5.0 mL) was added to the anode under an argon atmosphere. Triethylamine (300 μL) was added to the anode. The reaction was electrolyzed at -1.6 V vs. SCE in the dark and with an aluminum foil shield until current magnitude decreased $> -200\ \mu\text{A}$ after which the aluminum foil shield was removed and the reaction was irradiated at 405 nm for 12 hours. Temperature was maintained by electric fans cooling. After 12 hours GC analysis showed complete conversion of 4-chlorobiphenyl.

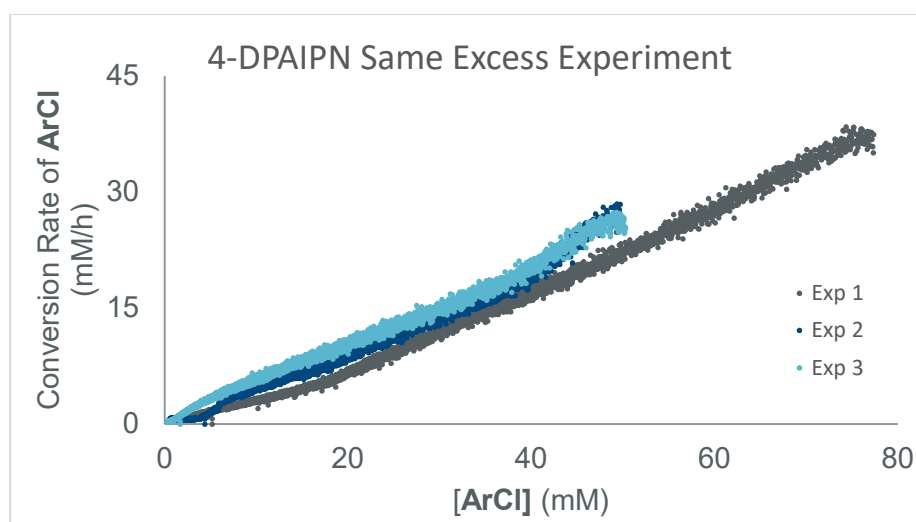
Experiment 1 [ArCl] = 0.08 M – 100 μL of stock solution A, carried out according to general procedure D

Experiment 2 $[ArCl] = 0.052\text{ M}$ – 60 μL of stock solution A, carried out according to general procedure D

Experiment 3 $[ArCl] = 0.052\text{ M}$ – 60 μL of stock solution A and biphenyl (21.6 mg, 0.14 mmol), carried out according to general procedure D

Experiment	Ending ArCl (mmol)	Correction factor
1	0	1.72
2	0	2.2
3	0	2.08

The $[ArCl]$ vs. Rate data for all three experiments were overlayed:



Perfectly overlapping traces indicates that the same amount of catalyst is active at a given concentration regardless of how many turnovers have taken place previously and it reveals that there is no catalyst decomposition taking place over the course of the reaction. A lack of overlay between rate traces from different starting concentrations suggests that there are different amounts of catalyst present at the same concentration despite both reactions starting with the same moles of catalyst. A different amount of active catalyst suggests that there is consumption of the catalyst throughout the reaction either through decomposition or through inhibitory effects from the formation of product.

In the above experiment, when substrate concentration is varied between standard reaction conditions (0.08 M) and a lower starting concentration (0.052 M) overlay of the rate profiles is very close. This suggests that there is some minor catalyst inhibition occurring in the reaction. When the profile for experiment three is compared to the previous two profiles, it does not overlap with experiment 1 indicating that the presence of product is not inhibiting the catalyst and that the lack of overlay is occurring due to minor catalyst decomposition.

Different Excess Experiment for **4DPAIPN**

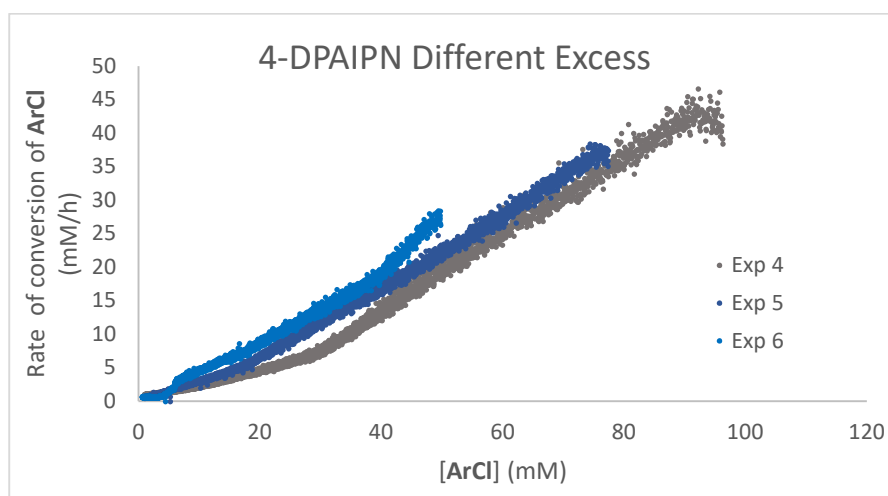
Experiment 4 $[\text{ArCl}] = 0.10 \text{ M}$ – 125 μL of stock solution A, carried out according to general procedure D

Experiment 5 $[\text{ArCl}] = 0.08 \text{ M}$ – 100 μL of stock solution A, carried out according to general procedure D

Experiment 6 $[\text{ArCl}] = 0.052 \text{ M}$ – 60 μL of stock solution A, carried out according to general procedure D

Experiment	Ending ArCl (mmol)	Correction factor
4	0	1.72
5	0	2.2
6	0	1.55

The $[\text{ArCl}]$ vs. Rate data (obtained and transformed as described above) for all three experiments were overlayed:



The nearly linear nature of the traces when plotted according to $[\text{ArCl}]$ as well as the closeness to overlaying is consistent with minor catalyst decomposition and the reaction being first order in aryl chloride substrate.

Same Excess Experiment for **NpMI**:

Stock solution C – 0.008 M **NpMI**, 0.5 M LiClO_4 in DMF was prepared in a 25 mL volumetric flask and transferred to a schlenk tube and degassed by 3 freeze/pump/thaw cycles and stored wrapped in tin foil.

General Procedure E: A flame dried large H-cell was equipped with stir bars and lithium perchlorate (266 mg, 2.5 mmol) was added to the anode chamber and an appropriate stock solution (see experiment details below) was added to the cathode. The cell was equipped with a three electrode setup and purged with a balloon of argon. Stock solution C (5.0 mL) was added to the cathode chamber with a reusable glass syringe at the same time as DMF (5.0 mL) was added to the anode under an argon atmosphere. Triethylamine (300 μL) was added to the

anode. The reaction was electrolyzed at -1.3 V vs. SCE in the dark and with an aluminum foil shield until current magnitude decreased $> -200 \mu\text{A}$ after which the aluminum foil shield was removed and the cathode was irradiated at 405 nm for 12 hours. Temperature was maintained by electric fan cooling. After 12 hours GC analysis showed incomplete consumption of ArCl however current had dropped to a negligible rate so electrolysis was stopped.

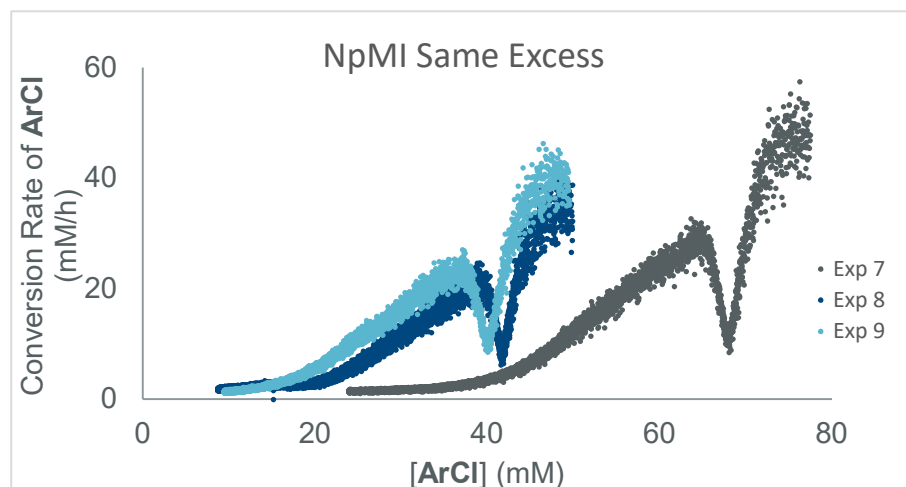
Experiment 7 $[\text{ArCl}] = 0.08 \text{ M}$ – 100 μL of stock solution A, carried out according to general procedure E

Experiment 8 $[\text{ArCl}] = 0.052 \text{ M}$ – 60 μL of stock solution A, carried out according to general procedure E

Experiment 9 $[\text{ArCl}] = 0.052 \text{ M}$ – 60 μL of stock solution A and biphenyl (21.6 mg, 0.14 mmol), carried out according to general procedure E.

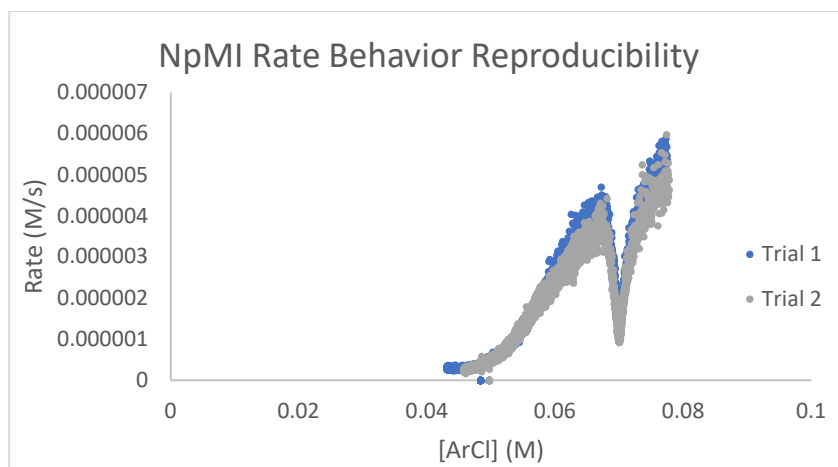
Experiment	Ending ArCl (mmol)	Correction factor
7	0.117	0.8
8	0.045	0.95
9	0.042	0.8

The $[\text{ArCl}]$ vs. Rate data (obtained and transformed as described above) for all three experiments were overlayed:



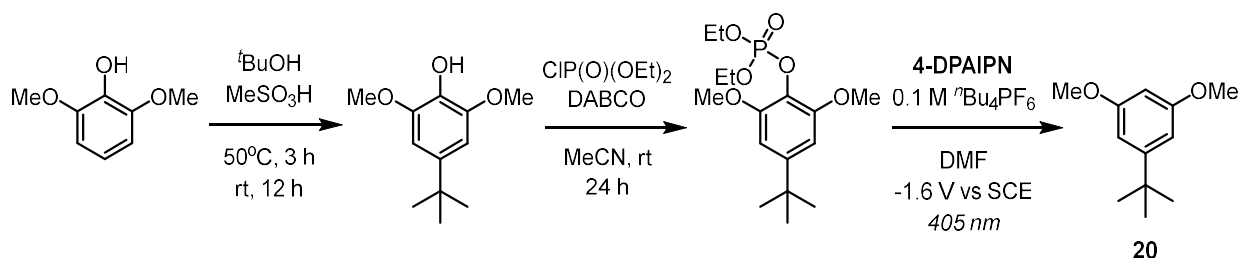
The lack of overlay observed between standard reaction conditions (0.08 M) and lower starting material concentration (0.052 M) indicates that there is a severe amount of catalyst death occurring in the reaction. Since adding biphenyl in to a reaction with a lower starting ArCl concentration does not restore overlay with standard reaction conditions, catalyst deactivation is occurring due to decomposition and not from inhibition by biphenyl.

The reaction rate profile obtained for NpMI was unusual and to confirm that it was reproducible and a result of NpMI's reactivity and not due to an error in electrochemical setup, replicate reactions were carried out to confirm the observed behavior's reproducibility. The unusual reaction profile shape was found to be reproducible.



The absence of overlay observed for the NpMI substrate is significantly more pronounced than what was observed for 4-DPAIPN suggesting that catalyst death and decomposition is a much more inhibitory problem for NpMI than for 4-DPAIPN. This increased proneness to decomposition could explain why reactivity with a challenging anilinium substrate was moderate for NpMI.

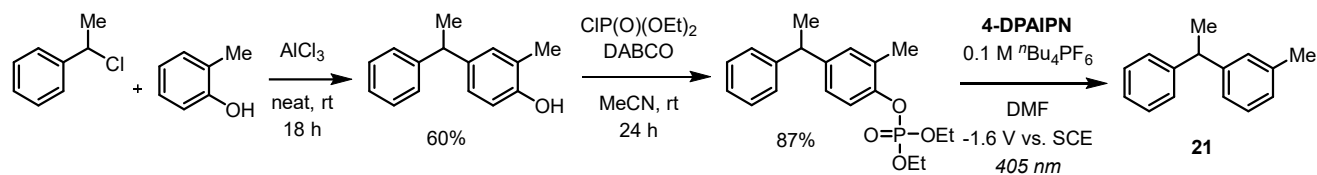
3.7.9 Syntheses using phenol as a traceless directing group



To a round bottom flask was added 2,6-dimethoxyphenol (1.54 g, 10.0 mmol, 1 equiv), *tert*-butanol (949 μ L, 10.0 mmol, 1 equiv) and methanesulfonic acid (2 mL). The reaction mixture was stirred at 50 $^{\circ}$ C for three hours after which the reaction was cooled to room temperature and stirred overnight. The reaction mixture was poured into ice water and extracted with dichloromethane (3x50 mL). The organic layers were combined and washed with brine and dried over MgSO_4 . Solvent was removed in vacuo and the crude reaction mixture to yield crude product as a yellow oil. The crude product mixture was purified by column chromatography to yield a colorless oil (1.73 g, 82%). $^1\text{H NMR}$ (400 MHz, CDCl_3) δ 6.63 (s, 2H), 5.39 (s, 1H), 3.92 (s, 6H), 1.33 (s, 9H), consistent with reported spectra (*J. Org. Chem.* **1982**, 47, 8, 1576-1578).

Aryl phosphate was obtained according to general procedure B with 1.73 g (8.2 mmol) phenol limiting reagent. Product was a white solid (2.48 g, 87%). $^1\text{H NMR}$ (400 MHz, CDCl_3) δ 6.61 (s, 2H), 4.33 (p, $J = 7.2$ Hz, 4H), 3.88 (s, 6H), 1.41 (t, $J = 7.0$ Hz, 6H), 1.32 (s, 8H), consistent with reported spectra (*J. Org. Chem.* **1982**, 47, 8, 1576-1578).

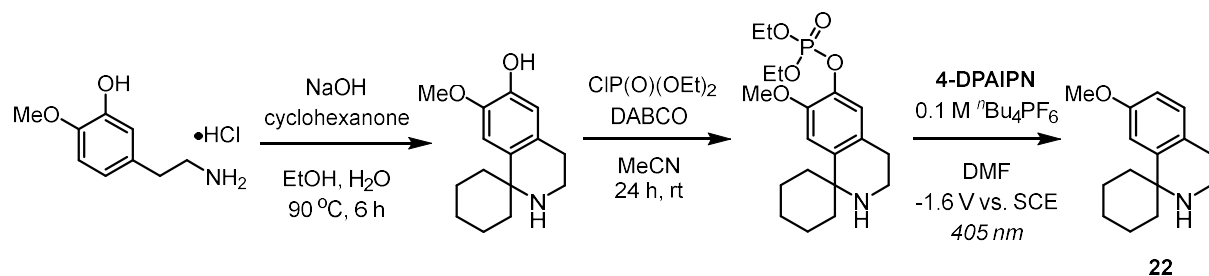
20 was obtained according to general procedure C on a 0.200 mmol scale with the following alterations: electrolyte loading was increased to 0.5 M TBAPF_6 (53% by NMR with a dibromomethane internal standard). $^1\text{HNMR}$ spectrum consistent with reported spectra (*J. Am. Chem. Soc.*, **2020**, 142, 22, 9938-9943).



A flame dried 10 mL schlenk flask was charged with o-cresol (757 mg, 7.0 mmol, 1 equiv) and (1-chloroethyl)benzene (1.18g, 8.4 mmol, 1.2 equiv) and placed under a flow of N₂. Aluminum trichloride (93 mg, 0.7 mmol, 0.1 equiv) was added under a positive pressure of nitrogen and the mixture was stirred at room temperature with the cap opened slightly to a flow of nitrogen for 1 hour to vent HCl gas buildup. The reaction tube was then sealed and stirred for 24 hours. The reaction mixture was quenched by pouring into ice water and extracting with ether (3x50 mL). The organic layer was washed with brine and dried over MgSO₄, concentrated and purified by column chromatography (hexanes:acetone) to yield pure product as a colorless oil (899 mg, 60%). **¹H NMR** (400 MHz, CDCl₃) δ 7.35 – 7.27 (m, 2H), 7.26 – 7.15 (m, 3H), 7.00 (d, J = 2.3 Hz, 1H), 6.96 (dd, J = 8.2, 2.3 Hz, 1H), 6.72 (d, J = 8.1 Hz, 1H), 4.09 (q, J = 7.2 Hz, 1H), 2.24 (s, 3H), 1.63 (d, J = 7.3 Hz, 3H), consistent with reported spectra (*Org. Lett.*, **2016**, 18, 19, 5034 – 5037).

Aryl phosphate was obtained according to general procedure B with 899 mg (4.2 mmol) phenol limiting reagent. Product was a colorless oil (1.29 g, 87%). **¹H NMR** (400 MHz, CDCl₃) δ **¹³C NMR** (126 MHz, CDCl₃) δ 147.49, 147.44, 146.25, 142.86, 130.51, 128.98, 128.92, 128.36, 127.56, 126.06, 119.49, 64.43, 44.13, 21.95, 16.49, 16.09. ; **³¹P NMR** (400 MHz, CDCl₃) δ -5.8 ppm; **HRMS** (ESI+) Calc: [M+H]⁺ (C₁₉H₂₅O₄P) 348.38; measured: 349.2

21 was obtained according to general procedure C on a 0.200 mmol scale (55% by NMR with a dibromomethane internal standard). **¹H NMR** spectrum consistent with reported spectra (*Angew. Chem. Int. Ed.* **2018**, 57, 2, 461-464).

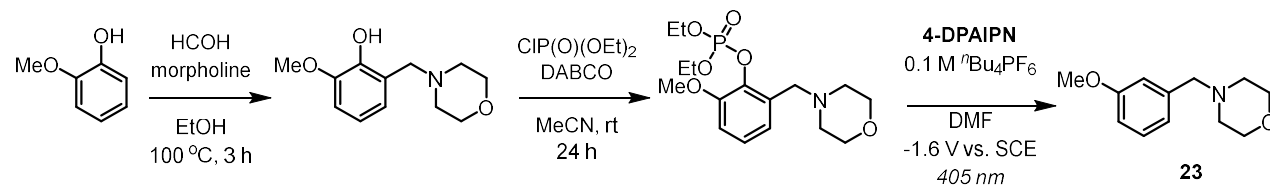


To a flask was added 5-(2-aminoethyl)-2-methoxyphenol-HCl (1.28 g, 7.0 mmol, 1 equiv.), sodium hydroxide (280 mg, 7.0 mmol, 1 equiv.), ethanol (7 mL) and water (1 mL). The solution was stirred until all of the sodium hydroxide had dissolved (10 minutes) and cyclohexanone (1.30 mL, 12.6 mmol, 1.8 equiv.) was added to the reaction mixture. The reaction mixture was stirred at 90 °C for six hours. The solution was cooled to room temperature and then added to a separatory funnel with water (100 mL). The aqueous layer was extracted with EtOAc (3x70 mL). The organic layers were washed with brine, dried over Mg₂SO₄, filtered and concentrated in vacuo. The crude product was purified by triturating with Et₂O and drying under vacuum for 48 hours. Pure product was obtained as an off-white solid (1.35 g, 78% yield). **¹H NMR** (400 MHz, CDCl₃) δ 6.64 (s, 1H), 6.53 (s, 1H), 3.81 (s, 3H), 2.96 (t, J = 5.9 Hz, 2H), 2.60 (t, J = 5.8 Hz, 2H),

1.75 – 1.56 (m, 9H), 1.23 (q, $J = 6.0, 5.2$ Hz, 1H), consistent with reported spectra (*J. Org. Chem.*, **2010**, 75, 24, 8542-8549).

Aryl phosphate was obtained according to general procedure B with 1.30 g (5.3 mmol) phenol limiting reagent. Product was a white solid (1.49 g, 74% yield). **^1H NMR** (400 MHz, CDCl_3) δ 6.87 (s, 1H), 6.72 (s, 1H), 4.18 (pd, $J = 7.2, 2.6$ Hz, 4H), 3.78 (s, 3H), 2.93 (t, $J = 5.8$ Hz, 2H), 2.59 (t, $J = 5.8$ Hz, 2H), 1.74 – 1.54 (m, 9H), 1.29 (t, $J = 7.1$ Hz, 6H), 1.26 – 1.12 (m, 1H), **^{13}C NMR** (126 MHz, CDCl_3) δ 171.13, 155.56, 153.60, 152.48, 137.01, 109.03, 107.96, 64.63, 63.96, 60.39, 56.40, 45.43, 21.04, 16.01, 14.20; **^{31}P NMR** (400 MHz, CDCl_3) δ -5.76 ppm; **HRMS** (ESI+) Calc: $[\text{M}+\text{H}]^+$ ($\text{C}_{19}\text{H}_{30}\text{NO}_5\text{P}$) 383.42; measured: 384.2

22 was obtained according to general procedure C on a 0.300 mmol scale with the following alterations: electrolyte loading was increased to 0.5 M TBAPF₆. Reaction solution was transferred to a separatory funnel with diethyl ether (50 mL) and 5 M HCl aqueous solution (60 mL). The aqueous layer was collected and the ether layer was washed with additional 5 M HCl (2x60 mL). The aqueous layers were combined and basified with concentrated NaOH solution until pH was 12. The basic aqueous layers were added to the separatory funnel and extracted with ether (3x50 mL). The ether layers from the basic extraction were combined, washed with brine, dried over Mg_2SO_4 and filtered. The solvent was removed in vacuo to give crude product mixture. The crude product was further purified by column chromatography to yield pure product as a colorless oil (43.0 mg, 62% yield). **^1H NMR** (400 MHz, CDCl_3) δ 7.04 – 6.98 (m, 1H), 6.83 (d, $J = 2.7$ Hz, 1H), 6.72 (dd, $J = 8.4, 2.7$ Hz, 1H), 3.82 (s, 3H), 3.05 (t, $J = 5.9$ Hz, 2H), 2.73 (t, $J = 5.8$ Hz, 2H), 1.86 – 1.64 (m, 9H), 1.33 (ddd, $J = 21.6, 13.2, 7.3$ Hz, 1H). **^{13}C NMR** (126 MHz, CDCl_3) δ 157.69, 146.06, 129.93, 127.25, 111.59, 111.21, 55.30, 54.76, 38.44, 37.86, 30.10, 25.73, 21.70. **HRMS** (ESI+) Calc: $[\text{M}+\text{H}]^+$ ($\text{C}_{15}\text{H}_{21}\text{NO}$) 231.34; measured: 232.2.

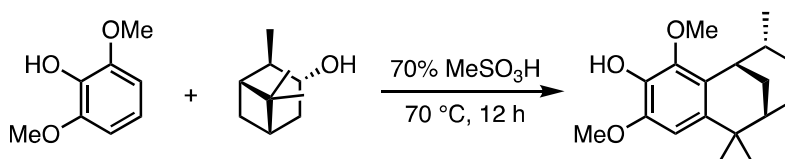


To a round bottom flask was added morpholine (1.48 g, 17.0 mmol, 1.7 equiv), ethanol (10 mL) and 36% aqueous formaldehyde (1.4 mL, 17.0 mmol, 1.7 equiv) followed by 2-methoxyphenol (1.12 mL, 10.0 mmol, 1 equiv). The solution was refluxed for 3 hours. The reaction mixture was cooled to room temperature and the solvent was removed in vacuo to give crude product mixture as a yellow oil. The crude product was purified by column chromatography to give the ortho alkylated arene as the major product as a colorless oil (1.36 g, 61%). **^1H NMR** (400 MHz, CDCl_3) δ 6.84 (dd, $J = 8.1, 1.6$ Hz, 1H), 6.77 (td, $J = 7.8, 1.7$ Hz, 1H), 6.63 (dd, $J = 7.6, 1.7$ Hz, 1H), 3.90 (d, $J = 1.7$ Hz, 3H), 3.76 (d, $J = 4.9$ Hz, 4H), 3.74 (d, $J = 1.7$ Hz, 2H), 2.60 (s, 4H), consistent with reported spectra (*J. Am. Chem. Soc.*, **2017**, 139, 36, 12390 – 12393).

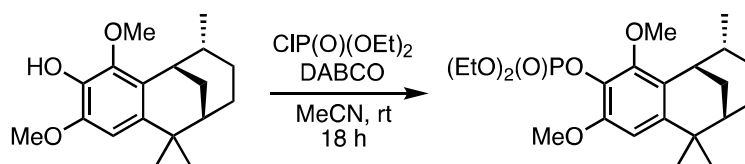
Aryl phosphate was obtained according to general procedure B with 1.35 g (6.05 mmol) phenol limiting reagent. Product was an off-white solid (1.54 g, 71%). **^1H NMR** (400 MHz, CDCl_3) δ 7.16 – 7.04 (m, 2H), 6.87 (dd, $J = 7.8, 1.9$ Hz, 1H), 4.37 – 4.20 (m, 4H), 3.88 (s, 3H), 3.76 – 3.69 (m, 4H), 3.66 (s, 2H), 2.53 – 2.46 (m, 4H), 1.39 (td, $J = 7.1, 1.2$ Hz, 6H). **^{13}C NMR** (126 MHz, CDCl_3) δ 151.16, 139.05, 131.04, 125.24, 122.33, 111.22, 67.09, 64.38, 56.82, 55.98, 53.61, 16.16; **^{31}P NMR** (400 MHz, CDCl_3) δ -6.0 ppm; **HRMS** (ESI+) Calc: $[\text{M}+\text{H}]^+$ ($\text{C}_{16}\text{H}_{26}\text{NO}_6\text{P}$) 359.36; measured: 360.2

23 was obtained according to general procedure C on a 0.200 mmol scale with the following alterations: electrolyte loading was increased to 0.5 M TBAPF₆, MgClO₄ (45 mg, 0.2 mmol, 1 equiv) was added to the cathode and the applied potential was lowered to -1.55 V vs. SCE (60% by NMR with a dibromomethane internal standard). ¹H NMR was consistent with reported spectra (*Tetrahedron*, **2014**, 70, 4, 880-885).

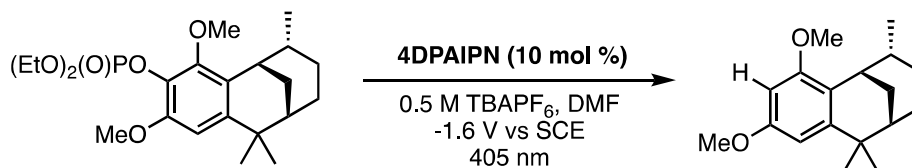
3.7.10 Synthesis of a tricyclic resorcinol derivative



To a flame dried 250 mL RBF with stir bar, added 2,6-dimethoxyphenol (1.7 g, 11 mmol, 1 equiv) and (-)-3-pinanol (2.0 g, 13.3 mmol, 1.2 equiv). The flask was capped with a septum and purged with an argon balloon. While under an Ar atmosphere, 70% aqueous methane sulfonic acid (51 mL, 0.2 M) was added. (70% solution was made from DI water and neat methane sulfonic acid. The solution was cooled to rt before adding to the reaction flask). The mixture was heated to 70 °C and stirred for 12 h. The reaction mixture was cooled to rt and poured into 150 mL ice cold water. Ice chips were added until the reaction cooled (Note: Adding water causes reaction to exotherm. Ensure reaction has cooled before adding ether). The product was extracted with diethyl ether (2x100 mL) followed by additional diethyl ether washes (2x50 mL). The organic layers were combined and washed with 100 mL brine and dried over Na₂SO₄. The dried organic layers were filtered and concentrated in vacuo to give crude product as a yellow oil. The crude product was purified by column chromatography (5-20% EtOAc in hexanes, R_f = 0.5 in 5:1 EtOAc:hexanes, stains blue with vanillin) to yield a white solid (1.46 g, 45%). ¹H NMR (400 MHz, CDCl₃) δ 6.61 (s, 1H), 5.38 (s, 1H), 3.88 (s, 3H), 3.87 (s, 3H), 2.88 (s, 1H), 1.97 (dt, J = 13.0, 3.2 Hz, 1H), 1.80 (ddt, J = 12.7, 9.9, 4.3 Hz, 2H), 1.74 – 1.65 (m, 2H), 1.57 (q, J = 3.4 Hz, 1H), 1.41 – 1.36 (m, 1H), 1.33 (s, 3H), 1.24 (s, 3H), 1.19 (d, J = 7.2 Hz, 3H), 0.98 (d, J = 13.6 Hz, 1H).

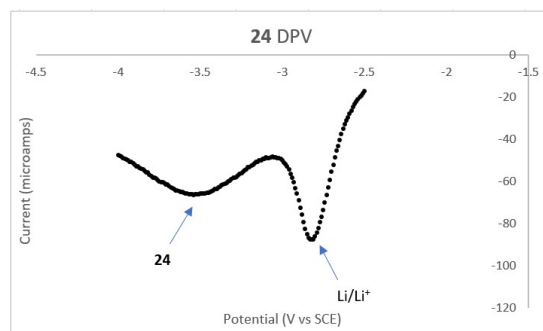


Aryl phosphate was obtained according to general procedure B. The crude product was purified by column chromatography (15-25% acetone in hexanes, R_f = 0.47 in 25% acetone in hexanes, stains blue with vanillin) to yield a colorless oil (1.44 g, 70%). ¹H NMR (600 MHz, CDCl₃) δ 6.65 (s, 1H), 4.26 (pd, J = 7.1, 4.6 Hz, 4H), 3.85 (s, 3H), 3.83 (s, 3H), 2.85 (s, 1H), 1.95 (dt, J = 13.1, 3.1 Hz, 1H), 1.80 – 1.64 (m, 4H), 1.56 (t, J = 3.5 Hz, 1H), 1.40 – 1.30 (m, 10H), 1.22 (s, 3H), 1.16 (d, J = 7.1 Hz, 3H), 0.96 (d, J = 13.4 Hz, 1H).

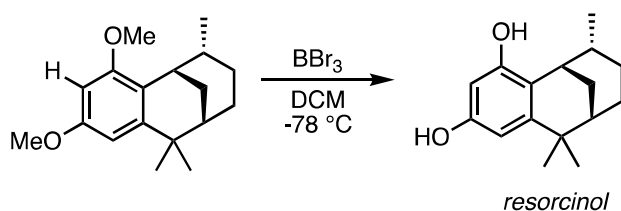


Phenol defunctionalization was obtained according to general procedure C except with 0.5 M $n\text{Bu}_4\text{PF}_6$ in anode and cathode. After 12 h, the contents from the cathode and anode were transferred to a separatory funnel with 70 mL 10% LiCl aq solution. Product was extracted with diethyl ether (3x50 mL). The organic layers were combined and washed with 100 mL 1M HCl and 100 mL brine and dried over Na_2SO_4 . The organic layers were filtered and concentrate in vacuo. The crude product was purified by column chromatography (1-20% acetone in hexanes, $R_f = 0.73$ in 15% acetone in hexanes) to yield a white solid (34 mg, 62%). **^1H NMR** (400 MHz, CDCl_3) δ 6.49 (d, $J = 2.5$ Hz, 1H), 6.29 (d, $J = 2.4$ Hz, 1H), 3.81 (s, 3H), 3.77 (s, 3H), 2.92 (s, $J = 3.7$ Hz, 1H), 1.96 (dt, $J = 13.2, 3.2$ Hz, 1H), 1.84 – 1.66 (m, 4H), 1.58 (t, $J = 3.5$ Hz, 1H), 1.45 – 1.39 (m, 1H), 1.34 (s, 3H), 1.26 (s, 3H), 1.17 (d, $J = 7.2$ Hz, 3H), 0.98 (d, $J = 15.7$ Hz, 1H).

Differential Pulse Voltammetry of **24**:



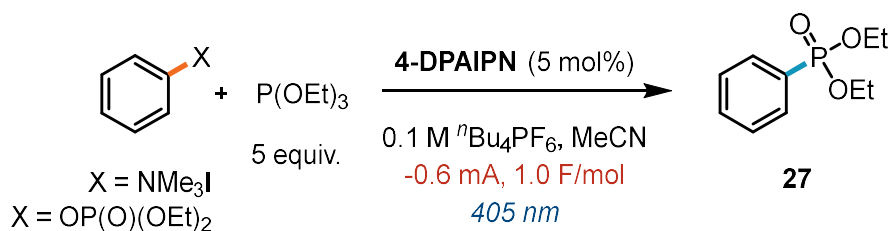
$$E_{\text{red}} = -3.54 \text{ V vs. SCE}$$



To a 2-dram vial was added **25** (34 mg, 0.124 mmol, 1 equiv) with a stir bar and a septum-lined cap. The vial was evacuated and backfilled with N_2 three times. While under active N_2 , anhydrous DCM (1.35 mL, 0.1 M) was added and the solution was cooled to -78°C using dry ice/acetone bath. To the solution was added slowly 1M BBr_3 in DCM (300 μL , 0.300 mmol, 2.4 equiv). The reaction solution was stirred overnight with gradual warming. The crude product was purified by column chromatography (30-50% diethyl ether in hexanes) to yield a white solid (28 mg, 91%). **^1H NMR** (600 MHz, CDCl_3) δ 6.42 (d, $J = 2.5$ Hz, 1H), 6.16 (d, $J = 2.4$ Hz, 1H), 4.84 (s, 2H), 2.76 (s, $J = 3.1$ Hz, 1H), 1.98 (dt, $J = 13.1, 3.2$ Hz, 1H), 1.83 – 1.66 (m, 4H), 1.58 (p, $J = 3.6$ Hz, 1H), 1.39 – 1.35 (m, 1H), 1.30 (s, 3H), 1.23 (s, 3H), 1.19 (d, $J = 7.2$ Hz, 3H), 1.01 (d, $J = 13.7$ Hz, 1H).

3.7.11 Redox neutral coupling reactions

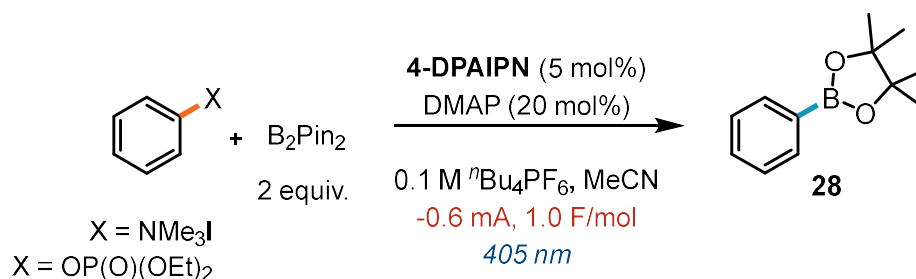
To confirm that the aryl radical intermediate generated during the reaction can be intercepted by classic radical trapping agents, we carried out several coupling reactions from the phenyl trimethylammonium iodide and phenyl diethyl phosphate ester.

Phosphonylation:

To the cathode of an H-typed divided cell was added tetrabutylammonium hexafluorophosphate (96 mg, 0.25 mmol, 1.2 equiv), 4-DPAIPN (8.0 mg, 0.01 mmol, 0.05 equiv.), and either phenyltrimethylammonium iodide (52.6 mg, 0.200 mmol, 1 equiv) or phenyl diethyl phosphate ester (46.0 mg, 0.200 mmol, 1 equiv). To the anode was added tetrabutylammonium hexafluorophosphate (96 mg, 0.25 mmol, 1.2 equiv). The cell was equipped with an electrode setup of RVC mounted on stainless steel. The cell was purged with a flow of N_2 for 10 minutes. To the cathode chamber was added triethylphosphite (172 μL , 1.00 mmol, 5 equiv.) and degassed acetonitrile (2 mL) was added to both the anode and cathode. Triethylamine (100 μL , 3.5 equiv.) was added to the anode and the electrode leads were connected to a potentiostat and electrolyzed at -0.6 mA for 9 hours (1 F/mol) and the cathode was irradiated with 405 nm LEDs.

After electrolysis, dibromomethane (7 μL , 0.1 mmol) was added to the cathode as an internal standard. A 100 μL aliquot was removed and added to 0.5 mL of a 10% LiCl aqueous solution and extracted into 200 μL CDCl_3 . An NMR spectrum was obtained of the organic extract to give an analytical yield:

X	Yield of 27
NMe_3I	75
$\text{OP}(\text{O})(\text{OEt})_2$	63

Borylation:

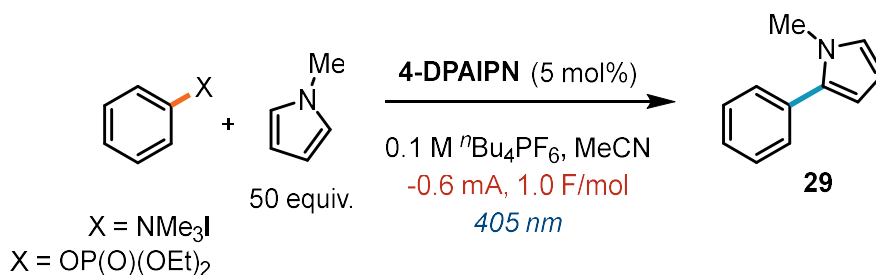
To the cathode of an H-typed divided cell was added tetrabutylammonium hexafluorophosphate (96 mg, 0.25 mmol, 1.2 equiv), 4-DPAIPN (8.0 mg, 0.01 mmol, 0.05 equiv.), dimethylaminopyridine (4.9 mg, 0.04 mmol, 0.20 equiv.), bis(pinacolato)diboron (102 mg, 0.400 mmol, 2 equiv.) and either phenyltrimethylammonium iodide (52.6 mg, 0.200 mmol, 1 equiv) or phenyl diethyl phosphate ester (46.0 mg, 0.200 mmol, 1 equiv). To the anode was added tetrabutylammonium hexafluorophosphate (96 mg, 0.25 mmol, 1.2 equiv). The cell was equipped with an electrode setup of RVC mounted on stainless steel. The cell was purged with a flow of N_2 for 10 minutes. To the cathode and anode chambers was added degassed

acetonitrile (2 mL). Triethylamine (100 μ L, 3.5 equiv.) was added to the anode and the electrode leads were connected to a potentiostat and electrolyzed at -0.6 mA for 9 hours (1 F/mol) and the cathode was irradiated with 405 nm LEDs.

After electrolysis, dibromomethane (7 μ L, 0.1 mmol) was added to the cathode as an internal standard. A 100 μ L aliquot was removed and added to 0.5 mL of a 10% LiCl aqueous solution and extracted into 200 μ L CDCl_3 . An NMR spectrum was obtained of the organic extract to give an analytical yield:

X	Yield of 28
NMe_3I	75
OP(O)(OEt)_2	57

Heteroarylation:

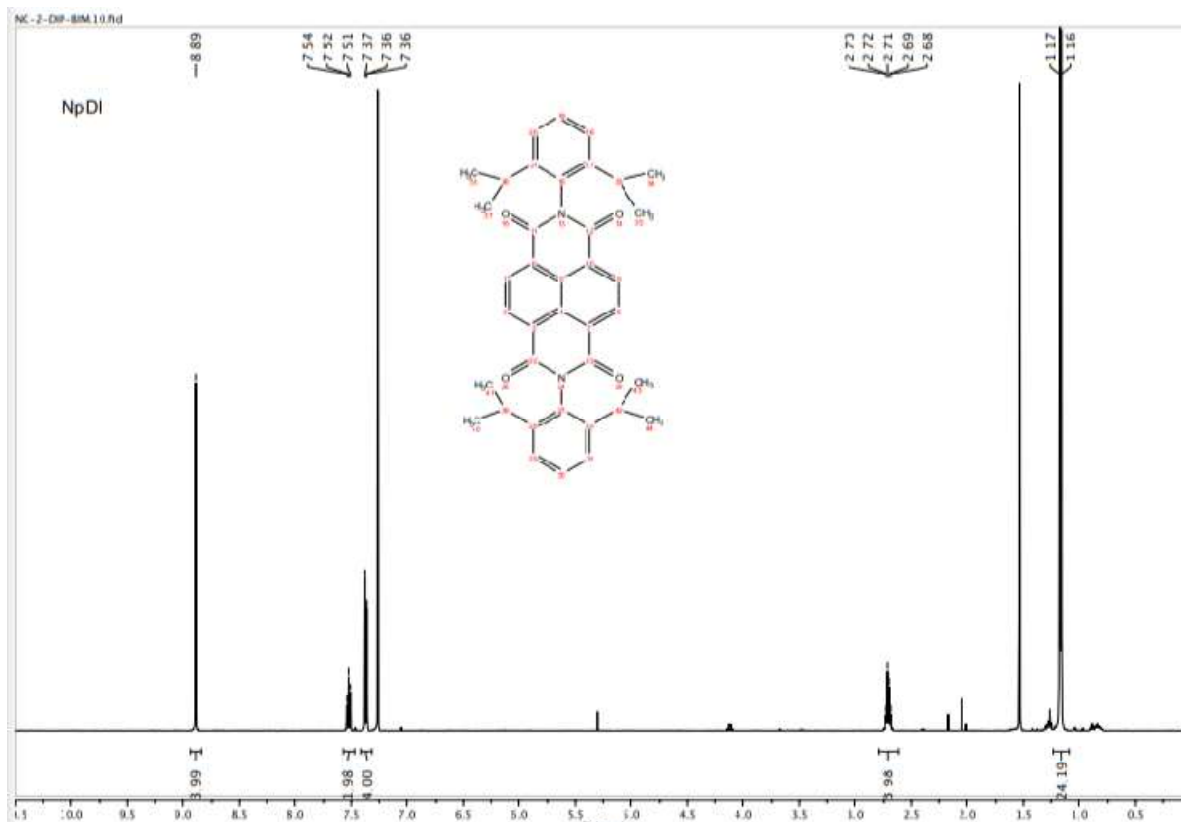
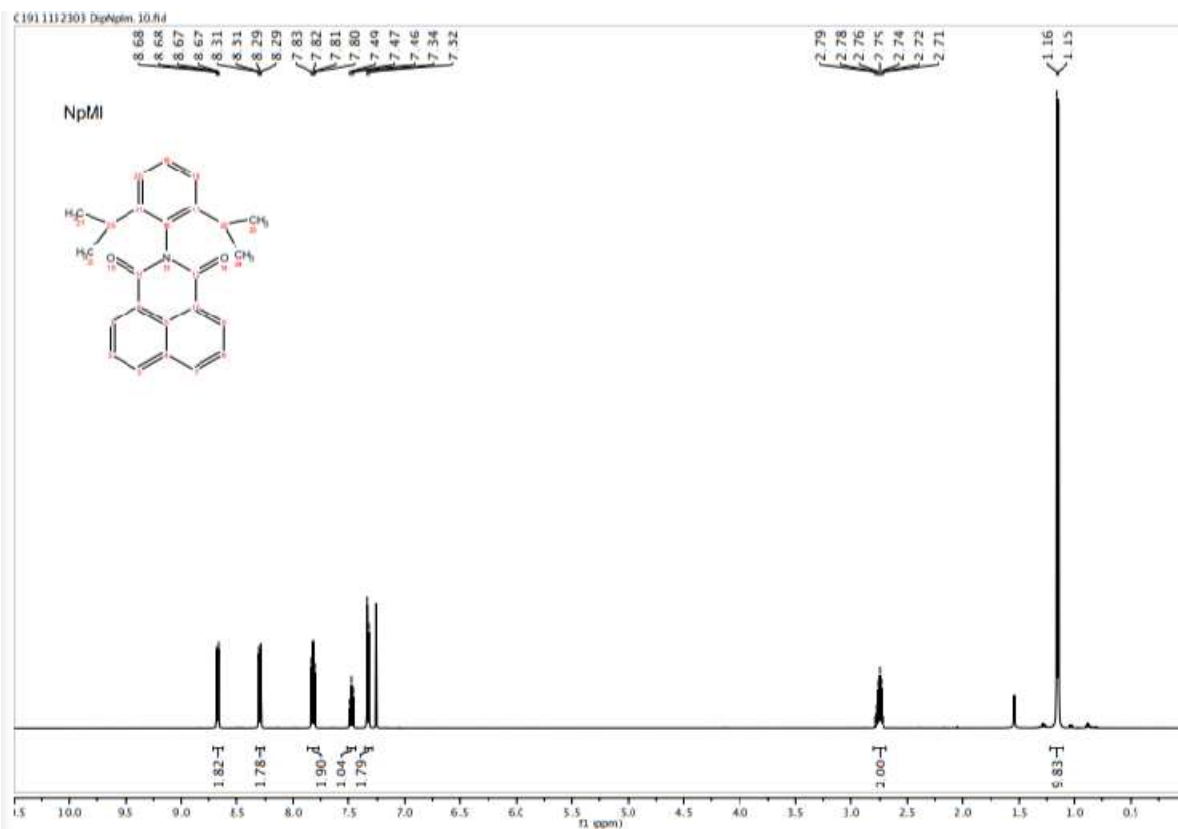


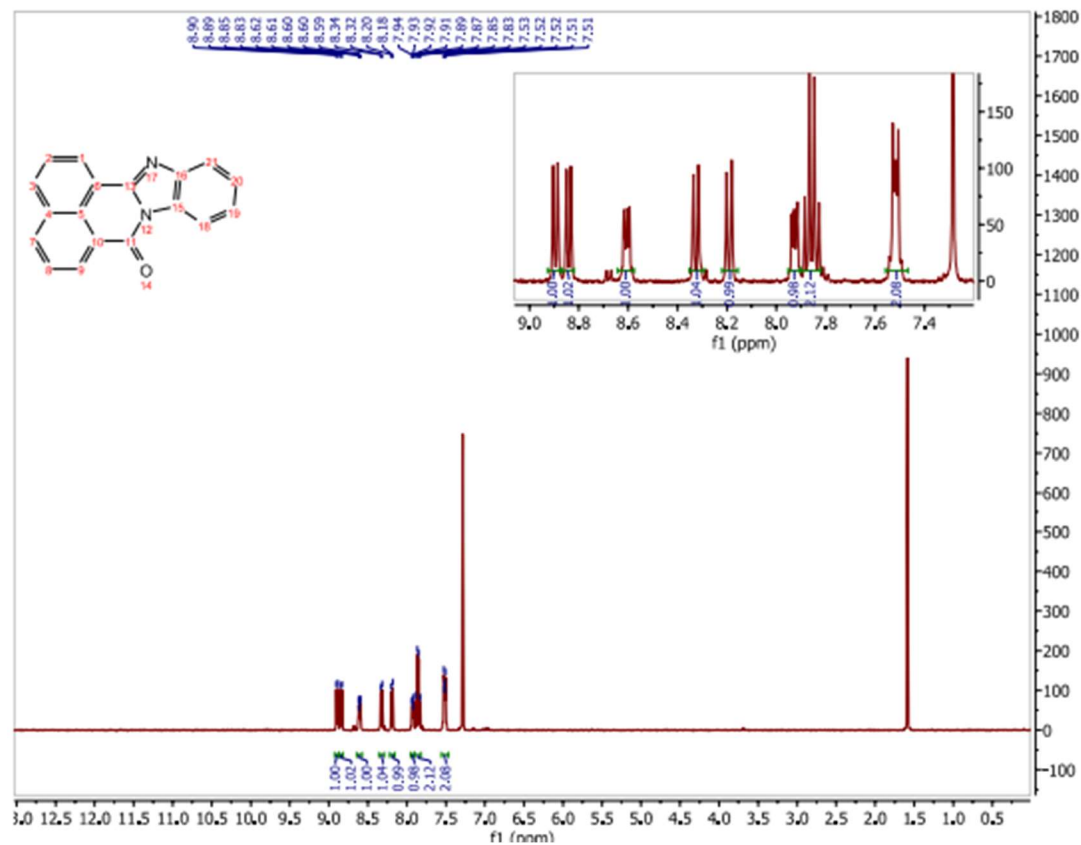
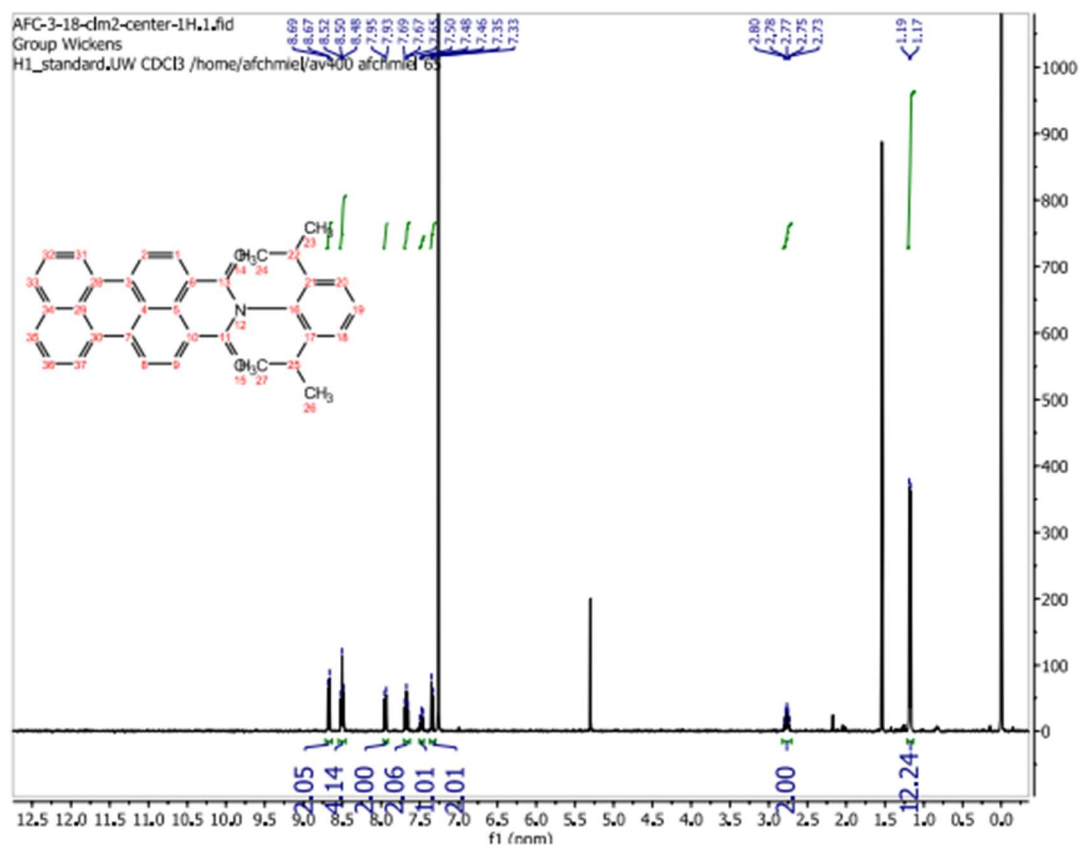
To the cathode of an H-typed divided cell was added tetrabutylammonium hexafluorophosphate (96 mg, 0.25 mmol, 1.2 equiv), 4-DPAIPN (8.0 mg, 0.01 mmol, 0.05 equiv.), and either phenyltrimethylammonium iodide (52.6 mg, 0.200 mmol, 1 equiv) or phenyl diethyl phosphate ester (46.0 mg, 0.200 mmol, 1 equiv). To the anode was added tetrabutylammonium hexafluorophosphate (96 mg, 0.25 mmol, 1.2 equiv). The cell was equipped with an electrode setup of RVC mounted on stainless steel. The cell was purged with a flow of N_2 for 10 minutes. To the cathode chamber was added N-methylpyrrole (888 μ L, 10.0 mmol, 50 equiv.) and degassed acetonitrile (1 mL) cathode. Triethylamine (100 μ L, 3.5 equiv.) and degassed acetonitrile (2 mL) was added to the anode and the electrode leads were connected to a potentiostat and electrolyzed at -0.6 mA for 9 hours (1 F/mol) and the cathode was irradiated with 405 nm LEDs.

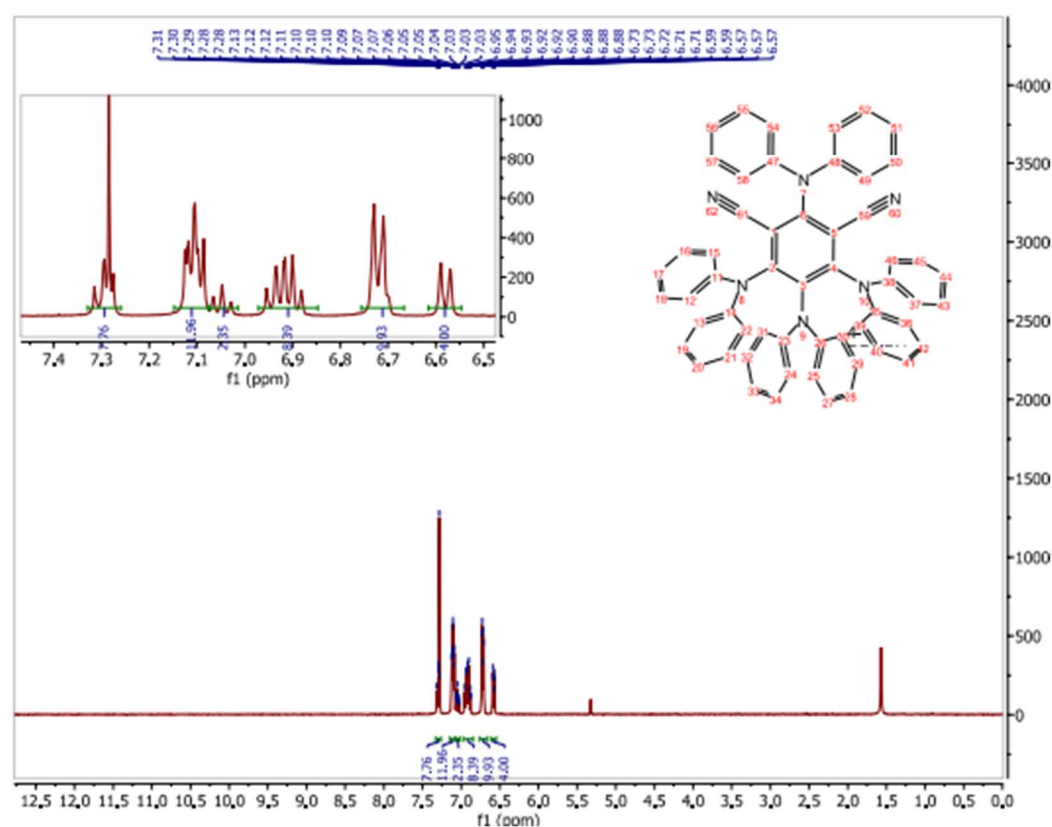
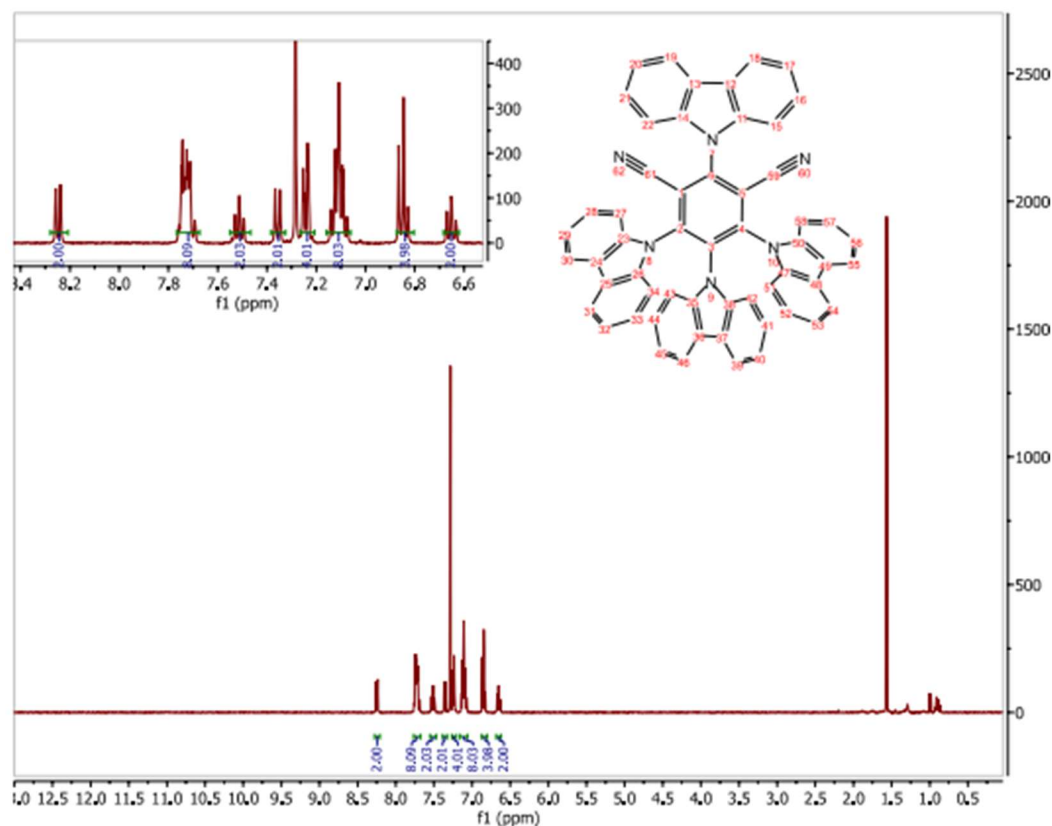
After electrolysis, dibromomethane (7 μ L, 0.1 mmol) was added to the cathode as an internal standard. A 100 μ L aliquot was removed and added to 0.5 mL of a 10% LiCl aqueous solution and extracted into 200 μ L CDCl_3 . An NMR spectrum was obtained of the organic extract to give an analytical yield:

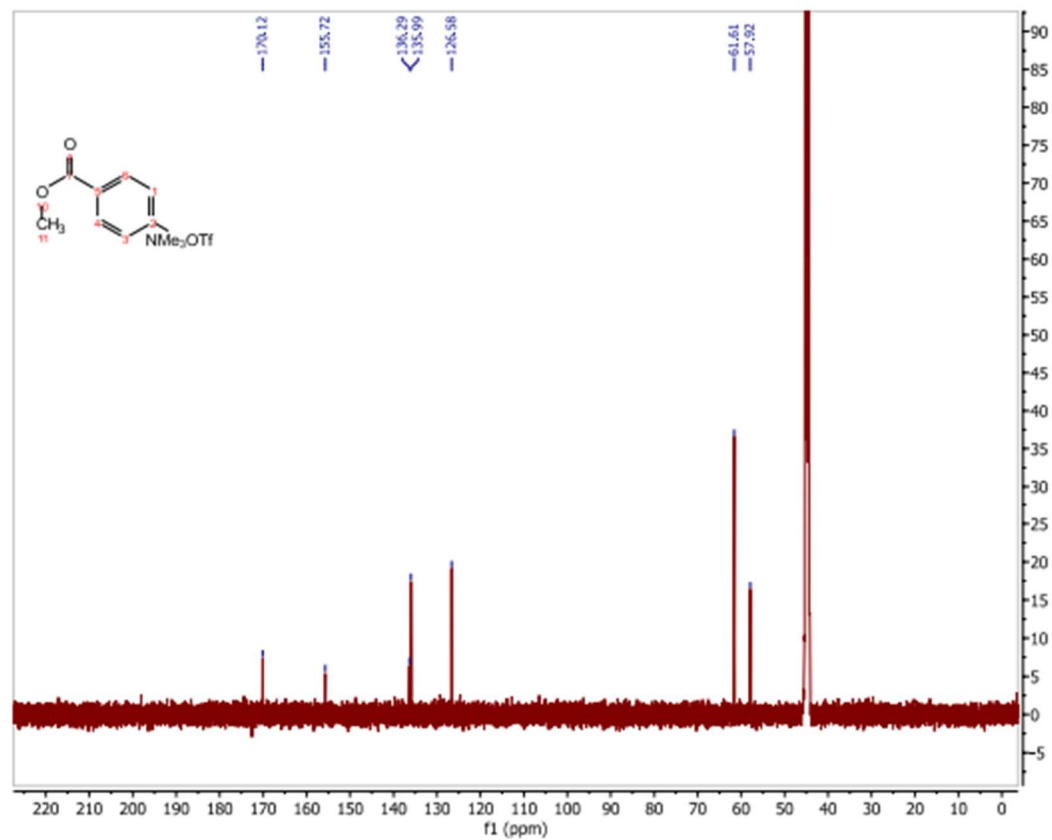
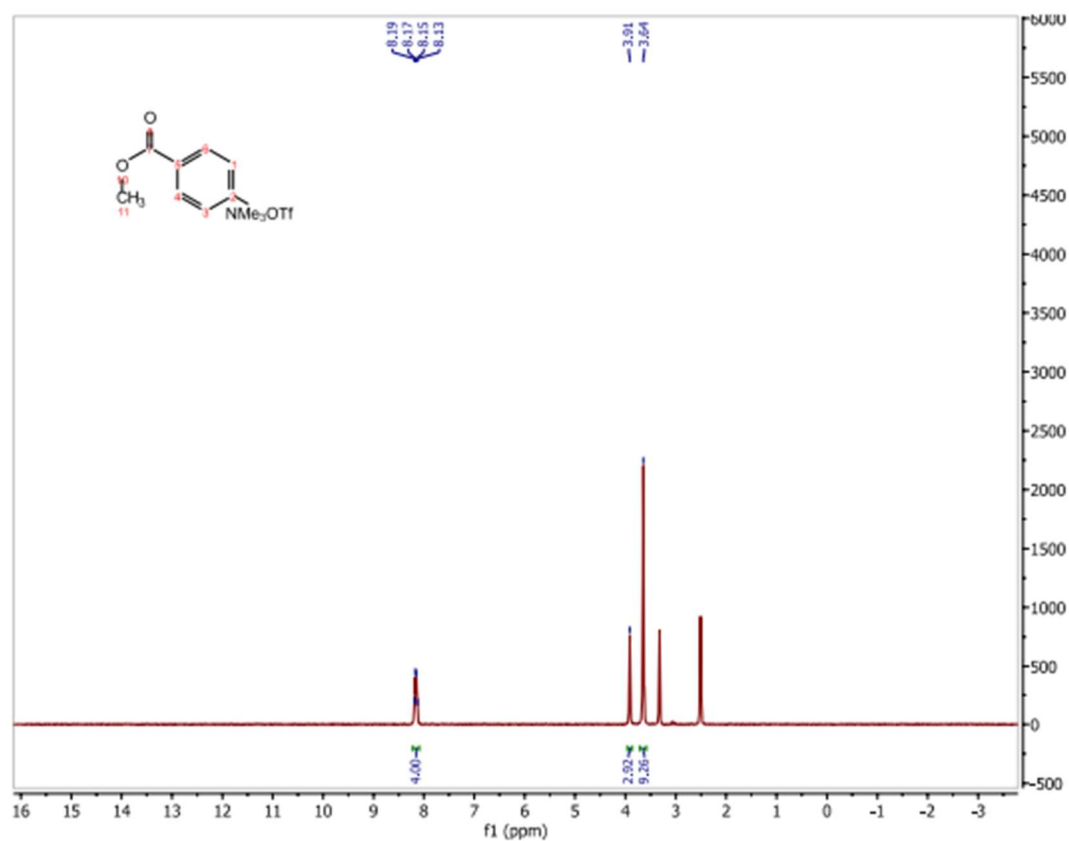
X	Yield of 29
NMe_3I	61
OP(O)(OEt)_2	42

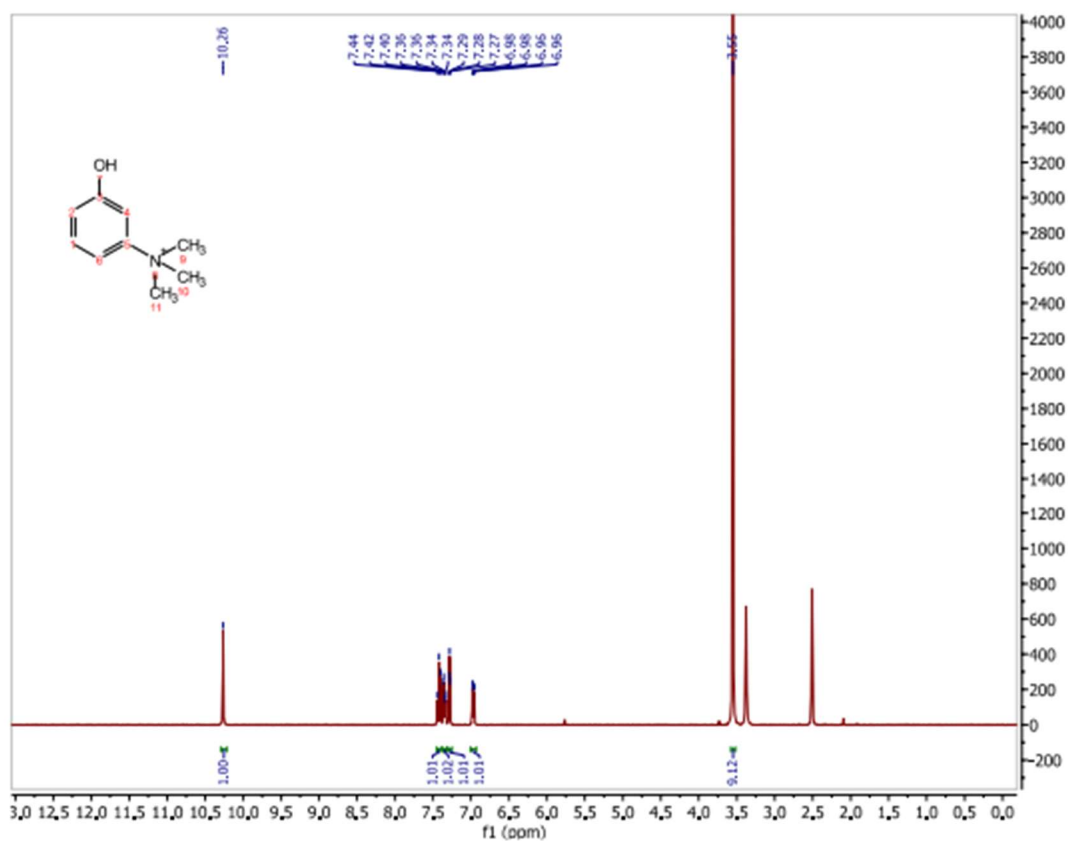
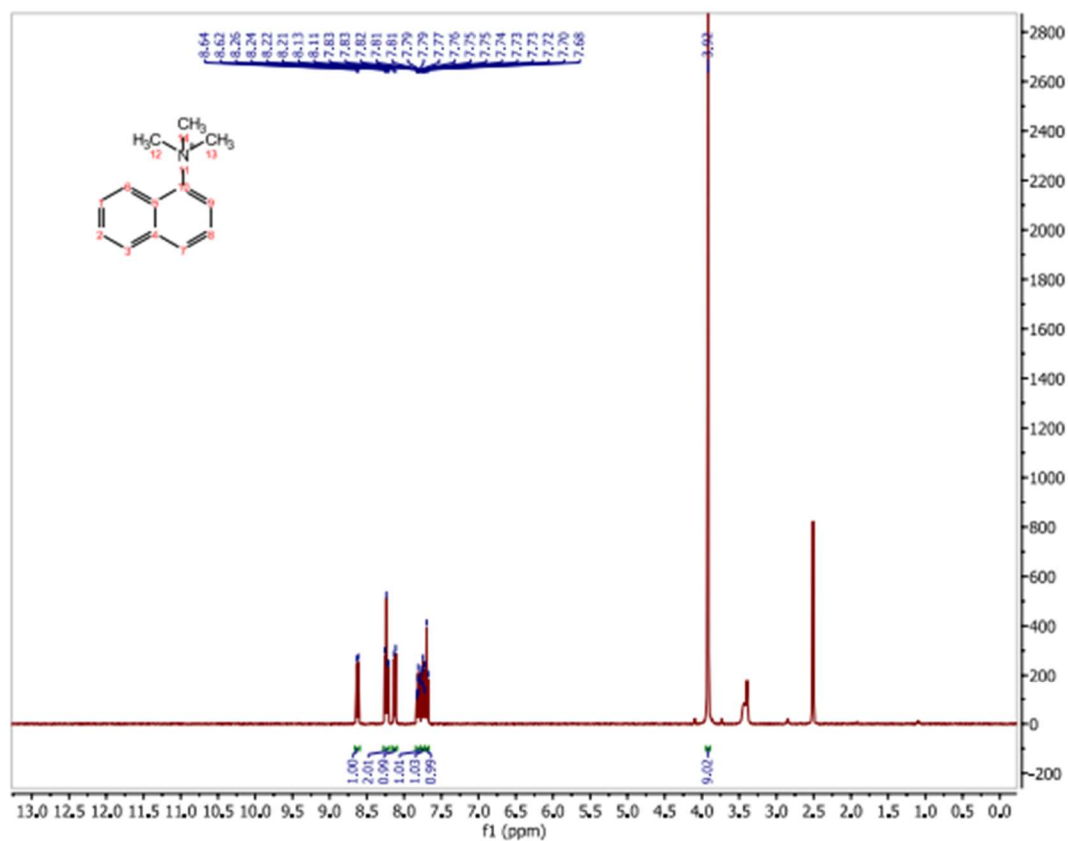
3.7.12 NMR spectra

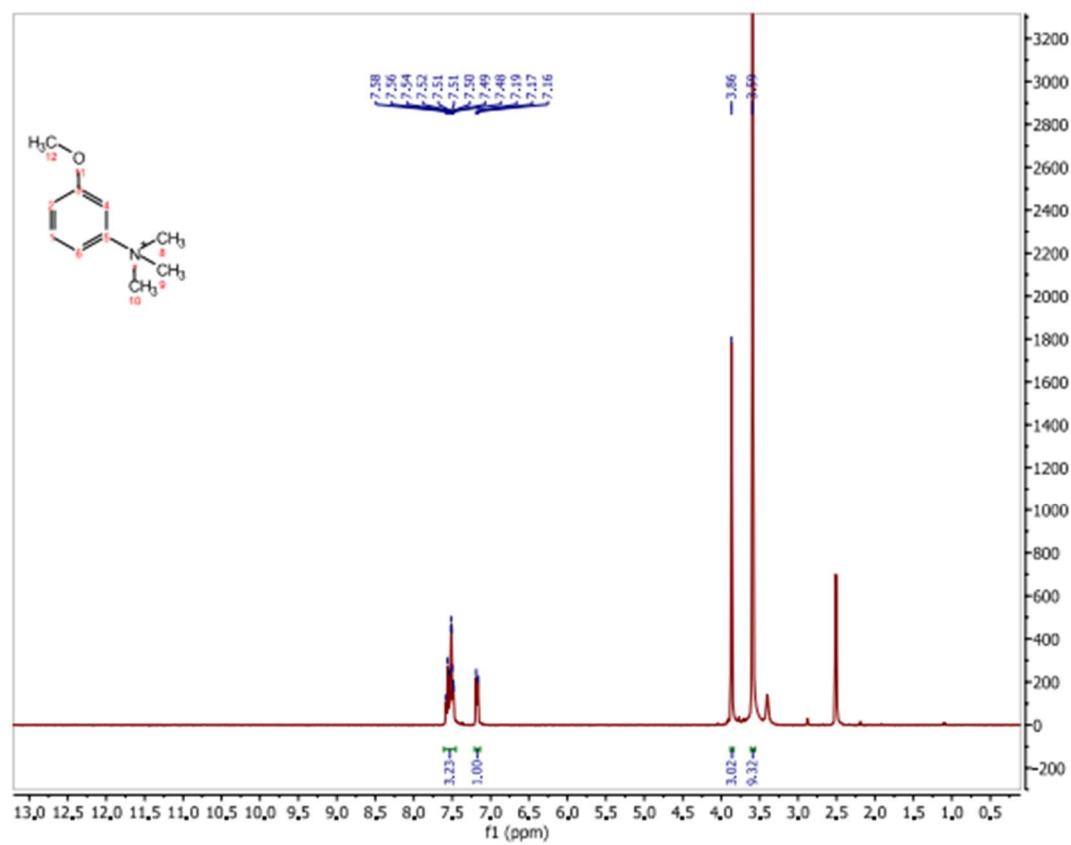
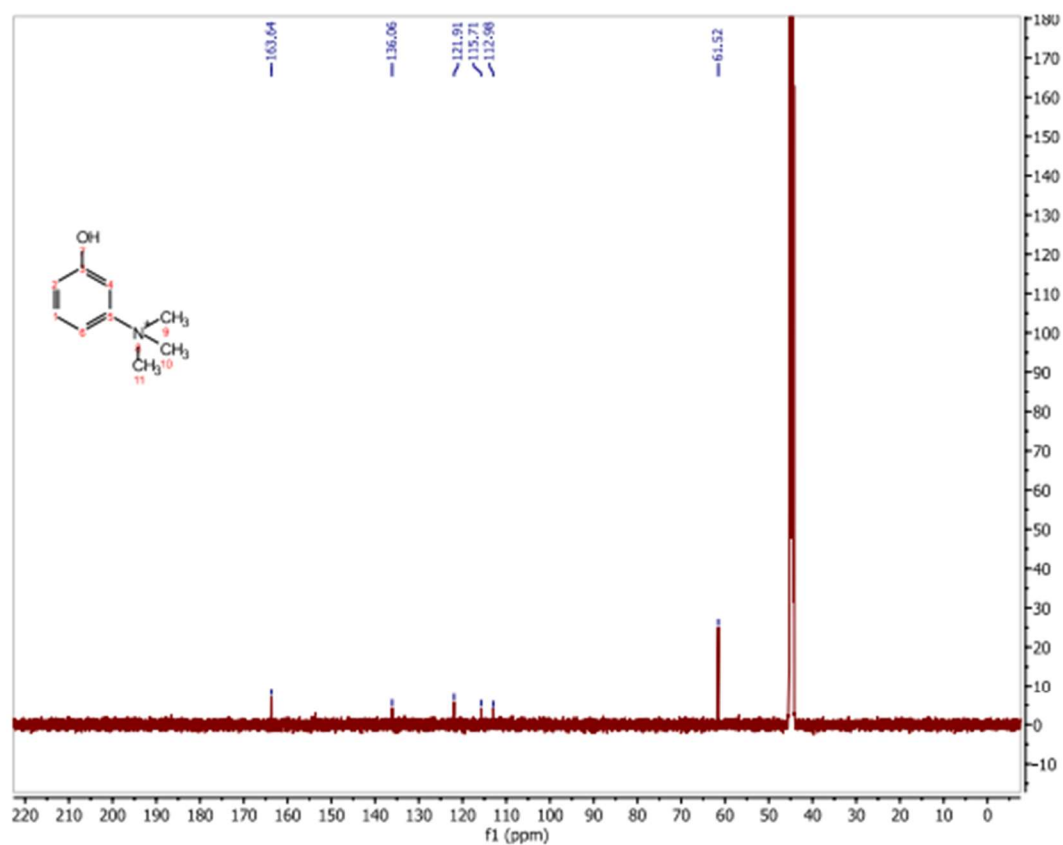


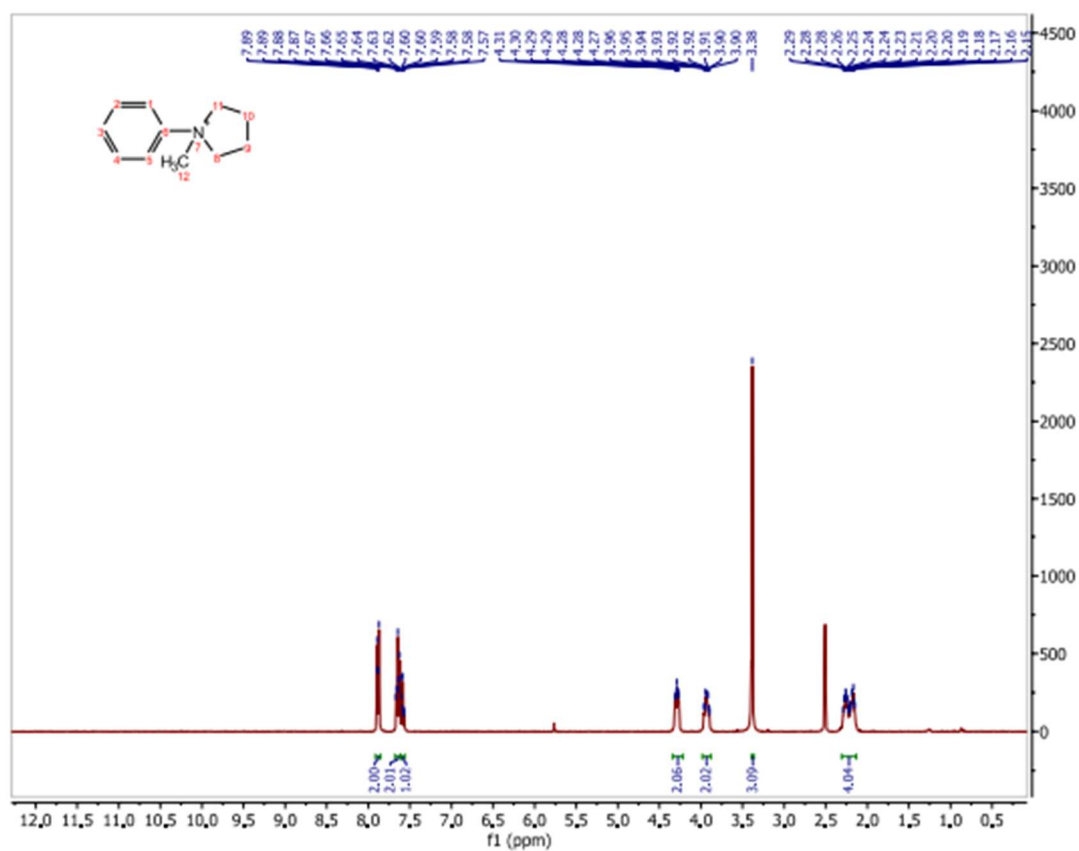
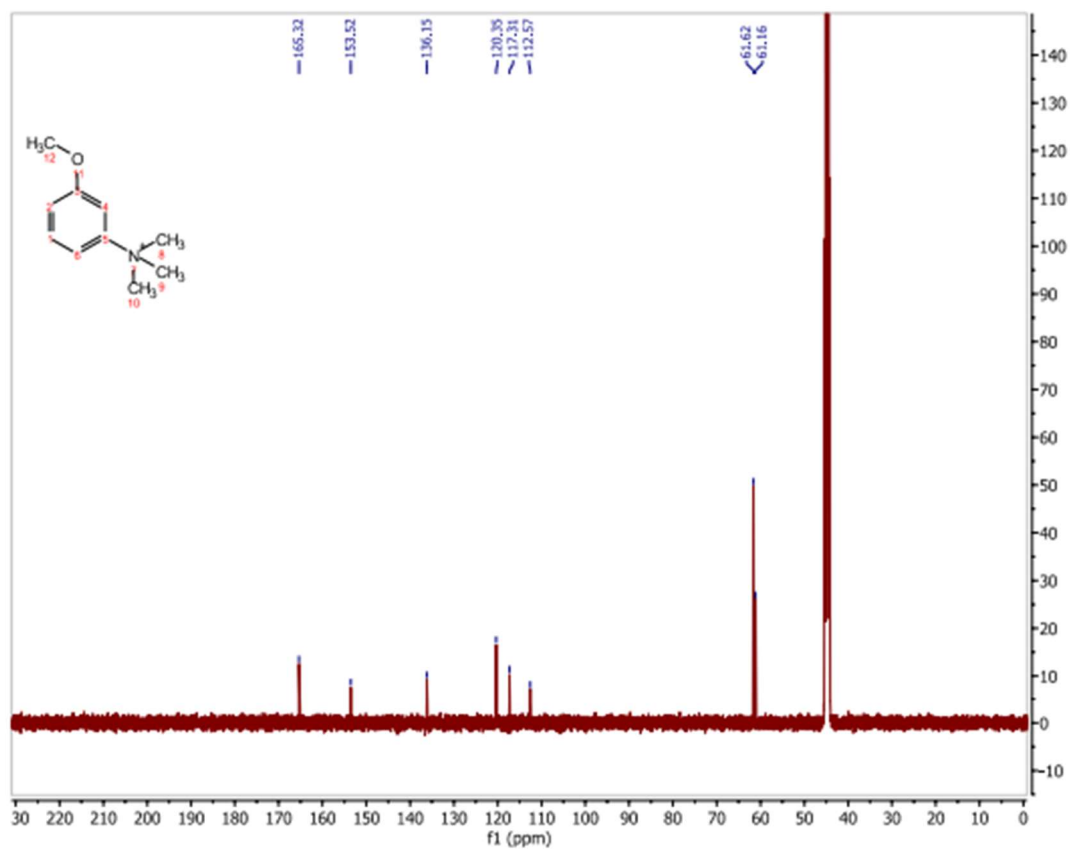


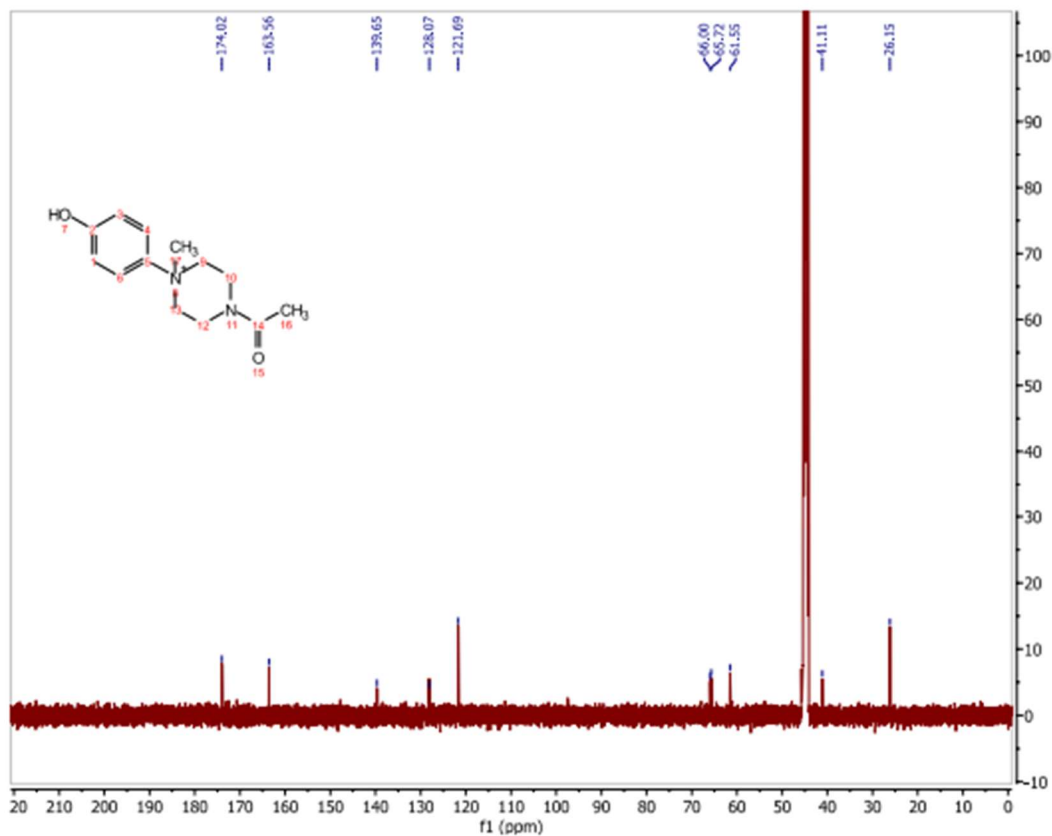
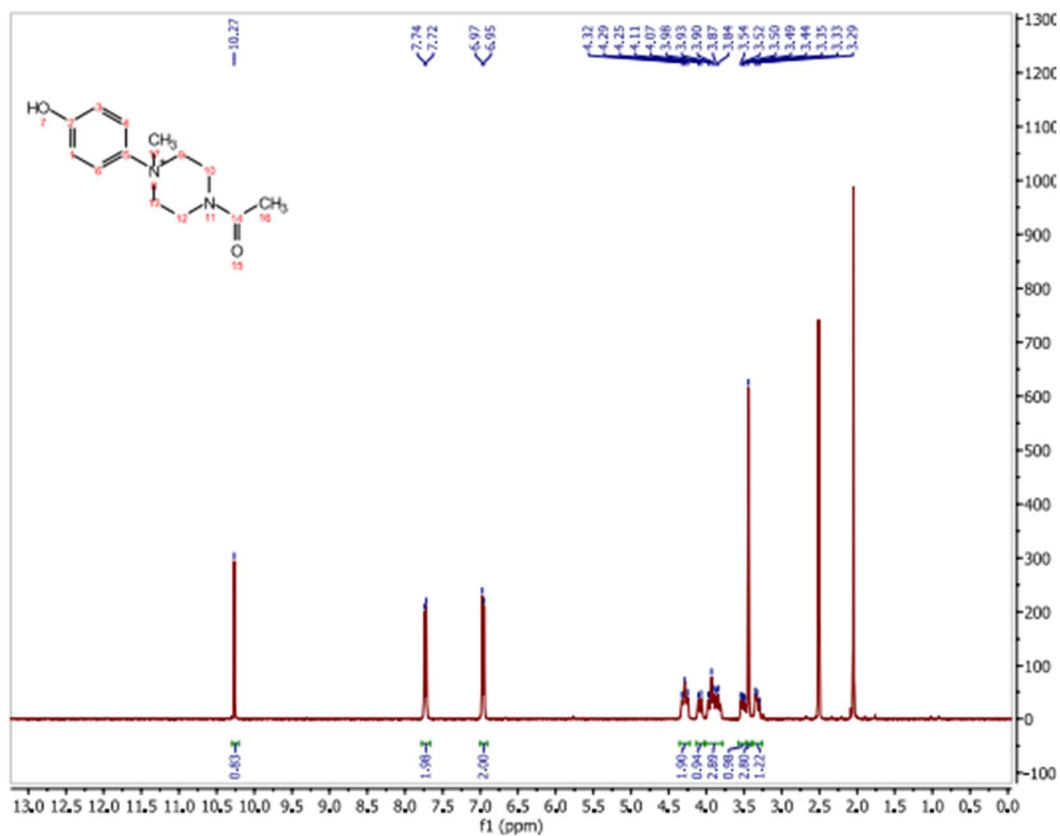


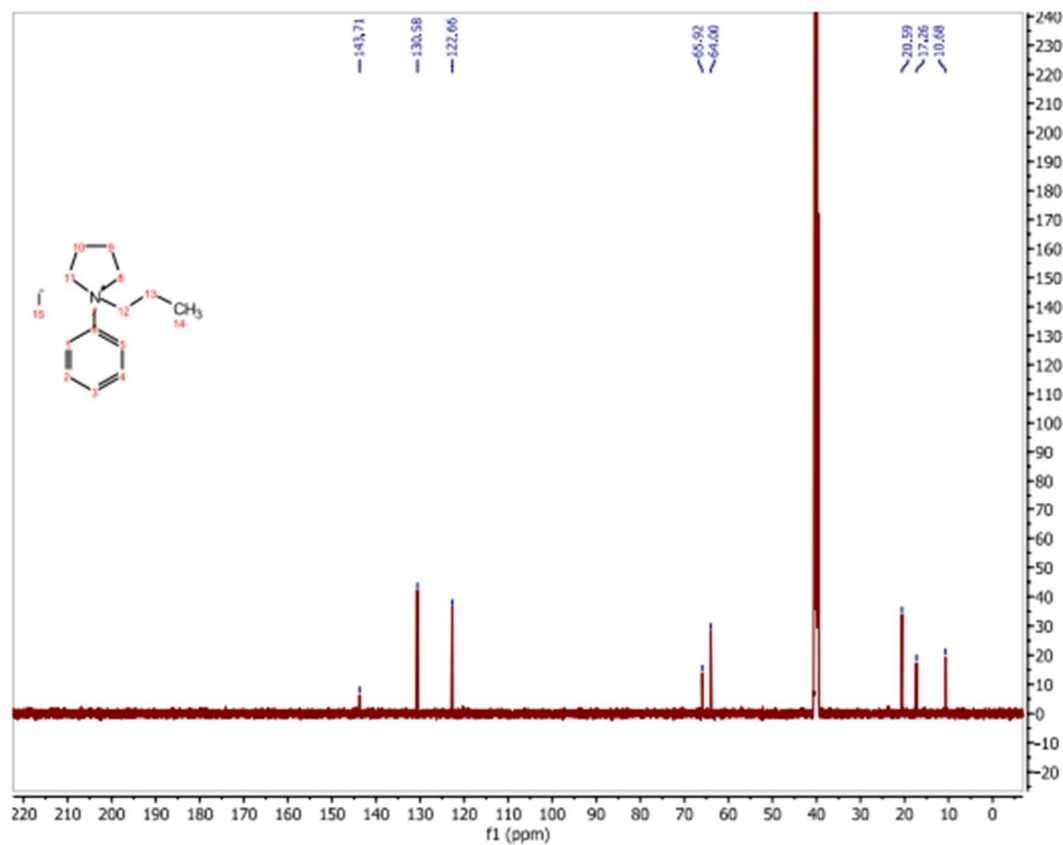
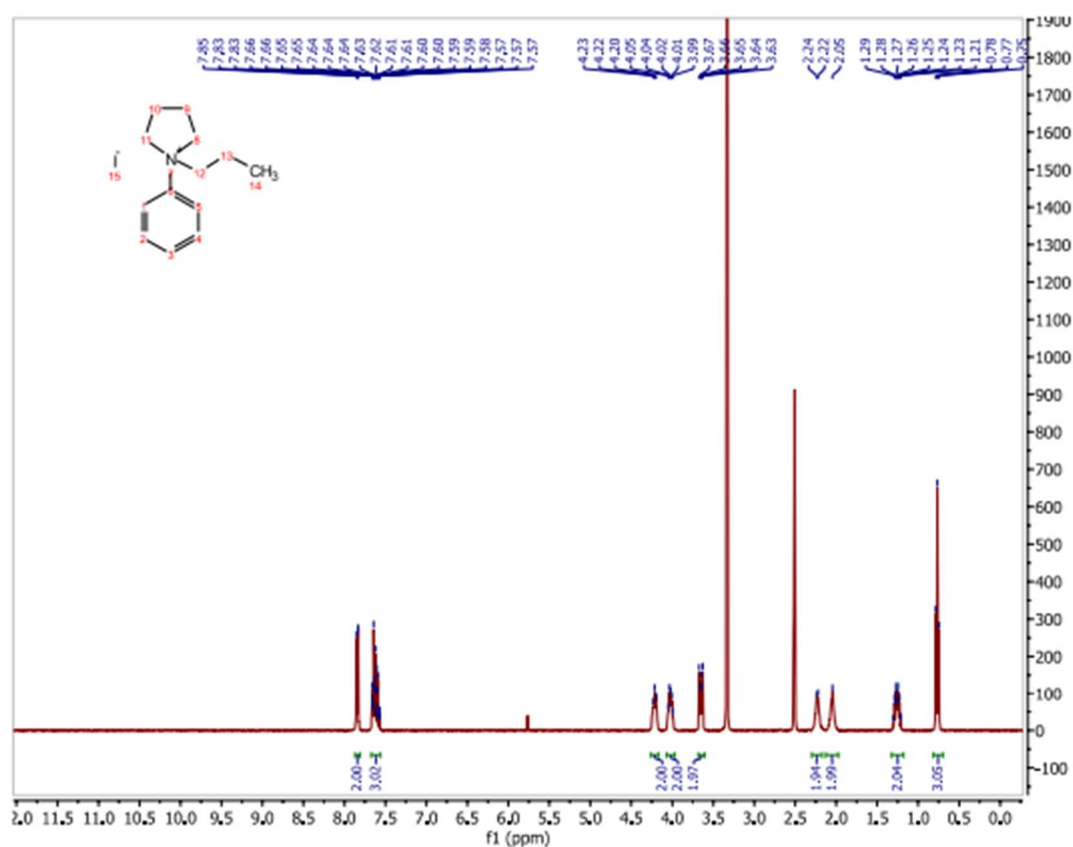


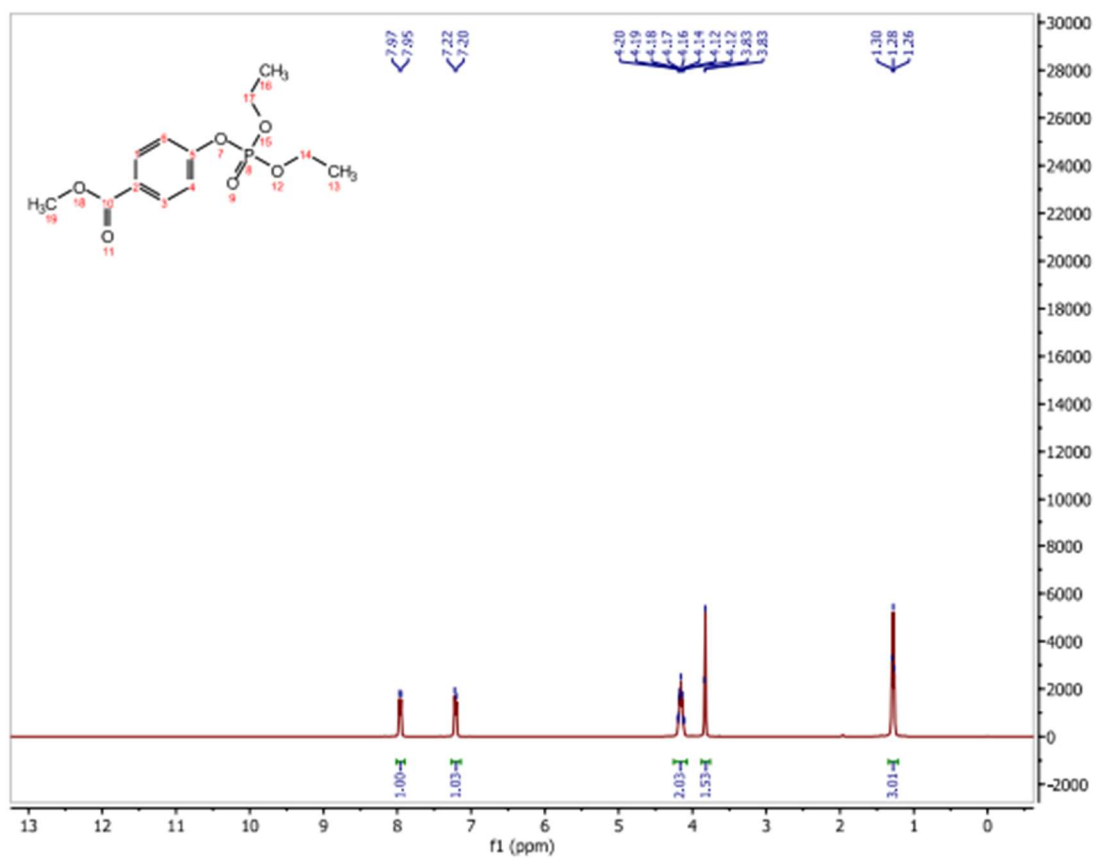
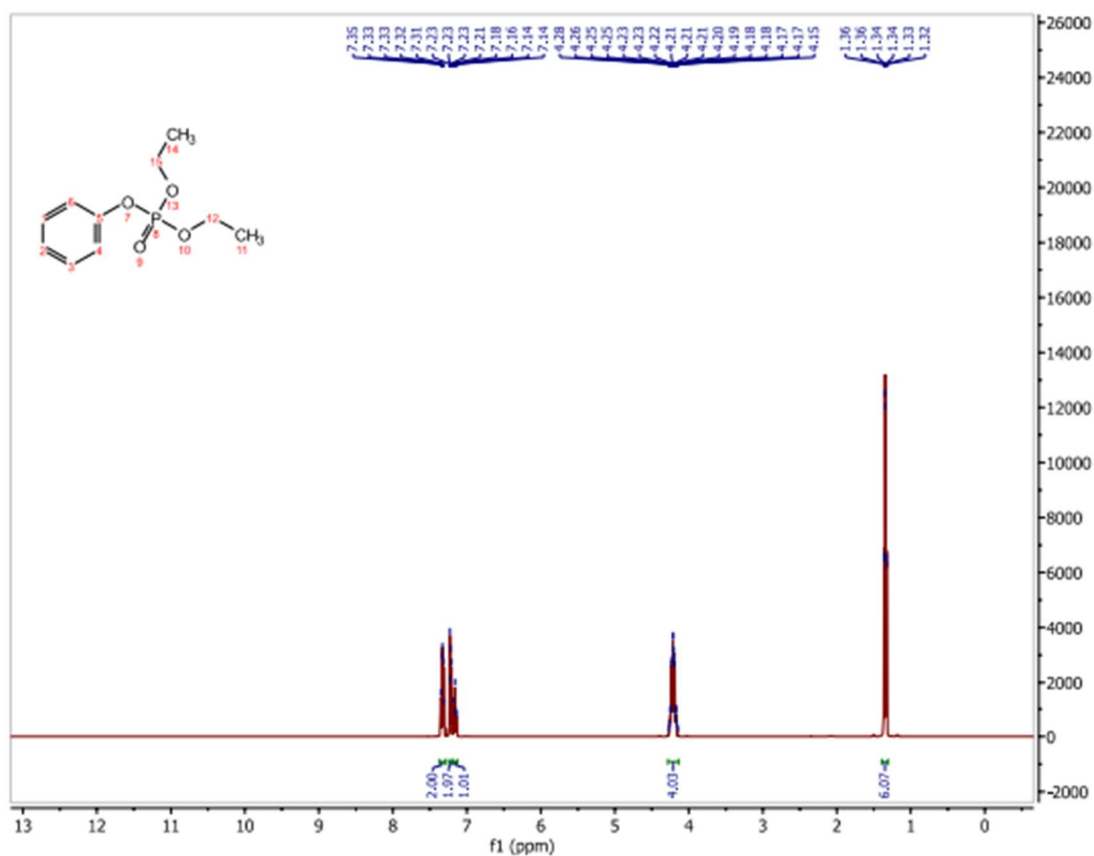


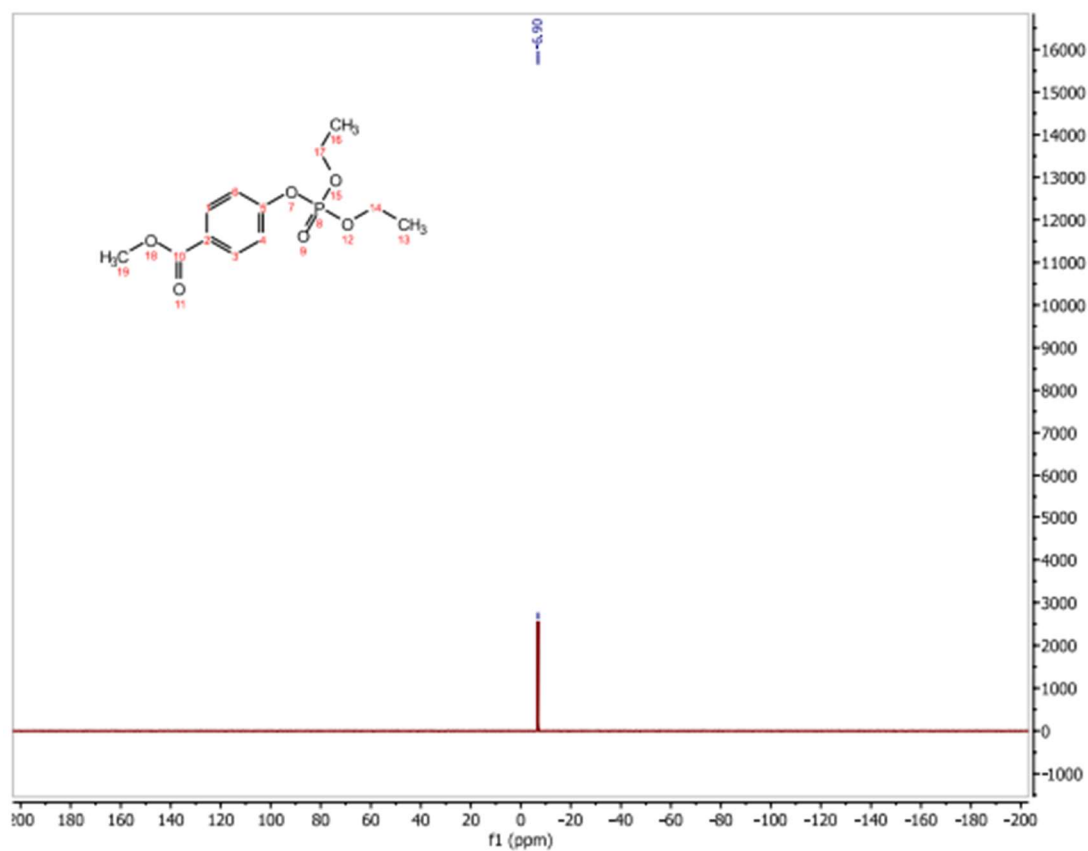
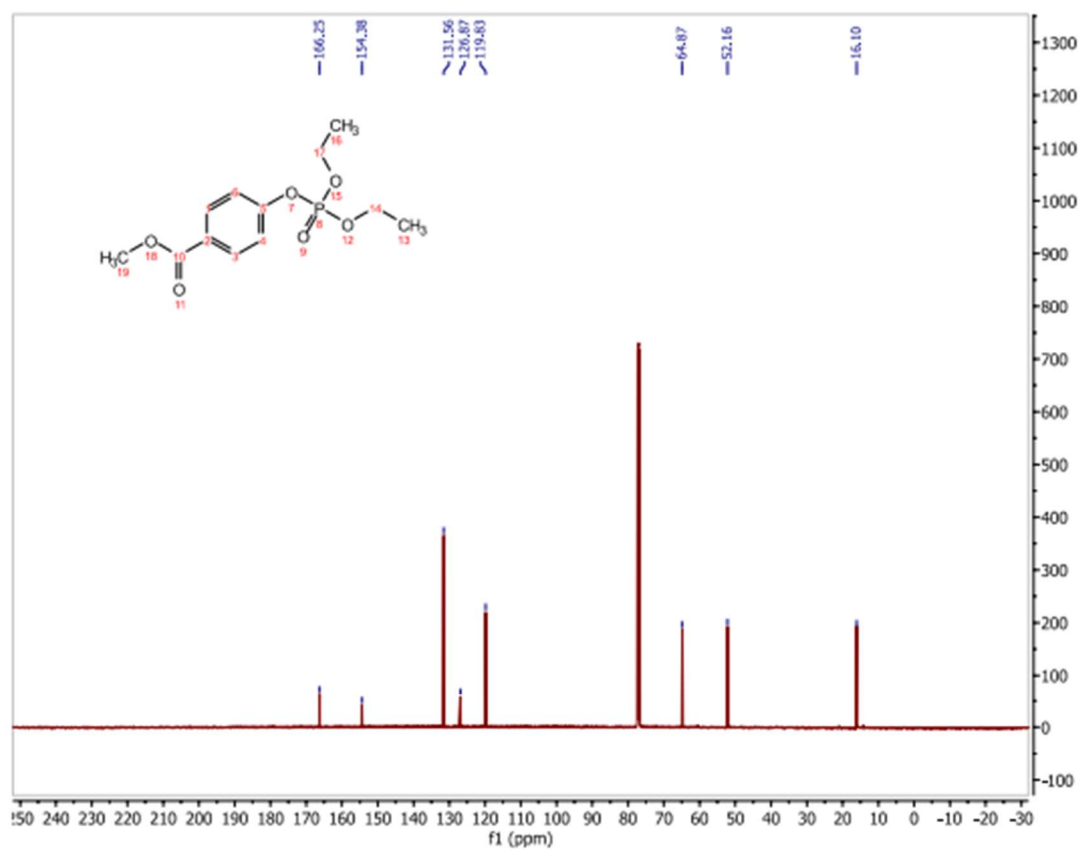


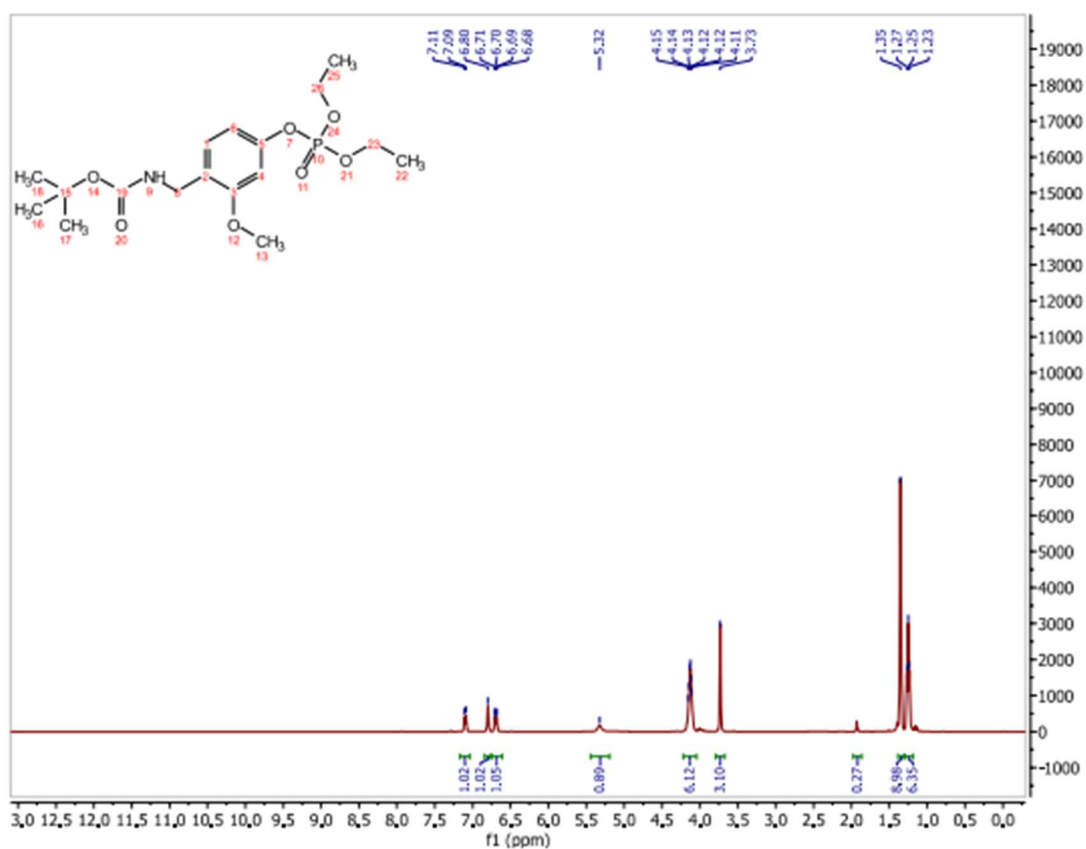
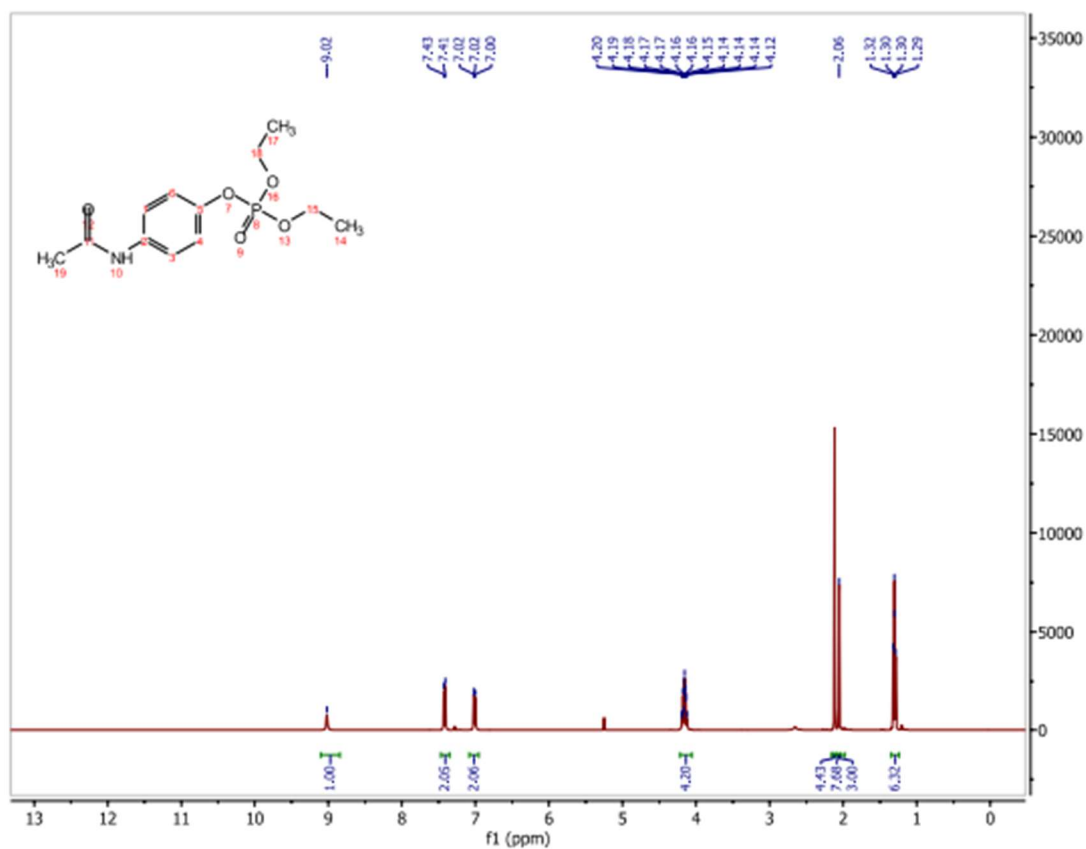


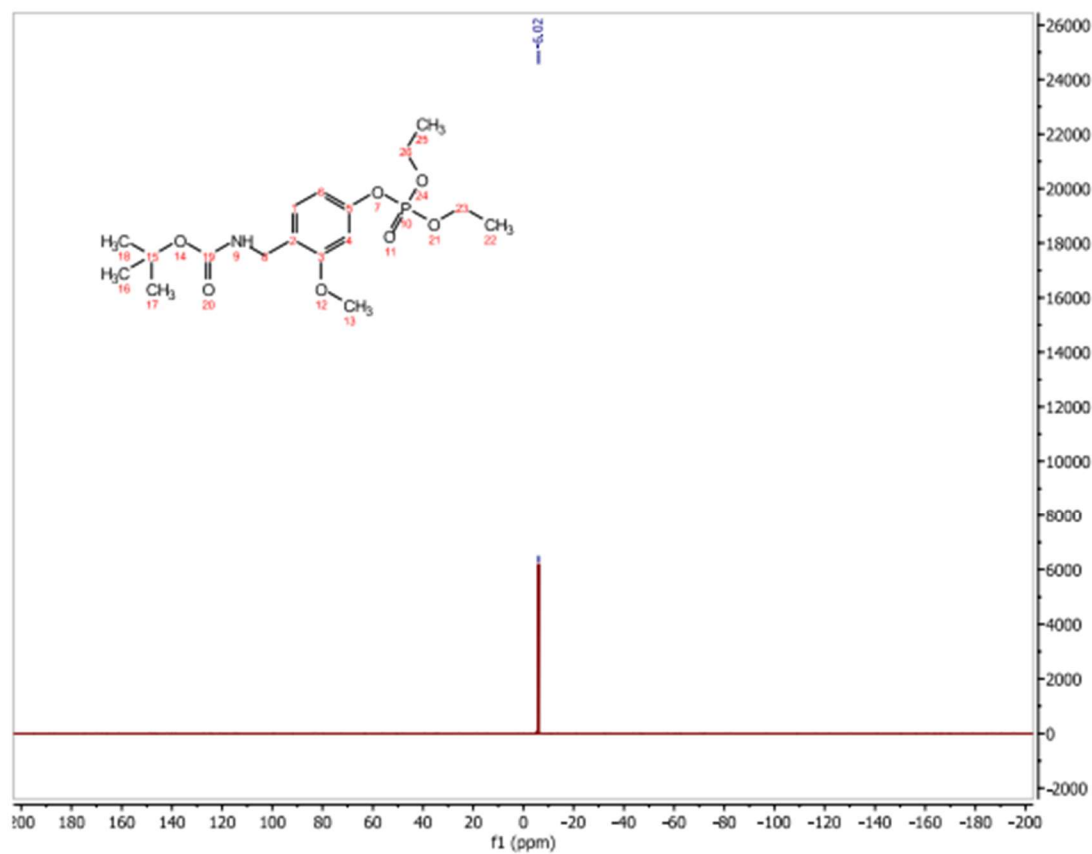
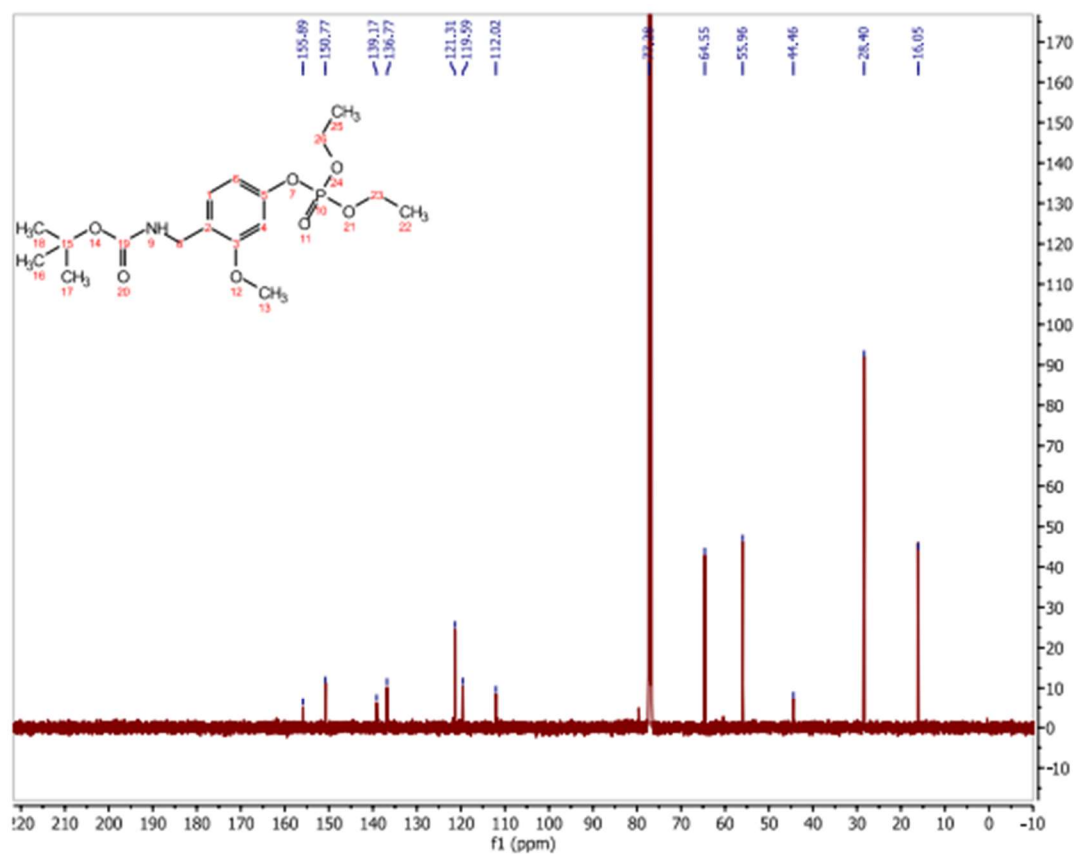


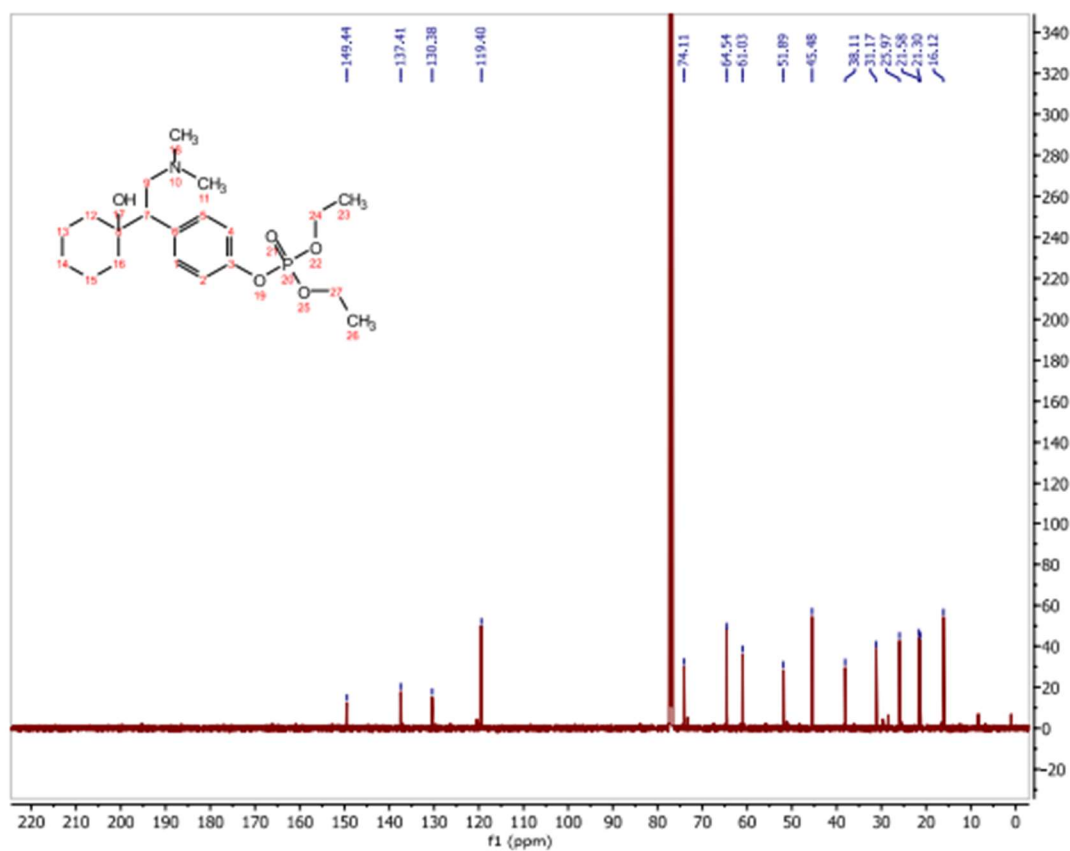
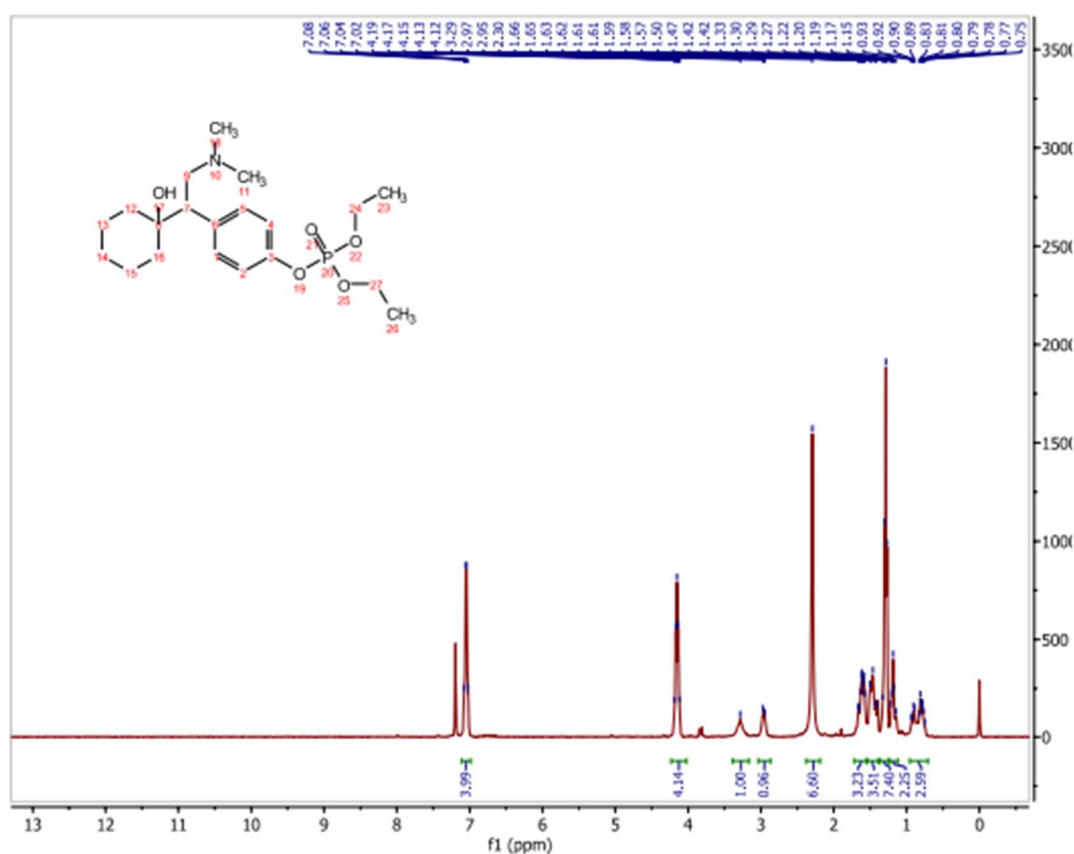


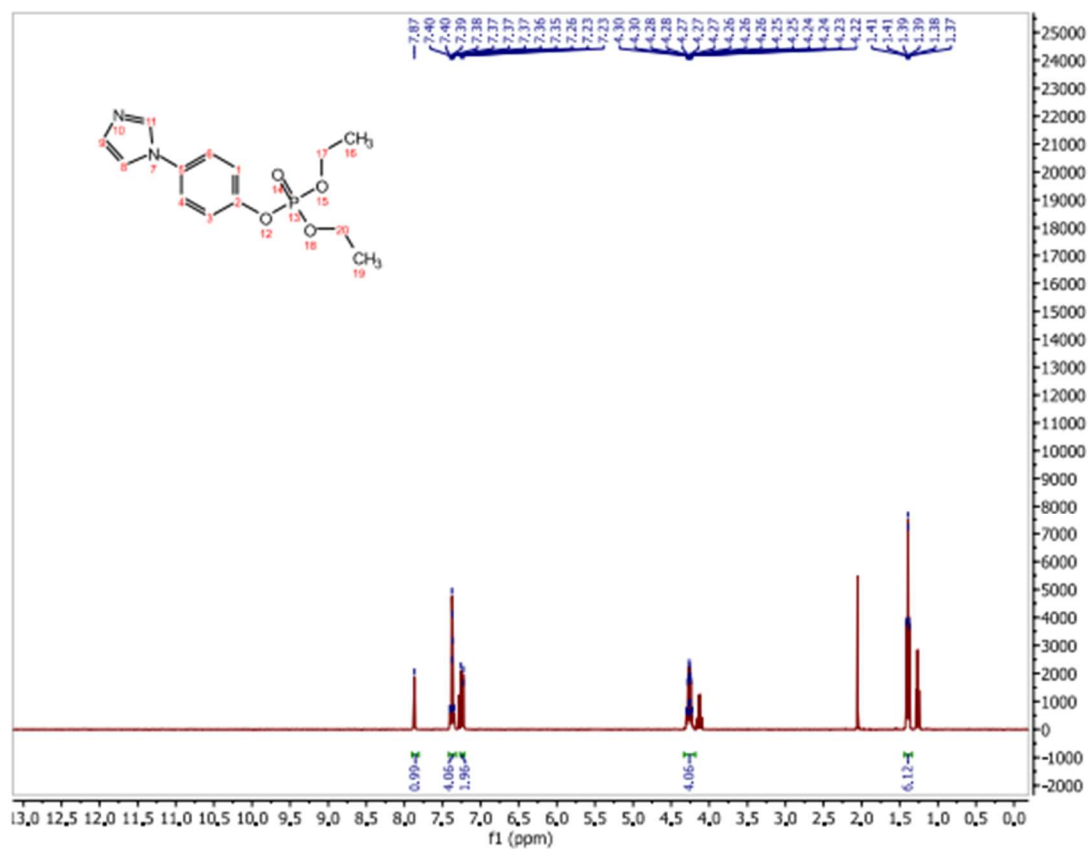
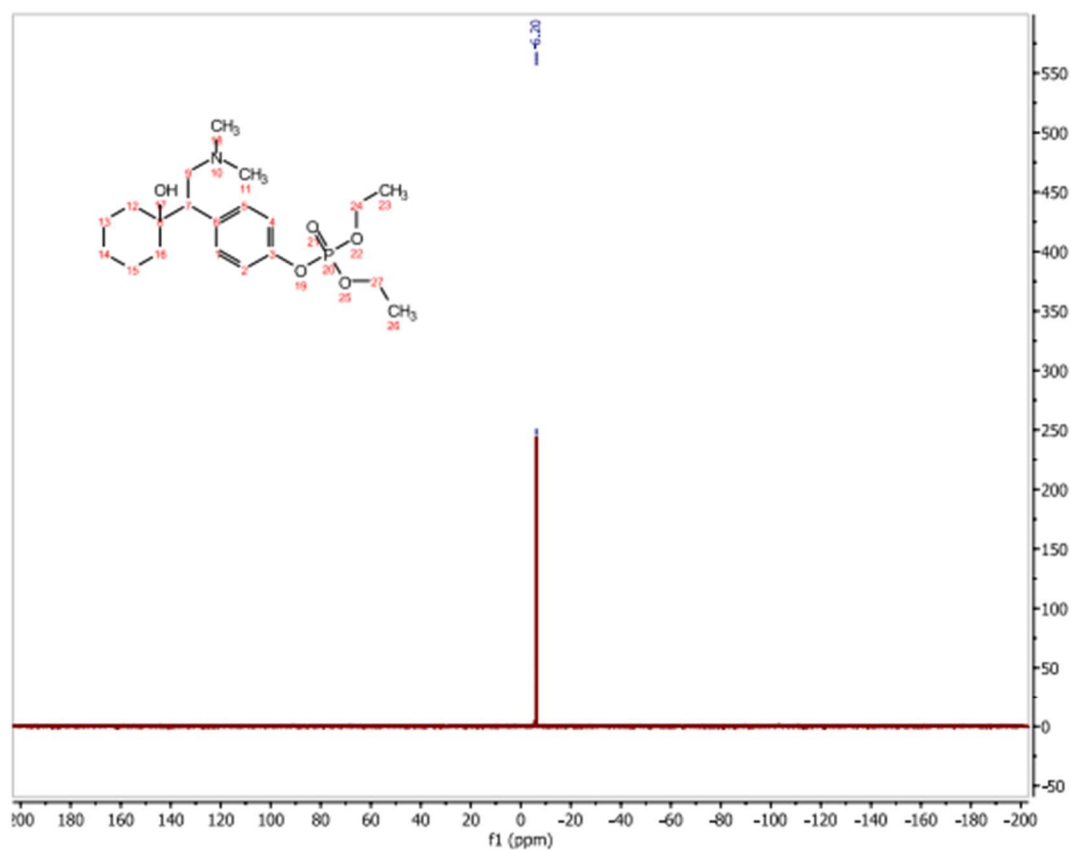


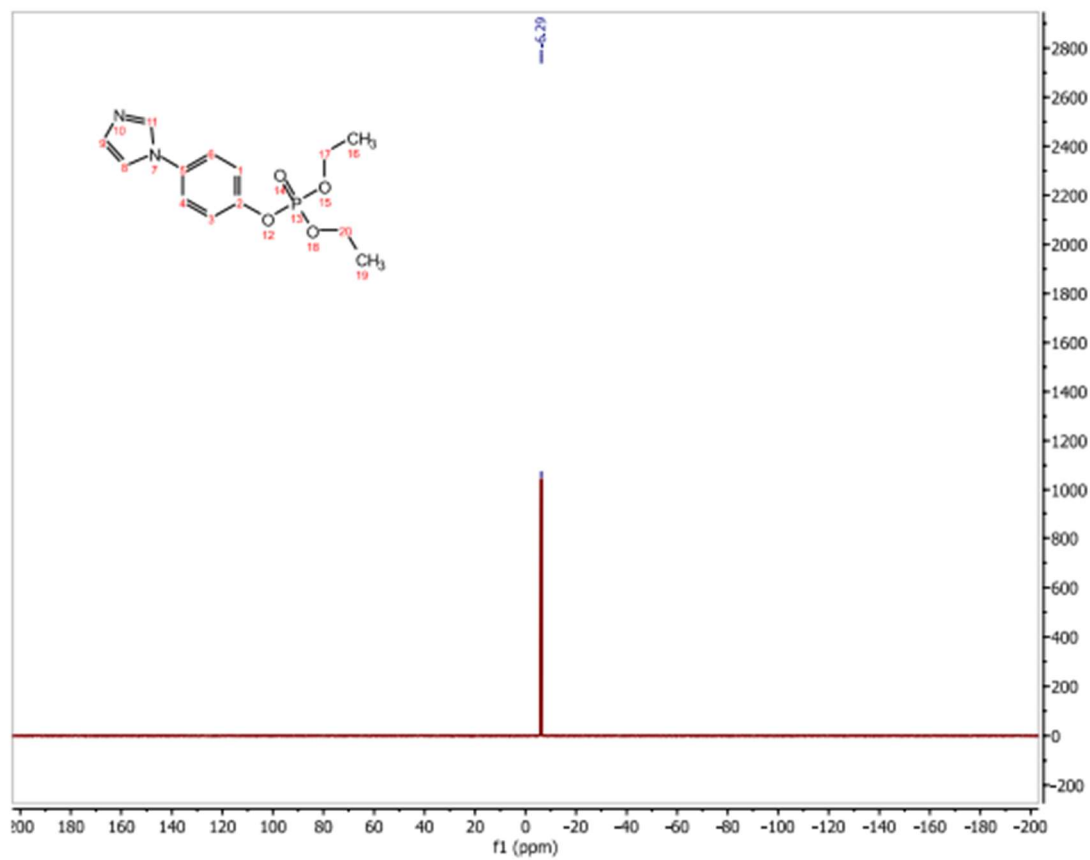
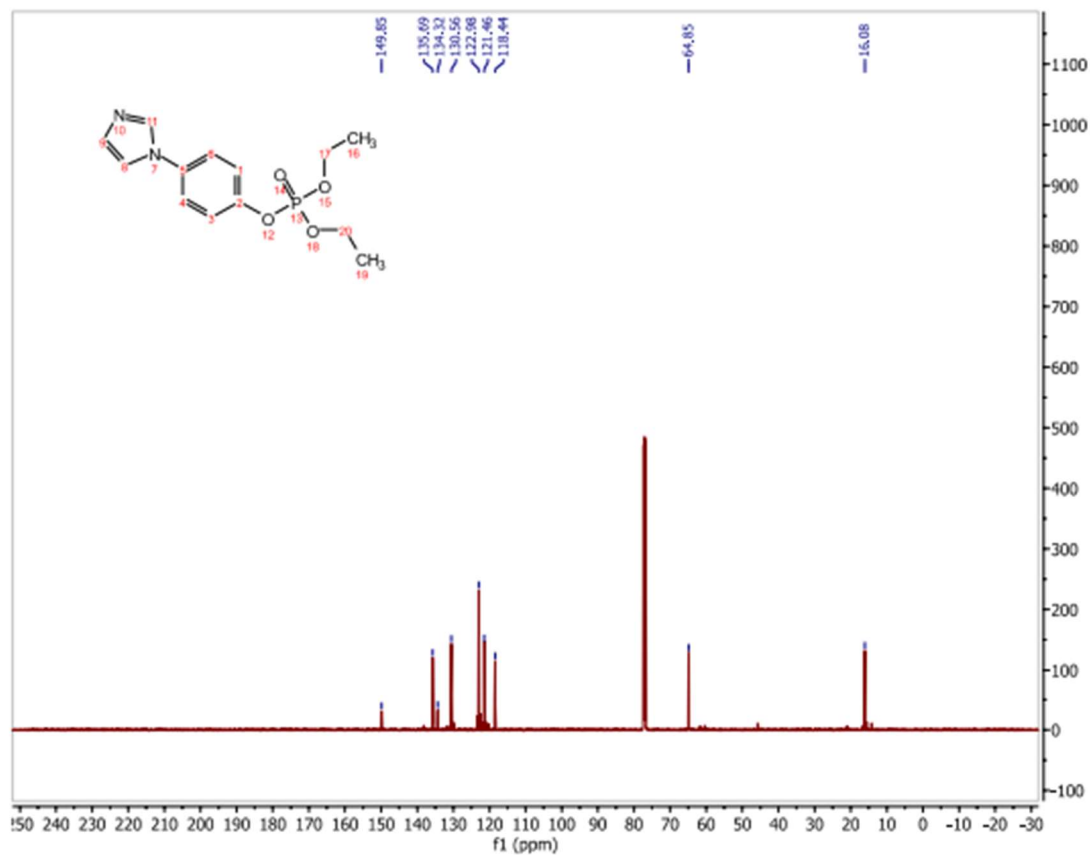


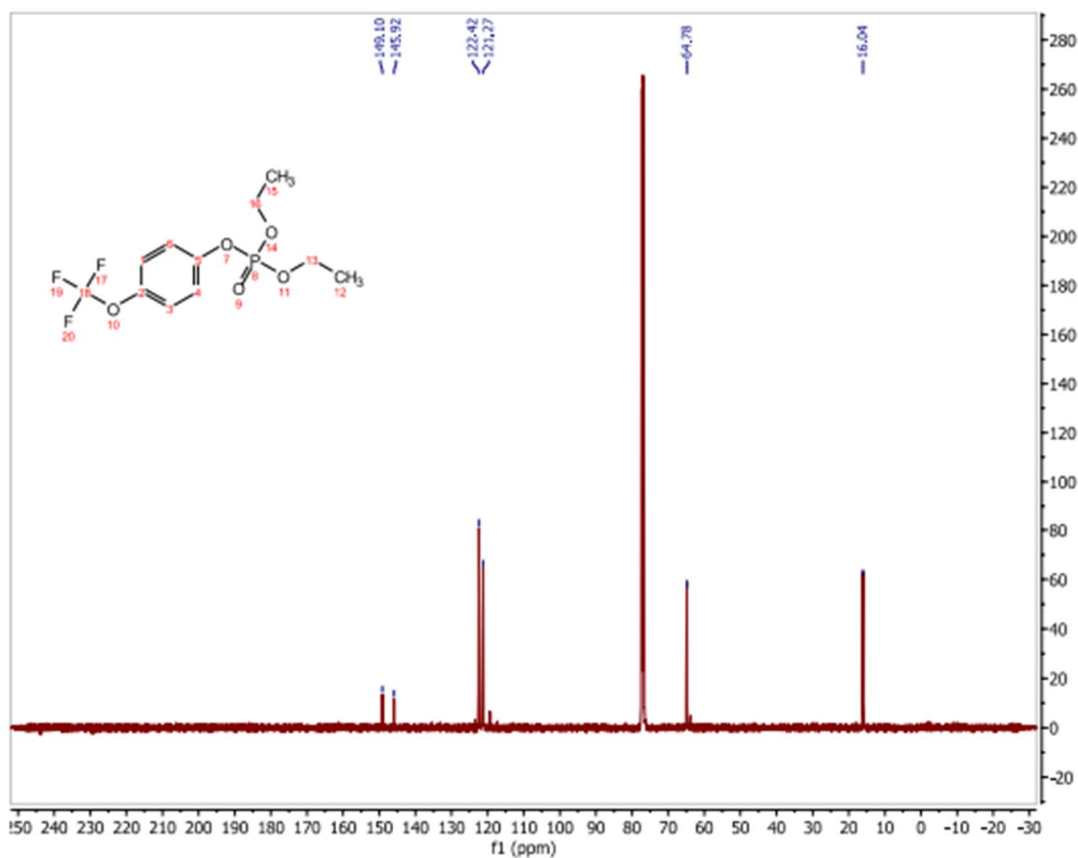
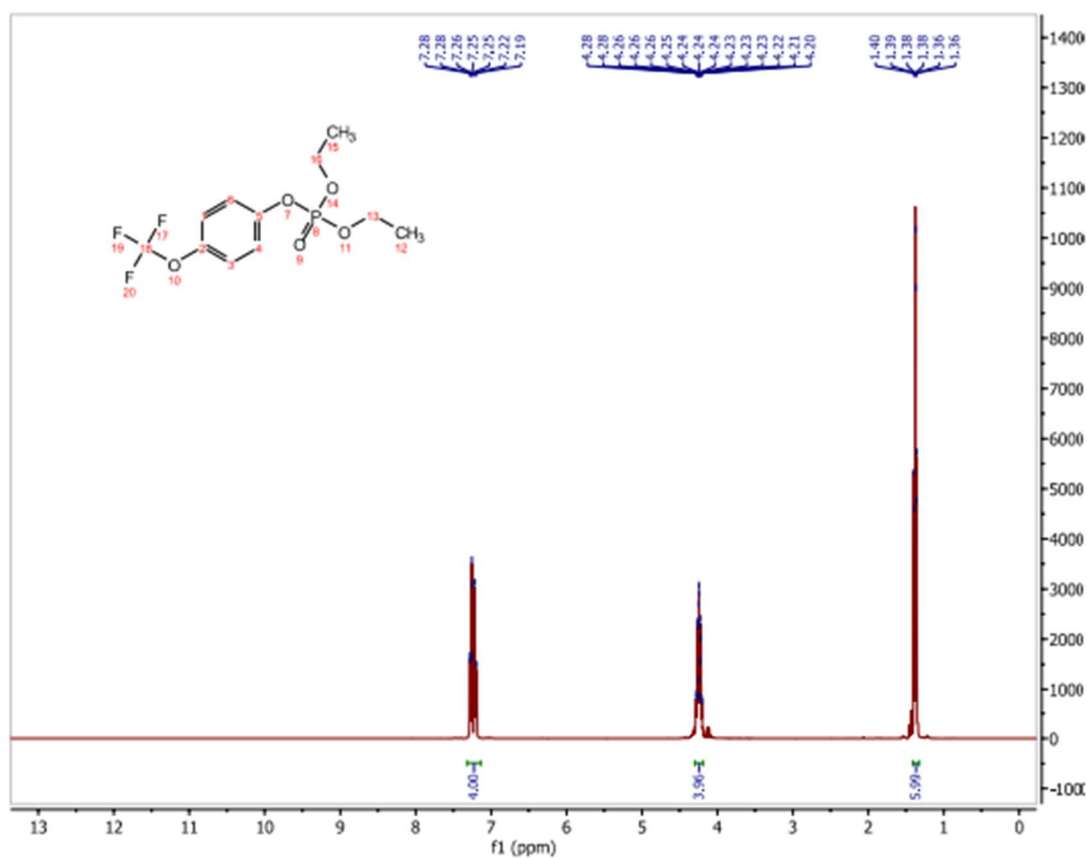


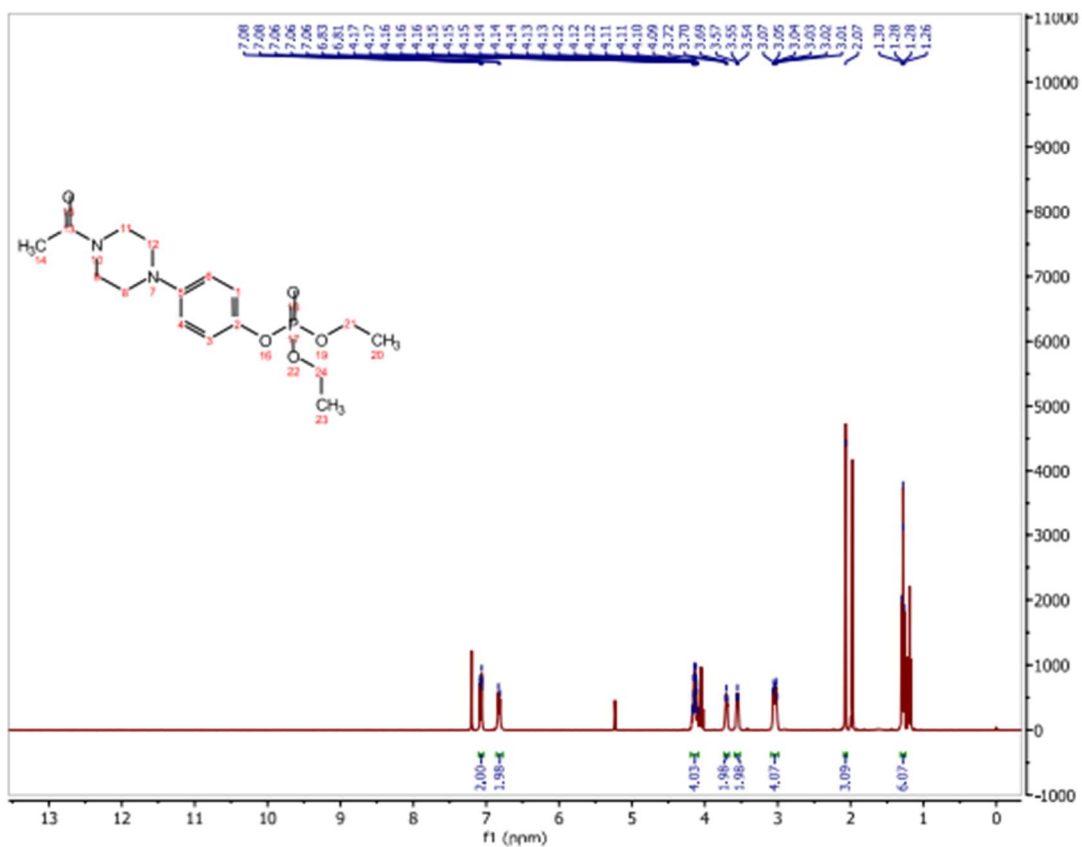


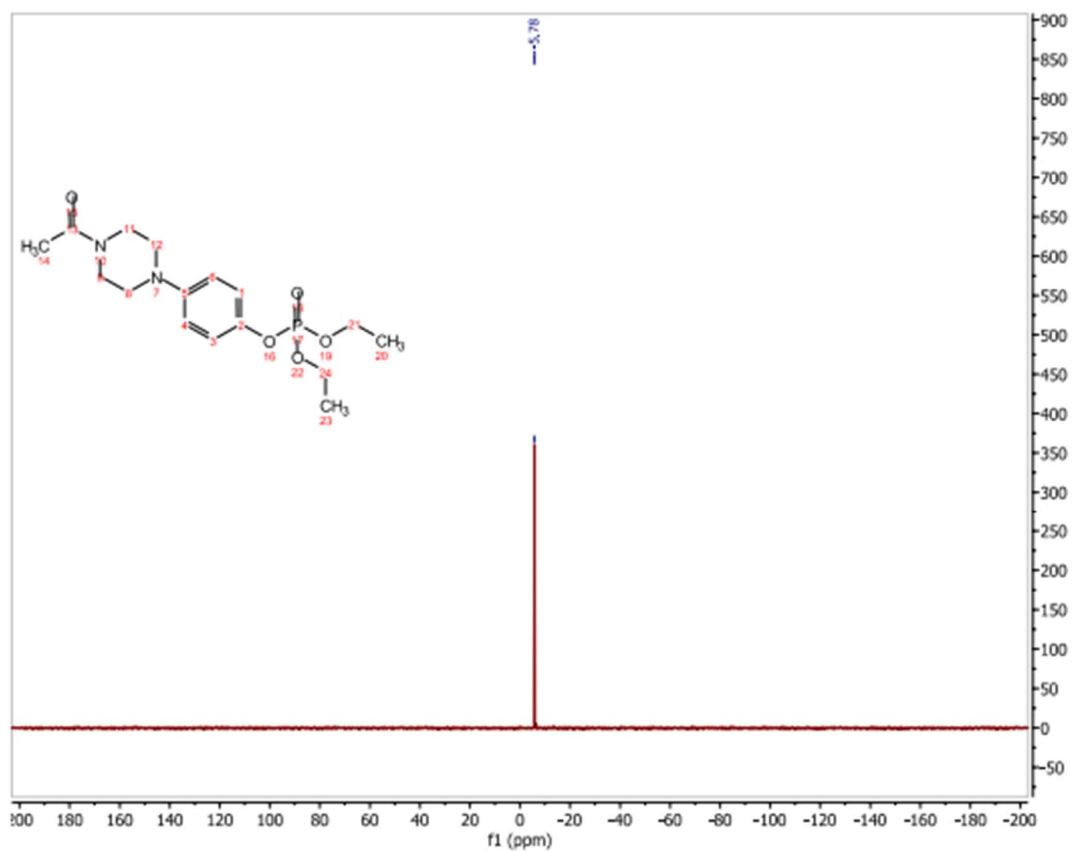
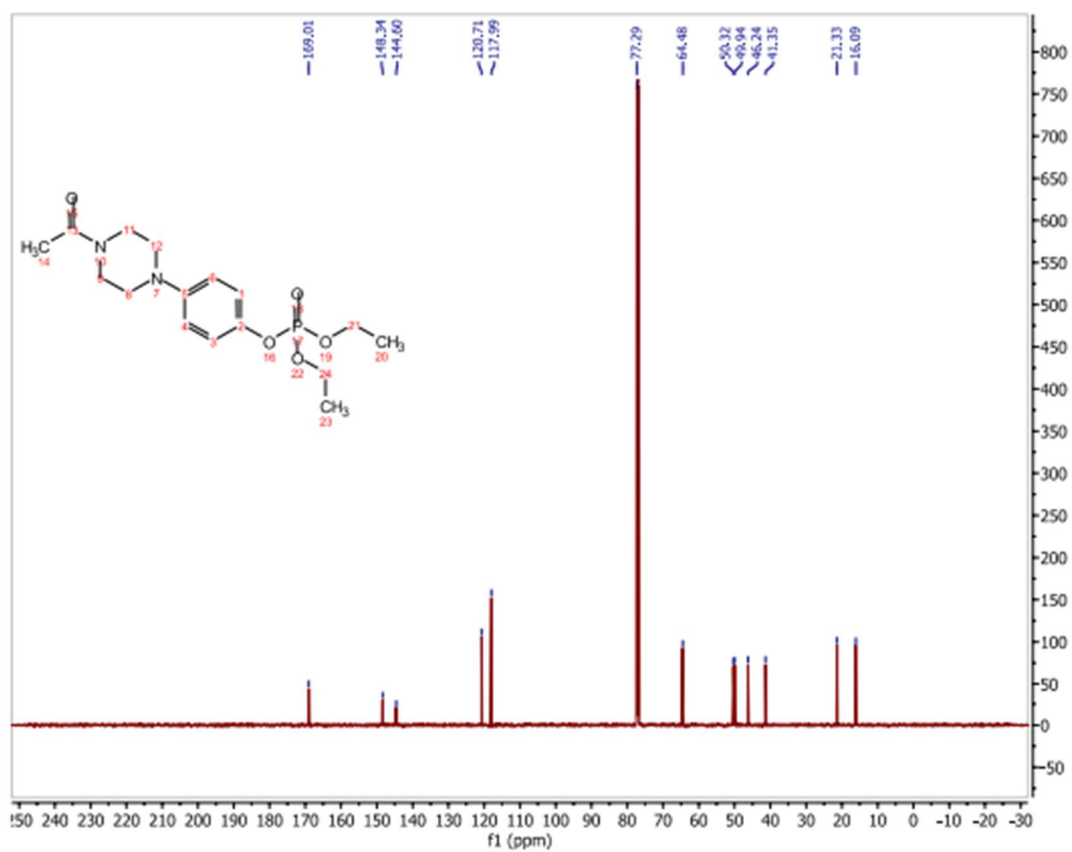


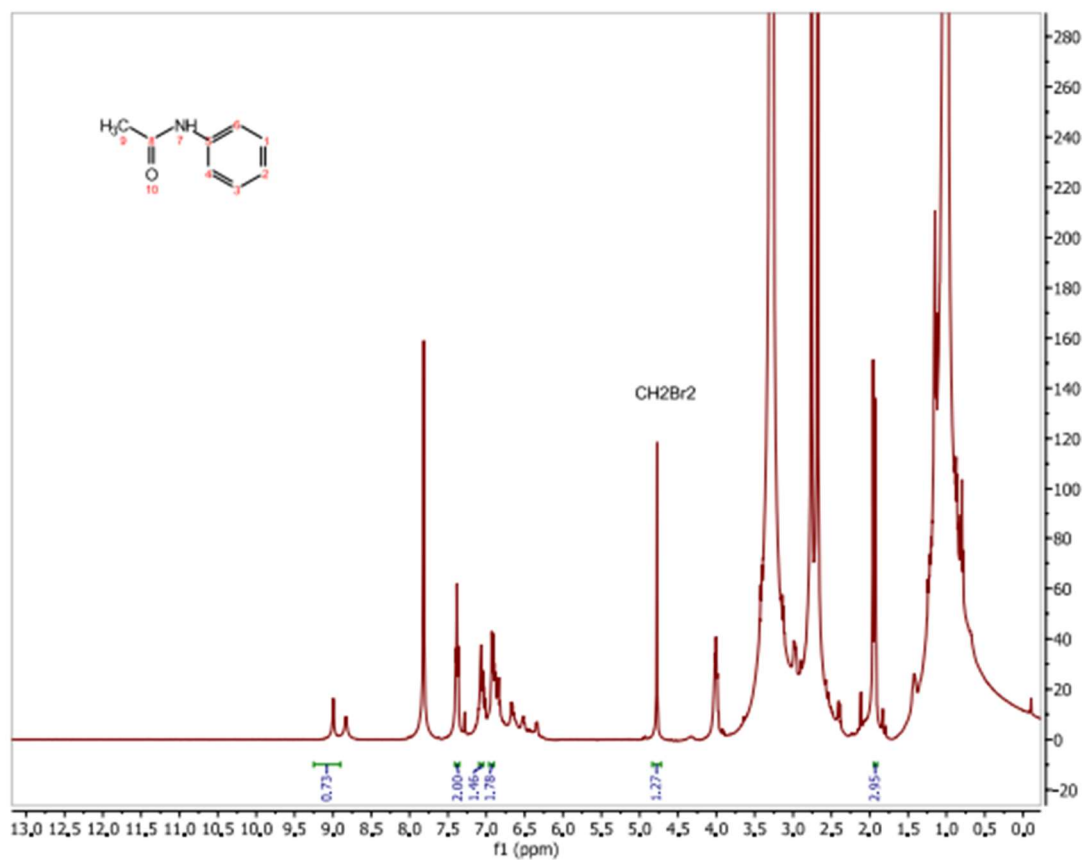
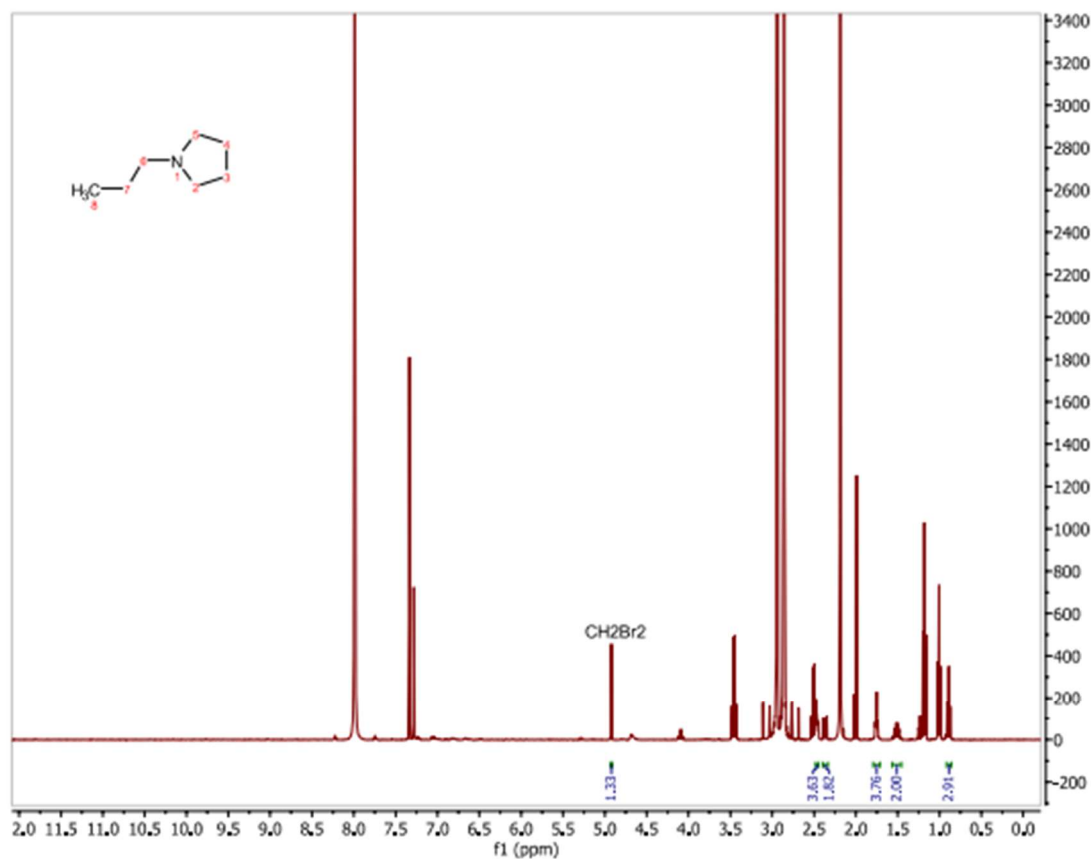


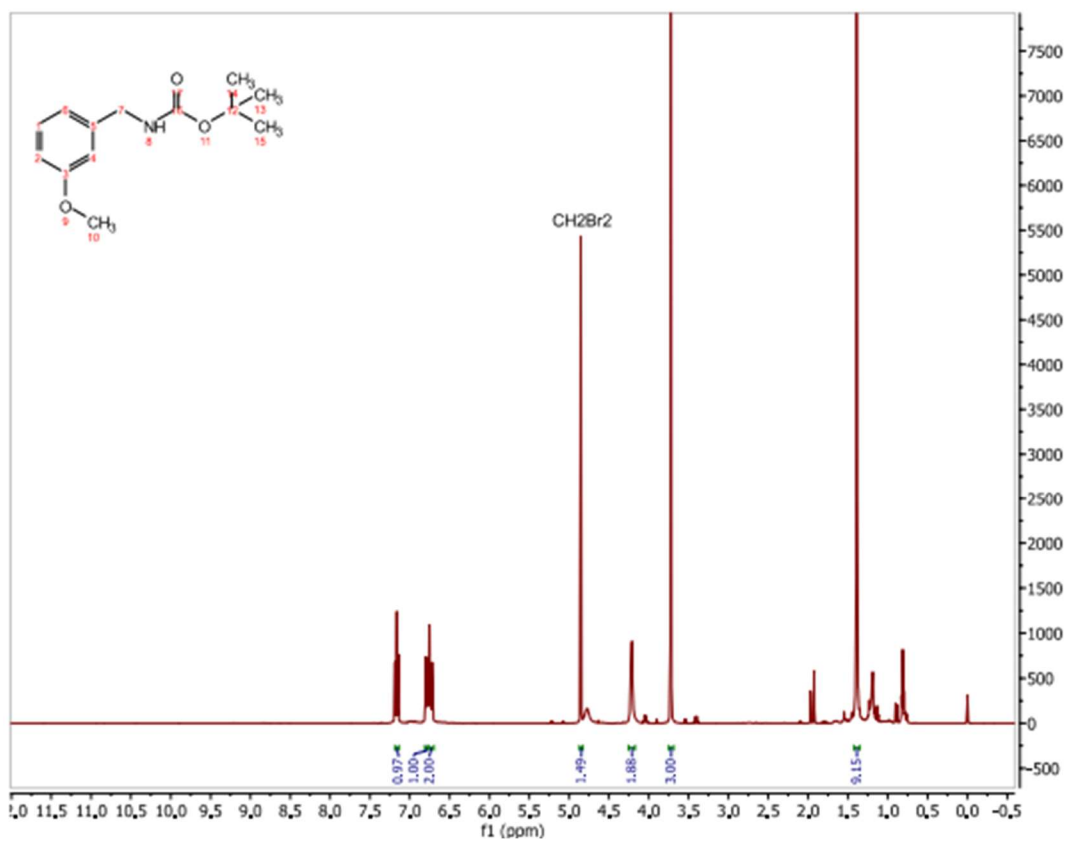
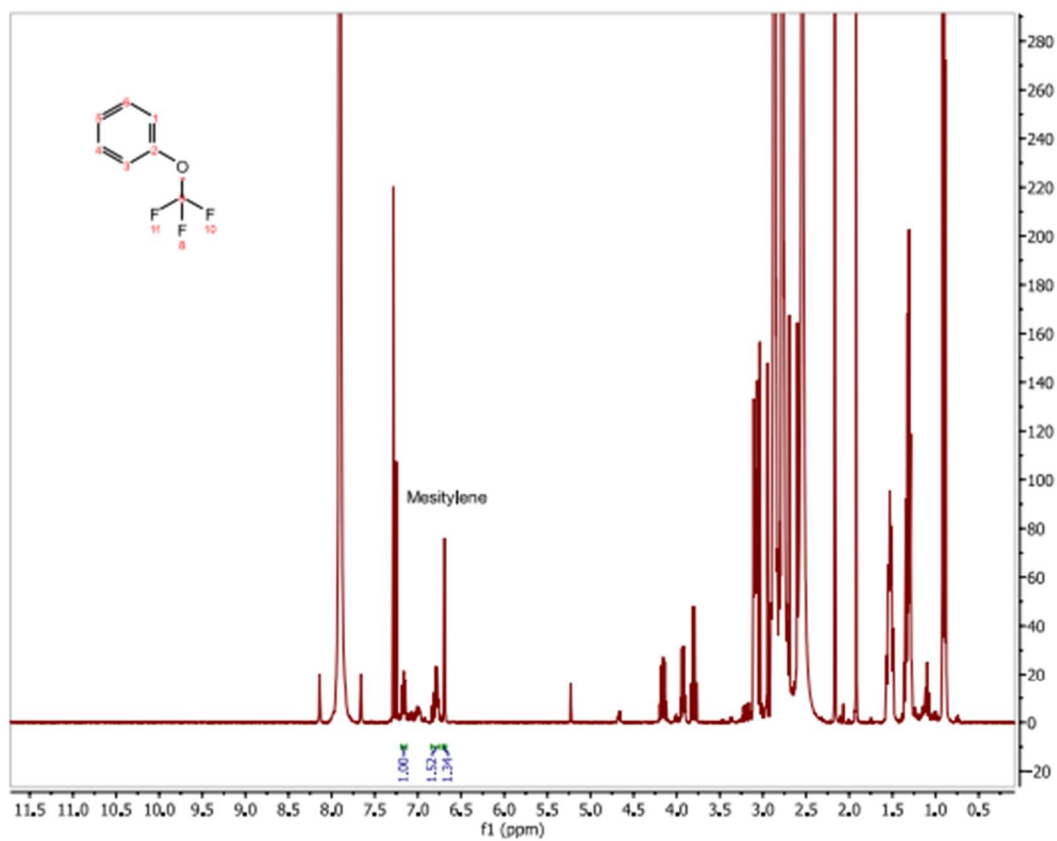


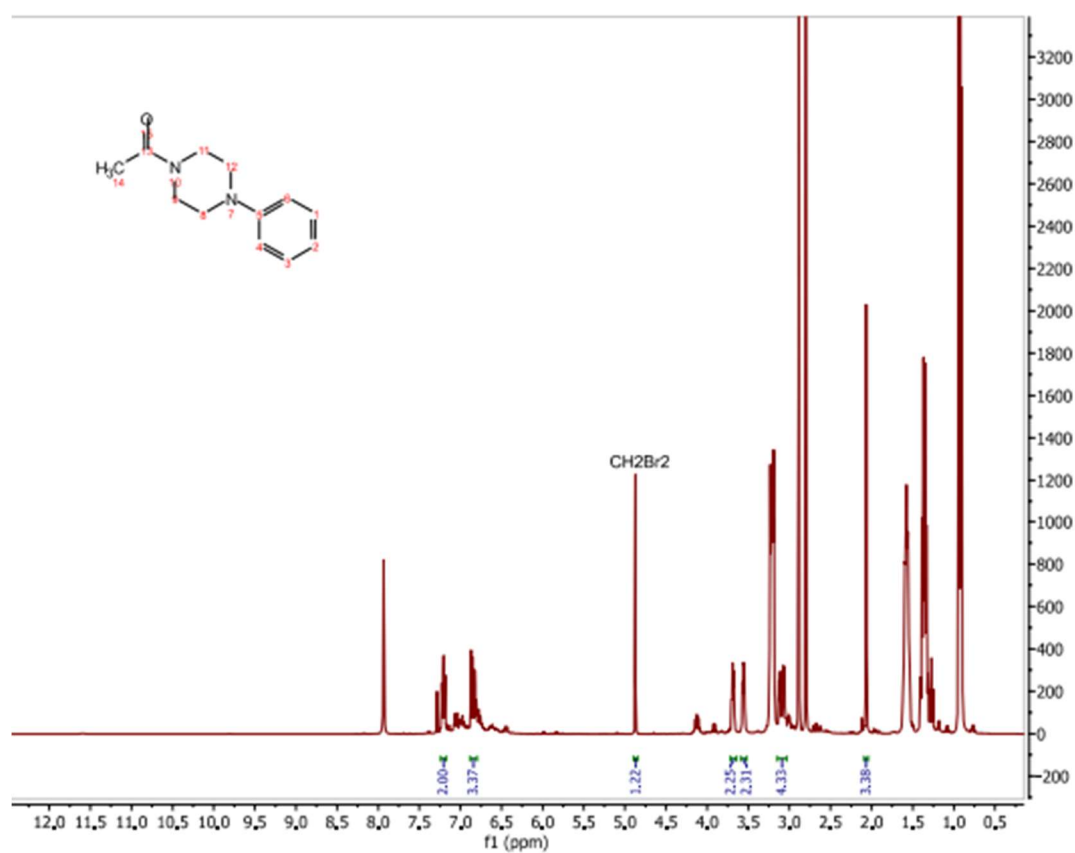
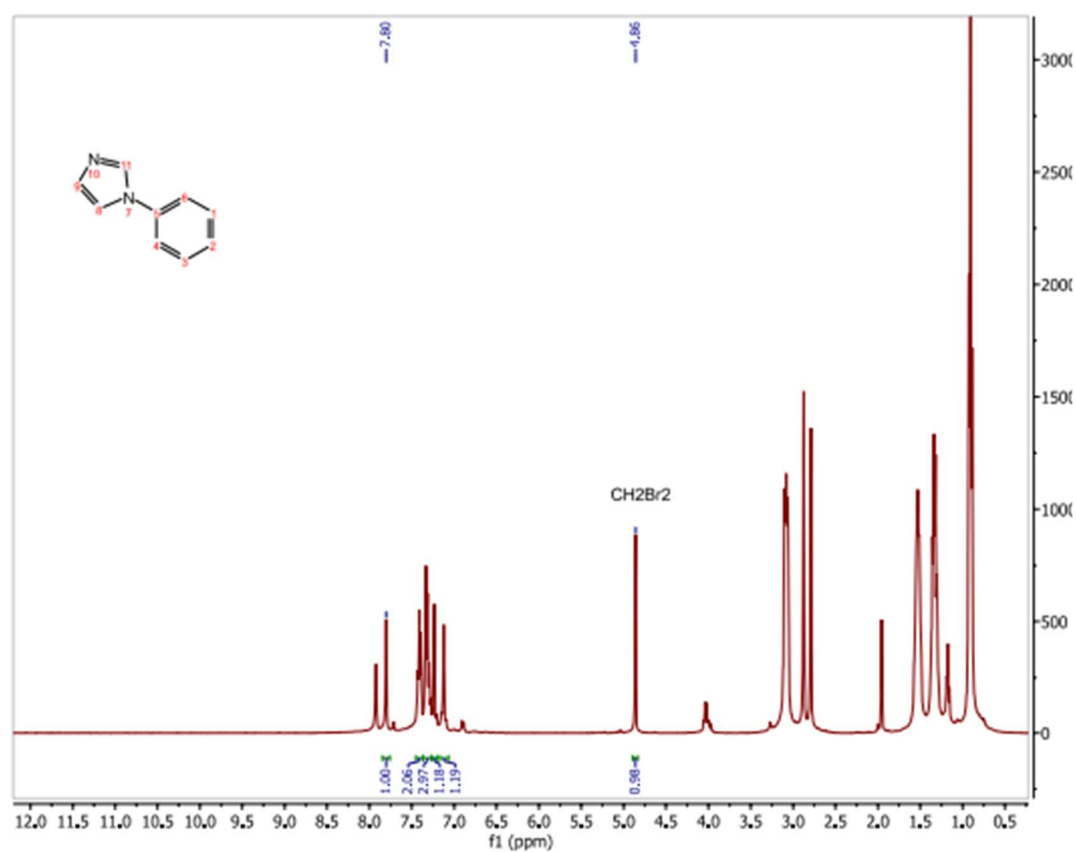


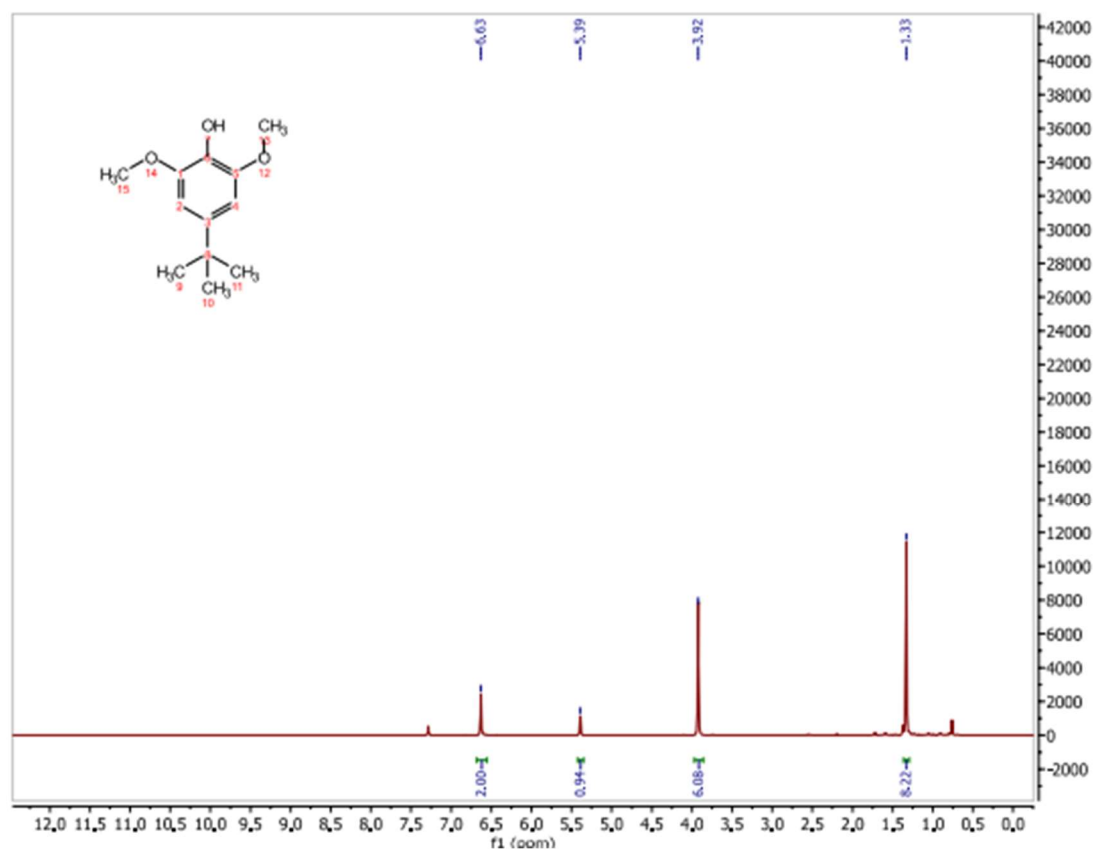
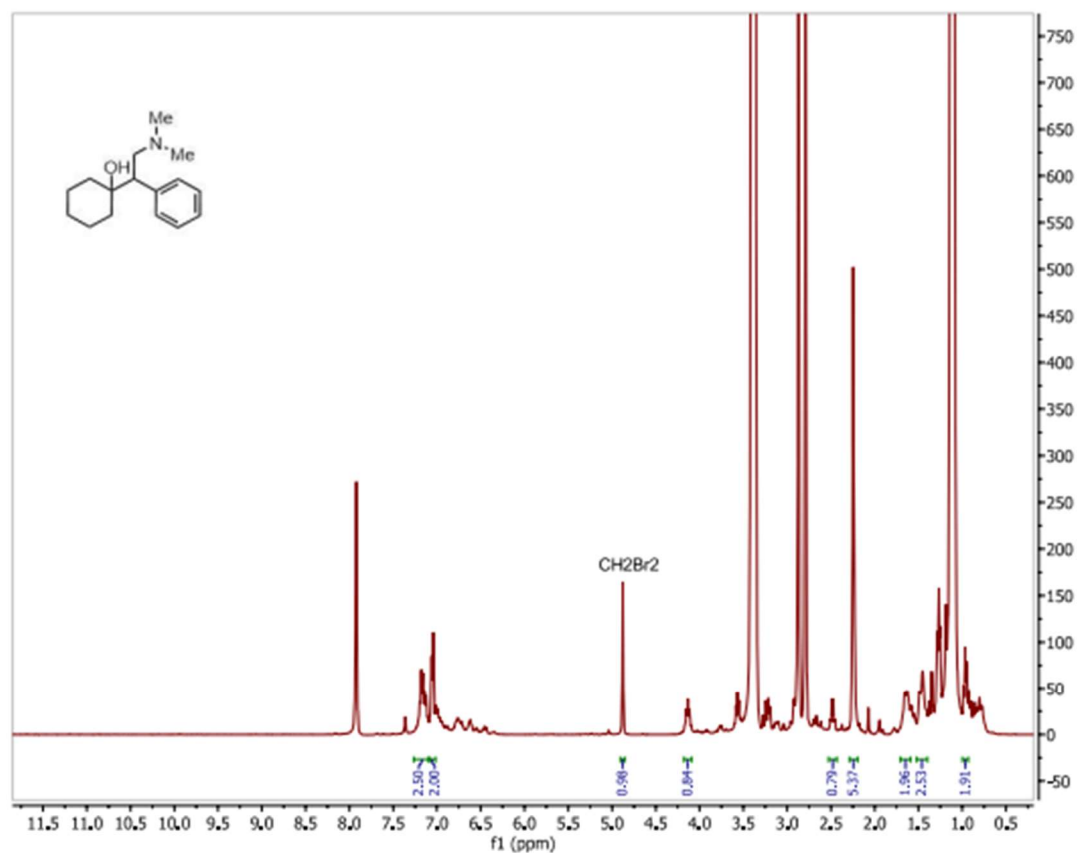


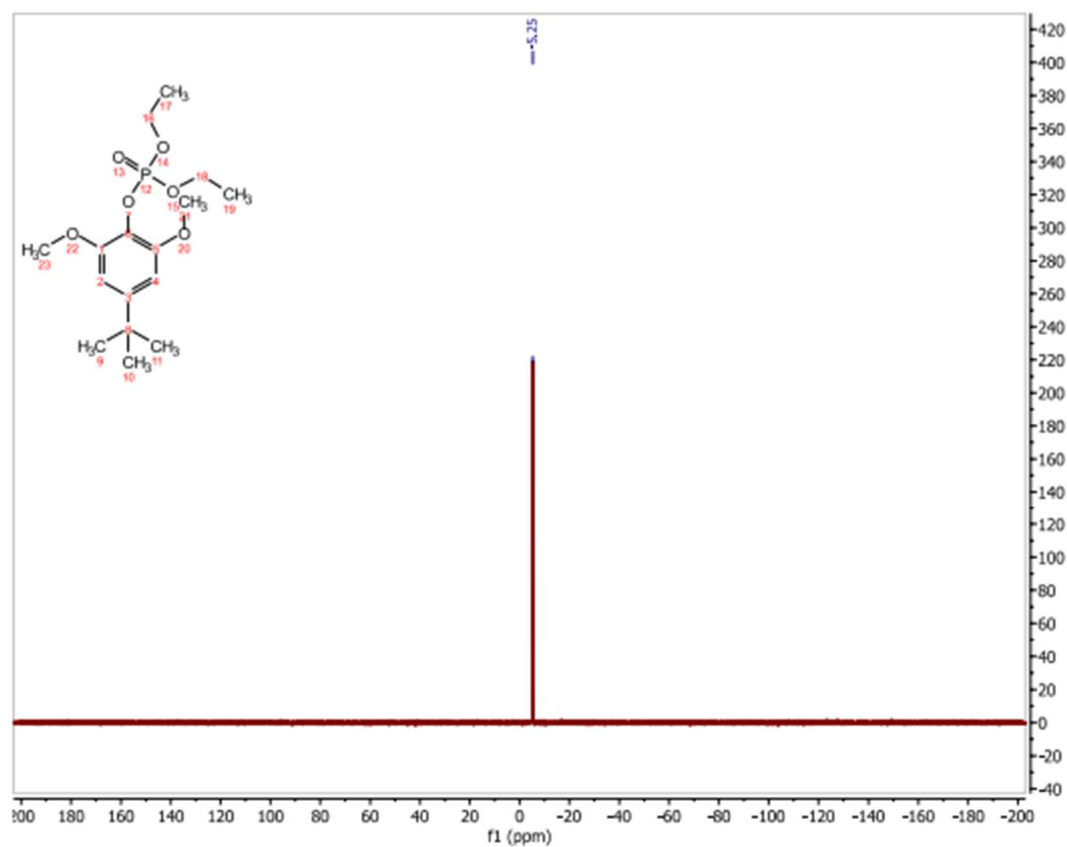
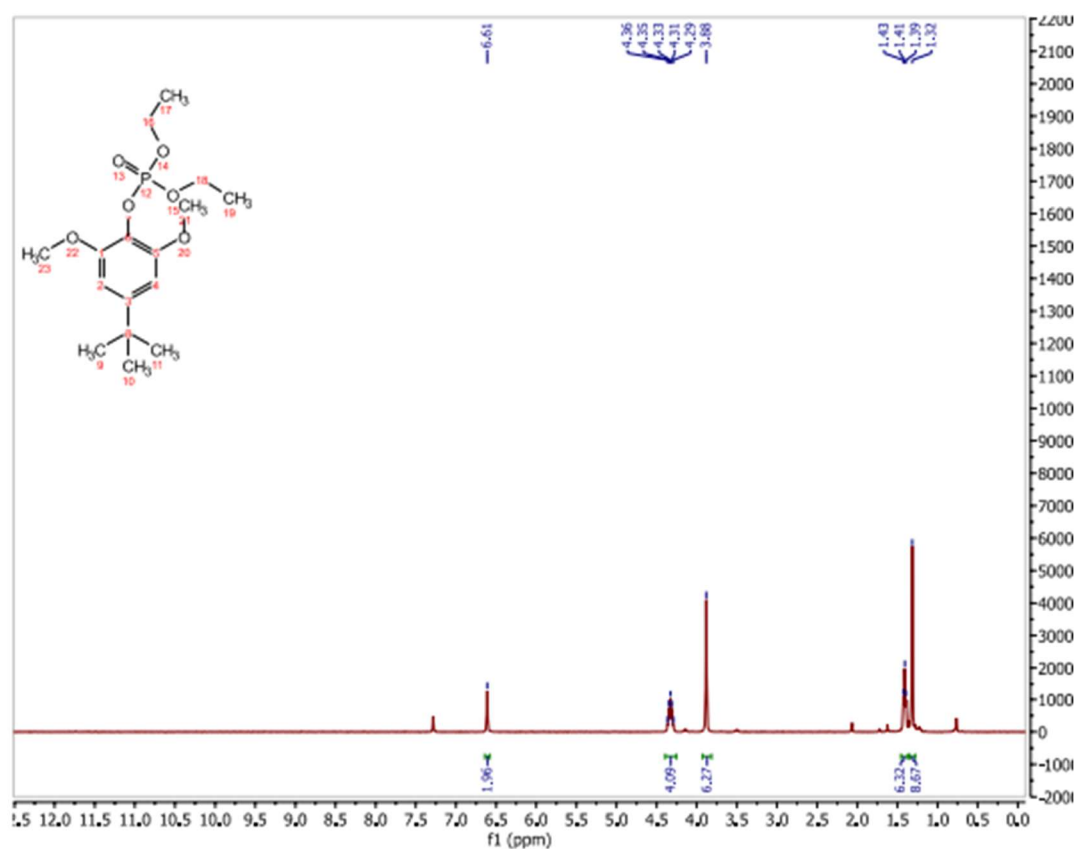


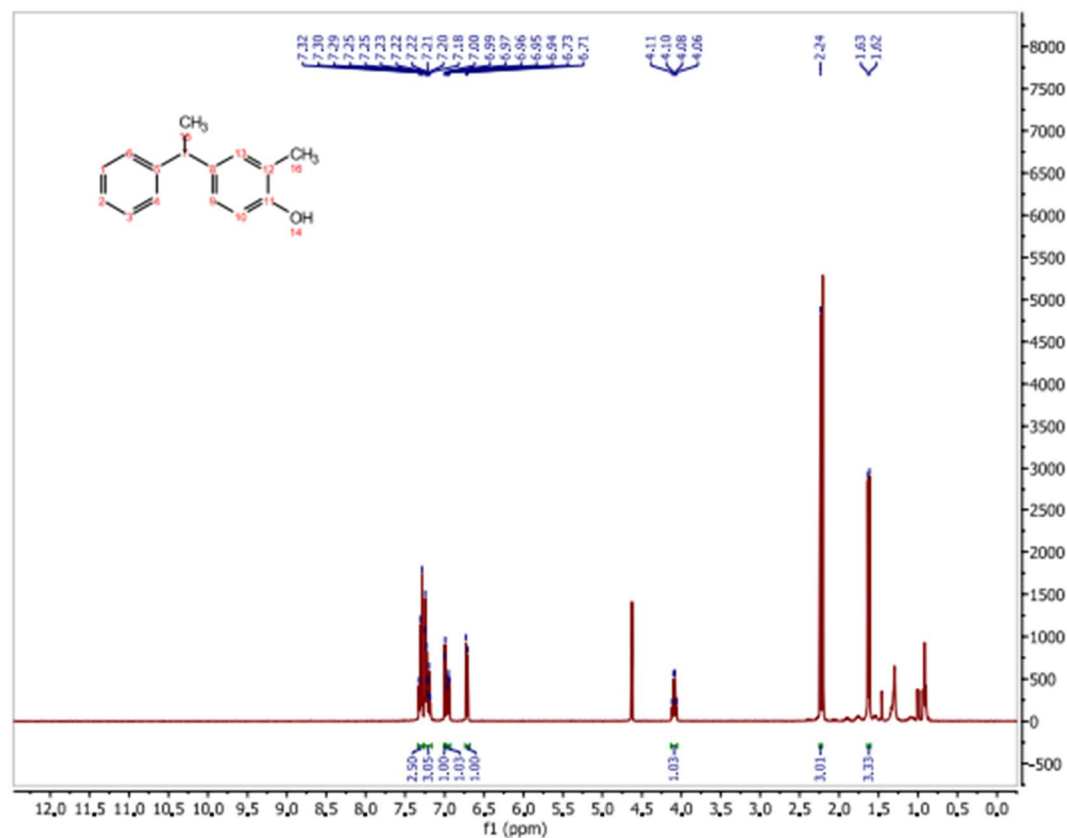
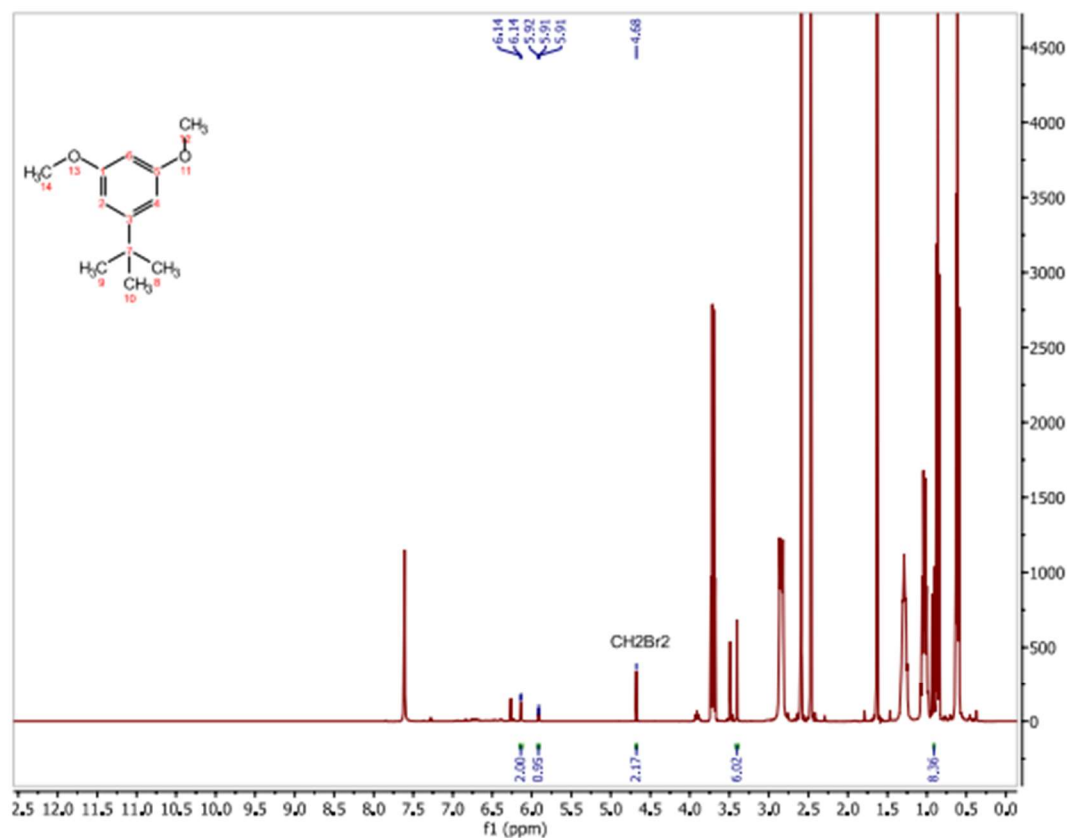


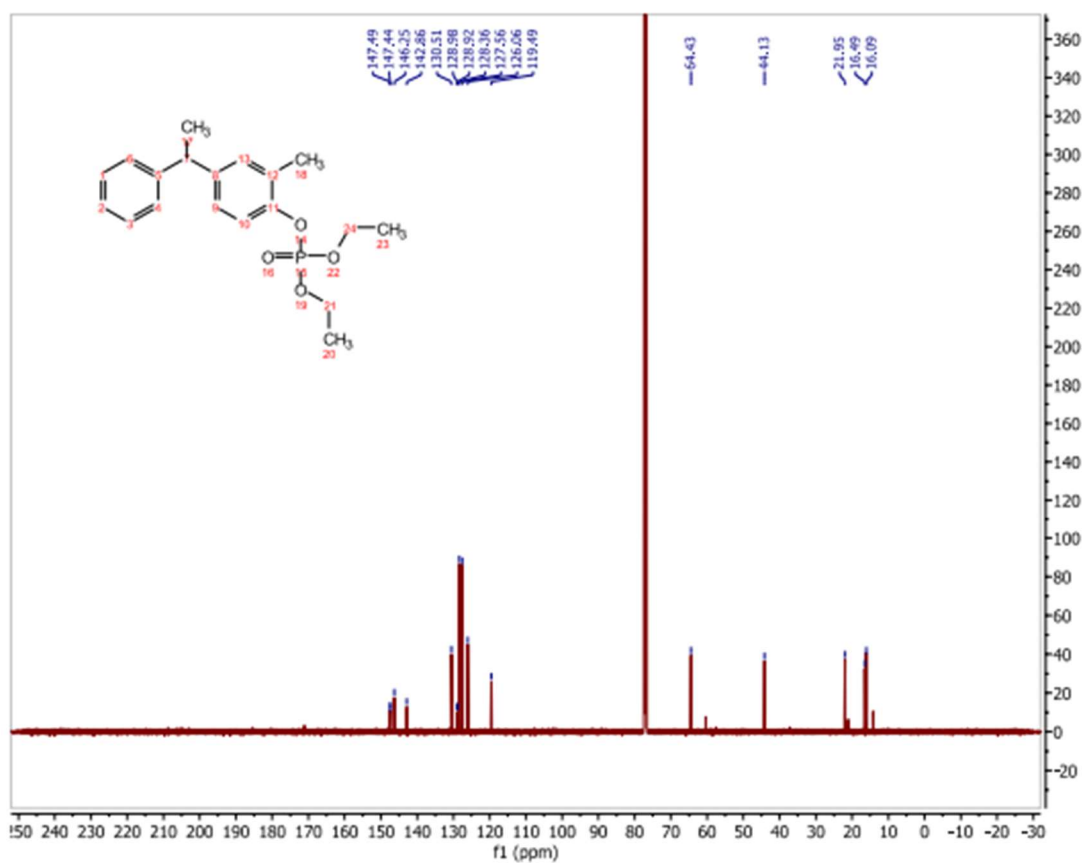
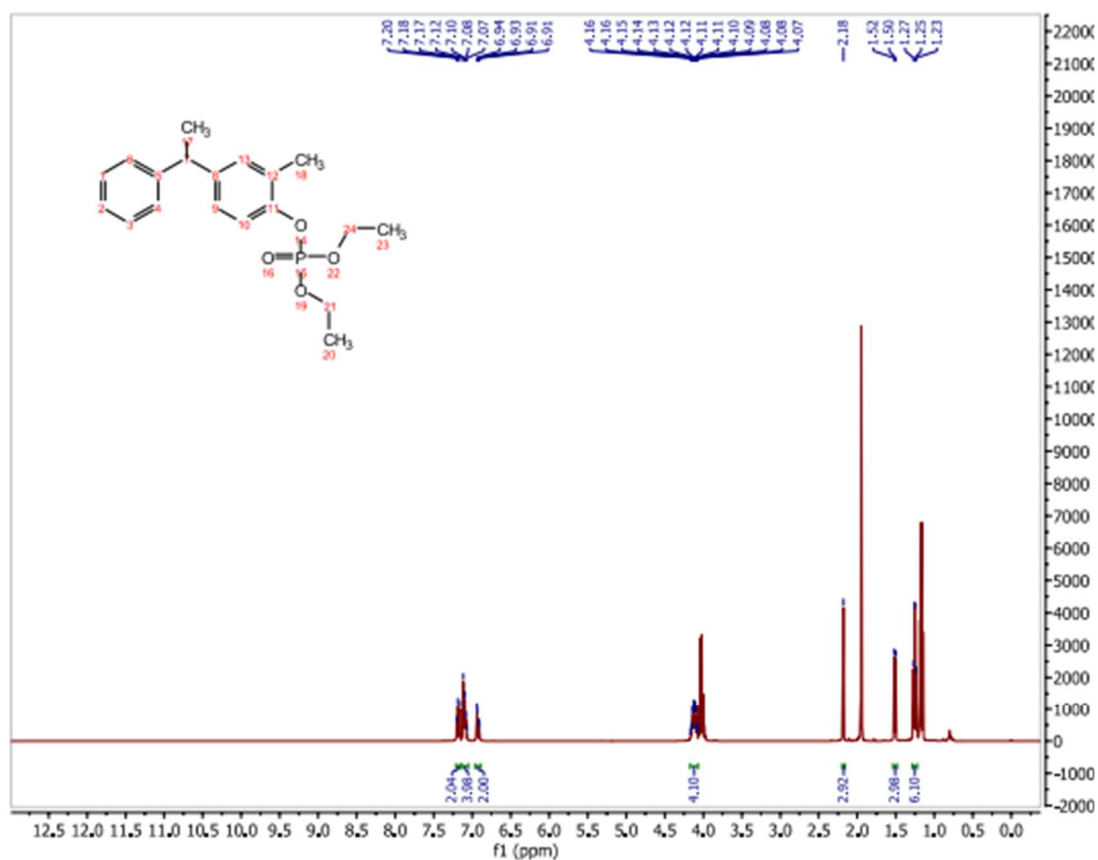


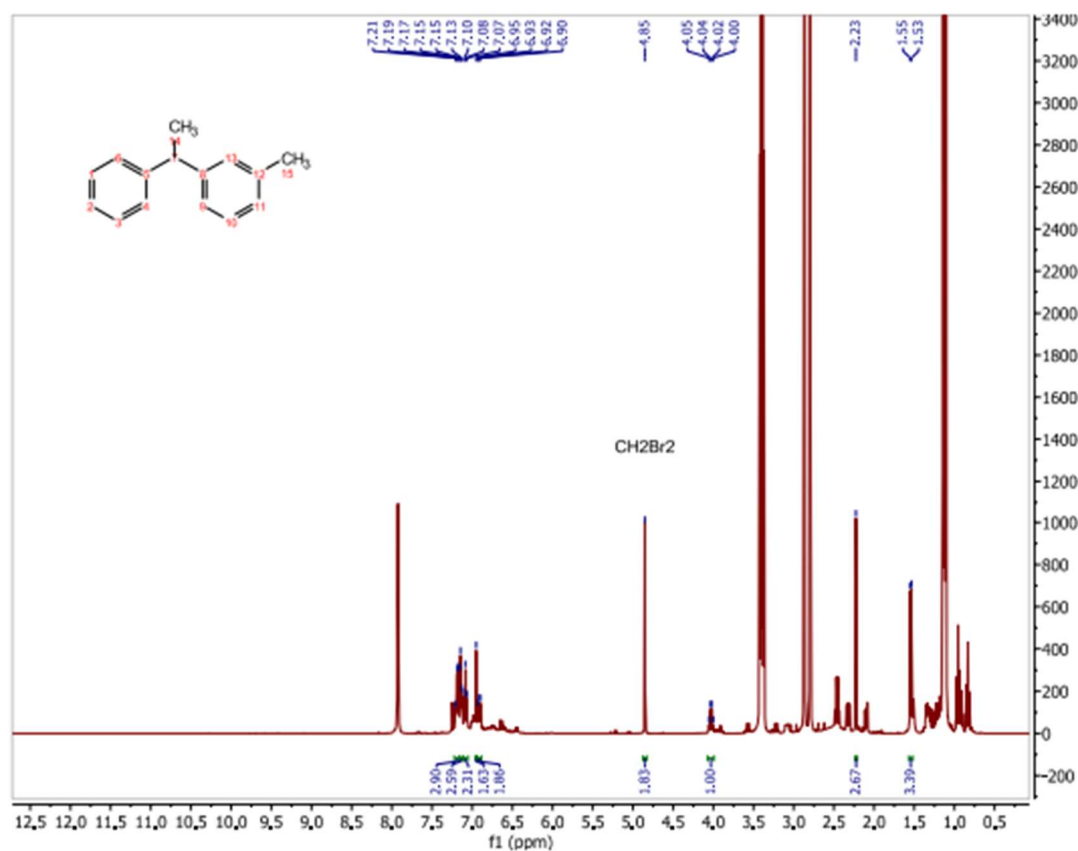
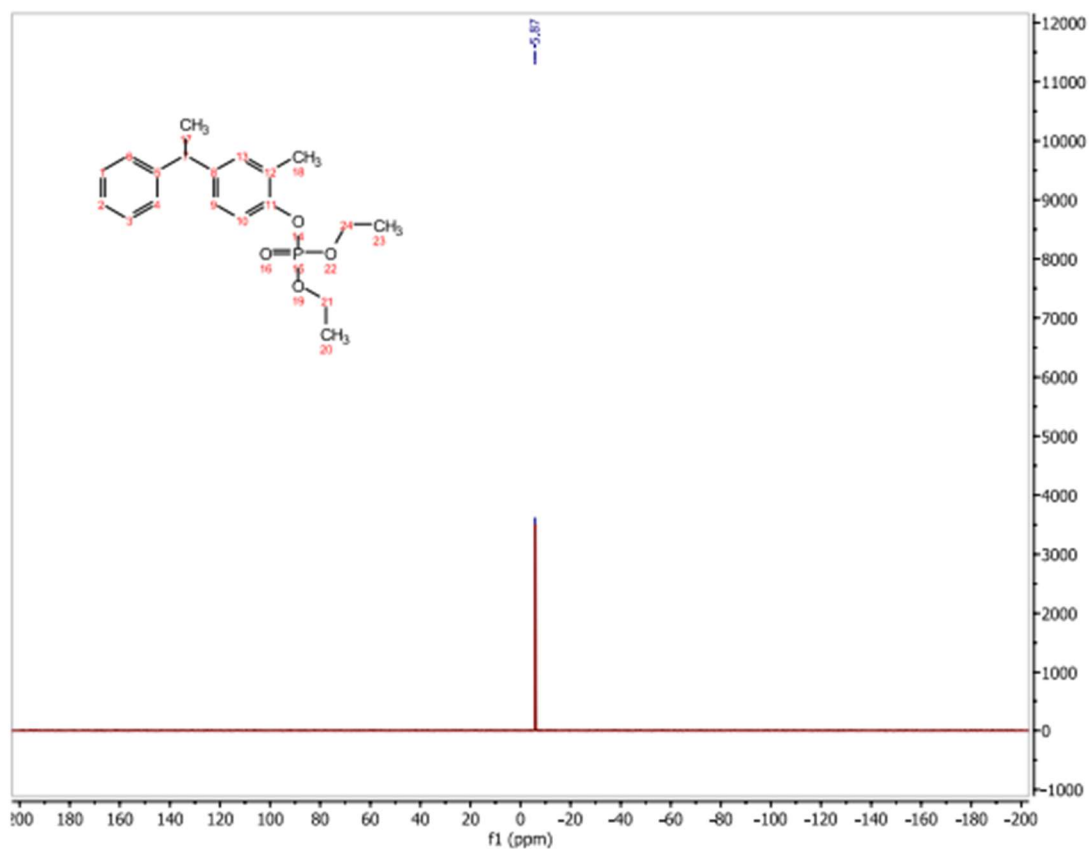


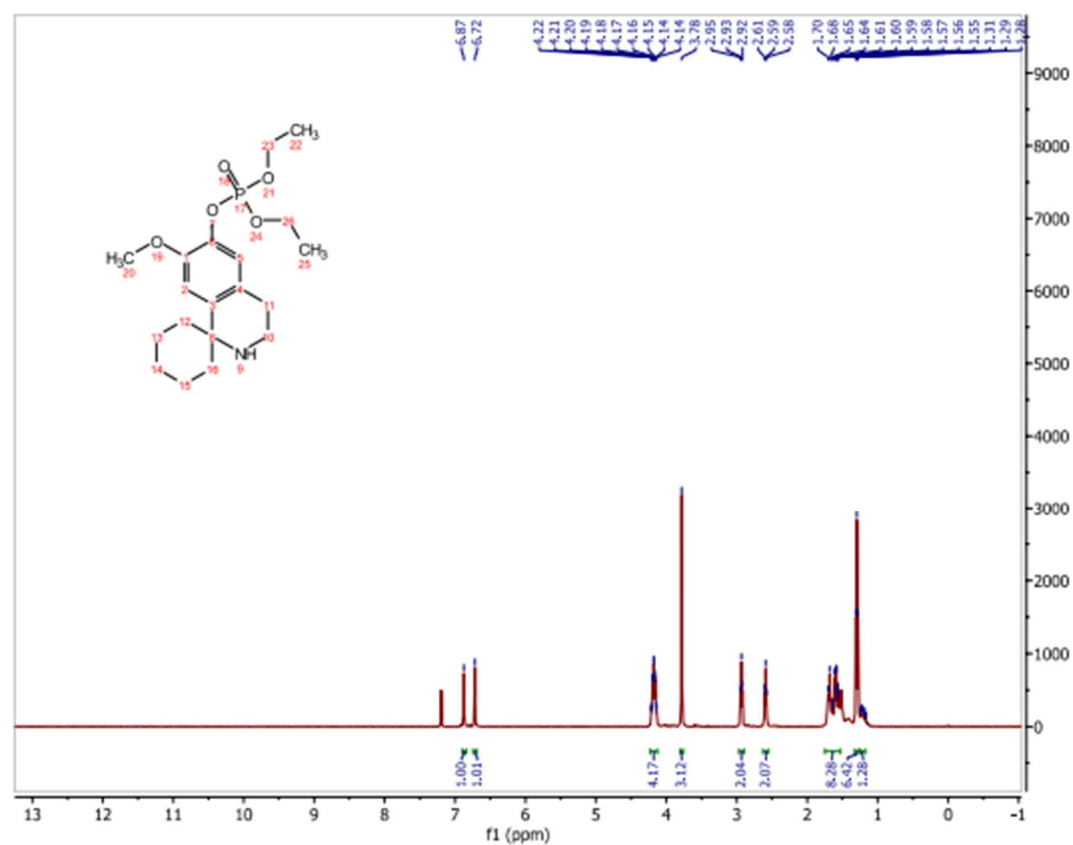
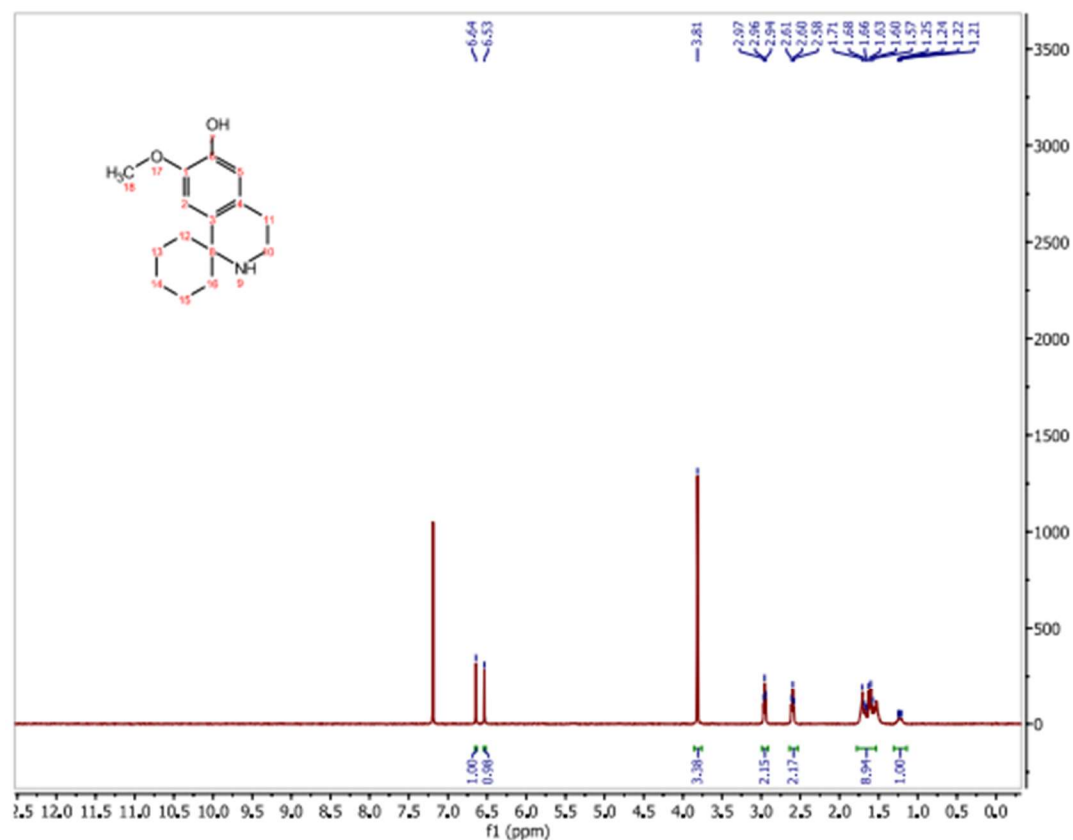


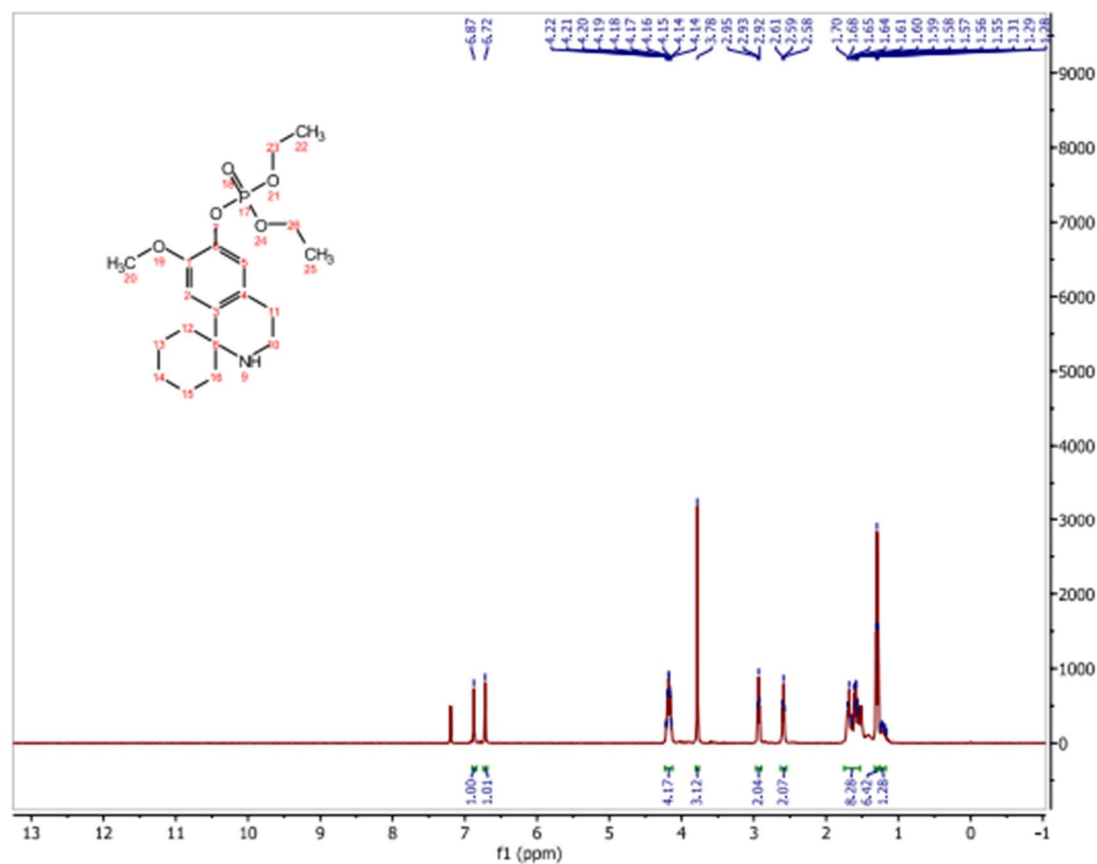
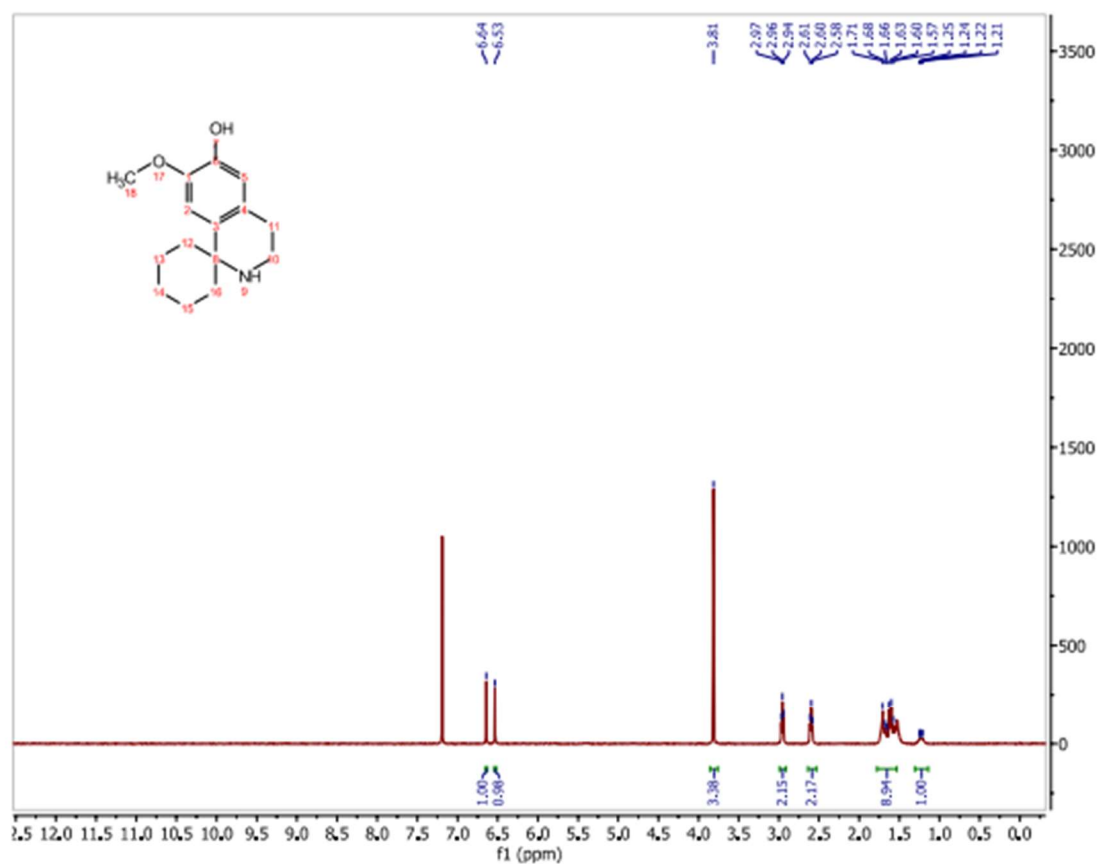


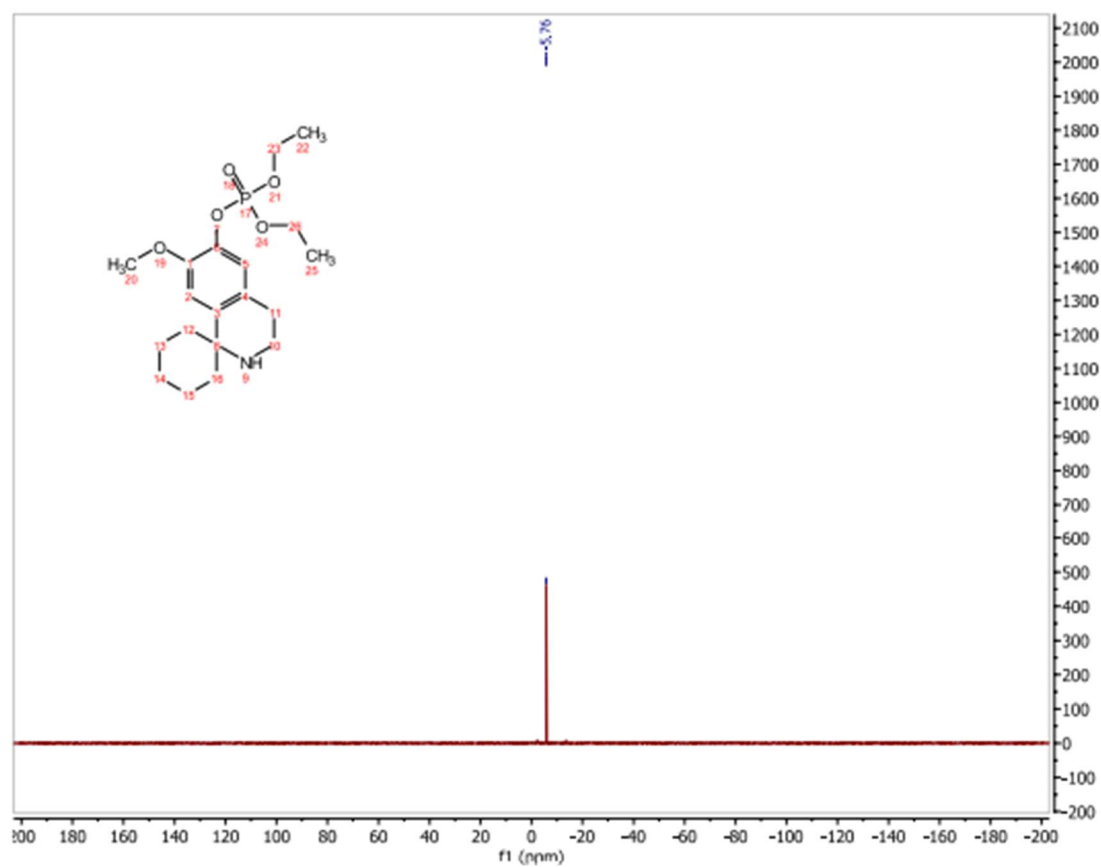
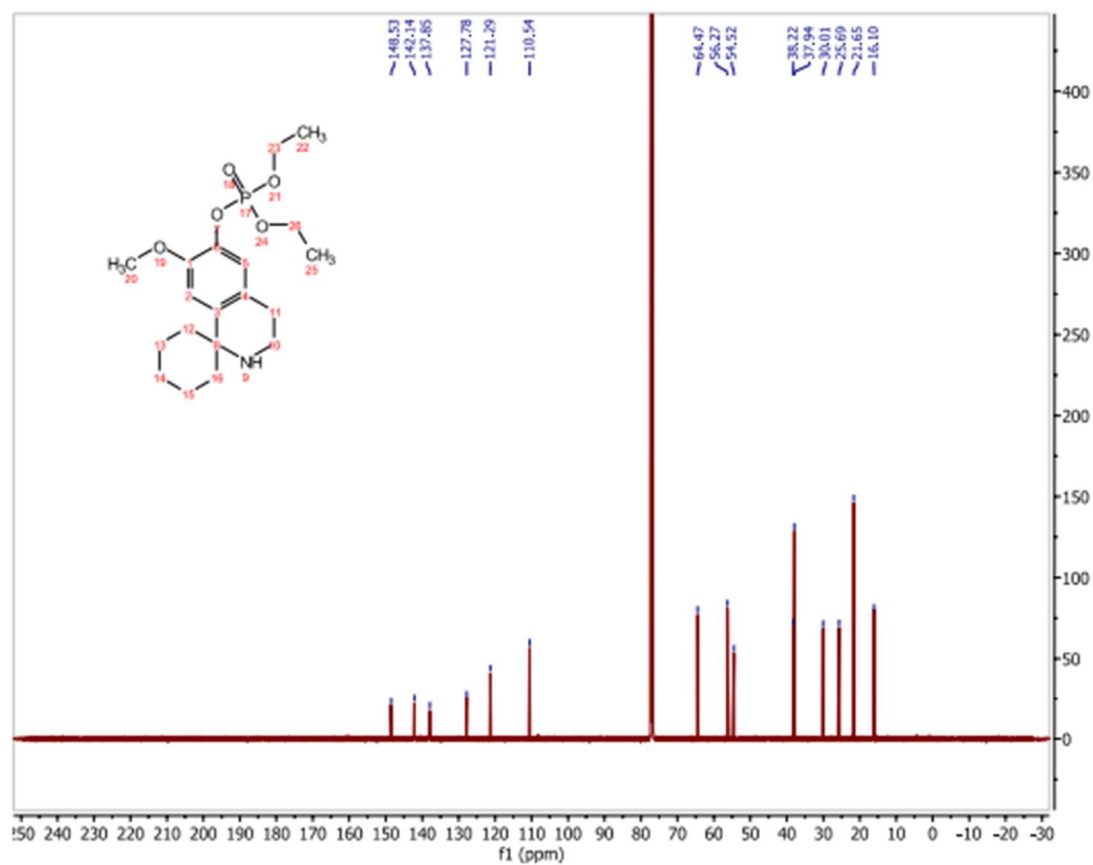


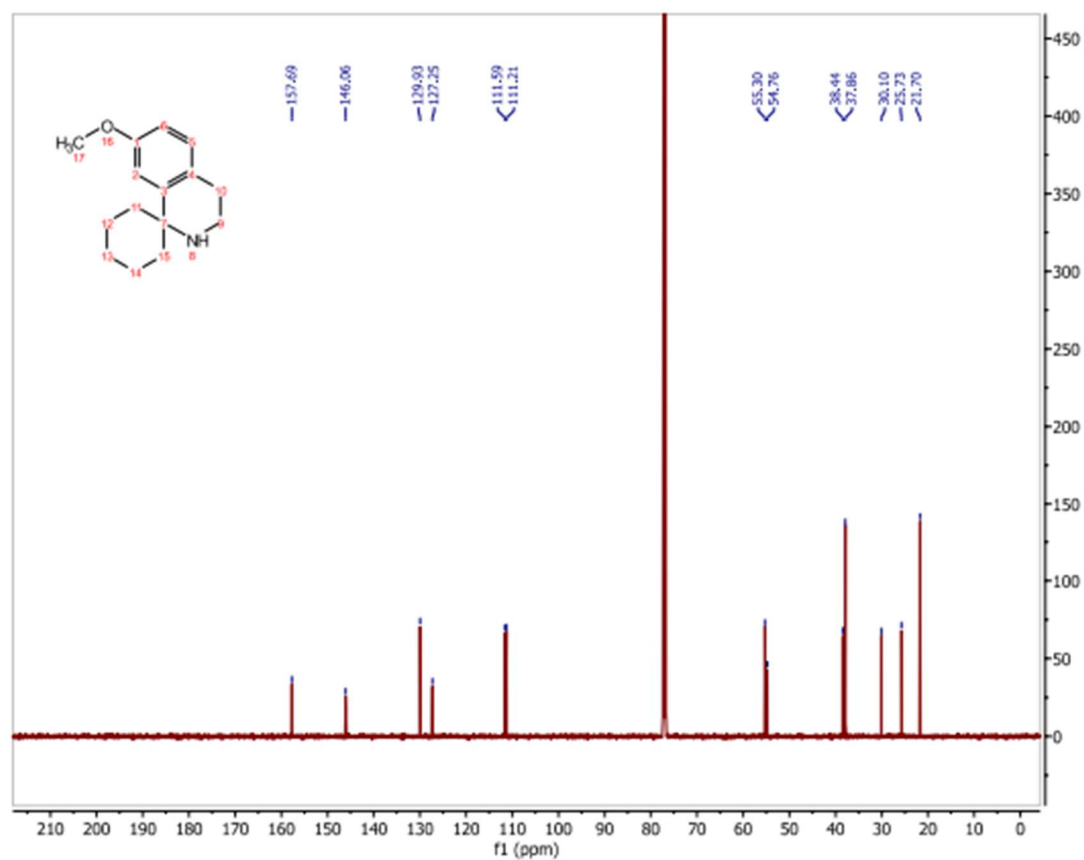
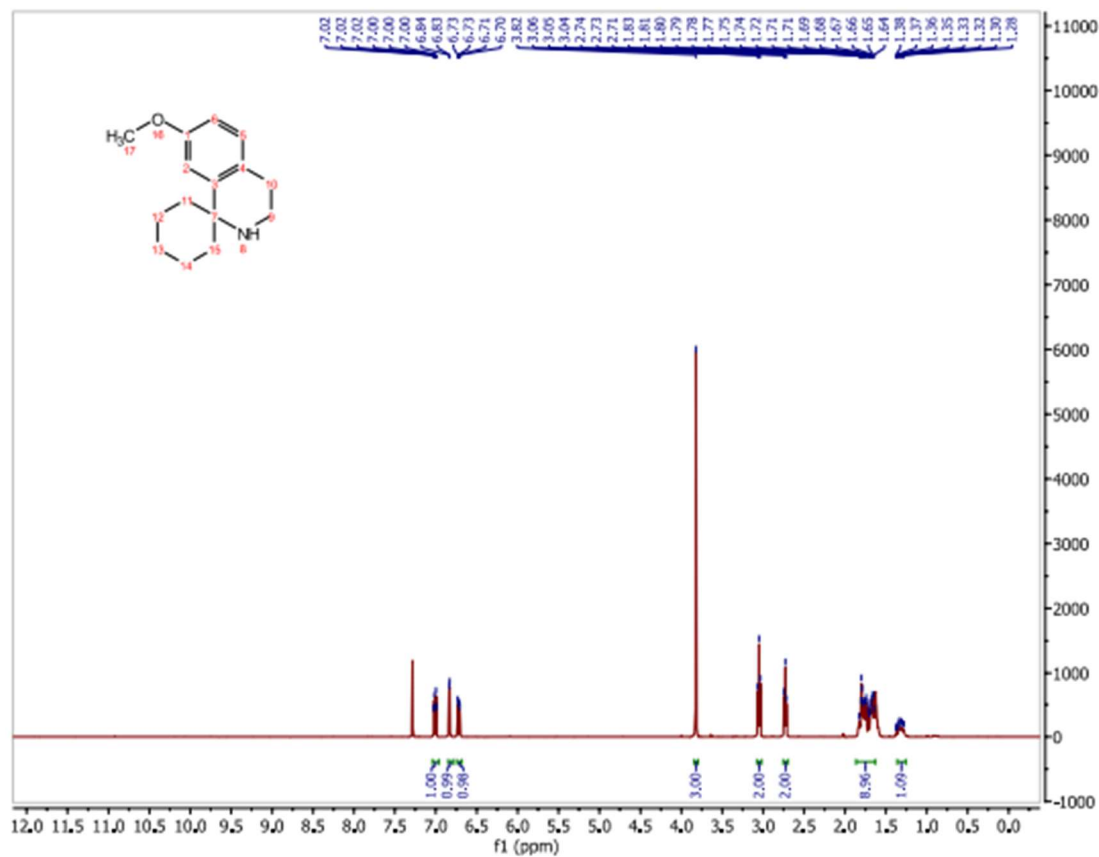


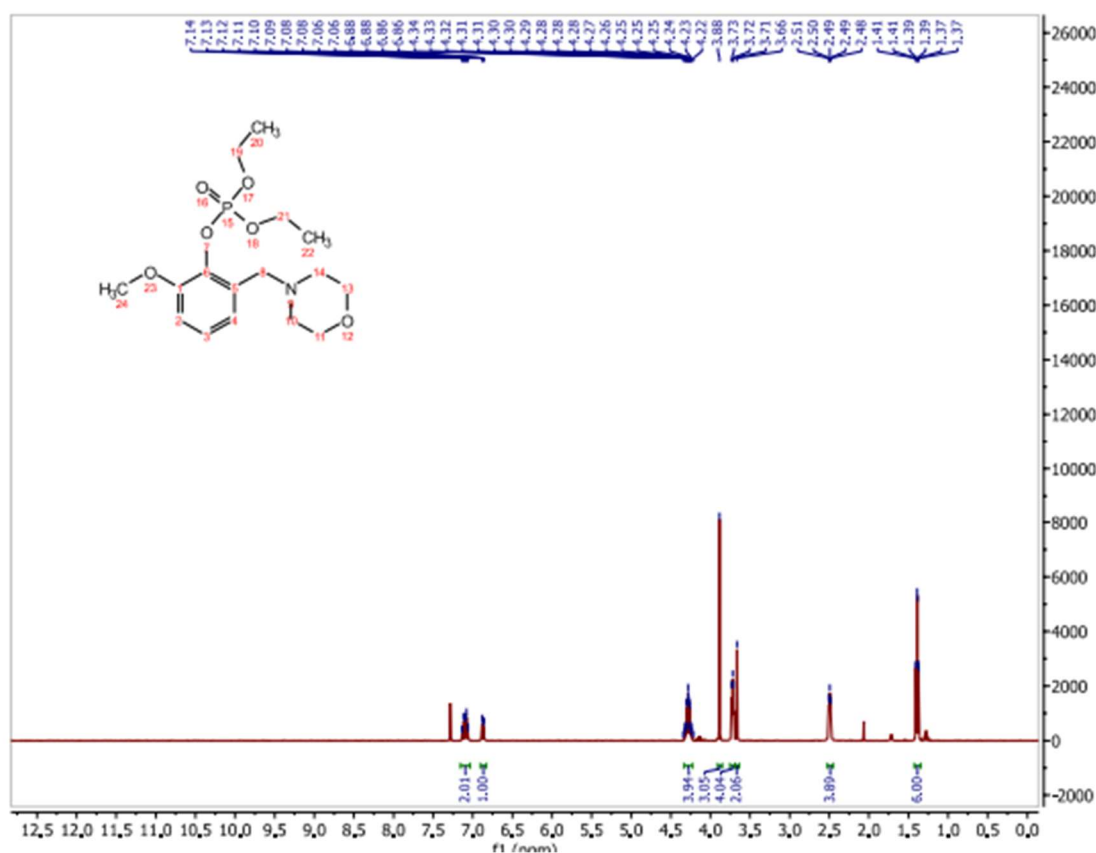
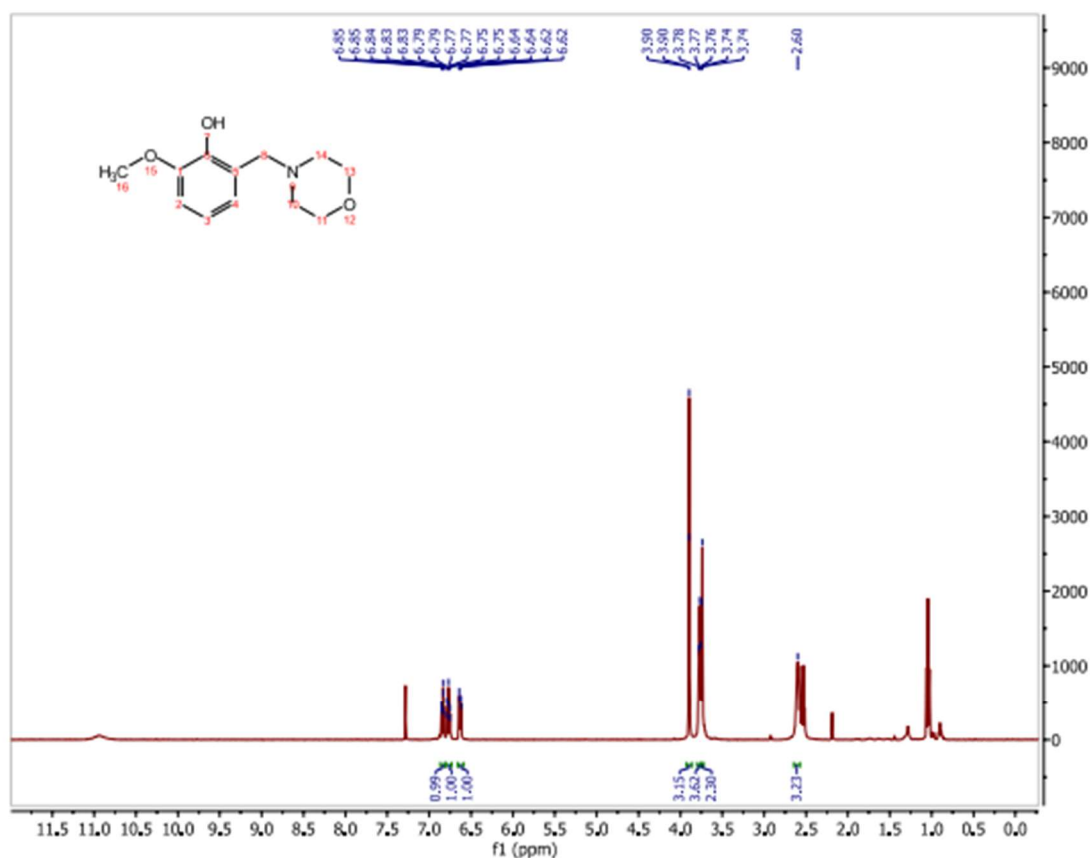


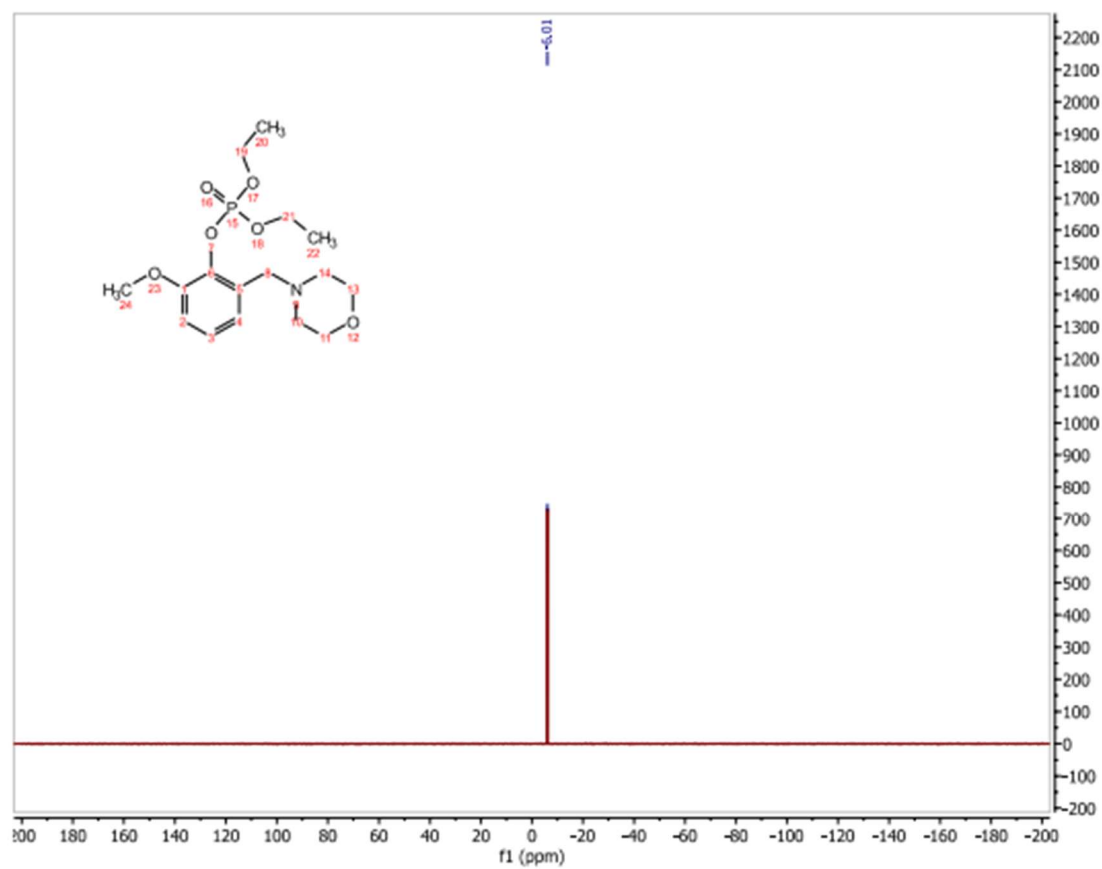
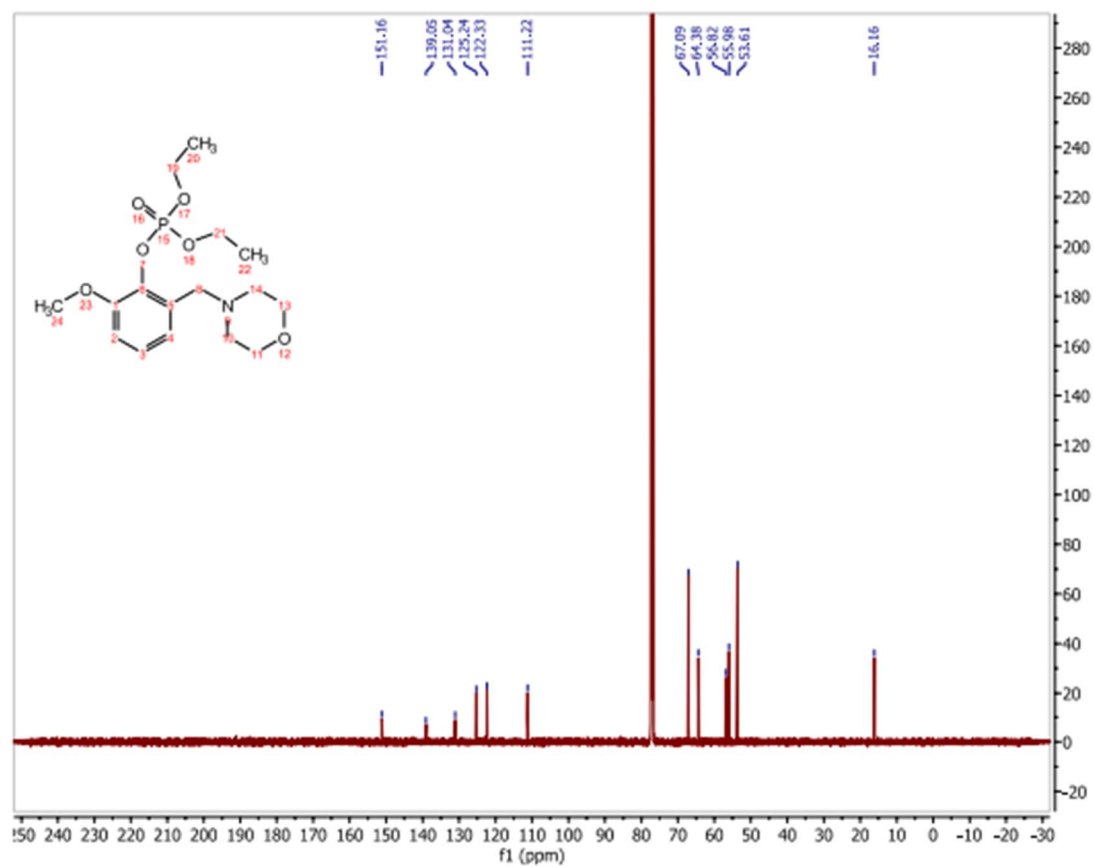


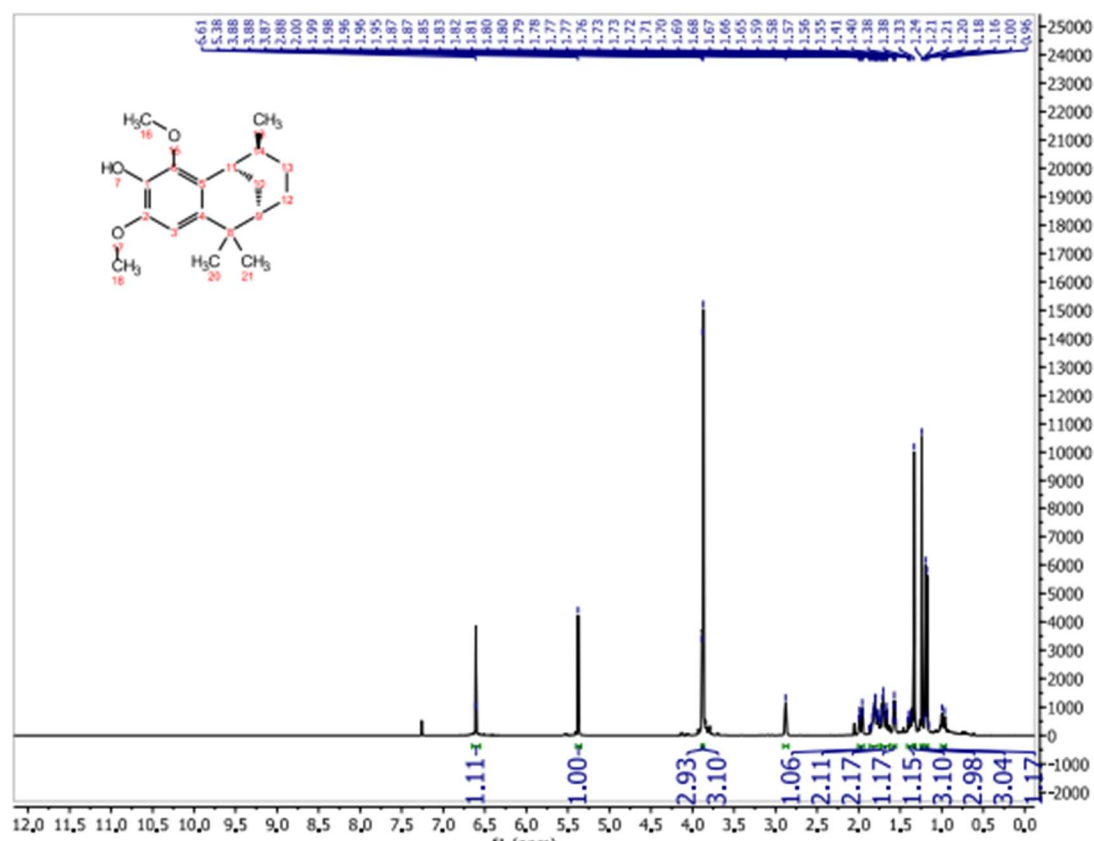
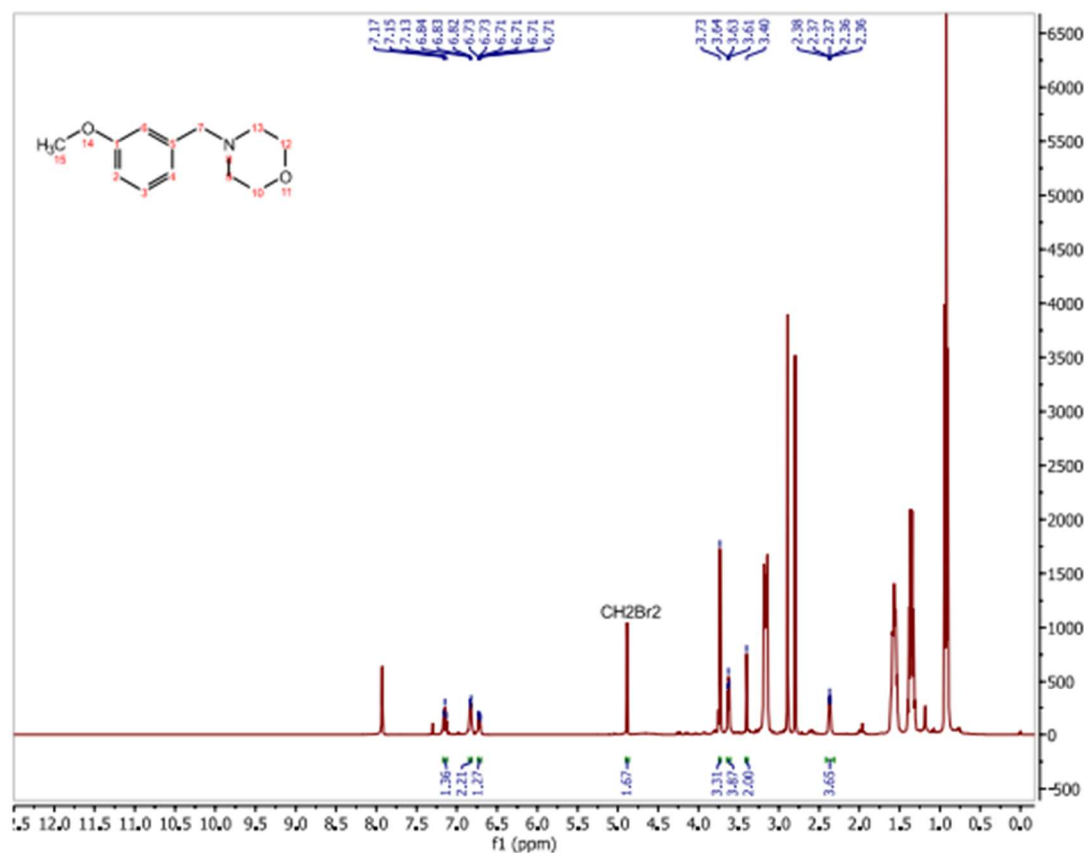


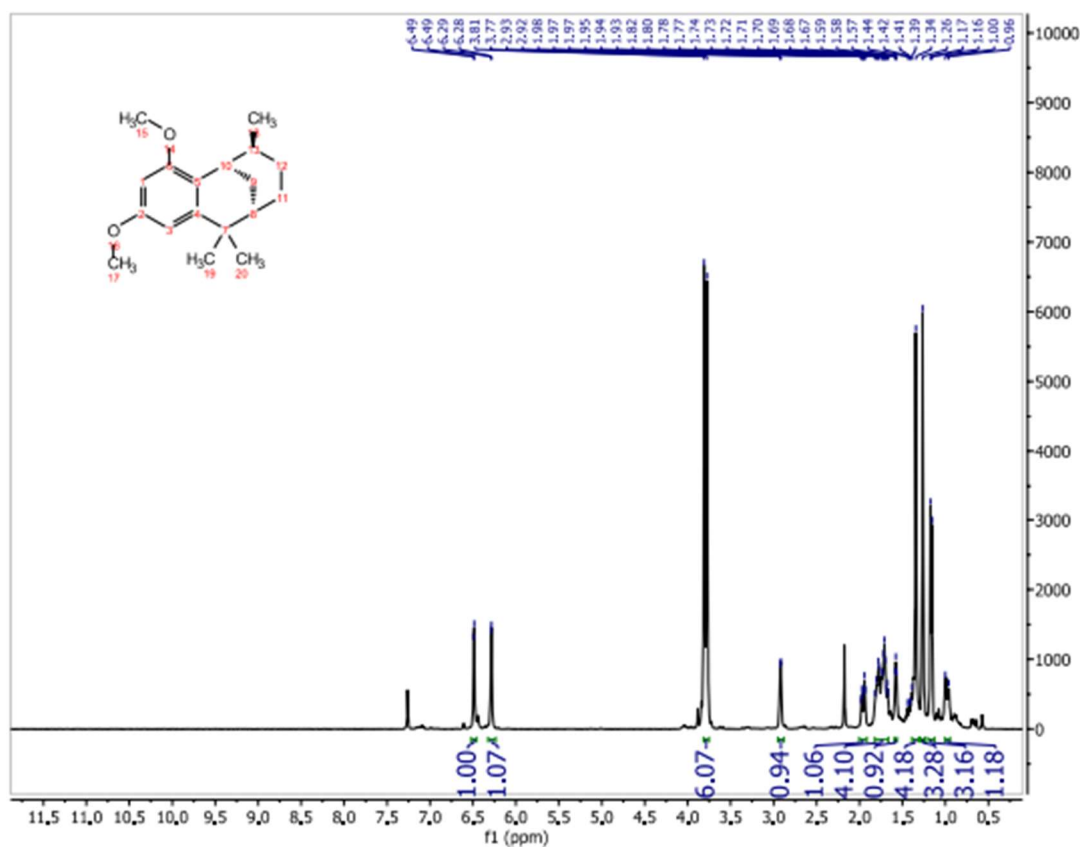
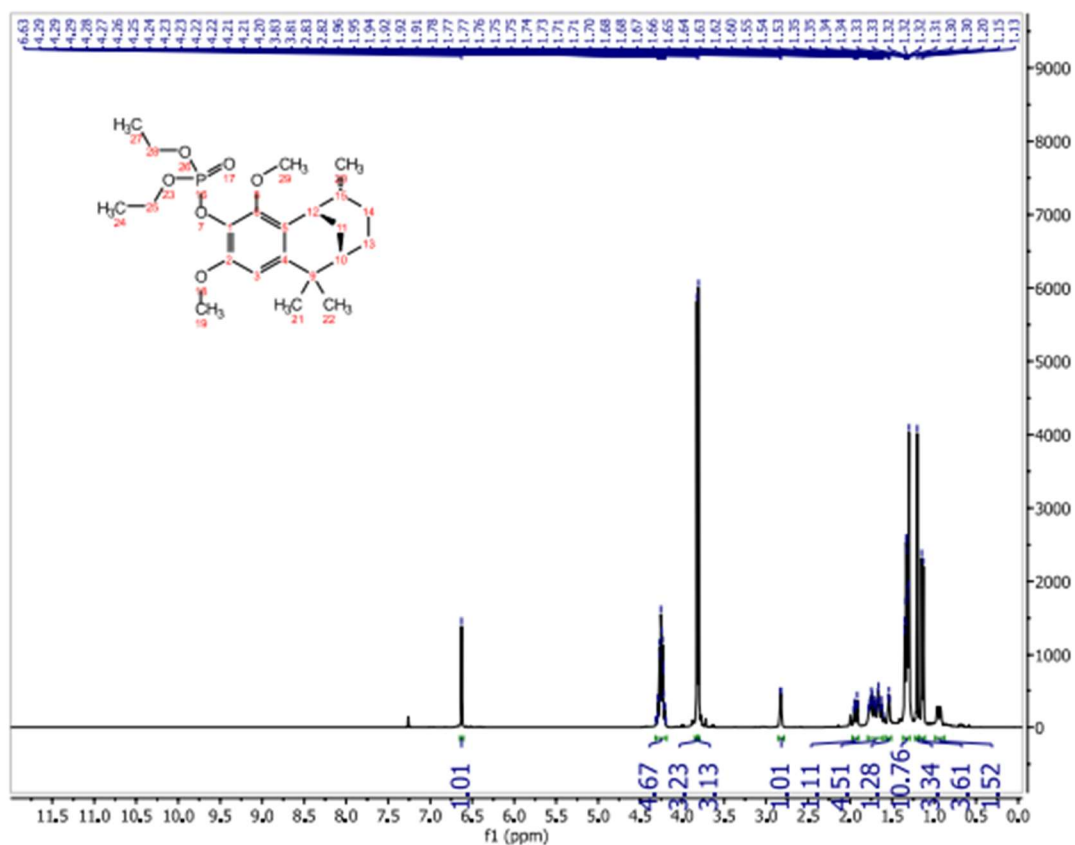


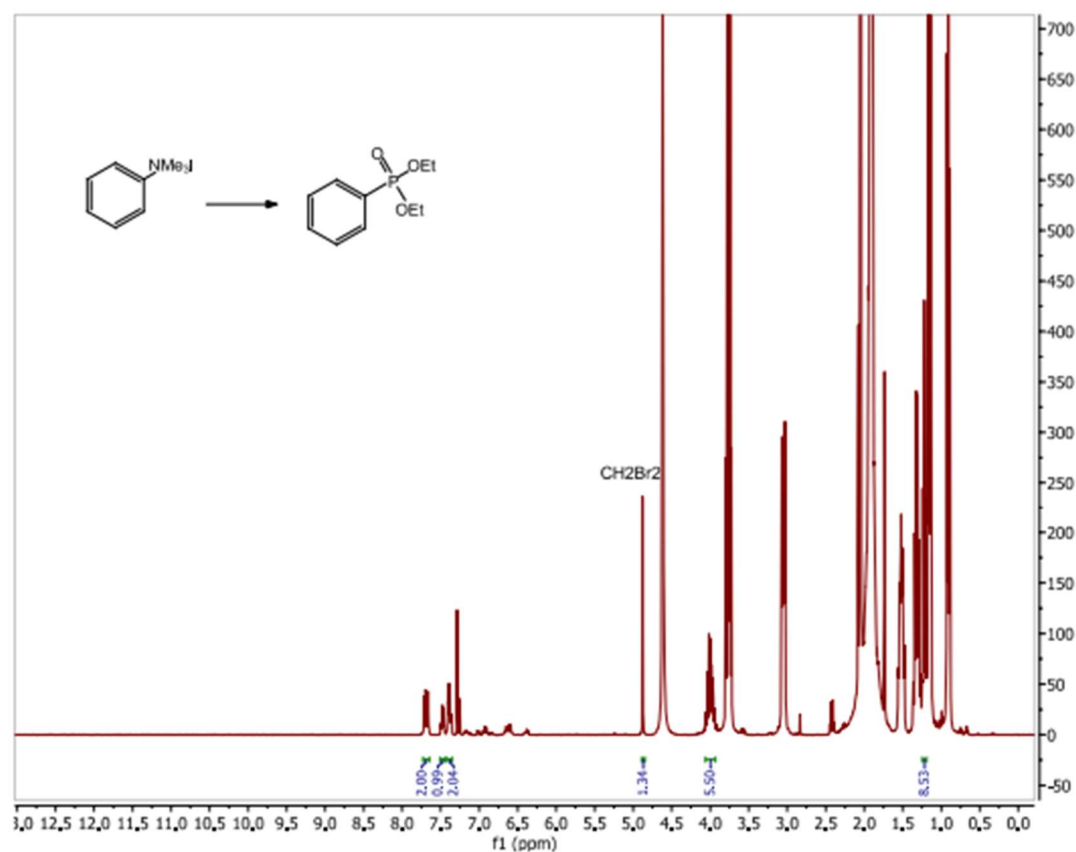
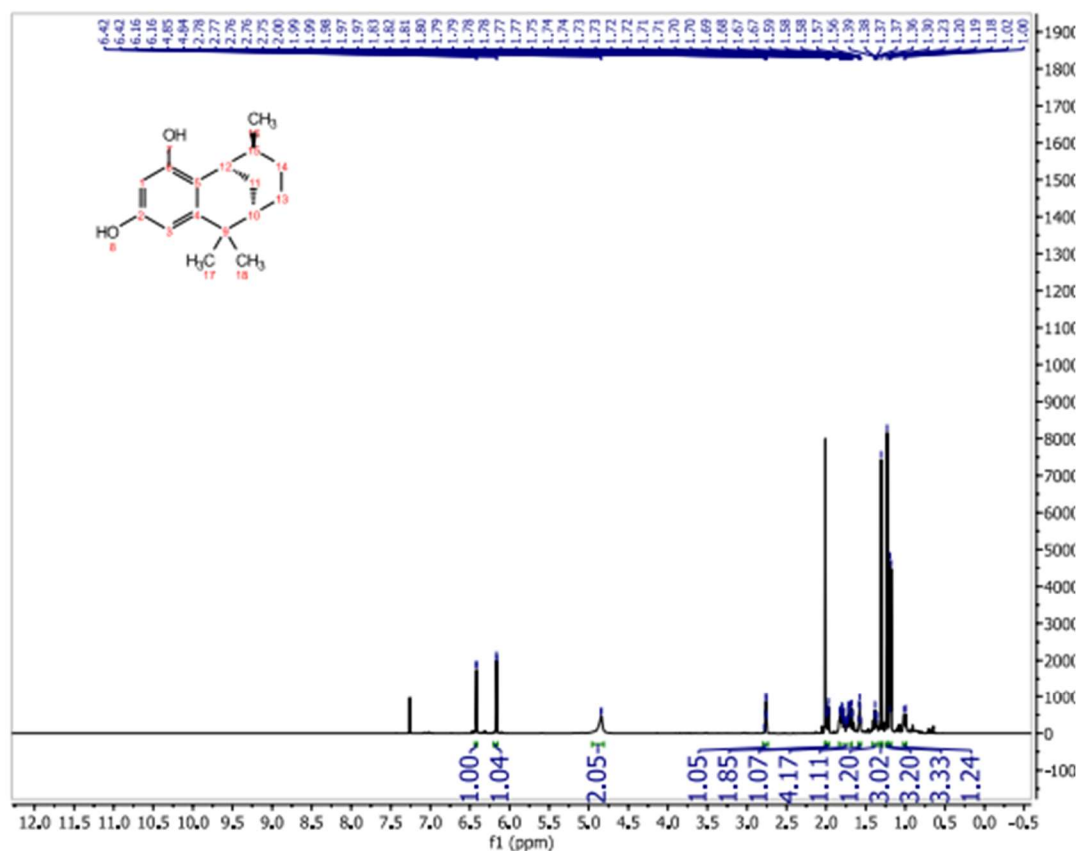


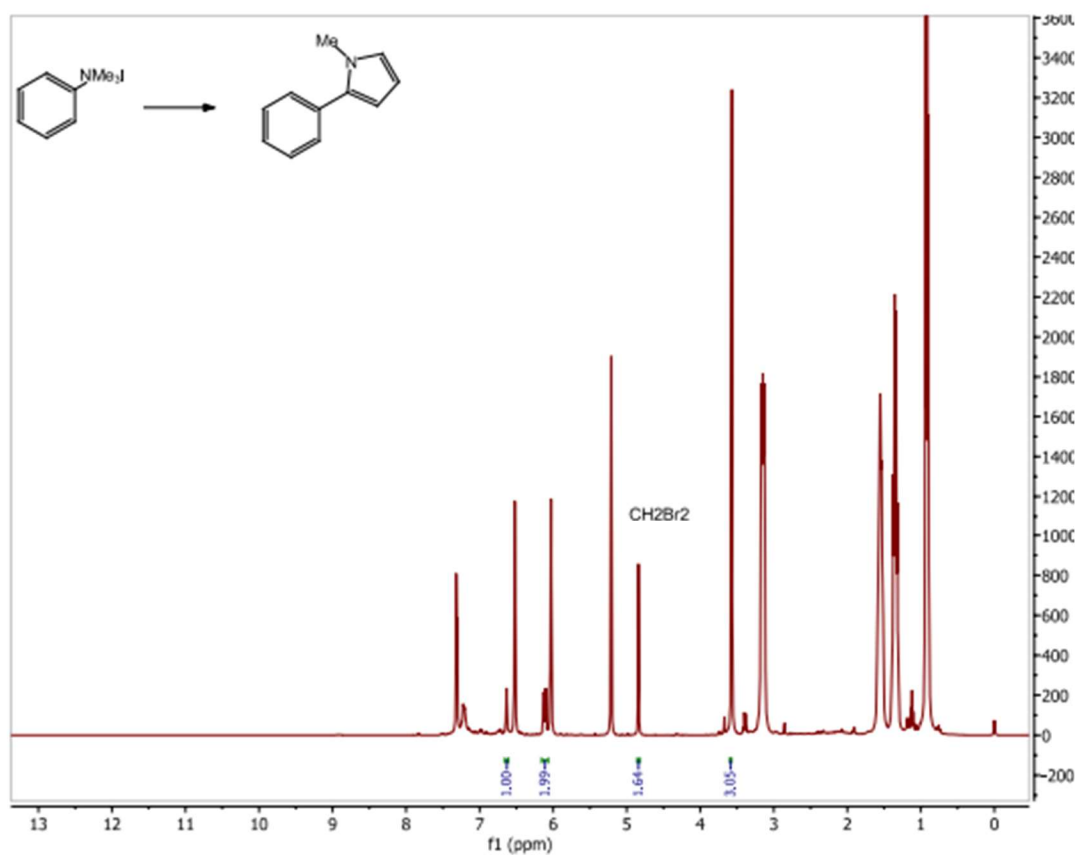
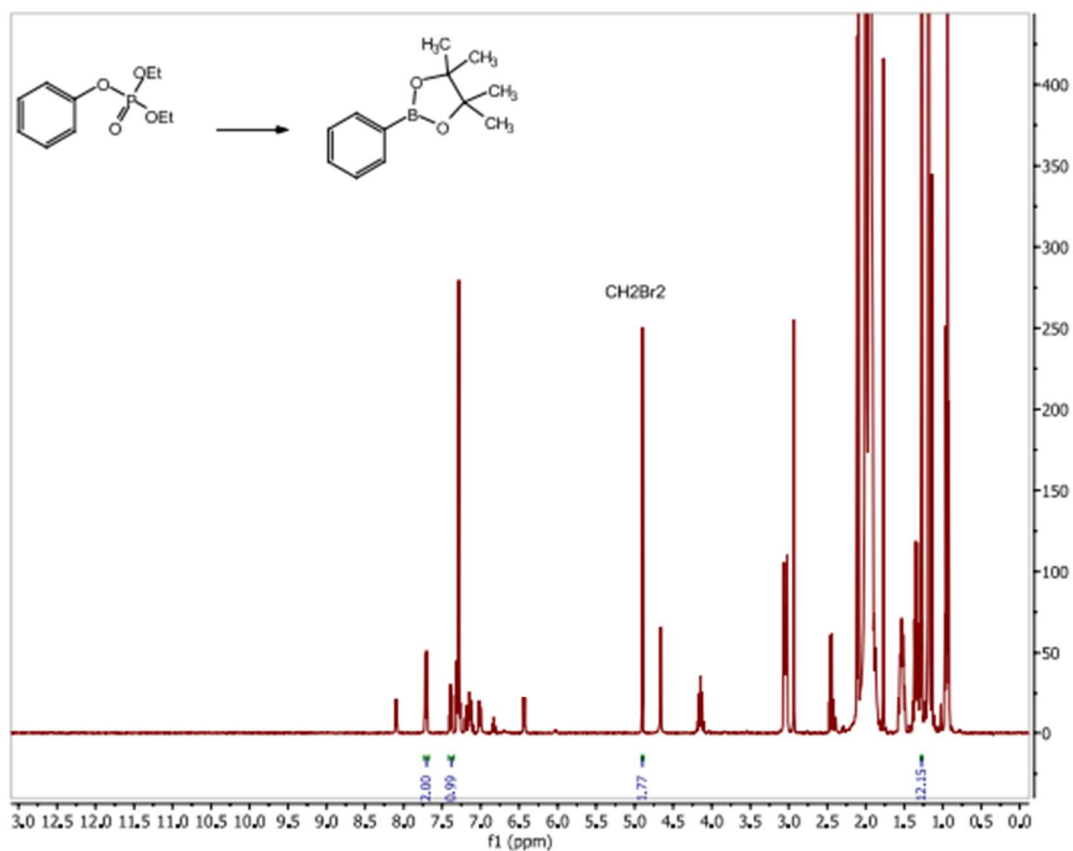












Chapter 4: Non-innocent Radical Ion Intermediates in Photoredox Catalysis: Parallel Reduction Modes Enable Coupling of Diverse Aryl Chlorides

This work is published: Chmiel, A.F.*; Williams, O.P.*; Chernowsky, C.P.; Yeung, C.S.; Wickens, Z.K. *J. Am. Chem. Soc.* **2021**, *143*, 10882-10889

(* denotes equal contribution)

4.1. Abstract

We describe a photocatalytic system that elicits potent photoreductant activity from conventional photocatalysts by leveraging radical anion intermediates generated in situ. The combination of an isophthalonitrile photocatalyst and sodium formate promotes diverse aryl radical coupling reactions from abundant but difficult to reduce aryl chloride substrates. Mechanistic studies reveal two parallel pathways for substrate reduction both enabled by a key terminal reductant byproduct, carbon dioxide radical anion.

4.2. Introduction

Reductive activation of organic molecules via single electron transfer (SET) is a fundamental elementary step that underpins diverse and powerful synthetic transformations.^{1–4} Photoredox catalysis promotes SET through conversion of energy from visible light into chemical redox potential and has enabled a suite of carbon–carbon and carbon-heteroatom bond-forming reactions.^{5–9} When considering whether a substrate will be suitable for photoredox reduction, two primary catalyst parameters are initially considered: (1) $E_{1/2}(\text{PC}^{++}/\text{PC}^{\bullet+})$ and (2) $E_{1/2}(\text{PC}/\text{PC}^{\bullet-})$.^{7,10,11} These values reflect redox potentials bounded by the energy of photons in the visible region, a limitation compounded by energy losses to intersystem crossing.¹² As a result, many abundant but challenging to reduce substrates are excluded from photoredox activation based on these guidelines (**Figure 4.1.(a)**).^{13–15}

Aryl radicals are reactive intermediates that engage in a myriad of synthetically valuable transformations.^{16–18} Classically, aryl radical intermediates are generated from aryl diazonium salts, iodides, or bromides.^{19–29} Aryl chlorides are rarely used as radical precursors despite the fact they comprise over two-thirds³⁰ of commercially available aryl halides (**Figure 4.1.(b)**).^{31–35} This is a consequence of their resistance to reductive activation,¹³ and high $\text{C}(\text{sp}^2)\text{--Cl}$ BDE.^{36,37} König recently pioneered an elegant strategy, termed consecutive photoinduced electron transfer (conPET), wherein a photochemically generated radical anion is subsequently excited.^{38,39} This

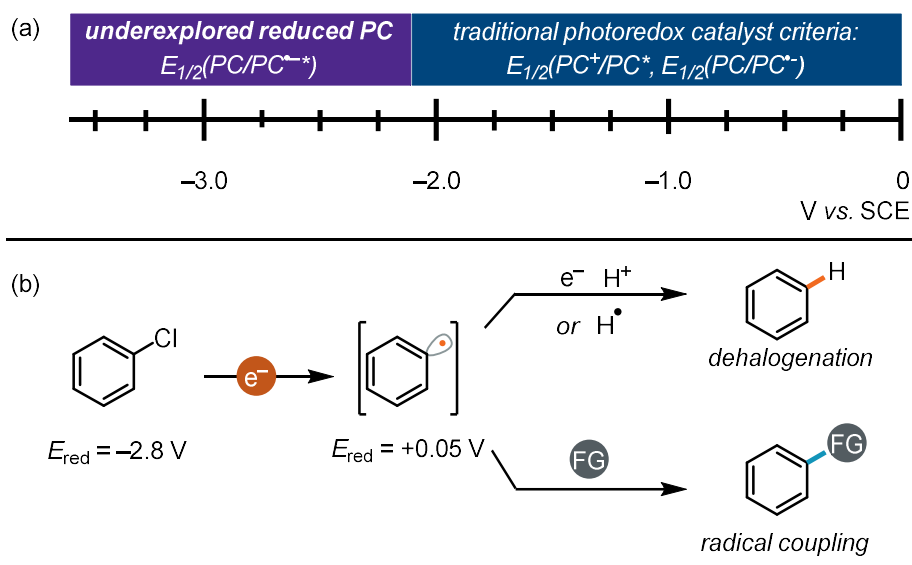


Figure 4.1. (a) Energy limitations for photoredox catalysis and electron-primed photoredox catalysis. (b) Aryl chlorides reactivity as aryl radical precursors. All V vs. SCE.

approach primes the photocatalyst with an electron prior to excitation and, in principle, can generate much deeper reduction potentials through $E_{1/2}(\text{PC}/\text{PC}^{\cdot-})$. Indeed, later implementations of this conPET strategy unlocked exceptionally challenging reductions.^{40,41} However, all recent advances in visible light photoredox methods that reduce electronically diverse chloroarenes have been limited to proteodefunctionalization and borylation reactions.^{40,42–45} Recent electrophotocatalytic^{46–49} approaches have directly generated these electron-primed photocatalysts cathodically.^{50,51} While this strategy has begun to expand the range of radical coupling reactions that engage aryl chlorides, a general approach to leverage the expansive pool of aryl chloride substrates in radical couplings has remained elusive and the need for electrochemical equipment remains a barrier in some settings.^{52,53} In particular, net-reductive radical coupling processes, such as alkene hydroarylation,^{54–56} have remained elusive for aryl chloride substrates for all modern methods. We suspect that the paucity of net-reductive processes is a consequence of the intrinsic challenges of circumventing premature reduction of the aryl radical intermediate ($E_{\text{red}}(\text{Ph}^{\cdot}/\text{Ph}^-) = +0.05 \text{ V vs SCE}$)⁵⁷ in the presence of a stoichiometric reductant.

Our group recently used electrochemistry to examine a diverse set of organic radical anions for photocatalytic activity in the reductive cleavage of strong C(sp²)-O and C(sp²)-N bonds.⁵⁸ These experiments revealed that numerous radical anions, including those derived from commonly employed photoredox catalysts, can serve as potent photocatalytic reductants upon cathodic reduction. These data fit into a growing body of literature from our group⁵⁹ and others^{40,60} that suggest photocatalyst-based redox events can engender more potent activity from conventional photocatalysts. Taken together, these data led us to consider whether we could redesign a photocatalytic system to favor formation of photoactive radical anion intermediates to elicit deeply reducing potentials and expand the repertoire of coupling reactions available from aryl chlorides under operationally simple conditions (**Figure 4.2.**). Herein, we disclose that selection of an appropriate reductant to generate and maintain an active electron-primed photoredox catalyst in situ enables reduction potentials far beyond those expected from conventional catalyst selection criteria. These new reduction conditions promote a diverse array of intermolecular coupling reactions, including net-reductive coupling processes, from readily available aryl chloride substrates.

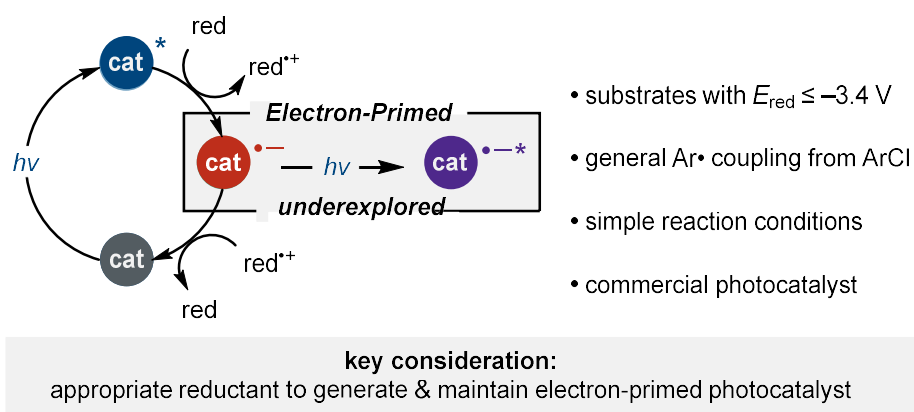


Figure 4.2. Exploiting non-innocent radical anion intermediates in photoredox cycles (this work)

4.3. Results and Discussion

We first evaluated a suite of organic compounds recently found to possess photocatalytically active radical anion congeners⁵⁸ for activity in the dehalogenation of PhCl ($E_{\text{red}} = -2.8 \text{ V}$ vs SCE). Considering only conventional photoredox catalyst selection parameters ($\text{PC}/\text{PC}^{\cdot-}$ and $\text{PC}^*/\text{PC}^{++}$), this reduction would be exceedingly endothermic ($>1 \text{ V}$) for the photocatalysts under investigation. Therefore, activity in this assay would implicate in situ formation of a distinct and potent reductant. Initially, we examined a range of trialkylamine reductants because these are common reductants in photoredox catalysis, including in conPET strategies (**Figure 4.3**).^{38,40,61} We found that each catalyst modestly promoted this energetically

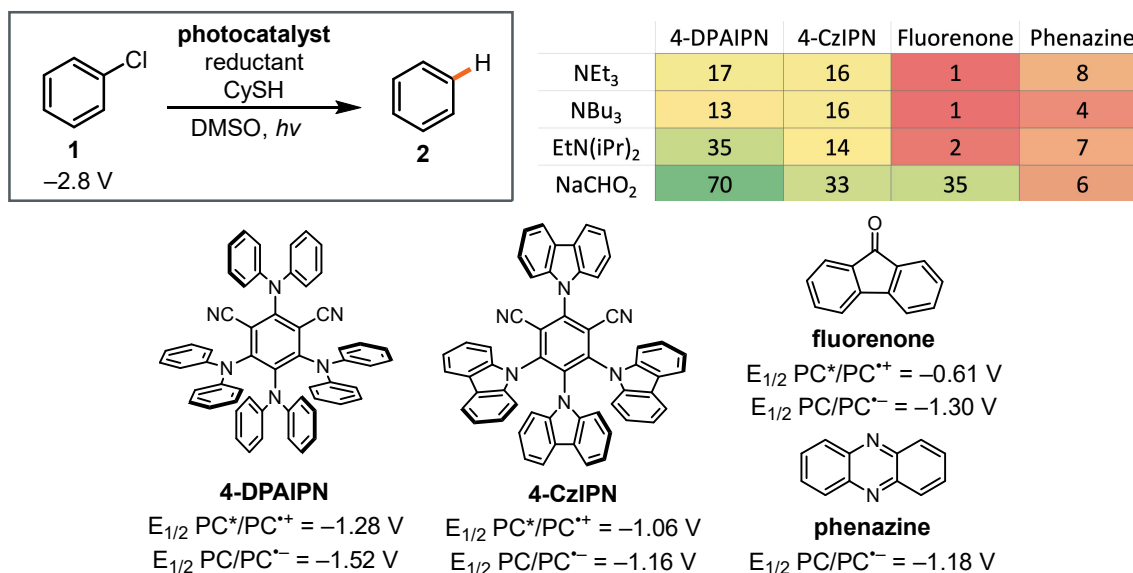


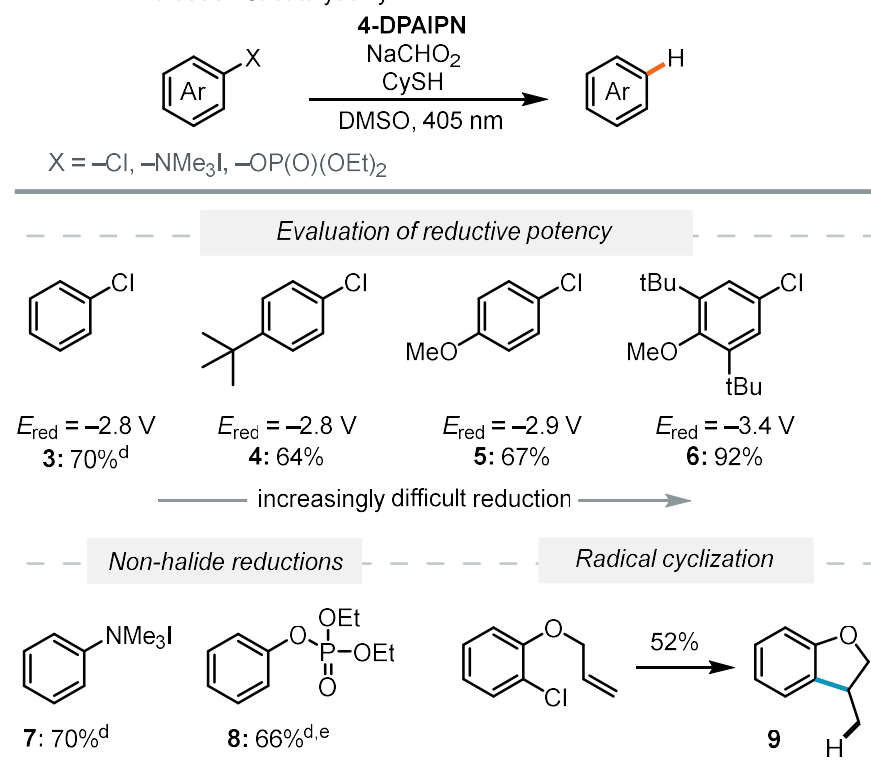
Figure 4.3. Unlocking radical anion photocatalyst reactivity by evaluation of reductant for catalyst activation. Reactions were conducted on 0.1 mmol scale with 10 mol % **4DPAIPN** and 3 equiv NaCHO_2 . All V vs. SCE.

demanding dehalogenation reaction. The isophthalonitrile catalysts, which are both excellent neutral chromophores⁶² as well as electron-primed photoredox catalysts,⁵⁸ promoted the reaction most efficiently albeit still in poor yield. To exclude halogen atom transfer (XAT) aryl radical generation,^{63–65} we examined the reductive defunctionalization of anilinium and aryl phosphate salts (**Table 4.1**). These are each challenging reductive cleavage reactions^{66,67} of nonpolarizable

leaving groups unlikely to undergo XAT processes. We found both substrates underwent productive defunctionalization, albeit in diminished yield (**Figure S13**).

A broader survey of reductants less commonly employed in photoredox catalysis (**Figure S14**) revealed that sodium formate substantially enhanced the photoreductant activity of **4DPAIPN** (**Figure 4.3**). We suspect this improvement occurs because formate salts undergo a second-order hydrogen atom transfer (HAT) process upon oxidation⁶⁸ that results in formic acid and carbon dioxide radical anion.^{69–72} As a consequence, a second reducing equivalent is liberated from formate after initial oxidation. We suspect that the carbon dioxide radical anion can either reduce another equivalent of photocatalyst or promote the reaction by direct reduction of substrate ($E_{1/2}(\text{CO}_2/\text{CO}_2^{\cdot-}) = -2.2 \text{ V vs SCE}$).⁷³ In each mechanistic manifold, the SET is rendered irreversible by the release of CO_2 gas. This scenario contrasts starkly with the trialkylamine

Table 4.1. Evaluation of catalytic system.^{a,b,c}



^aReactions were run on 0.1 mmol scale with 10 mol % **4-DPAIPN**, 3 equiv NaCHO_2 and 5 mol % CySH . ^bAll V vs. SCE. ^cNMR yield. ^dGC yield. ^e15 mol % **4-DPAIPN**.

reductants, which result in oxidizing amine radical cation intermediates ($E_{1/2}(\text{NR}_3^{++}/\text{NR}_3) = <1 \text{ V vs SCE}$) that could deactivate the radical anion photocatalyst via back electron transfer (**Figure 4.4**).^{61,74,75}

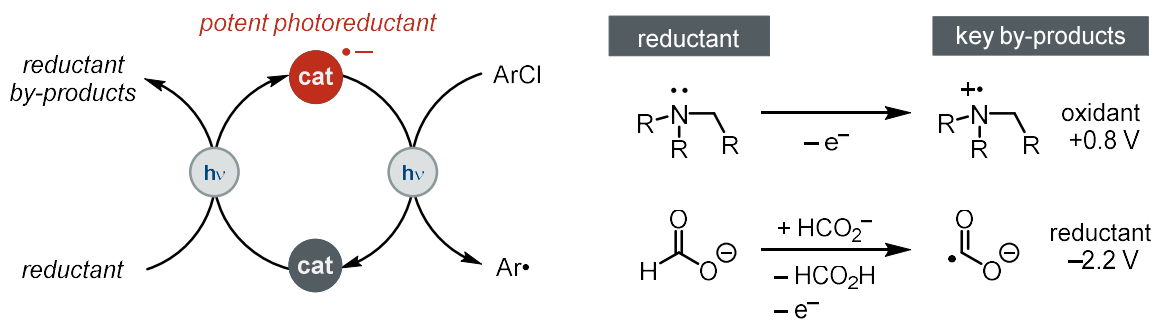


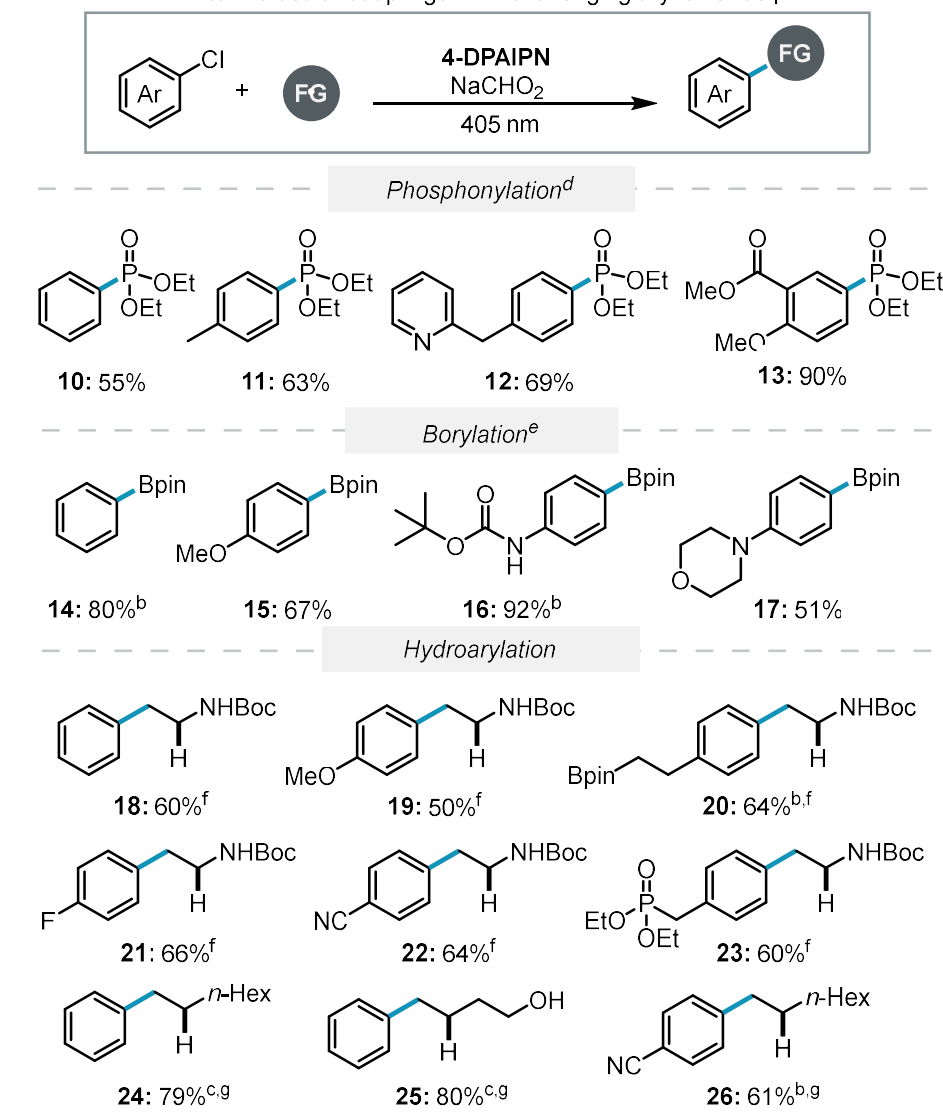
Figure 4.4. Overview of key considerations for chemical reductants as catalyst activators. All V vs. SCE.

We next evaluated the potency of this new catalytic system. Having established that chlorobenzene could be reduced (-2.8 V vs SCE), we probed dehalogenation of increasingly electron rich aryl chlorides. These experiments revealed that substrates with reduction potentials as low as -3.4 V vs SCE are efficiently reduced. Additionally, these conditions promoted the challenging reductive cleavage of both an anilinium and aryl phosphate substrate. Taken together, these data clearly implicate processes beyond a conventional photoredox manifold. For example, the reduction of **6** would be predicted to be endothermic by nearly 2 V ($>40 \text{ kcal/mol}$ at room temperature) based on the most reducing conventional redox couple of **4DPAIPN** ($E_{1/2}(\text{PC}/\text{PC}^{\cdot-}) = -1.5 \text{ V vs SCE}$).⁷⁶ We next attempted to validate the intermediacy of an aryl radical in this formate driven system. As anticipated, these conditions furnished the five-membered ring product **9** in high selectivity for radical cyclization. Despite its exceptionally reducing potentials, we suspected that this operationally simple procedure would be amenable to high-throughput techniques widely employed in medicinal chemistry. To this end, we rapidly evaluated the tolerance of complex drug-like scaffolds using a commercially available informer plate designed to challenge modern cross-coupling technology. We found that not only was photocatalytic activity

retained in the well-plate format but that several of these functional group rich molecules were effectively transformed (**Figure S16**).

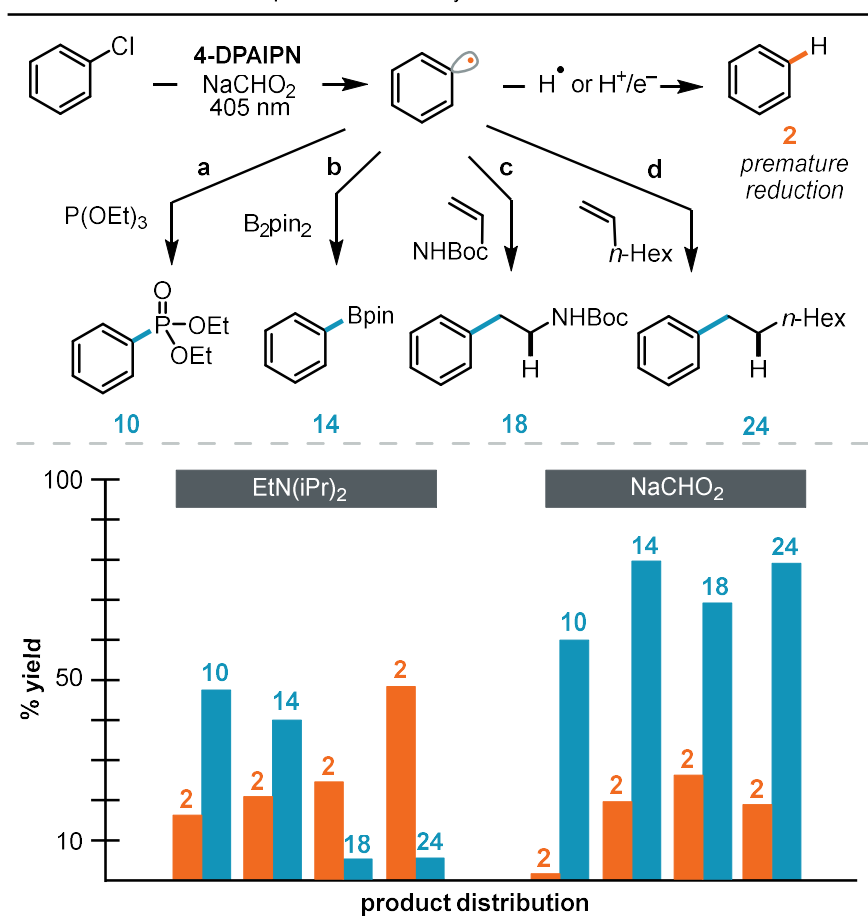
Although, in principle, aryl radicals are highly versatile synthetic intermediates, premature reduction precludes radical coupling reactions in many cases. This is particularly problematic when potent reductants are required. To evaluate selectivity for radical coupling, we targeted redox-neutral photo-Arbuzov and radical borylation processes. These established aryl radical transformations produce biologically relevant aryl phosphonates⁷⁷ and versatile organoboron products.⁷⁸ In both cases, we found that chloroarene substrates readily underwent the desired radical coupling process.⁷⁹ We found that both difficult to reduce electron-rich aryl chlorides and substrates bearing potentially reducible functional groups such as esters and amides were well-tolerated (**Table 4.2**). Furthermore, the catalytic system tolerated medically relevant heterocycles.

Next, we evaluated the reductive hydroarylation of alkenes. This challenging aryl radical reaction requires precise control over the relative rates of radical coupling versus protodehalogenation. HAT is mechanistically required to furnish product and cannot be simply suppressed. Initially, we targeted the synthesis of aryloethylamines via hydroarylation. Recently, Jui and co-workers reported that aryl radical intermediates productively couple with vinyl carbamates to produce the aryloethylamine pharmacophore.⁵⁶ Although one of the most reducing conventional photocatalysts was employed, the majority of the reaction scope was composed of aryl iodide substrates and only aryl chloride substrates bearing withdrawing groups were viable. Intriguingly, we found that although the vinylcarbamate substrate is thermodynamically easier to reduce than most chloroarenes ($E_{\text{red}} = -2.2 \text{ V vs SCE}$), these potent reductive conditions selectively transformed chlorobenzene into N-Boc phenethylamine in high yield. Even as the gap between the chloroarene and vinyl carbamate coupling partner widens, synthetically useful aryloethylamine yields are still observed. Similar to the other radical couplings, we found aryl

Table 4.2. Intermolecular couplings from challenging aryl chloride precursors.^a

^aReactions were run on 0.4 mmol scale. Isolated yield unless otherwise noted. ^bNMR yield. ^cGC yield. ^dReactions were run with **4-DPAIPN** (12–15 mol %), NaCHO₂ (3 equiv), P(OEt)₃ (5 equiv). ^eReactions were run with **4-DPAIPN** (5 mol %), NaCHO₂ (3 equiv), B₂pin₂ (3 equiv) and Cs₂CO₃ (3 equiv). ^fReactions were run with **4-DPAIPN** (6 mol %), NaCHO₂ (3 equiv), N-vinyl carbamate (2.5 equiv) and CySH (5 mol %). ^gReactions were run with **4-DPAIPN** (6 mol %), NaCHO₂ (3 equiv), alkene (5 equiv) and CySH (5 mol %).

chlorides bearing reductively sensitive functional groups were tolerated. We also found these conditions promoted the coupling of aryl chlorides and unactivated alkenes despite the fact that such a hydroarylation remains challenging with any aryl radical precursor.⁸⁰ Finally, we questioned whether formate was uniquely effective for each of these radical coupling reactions or whether alkylamines were suitable terminal reductants (**Table 4.3**). While EtN(*i*-Pr)₂ and

Table 4.3. Reductant Impact on Selectivity^e

Reactions were run on 0.4 mmol scale. Isolated yield. ^aReactions were run with **4-DPAIPN** (12-15 mol %), NaCHO₂ (3 equiv), P(OEt)₃ (5 equiv). ^bReactions were run with **4-DPAIPN** (5 mol %), NaCHO₂ (3 equiv), B₂pin₂ (3 equiv) and Cs₂CO₃ (3 equiv). ^cReactions were run with **4-DPAIPN** (6 mol %), NaCHO₂ (3 equiv), N-vinyl carbamate (2.5 equiv) and CySH (5 mol %). ^dReactions were run with **4-DPAIPN** (6 mol %), NaCHO₂ (3 equiv), alkene (5 equiv) and CySH (5 mol %). ^eReactions were run with conditions a-d, using either EtN(iPr)₂ or NaCHO₂ as the reductant. See the SI for details.

4DPAIPN promote photoreduction of chlorobenzene, both reactivity and radical selectivity were diminished in each coupling reaction. Of note, competitive protodehalogenation nearly precluded net-reductive hydroarylation when alkylamines were used.⁸¹

Having established a generally applicable catalytic system to engage aryl chloride substrates in radical coupling reactions, we next conducted a preliminary mechanistic investigation into the process. First, we probed whether an electron-primed photoredox mechanism—wherein the **4DPAIPN** radical anion is generated and subsequently excited—was

feasible under these conditions. We irradiated a mixture of **4DPAIPN** and sodium formate while monitoring speciation by absorption spectroscopy (**Figure 4.5**). This resulted in a decrease in **4DPAIPN** features and growth of new features consistent with electrochemically reduced **4DPAIPN** (**Figure S20**). Next, we probed the photoreduction of aryl chlorides. Chlorobenzene

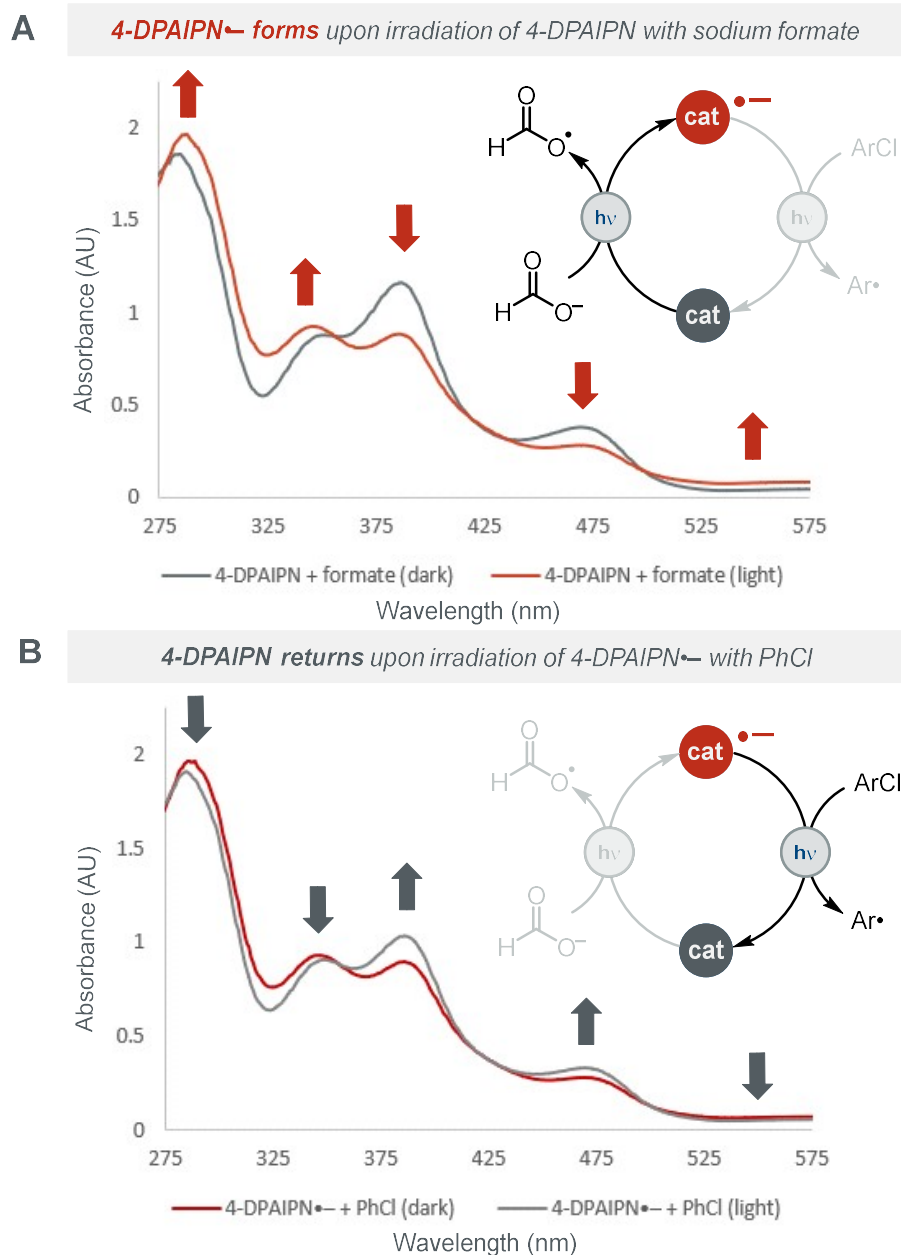


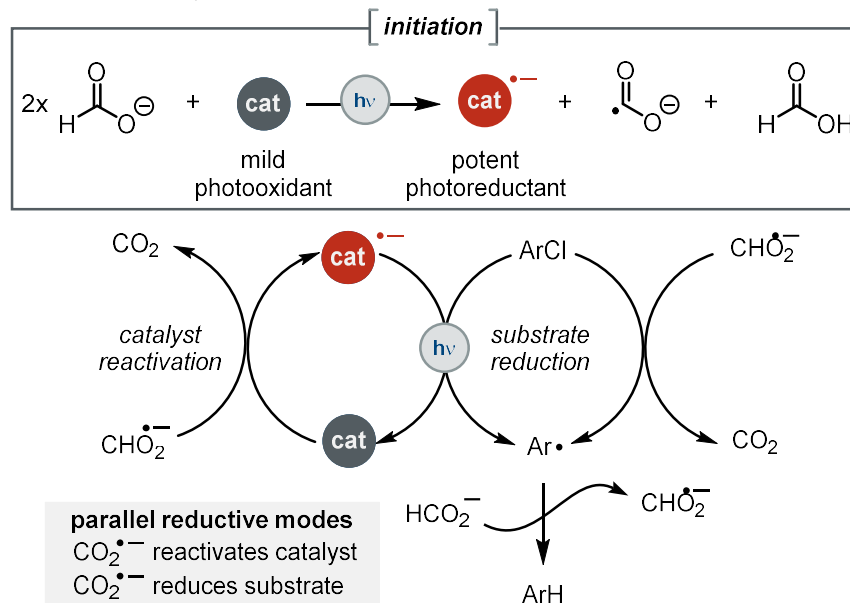
Figure 4.5. (A) UV-vis spectrum demonstrating $4\text{-DPAIPN}^{\bullet-}$ generation in the presence of sodium formate and light. (B) UV-vis spectrum demonstrating that $4\text{-DPAIPN}^{\bullet-}$ reverts to 4-DPAIPN upon exposure to PhCl and subsequent irradiation.

was added to the reaction mixture and, upon irradiation, the absorption features of **4DPAIPN** were restored (**Figure 4.5**). As expected based on the >1 V underpotential, no return of **4DPAIPN** was observed upon addition of chlorobenzene to **4DPAIPN** radical anion in the absence of light. Consistent with this mechanistic picture, Stern–Volmer analysis resulted in no measurable quenching of excited **4DPAIPN** by chlorobenzene. In contrast, formate salts did quench the excited state. Cyclohexanethiol, which was added to the net-reductive transformations as an HAT cocatalyst, also quenches the excited state and likely mediates the electron-transfer events in these systems by an analogous mechanism (**Figure S18**). Taken together, these experiments are consistent with our working hypothesis that photooxidation of formate results in the **4DPAIPN** radical anion, which can be subsequently excited to photoreduce chlorobenzene and return **4DPAIPN**.

While the UV–vis experiments indicate that an electron-primed photoredox mechanism is feasible, we recognized that carbon dioxide radical anion is sufficiently reducing ($E_{\text{red}}(\text{CO}_2/\text{CO}_2^{\cdot-}) = -2.2 \text{ V vs SCE}$)⁷³ to promote reductive fragmentation of some of the aryl chloride substrates studied without the intervention of an electron-primed photoredox manifold. To evaluate the relative contribution of direct substrate reduction by $\text{CO}_2^{\cdot-}$, we attempted to generate this radical anion directly by homolysis of $(\text{PhS})_2$ under 370 nm light in the absence of **4DPAIPN**.⁸² We envisioned thiyl radical could abstract a hydrogen atom from formate to directly generate $\text{CO}_2^{\cdot-}$ in situ (**Figure S23**).^{71,83,84} These conditions resulted in quantitative conversion of 4-chlorobenzonitrile ($E_{\text{red}} = -2.1 \text{ V vs SCE}$). However, only 9% conversion of chlorobenzene ($E_{\text{red}} = -2.8 \text{ V vs SCE}$) and <5% conversion of chloroanisole ($E_{\text{red}} = -2.9 \text{ V vs SCE}$) were observed under these photocatalyst-free conditions. In contrast, all three of these substrates are dehalogenated in comparable efficiency through use of the **4DPAIPN** conditions. We suspect both mechanisms operate in parallel for substrates within the bound of the potency of $\text{CO}_2^{\cdot-}$ (-2.2 V vs SCE) but that an electron-primed photoredox manifold supports more thermodynamically demanding reductions. In both cases, the $\text{CO}_2^{\cdot-}$ reductant byproduct plays an active role either (a) reducing

the substrate directly or (b) reducing the photocatalyst to reactivate it without requiring persistent multiphoton excitation (**Scheme 4.1**).

Scheme 4.1. Plausible mechanism for aryl chloride reduction and the roles of formate and its by-products.



4.4. Conclusions

Overall, we have illustrated that use of a formate-based terminal reductant in combination with an isophthalonitrile photocatalyst can engage aryl chlorides in diverse synthetically useful coupling reactions. We anticipate that these operationally simple reaction conditions comprise a broadly useful approach to photochemically induce difficult reductive processes. Beyond the immediate synthetic utility, these results are important because they challenge the notion that the terminal reductant can be viewed as merely an electron-source to turn over the photocatalyst. These data fit within a growing body of literature that suggests terminal reductant byproducts can play a non-innocent role in photoredox catalysis.^{64,65,74} We suspect that these results could also offer an alternative explanation for recent examples wherein isophthalonitrile catalysts have appeared to reduce substrates beyond their expected redox potentials^{65,85} and, more broadly, illustrate the importance of radical ion intermediates in photoredox catalysis.

4.5. Acknowledgments

We thank Prof. Alison Wendlandt for helpful suggestions. We thank the Stahl, Weix, Yoon, and Schomaker groups for sharing their chemical inventory. We thank Dr. Wesley Swords (Yoon group) for assistance with Stern–Volmer quenching experiments. We thank Sara Alektiar for cyclic voltammetry data. This work was financially supported by the Office of the Vice Chancellor for Research and Graduate Education at the University of Wisconsin–Madison with funding from the Wisconsin Alumni Research Foundation. Acknowledgement is made to the Donors of the American Chemical Society Petroleum Research Fund for partial funding of this research (60677-DNI1). Spectroscopic instrumentation was supported by a generous gift from Paul J. and Margaret M. Bender, NSF (CHE-1048642), and NIH (S10OD012245 and 1S10OD020022-1).

4.6. References

- (1) Ashby, E. C. Single-Electron Transfer, a Major Reaction Pathway in Organic Chemistry. An Answer to Recent Criticisms. *Acc. Chem. Res.* **1988**, *21* (11), 414–421. <https://doi.org/10.1021/ar00155a005>.
- (2) Zhang, N.; Samanta, S. R.; Rosen, B. M.; Percec, V. Single Electron Transfer in Radical Ion and Radical-Mediated Organic, Materials and Polymer Synthesis. *Chem. Rev.* **2014**, *114* (11), 5848–5958. <https://doi.org/10.1021/cr400689s>.
- (3) Broggi, J.; Terme, T.; Vanelle, P. Organic Electron Donors as Powerful Single-Electron Reducing Agents in Organic Synthesis. *Angew. Chem. Int. Ed.* **2014**, *53* (2), 384–413. <https://doi.org/10.1002/anie.201209060>.
- (4) Ebersson, L. Electron-Transfer Reactions in Organic Chemistry. In *Advances in Physical Organic Chemistry*; Gold, V., Bethell, D., Eds.; Academic Press, 1982; Vol. 18, pp 79–185. [https://doi.org/10.1016/S0065-3160\(08\)60139-2](https://doi.org/10.1016/S0065-3160(08)60139-2).
- (5) Prier, C. K.; Rankic, D. A.; MacMillan, D. W. C. Visible Light Photoredox Catalysis with Transition Metal Complexes: Applications in Organic Synthesis. *Chem. Rev.* **2013**, *113* (7), 5322–5363. <https://doi.org/10.1021/cr300503r>.
- (6) Shaw, M. H.; Twilton, J.; MacMillan, D. W. C. Photoredox Catalysis in Organic Chemistry. *J. Org. Chem.* **2016**, *81* (16), 6898–6926. <https://doi.org/10.1021/acs.joc.6b01449>.
- (7) Romero, N. A.; Nicewicz, D. A. Organic Photoredox Catalysis. *Chem. Rev.* **2016**, *116* (17), 10075–10166. <https://doi.org/10.1021/acs.chemrev.6b00057>.
- (8) Narayanam, J. M. R.; Stephenson, C. R. J. Visible Light Photoredox Catalysis: Applications in Organic Synthesis. *Chem. Soc. Rev.* **2010**, *40* (1), 102–113. <https://doi.org/10.1039/B913880N>.
- (9) Skubi, K. L.; Blum, T. R.; Yoon, T. P. Dual Catalysis Strategies in Photochemical Synthesis. *Chem. Rev.* **2016**, *116* (17), 10035–10074. <https://doi.org/10.1021/acs.chemrev.6b00018>.
- (10) Teegardin, K.; Day, J. I.; Chan, J.; Weaver, J. Advances in Photocatalysis: A Microreview of Visible Light Mediated Ruthenium and Iridium Catalyzed Organic

- Transformations. *Org. Process Res. Dev.* **2016**, *20* (7), 1156–1163. <https://doi.org/10.1021/acs.oprd.6b00101>.
- (11) Capaldo, L.; Ravelli, D. The Dark Side of Photocatalysis: One Thousand Ways to Close the Cycle: The Dark Side of Photocatalysis: One Thousand Ways to Close the Cycle. *Eur. J. Org. Chem.* **2020**, *2020* (19), 2783–2806. <https://doi.org/10.1002/ejoc.202000144>.
 - (12) Arias-Rotondo, D. M.; McCusker, J. K. The Photophysics of Photoredox Catalysis: A Roadmap for Catalyst Design. *Chem. Soc. Rev.* **2016**, *45* (21), 5803–5820. <https://doi.org/10.1039/C6CS00526H>.
 - (13) Roth, H.; Romero, N.; Nicewicz, D. Experimental and Calculated Electrochemical Potentials of Common Organic Molecules for Applications to Single-Electron Redox Chemistry. *Synlett* **2015**, *27* (05), 714–723. <https://doi.org/10.1055/s-0035-1561297>.
 - (14) *For a review on multi-photon excitation, which is not limited by the classic photocatalyst selection criteria, see: Glaser, F.; Kerzig, C.; Wenger, O. S. Multi-Photon Excitation in Photoredox Catalysis: Concepts, Applications, Methods. Angew. Chem., Int. Ed.* **2020**, *59* (26), 10266–10284.
 - (15) *For a review on photoelectrochemistry, which is not limited by the classic photocatalyst selection criteria, see: Liu, J.; Lu, L.; Wood, D.; Lin, S. New Redox Strategies in Organic Synthesis by Means of Electrochemistry and Photochemistry. ACS Cent. Sci.* **2020**, *6* (8), 1317–1340.
 - (16) Meerwein, H.; Büchner, E.; Emster, K. van. Über Die Einwirkung Aromatischer Diazoverbindungen Auf α,β -Ungesättigte Carbonylverbindungen. *J. Für Prakt. Chem.* **1939**, *152* (7–10), 237–266. <https://doi.org/10.1002/prac.19391520705>.
 - (17) Hanson, P.; Hammond, R. C.; Goodacre, P. R.; Purcell, J.; Timms, A. W. Sandmeyer Reactions. Part 2. Estimation of Absolute Rate Constants for Some Hydrogen-Transfer Reactions and for the Transfer of Water Ligands on CuII to Aryl Radicals by Use of a Pschorr Radical Clock. *J. Chem. Soc. Perkin Trans. 2* **1994**, No. 4, 691–696. <https://doi.org/10.1039/P29940000691>.
 - (18) Sainsbury, M. Modern Methods of Aryl-Aryl Bond Formation. *Tetrahedron* **1980**, *36* (23), 3327–3359. [https://doi.org/10.1016/0040-4020\(80\)80185-2](https://doi.org/10.1016/0040-4020(80)80185-2).
 - (19) Ghosh, I.; Marzo, L.; Das, A.; Shaikh, R.; König, B. Visible Light Mediated Photoredox Catalytic Arylation Reactions. *Acc. Chem. Res.* **2016**, *49* (8), 1566–1577. <https://doi.org/10.1021/acs.accounts.6b00229>.
 - (20) Wang, C.-S.; Dixneuf, P. H.; Soulé, J.-F. Photoredox Catalysis for Building C–C Bonds from C(Sp²)–H Bonds. *Chem. Rev.* **2018**, *118* (16), 7532–7585. <https://doi.org/10.1021/acs.chemrev.8b00077>.
 - (21) Discekici, E. H.; Treat, N. J.; Poelma, S. O.; Mattson, K. M.; Hudson, Z. M.; Luo, Y.; Hawker, C. J.; Alaniz, J. R. de. A Highly Reducing Metal-Free Photoredox Catalyst: Design and Application in Radical Dehalogenations. *Chem. Commun.* **2015**, *51* (58), 11705–11708. <https://doi.org/10.1039/C5CC04677G>.
 - (22) Devery, J. J.; Nguyen, J. D.; Dai, C.; Stephenson, C. R. J. Light-Mediated Reductive Debromination of Unactivated Alkyl and Aryl Bromides. *ACS Catal.* **2016**, *6* (9), 5962–5967. <https://doi.org/10.1021/acscatal.6b01914>.
 - (23) Boyington, A. J.; Riu, M.-L. Y.; Jui, N. T. Anti-Markovnikov Hydroarylation of Unactivated Olefins via Pyridyl Radical Intermediates. *J. Am. Chem. Soc.* **2017**, *139* (19), 6582–6585. <https://doi.org/10.1021/jacs.7b03262>.
 - (24) Cheng, Y.; Gu, X.; Li, P. Visible-Light Photoredox in Homolytic Aromatic Substitution: Direct Arylation of Arenes with Aryl Halides. *Org. Lett.* **2013**, *15* (11), 2664–2667. <https://doi.org/10.1021/ol400946k>.
 - (25) Shirakawa, E.; Hayashi, T. Transition-Metal-Free Coupling Reactions of Aryl Halides. *Chem. Lett.* **2012**, *41* (2), 130–134. <https://doi.org/10.1246/cl.2012.130>.

- (26) Galli, C. Radical Reactions of Arenediazonium Ions: An Easy Entry into the Chemistry of the Aryl Radical. *Chem. Rev.* **1988**, *88* (5), 765–792. <https://doi.org/10.1021/cr00087a004>.
- (27) Kvasovs, N.; Gevorgyan, V. Contemporary Methods for Generation of Aryl Radicals. *Chem. Soc. Rev.* **2021**, *50* (4), 2244–2259. <https://doi.org/10.1039/D0CS00589D>.
- (28) Heinrich, M. R. Intermolecular Olefin Functionalisation Involving Aryl Radicals Generated from Arenediazonium Salts. *Chem. – Eur. J.* **2009**, *15* (4), 820–833. <https://doi.org/10.1002/chem.200801306>.
- (29) Raviola, C.; Protti, S. Leaving Groups in Metal-Free Arylations: Make Your Choice! *Eur. J. Org. Chem.* **2020**, *2020* (33), 5292–5304. <https://doi.org/10.1002/ejoc.202000143>.
- (30) Weix and co-workers conducted an analysis of the commercially available aryl halides and found that aryl chlorides comprise more than two-thirds of the commercial substrates, see: Huang, L.; Ackerman, L. K. G.; Kang, K.; Parsons, A. M.; Weix, D. J. LiCl-Accelerated Multimetallic Cross-Coupling of Aryl Chlorides with Aryl Triflates. *J. Am. Chem. Soc.* **2019**, *141* (28), 10978–10983.
- (31) Electron-deficient aryl chlorides are viable substrates for the most reducing visible light photocatalysts. For examples, see refs 32–35.
- (32) Glaser, F.; Larsen, C. B.; Kerzig, C.; Wenger, O. S. Aryl Dechlorination and Defluorination with an Organic Super-Photoreductant. *Photochem. Photobiol. Sci.* **2020**, *19* (8), 1035–1041. <https://doi.org/10.1039/D0PP00127A>.
- (33) Shon, J.-H.; Kim, D.; Rathnayake, M. D.; Sittel, S.; Weaver, J.; Teets, T. S. Photoredox Catalysis on Unactivated Substrates with Strongly Reducing Iridium Photosensitizers. *Chem. Sci.* **2021**, *12* (11), 4069–4078. <https://doi.org/10.1039/D0SC06306A>.
- (34) Schmalzbauer, M.; Ghosh, I.; König, B. Utilising Excited State Organic Anions for Photoredox Catalysis: Activation of (Hetero)Aryl Chlorides by Visible Light-Absorbing 9-Anthrolate Anions. *Faraday Discuss.* **2019**, *215* (0), 364–378. <https://doi.org/10.1039/C8FD00176F>.
- (35) Ghosh, I.; Shaikh, R. S.; König, B. Sensitization-Initiated Electron Transfer for Photoredox Catalysis. *Angew. Chem. Int. Ed.* **2017**, *56* (29), 8544–8549. <https://doi.org/10.1002/anie.201703004>.
- (36) Blanksby, S. J.; Ellison, G. B. Bond Dissociation Energies of Organic Molecules. *Acc. Chem. Res.* **2003**, *36* (4), 255–263. <https://doi.org/10.1021/ar020230d>.
- (37) Costentin, C.; Robert, M.; Savéant, J.-M. Fragmentation of Aryl Halide π Anion Radicals. Bending of the Cleaving Bond and Activation vs Driving Force Relationships. *J. Am. Chem. Soc.* **2004**, *126* (49), 16051–16057. <https://doi.org/10.1021/ja045989u>.
- (38) Ghosh, I.; Ghosh, T.; Bardagi, J. I.; König, B. Reduction of Aryl Halides by Consecutive Visible Light-Induced Electron Transfer Processes. *Science* **2014**, *346* (6210), 725–728. <https://doi.org/10.1126/science.1258232>.
- (39) For later work introducing a second catalyst structure for conPET, see: Neumeier, M.; Sampedro, D.; Májek, M.; de la Peña O'Shea, V. A.; Jacobi von Wangelin, A.; Pérez-Ruiz, R. Dichromatic Photocatalytic Substitutions of Aryl Halides with a Small Organic Dye. *Chem. – Eur. J.* **2018**, *24* (1), 105–108.
- (40) MacKenzie, I. A.; Wang, L.; Onuska, N. P. R.; Williams, O. F.; Begam, K.; Moran, A. M.; Dunietz, B. D.; Nicewicz, D. A. Discovery and Characterization of an Acridine Radical Photoreductant. *Nature* **2020**, *580* (7801), 76–80. <https://doi.org/10.1038/s41586-020-2131-1>.
- (41) Cole, J. P.; Chen, D.-F.; Kudisch, M.; Pearson, R. M.; Lim, C.-H.; Miyake, G. M. Organocatalyzed Birch Reduction Driven by Visible Light. *J. Am. Chem. Soc.* **2020**, *142* (31), 13573–13581. <https://doi.org/10.1021/jacs.0c05899>.
- (42) Wang, S.; Wang, H.; König, B. Photo-Induced Thiolate Catalytic Activation of Inert Caryl-Hetero Bonds for Radical Borylation. *Chem* **2021**. <https://doi.org/10.1016/j.chempr.2021.04.016>.

- (43) Jin, S.; Dang, Hang. T.; Haug, G. C.; He, R.; Nguyen, V. D.; Nguyen, V. T.; Arman, H. D.; Schanze, K. S.; Larionov, O. V. Visible Light-Induced Borylation of C–O, C–N, and C–X Bonds. *J. Am. Chem. Soc.* **2020**, *142* (3), 1603–1613. <https://doi.org/10.1021/jacs.9b12519>.
- (44) Zhang, L.; Jiao, L. Visible-Light-Induced Organocatalytic Borylation of Aryl Chlorides. *J. Am. Chem. Soc.* **2019**, *141* (23), 9124–9128. <https://doi.org/10.1021/jacs.9b00917>.
- (45) Cybularczyk-Cecotka, M.; Szczepanik, J.; Giedyk, M. Photocatalytic Strategies for the Activation of Organic Chlorides. *Nat. Catal.* **2020**, *3* (11), 872–886. <https://doi.org/10.1038/s41929-020-00515-8>.
- (46) Barham, J. P.; König, B. Synthetic Photoelectrochemistry. *Angew. Chem. Int. Ed.* **2020**, *59* (29), 11732–11747. <https://doi.org/10.1002/anie.201913767>.
- (47) Novaes, L. F. T.; Liu, J.; Shen, Y.; Lu, L.; Meinhardt, J. M.; Lin, S. Electrocatalysis as an Enabling Technology for Organic Synthesis. *Chem. Soc. Rev.* **2021**. <https://doi.org/10.1039/D1CS00223F>.
- (48) Capaldo, L.; Quadri, L. L.; Ravelli, D. Merging Photocatalysis with Electrochemistry: The Dawn of a New Alliance in Organic Synthesis. *Angew. Chem. Int. Ed.* **2019**, *58* (49), 17508–17510. <https://doi.org/10.1002/anie.201910348>.
- (49) Yu, Y.; Guo, P.; Zhong, J.-S.; Yuan, Y.; Ye, K.-Y. Merging Photochemistry with Electrochemistry in Organic Synthesis. *Org. Chem. Front.* **2019**, *7* (1), 131–135. <https://doi.org/10.1039/C9QO01193E>.
- (50) Cowper, N. G. W.; Chernowsky, C. P.; Williams, O. P.; Wickens, Z. K. Potent Reductants via Electron-Primed Photoredox Catalysis: Unlocking Aryl Chlorides for Radical Coupling. *J. Am. Chem. Soc.* **2020**, *142* (5), 2093–2099. <https://doi.org/10.1021/jacs.9b12328>.
- (51) Kim, H.; Kim, H.; Lambert, T. H.; Lin, S. Reductive Electrophotocatalysis: Merging Electricity and Light To Achieve Extreme Reduction Potentials. *J. Am. Chem. Soc.* **2020**, *142* (5), 2087–2092. <https://doi.org/10.1021/jacs.9b10678>.
- (52) *For example, high-throughput experimentation (HTE) remains particularly difficult for electrochemical processes but is well established for photochemical systems. Recent work from Lin has advanced an attractive HTE plate for electrophotocatalysis in undivided cells. However, divided cells are required for all reductive electrophotocatalysis reported to-date, which would not be compatible with this technology; see ref 53.*
- (53) Rein, J.; Annand, J. R.; Wismer, M. K.; Fu, J.; Siu, J. C.; Klapars, A.; Strotman, N. A.; Kalyani, D.; Lehnher, D.; Lin, S. Unlocking the Potential of High-Throughput Experimentation for Electrochemistry with a Standardized Microscale Reactor. *ACS Cent. Sci.* **2021**, *7* (8), 1347–1355. <https://doi.org/10.1021/acscentsci.1c00328>.
- (54) *Aryl chlorides with electron-withdrawing groups are in these bounds and are viable substrates for the most reducing photoredox catalysts, albeit often in diminished yield. For selected examples, see refs 55 and 56.*
- (55) Li, H.; Liu, Y.; Chiba, S. Anti-Markovnikov Hydroarylation of Alkenes via Polysulfide Anion Photocatalysis. *Chem. Commun.* **2021**. <https://doi.org/10.1039/D1CC02185K>.
- (56) Boyington, A. J.; Seath, C. P.; Zearfoss, A. M.; Xu, Z.; Jui, N. T. Catalytic Strategy for Regioselective Arylethylamine Synthesis. *J. Am. Chem. Soc.* **2019**, *141* (9), 4147–4153. <https://doi.org/10.1021/jacs.9b01077>.
- (57) Andrieux, C. P.; Pinson, J. The Standard Redox Potential of the Phenyl Radical/Anion Couple. *J. Am. Chem. Soc.* **2003**, *125* (48), 14801–14806. <https://doi.org/10.1021/ja0374574>.
- (58) Chernowsky, C. P.; Chmiel, A. F.; Wickens, Z. K. Electrochemical Activation of Diverse Conventional Photoredox Catalysts Induces Potent Photoreductant Activity**. *Angew. Chem. Int. Ed.* **2021**, *60* (39), 21418–21425. <https://doi.org/10.1002/anie.202107169>.

- (59) Targos, K.; Williams, O. P.; Wickens, Z. K. Unveiling Potent Photooxidation Behavior of Catalytic Photoreductants. *J. Am. Chem. Soc.* **2021**, *143* (11), 4125–4132. <https://doi.org/10.1021/jacs.1c00399>.
- (60) Connell, T. U.; Fraser, C. L.; Czyz, M. L.; Smith, Z. M.; Hayne, D. J.; Doeven, E. H.; Agugiaro, J.; Wilson, D. J. D.; Adcock, J. L.; Scully, A. D.; Gómez, D. E.; Barnett, N. W.; Polyzos, A.; Francis, P. S. The Tandem Photoredox Catalysis Mechanism of [Ir(Ppy)₂(Dtb-Bpy)]⁺ Enabling Access to Energy Demanding Organic Substrates. *J. Am. Chem. Soc.* **2019**, *141* (44), 17646–17658. <https://doi.org/10.1021/jacs.9b07370>.
- (61) Hu, J.; Wang, J.; Nguyen, T. H.; Zheng, N. The Chemistry of Amine Radical Cations Produced by Visible Light Photoredox Catalysis. *Beilstein J. Org. Chem.* **2013**, *9* (1), 1977–2001. <https://doi.org/10.3762/bjoc.9.234>.
- (62) Speckmeier, E.; Fischer, T. G.; Zeitler, K. A Toolbox Approach To Construct Broadly Applicable Metal-Free Catalysts for Photoredox Chemistry: Deliberate Tuning of Redox Potentials and Importance of Halogens in Donor–Acceptor Cyanoarenes. *J. Am. Chem. Soc.* **2018**, *140* (45), 15353–15365. <https://doi.org/10.1021/jacs.8b08933>.
- (63) *Recent reports from Leonori and co-workers have illustrated that α -amino radicals formed in situ from alkylamine oxidation promote aryl radical reactions from aryl iodides and bromides via halogen atom transfer (XAT). However, the stronger and less polarizable C(sp²)–Cl bonds are expected to be less amenable to such a mechanism; see refs 64 and 65.*
- (64) Constantin, T.; Zanini, M.; Regni, A.; Sheikh, N. S.; Juliá, F.; Leonori, D. Aminoalkyl Radicals as Halogen-Atom Transfer Agents for Activation of Alkyl and Aryl Halides. *Science* **2020**, *367* (6481), 1021–1026. <https://doi.org/10.1126/science.aba2419>.
- (65) Constantin, T.; Juliá, F.; Sheikh, N. S.; Leonori, D. A Case of Chain Propagation: α -Aminoalkyl Radicals as Initiators for Aryl Radical Chemistry. *Chem. Sci.* **2020**, *11* (47), 12822–12828. <https://doi.org/10.1039/D0SC04387G>.
- (66) Azzena, U.; Denurra, T.; Melloni, G.; Fenude, E.; Rassu, G. Electron-Transfer-Induced Reductive Demethoxylation of Anisole: Evidence for Cleavage of a Radical Anion. *J. Org. Chem.* **1992**, *57* (5), 1444–1448. <https://doi.org/10.1021/jo00031a022>.
- (67) Xu, H.; Yu, B.; Zhang, H.; Zhao, Y.; Yang, Z.; Xu, J.; Han, B.; Liu, Z. Reductive Cleavage of Inert Aryl C–O Bonds to Produce Arenes. *Chem. Commun.* **2015**, *51* (61), 12212–12215. <https://doi.org/10.1039/C5CC03563E>.
- (68) *The oxidation potential of formate, +1.25 V vs SCE, is within the bounds of the excited state reduction potential of each catalyst. For the CV of formate, see SI.*
- (69) Gu, X.; Lu, S.; Fu, X.; Qiu, Z.; Sui, Q.; Guo, X. Carbon Dioxide Radical Anion-Based UV/S2O8²⁻/HCOOH Reductive Process for Carbon Tetrachloride Degradation in Aqueous Solution. *Sep. Purif. Technol.* **2017**, *172*, 211–216. <https://doi.org/10.1016/j.seppur.2016.08.019>.
- (70) Jacobsen, E.; Roberts, J. L.; Sawyer, D. T. Electrochemical Oxidation of Formate in Dimethylsulfoxide at Gold and Platinum Electrodes. *J. Electroanal. Chem. Interfacial Electrochem.* **1968**, *16* (3), 351–360. [https://doi.org/10.1016/S0022-0728\(68\)80083-X](https://doi.org/10.1016/S0022-0728(68)80083-X).
- (71) Grills, D. C.; Lyman, S. V. Radiolytic Formation of the Carbon Dioxide Radical Anion in Acetonitrile Revealed by Transient IR Spectroscopy. *Phys. Chem. Chem. Phys.* **2018**, *20* (15), 10011–10017. <https://doi.org/10.1039/C8CP00977E>.
- (72) Rosso, J. A.; Bertolotti, S. G.; Braun, A. M.; Mártire, D. O.; Gonzalez, M. C. Reactions of Carbon Dioxide Radical Anion with Substituted Benzenes. *J. Phys. Org. Chem.* **2001**, *14* (5), 300–309. <https://doi.org/10.1002/poc.365>.
- (73) Koppenol, W. H.; Rush, J. D. Reduction Potential of the Carbon Dioxide/Carbon Dioxide Radical Anion: A Comparison with Other C1 Radicals. *J. Phys. Chem.* **1987**, *91* (16), 4429–4430. <https://doi.org/10.1021/j100300a045>.

- (74) Sevrin, M. J.; Furst, L.; Nguyen, J. D.; Collins, J. L.; Stephenson, C. R. J. Lithium Bis-Catechol Borate as an Effective Reductive Quencher in Photoredox Catalysis. *Tetrahedron* **2018**, 74 (26), 3246–3252. <https://doi.org/10.1016/j.tet.2018.04.053>.
- (75) Beatty, J. W.; Stephenson, C. R. J. Amine Functionalization via Oxidative Photoredox Catalysis: Methodology Development and Complex Molecule Synthesis. *Acc. Chem. Res.* **2015**, 48 (5), 1474–1484. <https://doi.org/10.1021/acs.accounts.5b00068>.
- (76) Singh, P. P.; Srivastava, V. Recent Advances in Using 4DPAIPN in Photocatalytic Transformations. **2021**, 9.
- (77) Németh, G.; Greff, Z.; Sipos, A.; Varga, Z.; Székely, R.; Sebestyén, M.; Jászay, Z.; Béni, S.; Nemes, Z.; Pirat, J.-L.; Volle, J.-N.; Virieux, D.; Gyuris, Á.; Kelemenics, K.; Áy, É.; Minarovits, J.; Szathmary, S.; Kéri, G.; Örfi, L. Synthesis and Evaluation of Phosphorus Containing, Specific CDK9/CycT1 Inhibitors. *J. Med. Chem.* **2014**, 57 (10), 3939–3965. <https://doi.org/10.1021/jm401742r>.
- (78) Fyfe, J. W. B.; Watson, A. J. B. Recent Developments in Organoboron Chemistry: Old Dogs, New Tricks. *Chem* **2017**, 3 (1), 31–55. <https://doi.org/10.1016/j.chempr.2017.05.008>.
- (79) *We found for most of the reactions studied herein that the photocatalyst bleached over the course of the reaction and that adding photocatalyst in two batches provided improved yields; see SI for details. At this stage, a photocatalytically active decomposition product, either closed or open shell, cannot be excluded as a possibility. For an example of isophthalonitrile catalysts being attacked by radical intermediates, see: Grotjahn, S.; König, B. Org. Lett. 2021, 23, 3146–3150.*
- (80) *For an example of unactivated alkene hydroarylation, see ref 55.*
- (81) *While both alkylamine and formate reductants can act as hydrogen atom sources, we noted that sodium formate exhibits limited solubility under the reaction conditions. We suspect that the limited concentration of the reductant diminishes premature HAT to the aryl radical relative to homogeneous alkylamine reductants.*
- (82) Ito, O. Flash Photolysis Study on Reversible Addition Reactions of Thiyl Radicals. *Res. Chem. Intermed.* **1995**, 21 (1), 69–93. <https://doi.org/10.1163/156856795X00080>.
- (83) *For a proposed mechanism for CO₂ •– generation from PhSSPh, see SI. PhSSPh was used as the thiyl radical source to initiate the slightly endothermic HAT (BDE PhSH = 79 kcal/mol, BDE HCO₂– = 86 kcal/mol); see ref 84.*
- (84) Dénès, F.; Pichowicz, M.; Povie, G.; Renaud, P. Thiyl Radicals in Organic Synthesis. *Chem. Rev.* **2014**, 114 (5), 2587–2693. <https://doi.org/10.1021/cr400441m>.
- (85) McDaniel, K. A.; Blood, A. R.; Smith, G. C.; Jui, N. T. Dearomatization of Unactivated Arenes via Catalytic Hydroalkylation. *ACS Catal.* **2021**, 11 (9), 4968–4972. <https://doi.org/10.1021/acscatal.1c00732>.

4.7. Supplemental Information

4.7.1 General Methods and Materials

Unless otherwise noted, reactions were performed under an inert N₂ atmosphere in anhydrous DMSO thoroughly degassed by freeze-pump-thaw. Anhydrous DMSO was purchased from DriSolv. Crude mixtures were evaluated by thin-layer chromatography using EMD/Merck silica gel 60 F254 pre-coated plates (0.25 mm) and were visualized by UV, CAM, p- anisaldehyde, or KMnO₄ staining. Flash chromatography was performed with a Biotage Isolera One automated chromatography system with re-packed silica columns (technical grade silica, pore size 60 Å, 230-400 mesh particle size, 40-63 particle size). Purified materials were dried in vacuo (0.050 Torr) to remove trace solvent. ¹H, ¹³C, ³¹P Spectra were taken using a Bruker Avance-400 with a BBFO Probe or a Bruker Avance-500 with a DCH Cryoprobe. NMR data are reported relative to residual CHCl₃ (¹H, δ = 7.26 ppm), CDCl₃ (¹³C, δ = 77.16 ppm). Data for ¹H NMR spectra are reported as follows: chemical shift (δ ppm) (multiplicity, coupling constant (Hz), integration). Multiplicity and qualifier abbreviations are as follows: s = singlet, d = doublet, t = triplet, q = quartet, m = multiplet, br = broad. GC traces were taken on an Agilent 7890A GC with dual DB-5 columns (20 m \times 180 μ m \times 0.18 μ m), dual FID detectors, and hydrogen as the carrier gas.

4.7.2 Experimental Set-Up

LEDs used in this study were purchased from HepatoChem (PAR20- 18W LG 405 nm) and Kessil (KSPR160L-390, KSPR160L-440, KSPR160L-370).

Standard Reaction Set-Up

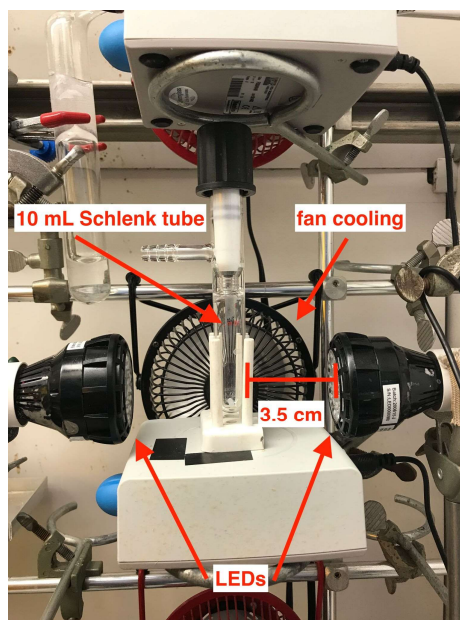
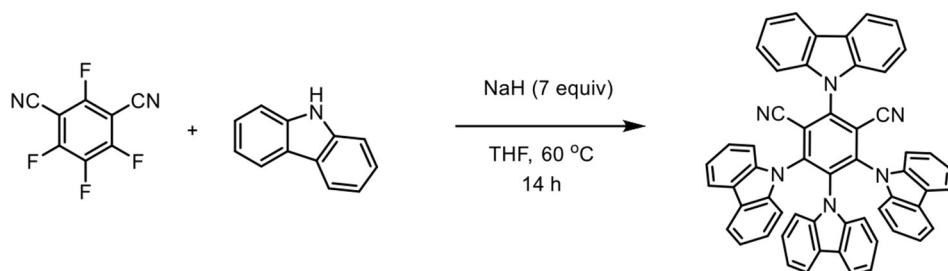


Figure S1. Standard setup for photoredox reactions with either 1 or 2 LEDs depending on the transformation. See **General Experimental Procedures for Photoredox Reductions** for details.

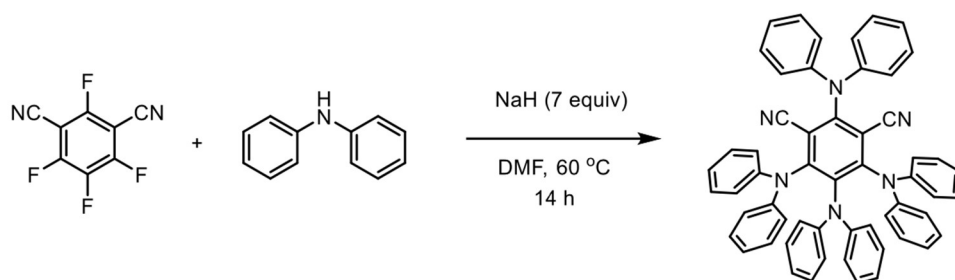
4.7.3 Preparation of Catalysts and Starting Materials

2,4,5,6-tetra(9H-carbazol-9-yl)isophthalonitrile (**4-CzIPN**)



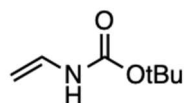
To a flame-dried flask under N₂, NaH (60% dispersion, 3.0 g, 75 mmol, 7 equiv) was added and evacuated then backfilled with N₂ three times. THF (100 mL) was added to the flask followed by 1-H-carbazole (8.4 g, 50 mmol, 5 equiv) in THF (25 mL). The carbazole solution was slowly added to the flask then heated to 60 °C and stirred for 1 hour. 2,4,5,6-tetrafluoroisophthalonitrile (2.0 g, 10 mmol, 1 equiv) in THF (25 mL) was slowly added to the reaction mixture. The solution was then cooled and stirred at 40 °C overnight. After cooling the reaction to room temperature, excess NaH was quenched with isopropanol. Water (200 mL) was then added to precipitate the crude product. The precipitate was filtered then washed with excess water and dried *in vacuo*. The crude product dissolved in DCM then filtered through a silica plug and recrystallized from DCM hexanes to provide pure product as a yellow solid (6.2 g, 8.2 mmol, 82 %). **¹H NMR** (500 MHz, CDCl₃) δ 8.24 (d, J = 7.8 Hz, 2H), 7.73 (m, 8H), 7.51 (ddd, J = 8.0, 6.7, 1.5 Hz, 2H), 7.35 (m, 2H), 7.25 (dd, J = 7.8, 1.4 Hz, 4H), 7.11 (tt, J = 7.4, 5.8 Hz, 8H), 6.85 (m, 4H), 6.65 (td, J = 7.7, 1.2 Hz, 2H), consistent with reported spectrum (Chem. Eur. J. 2016, 22, 4889-4898).

2,4,5,6-tetrakis(diphenylamino)isophthalonitrile (**4-DPAIPN**)

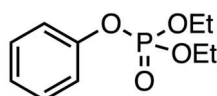


To a flame-dried flask under N₂, NaH (60% dispersion, 3.0 g, 75 mmol, 7 equiv) was added and evacuated then backfilled with N₂ three times. THF (100 mL) was added to the flask followed by diphenylamine (8.5 g, 50 mmol, 5 equiv) in THF (25 mL). The diphenylamine solution was slowly added to the flask then heated to 60 °C and stirred for 1 hour. 2,4,5,6-tetrafluoroisophthalonitrile (2.0 g, 10 mmol, 1 equiv) in THF (25 mL) was slowly added to the reaction mixture. The solution was then cooled and stirred at 40 °C overnight. After cooling the reaction to room temperature, excess NaH was quenched with isopropanol. Water (200 mL) was then added to precipitate the crude product. The precipitate was filtered then washed with excess water and dried *in vacuo*. The crude product dissolved in DCM then filtered through a silica plug and recrystallized from DCM hexanes to provide pure product as a yellow solid (5.0 g, 6.2 mmol, 62%). **¹H NMR** (400 MHz, CDCl₃) δ 7.31 – 7.23 (m, 4H), 7.14 – 6.97 (m, 14H), 6.95 – 6.83 (m, 8H), 6.73 – 6.65 (m,

10H), 6.59 – 6.51 (m, 4H), consistent with reported spectrum (Angew. Chem. Int. Ed. 2019, 131, 8266-8270).



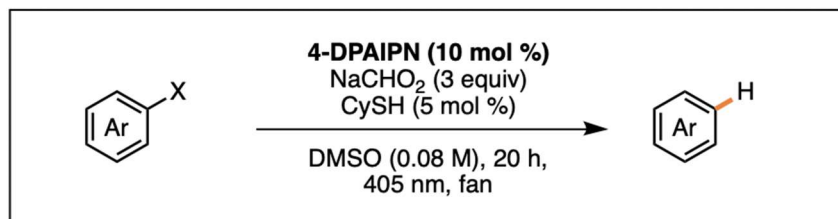
tert-butyl vinyl carbamate: Compound was synthesized according to a previous report (*J. Am. Chem. Soc.* 2019, 141, 9, 4147–4153) and 70% yield was obtained as a white crystalline solid. **¹H NMR** (400 MHz, CDCl₃) δ 6.66 (s, 1H), 6.28 (s, 1H), 4.40 (d, J = 15.7 Hz, 1H), 4.21 (d, J = 8.8 Hz, 1H), 1.47 (s, 9H).



diethyl phenyl phosphate: Compound was synthesized according to a previous report (Chernowsky, Colleen; Chmiel, Alyah; Wickens, Zachary (2021): Photocatalytic Activity of Diverse Organic Radical Anions: Catalyst Discovery Enables Cleavage of Strong C(sp²)–N and C(sp²)–O Bonds. ChemRxiv. Preprint. <https://doi.org/10.26434/chemrxiv.14710398.v1>) and 68% yield was obtained as a colorless oil. **¹H NMR** (400 MHz, CDCl₃) δ 7.33 (dd, J = 8.6, 7.2 Hz, 2H), 7.24 – 7.19 (m, 2H), 7.16 (t, J = 7.2 Hz, 1H), 4.29 – 4.14 (m, 4H), 1.34 (td, J = 7.1, 1.1 Hz, 6H).

4.7.4 General Experimental Procedures for Photoredox Reductions

General Procedure A — Dehalogenation

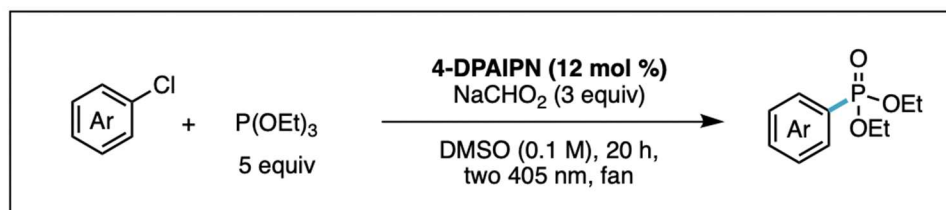


To an oven-dried 10 mL schlenk tube equipped with a stir bar, 4-DPAIPN (0.01 mmol, 10 mol %) and sodium formate (0.3 mmol, 3 equiv) were added. The tube was evacuated and backfilled with N₂ three times. While under active N₂, cyclohexylthiol (0.005 mmol, 5 mol %) and chlorobenzene (0.1 mmol, 1 equiv) were added to the schlenk tube followed by DMSO (1.25 mL, 0.08 M). The schlenk tube was sealed under N₂ then stirred and irradiated with a 405 nm LED (3.5 cm from glass surface with fan cooling for 20 hours).

For GC analyses: After reaction completion, mesitylene (14 μ L, 0.1 mmol, 1 equiv) was added as the internal standard to the crude mixture. 0.1 mL aliquot was removed from the crude and quenched with 1 mL water then extracted with 1 mL diethyl ether. Diethyl ether layer was filtered through a silica pipette plug then ran on the GC.

For NMR analyses: Added CH₂Br₂ as the internal standard (7 μ L, 0.1 mmol, 1 equiv) to crude reaction mixture. Took 0.1 mL aliquot and quenched with 1 mL water then extracted with 1 mL CDCl₃. Reactions were analyzed via ¹H NMR of the CDCl₃ layer.

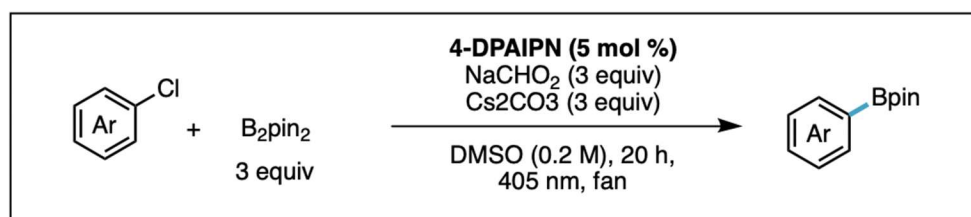
General Procedure B — Phosphonylation



To an oven-dried 10 mL schlenk tube equipped with a stir bar, 4-DPAIPN (0.048 mmol, 12 mol %) and sodium formate (1.2 mmol, 3 equiv) were added. Aryl chloride (0.4 mmol, 1 equiv) and triethyl phosphite (2.0 mmol, 5 equiv) were added to the schlenk tube followed by DMSO (4 mL, 0.1 M). The reaction mixture was freeze-pump-thawed then sealed under N_2 and stirred and irradiated with two 405 nm LEDs (4.5 cm from glass surface on each side of the tube with fan cooling) for 20 hours. After reaction completion, the reaction was quenched with 50 mL NaHCO_3 (aq) and extracted with 30 mL EtOAc three times. The combined EtOAc layer was washed with 50 mL brine then dried over Na_2SO_4 . The mixture was filtered and concentrated in vacuo then purified by flash chromatography with silica.

For NMR analyses: After reaction completion, CH_2Br_2 was added as the internal standard to crude reaction mixture. 0.1 mL aliquot was removed and quenched with 1 mL water then extracted with 1 mL CDCl_3 . Reactions were analyzed via ^1H NMR of the CDCl_3 layer.

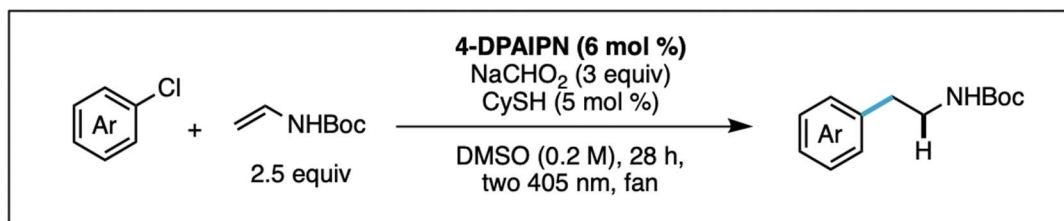
General Procedure C — Borylation



To an oven-dried 10 mL schlenk tube equipped with stir bar, 4-DPAIPN (0.01 mmol, 2.5 mol %), sodium formate (1.2 mmol, 3 equiv), B_2pin_2 (1.2 mmol, 3 equiv), and Cs_2CO_3 (1.2 mmol, 3 equiv) were added. The tube was evacuated and backfilled with N_2 three times. While under active N_2 , aryl chloride (0.4 mmol, 1 equiv) was added to the schlenk tube followed by DMSO (2 mL, 0.2 M). The schlenk tube was sealed under N_2 . Stirred and irradiated with two 405 nm LEDs (4.5 cm from glass surface on each side of the tube with fan cooling) for 20 hours total. At the 6 hour mark, an additional 2.5 mol % 4-DPAIPN was added as a stock solution (2.5 mol % 4-DPAIPN dissolved in 400 μL DMSO — then to the reaction vessel, evacuated and backfilled with N_2 on the side arm then while under active N_2 , added the stock solution). The tube was resealed under N_2 and stirred while irradiating for the remaining 14 hours. After reaction completion, the reaction was quenched with 50 mL NaHCO_3 (aq) and extracted with 30 mL EtOAc three times. The combined EtOAc layer was washed with 50 mL brine then dried over Na_2SO_4 . The mixture was filtered and concentrated in vacuo then purified by flash chromatography with silica.

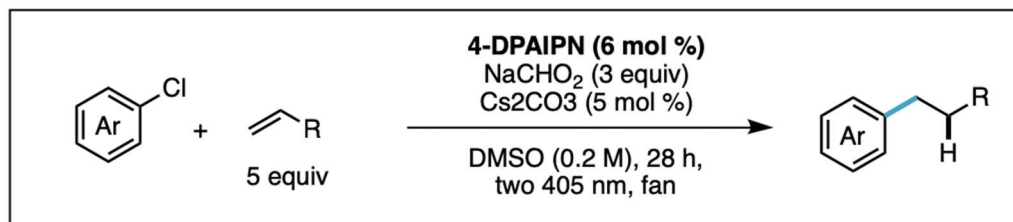
For NMR analyses: After reaction completion, CH_2Br_2 was added as the internal standard to crude reaction mixture. Took 0.1 mL aliquot and quenched with 1 mL water then extracted with 1 mL CDCl_3 . Reactions were analyzed via ^1H NMR of the CDCl_3 layer.

General Procedure D — Hydroarylation of Vinyl Carbamate



To an oven-dried 10 mL schlenk tube equipped with a stir bar, 4-DPAIPN (0.012 mmol, 3 mol %), sodium formate (1.2 mmol, 3 equiv), and vinyl carbamate (1.0 mmol, 2.5 equiv) were added. The tube was evacuated and backfilled with N₂ three times. While under active N₂, added cyclohexylthiol (0.02 mmol, 5 mol %) and aryl chloride (0.4 mmol, 1 equiv) to vial then DMSO (2 mL, 0.2 M). The tube was sealed under N₂ then stirred and irradiated with two 405 nm lamps (4.5 cm from glass surface on each side with fan cooling) for 28 hours total. At the 6 hour mark, an additional 3 mol % 4-DPAIPN was added as a stock solution (3 mol % 4-DPAIPN dissolved in 400 uL DMSO — then to the reaction vessel, evacuated and backfilled with N₂ on the side arm then while under active N₂, added the stock solution). The tube was resealed under N₂ and stirred while irradiating for the remaining 22 hours. After reaction completion, the reaction was quenched with 50 mL NaHCO₃ (aq) and extracted with 30 mL EtOAc three times. The combined EtOAc layer was washed with 50 mL brine then dried over Na₂SO₄. The mixture was filtered and concentrated in vacuo then purified by flash chromatography with silica.

General Procedure E — Hydroarylation of Unactivated Alkenes



To an oven-dried 10 mL schlenk tube equipped with a stir bar, 4-DPAIPN (0.012 mmol, 3 mol %) and sodium formate (1.2 mmol, 3 equiv) were added. The tube was evacuated and backfilled with N₂ three times. While under active N₂, cyclohexylthiol (0.02 mmol, 5 mol %), aryl chloride (0.4 mmol, 1 equiv), and alkene (2.0 mmol, 5 equiv) were added to the vial then DMSO (2 mL, 0.2 M). The tube was sealed under N₂ then stirred and irradiated with two 405 nm lamps (4.5 cm from glass surface on each side with fan cooling) for 28 hours total. At the 6 hour mark, an additional 3 mol % 4-DPAIPN was added as a stock solution (3 mol % 4-DPAIPN dissolved in 400 uL DMSO — then to the reaction vessel, evacuated and backfilled with N₂ on the side arm then while under active N₂, added the stock solution). The tube was resealed under N₂ and stirred while irradiating for the remaining 22 hours.

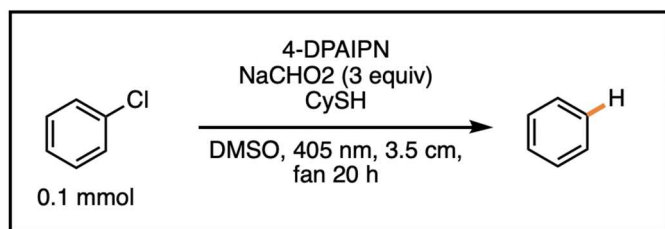
For GC analyses: After reaction completion, mesitylene was added as the internal standard to the crude mixture. 0.1 mL aliquot was removed from the crude and quenched with 1 mL water and extracted with 1 mL diethyl ether. The diethyl ether layer was filtered through a silica pipette plug then ran on the GC.

For NMR analyses: CH₂Br₂ was added as the internal standard to crude reaction mixture. 0.1 mL aliquot was removed and quenched with 1 mL water then extracted with 1 mL CDCl₃. Took Reactions were analyzed via ¹H NMR of the CDCl₃ layer.

4.7.5 Reaction Optimization

Dehalogenation

Following General Procedure A on 0.1 mmol scale, the following parameters were evaluated during optimization of this reaction. Reactions were analyzed via GCMS.

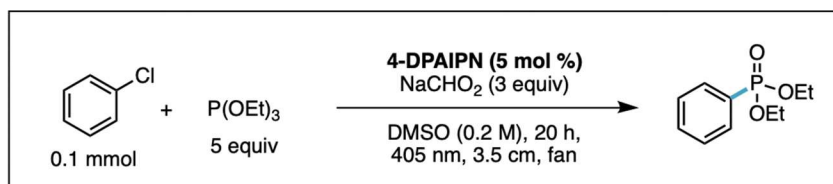


	PhH %
0.2 M DMSO, 5 mol % 4-DPAIPN (two 2.5 mol % batches)	62
0.08 M DMSO, 5 mol % 4-DPAIPN	62
0.08 M DMSO, 10 mol % 4-DPAIPN	74
0.2 M DMSO, 5 mol % 4-DPAIPN (two 2.5 mol % batches), no CySH	57
0.2 M DMF, 5 mol % 4-DPAIPN, no CySH	14
0.2 M THF, 5 mol % 4-DPAIPN (two 2.5 mol % batches), no CySH	0

Figure S2: Dehalogenation optimization.

Phosphonylation

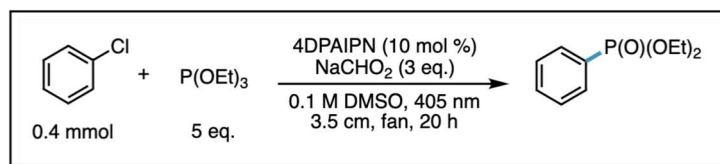
Following General Procedure B, the conditions below were used as the initial standard conditions. The following parameters were evaluated during optimization of this reaction. Reactions were analyzed via ¹H NMR using CH₂Br₂ as the internal standard.



	prdt
standard	30
2.5 mol % 4-DPAIPN	33
0.1 M DMSO, 2.5 mol % 4-DPAIPN	25
0.1 M DMSO, 5 mol % DPA (no batch addition)	40
0.1 M DMSO, 10 mol % DPA	55
0.1 M DMSO, 10 mol % DPA, FPT	53
10 eq phos, 2.5 mol % 4-DPAIPN	36
15 eq phos, 2.5 mol % 4-DPAIPN	36
0.067 M DMSO, 10 mol % 4-DPAIPN	30
0.1 M DMSO, 10 mol % 4-DPAIPN, 10 eq phos	50
0.067 M DMSO, 10 mol % 4-DPAIPN, 10 eq phos	46
0.1 M, 5 mol % 4-DPAIPN, 10 eq phos (no batch addition)	37

Figure S3: Phosphonylation optimization.

The remainder of optimization for the phosphonylation was performed on 0.4 mmol scale with the following standard conditions.

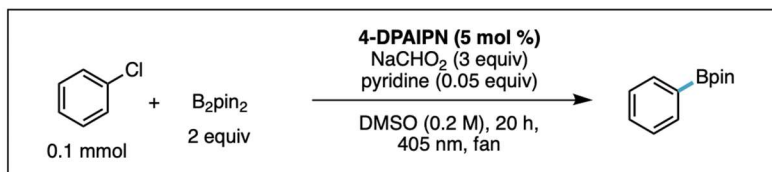


	prdt
standard	51
2 lights	55
photobox	51
12 mol % DPA	60
15 mol % DPA	61
12 mol % DPA, 0.08 M	50
15 mol % DPA, 0.08 M	63
12 mol % DPA, 0.05 M	47
15 mol % DPA, 0.05 M	52

Figure S4: Phosphonylation optimization on 0.4 mmol scale.

Borylation

Following General Procedure C on 0.1 mmol scale, the following parameters were evaluated during optimization of this reaction. Reactions were analyzed via ^1H NMR using CH_2Br_2 as the internal standard.



	prdt	PhH	prdt/PhH
standard	60	20	3
2.5 mol % 4-DPAIPN	50	15	3.33333333
0 eq pyr	50	28	1.78571429
0.05 eq pyr	68	27	2.51851852
0.5 eq pyr	68	22	3.09090909
1 eq B2pin2	54	18	3
3 eq B2pin2	67	25	2.68
4 eq B2pin2	67	11	6.09090909
5 eq B2pin2	70	15	4.66666667
0.1 M, 10 mol % 4-DPAIPN, 3 eq B2pin2, no batch	60	23	2.60869565
0.15 M, 5 mol % 4-DPAIPN, 3 eq B2pin2	68	19	3.57894737
DMF	15	10	1.5

Figure S5: Borylation optimization.

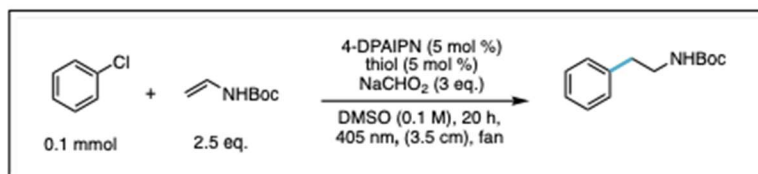
The remainder of borylation optimization was performed with chloroanisole as the substrate because electron-rich substrates were more challenging.

	prdt	Ar-H	rsm	prdt/Ar-H
standard	57	20	26	2.85
0.5 eq pyridine	54	22	30	2.45455
0.5 eq DMAP	58	25	14	2.32
no fan, 5 eq B2pin2, 0.5 eq pyridine	41	9	52	4.55556
10 mol % 4-DPAIPN, 0.08 M DMSO, 0.05 eq pyridine	50	32	21	1.5625
10 mol % 4-DPAIPN, 0.08 M DMSO, 1 eq pyridine	29	20	42	1.45
10 mol % 4-DPAIPN, 0.08 M DMSO, 1 eq DMAP	45	22	34	2.04545
10 mol % 4-DPAIPN, 0.08 M DMSO, 1 eq Cs2CO3	51	30	18	1.7
10 mol % 4-DPAIPN, 0.08 M DMSO, 1 eq tBuOK	41	29	8	1.41379
10 mol % 4-DPAIPN, 0.08 M DMSO, 1 eq K3PO4	37	24	26	1.54167
10 mol % 4-DPAIPN, 0.08 M DMSO, 1 eq pyridine, 5 eq B2pin2	34	9	54	3.77778
0.5 eq Cs2CO3	41	23	21	1.78261
1 eq Cs2CO3	49	20	18	2.45
2 eq Cs2CO3	61	23	11	2.65217
3 eq Cs2CO3	67	29	0	2.31034
4 eq Cs2CO4	66	33	0	2
3 eq Cs2CO3 with Cs formate	63	33	0	1.90909

Figure S6: Borylation optimization with chloroanisole as the substrate.

Hydroarylation of Vinyl Carbamate

Following General Procedure D on 0.1 mmol scale, the following parameters were evaluated during optimization of this reaction. Reactions were analyzed via GCMS.



catalyst	product %	product/PhH	conversion
NpMI (427 nm)	10	1.3	42
NpDI (467)	0	NA	0
DCA (525 nm)	0	NA	0
4-CzIPN (390 nm)	14	7.7	32
tBu-4-CzIPN	16	5.2	24
4-DPAPN	22	5.1	41
4-DPATPN	17	3.4	32
3-CN-3-Ph	0	NA	0
4-DPAIPN	55	4.2	97

Figure S7. Catalyst evaluation for hydroarylation.

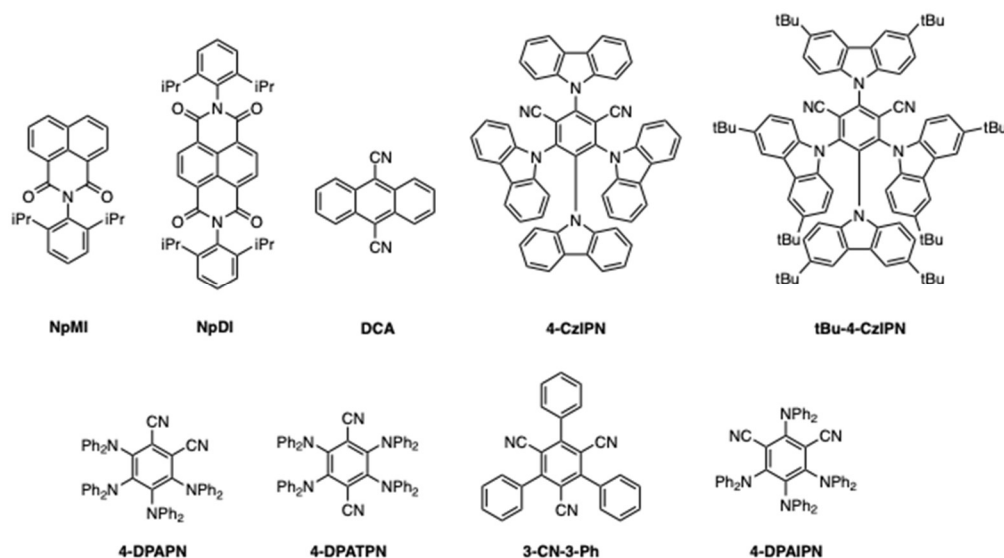


Figure S8: Catalyst structures.

	yield	prdt/PhH	conversion
DMSO	55	2.4	90
MeCN	18	1.6	46
DMF	21	0.7	52
acetone	4	0.5	25
HFIP	0	--	0
DCM	0	--	0
THF	0	(40% PhH)	58
0.05 M	32	0.8	85
0.10 M	50	2.4	90
0.20 M	27	6.2	35

Figure S9: Solvent evaluation for hydroarylation. All solvents tested were run 1:1 with DMSO.

		yield	prdt/PhH	conversion	MB
	no HAT	5	0.6	31	81
	2,6-di-tBu-4-OMe-PhOH	2	0.3	20	87
thiophenols	PhSH	41	2.4	80	83
	4-OMe-PhSH	53	2.4	89	87
alkyl thiols	decanethiol	54	2.1	89	91
	CySH	55	2.4	90	92
	tert-dodecylthiol	57	2.1	89	95

Figure S10: Thiol evaluation for hydroarylation.

reductant (3 equiv)	prdt	PhH	prdt/PhH
DIPEA	6	37	0.4
NPh ₃	0	0	--
Na-ascorbate	0	0	--
Li-formate	18	31	0.6
Cs-formate	53	24	2.3
K-formate	33	27	1.2
Na-formate	50	21	2.4
formic acid + NBu ₃	9	2	4.2
tBuOH	0	0	--
iPrOH	0	0	--
H ₂ O	0	0	--

Figure S11: Reductant evaluation for hydroarylation.

4.7.6 Photocatalyst and Reductant Evaluation

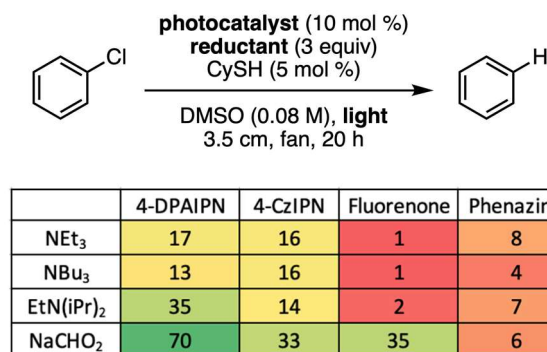


Figure S12. Catalyst and reductand matrix to unlock potent radical anion reactivity.

Following General Procedure A except varying the photocatalyst, reductant, and wavelength, the following yields were obtained via GC analysis using mesitylene as the internal standard. The light used for irradiation (4-DPAIPN = 405 nm, 4-CzIPN = 390 nm, fluorenone = 405 nm, phenazine = 440 nm) was determined from the optimal wavelength for the reduced congener of each photocatalyst, discovered in {Chernowsky, Colleen; Chmiel, Alyah; Wickens, Zachary (2021): Photocatalytic Activity of Diverse Organic Radical Anions: Catalyst Discovery Enables Cleavage of Strong C(sp²)-N and C(sp²)-O Bonds. ChemRxiv. Preprint. <https://doi.org/10.26434/chemrxiv.14710398.v1>}.

4.7.7 Evaluation of Leaving Groups not Susceptible to XAT

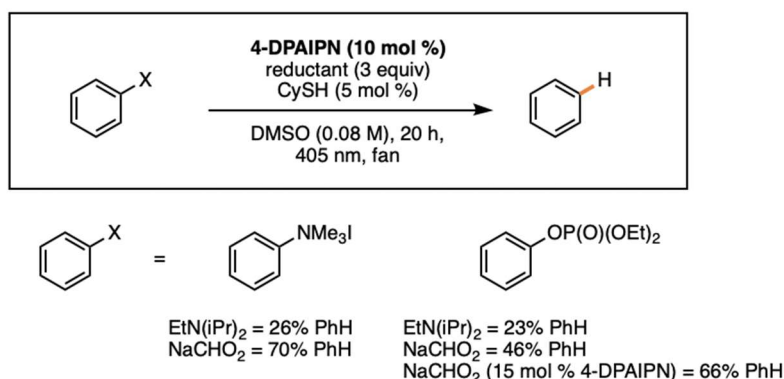


Figure S13. Testing non-halide leaving groups to rule out an XAT mechanism.

Following General Procedure A, the following yields were obtained via GC analysis. The alkyl amine promoted the desired reduction of the anilinium and phosphate in modest yields, supporting an electron-primed mechanism rather than halogen atom transfer (XAT). Furthermore, we see that the reduction becomes much more efficient upon employing sodium formate as the redox activator. Conversion of the phosphate can be increased by employing higher catalyst loading.

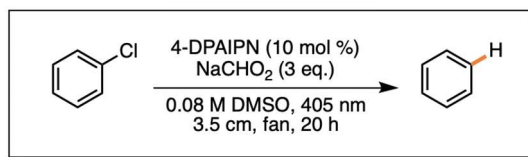
4.7.8 Reductants Evaluated with 4-DPAIPN

Below is a complete list of reductants that were tested with 4-DPAIPN as the photocatalyst, using General Procedure A. For reductants that lacked an H-atom (PPh₃, 4-OMe-NPh₃, Mn(0)), dimethylformamide was used as a co-solvent to act as an H-atom donor to the aryl radical that would be generated upon single electron reduction.

	% prdt
sodium oxalate	2
PPh ₃	7
4-OMe-NPh ₃	3
Mn(0)	1
sodium ascorbate	2
NEt ₃	17
NBu ₃	13
EtN(iPr) ₂	35
NaCHO ₂	70

Figure S14. Reductants tested with 4-DPAIPN for the dehalogenation of chlorobenzene.

4.7.9 Control Experiments



alterations	prdt	rsm
none	71	18
no light	< 2	99
no cat	< 2	94
no formate	<i>not detected</i>	98

The following control experiments were run using General Procedure A with the following deviations mentioned above. We see that light, catalyst, and formate are required.

4.7.10 Radical Clock Experiment

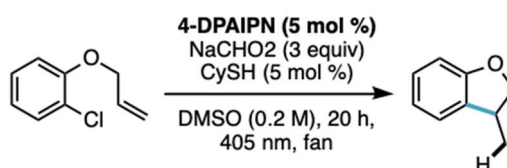


Figure S15. Radical clock experiment to support aryl radical intermediate.

To an oven-dried 10 mL schlenk tube equipped with a stir bar, 4-DPAIPN (0.0025 mmol, 2.5 mol %) and sodium formate (0.3 mmol, 3 equiv) were added. The flask was evacuated and backfilled with N₂ three times. While under active N₂ (if N₂ pressure is too low, then the reaction mixture was freeze-pump-thawed after addition of all reagents), added cyclohexylthiol (0.005 mmol, 5 mol %) and aryl chloride (0.1 mmol, 1 equiv) to vial then DMSO (0.5 mL, 0.2 M). Sealed tube under N₂. The reaction mixture was stirred and irradiated with a 405 nm lamp (3.5 cm from glass surface with fan cooling) for 20 hours total. At the 6 hour mark, an additional 2.5 mol % 4-DPAIPN (for a total of 5 mol % photocatalyst) was added as a stock solution (2.5 mol % 4-DPAIPN dissolved in 100 μ L DMSO — then to the reaction vessel, evacuated and backfilled with N₂ on the side arm then while under active N₂, added the stock solution). The tube was resealed under N₂ and the mixture stirred under irradiation for the remaining 14 hours. CH₂Br₂ (7 μ L, 0.1 mmol, 1 equiv) was added as the internal standard to crude reaction mixture. 0.1 mL aliquot was removed and quenched with 1 mL water then extracted with 1 mL CDCl₃. 52% yield was obtained via ¹H NMR. NMR consistent with reported spectrum (*J. Org. Chem.* 2018, 83, 16, 9381–9390).

4.7.11 High-Throughput Experimentation with Aryl Halide Informer Plate

Informer Plate was run at Merck.

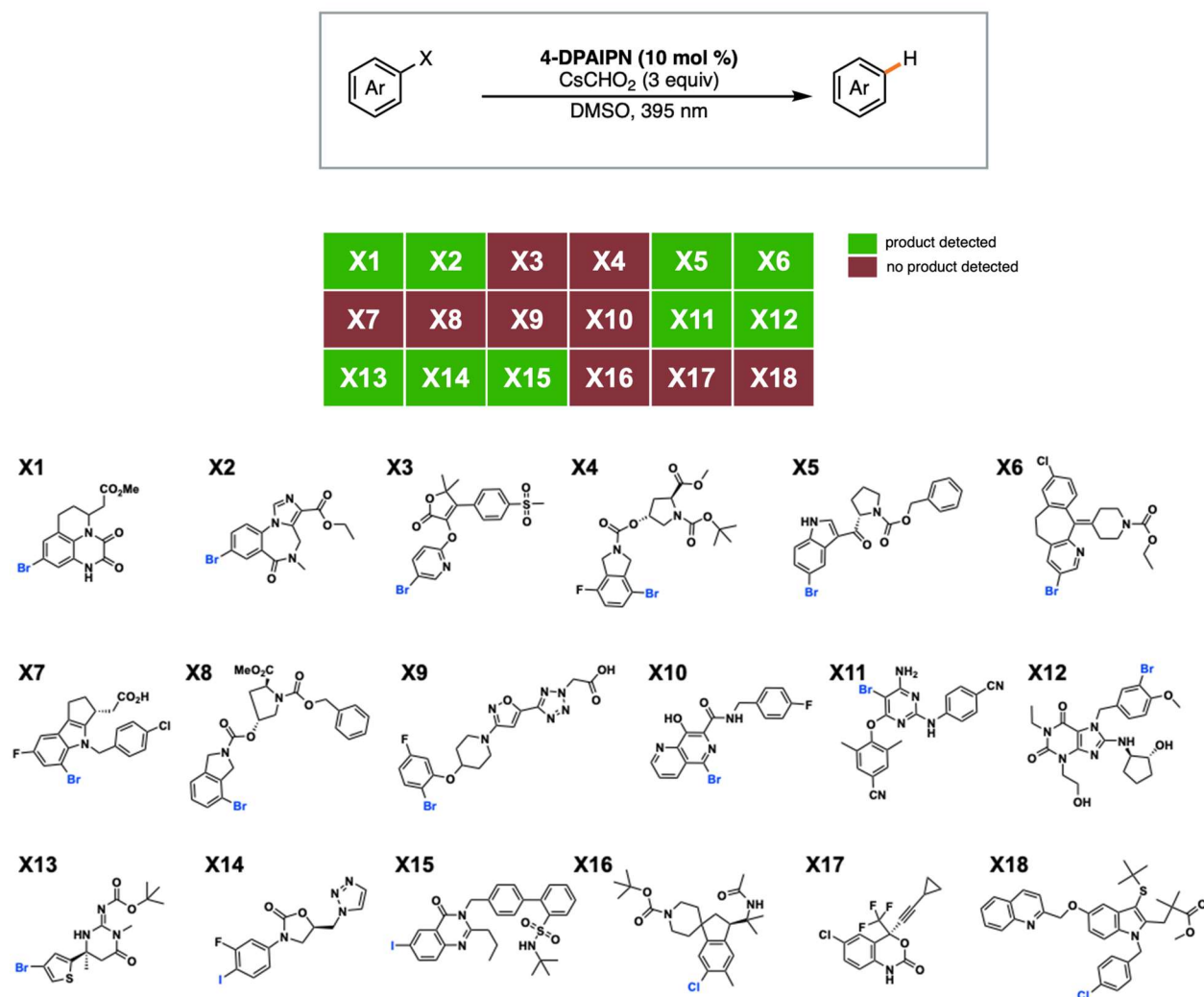


Figure S16. Aryl halide informer plate used in high-throughput experimentation to test the 4-DPAIPN and formate system, in collaboration with Merck.

To a 4 mL vial equipped with a stir bar, 4-DPAIPN (23.9 mg, 0.03 mmol) and cesium formate (0.9 mmol, 3 equiv) were added. Under active N₂, DMSO (3.75 mL) previously sparged with nitrogen for 5 min was added. The resulting suspension was vigorously stirred for 5–10 min. In a nitrogen inertion box, to each reaction well of a custom plated kit containing 10 μmol of the commercially available informers was added 125 μL of the suspension containing 4-DPAIPN (0.8 mg, 1 μmol), cesium formate (5.3 mg, 30 μmol). The reaction block was sealed, and the kit was stirred (by action of a tumble stirrer) under an active stream of nitrogen and irradiated with a 395 nm LED plate (Lumidox II, stage 3, 190 mW/well) equipped with an active cooling base for 8 hours. After completion, each reaction vial was analyzed on an LCMS. The HTE screen afforded hits as depicted in the following graphic showing conversion to the reduction product.

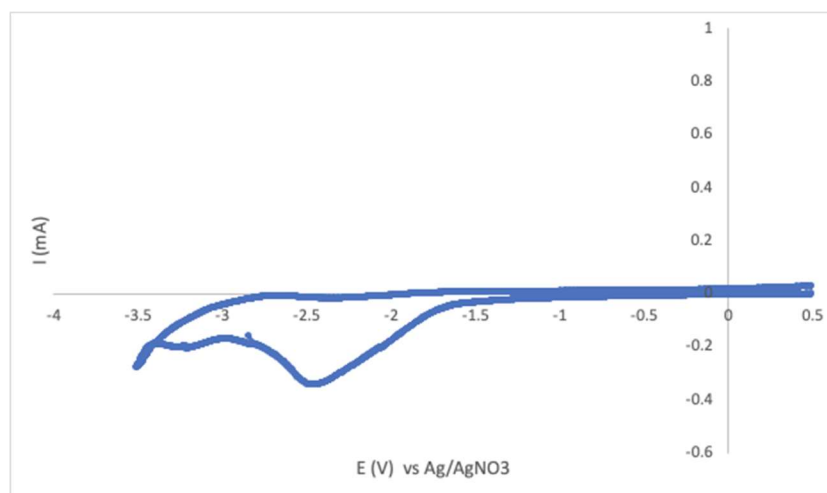
An advantage of using chemical reductants to generate electron-primed catalysts is that it allows for an operationally simple reaction setup as well as allows use of photoredox high-throughput experimentation technology. We demonstrated this using an aryl halide informer plate that contains a unique densely functionalized substrate in each well. Dehalogenation was chosen as the target reaction due to its analytical simplicity. We learned that this electron-primed system can reduce a variety of medicinally-relevant compounds using high-throughput experimentation. These compounds were detected as significant products via LCMS. HTE plate: Lumidox Gen II 24-Position LED Arrays, part no. LUM296DA395. Aryl halide informer plate: <https://www.sigmaaldrich.com/US/en/tech-docs/paper/970033>

To confirm the aforementioned hits, these reactions were repeated on a 0.1 mmol scale using a modified General Procedure A conducted with a Penn PhD Photoreactor M2 equipped with a 405 nm light source without cyclohexylthiol unless otherwise noted. See compounds **27-35**.

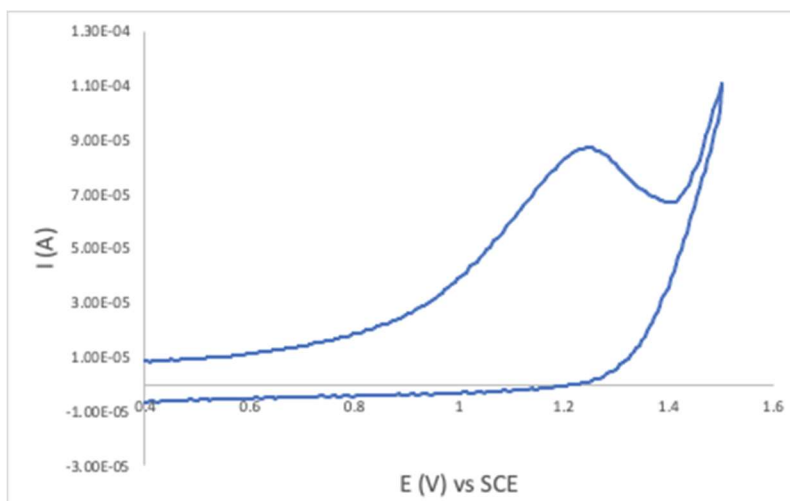
Additionally, a single informer (X2) was reacted on a 0.1 mmol scale using a modified General Procedure E conducted with a Penn PhD Photoreactor M2 equipped with a 405 nm light source. See compound **36**.

4.7.12 Cyclic Voltammetry

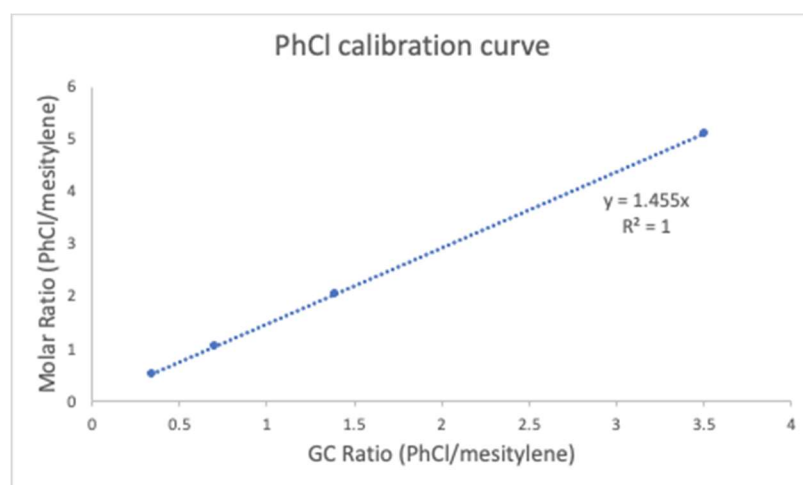
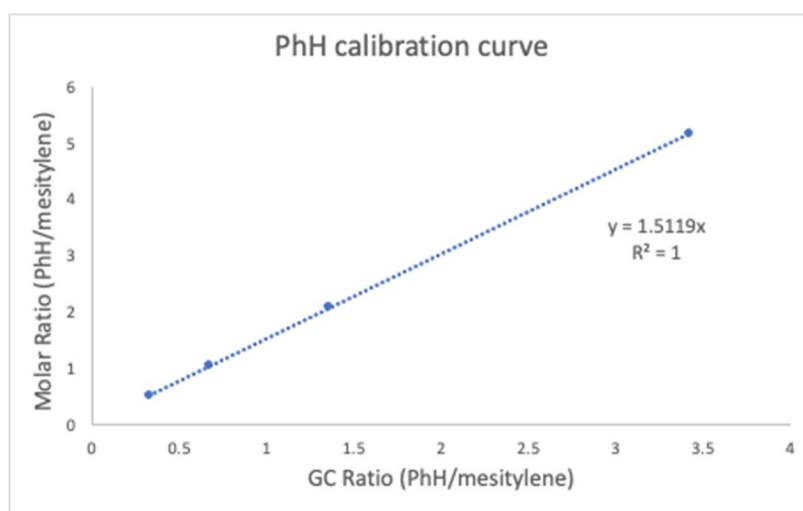
N-vinyl carbamate (0.1 M TBAPF₆) -- $E_{\text{red}} = -2.25 \text{ V vs SCE}$

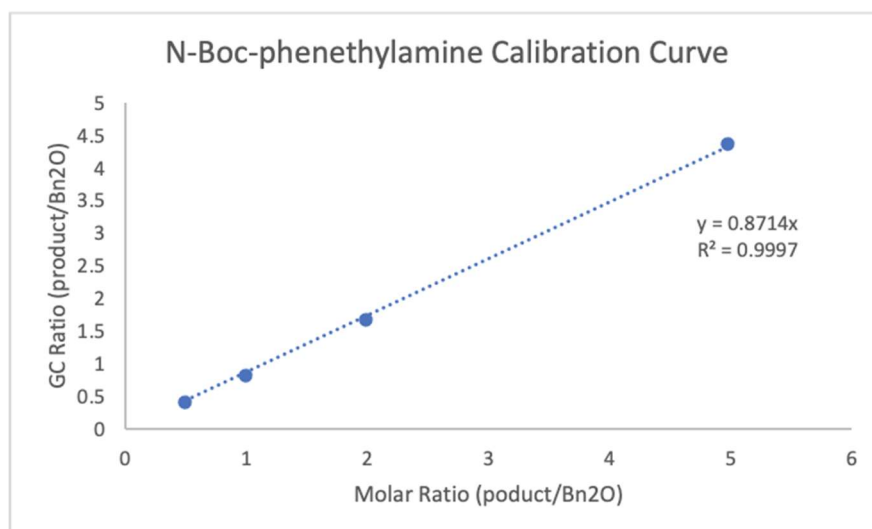
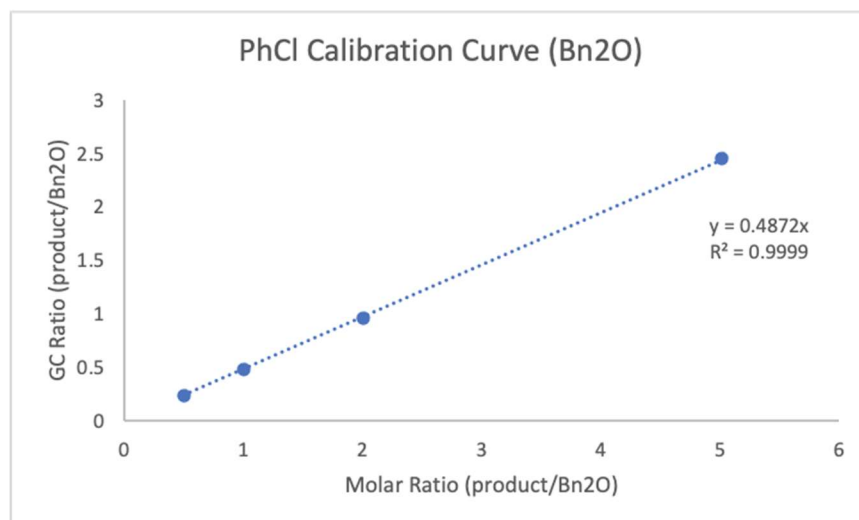
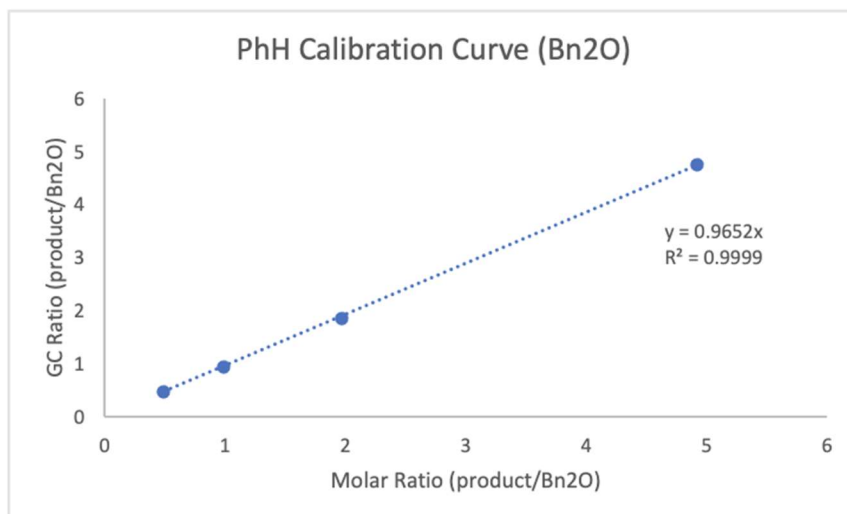


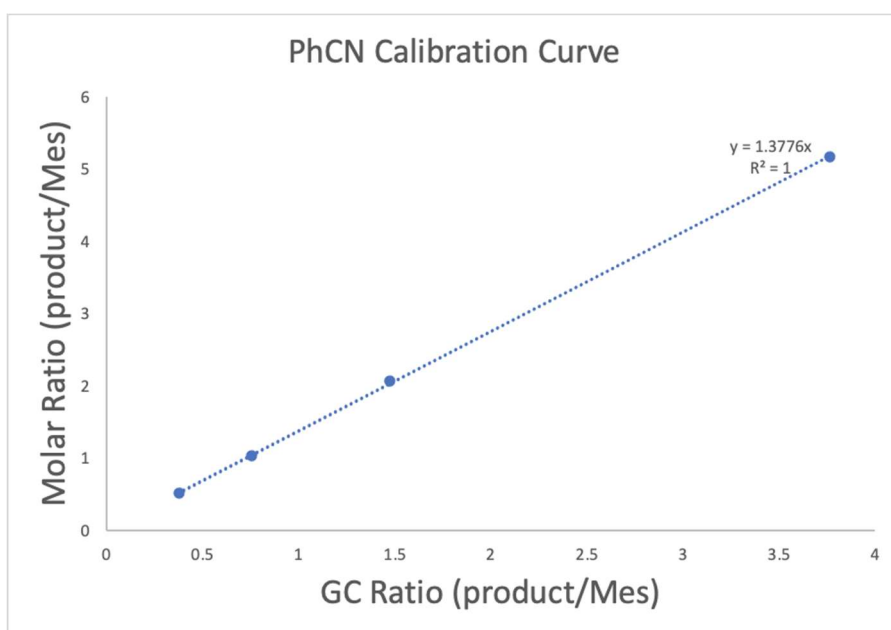
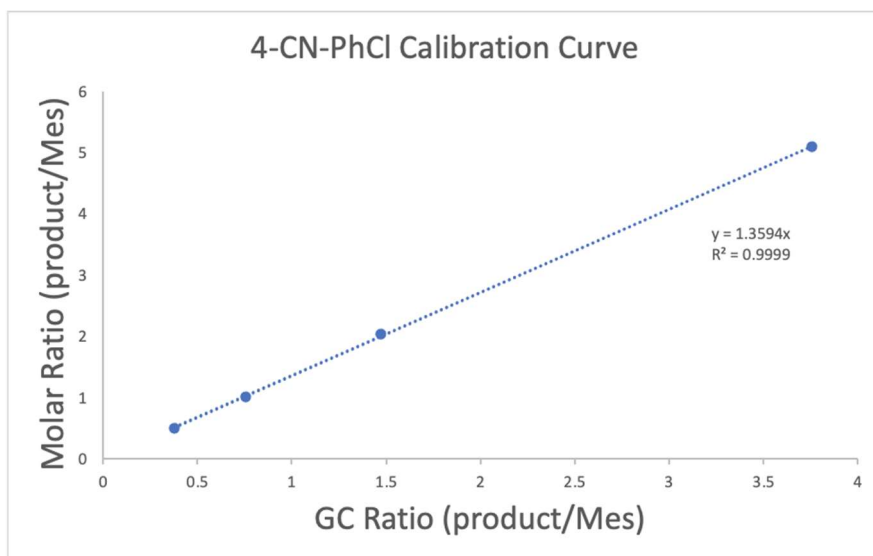
Sodium formate (0.1 M TBAPF₆) -- $E_{\text{ox}} = +1.25 \text{ V vs SCE}$

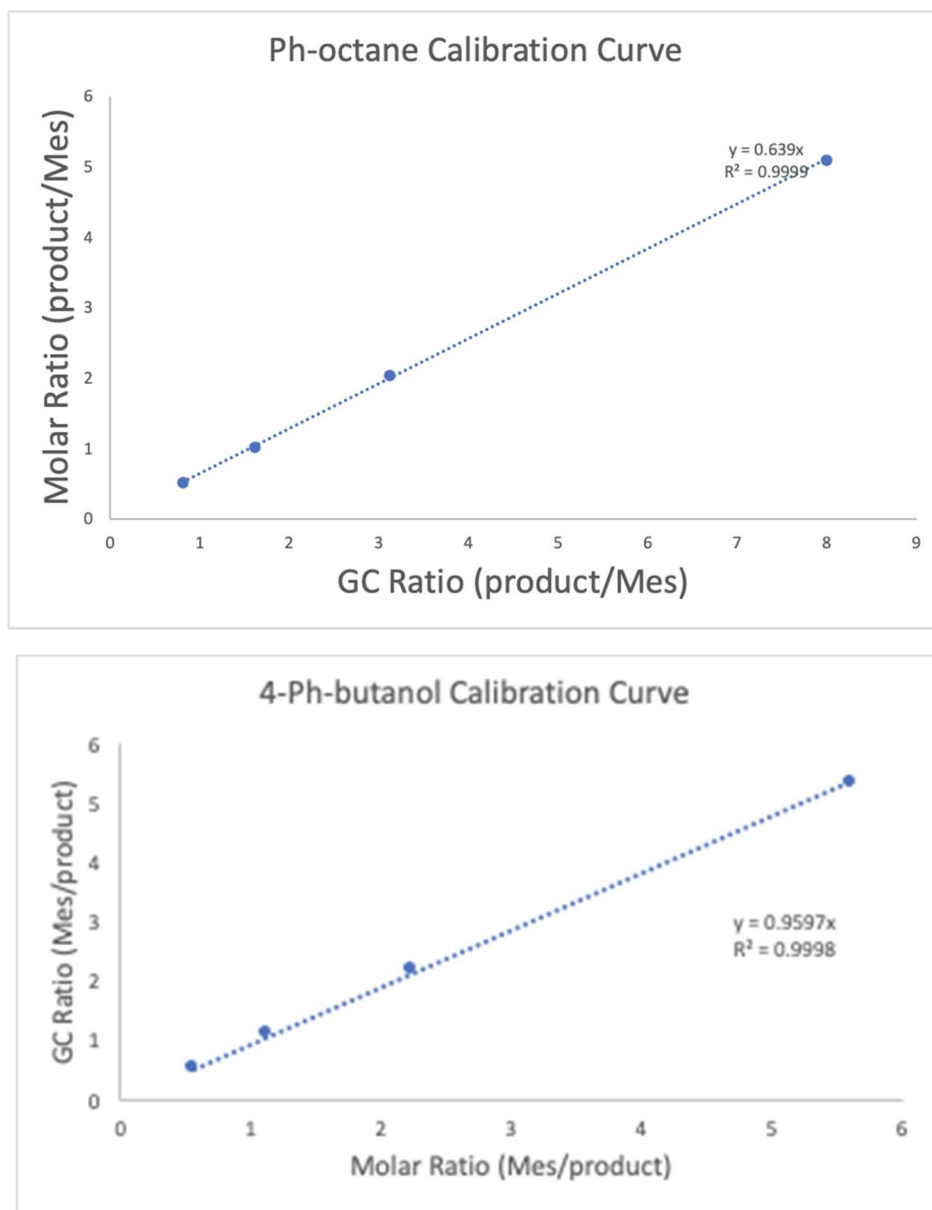


4.7.13 Gas Chromatography Calibration Curves









4.7.14 Stern Volmer and UV-Vis Data

Stern Volmer

In the glovebox, a 25 μM solution of 4-DPAIPN in DMSO was prepared with a given concentration of the quencher. The samples were irradiated at 435 nm and emission peak was measured at 525 nm. Quenching of 4-DPAIPN* was observed with tetrabutylammonium (TBA) formate and cyclohexylthiol, however no quenching was observed with chlorobenzene.

Note: TBA-formate was used instead of Na-formate because of poor solubility of the sodium counter ion. TBA-formate was tested as a reductant in the hydroarylation of the vinyl carbamate

(General Procedure D) to validate its reactivity. Lower conversion was observed (65% conversion) with undesired over-reduction (PhH) as the major by-product (55%).

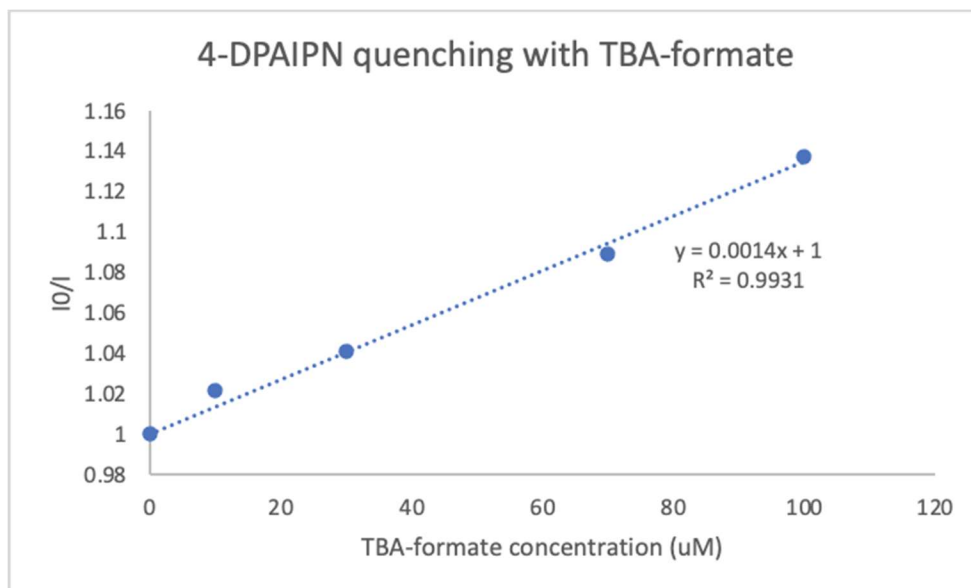


Figure S17. Stern-Volmer quenching of 4-DPAIPN with tetrabutylammonium formate.

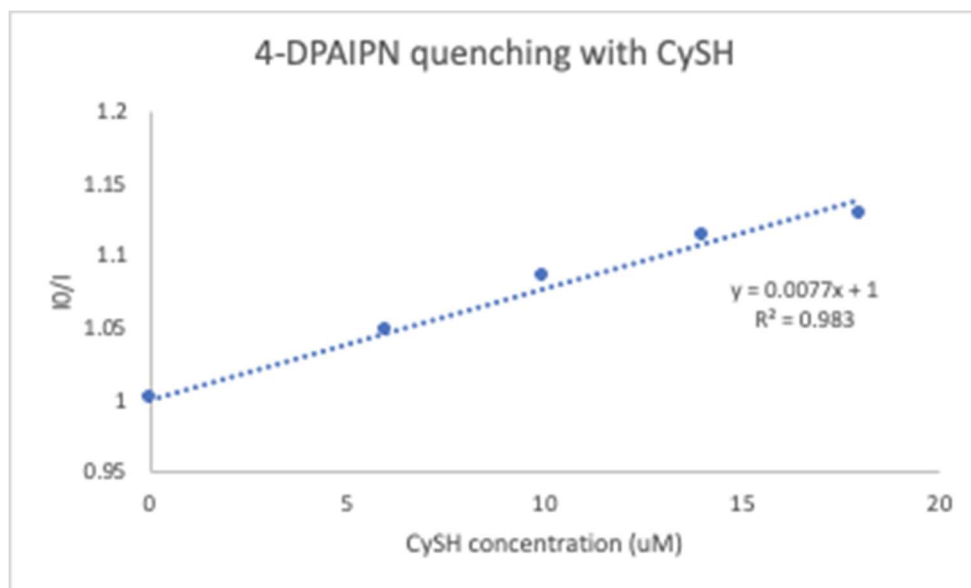


Figure S18. Stern-Volmer quenching of 4-DPAIPN with cyclohexylthiol.

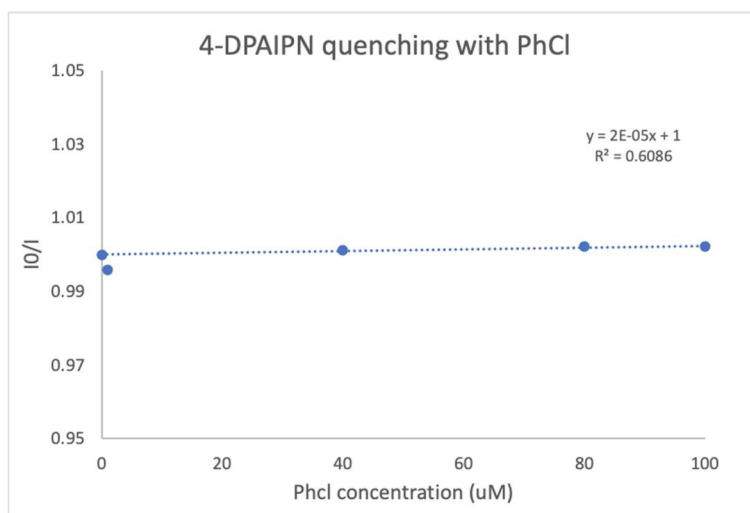


Figure S19. Stern-Volmer quenching of 4-DPAIPN with chlorobenzene.

UV-Vis

Under argon, a 25 μM solution of 4-DPAIPN and sodium formate in DMSO was prepared. The first UV/vis spectrum was taken. To the sample cuvette, a 405 nm LED was used to irradiate the mixture for 15 seconds while shaking. Following irradiation, the second UV/vis spectrum was taken which showed 4-DPAIPN \bullet^- features grow in. Next, chlorobenzene was added to the cuvette through the septum cap to give a 100 μM solution of chlorobenzene with the catalyst and formate mixture. The third UV/vis spectrum was recorded which showed no change in features, suggesting that 4-DPAIPN \bullet^- does not react on this time scale with chlorobenzene in the dark. Finally, the mixture was irradiated for 15 seconds with a 405 nm LED while shaking. The fourth UV/vis spectrum was taken and showed the 4-DPAIPN features grow in while the 4-DPAIPN \bullet^- features shrunk, suggesting that light is required for 4-DPAIPN \bullet^- to reduce chlorobenzene and revert to 4-DPAIPN.

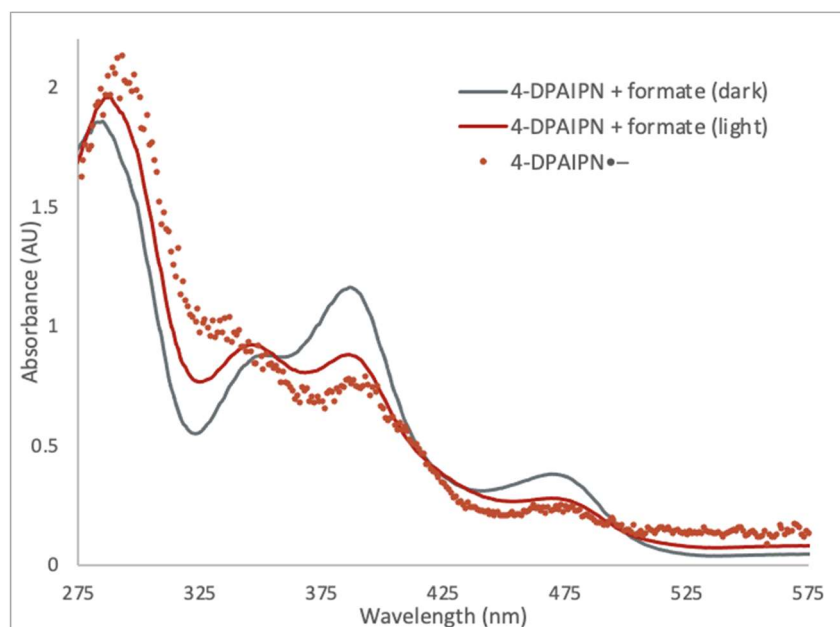


Figure S20. UV/vis of 4-DPAIPN•⁻ generated with formate + light, and electrochemically.

For electrochemically generated 4-DPAIPN:

An oven-dried divided electrochemical cell under N₂ was equipped with an electrode assembly consisting of rubber septa as caps with stainless steel wire and RVC for the cathode, a sacrificial zinc anode, and Ag/AgNO₃ reference electrode. TBAPF₆ (0.1 M in DMF) was added to the cell followed by 4-DPAIPN to make a 25 μ M solution. Using a dip-probe, the solution was electrolyzed at -2 V vs Ag/AgNO₃. The solution changed from bright yellow to dark green/brown/black. The UV/vis spectrum was then recorded.

4.7.15 NMR Experiment for 4-DPAIPN•⁻ Generation

In the glovebox, 4-DPAIPN (8 mg, 1 μ mol) and sodium formate (0.7 mg, 1 μ mol) were added to a J-young tube, followed by D₆-DMSO (0.4 mL) to give a bright yellow solution. The NMR tube was wrapped in foil during transport then the first NMR spectrum was recorded. The NMR tube was then irradiated with a 405 nm LED and shaken for 45 seconds until the solution turned brown/black. The NMR spectrum was recorded and revealed significant broadening on the catalyst signals, indicative of a radical species being generated. Finally, the NMR tube was opened to air to presumably oxidize the 4-DPAIPN•⁻ back to neutral 4-DPAIPN. The solution returned to bright yellow and the NMR spectrum was recorded, revealing the neutral 4-DPAIPN features had returned.

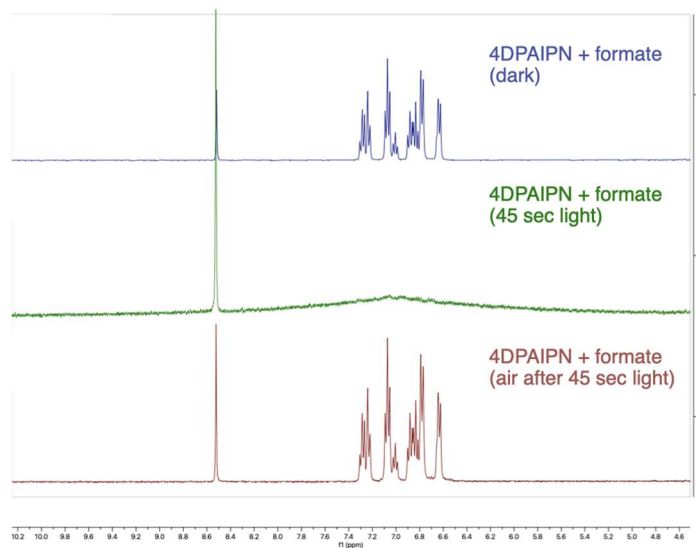


Figure S21: NMR experiment revealing evidence of 4-DPAIPN•⁻ generation in the presence of formate and light.

4.7.16 Plausible Mechanism for $\text{CO}_2^{\bullet-}$ Generation from Thiol Radical

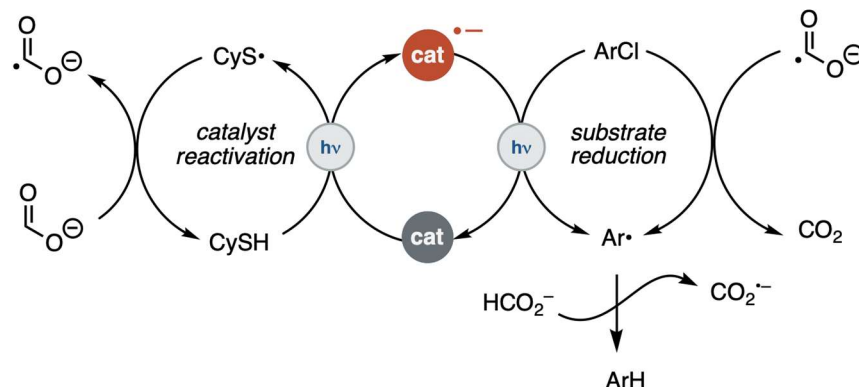
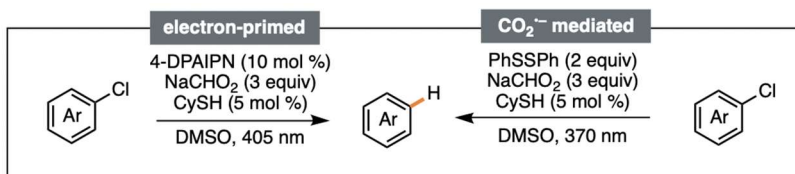


Figure S22. Mechanism of thiol generating $\text{CO}_2^{\bullet-}$

Based on quenching in Stern-Volmer experiments, a plausible mechanism when thiol is present in the net-reductive reactions could be oxidation of the thiol by the 4-DPAIPN* followed by electron-transfer/proton-transfer (ETPT) to generate a thiyl radical. That thiyl radical could then abstract an H• atom from formate to generate the $\text{CO}_2^{\bullet-}$ that can promote the reaction as shown in Scheme 1.

4.7.17 Probing Substrate Reduction by $\text{CO}_2^{\bullet-}$



	NC-C6H4-Cl -2.1 V	C6H5-Cl -2.7 V	MeO-C6H4-Cl -2.9 V
PhSSPh initiator (access to $\text{CO}_2^{\bullet-}$)	100	9	<5
4-DPAIPN (electron-primed)	80	75	67

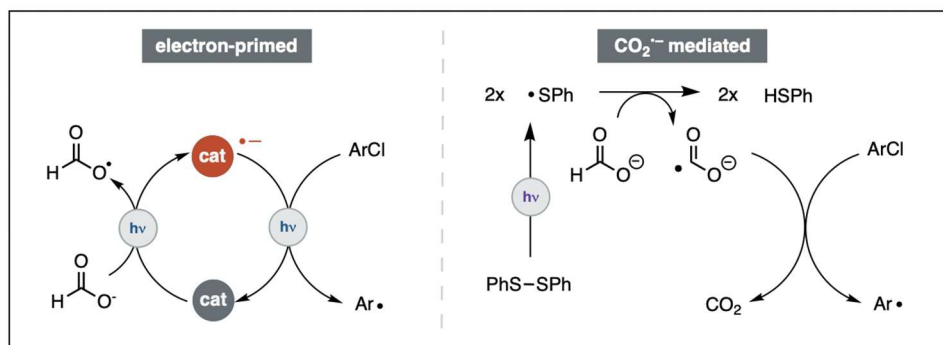
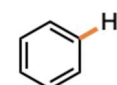


Figure S23. Evidence for $\text{CO}_2^{\bullet-}$ promoting substrate reduction at milder substrate E_{red} and electron-primed catalysis promoting substrate reduction at more challenging substrate E_{red} .

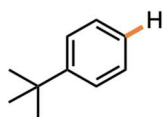
In an attempt to discriminate reduction of substrate via 4-DPAIPN radical anion excited state vs. CO_2 radical anion, the homolysis of the S–S bond of phenyl disulfide was explored as an alternative route to access $\text{CO}_2^{\bullet-}$ from formate. Conditions similar to the 4-DPAIPN-promoted reaction (General Procedure A) were used, replacing 4-DPAIPN with phenyl disulfide (2 equiv) and using 370 nm irradiation to homolyze the S–S bond, instead of 405 nm. The reactions were analyzed by measuring conversion of the aryl chloride via GCMS.

4.7.18 Product Characterization

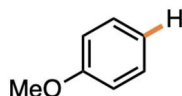


from PhCl

Benzene (3): 70% was obtained following General Procedure A, analyzed via GC analysis.



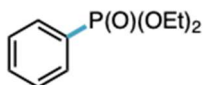
Tert-butylbenzene (4): 64% was obtained following General Procedure A, analyzed via ^1H NMR analysis. NMR consistent with reported spectrum (*J. Am. Chem. Soc.* 2013, 135, 2, 624–627).



Anisole (5): 67% was obtained following General Procedure A, analyzed via ^1H NMR analysis. NMR consistent with reported spectrum (*Angew. Chem. Int. Ed.* 2018, 57, 12906–12910).

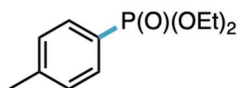


1,3-di-tert-butyl-2-methoxybenzene (6): 92% was obtained following General Procedure A, analyzed via ^1H NMR analysis. NMR consistent with reported spectrum (*Tetrahedron*, 69, 3, 2013, 1105-1111).

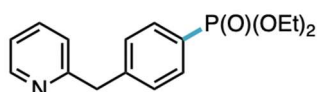


diethyl phenylphosphonate (10): 47 mg (55%) was obtained as a colorless oil following General Procedure B. Product was isolated via flash chromatography on silica using 2:1 hexanes/acetone. ^1H NMR (400 MHz, CDCl_3) δ 7.81 – 7.67 (m, 2H), 7.51 – 7.43 (m, 1H), 7.39 (tdd, J = 8.3, 4.2, 1.0

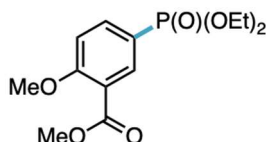
Hz, 2H), 4.19 – 3.90 (m, 4H), 1.25 (t, $J = 7.1$ Hz, 6H), consistent with reported spectrum (*Org. Lett.* 2013, 15, 20, 5362–5365).



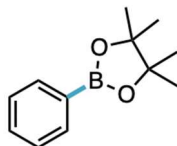
diethyl *p*-tolylphosphonate (11): 58 mg (63%) was obtained as a colorless oil following General Procedure B with the modification that 15 mol % 4-DPAIPN was used, first with the addition of 10 mol % photocatalyst followed by a batch of 5 mol % after 20 hours, giving a total 36 hour reaction time. Product was isolated via flash chromatography on silica using 2:1 hexanes/acetone. $^1\text{H NMR}$ (400 MHz, CDCl_3) δ 7.63 (dd, $J = 13.2, 8.1$ Hz, 2H), 7.32 – 7.10 (m, 2H), 4.19 – 3.88 (m, 4H), 2.33 (s, 3H), 1.24 (t, $J = 7.1$ Hz, 6H), consistent with reported spectrum (*Org. Lett.* 2018, 20, 14, 4164–4167).



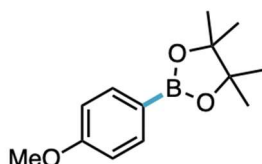
diethyl (4-(pyridin-2-ylmethyl)phenyl)phosphonate (12): 84 mg (69%) was obtained as a pale yellow oil following General Procedure B with the modification that 15 mol % 4-DPAIPN was used, first with the addition of 10 mol % photocatalyst followed by a batch of 5 mol % after 20 hours, giving a total 36 hour reaction time. Product was isolated via flash chromatography on silica using 20% MeOH in DCM. $^1\text{H NMR}$ (400 MHz, CDCl_3) δ 8.55 – 8.49 (m, 1H), 7.76 – 7.66 (m, 2H), 7.57 (td, $J = 7.7, 1.9$ Hz, 1H), 7.33 (dd, $J = 8.0, 3.9$ Hz, 2H), 7.09 (dd, $J = 7.8, 2.5$ Hz, 2H), 4.16 (s, 2H), 4.15 – 3.96 (m, 4H), 1.27 (t, $J = 7.1$ Hz, 6H). $^{13}\text{C NMR}$ (101 MHz, CDCl_3) δ 159.83, 149.51, 144.26 (d, $J = 3.2$ Hz), 136.73, 132.11 (d, $J = 10.3$ Hz), 129.18 (d, $J = 15.3$ Hz), 126.17 (d, $J = 189.7$ Hz), 123.28, 121.57, 62.03 (d, $J = 5.4$ Hz), 44.60, 16.31 (d, $J = 6.5$ Hz). $^{31}\text{P NMR}$ (162 MHz, CDCl_3) δ 19.05. **HRMS** (ESI^+) Calc: $[\text{M}+\text{H}]^+$ ($\text{C}_{16}\text{H}_{20}\text{NO}_3\text{P}$) 306.1253; measured 306.1247 = 2.0 ppm difference.



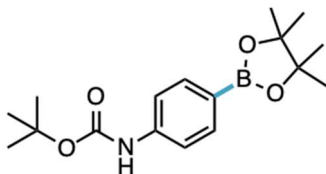
methyl 5-(diethoxyphosphoryl)-2-methoxybenzoate (13): 109 mg (90%) was obtained as a pale yellow oil following General Procedure B. Product was isolated via flash chromatography on silica using 30-60% acetone in hexanes. $^1\text{H NMR}$ (400 MHz, CDCl_3) δ 8.15 (dd, $J = 13.4, 2.1$ Hz, 1H), 7.85 (ddd, $J = 12.5, 8.6, 2.1$ Hz, 1H), 6.99 (dd, $J = 8.6, 3.2$ Hz, 1H), 4.15 – 3.95 (m, 4H), 3.89 (s, 3H), 3.83 (s, 3H), 1.25 (t, $J = 7.1$ Hz, 6H). $^{13}\text{C NMR}$ (101 MHz, CDCl_3) δ 165.67, 162.03 (d, $J = 3.3$ Hz), 137.28 (d, $J = 11.1$ Hz), 135.60 (d, $J = 12.2$ Hz), 120.32 (d, $J = 15.5$ Hz), 119.65 (d, $J = 196.4$ Hz), 111.93 (d, $J = 15.8$ Hz), 62.16 (d, $J = 5.4$ Hz), 56.19, 52.21, 16.32 (d, $J = 6.5$ Hz). $^{31}\text{P NMR}$ (162 MHz, CDCl_3) δ 18.00. **HRMS** (ESI^+) Calc: $[\text{M}+\text{H}]^+$ ($\text{C}_{13}\text{H}_{19}\text{O}_6\text{P}$) 303.0992; measured 303.0987 = 1.6 ppm difference.



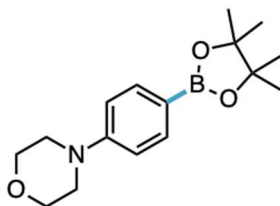
4,4,5,5-tetramethyl-2-phenyl-1,3,2-dioxaborolane (14): 80% was obtained following General Procedure C, analyzed via ^1H NMR analysis. NMR consistent with reported spectrum (*Org. Lett.* 2012, 14, 17, 4560–4563).



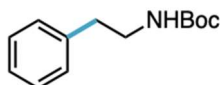
2-(4-methoxyphenyl)-4,4,5,5-tetramethyl-1,3,2-dioxaborolane (15): 63 mg (67%) was obtained as a white solid following General Procedure C. Product was isolated via flash chromatography on silica using 10 % ethyl acetate in hexanes. ^1H NMR (400 MHz, CDCl_3) δ 7.76 (d, J = 8.6 Hz, 2H), 6.90 (d, J = 8.6 Hz, 2H), 3.83 (s, 3H), 1.34 (s, 12H), consistent with reported spectrum (*Org. Lett.* 2012, 14, 17, 4560–4563).



tert-butyl (4-(4,4,5,5-tetramethyl-1,3,2-dioxaborolan-2-yl)phenyl)carbamate (16): 92% was obtained following General Procedure C, analyzed via ^1H NMR analysis. NMR consistent with reported spectrum (*J. Am. Chem. Soc.* 2020, 142, 5, 2087–2092).

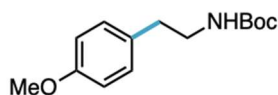


4-(4-(4,4,5,5-tetramethyl-1,3,2-dioxaborolan-2-yl)phenyl)morpholine (17): 59 mg (51%) was obtained as a white solid following General Procedure C. Product was isolated via flash chromatography on silica using 30% ethyl acetate in hexanes. ^1H NMR (400 MHz, CDCl_3) δ 7.73 (d, J = 8.6 Hz, 2H), 6.88 (d, J = 8.7 Hz, 2H), 3.92 – 3.78 (m, 4H), 3.34 – 3.17 (m, 4H), 1.33 (s, 12H), consistent with reported spectrum (*Org. Lett.* 2016, 18, 11, 2758–2761).

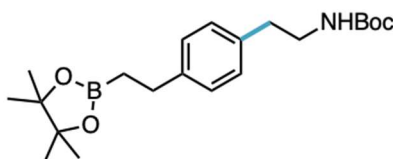


tert-butyl phenethylcarbamate (18): 53 mg (60%) was obtained following General Procedure D. Product was isolated via flash chromatography on silica using hexanes ethyl acetate. ^1H NMR (400 MHz, CDCl_3) δ 7.31 (dd, J = 8.0, 6.6 Hz, 2H), 7.20 (dd, J = 8.6, 7.1 Hz, 3H), 4.53 (s, 1H),

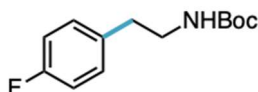
3.38 (q, $J = 6.8$ Hz, 2H), 2.80 (t, $J = 7.0$ Hz, 2H), 1.44 (s, 9H), consistent with reported spectrum (*Org. Lett.* 2019, 21, 8, 2818–2822).



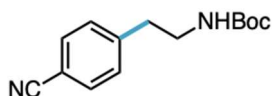
tert-butyl (4-methoxyphenethyl)carbamate (19): 50 mg (50%) was obtained following General Procedure D. Product was isolated via flash chromatography on silica using hexanes ethyl acetate. $^1\text{H NMR}$ (400 MHz, CDCl_3) δ 7.11 (d, $J = 8.6$ Hz, 2H), 6.84 (d, $J = 8.6$ Hz, 2H), 4.52 (s, 1H), 3.79 (s, 3H), 3.33 (t, $J = 6.8$ Hz, 2H), 2.73 (t, $J = 7.0$ Hz, 2H), 1.43 (s, 9H), consistent with reported spectrum (*Org. Lett.* 2019, 21, 8, 2818–2822).



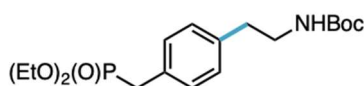
tert-butyl (4-(2-(4,4,5,5-tetramethyl-1,3,2-dioxaborolan-2-yl)ethyl)phenethyl)carbamate (20): 64% was obtained following General Procedure D. The product was partially purified on silica using hexanes ethyl acetate to verify product identity. $^1\text{H NMR}$ (400 MHz, CDCl_3) δ 7.08 (d, $J = 7.8$ Hz, 2H), 7.01 (d, $J = 7.7$ Hz, 2H), 3.28 (d, $J = 8.7$ Hz, 2H), 2.66 (dt, $J = 12.4, 7.5$ Hz, 4H), 1.36 (s, 9H), 1.15 (s, 12H), 1.06 (t, $J = 8.2$ Hz, 2H). $^{13}\text{C NMR}$ (126 MHz, CDCl_3) δ 155.89, 142.50, 136.02, 128.61, 128.21, 83.09, 63.63, 41.83, 38.80, 35.73, 34.25, 29.53, 28.42, 24.80. **HRMS** (ESI $^+$) Calc: $[\text{M}+\text{Na}]^+$ ($\text{C}_{21}\text{H}_{34}\text{BNO}_4$) 398.2477; measured 398.2469 = 2.0 ppm difference.



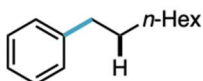
tert-butyl (4-fluorophenethyl)carbamate (21): 66% was obtained following General Procedure D and was analyzed via NMR analysis. The product was partially purified on silica using hexanes ethyl acetate to verify product identity. $^1\text{H NMR}$ was consistent with reported spectrum (*Molecules* 2016, 21(9), 1160).



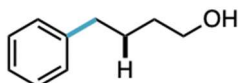
tert-butyl (4-cyanophenethyl)carbamate (22): 63 mg (64%) was obtained following General Procedure D. Product was isolated via flash chromatography on silica using hexanes ethyl acetate. $^1\text{H NMR}$ (400 MHz, CDCl_3) δ 7.60 (d, $J = 8.0$ Hz, 2H), 7.30 (d, $J = 8.0$ Hz, 2H), 3.39 (d, $J = 7.0$ Hz, 2H), 2.87 (t, $J = 7.0$ Hz, 2H), 1.43 (s, 9H), consistent with reported spectrum (*J. Med. Chem.* 2018, 61, 18, 8457–8467).



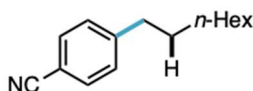
tert-butyl (4-((diethoxyphosphoryl)methyl)phenethyl)carbamate (23): 89 mg (60%) was obtained following General Procedure D. Product was isolated via flash chromatography on silica using hexanes ethyl acetate. $^1\text{H NMR}$ (400 MHz, CDCl_3) δ 7.24 (dd, $J = 8.1, 2.5$ Hz, 2H), 7.13 (d, $J = 7.8$ Hz, 2H), 4.51 (s, 1H), 4.10 – 3.95 (m, 4H), 3.36 (d, $J = 6.7$ Hz, 2H), 3.12 (d, $J = 21.5$ Hz, 2H), 2.77 (t, $J = 7.1$ Hz, 2H), 1.43 (s, 9H), 1.24 (t, $J = 7.1$ Hz, 6H), consistent with reported spectrum (*Angew. Chem. Int. Ed.* 2021, 60, 2393– 2397).



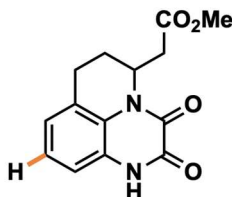
1-phenyloctane (24): 72% was obtained following General Procedure E and analyzed via GC.



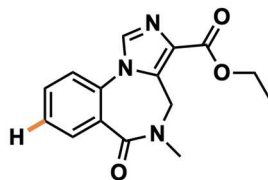
4-phenylbutan-1-ol (25): 80% was obtained following General Procedure E and analyzed via GC.



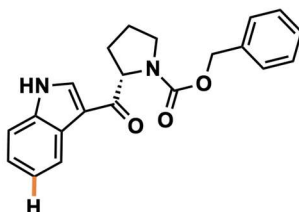
4-octylbenzonitrile (26): 61% was obtained following General Procedure E and analyzed via NMR analysis. Product confirmed with $^1\text{H NMR}$ of partial purification, consistent with reported spectrum (*J. Org. Chem.* 2013, 78, 15, 7436–7444). **HRMS** (ESI^+) Calc: $[\text{M}+\text{H}]^+$ ($\text{C}_{15}\text{H}_{21}\text{N}$) 216.1747; measured 216.1744 = 1.3 ppm difference.



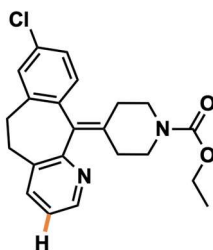
methyl 2-(2,3-dioxo-2,3,6,7-tetrahydro-1H,5H-pyrido[1,2,3-de]quinoxalin-5-yl)acetate (27): From **X1**, 16 mg (58%) was obtained following General Procedure A with the modification that a Penn PhD Photoreactor M2 equipped with a 405 nm light source was used to irradiate and no cyclohexylthiol was added. Product was isolated via mass-directed reversed phase chromatography using MeCN/ H_2O with an NH_4OH modifier. $^1\text{H NMR}$ (600 MHz, DMSO-d_6) δ 11.82 (s, 1H), 7.09 – 7.05 (m, 1H), 7.03 – 7.00 (m, 1H), 7.00 – 6.98 (m, 1H), 5.16 – 5.08 (m, 1H), 3.62 (s, 3H), 3.00 – 2.89 (m, 1H), 2.82 – 2.74 (m, 1H), 2.67 – 2.56 (m, 2H), 2.15 – 2.07 (m, 1H), 1.91 (tt, $J = 13.9, 4.6$ Hz, 1H). $^{13}\text{C NMR}$ (151 MHz, DMSO-d_6) δ 170.77, 154.19, 153.55, 125.64, 124.41, 123.25, 123.10, 122.56, 113.46, 51.69, 47.04, 34.96, 22.75, 21.08. **HRMS** (ESI^+) Calc: $[\text{M}+\text{H}]^+$ ($\text{C}_{14}\text{H}_{14}\text{N}_2\text{O}_4$) 275.1032; measured 275.1035 = 1.1 ppm difference.



ethyl 5-methyl-6-oxo-5,6-dihydro-4H-benzo[f]imidazo[1,5-a][1,4]diazepine-3-carboxylate (28): From **X2**, 13 mg (45%) was obtained as a white solid following General Procedure A with the modification that a Penn PhD Photoreactor M2 equipped with a 405 nm light source was used to irradiate and no cyclohexylthiol was added. Product was isolated via mass-directed reversed phase chromatography using MeCN/H₂O with an NH₄OH modifier. **¹H NMR** (600 MHz, DMSO-d₆) δ 8.37 (s, 1H), 7.93 – 7.89 (m, 1H), 7.76 – 7.72 (m, 2H), 7.61 – 7.55 (m, 1H), 4.98 (s, 1H), 4.47 (s, 1H), 4.32 (s, 2H), 3.10 (s, 3H), 1.33 (t, *J* = 7.1 Hz, 3H); consistent with reported spectrum (*Organic and Biomolecular Chemistry*, 2011, 9, 24, 8346–8355). **¹³C NMR** (151 MHz, DMSO-d₆) δ 165.74, 162.37, 136.42, 135.51, 132.68, 131.83, 131.73, 128.57, 128.16, 127.63, 122.82, 60.10, 42.00, 35.06, 14.22. **HRMS** (ESI+) Calc: [M+H]⁺ (C₁₅H₁₅N₃O₃) 286.1191; measured 286.1190 = –0.3 ppm difference.

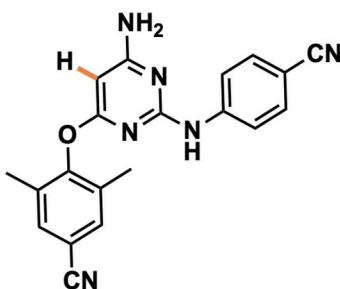


benzyl (S)-2-(1H-indole-3-carbonyl)pyrrolidine-1-carboxylate (29): From **X5**, 10 mg (22%) was obtained as a white solid following General Procedure A with the modification that a Penn PhD Photoreactor M2 equipped with a 405 nm light source was used to irradiate and 8 mol% cyclohexylthiol was added. Product was isolated via mass-directed reversed phase chromatography using MeCN/H₂O with an NH₄OH modifier. Compound is a roughly 1:1 mixture of two rotamers with distinct NMR signals. Peaks observed are reported (not assigned). **¹H NMR** (600 MHz, DMSO-d₆) δ 12.02 (d, *J* = 12.6 Hz, 1H), 8.44 (dd, *J* = 15.2, 3.1 Hz, 1H), 8.20 (dd, *J* = 30.8, 7.4 Hz, 1H), 7.51 – 7.47 (m, 1H), 7.38 (d, *J* = 4.6 Hz, 2H), 7.36 – 7.29 (m, 1H), 7.26 – 7.17 (m, 2H), 7.12 – 7.06 (m, 1H), 7.01 (t, *J* = 7.6 Hz, 1H), 5.22 (ddd, *J* = 30.3, 8.6, 3.5 Hz, 1H), 5.12 – 5.02 (m, 1H), 5.02 – 4.87 (m, 1H), 3.57 – 3.47 (m, 2H), 2.45 – 2.28 (m, 1H), 1.95 – 1.81 (m, 3H). **¹³C NMR** (151 MHz, DMSO-d₆) δ 193.65, 193.25, 153.83, 153.76, 137.17, 136.87, 136.54, 136.51, 133.87, 133.85, 128.40, 127.87, 127.75, 127.44, 127.23, 126.67, 125.75, 125.68, 122.94, 122.91, 121.85, 121.79, 121.39, 121.35, 113.73, 113.63, 112.15, 112.14, 65.75, 65.59, 61.95, 61.53, 47.27, 46.61, 31.84, 30.77, 23.99, 23.18. **HRMS** (ESI+) Calc: [M+H]⁺ (C₂₁H₂₀N₂O₃) 349.1552; measured 349.1557 = 1.4 ppm difference.

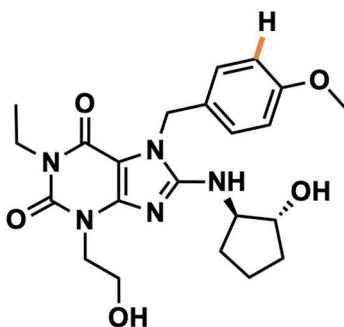


Ethyl-4-(8-chloro-5,6-dihydro-11H-benzo[5,6]cyclohepta[1,2-b]pyridin-11-ylidene)

piperidine-1-carboxylate (30): From **X6**, 13 mg (33%) was obtained as an off-white solid following General Procedure A with the modification that a Penn PhD Photoreactor M2 equipped with a 405 nm light source was used to irradiate and no cyclohexylthiol was added. Product was isolated via mass-directed reversed phase chromatography using MeCN/H₂O with an NH₄OH modifier. **¹H NMR** (600 MHz, DMSO-d₆) δ 8.34 (dd, J = 4.6, 1.3 Hz, 1H), 7.60 – 7.55 (m, 1H), 7.30 (d, J = 2.0 Hz, 1H), 7.25 – 7.17 (m, 2H), 7.09 (d, J = 8.2 Hz, 1H), 4.03 (q, J = 7.1 Hz, 2H), 3.67 – 3.55 (m, 2H), 3.33 – 3.24 (m, 2H), 3.23 – 3.12 (m, 2H), 2.81 (dq, J = 13.2, 6.1 Hz, 2H), 2.37 – 2.24 (m, 2H), 2.23 – 2.11 (m, 2H), 1.17 (t, J = 7.1 Hz, 3H); consistent with reported spectrum (*Journal of Organic Chemistry*, 1989. 54, 9, 2242–2244). **¹³C NMR** (151 MHz, DMSO-d₆) δ 156.80, 154.54, 146.37, 140.18, 137.84, 137.48, 136.48, 133.47, 133.25, 131.62, 130.70, 128.96, 125.69, 122.39, 60.69, 44.39, 44.31, 30.96, 30.55, 30.28, 30.18, 14.60. **HRMS** (ESI+) Calc: [M+H]⁺ (C₂₂H₂₃ClN₂O₂) 383.1526; measured 383.1533 = 1.8 ppm difference.

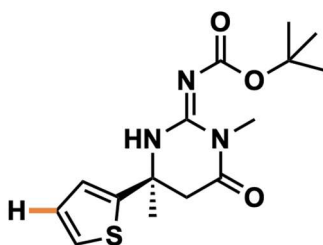
**4-((6-amino-2-((4-cyanophenyl)amino)pyrimidin-4-yl)oxy)-3,5-dimethylbenzonitrile (31):**

From **X11**, 22 mg (61%) was obtained following General Procedure A with the modification that a Penn PhD Photoreactor M2 equipped with a 405 nm light source was used to irradiate and no cyclohexylthiol was added. Product was isolated via mass-directed reversed phase chromatography using MeCN/H₂O with an NH₄OH modifier. **¹H NMR** (600 MHz, DMSO-d₆) δ 9.54 (s, 1H), 7.71 (s, 2H), 7.65 (d, J = 8.3 Hz, 2H), 7.46 (d, J = 8.8 Hz, 2H), 6.77 (s, 2H), 5.46 (s, 1H), 2.12 (s, 6H); consistent with reported spectrum (*Organic Process Research and Development*, 2010, 14, 3, 657–660). **¹³C NMR** (151 MHz, DMSO-d₆) δ 168.16, 166.41, 158.86, 153.90, 145.32, 132.93, 132.52, 132.45, 119.63, 118.69, 117.99, 108.01, 101.66, 78.66, 15.81. **HRMS** (ESI+) Calc: [M+H]⁺ (C₂₀H₁₆N₆O) 357.1464; measured 357.1474 = 2.7 ppm difference.

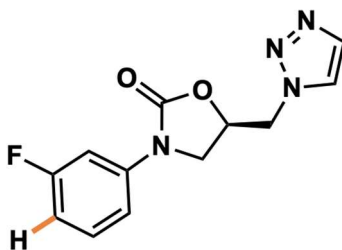


1-ethyl-8-(((1R,2R)-2-hydroxycyclopentyl)amino)-3-(2-hydroxyethyl)-7-(4-methoxybenzyl)-3,7-dihydro-1H-purine-2,6-dione (32): From **X12**, 23 mg (53%) was obtained following General Procedure A with the modification that a Penn PhD Photoreactor M2 equipped with a 405 nm light source was used to irradiate and no cyclohexylthiol was added. Product was isolated via mass-

directed reversed phase chromatography using MeCN/H₂O with an NH₄OH modifier. **¹H NMR** (600 MHz, DMSO-d₆) δ 7.23 (d, J = 8.3 Hz, 2H), 6.94 (d, J = 6.6 Hz, 1H), 6.87 (d, J = 8.2 Hz, 2H), 5.25 (s, 2H), 4.84 – 4.75 (m, 2H), 3.98 (t, J = 6.4 Hz, 3H), 3.87 (dq, J = 13.8, 6.5 Hz, 3H), 3.70 (s, 3H), 3.62 (q, J = 5.9 Hz, 2H), 2.05 (dq, J = 13.4, 7.6 Hz, 1H), 1.84 (dq, J = 14.2, 6.8 Hz, 1H), 1.64 (ddt, J = 21.7, 13.6, 7.4 Hz, 2H), 1.52 – 1.40 (m, 2H), 1.08 (t, J = 6.9 Hz, 3H). **¹³C NMR** (151 MHz, DMSO-d₆) δ 158.62, 153.45, 152.55, 150.42, 148.67, 129.22, 128.82, 113.86, 101.19, 76.10, 61.49, 57.80, 55.05, 44.63, 44.61, 35.13, 32.43, 29.90, 20.53, 13.34. **HRMS** (ESI⁺) Calc: [M+H]⁺ (C₂₂H₂₉N₅O₅) 444.2247; measured 444.2253 = 1.3 ppm difference.

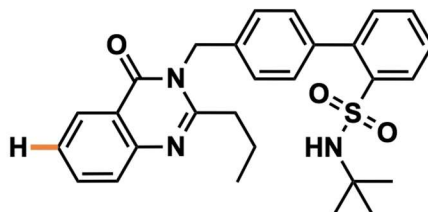


tert-butyl (S,Z)-(1,4-dimethyl-6-oxo-4-(thiophen-2-yl)tetrahydropyrimidin-2(1H)-ylidene) carbamate (33): From **X13**, 12 mg (38%) was obtained as a yellow oil following General Procedure A with the modification that a Penn PhD Photoreactor M2 equipped with a 405 nm light source was used to irradiate and no cyclohexylthiol was added. Product was isolated via mass-directed reversed phase chromatography using MeCN/H₂O with an NH₄OH modifier. **¹H NMR** (600 MHz, DMSO-d₆) δ 10.05 (s, 1H), 7.46 (d, J = 5.0 Hz, 1H), 7.06 – 7.03 (m, 1H), 7.00 (dd, J = 4.9, 3.7 Hz, 1H), 3.24 – 3.12 (m, 2H), 3.04 (s, 3H), 1.70 (s, 3H), 1.43 (s, 9H). **¹³C NMR** (151 MHz, DMSO-d₆) δ 167.63, 163.12, 156.84, 148.47, 127.51, 125.37, 124.09, 78.57, 52.88, 44.54, 31.31, 29.64, 27.92. **HRMS** (ESI⁺) Calc: [M+H]⁺ (C₁₅H₂₁N₃O₃S) 324.1382; measured 324.1379 = – 0.9 ppm difference.

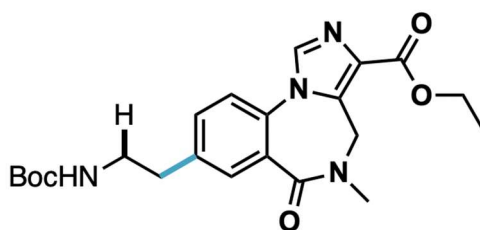


(R)-5-((1H-1,2,3-triazol-1-yl)methyl)-3-(3-fluorophenyl)oxazolidin-2-one (34): From **X14**, 16 mg (42%) was obtained as a white solid following General Procedure A with the modification that a Penn PhD Photoreactor M2 equipped with a 405 nm light source was used to irradiate and no cyclohexylthiol was added. Product was isolated via mass-directed reversed phase chromatography using MeCN/H₂O with an NH₄OH modifier. Alternatively, on a 0.022 mmol scale, 2.9 mg (50%) was obtained as a white solid following General Procedure A with the same modifications as mentioned above. **¹H NMR** (600 MHz, DMSO-d₆) δ 8.17 (d, J = 0.8 Hz, 1H), 7.77 – 7.75 (m, 1H), 7.46 – 7.39 (m, 2H), 7.26 (dd, J = 8.3, 1.5 Hz, 1H), 6.96 (td, J = 8.2, 2.3 Hz, 1H), 5.15 (dq, J = 10.9, 5.4 Hz, 1H), 4.84 (d, J = 5.2 Hz, 2H), 4.25 (t, J = 9.2 Hz, 1H), 3.91 (dd, J = 9.3, 5.7 Hz, 1H). **¹³C NMR** (151 MHz, DMSO-d₆) δ 162.22 (d, J = 241.8 Hz), 153.44, 139.78 (d, J = 11.0 Hz), 133.41, 130.65 (d, J = 9.5 Hz), 125.87, 113.73, 110.17 (d, J = 21.1 Hz), 105.07 (d, J =

26.9 Hz), 70.93, 51.70, 47.02. **HRMS** (ESI+) Calc: $[M+H]^+$ (C₁₂H₁₁FN₄O₂) 263.0944; measured 263.0945 = 0.3 ppm difference.

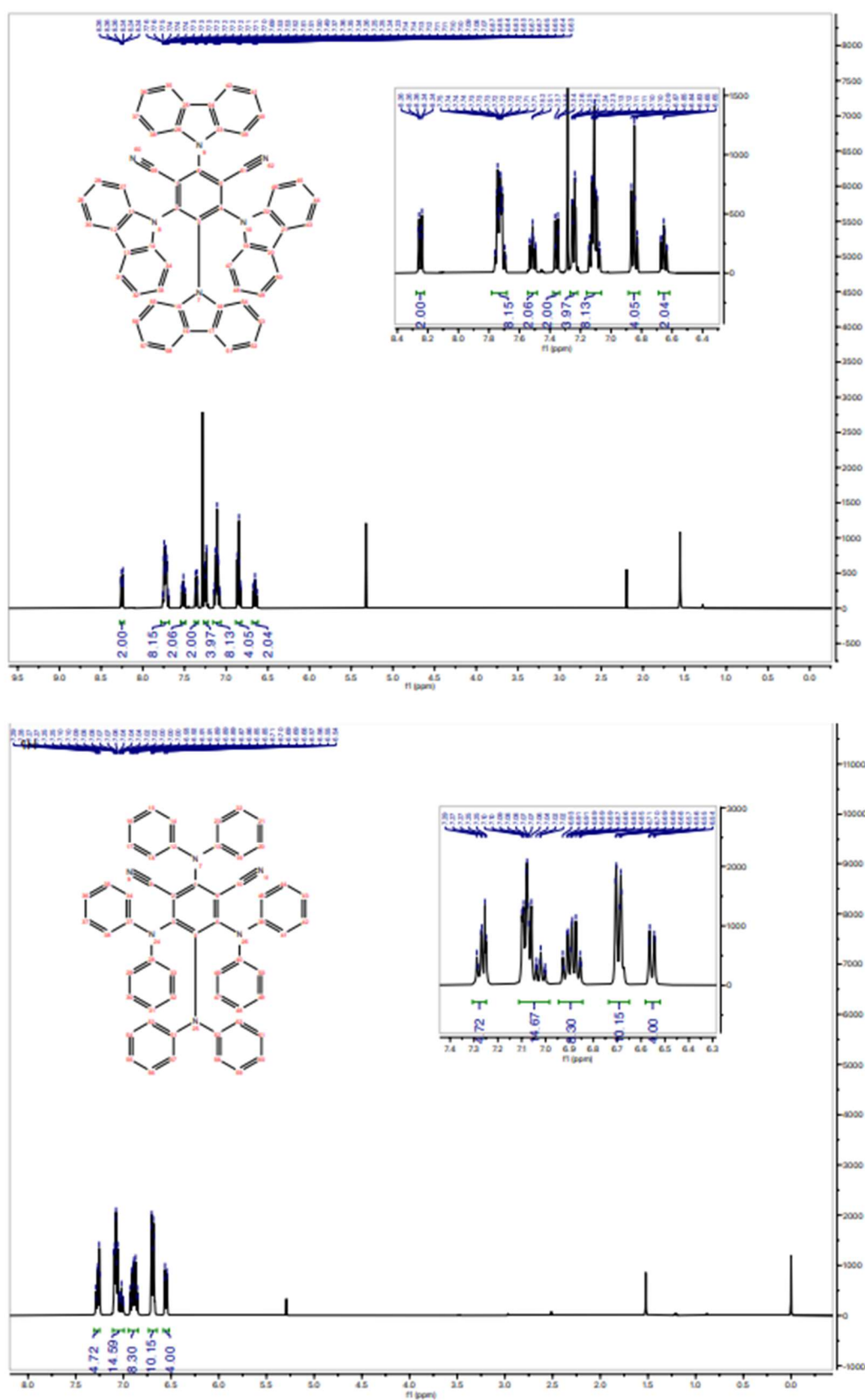


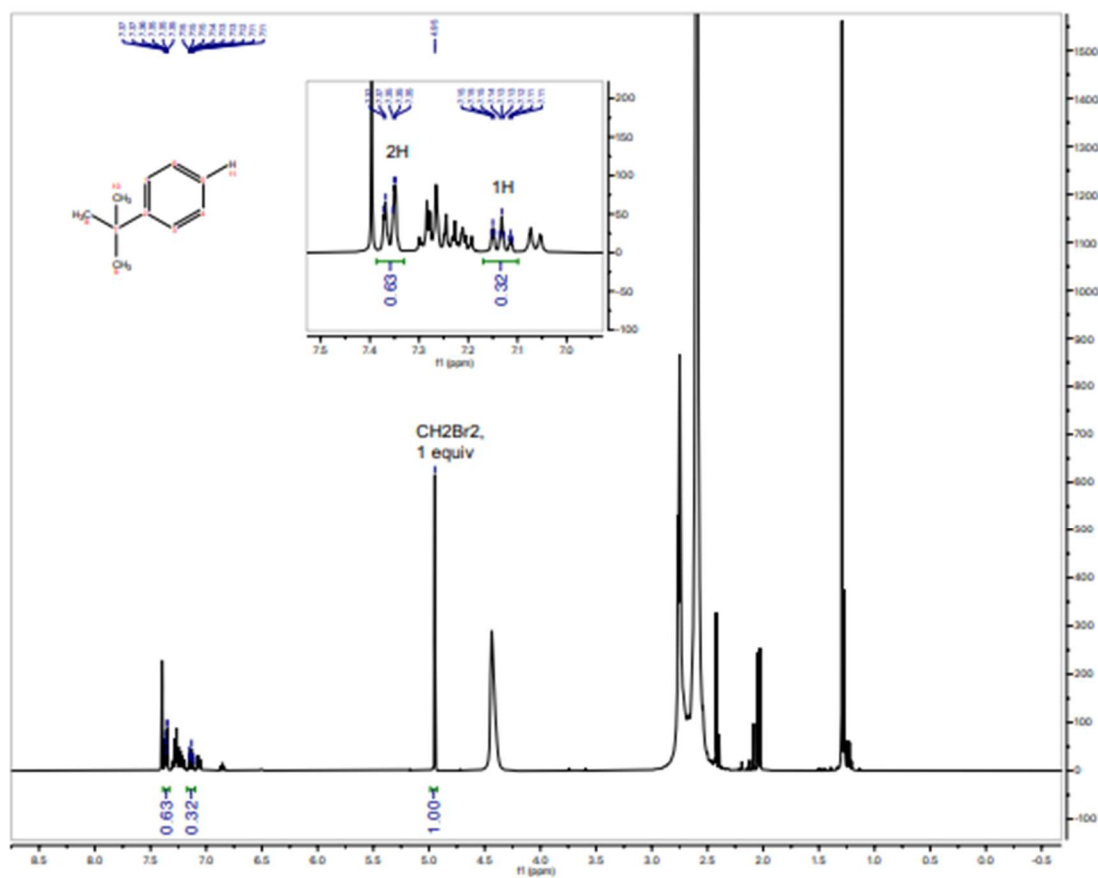
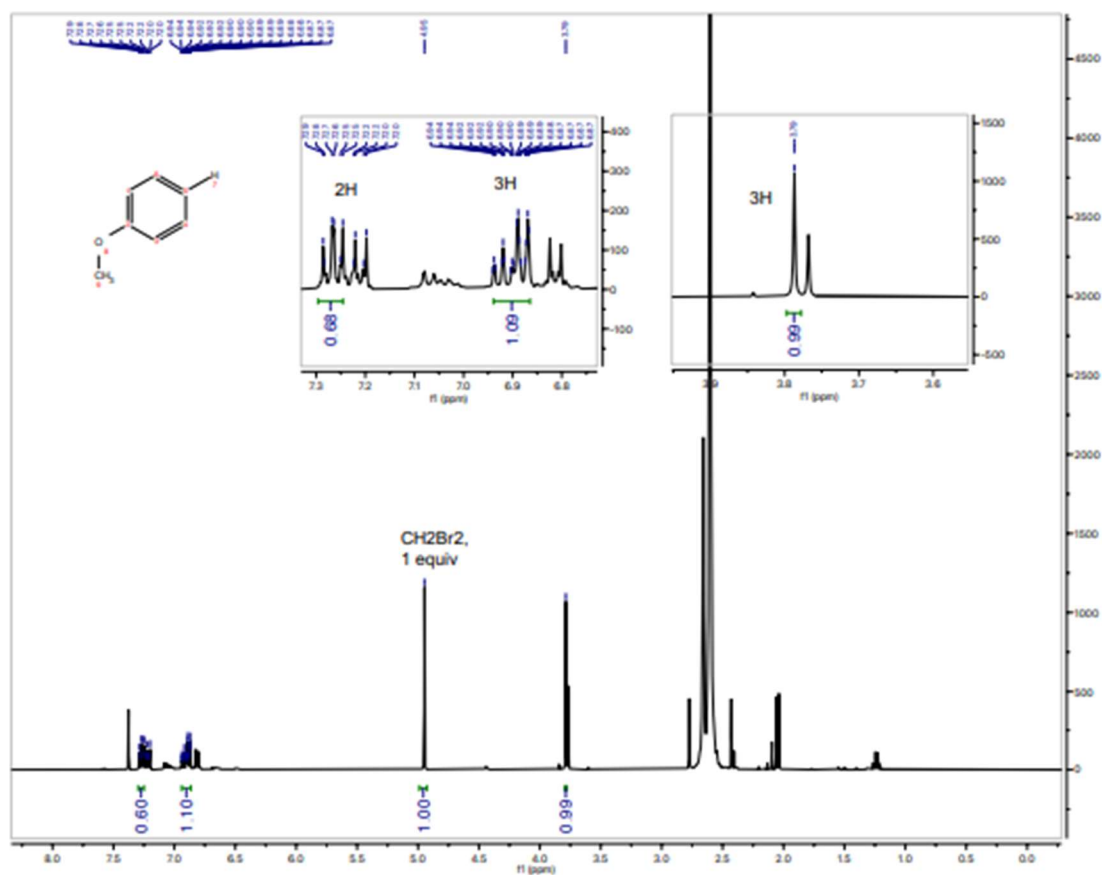
N-(tert-butyl)-4'-((4-oxo-2-propylquinazolin-3(4H)-yl)methyl)-[1,1'-biphenyl]-2-sulfonamide (35): From **X15**, 19 mg (39%) was obtained following General Procedure A with the modification that a Penn PhD Photoreactor M2 equipped with a 405 nm light source was used to irradiate and no cyclohexylthiol was added. Product was isolated via mass-directed reversed phase chromatography using MeCN/H₂O with an NH₄OH modifier. **¹H NMR** (600 MHz, DMSO-d₆) δ 8.18 (d, J = 7.9 Hz, 1H), 8.03 (d, J = 7.9 Hz, 1H), 7.83 (t, J = 7.7 Hz, 1H), 7.65 (d, J = 8.2 Hz, 1H), 7.61 (t, J = 7.4 Hz, 1H), 7.54 (q, J = 7.8 Hz, 2H), 7.38 (d, J = 6.9 Hz, 2H), 7.29 (d, J = 7.6 Hz, 1H), 7.21 (d, J = 7.3 Hz, 2H), 6.54 (s, 1H), 5.45 (s, 2H), 2.77 (t, J = 7.0 Hz, 2H), 1.76 (h, J = 7.2 Hz, 2H), 0.96 – 0.94 (m, 9H), 0.94 – 0.91 (m, 3H). **¹³C NMR** (151 MHz, DMSO-d₆) δ 161.66, 157.31, 146.99, 142.07, 139.58, 138.80, 135.78, 134.54, 132.58, 131.76, 129.65, 128.05, 127.74, 126.89, 126.50, 126.45, 125.58, 119.85, 53.35, 45.39, 35.79, 29.30, 19.41, 13.56. **HRMS** (ESI+) Calc: $[M+H]^+$ (C₂₈H₃₁N₃O₃S) 490.2164; measured 490.2172 = 1.6 ppm difference.

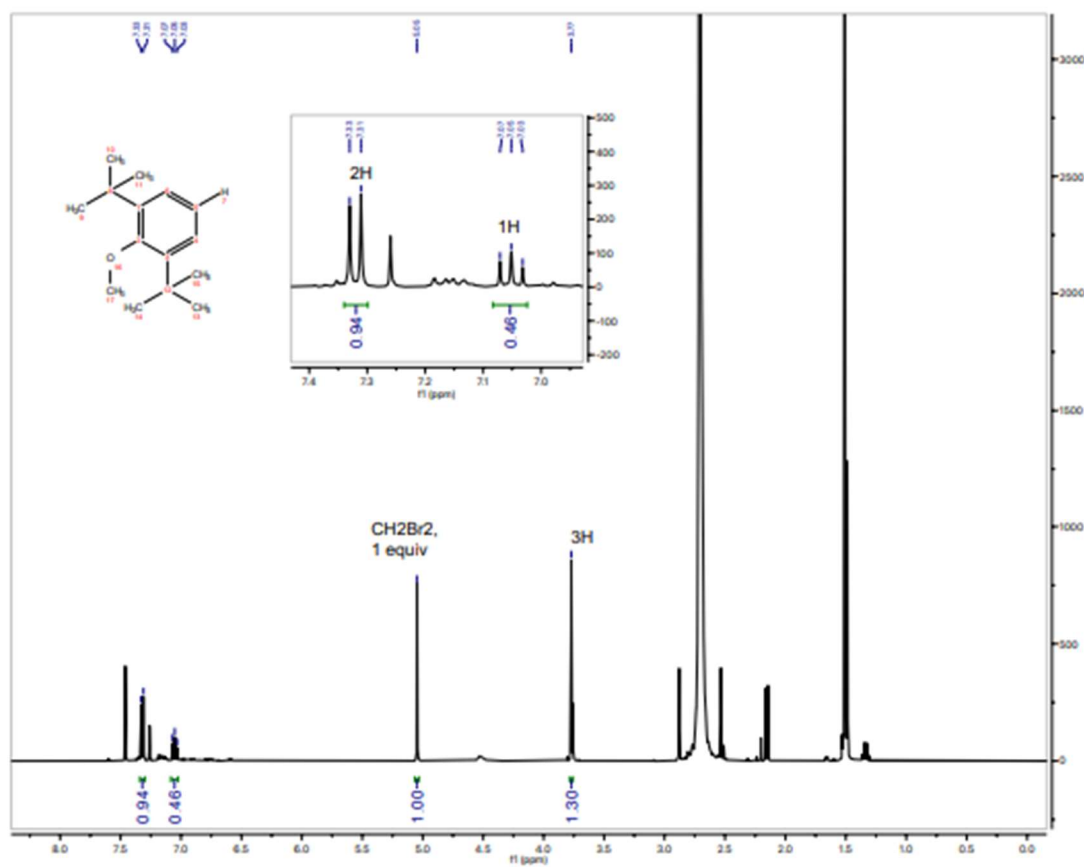
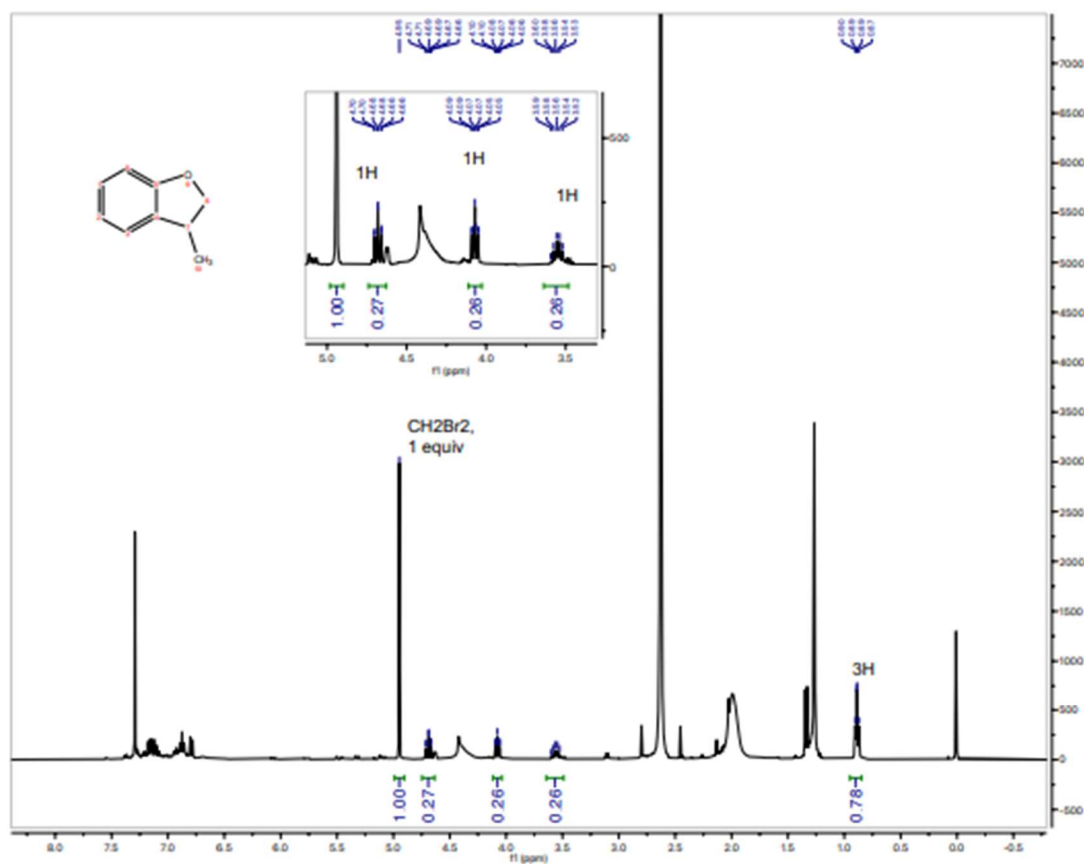


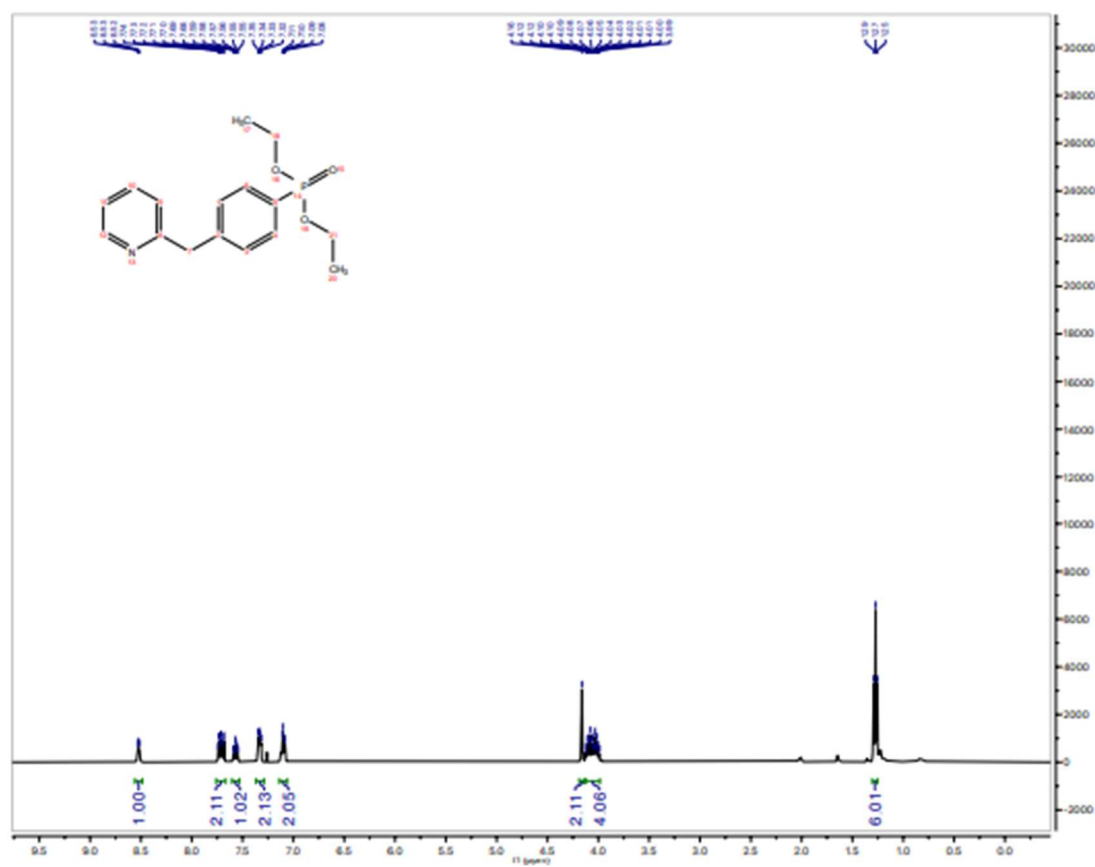
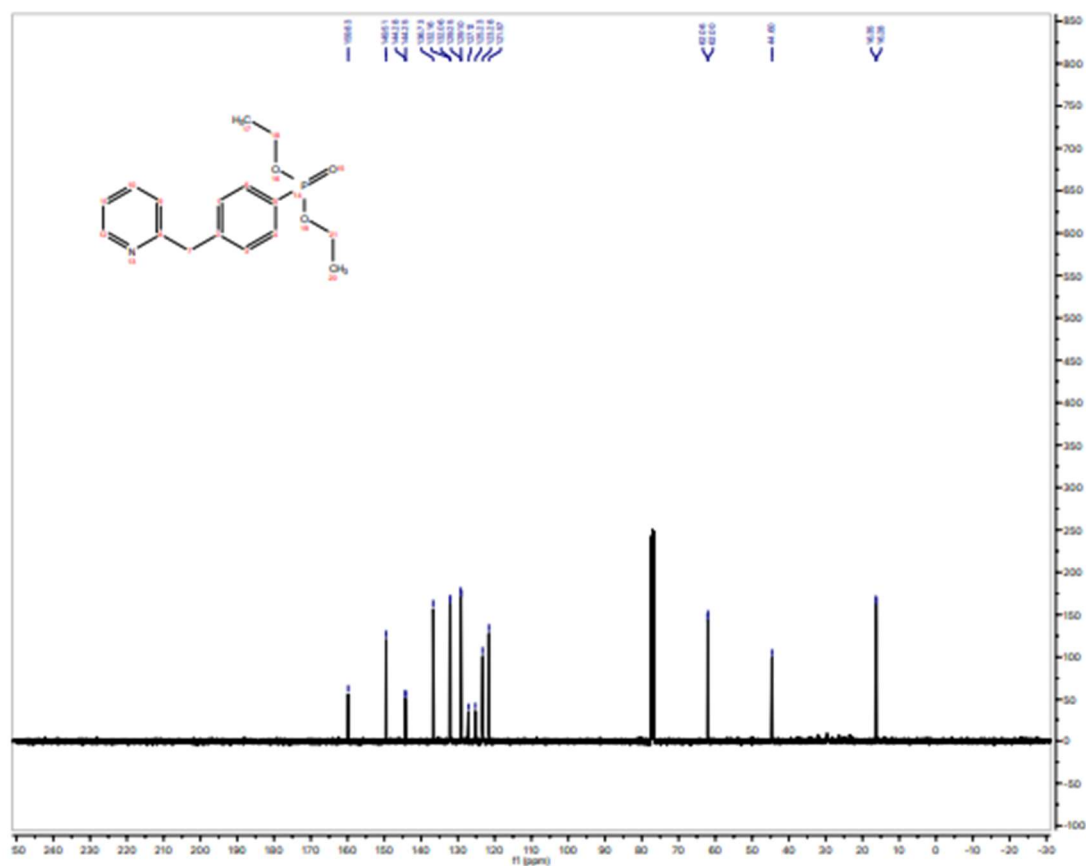
ethyl 8-(2-((tert-butoxycarbonyl)amino)ethyl)-5-methyl-6-oxo-5,6-dihydro-4H-benzo[f]imidazo[1,5-a][1,4]diazepine-3-carboxylate (36): From **X2**, 13 mg (29%) was obtained as a white solid following General Procedure E with the modification that a Penn PhD Photoreactor M2 equipped with a 405 nm light source was used to irradiate and 8 mol% cyclohexylthiol was added. In the reaction, an additional 4.4 mg (15%) of the reduction product was obtained as a white solid. Product was isolated via mass-directed reversed phase chromatography using MeCN/H₂O with an NH₄OH modifier. **¹H NMR** (600 MHz, DMSO-d₆) δ 8.33 (s, 1H), 7.73 (s, 1H), 7.66 (d, J = 8.2 Hz, 1H), 7.59 – 7.53 (m, 1H), 6.93 (t, J = 5.4 Hz, 1H), 4.98 (s, 1H), 4.41 (s, 1H), 4.32 (s, 2H), 3.20 (q, J = 6.8 Hz, 2H), 3.10 (s, 3H), 2.81 (t, J = 7.1 Hz, 2H), 1.36 (s, 9H), 1.33 (t, J = 7.1 Hz, 3H). **¹³C NMR** (151 MHz, DMSO-d₆) δ 165.75, 162.37, 155.57, 139.82, 136.31, 135.36, 132.97, 131.75, 130.06, 128.31, 127.54, 122.74, 77.61, 60.08, 42.01, 41.13, 35.09, 34.67, 28.23, 14.23. **HRMS** (ESI+) Calc: $[M+H]^+$ (C₂₂H₂₈N₄O₅) 429.2138; measured 429.2146 = 1.8 ppm difference.

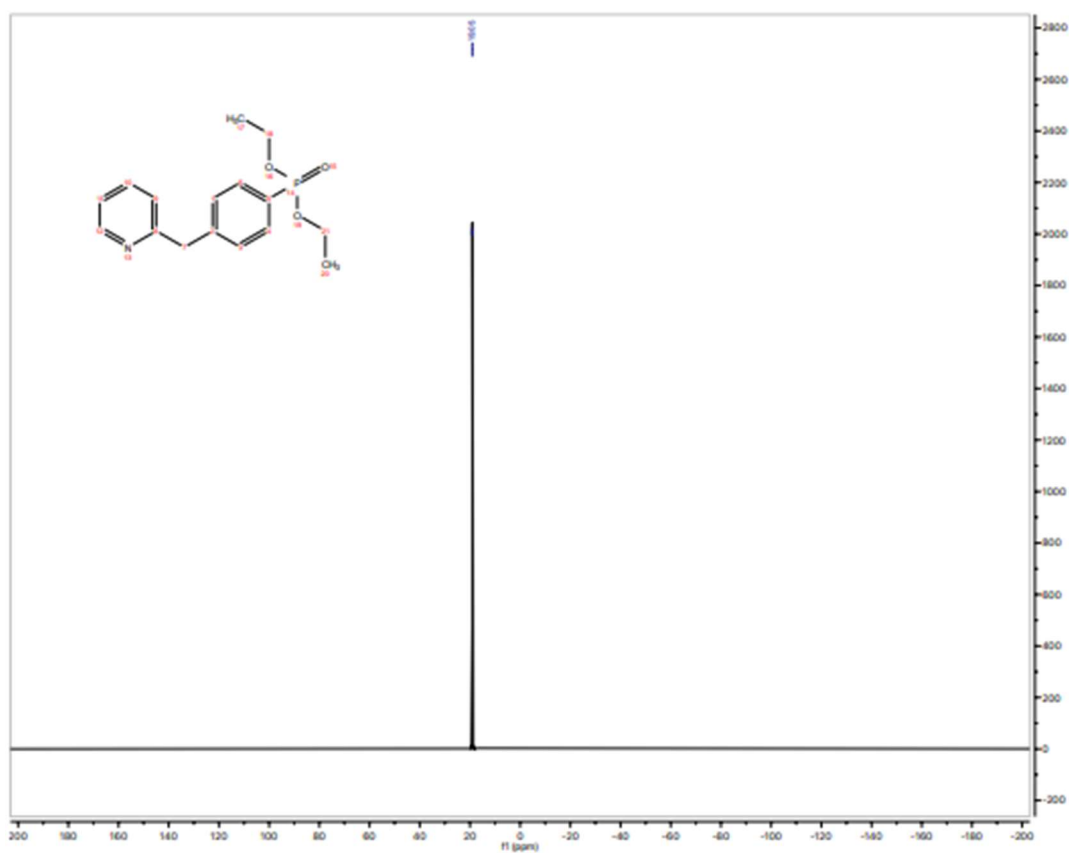
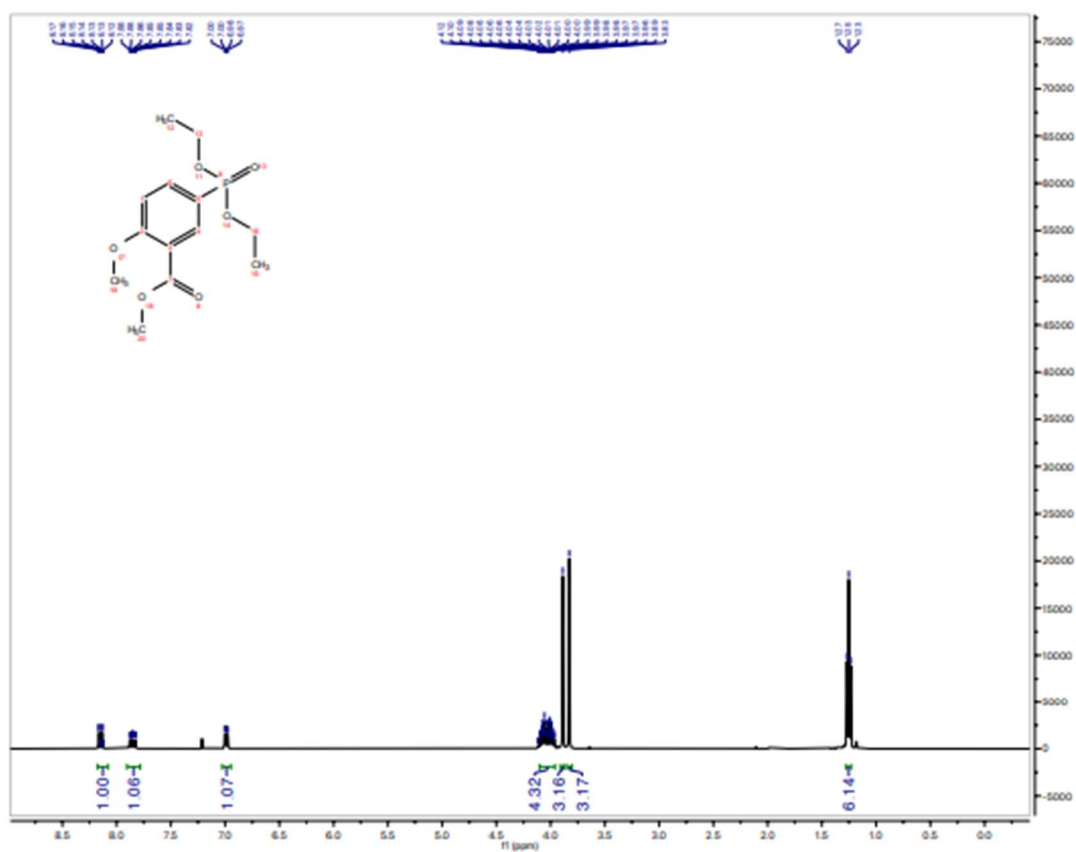
4.7.19 NMR Spectra

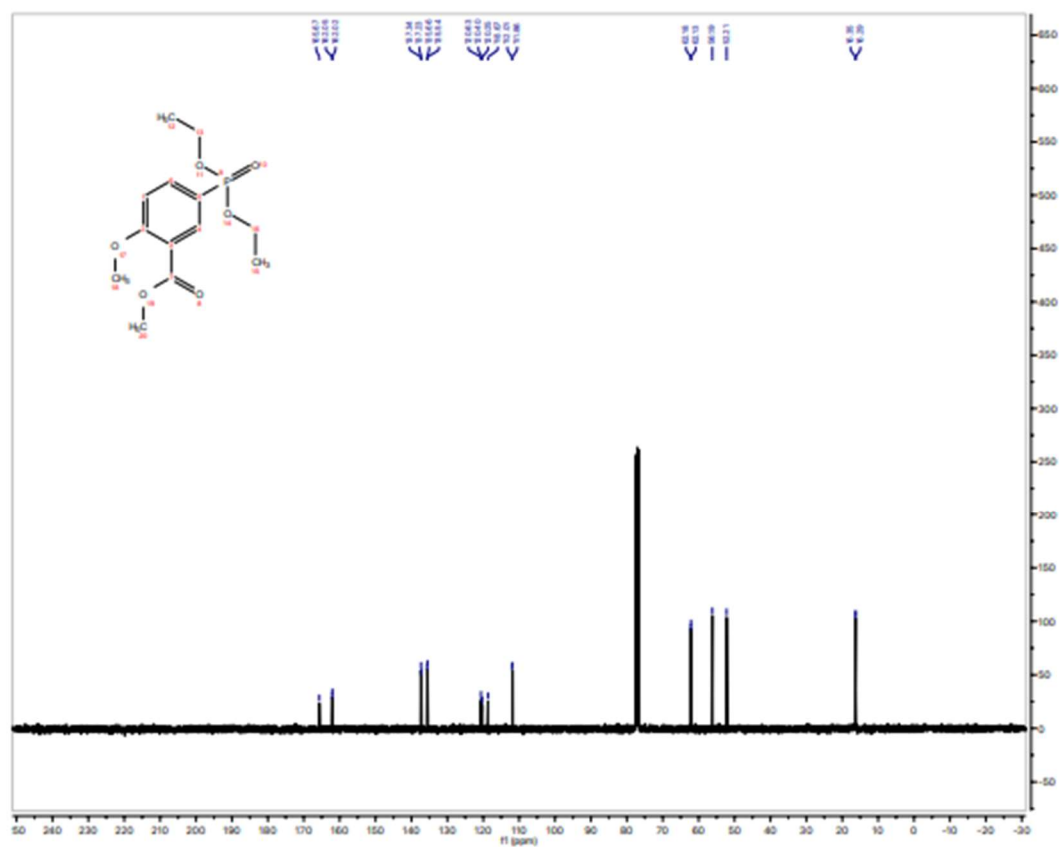
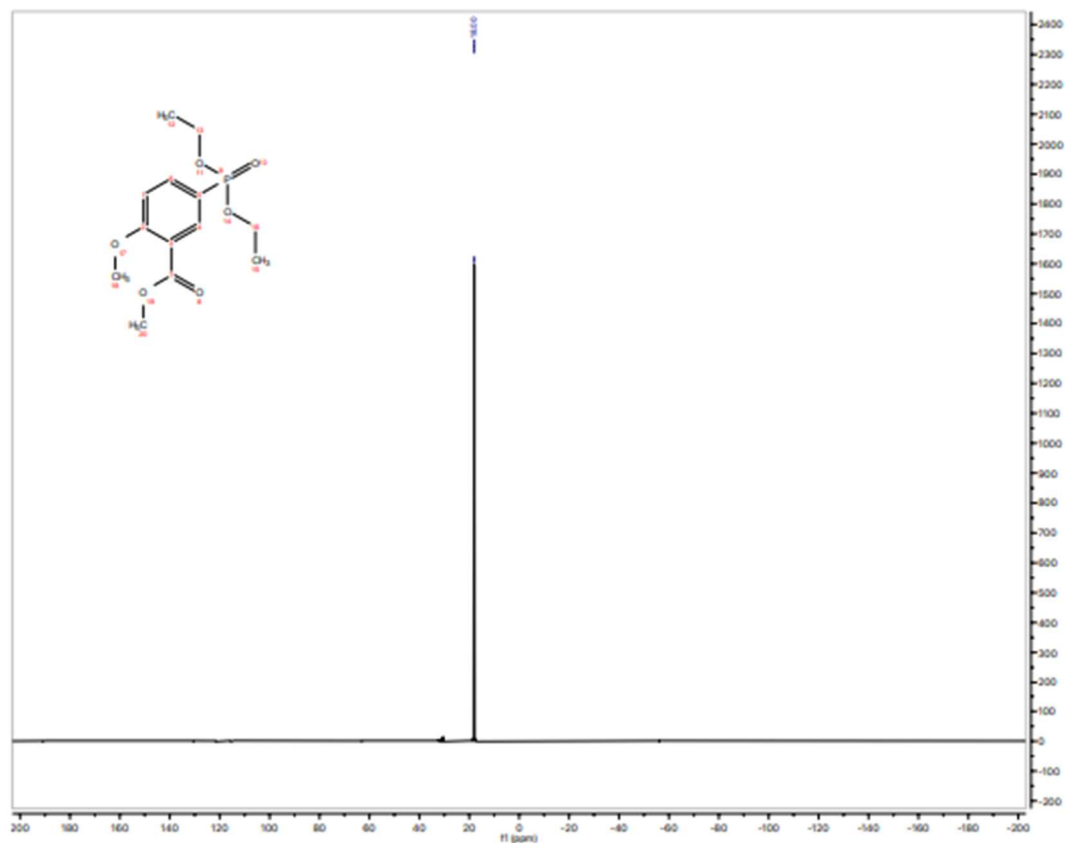


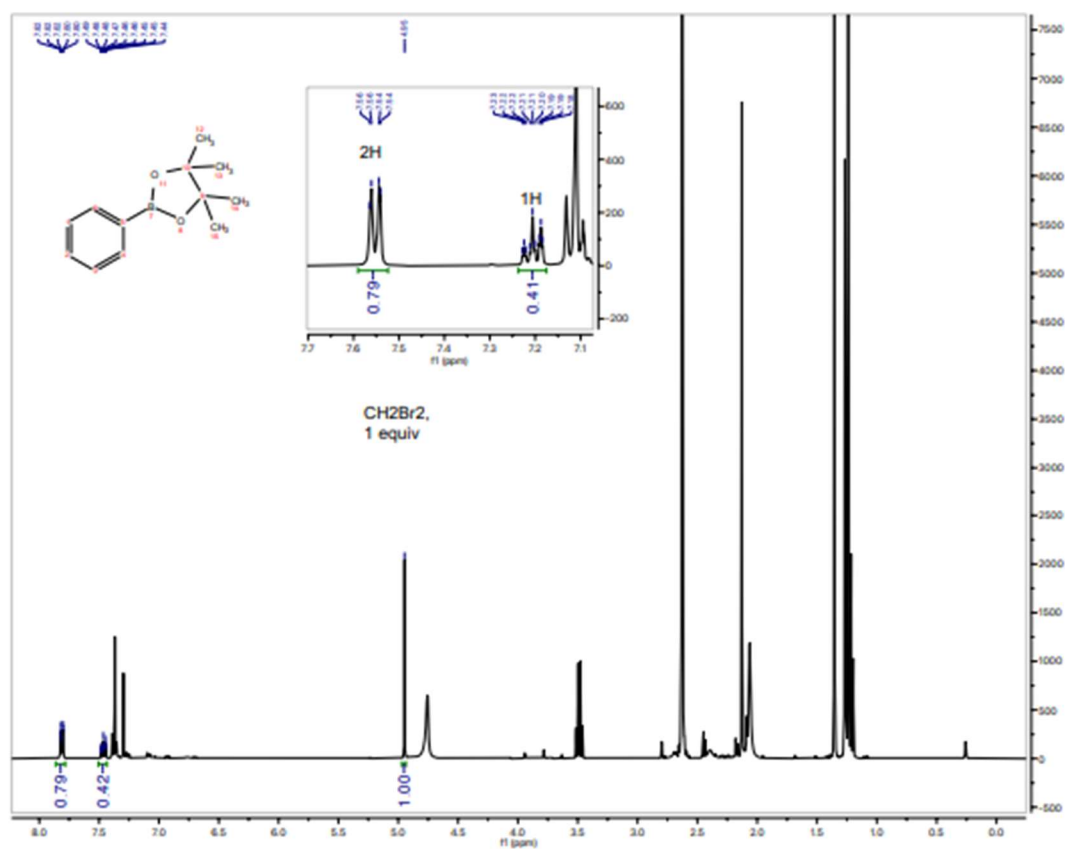
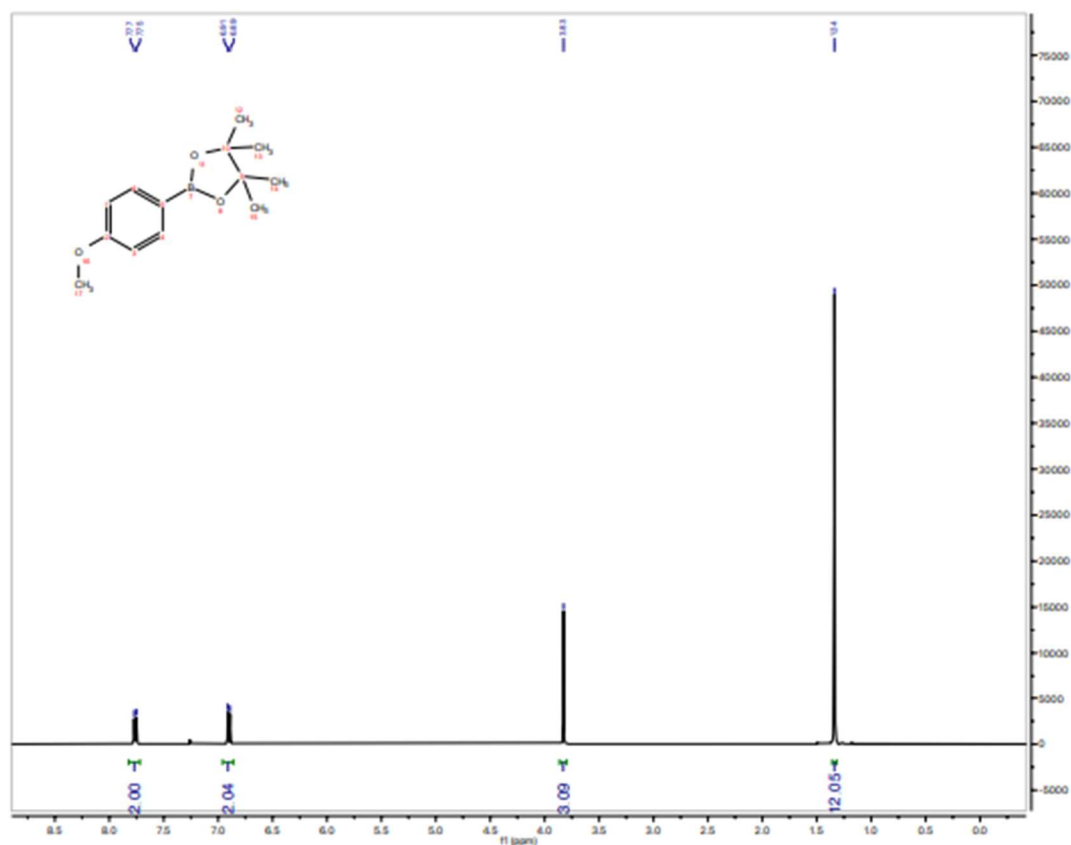


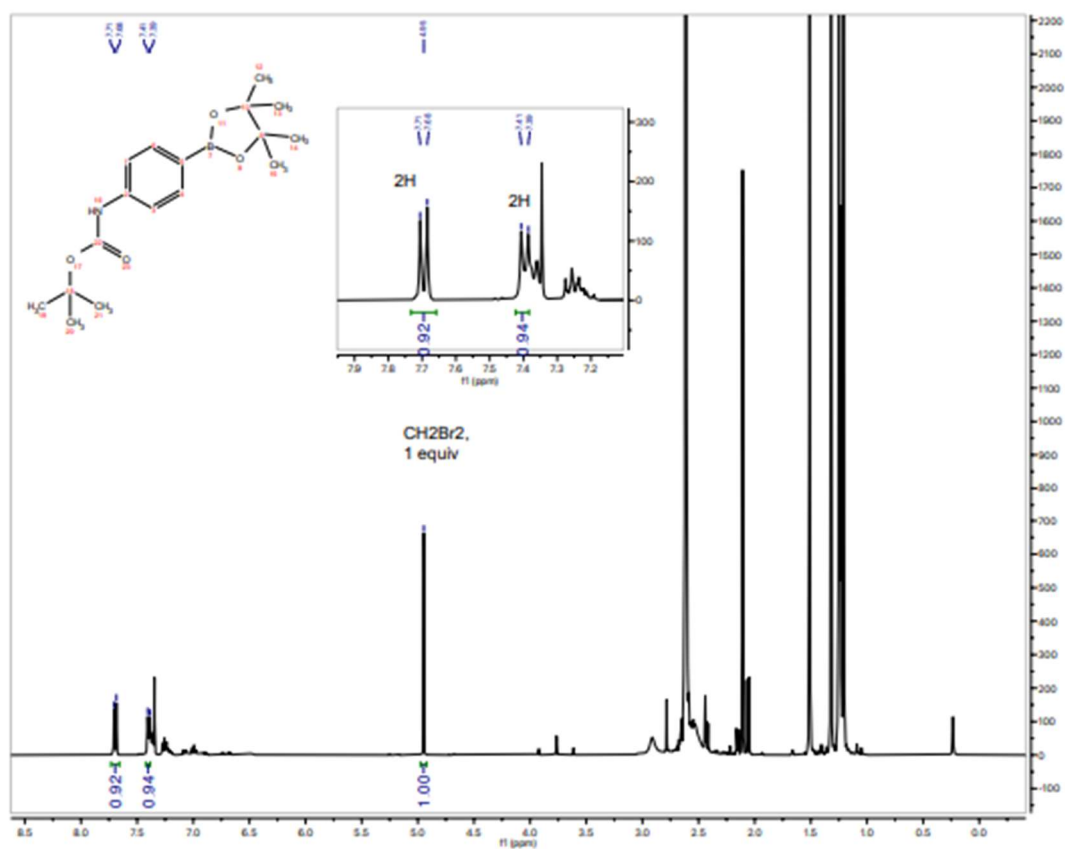
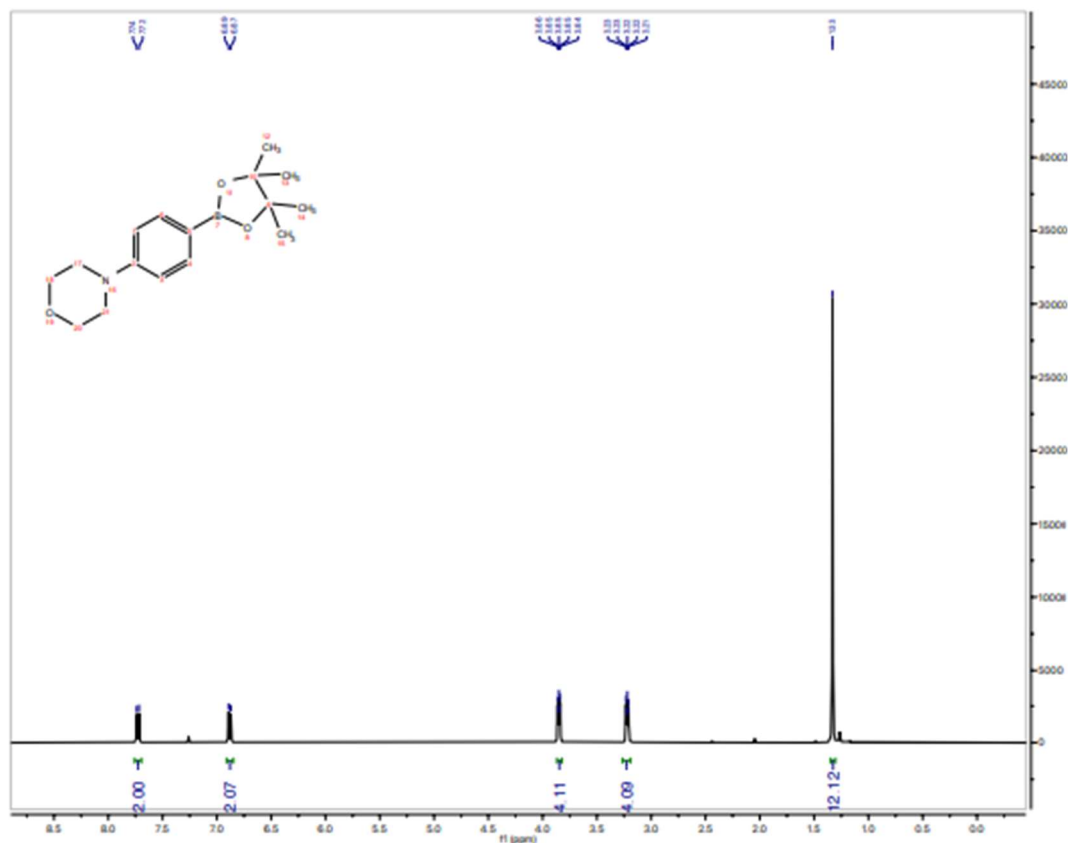


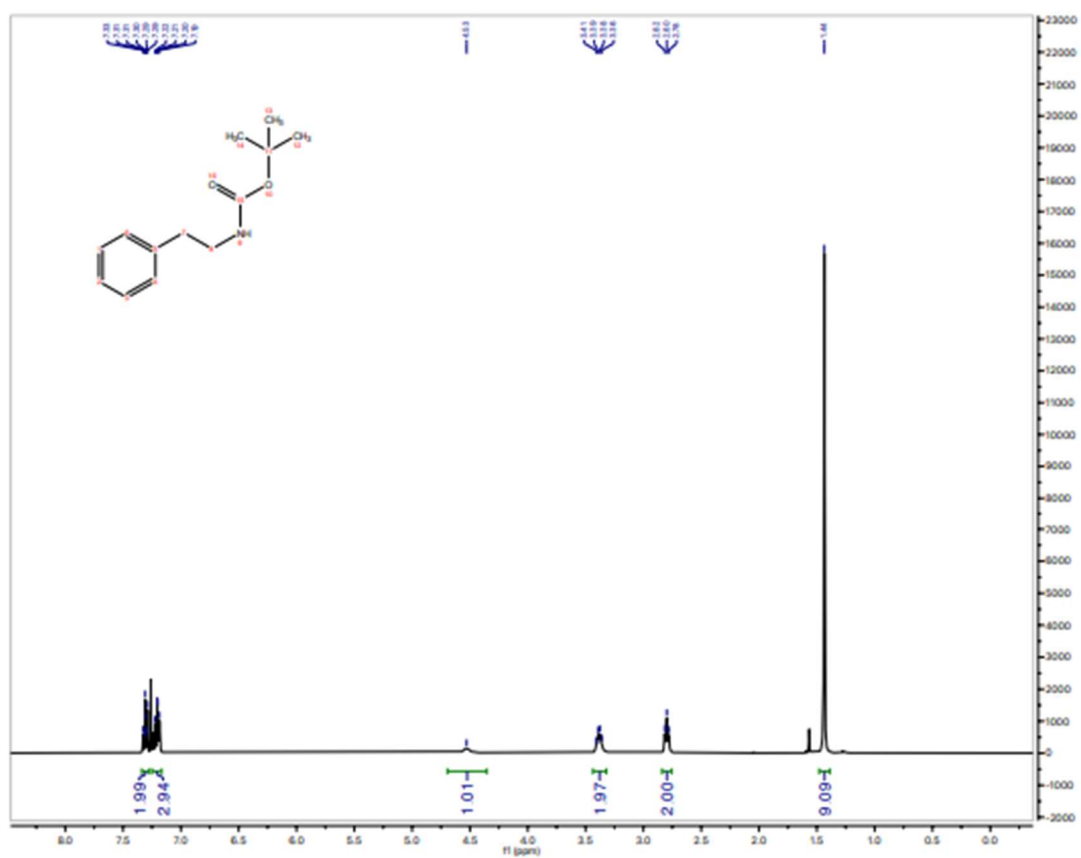
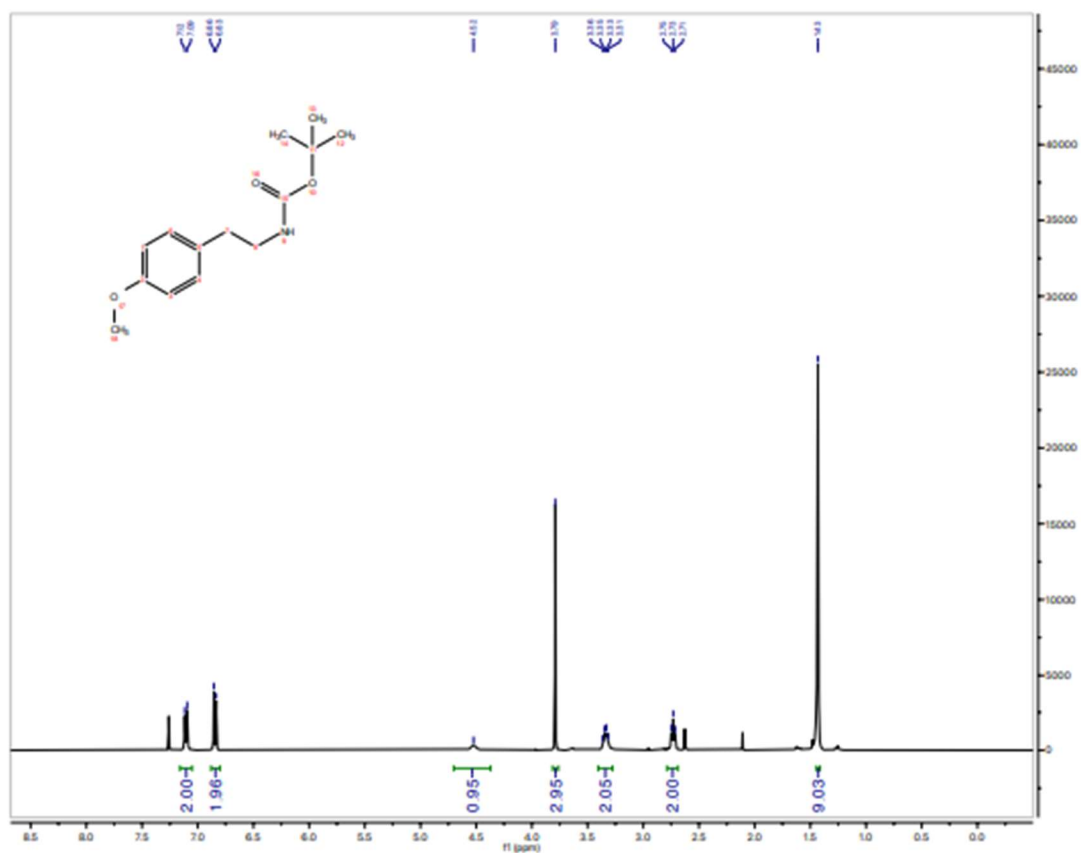


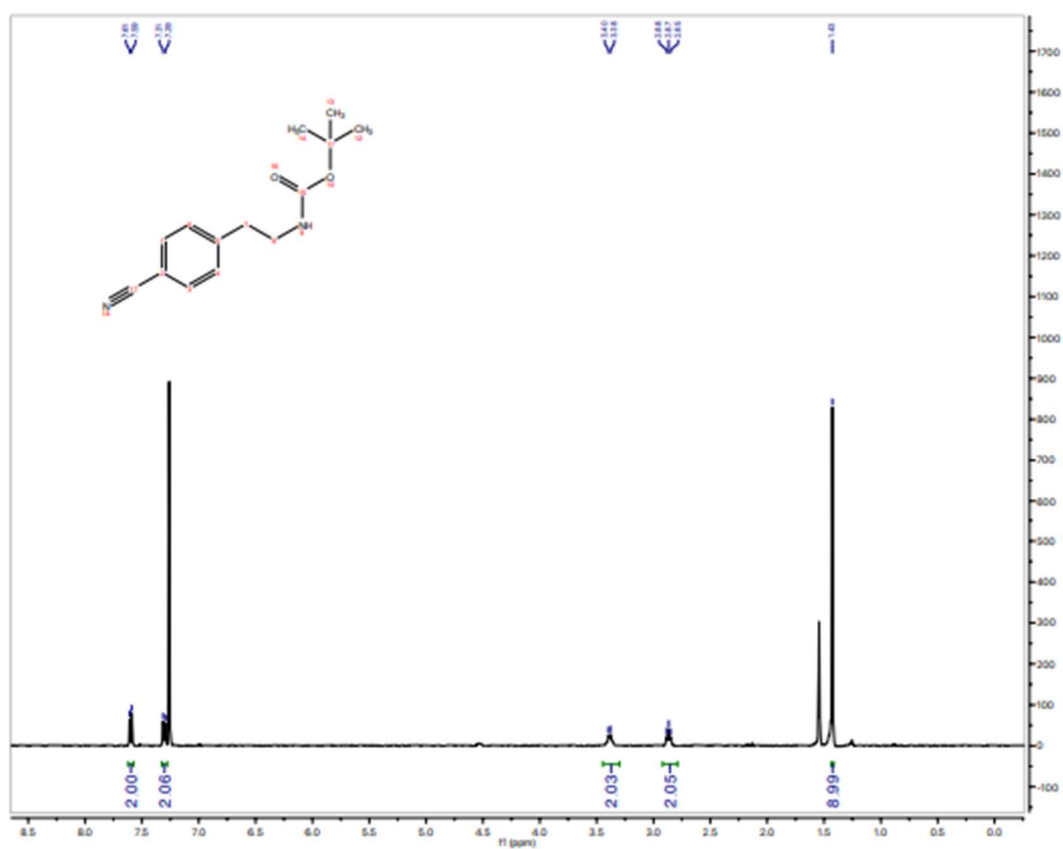
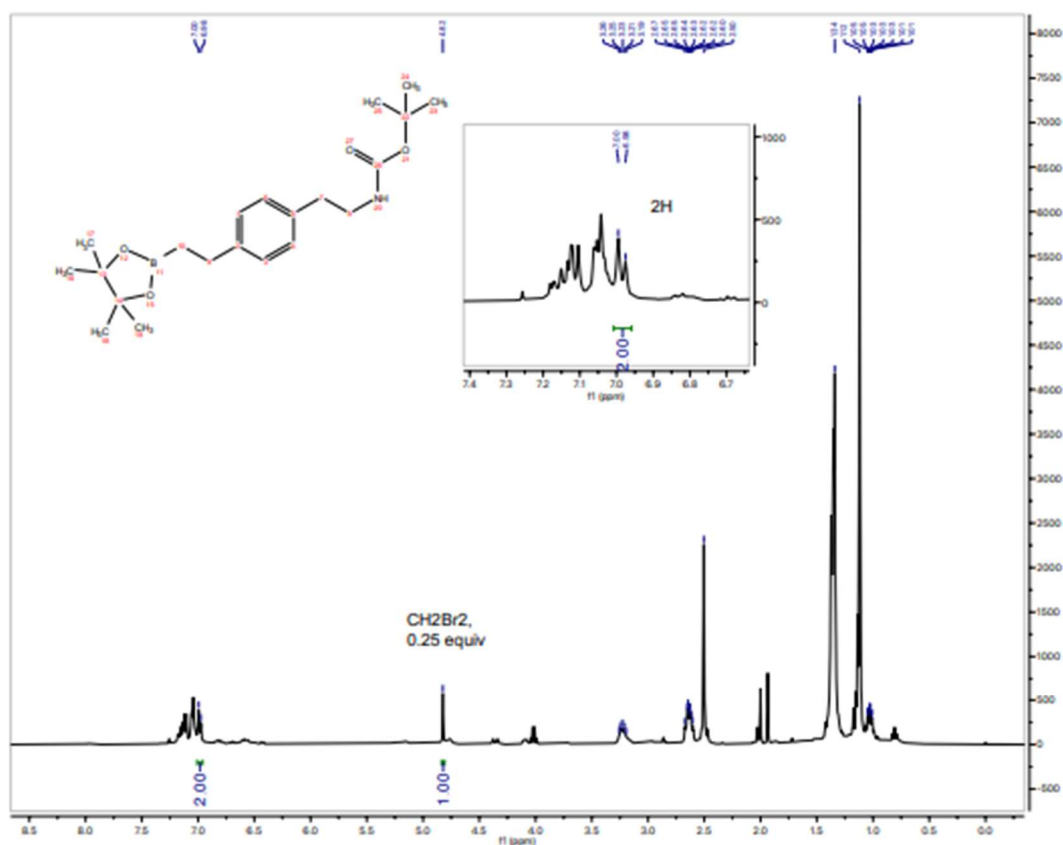


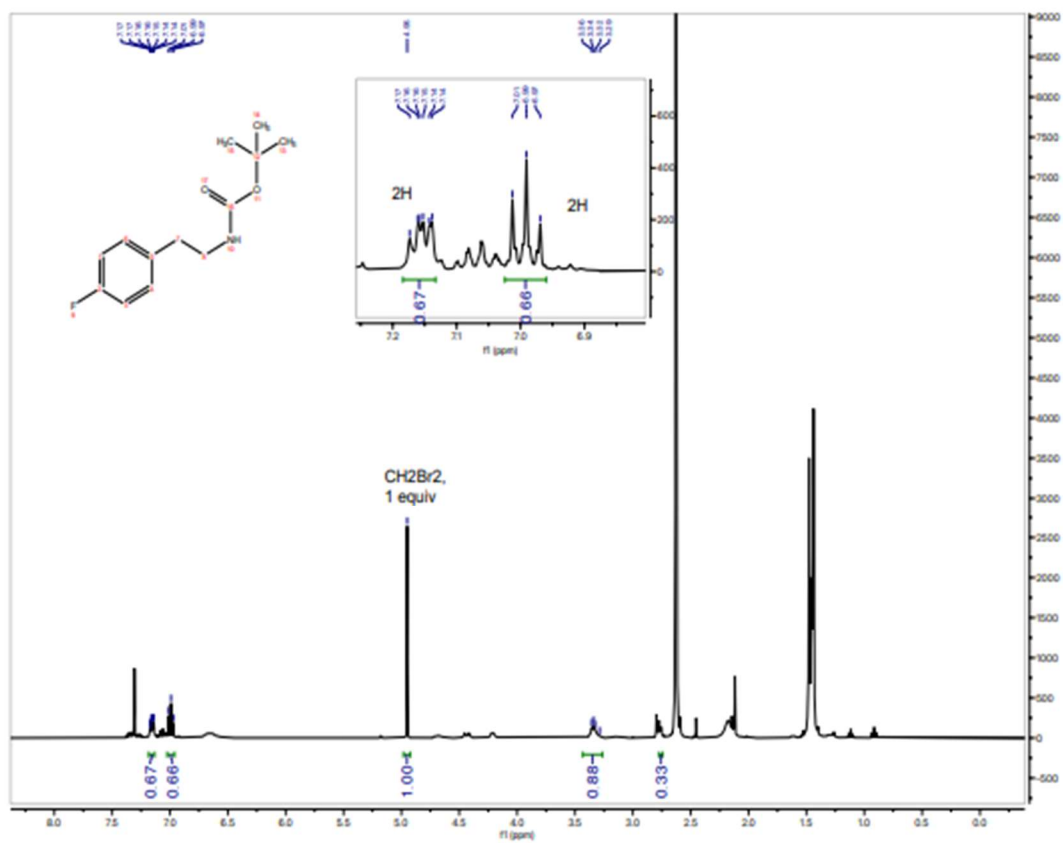
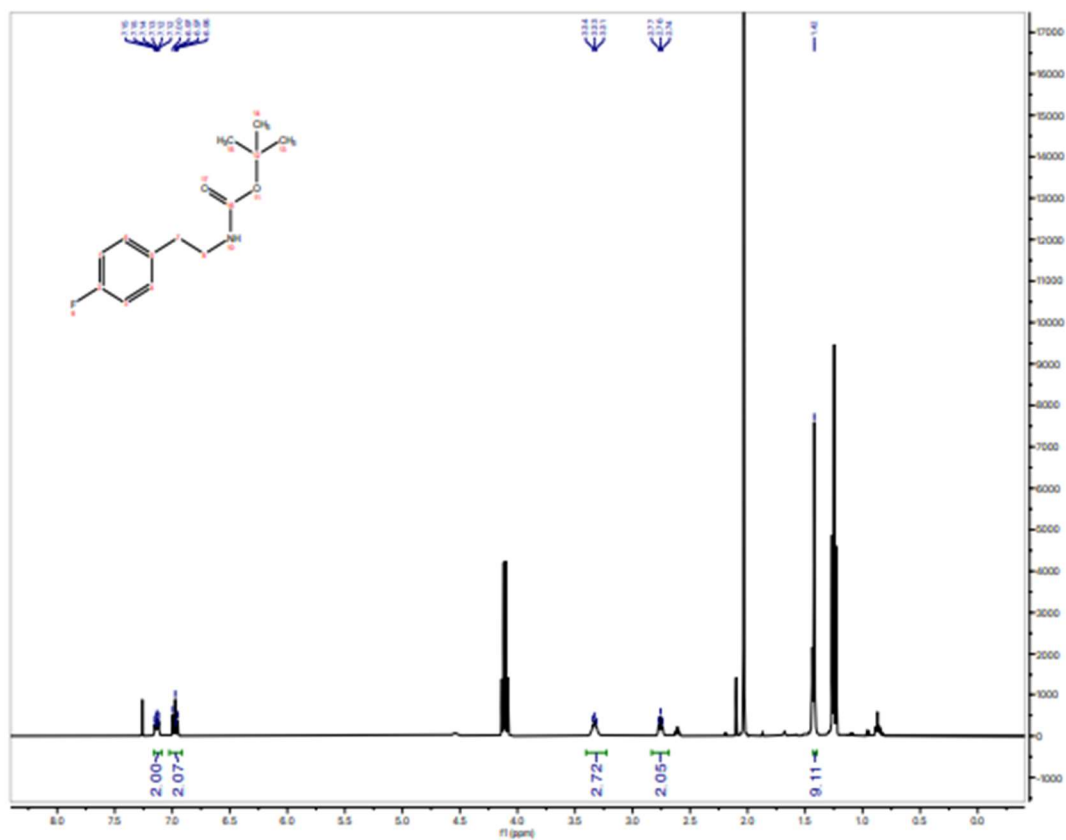


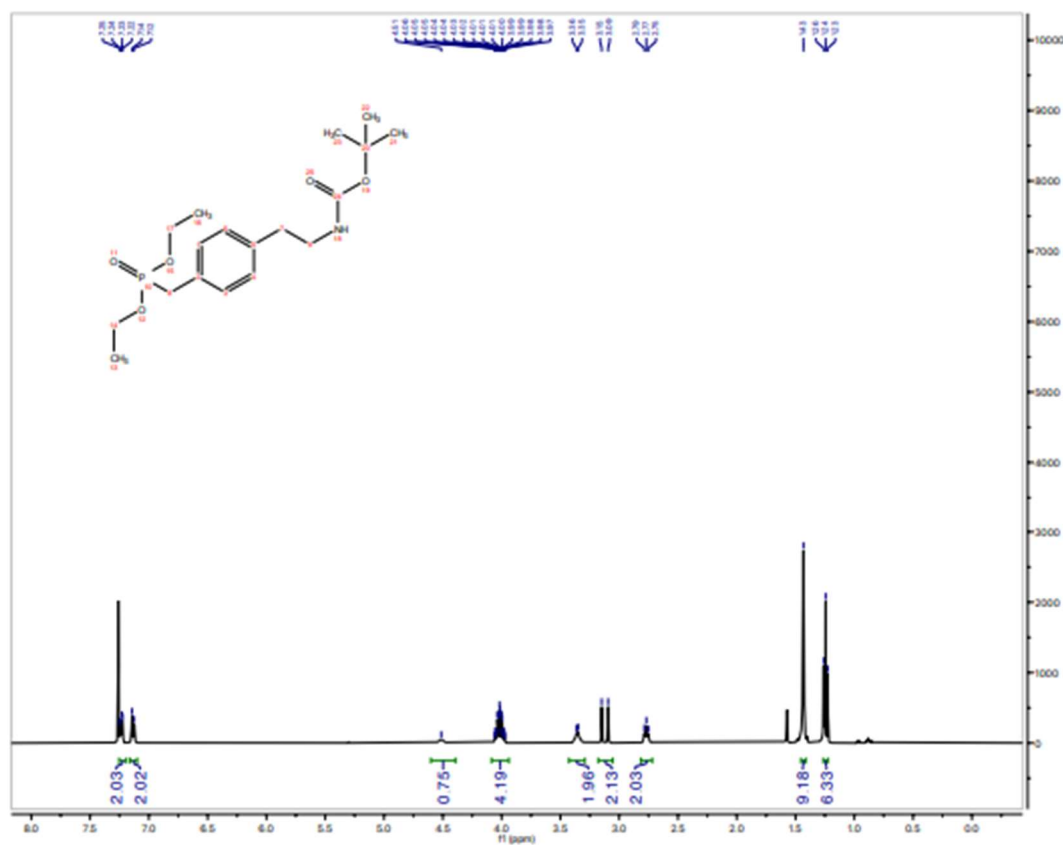
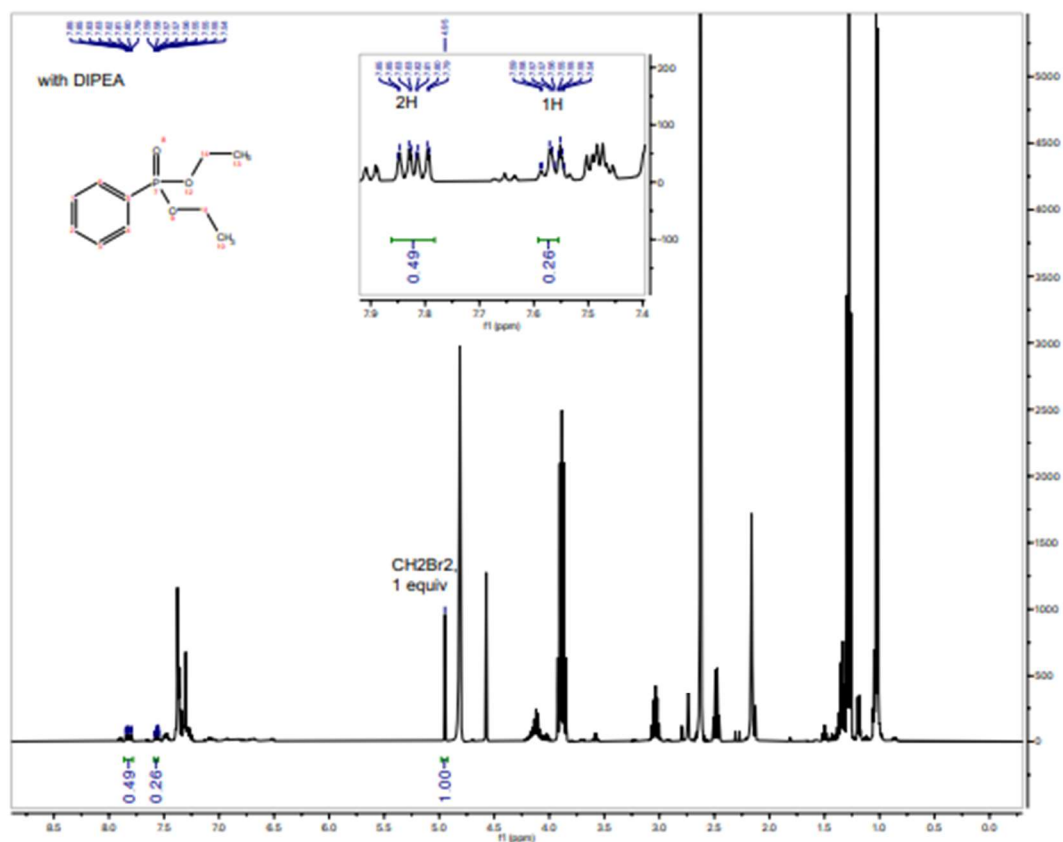


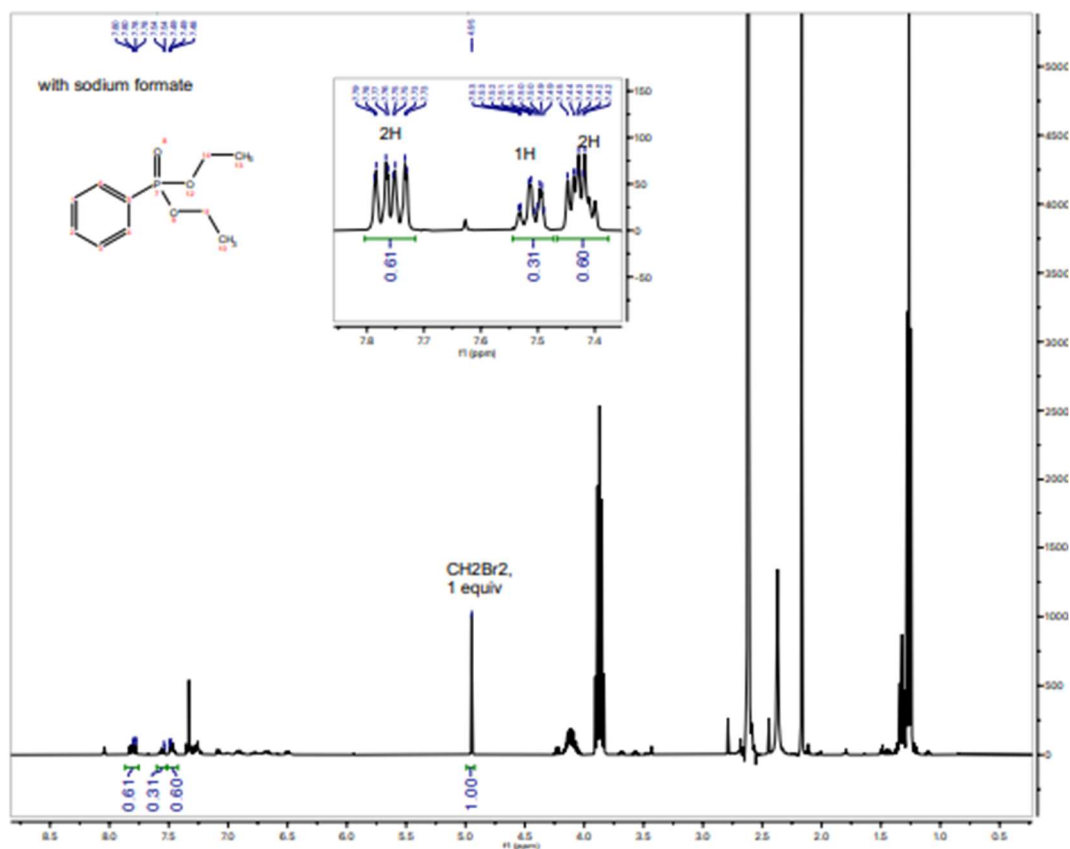
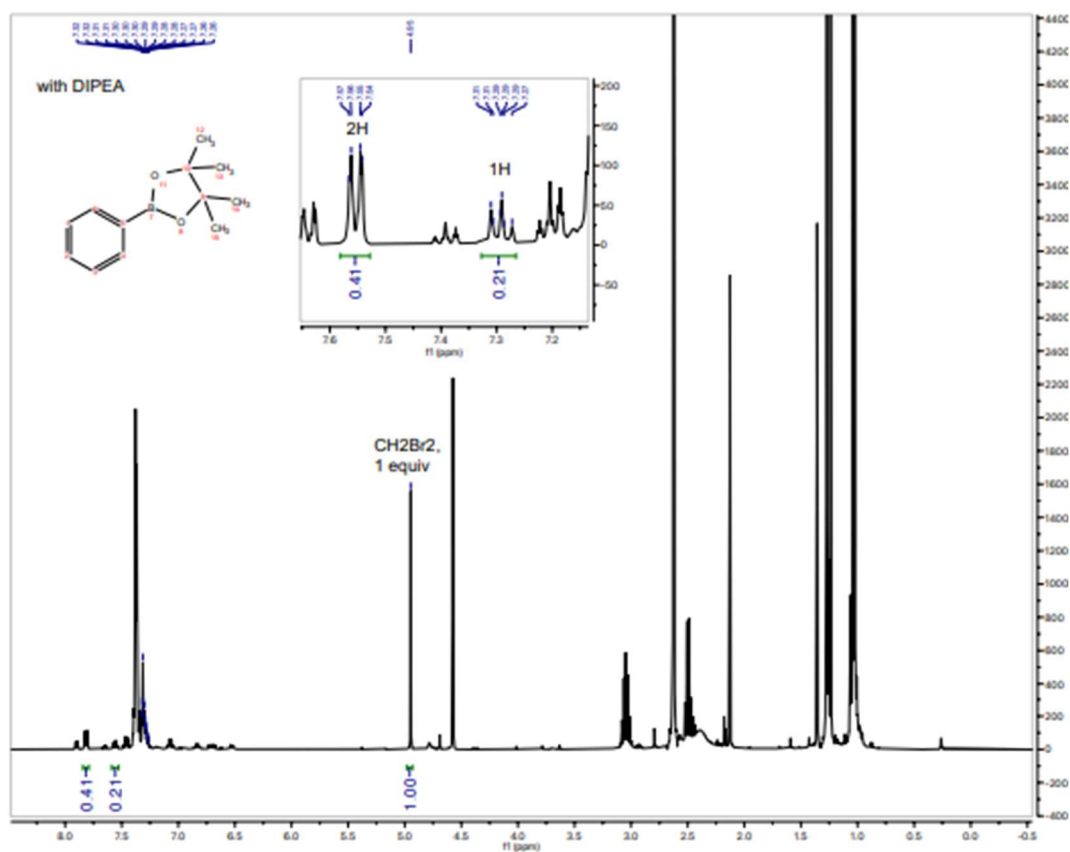


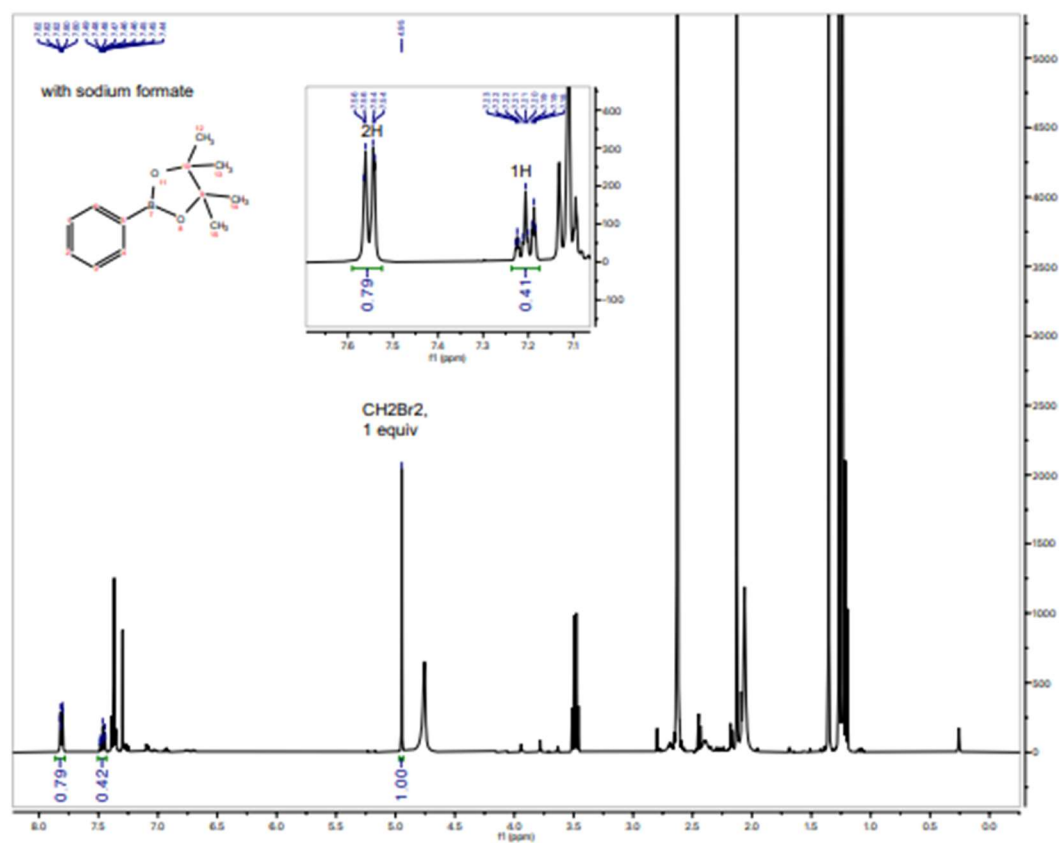
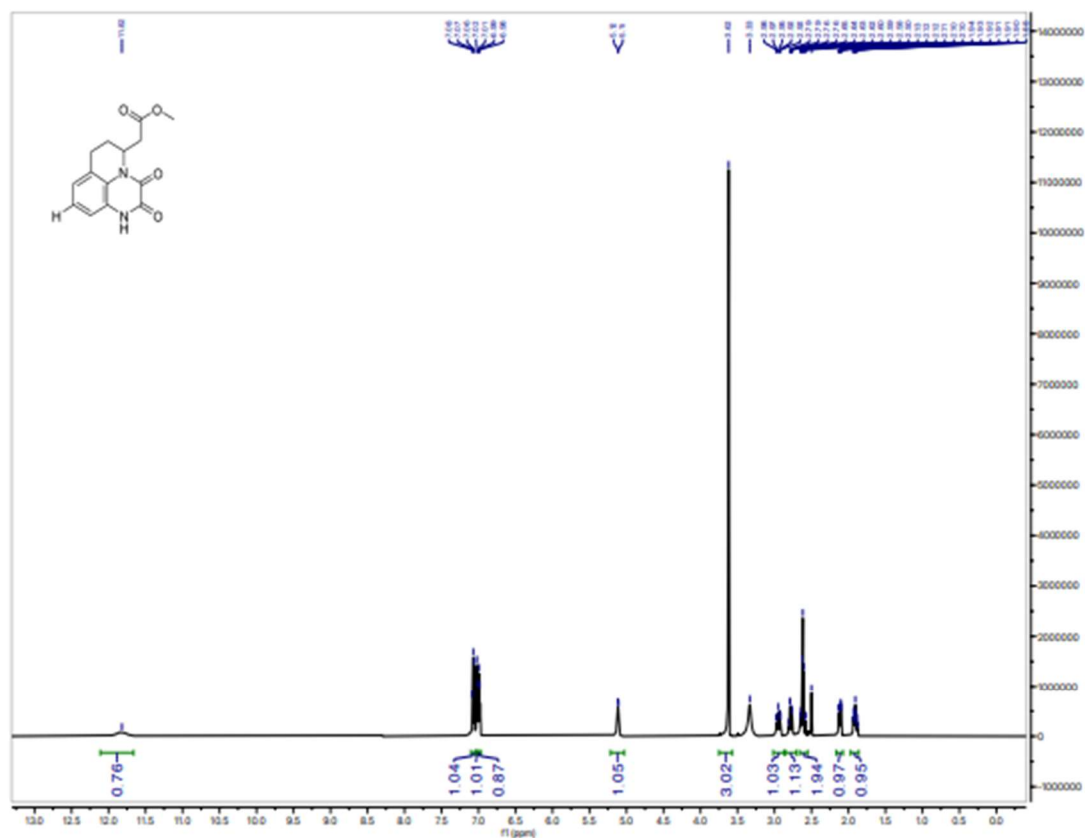


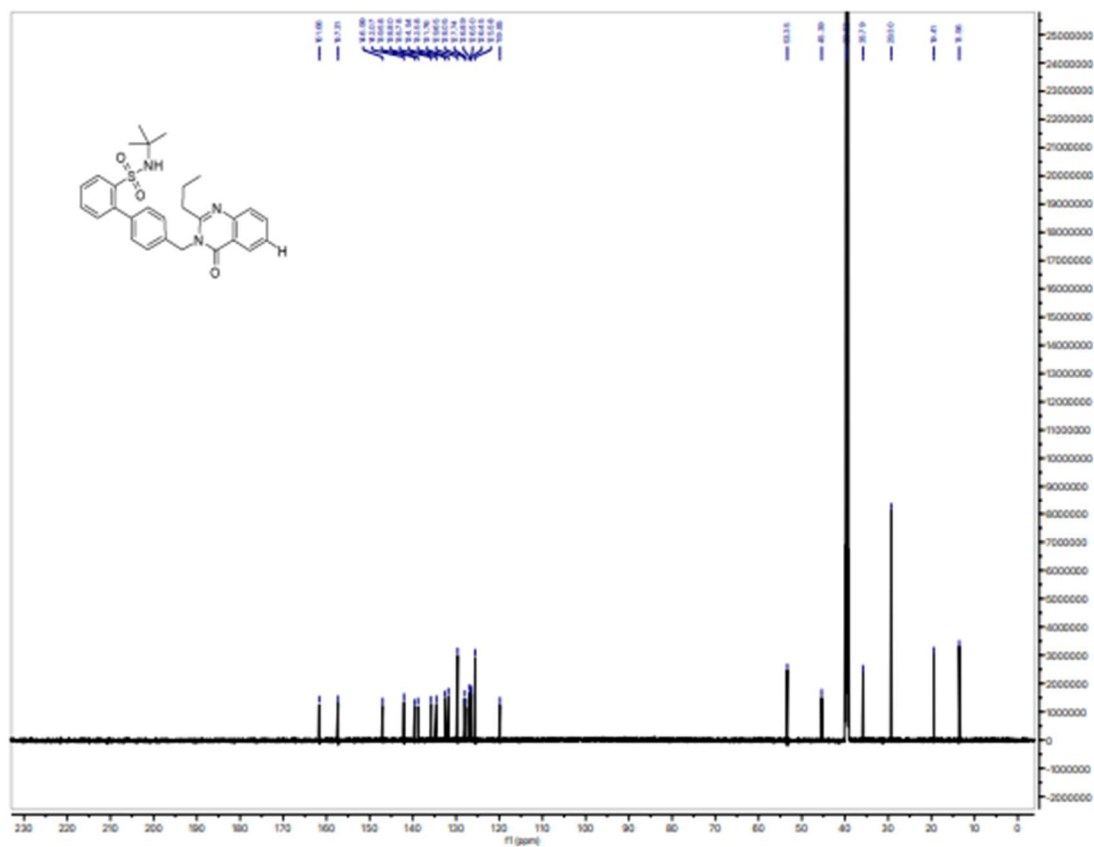
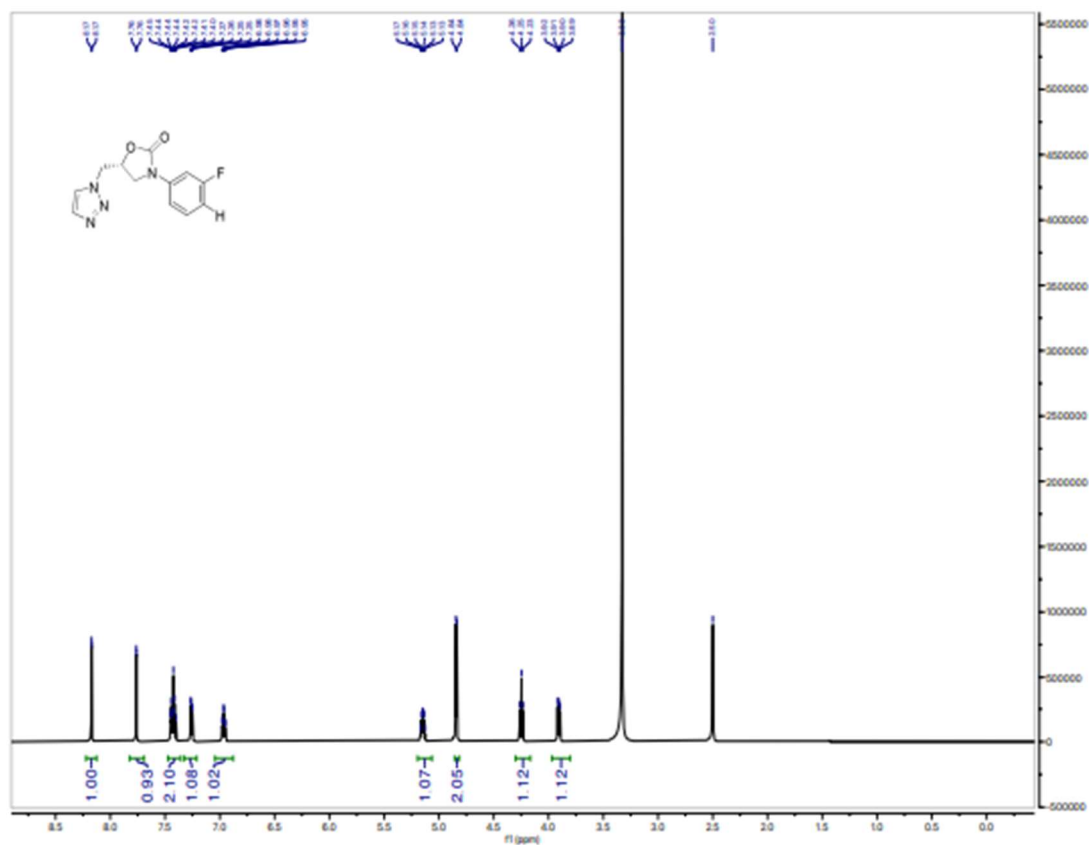


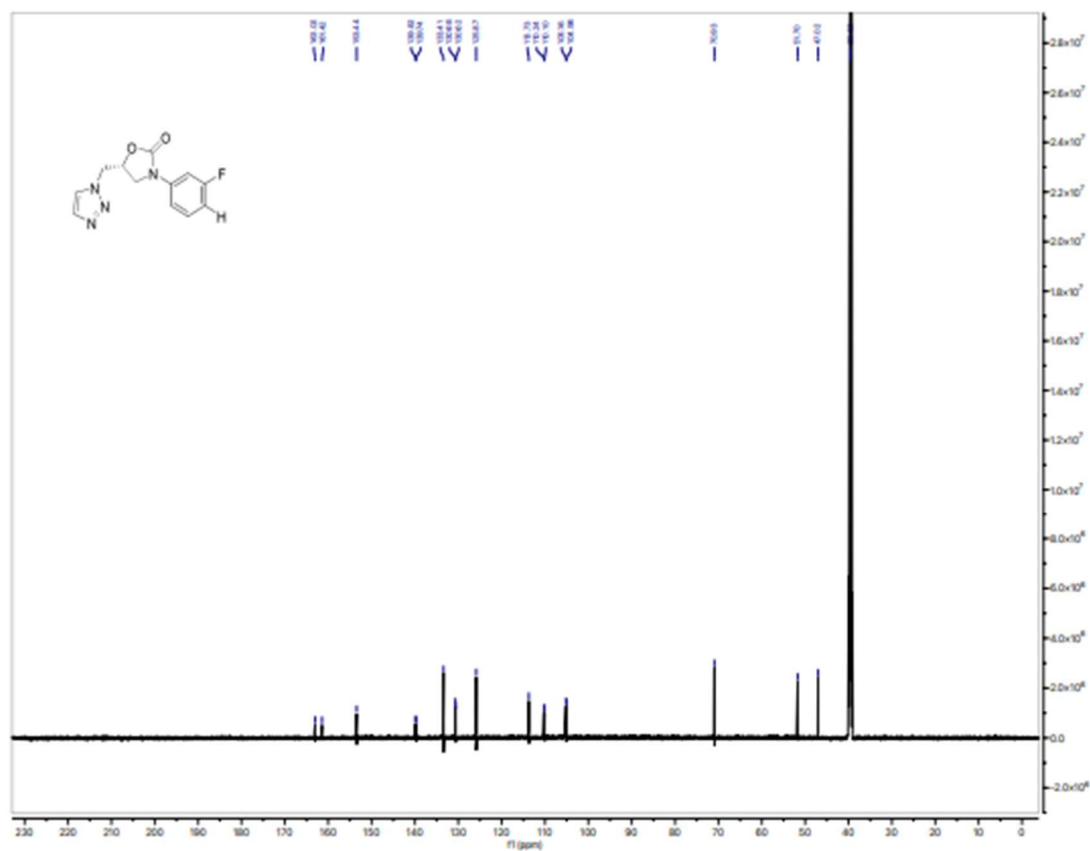
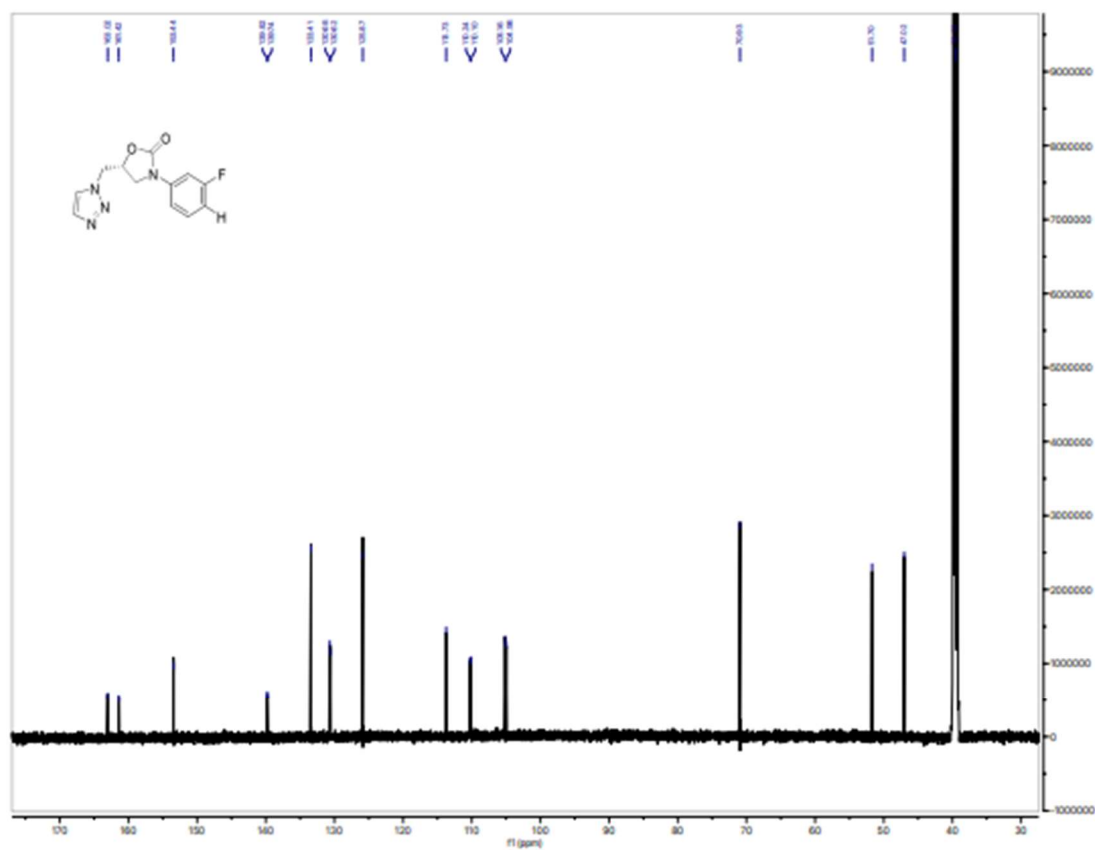


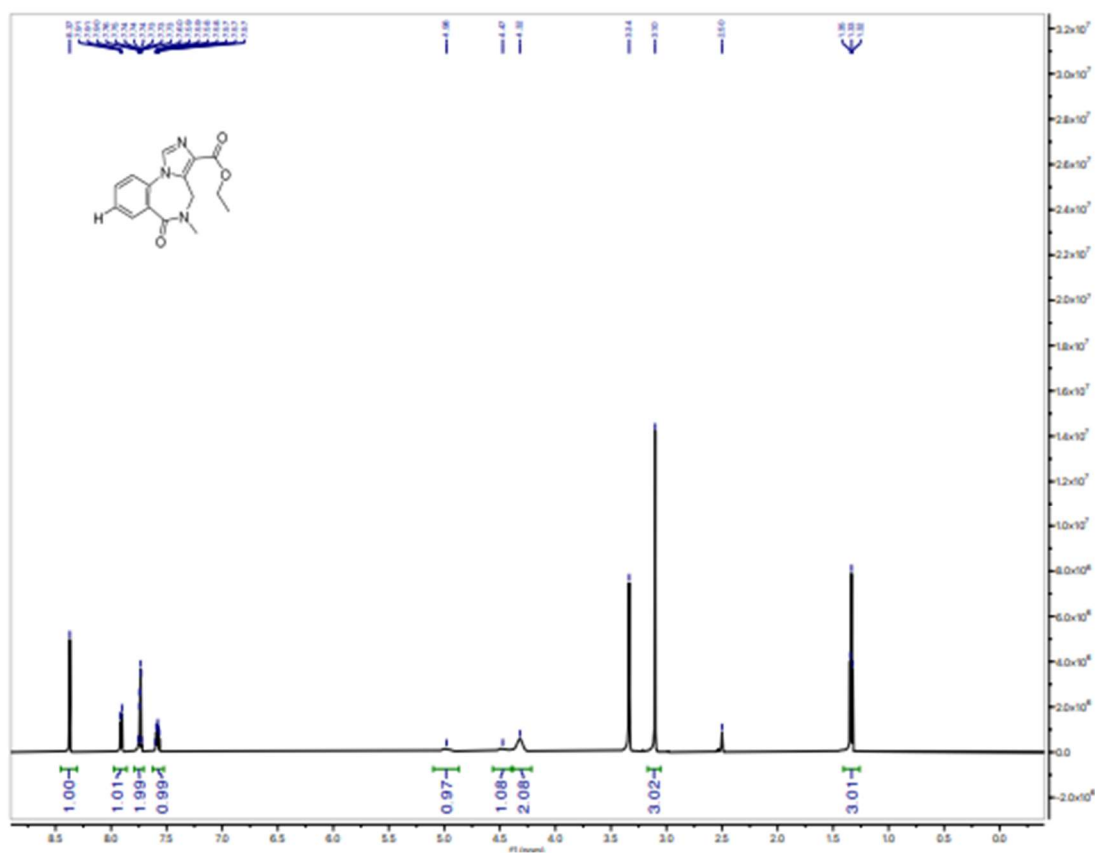
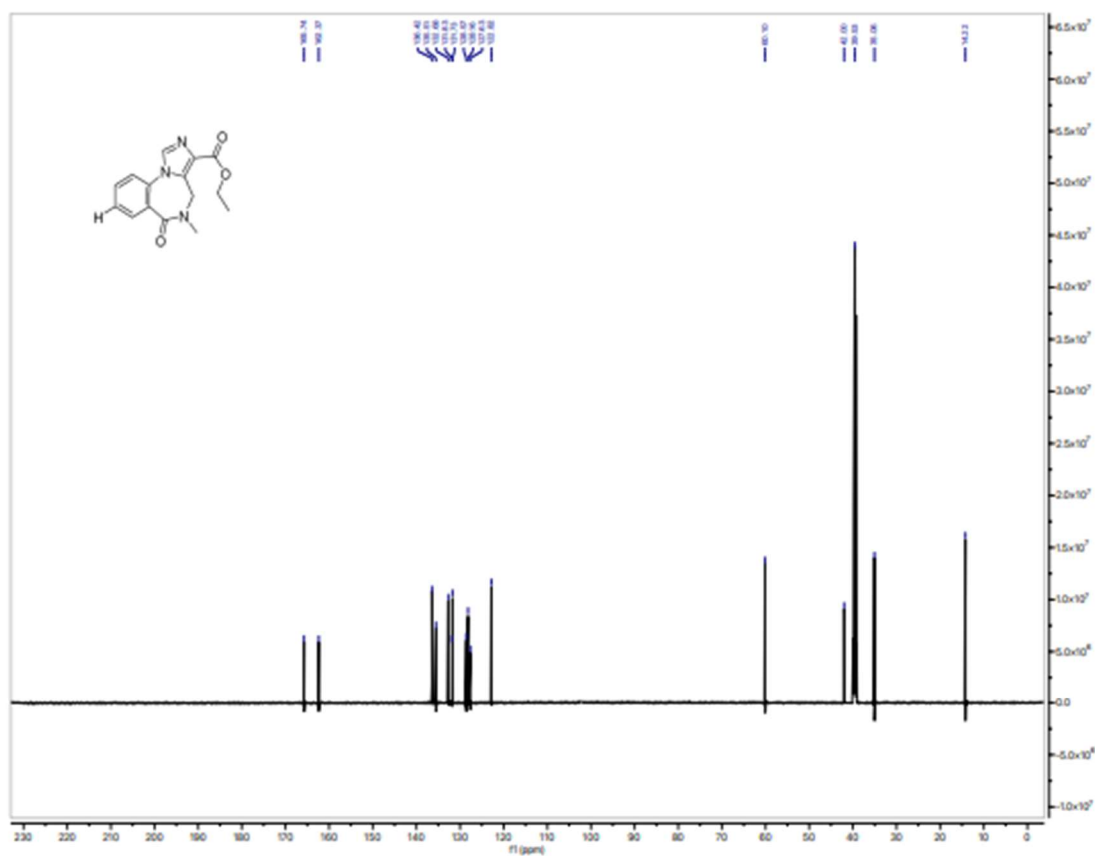


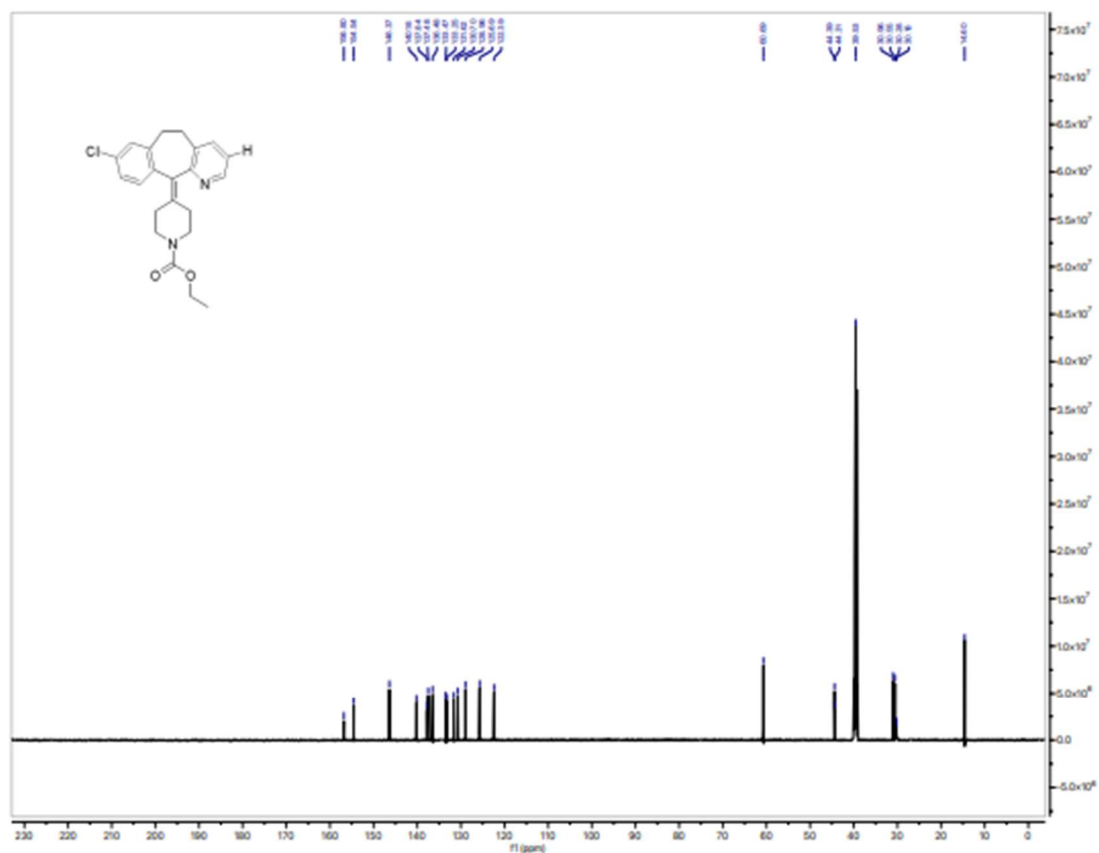


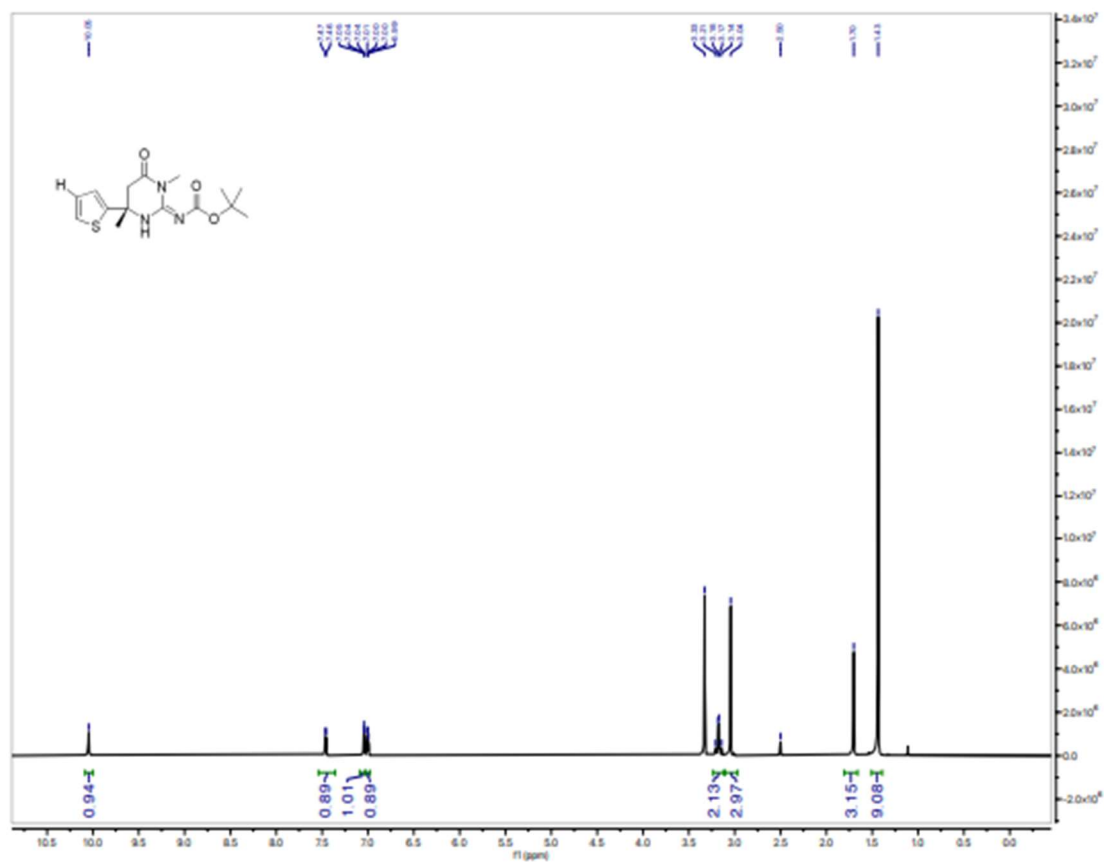
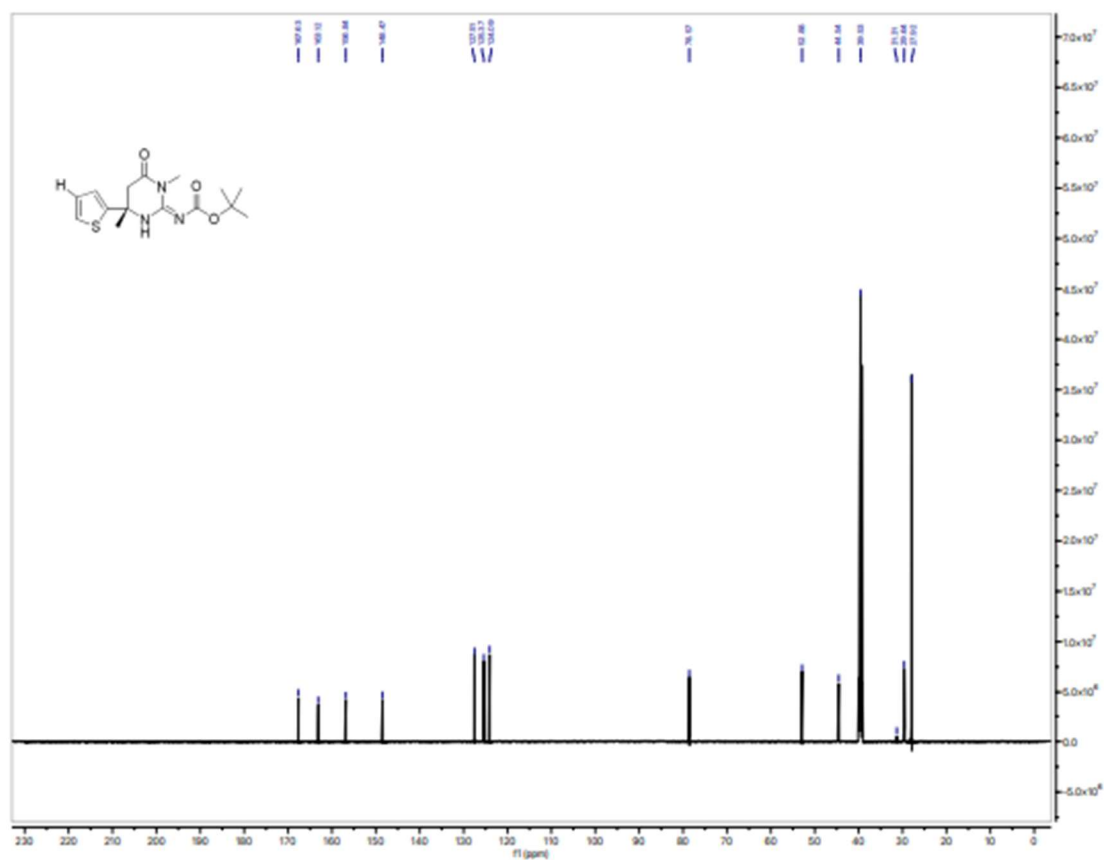


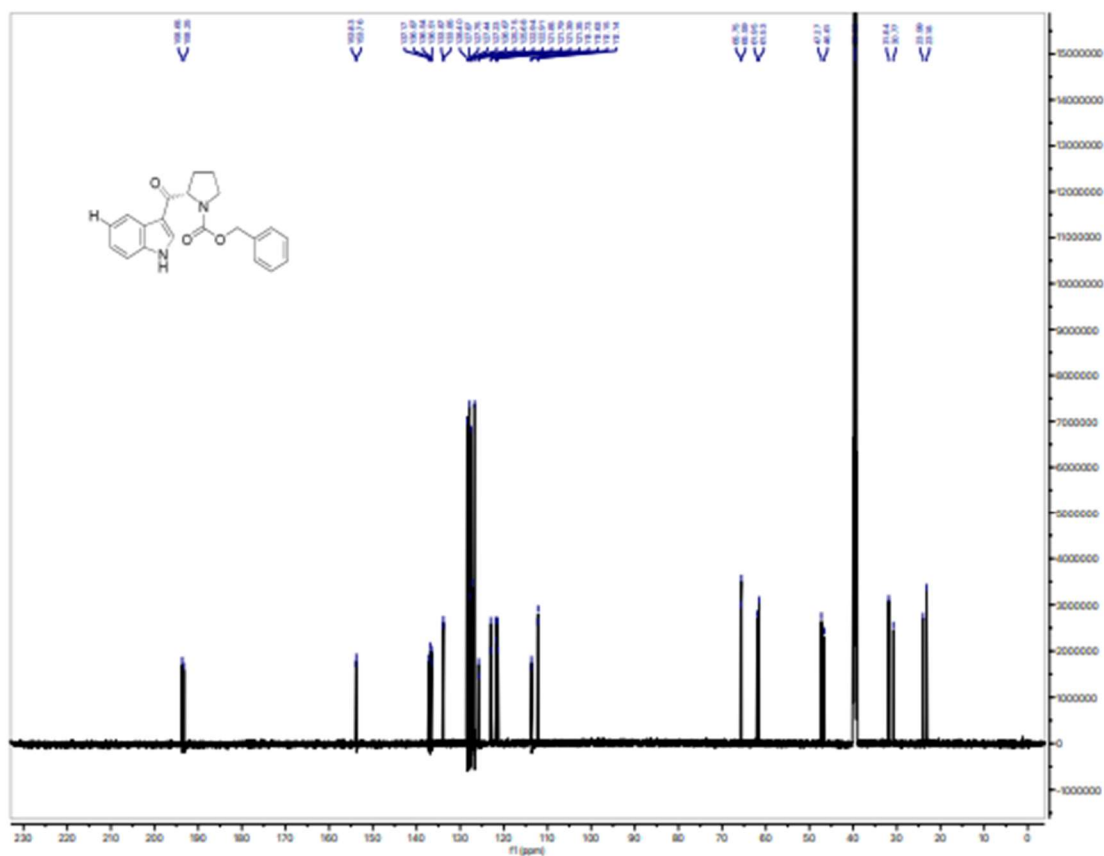
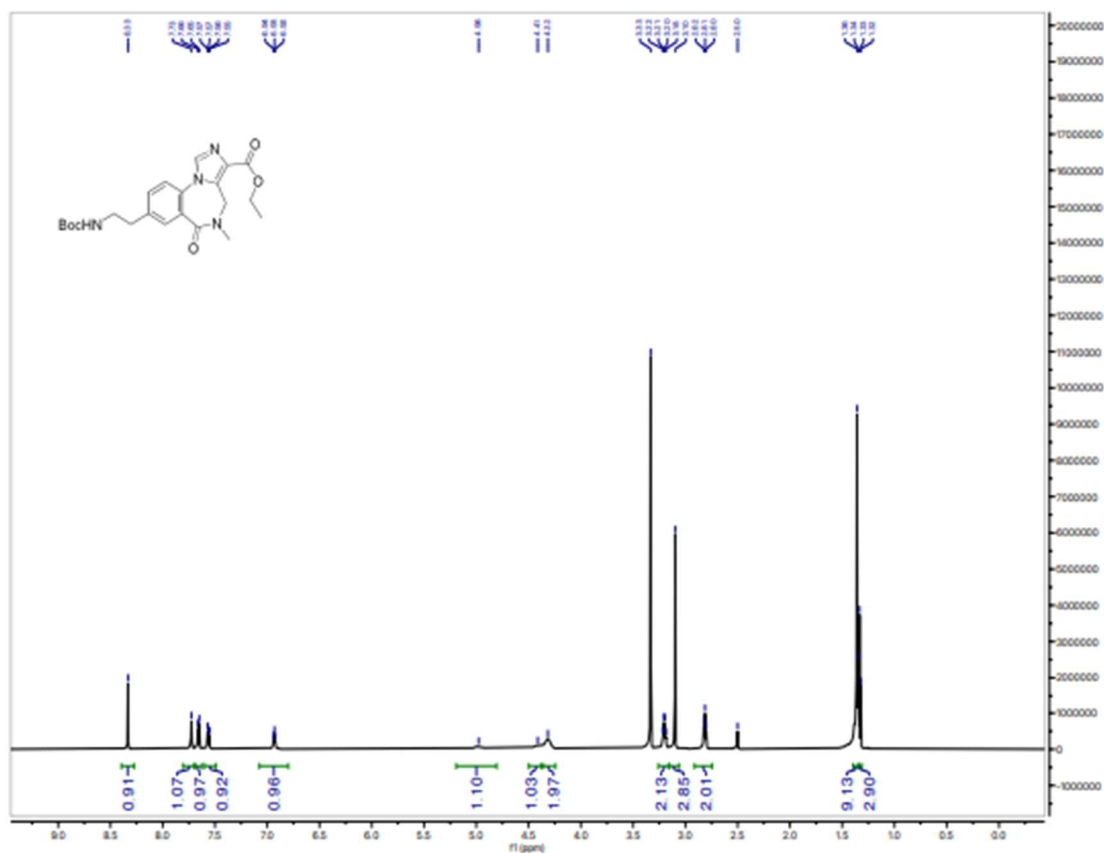


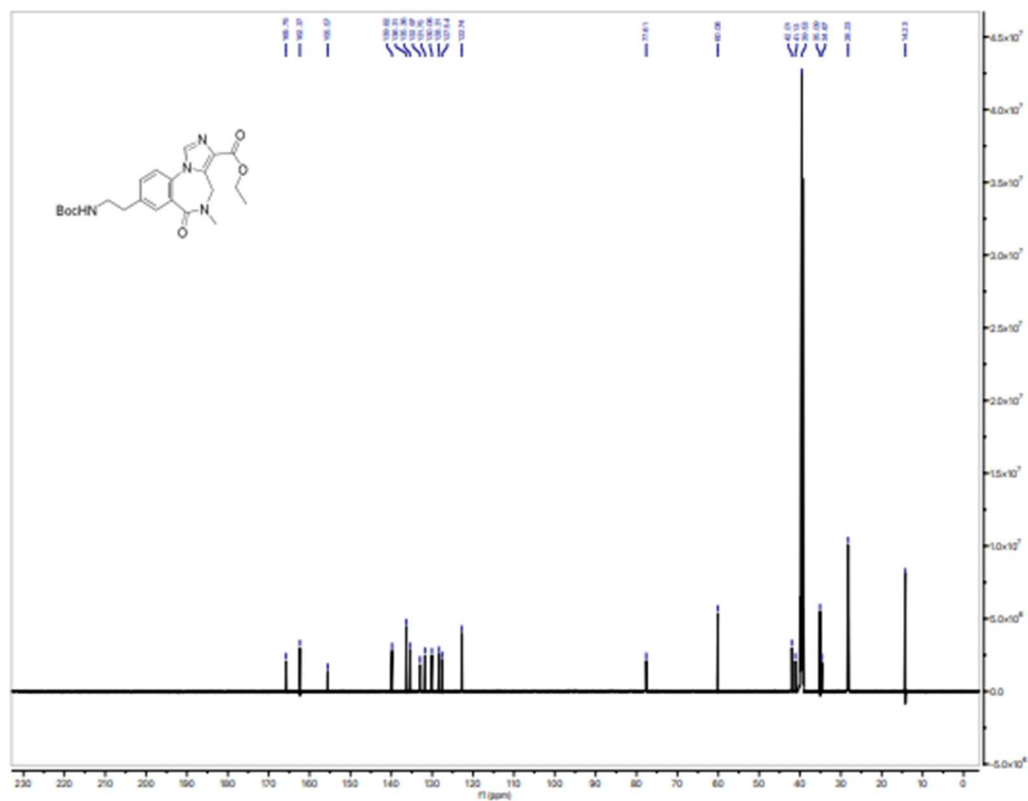












Chapter 5: *E*-Selective Semi-Hydrogenation of Alkynes via Electron-Primed Photoredox Catalysis

This work is unpublished: Chernowsky, C.P.; Sowin, J.A.; Wickens, Z.K.

5.1 Abstract

E-selective semi-hydrogenation of alkynes is a valuable transformation often leveraged in the synthesis of natural products and complex structures. Unfortunately, there is a lack of strategies to promote this transformation outside of harsh sodium dissolving metal conditions. Herein, we report a system that provides selective semi-hydrogenation of alkynes via electron-primed photoredox catalysis. Preliminary data revealed that both aromatic and aliphatic alkynes are reduced to their respective alkenes with an appropriate catalyst structure, however, a balance is required to minimize affinity of the neutral catalyst structures for triplet energy transfer while maintaining the reductive potency of the excited state radical anion.

5.2 Introduction

Reductive single electron transfer (SET) is a vital elementary step and is a cornerstone to many important transformations.^{1–5} Classically, SET has been initiated through the use of harsh stoichiometric metals such as lithium or sodium.^{6–8} While progress has been made in replacing many of these hazardous techniques with more mild photochemical systems,^{9–16} dissolving metal conditions remain a standard for numerous reductive reactions.^{17–22} These reactions include the reduction of pi bonds such as semi-hydrogenation of alkynes which is carried out with sodium metal reductants to afford *E*-alkenes as the main products (**Figure 5.1 (a)**).^{23,24} To avoid the use of harsh dissolving metal conditions, various strategies leveraging metal-hydride transfer^{25–30} have been developed for alkyne semi-hydrogenation, however, these reactions are selective for formation of *Z*-alkene products due to the key migratory insertion step of metal hydride species into alkynes (**Figure 5.1 (b)**). In these reactions, the *E* isomer is often obtained via isomerization of the initial *Z*-alkene products^{31–36} and unfortunately, either scopes remain limited or the isomerization step does not proceed to completion and leads to a mixture of diastereomers. A semi-hydrogenation strategy that avoids an isomerization step and provides excellent *E* selectivity was developed by Fürstner leveraging ruthenium catalysis and hydrogen gas (**Figure 5.1 (c)**). While these conditions are effective at promoting *E*-selective alkyne semi-hydrogenation, the

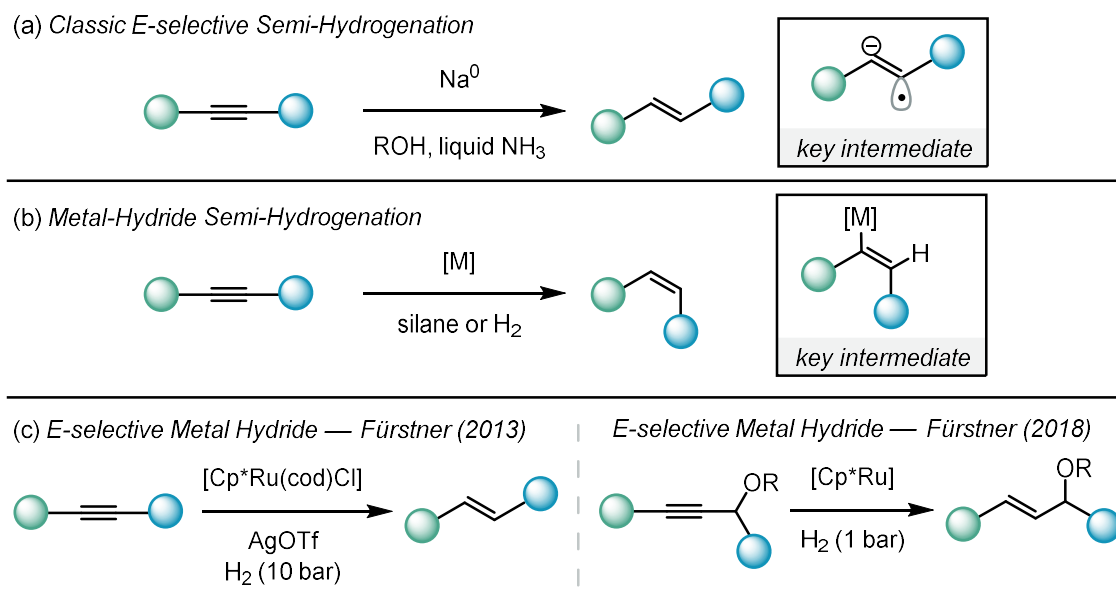


Figure 5.1. Established methods for alkyne semi-hydrogenation

scope remains limited as either a chelating directing group^{37–39} is required on the substrate or high pressures of hydrogen gas^{40,41} are necessary for hydrogenation. Furthermore, metal hydride catalysis is mechanistically distinct from radical based SET reduction strategies. Despite advances in metal-hydride catalysis, reduction via dissolving metal conditions remains the primary strategy for promoting *E*-selective semi-hydrogenation of alkynes and to date, no mild SET analog to dissolving metal reductions has been reported for this transformation.

Our group,^{42–44} and several others,^{45–52} have developed an electron-primed photocatalytic strategy that leverages photoexcitation of radical anion catalysts to achieve highly reducing excited states. This photocatalytic platform has proven a powerful method for single electron transfer under mild conditions and has been successful at promoting reductive transformations previously carried out with lithium metal.⁵³ The reduction of various neutral catalyst structures to their radical anions have been successfully engaged under both consecutive photoinduced electron transfer (conPET)^{43,46,47,49,50} as well as electrochemical reduction^{42,44,48,51} offering versatility in the design of a reductive SET system. Despite this versatility, previous reports from our group have focused exclusively on the reduction and mesolytic cleavage of functionalized arenes to generate aryl radical intermediates. We proposed that electron-primed photoredox

catalysis would serve as an effective SET reductive strategy to engage alkyne substrates in *E*-selective semi-hydrogenation. Additionally, this reaction would also provide a context in which to expand the reactivity of electron-primed photoredox catalysis beyond arenes substrates that can undergo mesolytic cleavage. Herein, preliminary studies are disclosed into developing a catalytic platform for *E*-selective semi-hydrogenation of alkynes promoted by electron-primed photoredox catalysis under constant potential electrolysis (**Figure 5.2**).

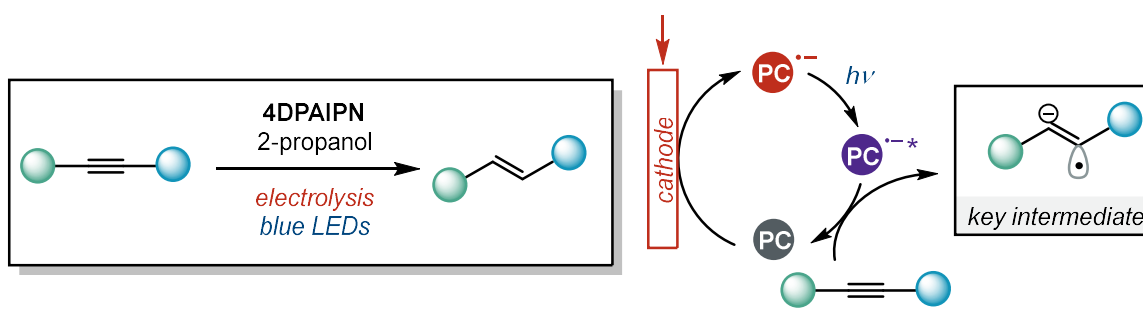


Figure 5.2. *This work:* electron-primed photoredox catalysis *E*-selective Semi-Hydrogenation

5.3 Results and Discussion

We initiated our studies to design a catalytic system for *E*-selective alkyne semi-hydrogenation with 1-phenyl-1-propyne (**1**) as a model substrate. Several engines have been developed in recent years to promote electron-primed photoredox catalysis⁵³ and reduction of **1** was studied under each potential system with **4DPAIPN** as the catalyst, selected for its success as an electron-primed photocatalyst in previous studies conducted by our group (**Figure 5.3**).^{43,44} Unfortunately, a conPET system with a trialkylamine reductant, DIPEA, was unsuccessful and provided no desired semi-hydrogenation yield or conversion of **1**. While exchanging the reductant for a formate salt (previously shown to be a more efficient reductant than a trialkylamine⁴³) did result in high conversion of **1**, no semi-hydrogenation was observed. We hypothesized that the majority of the mass was converting to an intractable mixture of carboxylated products due to the generation of CO₂^{•-} upon formate oxidation which was previously demonstrated by our group⁵⁴ to readily add into styrenes and other activated pi bonds (see the SI for mechanistic details). Excitingly, attempting reduction of **1** with electrolysis at an applied potential equivalent to the E_{red}

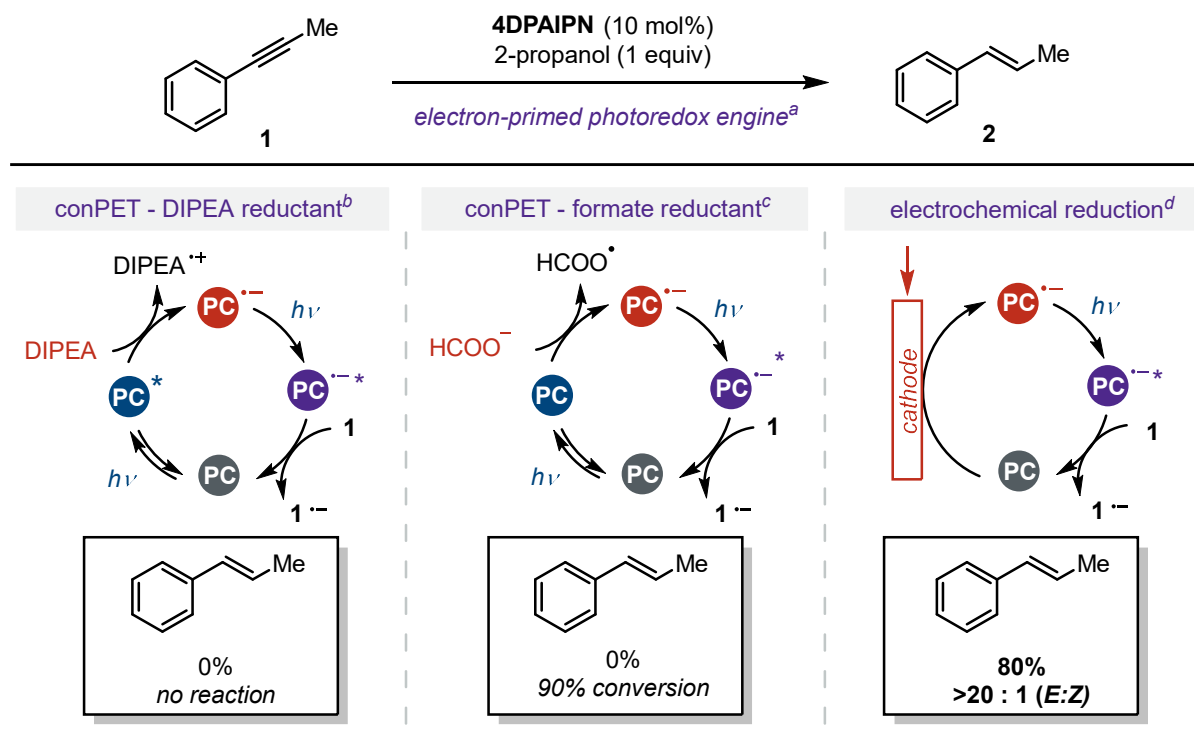


Figure 5.3. Testing different electron-primed photoredox engines for semi-hydrogenation. ^a all reactions irradiated at 405 nm for 8 hr, NMR analysis. ^b DIPEA (2 equiv), DMF (0.1 M). ^c Na formate (3 equiv), CySH (5 mol%), DMSO (0.08 M), dicarboxylation = 2-methyl-3-phenylsuccinate. ^d 0.1 M *n*-Bu₄NPF₆, DMF (0.1 M), -1.6 V vs SCE.

of **4DPAIPN** provided the desired styrene product (**2**) in 80% yield with an *E:Z* ratio of >20:1. Control experiments revealed that indeed both electrolysis at the E_{red} of **4DPAIPN** as well as irradiation was required for reactivity, supporting the proposed electron-primed photoredox mechanism (see the SI for details). Semi-hydrogenation was the exclusive product observed under these conditions, however, a switch in selectivity could be achieved to instead favor exhaustive hydrogenation (**3**) when the amount of isopropanol added to the system was increased from one equivalent to four (**Table 5.1**). This result was confirmed by subjecting β -methyl styrene to standard reaction conditions with four equivalence of isopropanol and observing the hydrogenated propyl benzene product in 83% yield. These results confirm that the extent of hydrogenation can be modulated via simple variation in the alcohol equivalence.

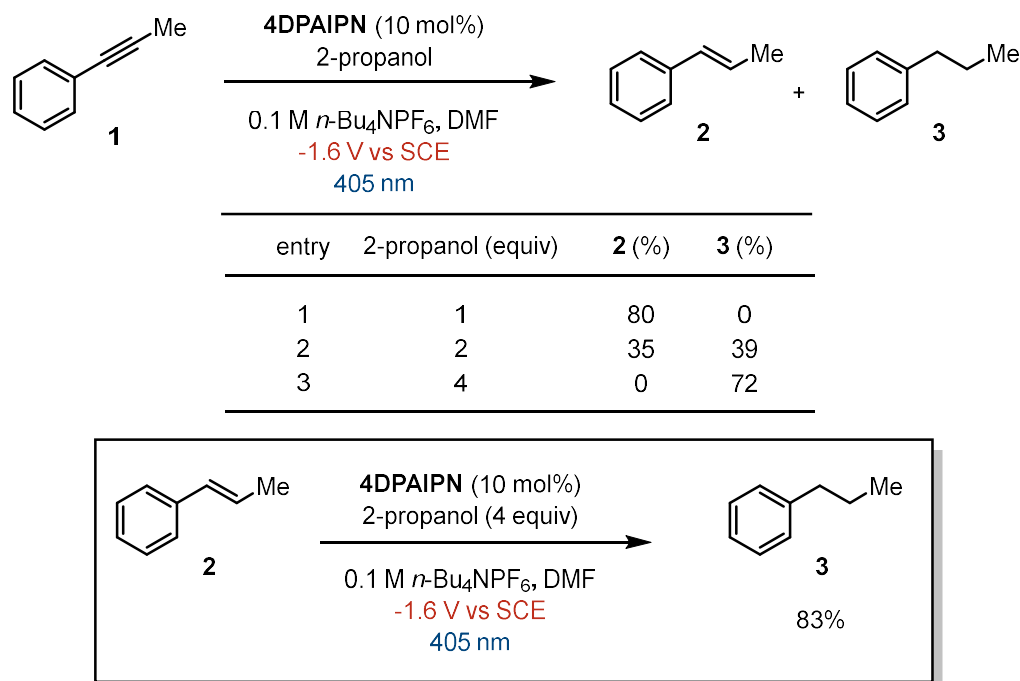


Table 5.1. Selectivity in degree of hydrogenation based on isopropanol equivalence. Reactions run on 0.2 mmol scale for 8 h and analyzed by NMR.

We next turned our attention to engaging aliphatic alkynes in semi-hydrogenation. Unfortunately, adopting the reaction conditions developed for the reduction of **1** provided no conversion of 1-phenyl-3-pentyne (**4**) and variations in reaction parameters with **4DPAIPN** as the catalyst were unsuccessful at promoting reactivity. However, when **4DPAIPN** was exchanged for a catalyst with a higher energy radical anion ground state, pyrene,^{55,56} semi-hydrogenation was observed in 27% yield (**Figure 5.4**) (see the SI for catalyst screening details). While yields remain low and further investigation is required, these initial data indicate that aliphatic alkynes

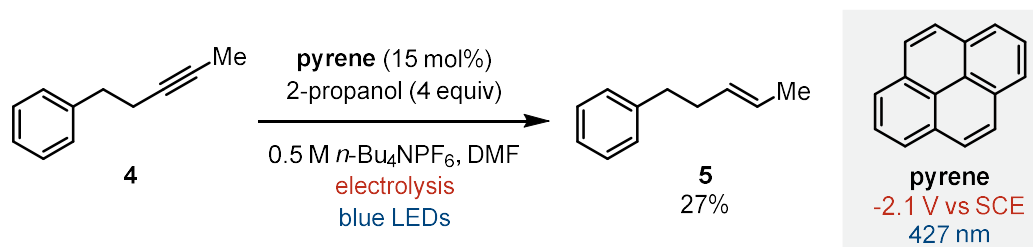


Figure 5.4. Preliminary data on semi-hydrogenation of an aliphatic alkyne. Reaction run at constant working potential for 12 h and analyzed by NMR. (See the SI for catalyst screening details)

are indeed a viable substrate class that can undergo semi-hydrogenation with electron-primed photoredox conditions.

With reaction conditions in hand, we next investigated the scope for *E*-selective semi-hydrogenation of aromatic alkynes (**Table 5.2**). Preliminary studies revealed that both electron poor and electron rich substrates can be reduced to the alkene with tolerance for functional groups like pendant alkenes (**6**), carboxylic acids (**7**), nitriles (**7**), and Boc amines (**11**). Saturated heterocycles such as morpholine (**10**) or piperazine (**11**) were also well tolerated. While these substrates were all successfully reduced, we noted that when the arene was electron rich, diastereomeric ratios of the *E* and *Z* isomers were being formed (**8** – **11**). To gain insight into

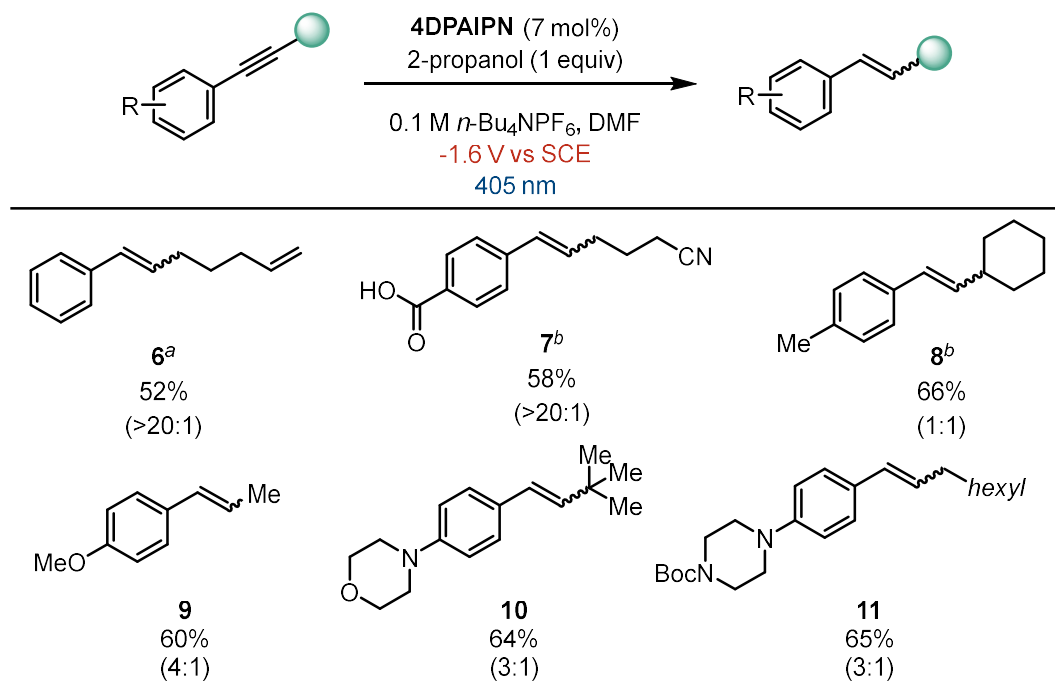


Table 5.2. Preliminary scope of alkyne semi-hydrogenation. Ratios given are for *E*:*Z* ratios. All reactions conducted on a 0.2 mmol scale, run for 12 h and analyzed by H NMR. ^aRun with 2 mol% catalyst. ^bRun with 5 mol% catalyst.

when the undesired *Z* isomer was being formed, a time course was conducted that showed a constant rate of *Z* alkene formation throughout the reaction. However, this time course also revealed that over time, the desired *E* isomer formed early in the reaction slowly converted to the undesired *Z* isomer resulting in a near 1:1 mixture of products at the end of the reaction (**Figure**

5.5). We proposed that this isomerization occurs due to catalyst promoted triplet energy transfer^{57–60} upon prolonged exposure to irradiation. Triplet energy transfer is a pathway that has been leveraged to convert *E* alkenes to their *Z* isomers^{61–64} via the alkene excited state and the literature shows **4DPAIPN** to be capable of catalyzing reactions that proceed through triplet energy transfer pathways.⁶⁵ Based on this precedent, we concluded that **4DPAIPN** could be catalyzing a background isomerization pathway in addition to the desired SET reduction pathway (see the SI for details).

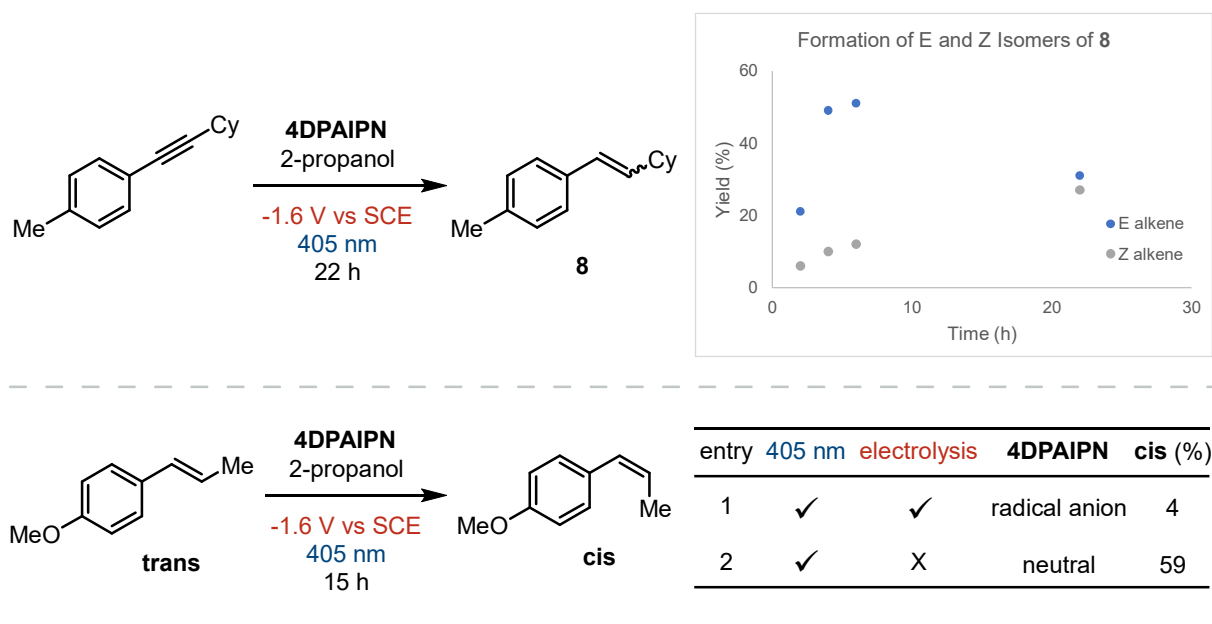


Figure 5.5. Investigations into isomerization of alkene products. All reactions run on 0.200 mmol scale, with 0.1 M *n*-Bu₄NPF₆ in DMF (0.1 M).

We next set out to test the hypothesis of **4DPAIPN** promoted triplet energy transfer and to determine if this pathway is a property of exclusively the neutral catalyst or if energy transfer could also be promoted by the radical anion congener. We subjected (*trans*)-4-methoxy-β-methylstyrene to standard reaction conditions where the catalyst is fully reduced to the radical anion and obtained only 4% isomerization to the *cis* isomer (**Figure 5.5**). In contrast, when electrolysis is absent and the catalyst remains neutral **4DPAIPN** under irradiation, the *trans* alkene is isomerized to the *cis* isomer in 59% yield. Given these data, we concluded that the *E*:*Z* isomerization observed was primarily due to the generation of neutral **4DPAIPN** upon SET with

substrate before the catalyst can be re-reduced at the electrode. Unfortunately, due to the nature of the catalytic cycle, neutral **4DPAIPN** will never be fully removed from the system and UV-Vis experiments revealed that there is no wavelength of excitation where the radical anion congener has a higher absorption than the neutral catalyst (see the SI for details). We concluded from these data that despite the effective reactivity for semi-hydrogenation, the challenges with *E* to *Z* isomerization for electron rich substrates will persist with **4DPAIPN** as the catalyst under the current reaction conditions and further exploration is necessary for this system to reach its full potential. Inspired by the range in the degree of stilbene isomerization that has been reported for different nitrile photocatalysts,⁶⁵ current efforts are centered on investigating alternative phthalonitrile derivatives and isomers to identify a catalyst that has a lower affinity for triplet energy transfer as the neutral structure but is still a potent photoreductant as the radical anion congener.

5.4. Conclusions

Overall, we have demonstrated that alkynes can undergo semi-hydrogenation to alkene products under electron-primed photoredox conditions and selectivity can be modulated between partial and exhaustive hydrogenation through controlled equivalence of a proton source. Initial studies revealed that aromatic alkynes are reduced in the presence of **4DPAIPN** in good yields and preliminary data indicates that aliphatic alkynes are reduced when the catalyst is exchanged for pyrene. While overall good yields were achieved for semi-hydrogenation products, unexpected isomerization to *Z* isomers was observed for electron rich substrates due to a triplet energy transfer pathway catalyzed by neutral **4DPAIPN**. Future efforts to optimize away from this isomerization pathway include investigation of alternative phthalonitrile structures that are poor triplet energy catalysts as the neutral structure but are capable of difficult SET reductions from an excited state radical anion.

5.5. Acknowledgments

We thank the Weix, Yoon, Stahl, and Schomaker groups for sharing their chemical inventory and laboratory equipment. We thank the Martell group for sharing their lab space during

the completion of this work. Tracy Drier is acknowledged for electrochemical glassware fabrication. Dr. Blaise Thompson is acknowledged for construction of constant potential electrochemical equipment. This work was financially supported by the Office of the Vice Chancellor for Research and Graduate Education at the University of Wisconsin–Madison with funding from the Wisconsin Alumni Research Foundation. This material is based upon work supported by the National Science Foundation under Grant No. (2047108). Acknowledgment is made to the Donors of the American Chemical Society Petroleum Research Fund for partial funding of this research (60677-DNI1). Spectroscopic instrumentation was supported by a generous gift from Paul. J. and Margaret M. Bender, NSF (CHE-1048642), and NIH (1S10 OD020022-1).

5.6. References

- (1) Ashby, E. C. Single-Electron Transfer, a Major Reaction Pathway in Organic Chemistry. An Answer to Recent Criticisms. *Acc. Chem. Res.* **1988**, *21* (11), 414–421. <https://doi.org/10.1021/ar00155a005>.
- (2) Zhang, N.; Samanta, S. R.; Rosen, B. M.; Percec, V. Single Electron Transfer in Radical Ion and Radical-Mediated Organic, Materials and Polymer Synthesis. *Chem. Rev.* **2014**, *114* (11), 5848–5958. <https://doi.org/10.1021/cr400689s>.
- (3) Broggi, J.; Terme, T.; Vanelle, P. Organic Electron Donors as Powerful Single-Electron Reducing Agents in Organic Synthesis. *Angewandte Chemie International Edition* **2014**, *53* (2), 384–413. <https://doi.org/10.1002/anie.201209060>.
- (4) Girard, P.; Namy, J. L.; Kagan, H. B. Divalent Lanthanide Derivatives in Organic Synthesis. 1. Mild Preparation of Samarium Iodide and Ytterbium Iodide and Their Use as Reducing or Coupling Agents. *J. Am. Chem. Soc.* **1980**, *102* (8), 2693–2698. <https://doi.org/10.1021/ja00528a029>.
- (5) Ebersson, L. Electron-Transfer Reactions in Organic Chemistry. In *Advances in Physical Organic Chemistry*; Gold, V., Bethell, D., Eds.; Academic Press, 1982; Vol. 18, pp 79–185. [https://doi.org/10.1016/S0065-3160\(08\)60139-2](https://doi.org/10.1016/S0065-3160(08)60139-2).
- (6) Birch, A. J. 117. Reduction by Dissolving Metals. Part I. *J. Chem. Soc.* **1944**, No. 0, 430–436. <https://doi.org/10.1039/JR94400000430>.
- (7) Zimmerman, H. E. Orientation in Metal Ammonia Reductions. *Tetrahedron* **1961**, *16* (1), 169–176. [https://doi.org/10.1016/0040-4020\(61\)80067-7](https://doi.org/10.1016/0040-4020(61)80067-7).
- (8) Rabideau, P. W. The Metal-Ammonia Reduction of Aromatic Compounds. *Tetrahedron* **1989**, *45* (6), 1579–1603. [https://doi.org/10.1016/S0040-4020\(01\)80022-3](https://doi.org/10.1016/S0040-4020(01)80022-3).
- (9) Prier, C. K.; Rankic, D. A.; MacMillan, D. W. C. Visible Light Photoredox Catalysis with Transition Metal Complexes: Applications in Organic Synthesis. *Chem. Rev.* **2013**, *113* (7), 5322–5363. <https://doi.org/10.1021/cr300503r>.
- (10) Shaw, M. H.; Twilton, J.; MacMillan, D. W. C. Photoredox Catalysis in Organic Chemistry. *J. Org. Chem.* **2016**, *81* (16), 6898–6926. <https://doi.org/10.1021/acs.joc.6b01449>.

- (11) Romero, N. A.; Nicewicz, D. A. Organic Photoredox Catalysis. *Chem. Rev.* **2016**, *116* (17), 10075–10166. <https://doi.org/10.1021/acs.chemrev.6b00057>.
- (12) Skubi, K. L.; Blum, T. R.; Yoon, T. P. Dual Catalysis Strategies in Photochemical Synthesis. *Chem. Rev.* **2016**, *116* (17), 10035–10074. <https://doi.org/10.1021/acs.chemrev.6b00018>.
- (13) DiRocco, D. A.; Dykstra, K.; Krska, S.; Vachal, P.; Conway, D. V.; Tudge, M. Late-Stage Functionalization of Biologically Active Heterocycles Through Photoredox Catalysis. *Angewandte Chemie International Edition* **2014**, *53* (19), 4802–4806. <https://doi.org/10.1002/anie.201402023>.
- (14) Narayanam, J. M. R.; Stephenson, C. R. J. Visible Light Photoredox Catalysis: Applications in Organic Synthesis. *Chem. Soc. Rev.* **2010**, *40* (1), 102–113. <https://doi.org/10.1039/B913880N>.
- (15) Speckmeier, E.; Fischer, T. G.; Zeitler, K. A Toolbox Approach To Construct Broadly Applicable Metal-Free Catalysts for Photoredox Chemistry: Deliberate Tuning of Redox Potentials and Importance of Halogens in Donor–Acceptor Cyanoarenes. *J. Am. Chem. Soc.* **2018**, *140* (45), 15353–15365. <https://doi.org/10.1021/jacs.8b08933>.
- (16) Joshi-Pangu, A.; Lévesque, F.; Roth, H. G.; Oliver, S. F.; Campeau, L.-C.; Nicewicz, D.; DiRocco, D. A. Acridinium-Based Photocatalysts: A Sustainable Option in Photoredox Catalysis. *J. Org. Chem.* **2016**, *81* (16), 7244–7249. <https://doi.org/10.1021/acs.joc.6b01240>.
- (17) Chuang, K. V.; Xu, C.; Reisman, S. E. A 15-Step Synthesis of (+)-Ryanodol. *Science* **2016**, *353* (6302), 912–915. <https://doi.org/10.1126/science.aag1028>.
- (18) Liu, Y.-T.; Li, L.-P.; Xie, J.-H.; Zhou, Q.-L. Divergent Asymmetric Total Synthesis of Mulinane Diterpenoids. *Angewandte Chemie International Edition* **2017**, *56* (41), 12708–12711. <https://doi.org/10.1002/anie.201706994>.
- (19) He, C.; Stratton, T. P.; Baran, P. S. Concise Total Synthesis of Herquelines B and C. *J. Am. Chem. Soc.* **2019**, *141* (1), 29–32. <https://doi.org/10.1021/jacs.8b13029>.
- (20) Joshi, D. K.; Sutton, J. W.; Carver, S.; Blanchard, J. P. Experiences with Commercial Production Scale Operation of Dissolving Metal Reduction Using Lithium Metal and Liquid Ammonia. *Org. Process Res. Dev.* **2005**, *9* (6), 997–1002. <https://doi.org/10.1021/op050155x>.
- (21) Paquette, L. A.; Fuhr, K. H. Intramolecular Epoxide Cleavage by Dissolving Metal Reduction of Proximal Cyclopropane Rings. *J. Am. Chem. Soc.* **1972**, *94* (26), 9221–9222. <https://doi.org/10.1021/ja00781a040>.
- (22) Huffman, J. W.; McWhorter, W. W. Dissolving Metal Reduction of Cyclic Ketones. *J. Org. Chem.* **1979**, *44* (4), 594–599. <https://doi.org/10.1021/jo01318a023>.
- (23) Han, M.; Ding, Y.; Yan, Y.; Li, H.; Luo, S.; Adijiang, A.; Ling, Y.; An, J. Transition-Metal-Free, Selective Reductive Deuteration of Terminal Alkynes with Sodium Dispersions and EtOD-D1. *Org. Lett.* **2018**, *20* (10), 3010–3013. <https://doi.org/10.1021/acs.orglett.8b01036>.
- (24) Dias, L. C.; de Oliveira, L. G.; de Sousa, M. A. Total Synthesis of (–)-Pironetin. *Org. Lett.* **2003**, *5* (3), 265–268. <https://doi.org/10.1021/ol027211o>.
- (25) Li, K.; Yang, C.; Chen, J.; Pan, C.; Fan, R.; Zhou, Y.; Luo, Y.; Yang, D.; Fan, B. Anion Controlled Stereodivergent Semi-Hydrogenation of Alkynes Using Water as Hydrogen Source. *Asian Journal of Organic Chemistry* **2021**, *10* (8), 2143–2146. <https://doi.org/10.1002/ajoc.202000716>.
- (26) Shen, R.; Chen, T.; Zhao, Y.; Qiu, R.; Zhou, Y.; Yin, S.; Wang, X.; Goto, M.; Han, L.-B. Facile Regio- and Stereoselective Hydrometalation of Alkynes with a Combination of Carboxylic Acids and Group 10 Transition Metal Complexes: Selective Hydrogenation of Alkynes with Formic Acid. *J. Am. Chem. Soc.* **2011**, *133* (42), 17037–17044. <https://doi.org/10.1021/ja2069246>.

- (27) Li, K.; Khan, R.; Zhang, X.; Gao, Y.; Zhou, Y.; Tan, H.; Chen, J.; Fan, B. Cobalt Catalyzed Stereodivergent Semi-Hydrogenation of Alkynes Using H₂O as the Hydrogen Source. *Chem. Commun.* **2019**, 55 (39), 5663–5666. <https://doi.org/10.1039/C9CC01970G>.
- (28) Gorgas, N.; Brünig, J.; Stöger, B.; Vanicek, S.; Tilset, M.; Veiros, L. F.; Kirchner, K. Efficient Z-Selective Semihydrogenation of Internal Alkynes Catalyzed by Cationic Iron(II) Hydride Complexes. *J. Am. Chem. Soc.* **2019**, 141 (43), 17452–17458. <https://doi.org/10.1021/jacs.9b09907>.
- (29) Johnson, C.; Albrecht, M. Z-Selective Alkyne Semi-Hydrogenation Catalysed by Piano-Stool N-Heterocyclic Carbene Iron Complexes. *Catal. Sci. Technol.* **2018**, 8 (11), 2779–2783. <https://doi.org/10.1039/C8CY00681D>.
- (30) Gnaim, S.; Bauer, A.; Zhang, H.-J.; Chen, L.; Gannett, C.; Malapit, C. A.; Hill, D. E.; Vogt, D.; Tang, T.; Daley, R. A.; Hao, W.; Zeng, R.; Quertenmont, M.; Beck, W. D.; Kandahari, E.; Vantourout, J. C.; Echeverria, P.-G.; Abruna, H. D.; Blackmond, D. G.; Minter, S. D.; Reisman, S. E.; Sigman, M. S.; Baran, P. S. Cobalt-Electrocatalytic HAT for Functionalization of Unsaturated C–C Bonds. *Nature* **2022**, 605 (7911), 687–695. <https://doi.org/10.1038/s41586-022-04595-3>.
- (31) Luo, F.; Pan, C.; Wang, W.; Ye, Z.; Cheng, J. Palladium-Catalyzed Reduction of Alkynes Employing HSiEt₃: Stereoselective Synthesis of Trans- and Cis-Alkenes. *Tetrahedron* **2010**, 66 (6), 1399–1403. <https://doi.org/10.1016/j.tet.2009.11.098>.
- (32) Hale, D. J.; Ferguson, M. J.; Turculet, L. (PSiP)Ni-Catalyzed (E)-Selective Semihydrogenation of Alkynes with Molecular Hydrogen. *ACS Catal.* **2022**, 12 (1), 146–155. <https://doi.org/10.1021/acscatal.1c04537>.
- (33) Zhao, C.-Q.; Chen, Y.-G.; Qiu, H.; Wei, L.; Fang, P.; Mei, T.-S. Water as a Hydrogenating Agent: Stereodivergent Pd-Catalyzed Semihydrogenation of Alkynes. *Org. Lett.* **2019**, 21 (5), 1412–1416. <https://doi.org/10.1021/acs.orglett.9b00148>.
- (34) Gong, D.; Hu, B.; Yang, W.; Kong, D.; Xia, H.; Chen, D. A Bidentate Ru(II)-NC Complex as a Catalyst for Semihydrogenation of Alkynes to (E)-Alkenes with Ethanol. *Organometallics* **2020**, 39 (6), 862–869. <https://doi.org/10.1021/acs.organomet.0c00074>.
- (35) Karunananda, M. K.; Mankad, N. P. E-Selective Semi-Hydrogenation of Alkynes by Heterobimetallic Catalysis. *J. Am. Chem. Soc.* **2015**, 137 (46), 14598–14601. <https://doi.org/10.1021/jacs.5b10357>.
- (36) Higashida, K.; Mashima, K. E-Selective Semi-Hydrogenation of Alkynes with Dinuclear Iridium Complexes under Atmospheric Pressure of Hydrogen. *Chem. Lett.* **2016**, 45 (8), 866–868. <https://doi.org/10.1246/cl.160410>.
- (37) Biberger, T.; Gordon, C. P.; Leutzsch, M.; Peil, S.; Guthertz, A.; Copéret, C.; Fürstner, A. Alkyne Gem-Hydrogenation: Formation of Piano-Stool Ruthenium Carbene Complexes and Analysis of Their Chemical Character. *Angewandte Chemie International Edition* **2019**, 58 (26), 8845–8850. <https://doi.org/10.1002/anie.201904255>.
- (38) Guthertz, A.; Leutzsch, M.; Wolf, L. M.; Gupta, P.; Rummelt, S. M.; Goddard, R.; Farès, C.; Thiel, W.; Fürstner, A. Half-Sandwich Ruthenium Carbene Complexes Link Trans-Hydrogenation and Gem-Hydrogenation of Internal Alkynes. *J. Am. Chem. Soc.* **2018**, 140 (8), 3156–3169. <https://doi.org/10.1021/jacs.8b00665>.
- (39) Peil, S.; Bistoni, G.; Goddard, R.; Fürstner, A. Hydrogenative Metathesis of Enynes via Piano-Stool Ruthenium Carbene Complexes Formed by Alkyne Gem-Hydrogenation. *J. Am. Chem. Soc.* **2020**, 142 (43), 18541–18553. <https://doi.org/10.1021/jacs.0c07808>.
- (40) Radkowski, K.; Sundararaju, B.; Fürstner, A. A Functional-Group-Tolerant Catalytic Trans Hydrogenation of Alkynes. *Angewandte Chemie International Edition* **2013**, 52 (1), 355–360. <https://doi.org/10.1002/anie.201205946>.
- (41) Fuchs, M.; Fürstner, A. Trans-Hydrogenation: Application to a Concise and Scalable Synthesis of Brefeldin A. *Angewandte Chemie International Edition* **2015**, 54 (13), 3978–3982. <https://doi.org/10.1002/anie.201411618>.

- (42) Cowper, N. G. W.; Chernowsky, C. P.; Williams, O. P.; Wickens, Z. K. Potent Reductants via Electron-Primed Photoredox Catalysis: Unlocking Aryl Chlorides for Radical Coupling. *J. Am. Chem. Soc.* **2020**, *142* (5), 2093–2099. <https://doi.org/10.1021/jacs.9b12328>.
- (43) Chmiel, A. F.; Williams, O. P.; Chernowsky, C. P.; Yeung, C. S.; Wickens, Z. K. Non-Innocent Radical Ion Intermediates in Photoredox Catalysis: Parallel Reduction Modes Enable Coupling of Diverse Aryl Chlorides. *J. Am. Chem. Soc.* **2021**, *143* (29), 10882–10889. <https://doi.org/10.1021/jacs.1c05988>.
- (44) Chernowsky, C. P.; Chmiel, A. F.; Wickens, Z. K. Electrochemical Activation of Diverse Conventional Photoredox Catalysts Induces Potent Photoreductant Activity**. *Angewandte Chemie International Edition* **2021**, *60* (39), 21418–21425. <https://doi.org/10.1002/anie.202107169>.
- (45) Cabby, S.; Bouchet, L. M.; Argüello, J. E.; Rossi, R. A.; Bardagi, J. I. Excitation of Radical Anions of Naphthalene Diimides in Consecutive- and Electro-Photocatalysis**. *ChemCatChem* **2021**, *13* (13), 3001–3009. <https://doi.org/10.1002/cctc.202100359>.
- (46) König, B.; Ghosh, I.; Ghosh, T.; Bardagi, J. I. Reduction of Aryl Halides by Consecutive Visible Light-Induced Electron Transfer Processes. *Science* **2014**, *346* (6210), 725–728. <https://doi.org/10.1126/science.1258232>.
- (47) Neumeier, M.; Sampedro, D.; Májek, M.; de la Peña O'Shea, V. A.; Jacobi von Wangelin, A.; Pérez-Ruiz, R. Dichromatic Photocatalytic Substitutions of Aryl Halides with a Small Organic Dye. *Chemistry – A European Journal* **2018**, *24* (1), 105–108. <https://doi.org/10.1002/chem.201705326>.
- (48) Kim, H.; Kim, H.; Lambert, T. H.; Lin, S. Reductive Electrophotocatalysis: Merging Electricity and Light To Achieve Extreme Reduction Potentials. *J. Am. Chem. Soc.* **2020**, *142* (5), 2087–2092. <https://doi.org/10.1021/jacs.9b10678>.
- (49) MacKenzie, I. A.; Wang, L.; Onuska, N. P. R.; Williams, O. F.; Begam, K.; Moran, A. M.; Dunietz, B. D.; Nicewicz, D. A. Discovery and Characterization of an Acridine Radical Photoreductant. *Nature* **2020**, *580* (7801), 76–80. <https://doi.org/10.1038/s41586-020-2131-1>.
- (50) Cole, J. P.; Chen, D.-F.; Kudisch, M.; Pearson, R. M.; Lim, C.-H.; Miyake, G. M. Organocatalyzed Birch Reduction Driven by Visible Light. *J. Am. Chem. Soc.* **2020**, *142* (31), 13573–13581. <https://doi.org/10.1021/jacs.0c05899>.
- (51) Tian, X.; Karl, T. A.; Reiter, S.; Yakubov, S.; de Vivie-Riedle, R.; König, B.; Barham, J. P. Electro-Mediated PhotoRedox Catalysis for Selective C(Sp³)–O Cleavages of Phosphinated Alcohols to Carbanions. *Angewandte Chemie International Edition* **2021**, *60* (38), 20817–20825. <https://doi.org/10.1002/anie.202105895>.
- (52) Xu, J.; Cao, J.; Wu, X.; Wang, H.; Yang, X.; Tang, X.; Toh, R. W.; Zhou, R.; Yeow, E. K. L.; Wu, J. Unveiling Extreme Photoreduction Potentials of Donor–Acceptor Cyanoarenes to Access Aryl Radicals from Aryl Chlorides. *J. Am. Chem. Soc.* **2021**, *143* (33), 13266–13273. <https://doi.org/10.1021/jacs.1c05994>.
- (53) Wu, S.; Kaur, J.; Karl, T. A.; Tian, X.; Barham, J. P. Synthetic Molecular Photoelectrochemistry: New Frontiers in Synthetic Applications, Mechanistic Insights and Scalability. *Angewandte Chemie International Edition* **2022**, *61* (12), e202107811. <https://doi.org/10.1002/anie.202107811>.
- (54) Alektiar, S. N.; Wickens, Z. K. Photoinduced Hydrocarboxylation via Thiol-Catalyzed Delivery of Formate Across Activated Alkenes. *J. Am. Chem. Soc.* **2021**, *143* (33), 13022–13028. <https://doi.org/10.1021/jacs.1c07562>.
- (55) Lund, H.; Carlsson, H. S.; Nishida, T.; Enzell, C. R.; Matsuno, T. Photochemistry of Radical Ions. *Acta Chem. Scand.* **1978**, *32b*, 505–509. <https://doi.org/10.3891/acta.chem.scand.32b-0505>.

- (56) Francke, R.; Little, R. D. Redox Catalysis in Organic Electrosynthesis: Basic Principles and Recent Developments. *Chem. Soc. Rev.* **2014**, *43* (8), 2492–2521. <https://doi.org/10.1039/C3CS60464K>.
- (57) Strieth-Kalthoff, F.; Glorius, F. Triplet Energy Transfer Photocatalysis: Unlocking the Next Level. *Chem* **2020**, *6* (8), 1888–1903. <https://doi.org/10.1016/j.chempr.2020.07.010>.
- (58) Chen, D.-F.; Chrisman, C. H.; Miyake, G. M. Bromine Radical Catalysis by Energy Transfer Photosensitization. *ACS Catal.* **2020**, *10* (4), 2609–2614. <https://doi.org/10.1021/acscatal.0c00281>.
- (59) Strieth-Kalthoff, F.; James, M. J.; Teders, M.; Pitzer, L.; Glorius, F. Energy Transfer Catalysis Mediated by Visible Light: Principles, Applications, Directions. *Chem. Soc. Rev.* **2018**, *47* (19), 7190–7202. <https://doi.org/10.1039/C8CS00054A>.
- (60) Hammond, G. S.; Turro, N. J.; Leermakers, P. A. The Mechanisms of Photoreactions in Solution. IX. Energy Transfer from the Triplet States of Aldehydes and Ketones to Unsaturated Compounds. *J. Phys. Chem.* **1962**, *66* (6), 1144–1147. <https://doi.org/10.1021/j100812a041>.
- (61) Metternich, J. B.; Gilmour, R. A Bio-Inspired, Catalytic E → Z Isomerization of Activated Olefins. *J. Am. Chem. Soc.* **2015**, *137* (35), 11254–11257. <https://doi.org/10.1021/jacs.5b07136>.
- (62) Nevesely, T.; Wienhold, M.; Molloy, J. J.; Gilmour, R. Advances in the E → Z Isomerization of Alkenes Using Small Molecule Photocatalysts. *Chem. Rev.* **2021**. <https://doi.org/10.1021/acs.chemrev.1c00324>.
- (63) Kudo, E.; Sasaki, K.; Kawamata, S.; Yamamoto, K.; Murahashi, T. Selective E to Z Isomerization of 1,3-Dienes Enabled by A Dinuclear Mechanism. *Nat Commun* **2021**, *12* (1), 1473. <https://doi.org/10.1038/s41467-021-21720-4>.
- (64) Xu, J.; Liu, N.; Lv, H.; He, C.; Liu, Z.; Shen, X.; Cheng, F.; Fan, B. Photocatalyst-Free Visible Light Promoted E → Z Isomerization of Alkenes. *Green Chem.* **2020**, *22* (9), 2739–2743. <https://doi.org/10.1039/C9GC04303A>.
- (65) Lu, J.; Pattengale, B.; Liu, Q.; Yang, S.; Shi, W.; Li, S.; Huang, J.; Zhang, J. Donor–Acceptor Fluorophores for Energy-Transfer-Mediated Photocatalysis. *J. Am. Chem. Soc.* **2018**, *140* (42), 13719–13725. <https://doi.org/10.1021/jacs.8b07271>.

5.7 Supplemental Information

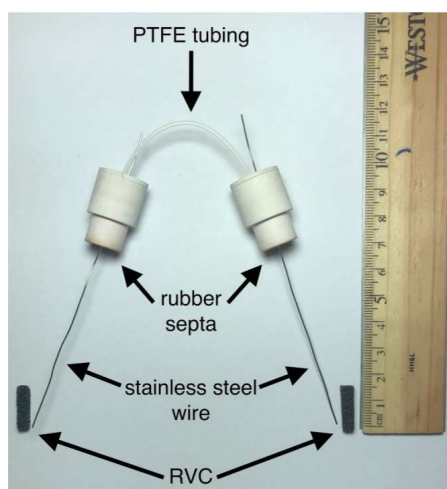
5.71. General Methods and Materials

Unless otherwise noted, reactions were performed under an inert N₂ atmosphere in an anhydrous solvent thoroughly degassed by freeze-pump-thaw. DMF was dried by passing through activated alumina columns. DMSO was purchased anhydrous in sure-seal bottles. All tetra-butylammonium electrolyte salts and lithium perchlorate electrolyte salts were recrystallized from hot ethyl acetate prior to use. Unless otherwise noted, other commercially-available reagents were used as received. Crude mixtures were evaluated by thin-layer chromatography using EMD/Merck silica gel 60 F254 pre-coated plates (0.25 mm) and were visualized by UV, CAM, p-anisaldehyde, or KMnO₄ staining. Flash chromatography was performed with a Biotage Isolera One automated chromatography system with re-packed silica columns (technical grade silica, pore size 40 Å, 230-400 mesh particle size, 40-63 particle size). Purified materials were dried in vacuo (0.050 Torr) to remove trace solvent. ¹H, ¹³C, ³¹P Spectra were taken using a Bruker Avance-400 with a BBFO Probe or a Bruker Avance-500 with a DCH Cryoprobe. NMR data are reported relative to residual CHCl₃ (¹H, δ = 7.26 ppm), CDCl₃ (¹³C, δ = 77.16 ppm). Data for ¹H NMR spectra are reported as follows: chemical shift (δ ppm) (multiplicity, coupling constant (Hz), integration). Multiplicity and qualifier abbreviations are as follows: s = singlet, d = doublet, t = triplet, q = quartet, m = multiplet, br = broad.

5.7.2. Electrochemical Equipment and Experimental Set-Up

All cyclic voltametric and controlled potential measurements were performed at room temperature using a Pine WaveNowXV. The CV experiments were carried out in a three-electrode cell configuration with a glassy carbon (GC) working electrode (3 mm diameter, unless otherwise stated) and a platinum wire counter electrode. CV experiments were carried out with a 0.1 M ⁿBu₄NPF₆ in DMF solution. Bulk constant potential experiments were carried out in divided H cells with RVC (10 × 5 × 5mm) as working and counter electrodes affixed to stainless steel wire. The potentials were measured versus an Ag/AgNO₃ (0.01 M in MeCN with 0.01M ⁿBu₄NPF₆) reference electrode (all electrodes from Pine Research). LEDs (PAR20-18W LG 405 nm) used in this study were purchased from HepatoChem (PAR20-18W LG 405 nm) and Kessil (KSPR160L-390, KSPR160L-427, KSPR160L-440).

Electrode Assembly and Fabrication:



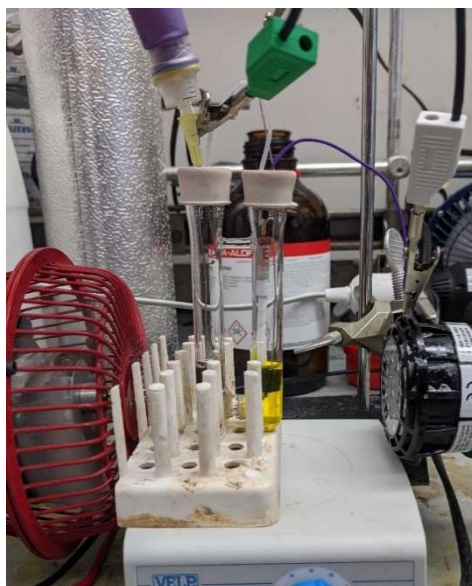
Polytetrafluoroethylene (PTFE) tubing purchased from Cole-Parmer; 1/32" ID, 1/16" OD, item number EW-06407-41. 14/20 Rubber septa purchased from VWR, item number 89064-940. Stainless steel wire purchased from Grainger; stainless steel lockwire, 0.025" diameter, item number 16Y043. Reticulated vitreous carbon (RVC) purchased from SELEE Corporation; 80 ppi, 04-07 g/cc, cut into 15×3×5 mm pieces.

H-Type Cell Fabrication:



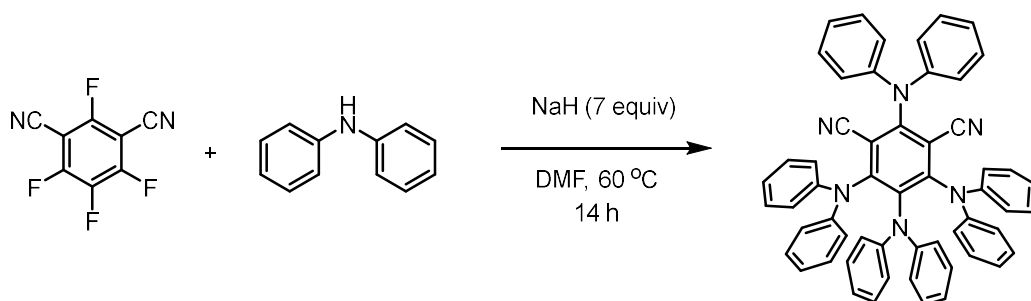
Divided cell fabricated in-house (*FUSION, Journal of the ASGS*, **2020**, 67, 4, 19-26). Porosity E glass filter disc purchased from Ace Glass; 8 mm diameter, part number 7176-21.

Standard reaction setup:



5.7.3. Catalyst Synthesis

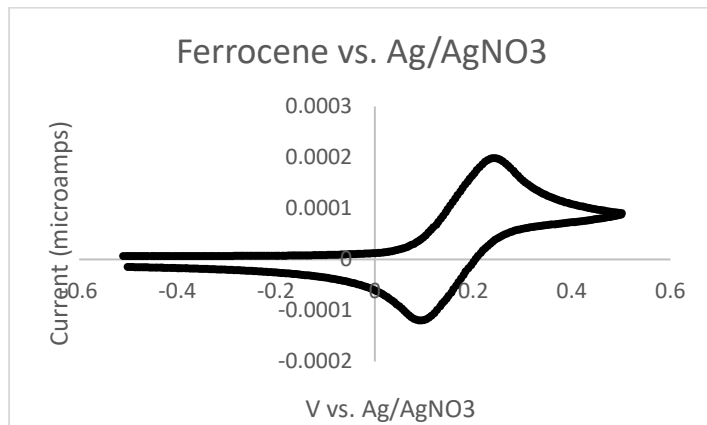
2,4,5,6-tetrakis(diphenylamino)isophthalonitrile (**4-DPAIPN**)



A flame dried RBF was charged with NaH (60% dispersion, 3.0 g, 75 mmol, 7 equiv) and placed under nitrogen atmosphere and DMF (100 mL) was added to the flask. In a separate flask, diphenylamine (8.5 g, 50 mmol, 5 equiv) was dissolved in DMF (25 mL) and the solution was added dropwise to the reaction flask and the solution was heated to 60 °C and stirred for 1 hour. In a separate flask, 2,4,5,6-tetrafluoroisophthalonitrile (2.0 g, 10 mmol, 1 equiv) was dissolved in DMF (25 mL) and the solution was added dropwise to the reaction vessel and the solution was cooled and stirred at 40 °C overnight. Reaction was cooled to room temperature and excess NaH was quenched by adding isopropanol dropwise. Water (200 mL) was added to precipitate crude product. Precipitate was collected by filtration and washed with water and dried *in vacuo*. Crude product was purified by dissolving in DCM passing through a silica plug and recrystallized from DCM/hexanes to provide pure product as a yellow solid (5.2 g, 6.6 mmol, 66%). **¹H NMR** (500 MHz, CDCl₃) δ 7.35 – 7.24 (m, 4H), 7.15 – 7.07 (m, 12H), 7.07 – 7.01 (m, 2H), 6.97 – 6.86 (m, 8H), 6.75 – 6.69 (m, 10H), 6.58 (d, J = 7.5 Hz, 4H). Consistent with reported spectra (*Angew. Chem. Int. Ed.* **2019**, 131, 8266-8270).

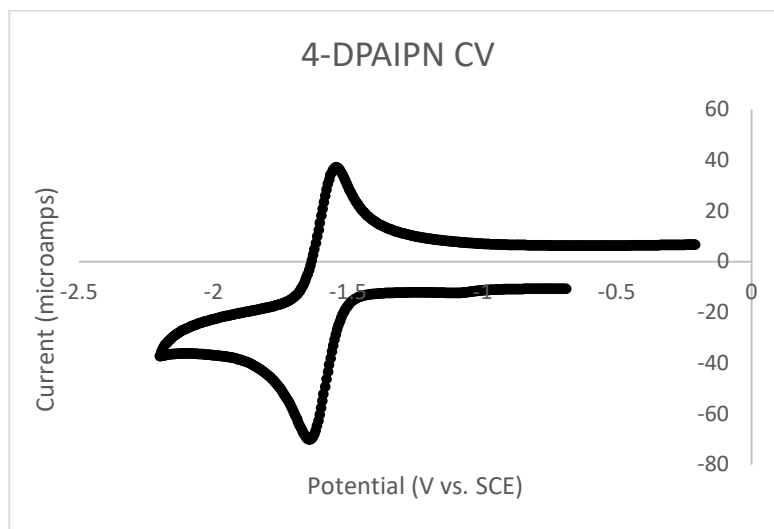
5.7.4. Cyclic Voltammetry

All CV measurements were conducted in DMF against Ag/AgNO₃ (0.01 M in MeCN) reference cell and 0.1 M ⁿBu₄NPF₆ supporting electrolyte. Analyte was measured in 10 mM concentration. Conversion from the Ag/AgNO₃ reference used for measurements to standard SCE reference was obtained by measuring the ferrocene redox couple and using standard conversion values between ferrocene and SCE.



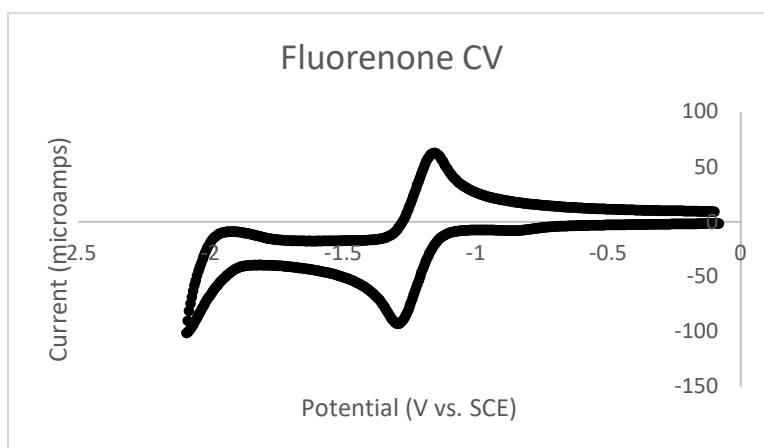
$\text{Fc/Fc}^+ E_{1/2} = 0.17 \text{ V vs. Ag/AgNO}_3$ (Ag/AgNO₃ to SCE conversion = 300 mV)

4DPAIPN



4DPAIPN $E_{\text{red}} = -1.64 \text{ V vs. SCE}$

Fluorenone



Fluorenone $E_{\text{red}} = -1.28 \text{ V vs SCE}$

Literature values were used for the following structures:

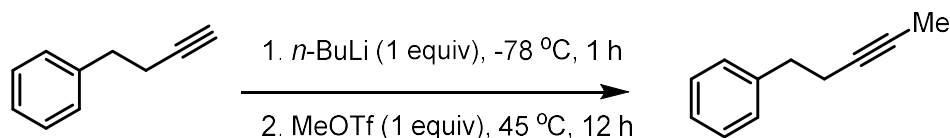
Pyrene $E_{\text{red}} = -2.1 \text{ V vs SCE}$ (*Acta. Chem. Sca. B.*, **19787**, 505-509)

Rubrene = -1.84 V vs SCE (*J.Phys.Chem.*, **2022**, 126, 40, 7147-7158)

Acridine Orange $E_{\text{red}} = -2.4 \text{ V vs SCE}$ (*Chem.Rev.*, **2016**, 116, 17, 10075-10166)

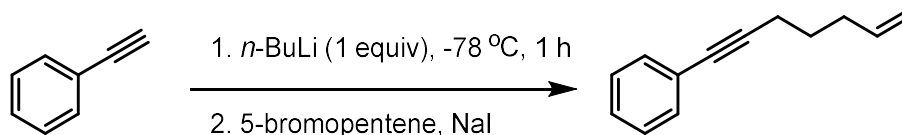
5.7.5. Synthesis of Non-Commercial Substrates

1-phenyl-3-pentyne (4)



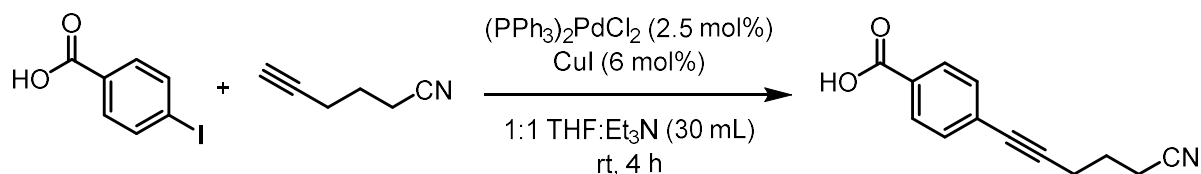
To a flame dried 50 mL round bottom flask was added 1-phenyl-3-butyne (2.8 mL, 20 mmol, 1 equiv) and diethyl ether (15 mL) and cooled to -78 °C and *n*-BuLi solution (6.7 mL of a 2.2 M solution in hexanes, 1 equiv) was added dropwise under and atmosphere of N₂. The solution was stirred for 1 hour. To the solution was added methyl triflate (2.2 mL, 20 mmol, 1 equiv) dropwise and the solution was warmed to room temperature before heating to 45 °C overnight. The reaction mixture was quenched with sat. NH₄Cl (5 mL) and diluting with water (50 mL). The organic layer was extracted with hexanes (3x60 mL) and washed with 1 M HCl (20 mL) and brine before drying over Mg(SO₄)₂ and concentration. The crude product mixture was purified by vacuum distillation (starting material distilled at 70 °C and product **4** distilled at 85 °C. Pure product was recovered as a colorless liquid (1.16 g, 48%). ¹H NMR (500 MHz, CDCl₃) δ 7.21 (dd, *J* = 8.0, 6.8 Hz, 2H), 7.13 (d, *J* = 7.1 Hz, 3H), 2.72 (t, *J* = 7.7 Hz, 2H), 2.34 (tq, *J* = 7.5, 2.5 Hz, 2H), 1.70 (t, *J* = 2.5 Hz, 3H). Consistent with reported spectra (*J. Am. Chem. Soc.* **2018**, 140, 18, 6006-6013).

Hept-6-en-1-ynylbenzene



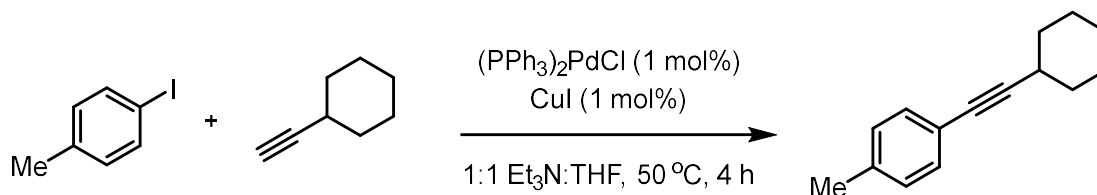
To a flame dried 100 mL round bottom flask was added 1-phenyl-ethyne (1.10 mL, 10 mmol, 1.4 equiv) and THF (15 mL) and cooled to -78 °C. To the solution was added *n*-BuLi (2.9 mL of a 2.5 M solution in hexanes, 1 equiv) dropwise and stirred for 1 hour. To the solution was added 5-bromopentene (845 μL, 7.1 mmol, 1 equiv) and sodium iodide (53 mg, 0.3 mmol, 0.05 equiv) and the solution was warmed to room temperature and stirred at 80 °C for 48 h. The reaction mixture was quenched with sat. NH₄Cl (5 mL) and diluting with water (50 mL). The organic layer was extracted with hexanes (3x60 mL) and washed with 1 M HCl (20 mL) and brine before drying over Mg(SO₄)₂ and concentration. The crude product mixture was purified by column chromatography to give pure product as a colorless liquid (950 mg, 78%). ¹H NMR (500 MHz, CDCl₃) δ 7.45 – 7.40 (m, 2H), 7.34 – 7.26 (m, 3H), 5.87 (ddt, *J* = 17.0, 10.2, 6.7 Hz, 1H), 5.11 (dq, *J* = 17.2, 1.7 Hz, 1H), 5.04 (ddt, *J* = 10.2, 2.3, 1.2 Hz, 1H), 2.46 (t, *J* = 7.1 Hz, 2H), 2.31 – 2.21 (m, 2H), 1.74 (p, *J* = 7.2 Hz, 2H). Consistent with reported spectra (*Org. Lett.* **2019**, 21, 16, 6552-6556).

4-(5-cyanopent-1-yn-1-yl)benzoic acid



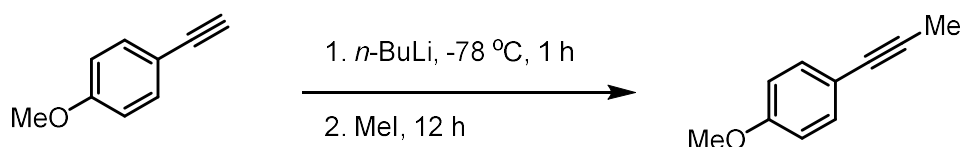
To a flame dried flask was added bis(triphenylphosphine)palladium (II) dichloride, copper iodide, and 4-iodobenzoic acid and placed under an inert atmosphere. Nitrogen gas was bubbled through THF and triethylamine for fifteen minutes and the degassed THF and Et₃N were added to the reaction flask followed by 5-hexynenitrile. The solution was stirred at room temperature for four hours after which 1 M aqueous HCl (70 mL) was added and the mixture was extracted with diethyl ether (3x50 mL). The organic layers were combined, washed with brine and dried over MgSO₄. The crude reaction mixture was purified by column chromatography followed by recrystallization from DCM:hexanes to yield pure product as a pale yellow solid (489 mg, 69% yield). ¹H NMR (500 MHz, CDCl₃) δ 8.06 (d, *J* = 8.4 Hz, 2H), 7.51 (d, *J* = 8.2 Hz, 2H), 2.68 (t, *J* = 6.8 Hz, 2H), 2.60 (t, *J* = 7.1 Hz, 2H), 2.02 (p, *J* = 7.0 Hz, 2H).

1-(cyclohexylethynyl)-4-methylbenzene



To a 100 mL flame dried round bottom flask was added 4-iodotoluene (1.09 g, 5.00 mmol, 1 equiv), bis-(triphenylphosphino)-palladium chloride (35 mg, 0.05 mmol, 0.01 equiv), copper iodide (9.5 mg, 0.05 mmol, 0.01 equiv) and THF (8 mL). To the solution was added cyclohexylacetylene (653 μL, 5.00 mmol, 1 equiv) and triethylamine (8 mL) under a nitrogen atmosphere. The mixture was stirred at 50 °C for 4 hours. The crude reaction mixture was filtered with a short silica pad and concentrated. The residue was purified by column chromatography to give the pure product as a colorless oil (900 mg, 90%). ¹H NMR (400 MHz, CDCl₃) δ 7.31 (d, *J* = 8.1 Hz, 2H), 7.10 (d, *J* = 7.9 Hz, 2H), 2.60 (tt, *J* = 8.8, 3.8 Hz, 1H), 2.35 (s, 3H), 1.94 – 1.86 (m, 2H), 1.84 – 1.70 (m, 2H), 1.60 – 1.51 (m, 3H), 1.37 (p, *J* = 7.0, 5.9 Hz, 3H). Consisted with reported spectra (*J.Am.Chem.Soc.*, **2016**, 138, 5, 1514-1517).

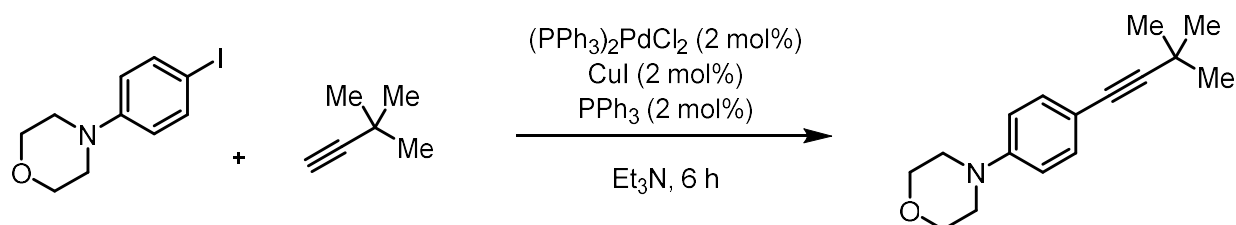
1-methoxy-4-(prop-1-yn-1-yl)benzene



To a flame dried 100 mL round bottom flask was added 4-methoxy phenyl acetylene (1.3 mL, 10 mmol, 1 equiv) and THF (20 mL) under an atmosphere of N₂ and cooled to -78 °C. To the solution was added *n*-BuLi (4.2 mL of a 2.5 M solution in hexanes, 1.05 equiv) dropwise and stirred for 1 h. To the solution was added methyl iodide (685 μL, 11 mmol, 1.1 equiv) dropwise and the solution was warmed to room temperature and stirred overnight. The reaction was

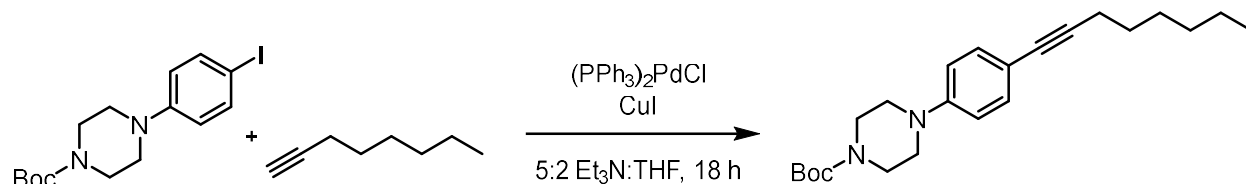
quenched with saturated NH_4Cl (5 mL), and diluted with water (50 mL). The organic layer was extracted with hexanes (3 x 100 mL), washed with brine, dried over $\text{Mg}(\text{SO}_4)_2$, and concentrated. Crude product was purified by vacuum distillation and pure product was isolated as a colorless oil (1.4 g, 99%). **$^1\text{H NMR}$** (500 MHz, CDCl_3) δ 7.35 (d, J = 8.8 Hz, 2H), 6.84 (d, J = 8.8 Hz, 2H), 3.82 (s, 3H), 2.06 (s, 3H). Consistent with reported spectra (*J. Am. Chem. Soc.*, **2022**, 144, 30, 13961-13972).

4-(4-(3,3-dimethylbut-1-yn-1-yl)phenyl)morpholine



To a 100 mL flame dried round bottom flask was added 4-iodophenylmorpholine (867 mg, 3.00 mmol, 1 equiv), bis-(triphenylphosphino)-palladium dichloride (42 mg, 0.04 mmol, 0.02 equiv), copper iodide (11 mg, 0.04 mmol, 0.02 equiv) and Et_3N (25 mL). To the solution was added tert-butylacetylene (554 μL , 4.5 mmol, 1.5 equiv) under a nitrogen atmosphere and the mixture was stirred at room temperature for 6 hours. The reaction was quenched with saturated NH_4Cl (5 mL), and diluted with water (50 mL). The organic layer was extracted with ethyl acetate (3 x 50 mL), washed with brine, dried over $\text{Mg}(\text{SO}_4)_2$, and concentrated. Crude product was purified by column chromatography to give pure product as a white solid (633 mg, 87%). **$^1\text{H NMR}$** (500 MHz, CDCl_3) δ 7.32 (d, J = 8.9 Hz, 2H), 6.82 (d, J = 8.4 Hz, 2H), 3.95 – 3.81 (m, 4H), 3.23 – 3.13 (m, 4H), 1.33 (s, 9H).

tert-butyl 4-(4-(oct-1-yn-1-yl)phenyl)piperazine-1-carboxylate



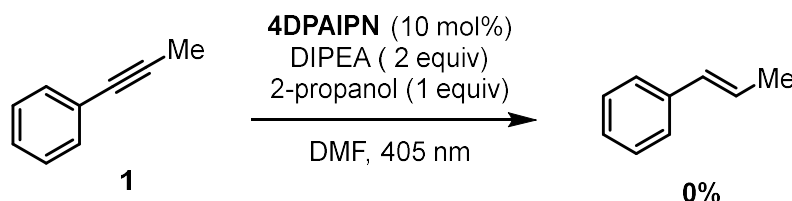
To a 50 mL flame dried round bottom flask was added tert-butyl-4-(4-iodophenyl)piperazine-1-carboxylate (582 mg, 1.5 mmol, 1 equiv), bis-(triphenylphosphino)-palladium dichloride (10 mg, 0.015 mmol, 0.01 equiv), copper iodide (2.9 mg, 0.015 mmol, 0.01 equiv) and THF (2 mL). To the solution was added 1-octyne (221 μL , 1.5 mmol, 1 equiv) and Et_3N (5 mL) under a nitrogen atmosphere and the mixture was stirred at room temperature for 9 hours. Additional bis-(triphenylphosphino)-palladium dichloride (10 mg, 0.015 mmol, 0.01 equiv) and copper iodide (2.9 mg, 0.015 mmol, 0.01 equiv) was added under N_2 and the reaction was stirred for an additional 9 h. The reaction was quenched with saturated NH_4Cl (5 mL), and diluted with water (50 mL). The organic layer was extracted with ethyl acetate (3 x 50 mL), washed with brine, dried over $\text{Mg}(\text{SO}_4)_2$, and concentrated. Crude product was purified by column chromatography to give pure product as a white solid (351 mg, 63%). **$^1\text{H NMR}$** (500 MHz, CDCl_3) δ 7.32 (d, J = 8.8 Hz, 2H), 6.88 – 6.78 (m, 2H), 3.59 (t, J = 5.1 Hz, 4H), 3.17 (t, J = 5.2 Hz, 4H), 2.40 (t, J = 7.1 Hz, 2H), 1.60 (dd, J = 13.9, 6.3 Hz, 2H), 1.50 (m, 11H), 1.38 – 1.29 (m, 4H), 0.98 – 0.88 (m, 3H).

5.7.6. Screening Engines for Electron-Primed Photoredox Catalysis

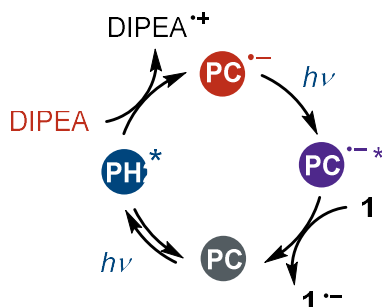
conPET Systems

To a 10 mL Schlenk flask was added 1-phenyl-1-propyne (12.5 μ L, 0.1 mmol 1 equiv), **4DPAIPN** (8 mg, 0.01 mmol, 0.1 equiv), diisopropylethylamine (35 μ L, 0.2 mmol, 2 equiv), 2-propanol (7.7 μ L, 0.1 mmol, 1 equiv) and DMF (2 mL). The solution was degassed by freeze, pump, thaw cycles (3x) and irradiated at 405 nm for 8 hours.

Aliquot workup: To the crude reaction mixture was added mesitylene (18 μ L, 0.13 mmol) as an internal standard. 0.1 mL of the reaction mixture was placed in a vial and diluted with brine (1 mL) before being extracted with deuterated chloroform for analysis by NMR.



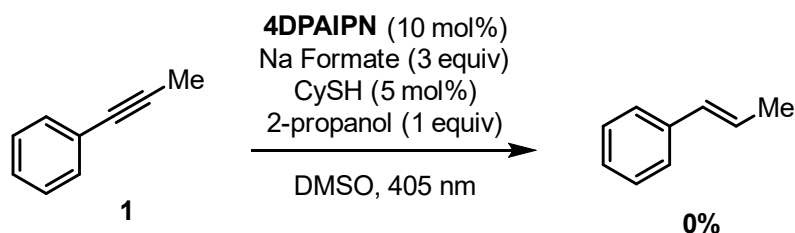
Electron-Primed engine:



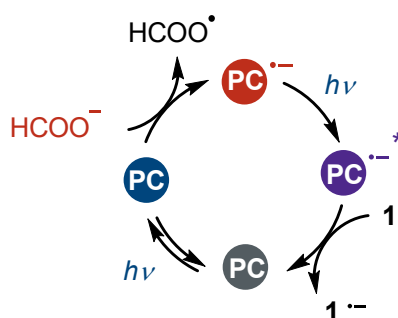
Conditions adapted from *J. Am. Chem. Soc.*, **2021**, 143, 10882-10889:

To a 10 mL Schlenk flask was added 1-phenyl-1-propyne (12.5 μ L, 0.1 mmol 1 equiv), **4DPAIPN** (4 mg, 0.005 mmol, 0.05 equiv), sodium formate (20mg, 0.3 mmol, 3 equiv), cyclohexane thiol (0.6 μ L, 0.005 mmol, 0.05 equiv), 2-propanol (7.7 μ L, 0.1 mmol, 1 equiv) and DMSO (1.25 mL). The reaction solution was degassed by freeze/pump/thaw cycles (x3) and irradiated at 405 nm for 16 hours.

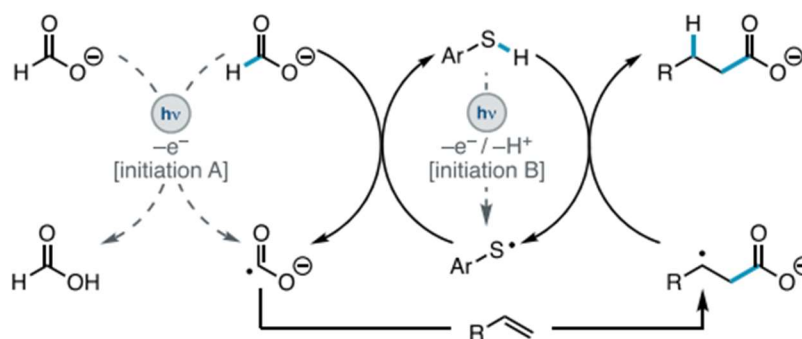
Aliquot workup: To the crude reaction mixture was added mesitylene (18 μ L, 0.13 mmol) as an internal standard. 0.1 mL of the reaction mixture was placed in a vial and diluted with brine (1 mL) before being extracted with deuterated chloroform for analysis by NMR.



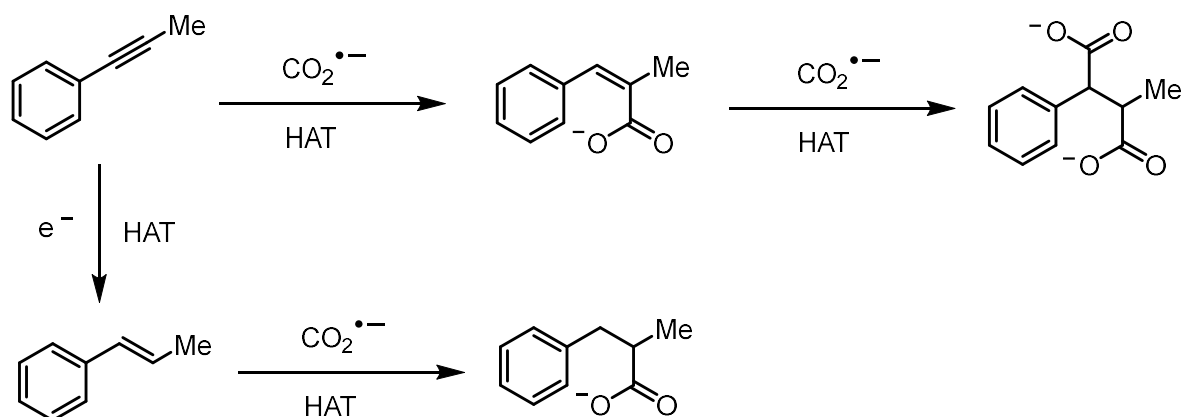
Electron-Primed engine:



High substrate conversion was observed but no product formation. We hypothesize that the majority of mass balance is going to a variety of carboxylated products that are not soluble in the chloroform NMR solvent and were not observed in the crude NMR analysis. This hypothesis comes from work published by our group (*J.Am.Chem.Soc.* **2021**, 143, 33, 13022-13028) showing that $\text{CO}_2^{\bullet-}$, generated when formate is used as a terminal oxidant, can add into activated pi bonds via radical addition. The mechanism proposed in this work is below:



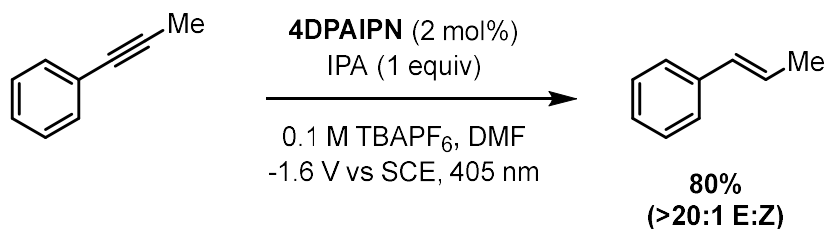
Possible carboxylated products derived from **1** could form by numerous mechanisms including $\text{CO}_2^{\bullet-}$ -addition to the alkyne followed by HAT to give a mono-carboxylated styrene. This intermediate could then undergo a second carboxylation to 2-methyl-3-phenylsuccinate. Alternatively, semi-hydrogenation could be promoted and the styrene product could undergo hydrocarboxylation. The possible pathways are summarized below:



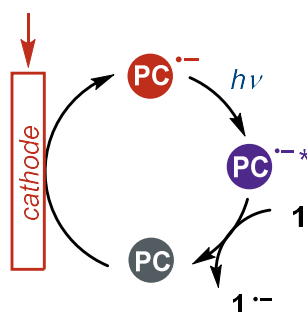
Electrochemical System

An oven dried, H-type divided cell with a glass frit was equipped with stir bars and 1-phenyl-1-propyne (25 μ L, 0.2 mmol, 1 equiv), 4DPAIPN (2.1 mg, 0.004 mmol, 0.02 equiv.), 2-propanol (15.3 μ L, 0.2 mmol, 1 equiv) and n Bu₄PF₆ (0.2 mmol, 77 mg) were added to the cathodic chamber while n Bu₄PF₆ (0.2 mmol, 77 mg) was added to the anodic chamber. A three-electrode setup was assembled with a RVC cathode and anode and a reference cell wrapped in Teflon. The divided cell was equipped with the electrode assembly, sealed with septa and purged with a flow of N₂ for 10 minutes (inlet needle in the anode, outlet needle in the cathode). To the anode and then cathode was added DMF (2 mL) and triethylamine (220 μ L, 1.6 mmol, 4 equiv) was added to the anode. Electrodes were connected to a WaveNow potentiostat and electrolyzed at -1.6 V vs. SCE and irradiated with HepatoChem 405 nm LEDs for 12 hours. Temperature was maintained by electric fans cooling.

Aliquot workup: To the crude reaction mixture was added mesitylene (18 μ L, 0.13 mmol) as an internal standard. 0.1 mL of the reaction mixture was placed in a vial and diluted with brine (1 mL) before being extracted with deuterated chloroform for analysis by NMR.



Electron-Primed engine:

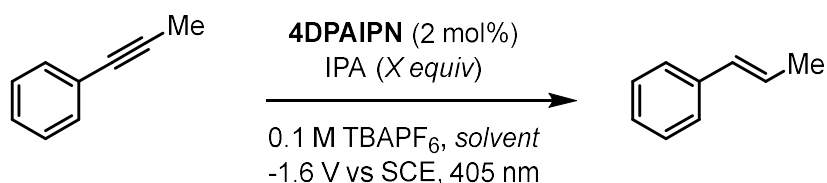


5.7.7. Controlling the Degree of Hydrogenation

The amount of isopropanol added to a reaction was varied, following the following procedure:

An oven dried, H-type divided cell with a glass frit was equipped with stir bars and 1-phenyl-1-propyne (25 μ L, 0.2 mmol, 1 equiv), 4DPAIPN (2.1 mg, 0.004 mmol, 0.02 equiv.), 2-propanol (*varying amounts*) and n Bu₄PF₆ (0.2 mmol, 77 mg) were added to the cathodic chamber while n Bu₄PF₆ (0.2 mmol, 77 mg) was added to the anodic chamber. A three-electrode setup was assembled with a RVC cathode and anode and a reference cell wrapped in Teflon. The divided cell was equipped with the electrode assembly, sealed with septa and purged with a flow of N₂ for 10 minutes (inlet needle in the anode, outlet needle in the cathode). To the anode and then cathode was added solvent (2 mL) and triethylamine (220 μ L, 1.6 mmol, 4 equiv) was added to the anode. Electrodes were connected to a WaveNow potentiostat and electrolyzed at -1.6 V vs. SCE and irradiated with HepatoChem 405 nm LEDs for 12 hours. Temperature was maintained by electric fans cooling.

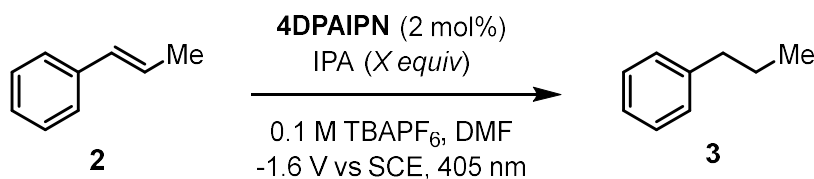
Aliquot workup: To the crude reaction mixture was added mesitylene (18 μ L, 0.13 mmol) as an internal standard. 0.1 mL of the reaction mixture was placed in a vial and diluted with brine (1 mL) before being extracted with deuterated chloroform for analysis by NMR.



entry	solvent	IPA (equiv)	2	3
1	DMF	1	78	0
2	DMF	2	35	39
3	DMF	4	0	72
4	MeCN	1	51	1
5	MeCN	2	47	2
6	MeCN	4	0	53

To test the conditions that resulted in exhaustive hydrogenation, we repeated the experiment but replaced 1-phenyl-1-propyne with *trans*- β -methylstyrene, following the same procedure.

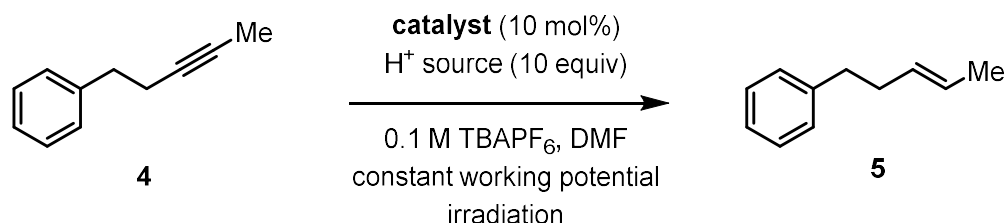
Reduction of styrene derivatives



entry	IPA (equiv)	3
1	1	1
2	2	2
3	4	83

5.7.8. Semi-Hydrogenation of Aliphatic Alkynes

1-phenyl-3-pentyne was selected as the model substrate, however, standard reaction conditions optimized for semi-hydrogenation of 1-phenyl-1-pentyne resulted in no conversion. We conducted a screen of structurally diverse photocatalysts to attempt to uncover a more effective system for aliphatic alkynes.

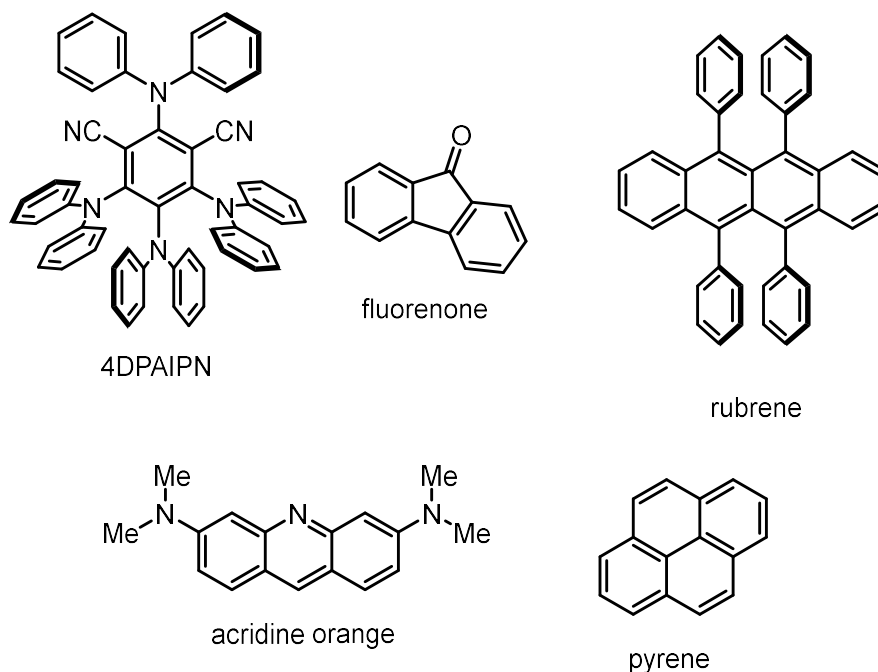


Each catalyst was studied under a constant applied potential equal to that of the E_{red} found via cyclic voltammetry.

The optimal wavelength was found for each catalyst studied by observing the current response on the potentiostat computer when subjected to different wavelengths of light. Since current is a measure of rate of electrons being passed and proportional to the rate of catalysis, the wavelength that resulted in the highest magnitude current readout was selected as the irradiation wavelength for each catalyst.

All reactions run on a 0.200 mmol scale and analyzed by NMR.

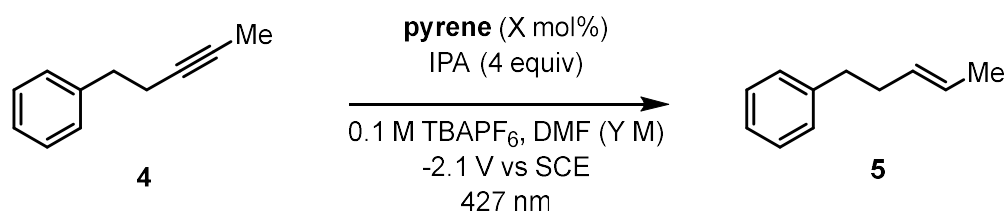
The catalysts tested are listed below:



Entry	Catalyst	Optimal λ (nm)	E_{red} (V vs SCE)	H^+ source	5 (%)
1	4DPAIPN	405	-1.6	IPA	0
2	Fluorenone	405	-1.3	water	0
3	Rubrene	456	-1.5	IPA	0
4	Acridine orange	405	-2.0	water	4
5	pyrene	427	-2.1	water	18

We moved forward with pyrene as the optimal catalyst as it gave the highest semi-hydrogenation yield. We next varied some of the reaction conditions including concentration, catalyst loading and changed the H^+ source from water to IPA because this alcohol source was uniformly better than water when optimizing aromatic alkyne semi-hydrogenation.

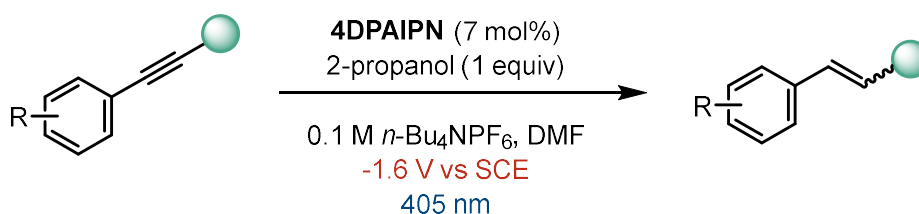
Reactions all conducted on a 0.200 mmol scale and analyzed by NMR.



entry	[] (M)	pyrene (mol %)	5 (%)
1	0.1	5	0
2	0.1	10	21
3	0.1	15	27
4	0.05	5	4
5	0.05	10	6
6	0.05	15	14

No further attempts to optimize this reaction were made at the time of writing this report.

5.7.9. Preliminary Scope Investigations

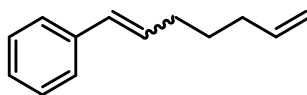


General Procedure:

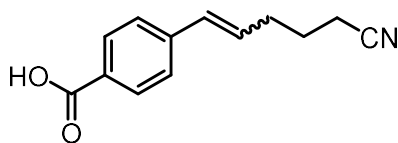
An oven dried, H-type divided cell with a glass frit was equipped with stir bars and aryl alkyne (0.2 mmol, 1 equiv), 4DPAIPN (11 mg, 0.014 mmol, 0.07 equiv.), 2-propanol (15.3 μ L, 0.2 mmol, 1 equiv) and ⁿBu₄PF₆ (0.2 mmol, 77 mg) were added to the cathodic chamber while ⁿBu₄PF₆ (0.2 mmol, 77 mg) was added to the anodic chamber. A three-electrode setup was assembled with a RVC cathode and anode and a reference cell wrapped in Teflon. The divided cell was equipped with the electrode assembly, sealed with septa and purged with a flow of N₂ for 10 minutes (inlet needle in the anode, outlet needle in the cathode). To the anode and then cathode was added DMF (2 mL) and triethylamine (220 μ L, 1.6 mmol, 4 equiv) was added to the anode. Electrodes were connected to a WaveNow potentiostat and electrolyzed at -1.6 V vs. SCE and irradiated with HepatoChem 405 nm LEDs for 15 hours. Temperature was maintained by electric fans cooling.

Aliquot workup: To the crude reaction mixture was added mesitylene (18 μ L, 0.13 mmol) as an internal standard. 0.1 mL of the reaction mixture was placed in a vial and diluted with brine (1 mL) before being extracted with deuterated chloroform for analysis by NMR.

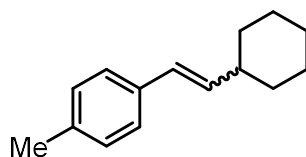
Hepta-1,6-dien-1-ylbenzene (**6**)



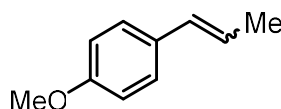
Hept-6-en-1-ynylbenzene underwent semi-hydrogenation according to the general procedure. NMR analysis of the crude reaction mixture showed semi-hydrogenation in 52% yield with an E:Z ratio of >20:1.

4-(5-cyanopent-1-en-1-yl)benzoic acid (**7**)

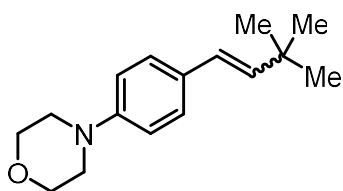
4-(5-cyanopent-1-yn-1-yl)benzoic acid underwent semi-hydrogenation according to the general procedure with the following adjustments: 4DPAIPN loading was reduced to 5 mol% and overall reaction concentration was reduced to 0.05 M. NMR analysis of the crude reaction mixture showed semi-hydrogenation in 58% yield with an E:Z ratio of >20:1.

1-(2-cyclohexylvinyl)-4-methylbenzene (**8**)

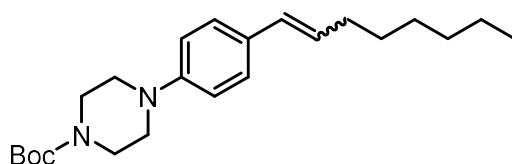
1-(cyclohexylethynyl)-4-methylbenzene underwent semi-hydrogenation according to the general procedure. NMR analysis of the crude reaction mixture showed semi-hydrogenation in 66% yield with an E:Z ratio of 1:1.

1-methoxy-4-(prop-1-en-1-yl)benzene (**9**)

1-methoxy-4-(prop-1-yn-1-yl)benzene underwent semi-hydrogenation according to the general procedure. NMR analysis of the crude reaction mixture showed semi-hydrogenation in 66% yield with an E:Z ratio of 4:1.

4-(4-(3,3-dimethylbut-1-en-1-yl)phenyl)morpholine (**10**)

4-(4-(3,3-dimethylbut-1-yn-1-yl)phenyl)morpholine underwent semi-hydrogenation according to the general procedure. NMR analysis of the crude reaction mixture showed semi-hydrogenation in 64% yield with an E:Z ratio of 3:1.

tert-butyl 4-(4-(oct-1-en-1-yl)phenyl)piperazine-1-carboxylate (**11**)

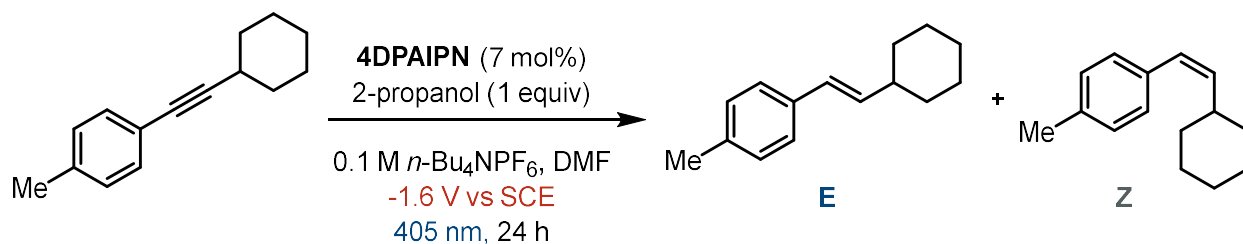
tert-butyl 4-(4-(oct-1-yn-1-yl)phenyl)piperazine-1-carboxylate underwent semi-hydrogenation according to the general procedure. NMR analysis of the crude reaction mixture showed semi-hydrogenation in 65% yield with an E:Z ratio of 3:1.

5.7.10. Investigation of Isomerization Mechanism

Time Course

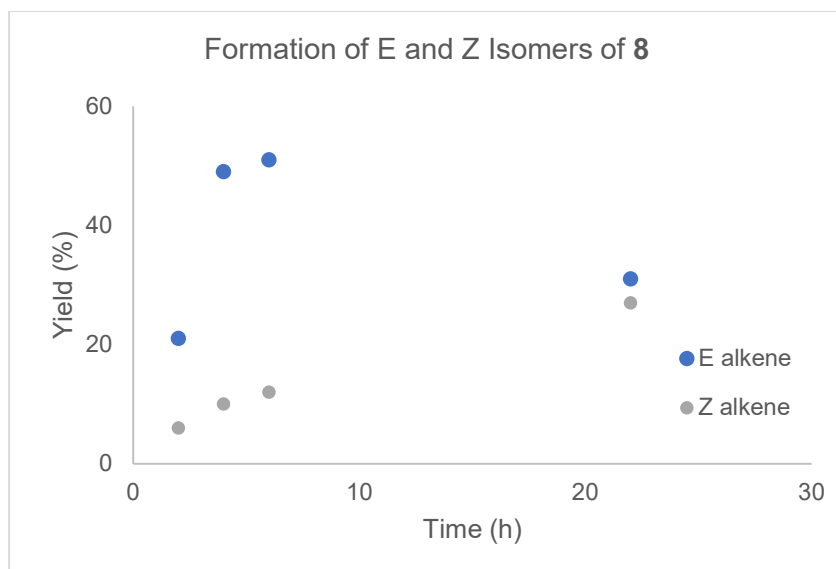
The mixture of E:Z isomers observed for electron rich substrates could be forming by either a constant ratio over the course of the whole reaction as a result of the outcome of the SET reduction of alkynes or the E isomer can be slowly isomerizing to the Z product through an energy transfer mechanism.

To determine when the undesired Z isomer is being formed and if it is coming from the reduction or through isomerization, a time course was run of a standard reaction with an electron rich substrate.

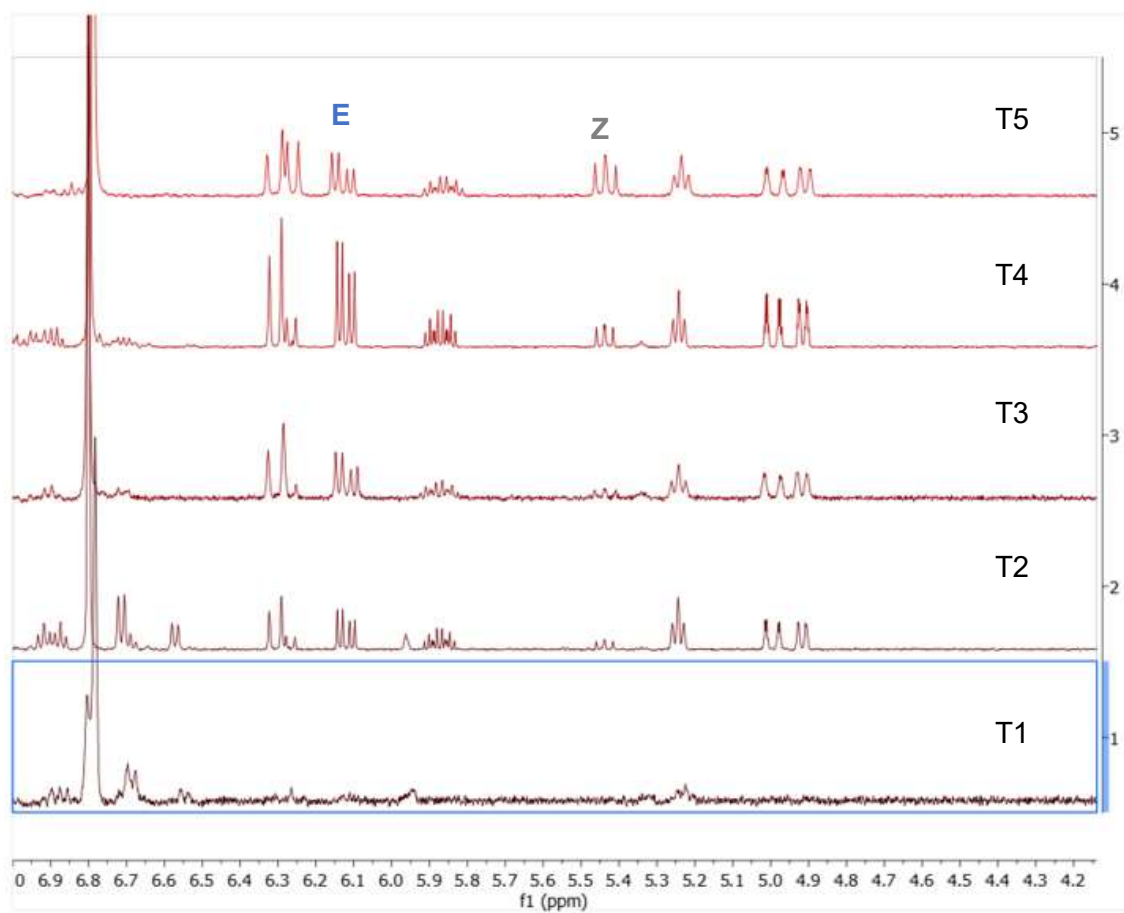


1-(cyclohexylethynyl)-4-methylbenzene was subjected to standard reaction conditions according to the general procedure with the addition of mesitylene (18 μL , 0.13 mmol) as an internal standard. Time points were taken throughout the reaction and analyzed by NMR. The data is summarized below:

Entry	Time (h)	E (%)	Z (%)	Ratio (E:Z)
1	1.25	0	0	0
2	2.18	21	6	3 : 1
3	4.80	49	10	5 : 1
4	6.10	51	12	4 : 1
5	22.0	31	27	1 : 1



The NMR spectra for the time points showing the region with the distinctive E and Z isomers are shown stacked below:



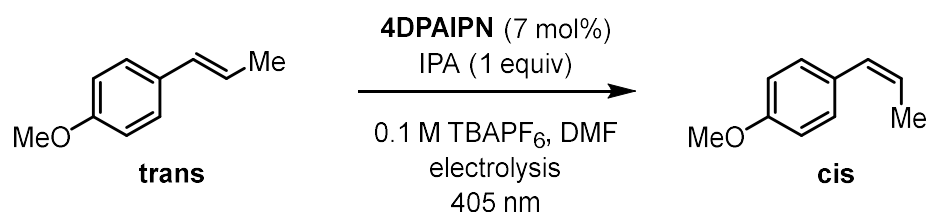
Alkene Isomerization

We propose that alkene isomerization is occurring via triplet energy transfer catalysis. We probed if the energy transfer is a characteristic of the neutral state of **4DPAIPN** or of the radical anion of **4DPAIPN** or if both states of the catalyst are capable of catalyzing an energy transfer pathway.

To test the amount of isomerization observed as a function of the catalyst speciation, we subjected an electron rich styrene, (E)-1-methoxy-4-(prop-1-en-1-yl)benzene to irradiation with no electrolysis where the catalyst distribution is exclusively neutral **4DPAIPN**.

To test **4DPAIPN** radical anion we tested the same electron rich substrate under irradiation but now at the $E_{1/2}$ of **4DPAIPN** where the catalyst distribution is 1:1 neutral **4DPAIPN** and **4DPAIPN** radical anion and at the E_{red} where the catalyst distribution is now exclusively the radical anion.

General Procedure:



An oven dried, H-type divided cell with a glass frit was equipped with stir bars and (E)-1-methoxy-4-(prop-1-en-1-yl)benzene (29.6 mg, 0.2 mmol, 1 equiv), **4DPAIPN** (11 mg, 0.014 mmol, 0.07 equiv.), 2-propanol (15.3 μ L, 0.2 mmol, 1 equiv) and $n\text{Bu}_4\text{PF}_6$ (0.2 mmol, 77 mg) were added to the cathodic chamber while $n\text{Bu}_4\text{PF}_6$ (0.2 mmol, 77 mg) was added to the anodic chamber. A three-electrode setup was assembled with a RVC cathode and anode and a reference cell wrapped in Teflon. The divided cell was equipped with the electrode assembly, sealed with septa and purged with a flow of N_2 for 10 minutes (inlet needle in the anode, outlet needle in the cathode). To the anode and then cathode was added DMF (2 mL) and triethylamine (220 μ L, 1.6 mmol, 4 equiv) was added to the anode.

Reactions were either irradiated or electrolyzed and irradiated according to the experiments described below.

Aliquot workup: To the crude reaction mixture was added mesitylene (18 μ L, 0.13 mmol) as an internal standard. 0.1 mL of the reaction mixture was placed in a vial and diluted with brine (1 mL) before being extracted with deuterated chloroform for analysis by NMR.

Experiment 1: electrolysis at the $E_{1/2}$ of **4DPAIPN**

4DPAIPN distribution: 50% neutral catalyst, 50% radical anion catalyst

Experiment 2: electrolysis at the E_{red} of **4DPAIPN**

4DPAIPN distribution: 100% radical anion catalyst

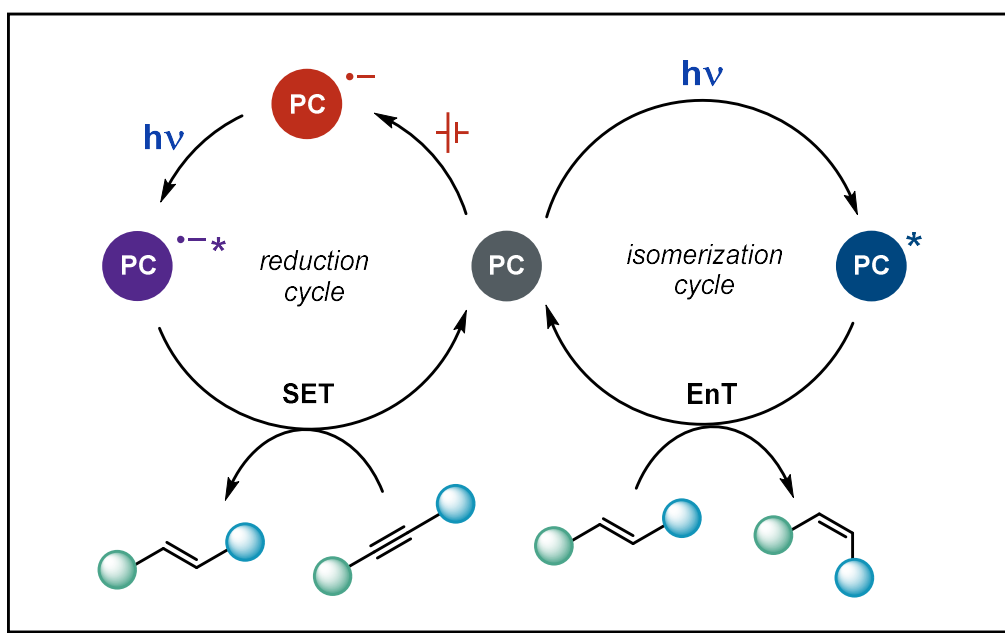
Experiment 3: no electrolysis

4DPAIPN distribution: 100% neutral catalyst

entry	Potential (V vs SCE)	4DPAIPN distribution	trans (%)	cis (%)	ratio (E:Z)	hydrogenation (%)
1	-1.55	mixed	72	18	4 : 1	5
2	-1.64	radical anion	82	4	20 : 1	6
3	Non	Neutral	16	59	1: 4	0

Significant isomerization is observed when **4DPAIPN** remains as the neutral catalyst while only a small amount of isomerization is observed when **4DPAIPN** is electrolyzed to the radical anion. Based on these observations we propose that energy transfer catalysis that is responsible for the E:Z isomerization we observe with electron rich substrates is the result of neutral **4DPAIPN** in the reaction.

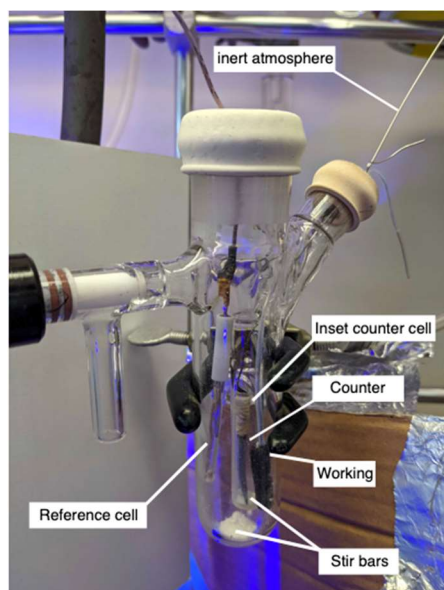
The proposed operative catalytic cycles are summarized below:



5.7.11. UV-Vis of 4DPAIPN

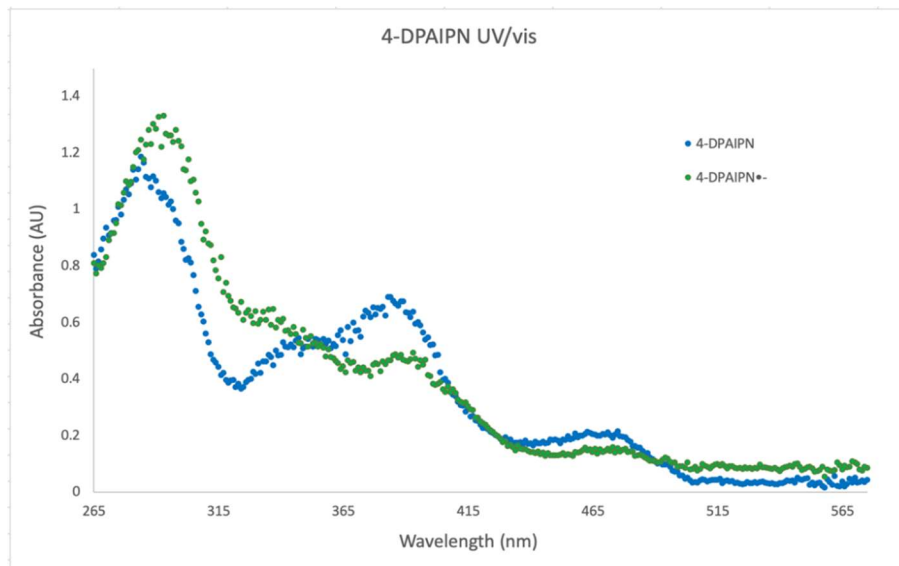
Electro-UV-Vis Sample preparation

To the oven-dried electrochemical cell with stir bars was added ⁿBu₄PF₆ (200 mg, 0.05 M) to each the anode and cathode. A three-electrode setup was assembled with a RVC cathode, a platinum sacrificial anode, and a reference cell wrapped in Teflon. The divided cell was equipped with the electrode assembly, sealed with septa and purged with a flow of Ar for 10 minutes. While under Ar, degassed DMF (8 mL, 0.05 M) was added to the cell. In a separate flame-dried vial, 4-DPAIPN (16 mg, 20 μmol) was added then flushed vial with Ar for 5 minutes. DMF (1 mL) was added to the vial of catalyst.

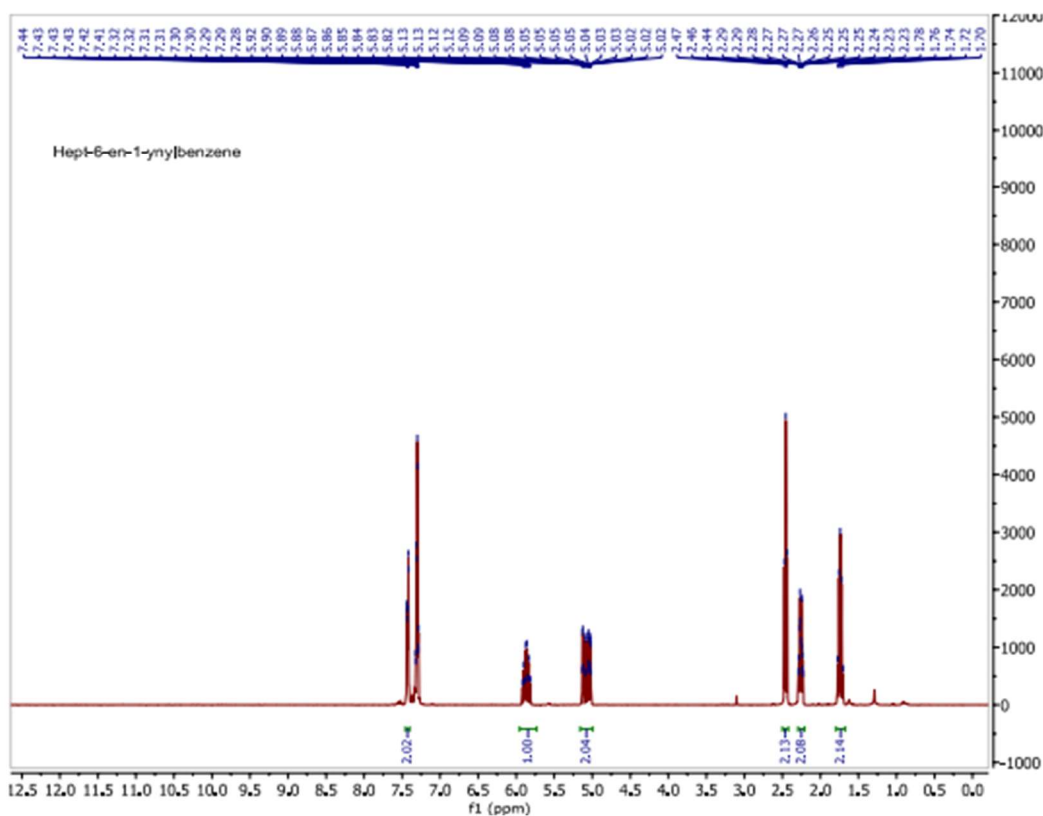
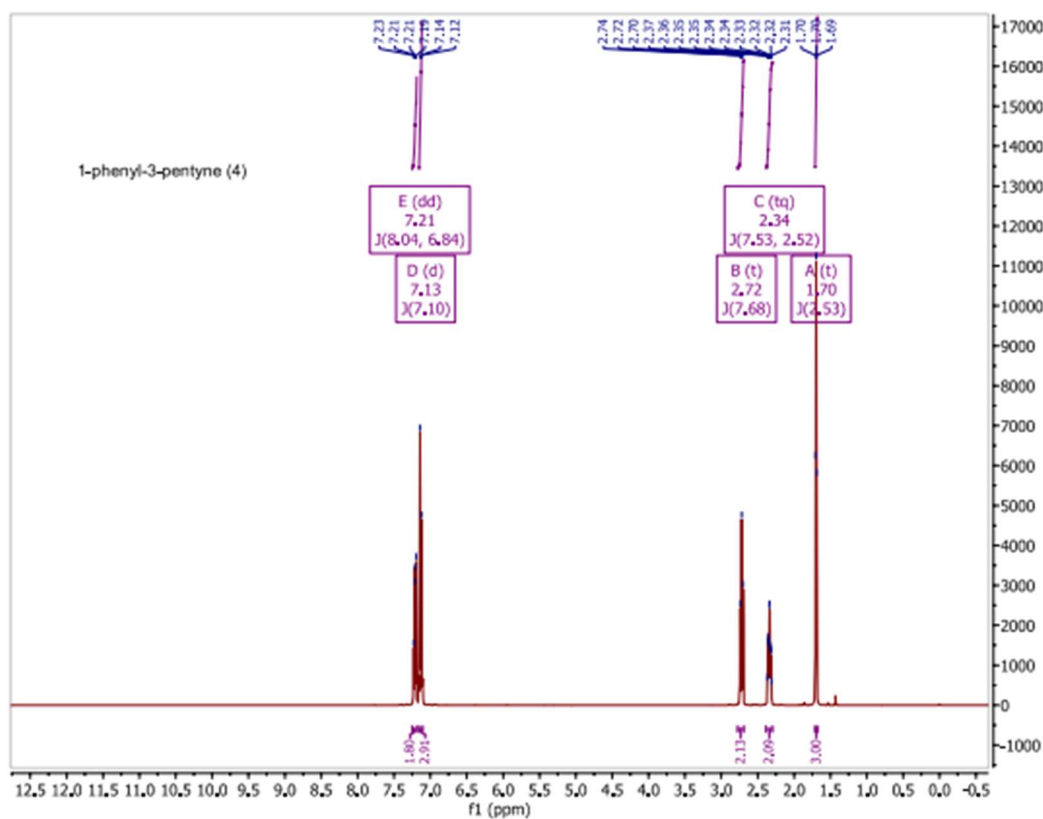


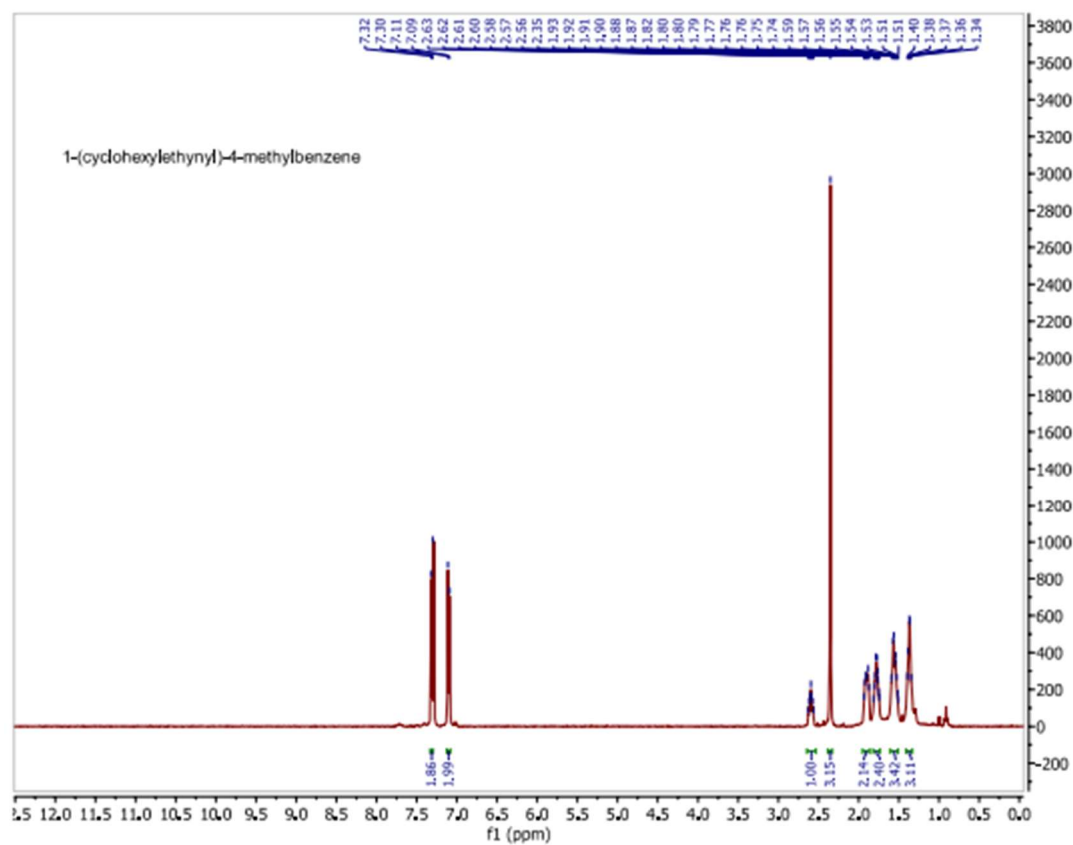
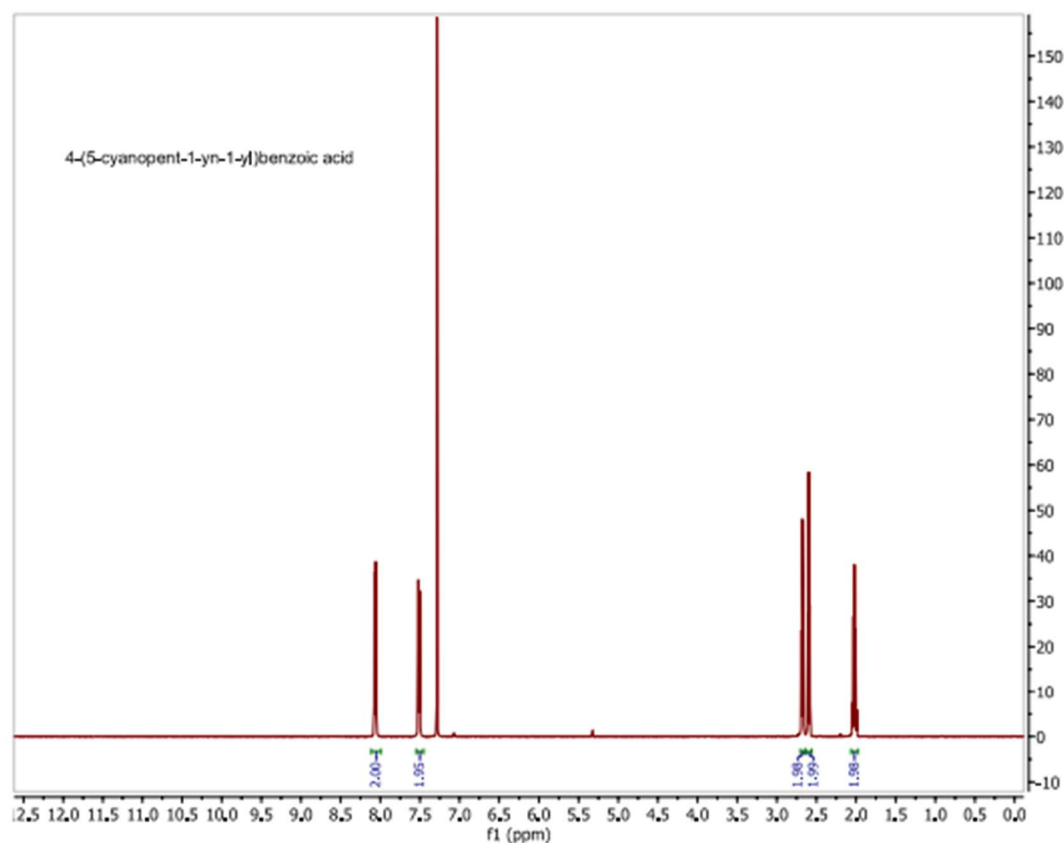
Electrochemical reduction and UV/Vis measurements

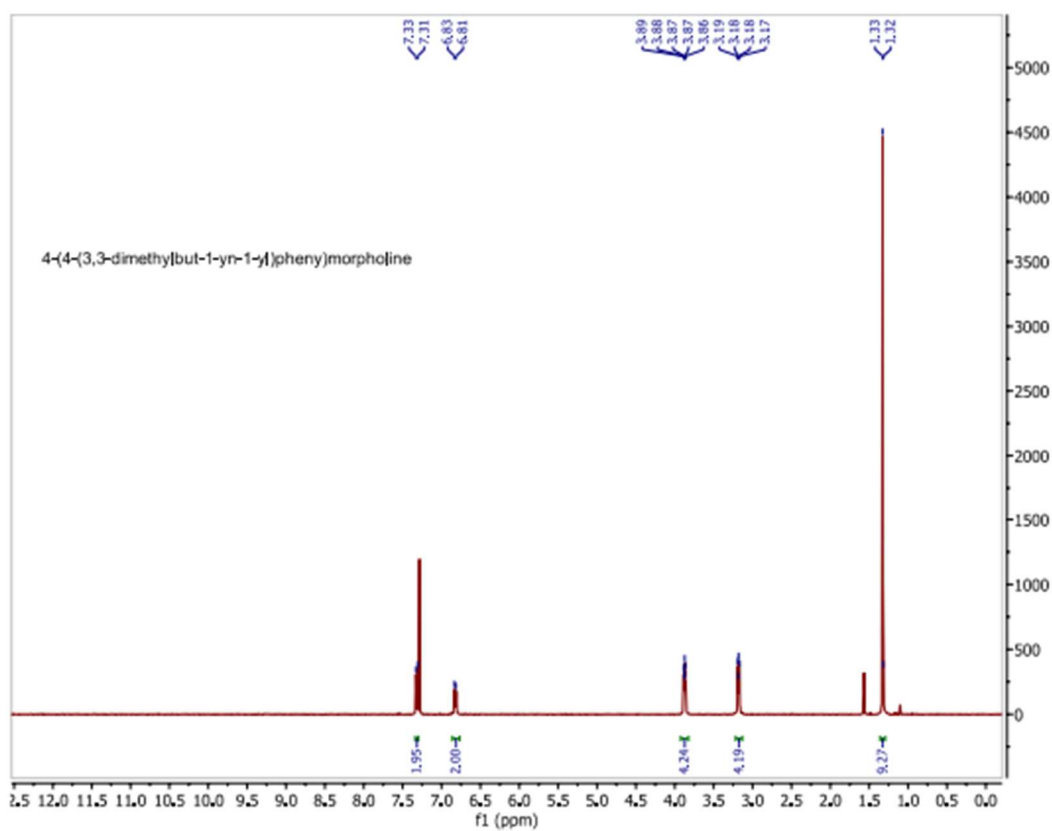
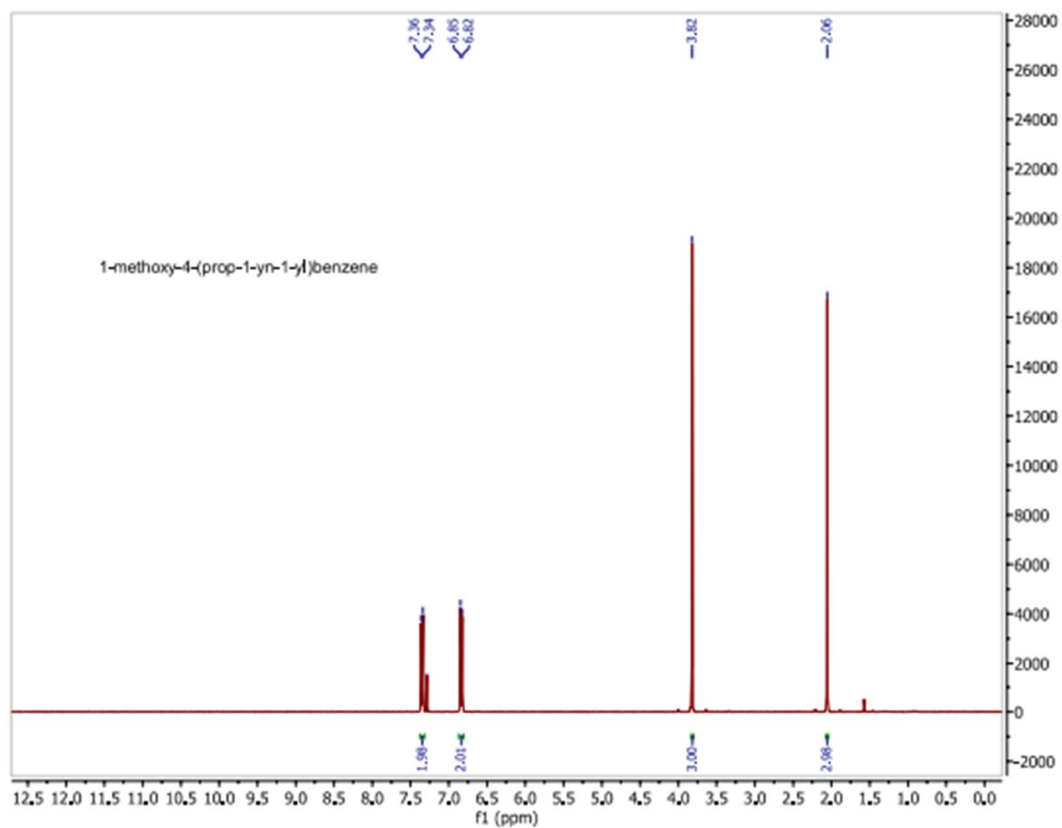
A fiberoptic dip-probe was inserted through the septum and into the electrolyte solution. After measuring a blank UV/Vis of the electrolyte solution, 4-DPAIPN stock solution (25 μ L, 0.5 μ mol) was added to the cell. A UV/Vis measurement was taken of neutral 4-DPAIPN. Finally, the solution was electrolyzed at -1.6 V vs. SCE until the yellow solution turned black. A measurement was taken of the solution to reveal the UV/Vis spectrum of 4-DPAIPN \bullet^- .

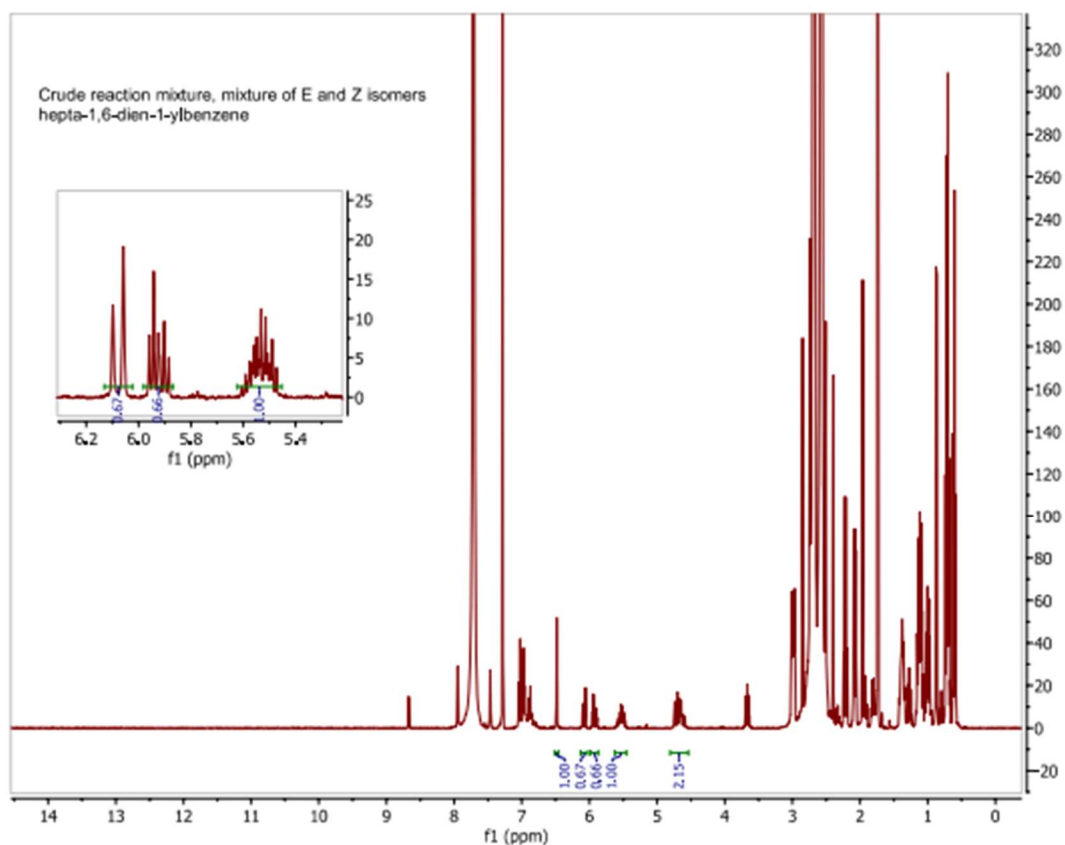
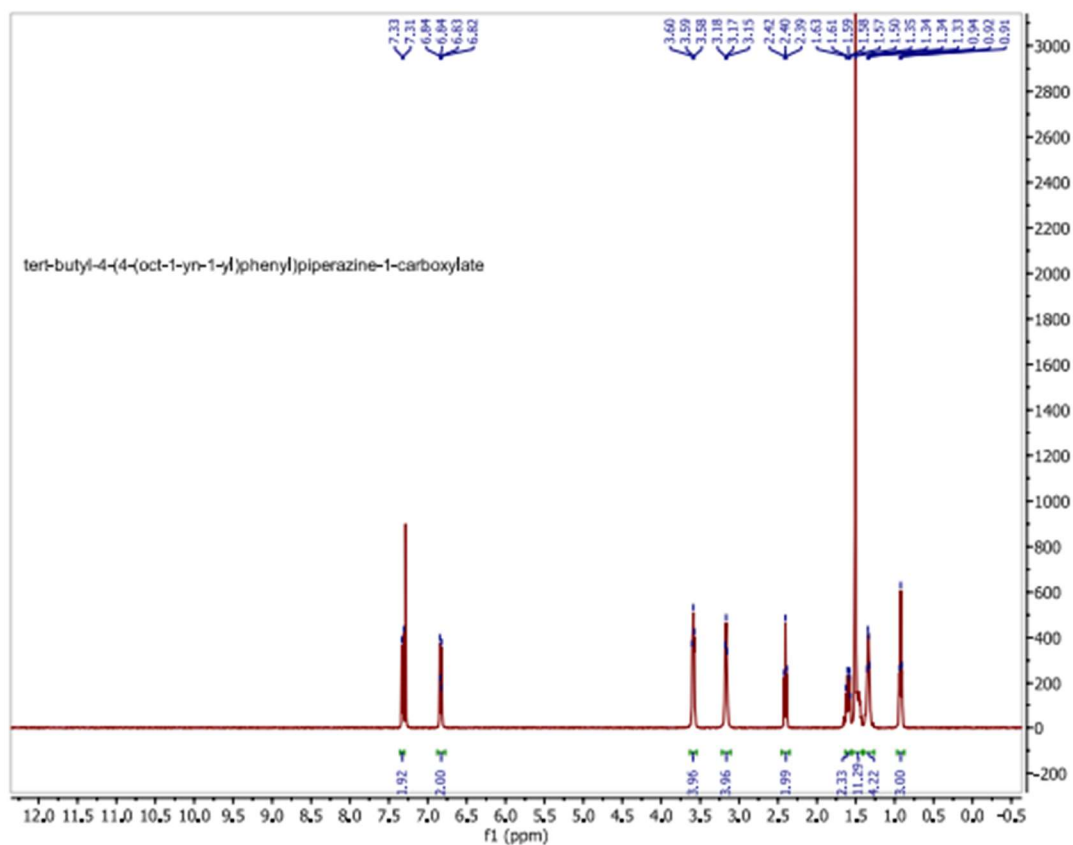


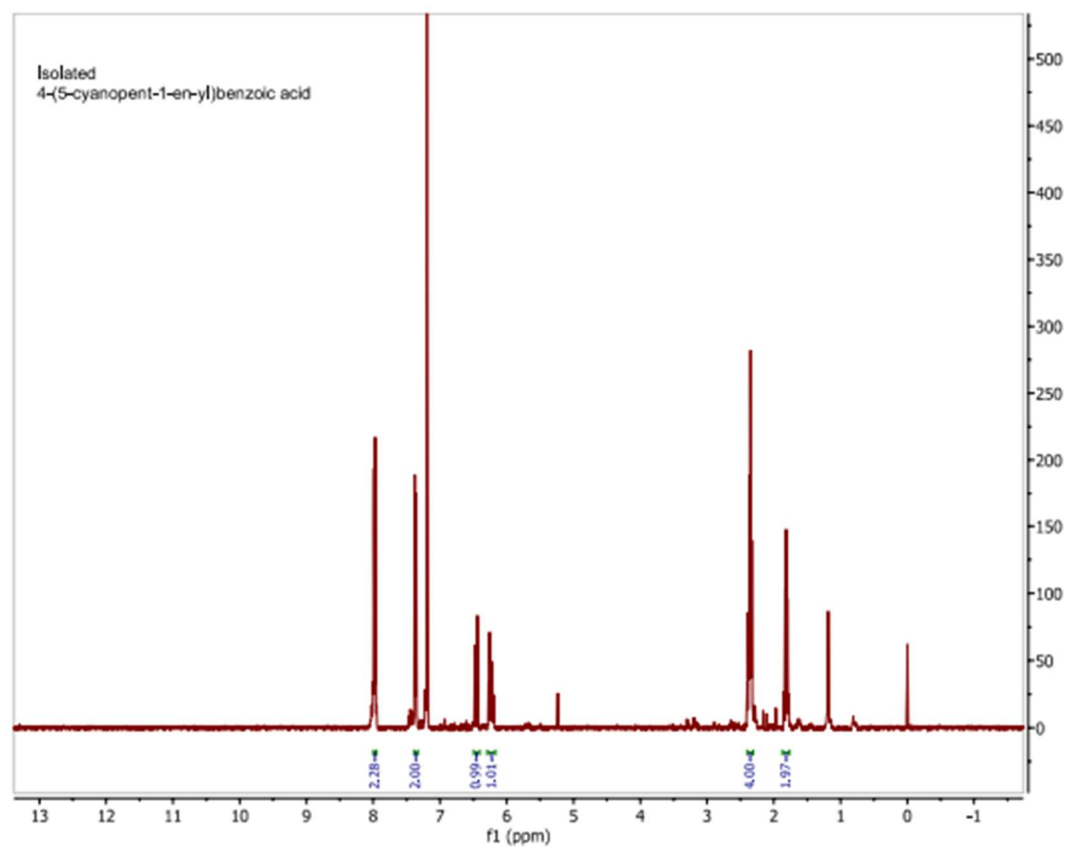
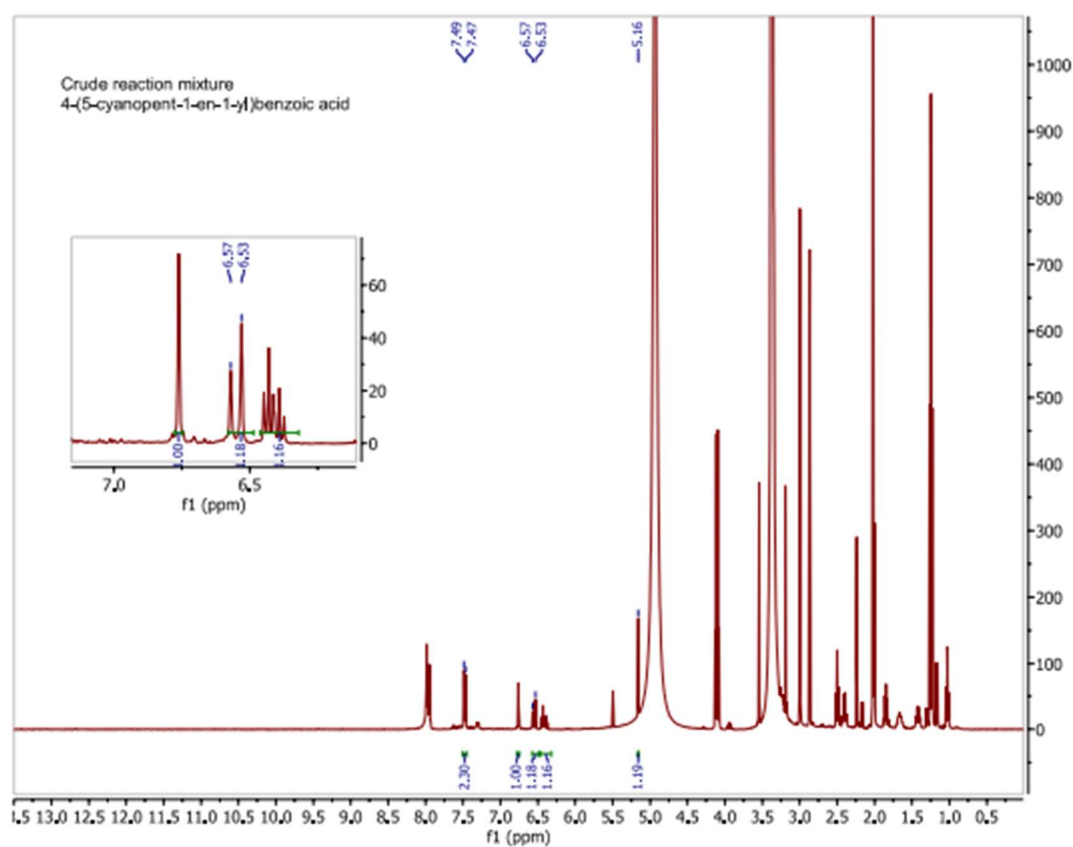
5.7.12. NMR Spectra

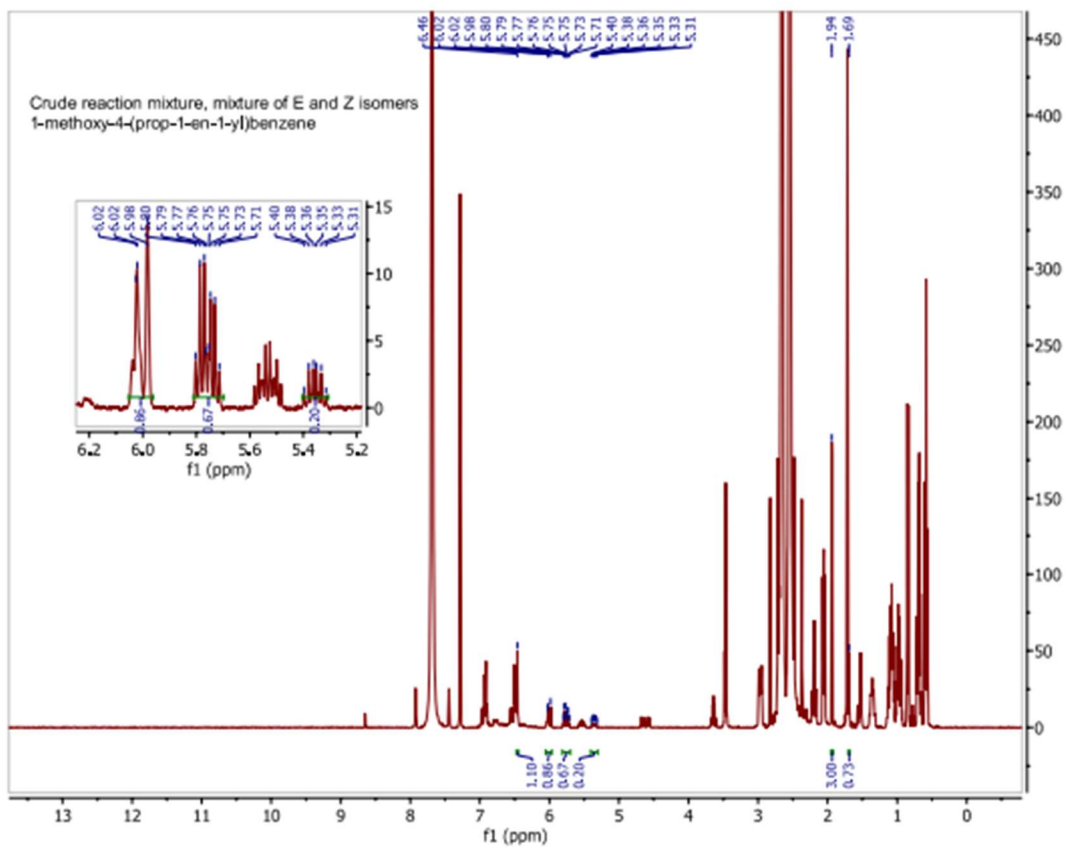
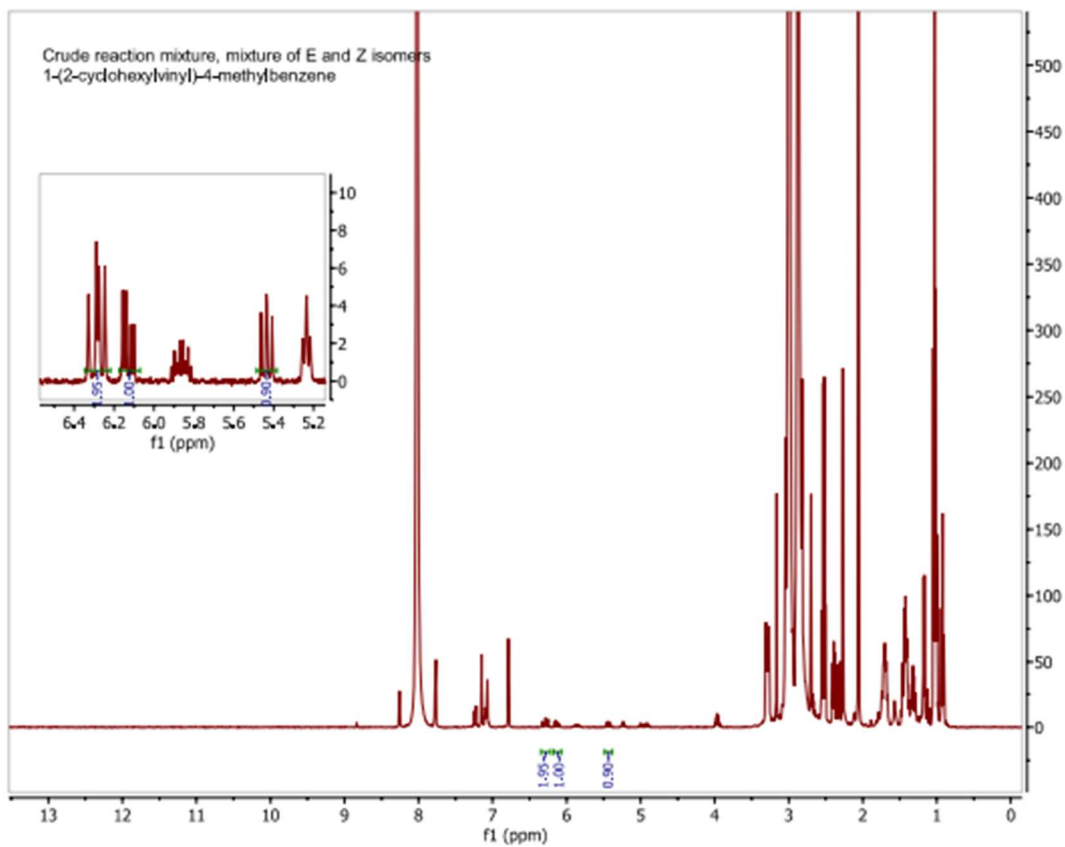


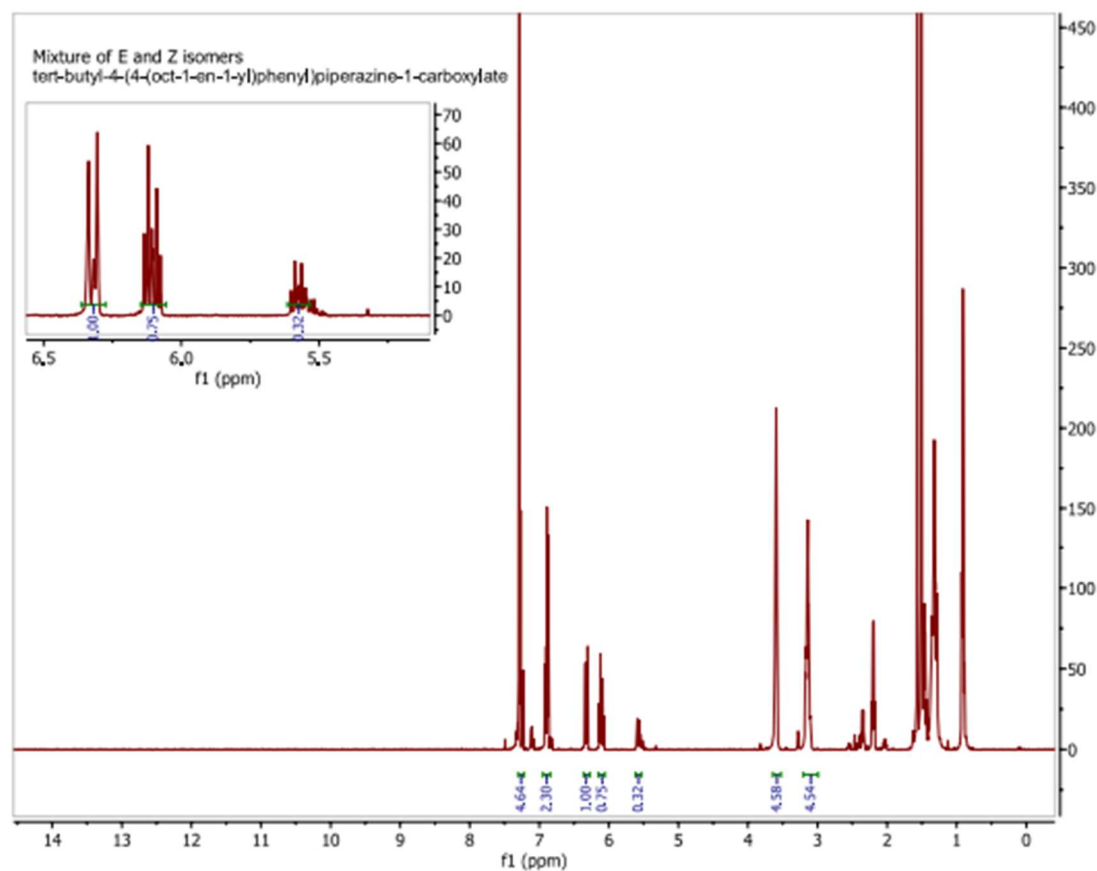
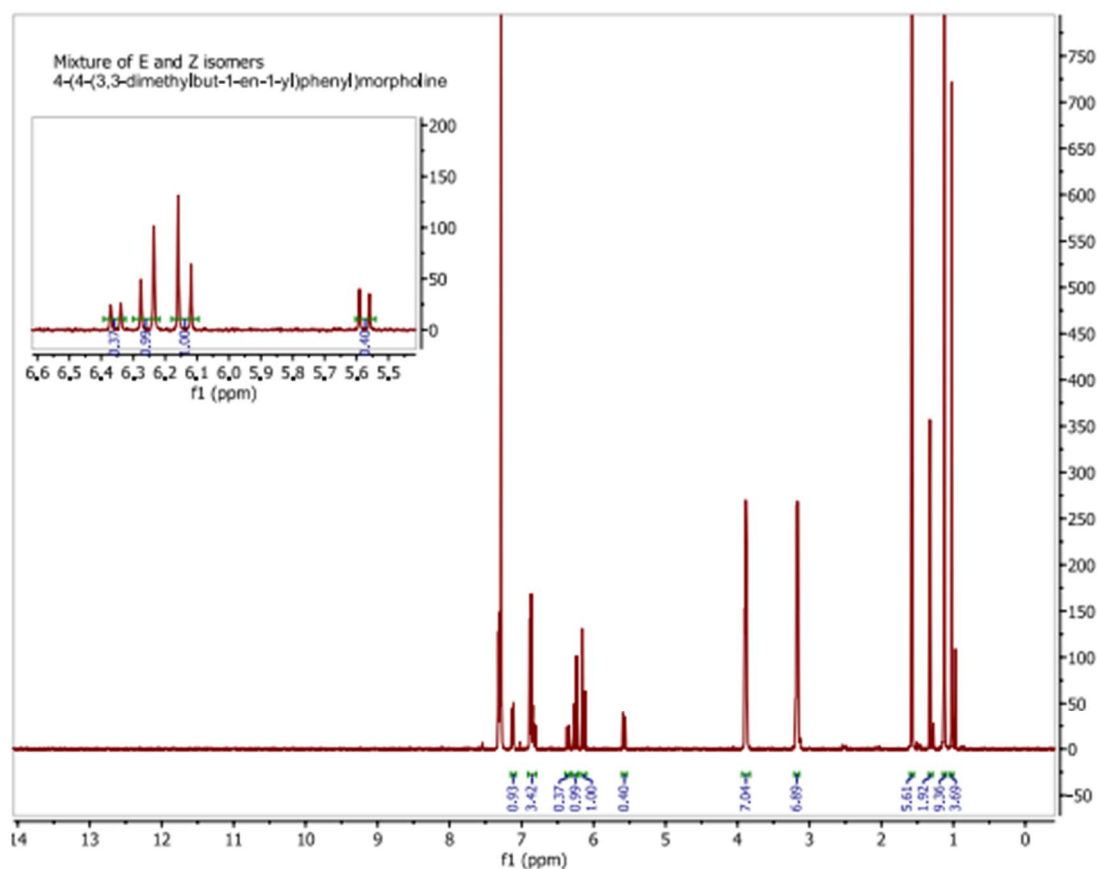












Chapter 6: An Electrochemical Copper Strategy for Mild and Selective Nitrile Reduction

This work is unpublished: Chernowsky, C.P.; Wickens, Z.K.

6.1. Abstract

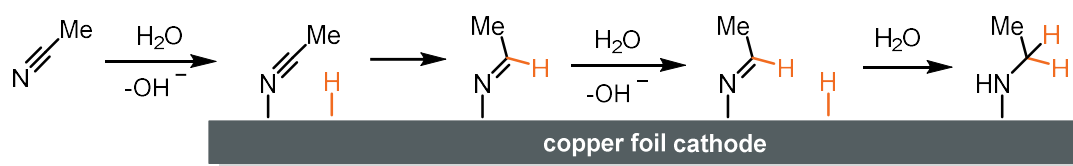
Nitrile reduction is an important reaction in organic synthesis, however, reduction strategies outside of harsh lithium aluminum hydride reagents are lacking, particularly for aliphatic nitriles. Herein, an electrochemical strategy is developed for nitrile reduction that takes advantage of both oxidative and reductive half reactions of an electrochemical cell. Copper anode oxidation to generate homogeneous copper ions and cathodic hydrogen evolution enable reduction of both aromatic and aliphatic nitriles with excellent selectivity for the primary amine product and tolerance of reductively sensitive functional groups.

6.2. Introduction

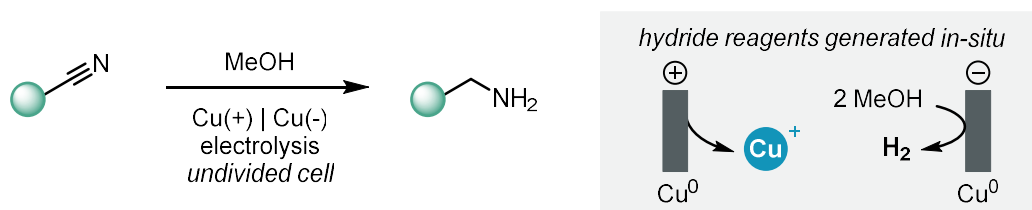
Nitrile reduction is a valuable strategy to generate amines which are among the most commonly occurring functional groups in organic molecules.^{1–3} Nitriles serve as an effective protecting group for primary amines that can be unmasked via reduction and further derivatized in late-stage synthesis.^{4–7} Additionally, cyanide is a competent nucleophile that can easily be installed in molecules with numerous reactions^{8–11} and can furnish aminated products upon reduction.¹² Nitrile reduction is classically promoted with lithium aluminum hydride (LiAlH_4),^{13,14} which is a powerful but unselective hydride reagent capable of reducing carbonyls, halides, or epoxide functional groups in addition to nitriles (**Figure 6.1(a)**).^{15–17} Challenges with functional group compatibility are exacerbated by the stoichiometric or super-stoichiometric quantities that are typically required. Additionally, LiAlH_4 is a pyrophoric reagent that introduces significant safety hazards¹⁸ to large scale synthesis. However, despite the hazards and selectivity challenges, reductions with LiAlH_4 are still routinely used in synthesis for nitrile reduction to amines.^{12,19,20} While there has been progress in developing nitrile reduction strategies without the use of LiAlH_4 , retaining selectivity for primary amine products and limitations in scope remain a challenge.²¹ Metal catalysts including but not limited to ruthenium, iron, or cobalt have been successfully used to facilitate hydride transfer from more mild reagents like hydrogen gas, silanes or borohydride reductants (**Figure 6.1(b)**).^{22–28} Unfortunately, metal-hydride catalysis not only necessitates super

enables slow addition of the hydride reagent over time and could improve functional group tolerance. The limited exploration of electrochemical nitrile reduction in the literature has relied on copper as the cathode material which enabled nitrile adsorption to the electrode in combination with HER to generate a hydride reductant (**Figure 6.2(a)**).^{40,41} Nitrile coordination also prevented secondary and tertiary amine byproduct formation due to the binding affinity of the primary amine products to the copper cathode surface. While this strategy has been effective for the reduction of acetonitrile solvent to ethylamine and a very limited scope of small molecule nitriles, it has not been explored outside the context of bulk commodity chemical synthesis or hydrogen uptake energy storage. We sought to adapt this appealing strategy to organic synthesis and enable selective nitrile reduction of a broad range of aromatic and aliphatic nitriles under mild reaction conditions with cheap and benign reagents (**Figure 6.2(b)**).

(a) Industrial reduction of acetonitrile



(b) This work: electrochemical copper reduction of nitriles



safe and simple starting materials • primary amine selective • functional group tolerant

Figure 6.2. Electrochemical reduction of nitriles

6.3. Results and Discussion

We investigated the reduction of an aliphatic nitrile, 4-phenylbutyronitrile, as a model substrate. Unfortunately, conditions adopted from the literature⁴⁰ consisting of a divided cell with a copper cathode and 1 M NaOH aqueous solvent resulted in no conversion of the substrate

under constant current electrolysis. Using a more organic electrolyte, tetraethylammonium hexafluorophosphate, in water was also unsuccessful in promoting reactivity. However, when the reaction setup was altered to an undivided cell, selective nitrile reduction was observed in 10% conversion to the primary amine product. A screen of alcohol solvents and organic co-solvents revealed that methanol provided the best results, generating product in 46% yield (see SI for screening details). Dilution of both the electrolyte and overall reaction concentration further improved yield to 69%. Under these more dilute conditions, lengthening the electrolysis time resulted in an increase in product formation to 83% (**Table 6.1**). Importantly, nitrile reduction always yielded the desired primary amine product with no secondary or tertiary side products observed. The optimized reaction conditions could easily be applied to benzonitrile by reducing the reaction time and resulted in 85% benzylamine product.

entry	solvent (M)	conditions	2 (%)
1	water (0.1)	5 F/mol	10
2	MeOH (0.1)	5 F/mol	46
3	MeOH (0.1)	7 F/mol	57
4	MeOH (0.05)	7 F/mol	69
5	MeOH (0.05)	7 F/mol, 30°C	57
6	MeOH (0.05)	13 F/mol	82
7	MeOH (0.05)	13 F/mol, 10 equiv water	64

not observed

Table 6.1. Optimization of aliphatic nitrile reduction.

With optimized reaction conditions in hand, we next turned our attention to probing the functional group compatibility, particularly with respect to carbonyl derivatives and other functional groups that are incompatible with traditional LiAlH_4 reaction conditions.¹⁷ To this end, we carried out a Glorius screen⁴² (**Table 6.2**) where several reactions were conducted under standard conditions with one equivalent of an additional substrate containing a functional group of interest.

Excitingly, reductively sensitive functional groups including styrene (**3**), esters (**4**), and amides (**5**) were tolerated in near quantitative retention. While aromatic ketones (**9**) and aldehydes (**10**) were consumed, we were excited to observe that an aliphatic ketone (**6**) was retained in high yields. Surprisingly, alkyne containing substrates that are prone to reduction in the presence of copper hydride species^{43,44} were only partially consumed (**7** and **8**), however, when a pendent chelating alcohol was present (**13**) the alkyne functionality was fully reduced. Overall, these data suggest that electrochemical copper reduction of nitriles is a highly selective strategy that improves functional group tolerance when compared to LiAlH_4 reduction or many of the established metal-hydride catalytic systems. We attribute this selectivity to the high binding affinity of copper for nitrogen over other coordinating functional groups like carbonyls, alkenes or alkynes.

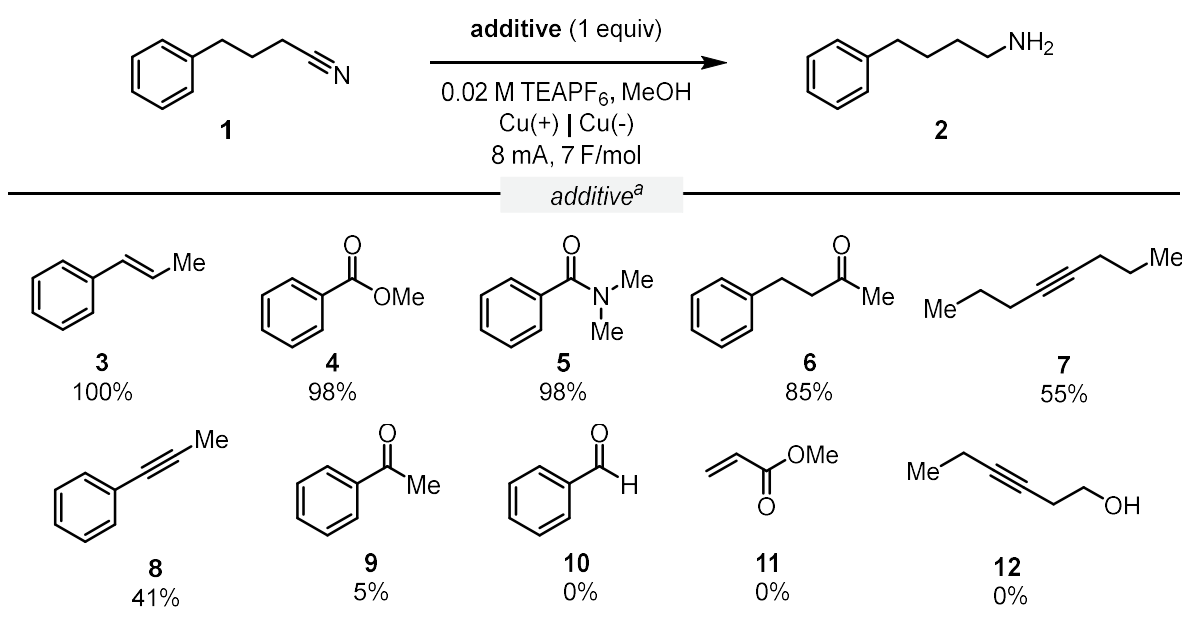
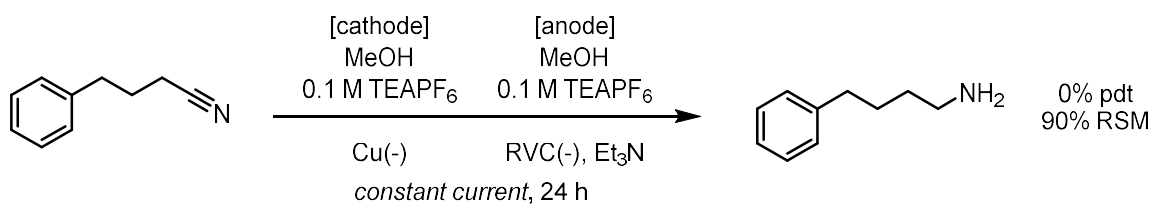


Table 6.2. A Glorius screen of additives under standard reaction conditions. ^aPercentages given are the percentage of the additive retained at the end of the reaction time.

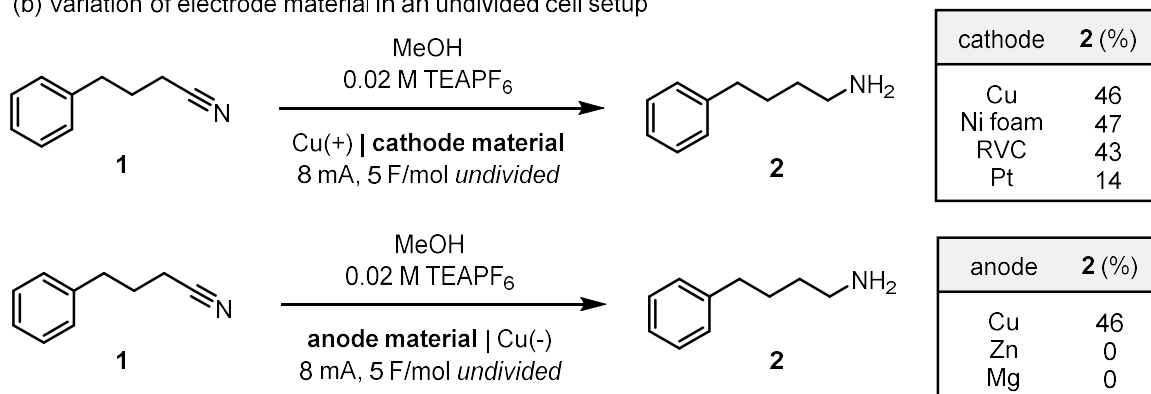
Next, we investigated the proposed mechanism for electrochemical nitrile reduction. While our initial hypothesis consisted of a heterogeneous reduction taking place on the surface of the cathode in conjunction with HER, a control experiment where nitrile reduction was attempted in the cathode of a divided cell yielded no conversion of the substrate even after 24 hours (**Figure 6.3 (a)**). This lack of reactivity suggests that the mode of reduction is more complex than simply

cathodic adsorption and reduction. Additional undivided cell experiments revealed that the cathode material can be exchanged for nickel foam, platinum or RVC with no effect on reactivity (**Figure 6.3 (b)**). The material of the cathode in an undivided cell being interchangeable coupled with the lack of conversion observed in a divided cell cathode led us to rule out a copper electrode promoted heterogeneous mechanism. Surprisingly, when the anode material in an undivided cell was changed from copper to an alternate sacrificial electrode material like zinc or magnesium, no conversion was observed (**Figure 6.3 (b)**).

(a) Divided cell setup with substrate in the cathode



(b) Variation of electrode material in an undivided cell setup



(c) Proposed mechanism

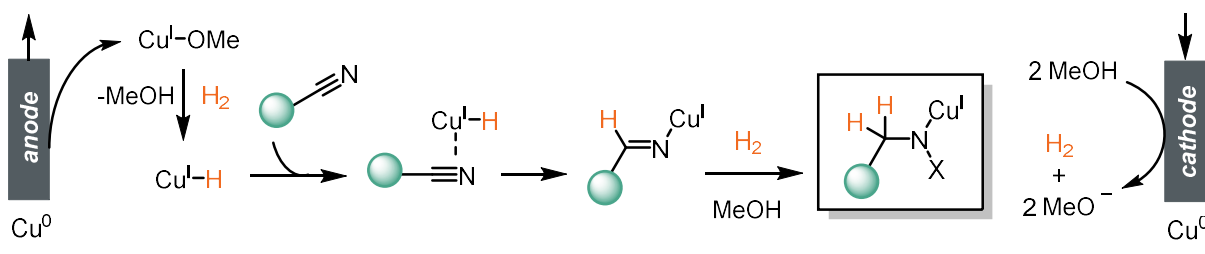


Figure 6.5. Mechanistic investigations. See the SI for experimental details

The importance of having a sacrificial copper anode suggests that generation of homogeneous copper ions in solution is important to the mechanism of nitrile reduction. Additionally, analysis of

the crude reaction mixture revealed that the amine products were coordinated to copper and the complexes formed were homogeneous in solution. We hypothesized that this copper coordination in solution is responsible for selective primary amine formation rather than our initial hypothesis of adsorption on the electrode. The data from these preliminary mechanistic studies led us to a new proposed mechanism summarized in **Figure 6.3 (c)** that relies on copper ions generated at the anode and hydrogen gas generated via HER at the cathode.

6.4. Conclusion

Overall, we have developed a simple and safe system for nitrile reduction that is selective for formation of primary amine products. Excitingly, this method circumvents the need for harsh stoichiometric hydride reagents by taking advantage of both half reactions in an electrochemical cell and generating the active reductants in-situ from simple copper wire and methanol solvent. Both aromatic and aliphatic nitriles are efficiently reduced under these conditions and while more thorough scope investigations are ongoing, initial studies into chemoselectivity reveal a high selectivity for nitriles in the presence of functional groups prone to hydride reduction under previously established methods. We anticipate electrochemical copper promote hydride reduction to be a valuable synthetic tool for selectively reducing nitrile substrates to primary amines across a wide range of diverse substrates.

6.5. Acknowledgements

Dr. Blaise Thompson is acknowledged for construction of galvanostat electrochemical equipment. Tracy Drier is acknowledged for fabrication of divided cell electrochemical glassware. This work was financially supported by the Office of the Vice Chancellor for Research and Graduate Education at the University of Wisconsin–Madison with funding from the Wisconsin Alumni Research Foundation. This material is based upon work supported by the National Science Foundation under Grant No. (2047108).). Spectroscopic instrumentation was supported

by a generous gift from Paul. J. and Margaret M. Bender, NSF (CHE-1048642), and NIH (1S10 OD020022-1).

6.6. References

- (1) Synthesis and Chemistry of Agrochemicals II: Developed from Symposia Sponsored by the Division of Agrochemicals, of the American Chemical Society; Baker, D. R., Fenyves, J. G., Moberg, W. K., American Chemical Society, Eds.; ACS symposium series; American Chemical Society: Washington, DC, 1991.
- (2) Adams, J. P. Imines, Enamines and Oximes. *J. Chem. Soc., Perkin Trans. 1* **2000**, No. 2, 125–139. <https://doi.org/10.1039/A808142E>.
- (3) Lawrence, S. A. *Amines: Synthesis, Properties and Applications*; Cambridge University Press, 2004.
- (4) Varela, J. A.; Saá, C. Construction of Pyridine Rings by Metal-Mediated [2 + 2 + 2] Cycloaddition. *Chem. Rev.* **2003**, 103 (9), 3787–3802. <https://doi.org/10.1021/cr030677f>.
- (5) Yan, H.; Suk Oh, J.; Lee, J.-W.; Eui Song, C. Scalable Organocatalytic Asymmetric Strecker Reactions Catalysed by a Chiral Cyanide Generator. *Nat Commun* **2012**, 3 (1), 1212. <https://doi.org/10.1038/ncomms2216>.
- (6) Wan, S.; Wu, F.; Rech, J. C.; Green, M. E.; Balachandran, R.; Horne, W. S.; Day, B. W.; Floreancig, P. E. Total Synthesis and Biological Evaluation of Pederin, Psymberin, and Highly Potent Analogs. *J. Am. Chem. Soc.* **2011**, 133 (41), 16668–16679. <https://doi.org/10.1021/ja207331m>.
- (7) Kende, A. S.; Deng, W.-P.; Zhong, M.; Guo, X.-C. Enantioselective Total Synthesis and Structure Revision of Spirodihydrobenzofuranlactam 1. Total Synthesis of Stachybotrylactam. *Org. Lett.* **2003**, 5 (10), 1785–1788. <https://doi.org/10.1021/ol030039j>.
- (8) Zhang, X.; Tan, C.-H. Stereospecific and Stereoconvergent Nucleophilic Substitution Reactions at Tertiary Carbon Centers. *Chem* **2021**, 7 (6), 1451–1486. <https://doi.org/10.1016/j.chempr.2020.11.022>.
- (9) Lanke, V.; Marek, I. Stereospecific Nucleophilic Substitution at Tertiary and Quaternary Stereocentres. *Chemical Science* **2020**, 11 (35), 9378–9385. <https://doi.org/10.1039/D0SC02562C>.
- (10) Cohen, D. T.; Buchwald, S. L. Mild Palladium-Catalyzed Cyanation of (Hetero)Aryl Halides and Triflates in Aqueous Media. *Org. Lett.* **2015**, 17 (2), 202–205. <https://doi.org/10.1021/ol5032359>.
- (11) Fang, X.; Yu, P.; Morandi, B. Catalytic Reversible Alkene-Nitrile Interconversion through Controllable Transfer Hydrocyanation. *Science* **2016**, 351 (6275), 832–836. <https://doi.org/10.1126/science.aae0427>.
- (12) Adams, G. L.; Carroll, P. J.; Smith, A. B. I. Access to the Akuammiline Family of Alkaloids: Total Synthesis of (+)-Scholarisine A. *J. Am. Chem. Soc.* **2013**, 135 (1), 519–528. <https://doi.org/10.1021/ja3111626>.
- (13) Amundsen, L. H.; Nelson, L. S. Reduction of Nitriles to Primary Amines with Lithium Aluminum Hydride ¹. *J. Am. Chem. Soc.* **1951**, 73 (1), 242–244. <https://doi.org/10.1021/ja01145a082>.
- (14) Nystrom, R. F. Reduction of Organic Compounds by Mixed Hydrides. I. Nitriles. *J. Am. Chem. Soc.* **1955**, 77 (9), 2544–2545. <https://doi.org/10.1021/ja01614a053>.
- (15) Walker, E. R. H. The Functional Group Selectivity of Complex Hydride Reducing Agents. *Chem. Soc. Rev.* **1976**, 5 (0), 23–50. <https://doi.org/10.1039/CS9760500023>.

- (16) Magano, J.; Dunetz, J. R. Large-Scale Carbonyl Reductions in the Pharmaceutical Industry. *Org. Process Res. Dev.* **2012**, 16 (6), 1156–1184. <https://doi.org/10.1021/op2003826>.
- (17) Nystrom, R. F.; Brown, W. G. Reduction of Organic Compounds by Lithium Aluminum Hydride. I. Aldehydes, Ketones, Esters, Acid Chlorides and Acid Anhydrides. *J. Am. Chem. Soc.* **1947**, 69 (5), 1197–1199. <https://doi.org/10.1021/ja01197a060>.
- (18) Merlic, C. A.; Ferber, C. J.; Schröder, I. Lessons Learned—Lithium Aluminum Hydride Fires. *ACS Chem. Health Saf.* **2022**, 29 (4), 362–365. <https://doi.org/10.1021/acs.chas.2c00035>.
- (19) Varseev, G. N.; Maier, M. E. Total Synthesis of (±)-Symbioimine. *Angewandte Chemie International Edition* **2006**, 45 (29), 4767–4771. <https://doi.org/10.1002/anie.200601418>.
- (20) Horst, B.; Verdoorn, D. S.; Hennig, S.; van der Heijden, G.; Ruijter, E. Enantioselective Total Synthesis of (–)-Limaspermidine and (–)-Kopsinine by a Nitroaryl Transfer Cascade Strategy. *Angewandte Chemie* **2022**, 134 (42), e202210592. <https://doi.org/10.1002/ange.202210592>.
- (21) Constable, D. J. C.; Dunn, P. J.; Hayler, J. D.; Humphrey, G. R.; Johnnie L. Leazer, J.; Linderman, R. J.; Lorenz, K.; Manley, J.; Pearlman, B. A.; Wells, A.; Zaks, A.; Zhang, T. Y. Key Green Chemistry Research Areas—a Perspective from Pharmaceutical Manufacturers. *Green Chem.* **2007**, 9 (5), 411–420. <https://doi.org/10.1039/B703488C>.
- (22) Sharma, D. M.; Punji, B. 3 d Transition Metal-Catalyzed Hydrogenation of Nitriles and Alkynes. *Chemistry – An Asian Journal* **2020**, 15 (6), 690–708. <https://doi.org/10.1002/asia.201901762>.
- (23) Lévy, K.; Tóth, K. D.; Kárpáti, T.; Hegedűs, L. Heterogeneous Catalytic Hydrogenation of 3-Phenylpropionitrile over Palladium on Carbon. *ACS Omega* **2020**, 5 (10), 5487–5497. <https://doi.org/10.1021/acsomega.0c00125>.
- (24) Bornschein, C.; Werkmeister, S.; Wendt, B.; Jiao, H.; Alberico, E.; Baumann, W.; Junge, H.; Junge, K.; Beller, M. Mild and Selective Hydrogenation of Aromatic and Aliphatic (Di)Nitriles with a Well-Defined Iron Pincer Complex. *Nat Commun* **2014**, 5 (1), 1–11. <https://doi.org/10.1038/ncomms5111>.
- (25) Lévy, K.; Hegedűs, L. Recent Achievements in the Hydrogenation of Nitriles Catalyzed by Transitional Metals. *Current Organic Chemistry* 23 (18), 1881–1900.
- (26) Lu, Q.; Liu, J.; Ma, L. Recent Advances in Selective Catalytic Hydrogenation of Nitriles to Primary Amines. *Journal of Catalysis* **2021**, 404, 475–492. <https://doi.org/10.1016/j.jcat.2021.10.028>.
- (27) Lévy, K.; Hegedűs, L. Selective Heterogeneous Catalytic Hydrogenation of Nitriles to Primary Amines. *Periodica Polytechnica Chemical Engineering* **2018**, 62 (4), 476–488. <https://doi.org/10.3311/PPch.12787>.
- (28) Garduño, J. A.; García, J. J. Toward Amines, Imines, and Imidazoles: A Viewpoint on the 3d Transition-Metal-Catalyzed Homogeneous Hydrogenation of Nitriles. *ACS Catal.* **2020**, 10 (14), 8012–8022. <https://doi.org/10.1021/acscatal.0c02283>.
- (29) Caddick, S.; Judd, D. B.; Lewis, A. K. de K.; Reich, M. T.; Williams, M. R. V. A Generic Approach for the Catalytic Reduction of Nitriles. *Tetrahedron* **2003**, 59 (29), 5417–5423. [https://doi.org/10.1016/S0040-4020\(03\)00858-5](https://doi.org/10.1016/S0040-4020(03)00858-5).
- (30) Caddick, S.; de K. Haynes, A. K.; Judd, D. B.; Williams, M. R. V. Convenient Synthesis of Protected Primary Amines from Nitriles. *Tetrahedron Letters* **2000**, 41 (18), 3513–3516. [https://doi.org/10.1016/S0040-4039\(00\)00410-X](https://doi.org/10.1016/S0040-4039(00)00410-X).
- (31) Sharma, D. M.; Punji, B. Selective Synthesis of Secondary Amines from Nitriles by a User-Friendly Cobalt Catalyst. *Advanced Synthesis & Catalysis* **2019**, 361 (17), 3930–3936. <https://doi.org/10.1002/adsc.201900586>.

- (32) Shao, Z.; Fu, S.; Wei, M.; Zhou, S.; Liu, Q. Mild and Selective Cobalt-Catalyzed Chemodivergent Transfer Hydrogenation of Nitriles. *Angewandte Chemie* **2016**, 128 (47), 14873–14877. <https://doi.org/10.1002/ange.201608345>.
- (33) Geri, J. B.; Szymczak, N. K. A Proton-Switchable Bifunctional Ruthenium Complex That Catalyzes Nitrile Hydroboration. *J. Am. Chem. Soc.* **2015**, 137 (40), 12808–12814. <https://doi.org/10.1021/jacs.5b08406>.
- (34) Bhattacharjee, J.; Harinath, A.; Bano, K.; Panda, T. K. Highly Chemoselective Hydroboration of Alkynes and Nitriles Catalyzed by Group 4 Metal Amidophosphine–Borane Complexes. *ACS Omega* **2020**, 5 (3), 1595–1606. <https://doi.org/10.1021/acsomega.9b03598>.
- (35) Hayrapetyan, D.; Khalimon, A. Y. Catalytic Nitrile Hydroboration: A Route to N,N-Diborylamines and Uses Thereof. *Chemistry – An Asian Journal* **2020**, 15 (17), 2575–2587. <https://doi.org/10.1002/asia.202000672>.
- (36) Murai, T.; Sakane, T.; Kato, S. Cobalt Carbonyl Catalyzed Hydrosilylation of Nitriles: A New Preparation of N,N-Disilylamines. *J. Org. Chem.* **1990**, 55 (2), 449–453. <https://doi.org/10.1021/jo00289a014>.
- (37) Reddy, N. P.; Uchimar, Y.; Lautenschlager, H.-J.; Tanaka, M. Platinum-Catalyzed Novel Reactions of Nitriles and an Azirine with o-Bis(Dimethylsilyl)Benzene. *Chem. Lett.* **1992**, 21 (1), 45–48. <https://doi.org/10.1246/cl.1992.45>.
- (38) Sharifi-Asl, S.; Macdonald, D. D. Investigation of the Kinetics and Mechanism of the Hydrogen Evolution Reaction on Copper. *J. Electrochem. Soc.* **2013**, 160 (6), H382. <https://doi.org/10.1149/2.143306jes>.
- (39) Lasia, A. Hydrogen Evolution Reaction. In *Handbook of Fuel Cell Technology*; 2003; Vol. 2, pp 414–440. <https://doi.org/10.1002/9780470974001.f204033>.
- (40) Xia, R.; Tian, D.; Kattel, S.; Hasa, B.; Shin, H.; Ma, X.; Chen, J. G.; Jiao, F. Electrochemical Reduction of Acetonitrile to Ethylamine. *Nat Commun* **2021**, 12 (1), 1949. <https://doi.org/10.1038/s41467-021-22291-0>.
- (41) Zhang, D.; Chen, J.; Hao, Z.; Jiao, L.; Ge, Q.; Fu, W.-F.; Lv, X.-J. Highly Efficient Electrochemical Hydrogenation of Acetonitrile to Ethylamine for Primary Amine Synthesis and Promising Hydrogen Storage. *Chem Catalysis* **2021**, 1 (2), 393–406. <https://doi.org/10.1016/j.checat.2021.03.012>.
- (42) Collins, K. D.; Glorius, F. A Robustness Screen for the Rapid Assessment of Chemical Reactions. *Nature Chem* **2013**, 5 (7), 597–601. <https://doi.org/10.1038/nchem.1669>.
- (43) Wakamatsu, T.; Nagao, K.; Ohmiya, H.; Sawamura, M. Copper-Catalyzed Semihydrogenation of Internal Alkynes with Molecular Hydrogen. *Organometallics* **2016**, 35 (10), 1354–1357. <https://doi.org/10.1021/acs.organomet.6b00126>.
- (44) Wang, G.-H.; Bin, H.-Y.; Sun, M.; Chen, S.-W.; Liu, J.-H.; Zhong, C.-M. Copper-Catalyzed Z-Selective Semihydrogenation of Alkynes with Hydrosilane: A Convenient Approach to Cis-Alkenes. *Tetrahedron* **2014**, 70 (12), 2175–2179. <https://doi.org/10.1016/j.tet.2014.01.053>.

6.7. Supplemental Information

6.7.1. General Methods and Materials

Unless otherwise noted, reactions were performed with no efforts to exclude air or water. Unless otherwise noted, other commercially-available reagents and solvents were used as received. Flash chromatography was performed with a Biotage Isolera One automated chromatography system with re-packed silica columns (technical grade silica, pore size 40 Å, 230-400 mesh particle size, 40-63 particle size). ^1H , ^{13}C , ^{31}P Spectra were taken using a Bruker Avance-400 with a BBFO Probe or a Bruker Avance-500 with a DCH Cryoprobe. NMR data are reported relative to residual CHCl_3 (^1H , $\delta = 7.26$ ppm), CDCl_3 (^{13}C , $\delta = 77.16$ ppm). Data for ^1H NMR spectra are reported as follows: chemical shift (δ ppm) (multiplicity, coupling constant (Hz), integration). Multiplicity and qualifier abbreviations are as follows: s = singlet, d = doublet, t = triplet, q = quartet, m = multiplet, br = broad.

6.7.2. Electrochemical Equipment and Experimental Set-Up

All controlled potential measurements were performed at room temperature using a Pine WaveNowXV. Bulk electrolysis experiments were carried out in divided H cells when requiring a divided cell setup and 16x100 disposable test tubes when requiring an undivided cell.

Electrode equipment:

Cu – 20 gauge wire coiled to a length of 1 cm (coil made by wrapping around a 16G purple disposable needle)

RVC – RVC (10 x 5 x 5 mm) affixed to stainless steel wire

Zn – 5 mm diameter zinc rods cut 3 cm in length affixed to stainless steel wire wrapped around one end and secured with teflon tape

Mg – 10 mm diameter Mg rods cut 3 cm in length affixed to stainless steel wire wrapped around one end and secured with teflon tape

Pt – Platinum plate (1 x 2 cm) affixed to stainless steel wire wrapped around one end and secured with Teflon tape.

When a divided cell is specified the following cell is used:

H-Type Cell Fabrication:



Divided cell fabricated in-house (*FUSION, Journal of the ASGS*, **2020**, 67, 4, 19-26). Porosity E glass filter disc purchased from Ace Glass; 8 mm diameter, part number 7176-21.

Low-current Power Supply:

Original design and fabrication by Dr. Blaise J. Thompson. Provides an operational range of ± 0.01 – 14.99 mA, tunable by variable resistor, delivering power to banana socket pair. The power supply is limited to ± 15 V for bulk electrolysis and is powered by an 18 V wall wart. Circuitry is housed within an aluminum enclosure. For additional specifications, see: *J. Am. Chem. Soc.* **2020** 142, 2093–2099 and *Nature* **2021** 596, 74–79.

6.7.3. Reaction Optimization

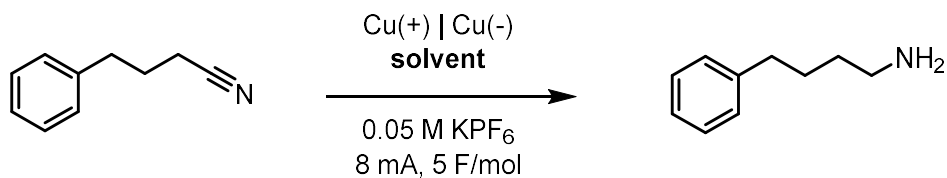
General Procedure:

To a 16x100 mm test tube was added potassium hexafluorophosphate (18 mg, 0.1 mmol, 0.5 equiv) and stir bar and 4-phenyl-1-butyronitrile (29.8 μ L, 0.2 mmol, 1 equiv) and solvent (total volume of 2 mL) with no attempts to exclude air or exogenous water. A 14/24 setpa equipped with copper wire electrodes was affixed to the reaction vessel and the electrodes were connected to a galvanostat set to deliver 8 mA. The reaction was electrolyzed at constant current for 3.25 hours (to deliver 5 F/mol).

Workup: To the reaction solution was added mesitylene (18 μ L, 0.13 mmol) as an internal standard. A 0.2 mL aliquot of the reaction solution was transferred to a vial and diluted with 2 mL of a 25% EDTA aqueous solution. The mixture was stirred for 1 hour and deuterated chloroform was added to the solution, mixed and extracted for NMR analysis.

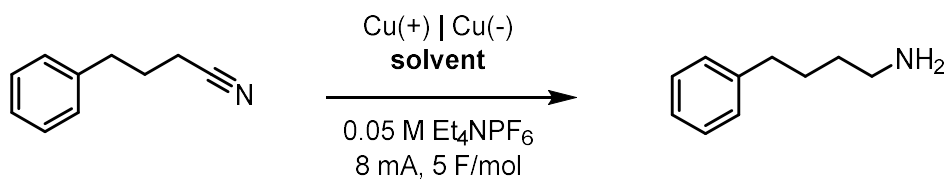
Solvent and electrolyte dependence:

Solvent blends listed below are mixtures of 1:1 organic solvent:ROH.



entry	organic solvent	ROH	yield (%)
1	none	water	13
2	none	MeOH	40
3	none	EtOH	0
4	none	iPrOH	0
5	none	tAmylOH	0
6	none	tBuOH	0
7	THF	water	46
8	THF	MeOH	20
9	THF	EtOH	0
10	THF	iPrOH	0
11	THF	tAmylOH	0
12	THF	tBuOH	0
13	DMF	water	54
14	DMF	MeOH	35
15	DMF	EtOH	34
16	DMF	iPrOH	14
17	DMF	tAmylOH	14
18	DMF	tBuOH	27

While the combination of DMF:water gave the highest yield, these reaction conditions were not selected moving forward as they resulted in an extremely viscous solution with inconsistent reproducibility.

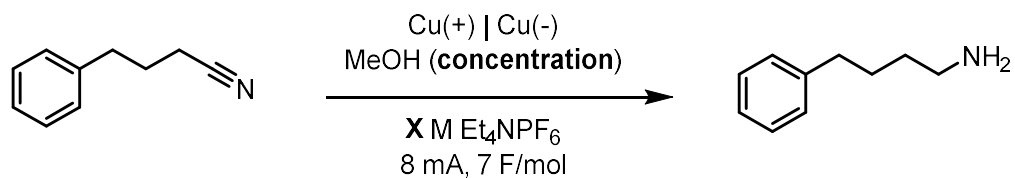


entry	organic solvent	ROH	yield (%)
1	none	water	10
2	none	MeOH	46
3	none	EtOH	0
4	none	iPrOH	0
5	none	tAmylOH	0
6	none	tBuOH	0
7	THF	water	27
8	THF	MeOH	17
9	THF	EtOH	0
10	THF	iPrOH	0
11	THF	tAmylOH	0
12	THF	tBuOH	0
13	DMF	water	22
14	DMF	MeOH	24
15	DMF	EtOH	20
16	DMF	iPrOH	20
17	DMF	tAmylOH	0
18	DMF	tBuOH	0

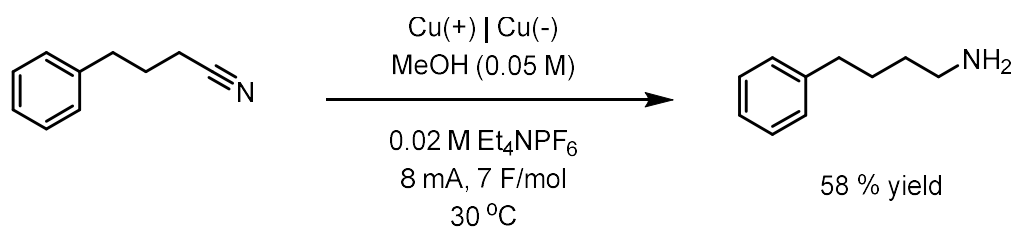
Methanol as the solvent with Et₄NPF₆ were selected as the reaction conditions moving forward for further optimization.

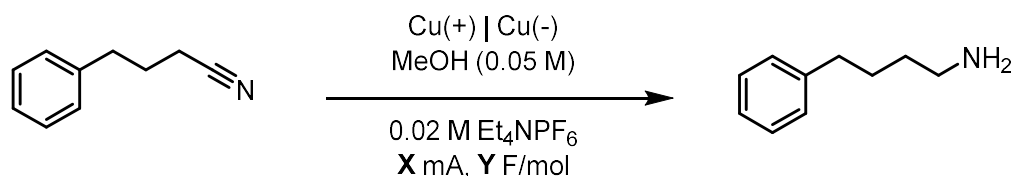
Reaction concentration and electrolyte concentration:

Reaction time was extended to 7 F/mol



entry	rxn [] (M)	electrolyte [] (M)	yield (%)
1	0.067	0.05	60
2	0.1	0.05	54
3	0.13	0.05	53
4	0.1	0.02	57
5	0.1	0.1	55
6	0.1	0.15	53
7	0.067	0.02	57
8	0.05	0.02	69
9	0.04	0.02	57
10	0.05	0.01	50
11	0.05	0.005	29

Temperature (conditions compare to entry 8 in above table):

Current versus F/mol:

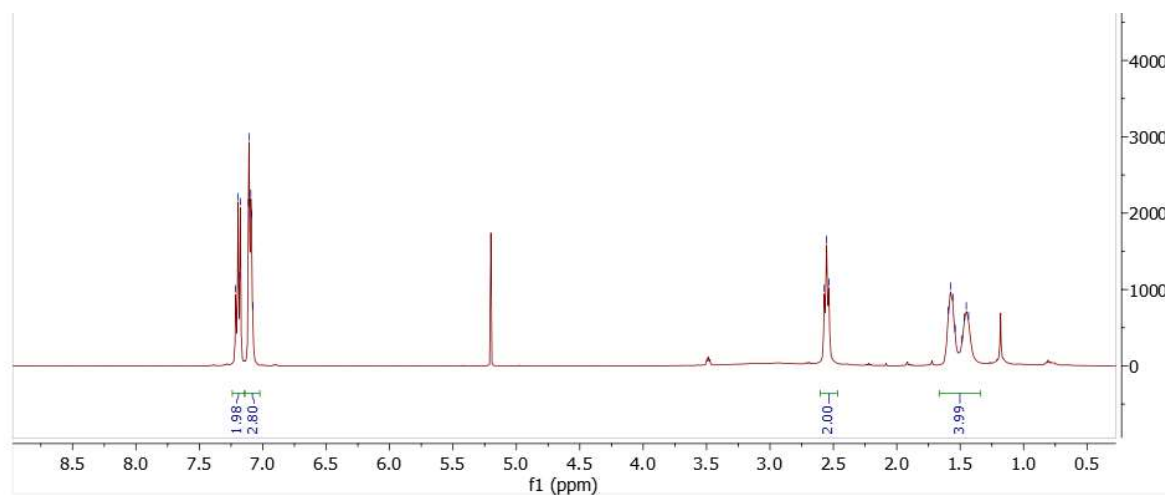
entry	current (mA)	F/mol	yield (%)
1	6	7	59
2	6	14	78
3	8	7	69
4	8	13	82
5	10	7	53
6	10	14	83

A lower current of 8 mA was selected over 10 mA in anticipation of lower current having better selectivity for reductively sensitive functional groups.

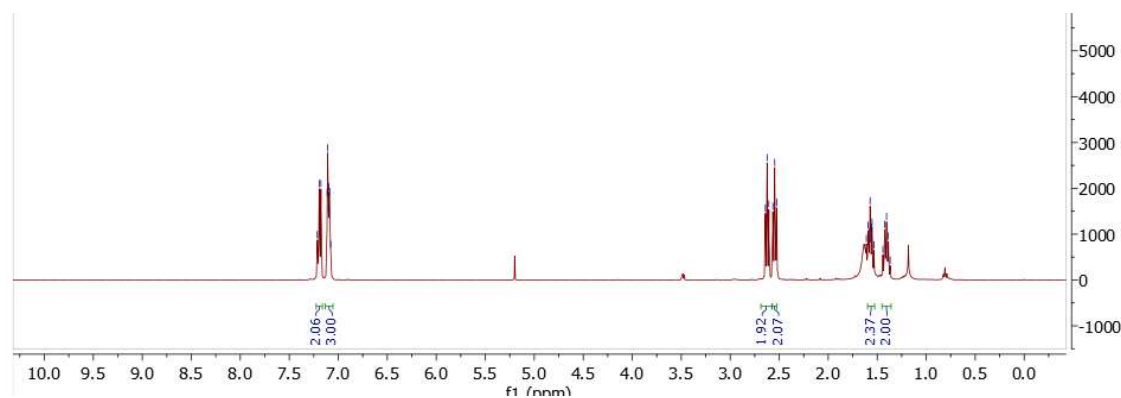
Product Confirmation by isolation:

Crude reaction mixtures were combined to isolate amine product for structure confirmation. Crude reactions were diluted with aqueous 25% EDTA solution and extracted with DCM (3x50 mL), dried with brine and $\text{Mg}(\text{SO}_4)_2$ and concentrated. Crude NMR analysis showed both product and starting material present. The combined organic layers were taken up in DCM again (50 mL) and 1 M HCl solution (70 mL) and the aqueous layer was washed with DCM (3 x 50 mL). The aqueous layer was basified with sodium bicarbonate and the organic product was extracted with DCM (3x50 mL). The combined organic layers were dried with brine and $\text{Mg}(\text{SO}_4)_2$ and concentrated. NMR analysis showed product present but the methylene signal alpha to the nitrogen was suppressed. We attributed this signal suppression to be due to residual copper coordination. An additional wash with 25% EDTA aqueous solution removed the copper and the alpha amine methylene signal was recovered by ^1H NMR. **^1H NMR** (400 MHz, CDCl_3) δ 7.22 – 7.17 (m, 2H), 7.10 (dt, J = 9.2, 3.0 Hz, 3H), 2.62 (t, J = 7.1 Hz, 2H), 2.55 (t, J = 7.6 Hz, 2H), 1.62 – 1.51 (m, 2H), 1.40 (p, J = 7.2 Hz, 2H). Consistent with reported spectra (*J. Am. Chem. Soc.* **2020**, 142, 29, 12708-12714)

^1H NMR after an acid/base extraction:

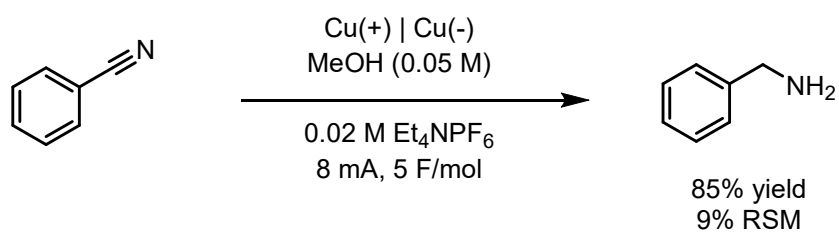


^1H NMR after an additional EDTA wash:



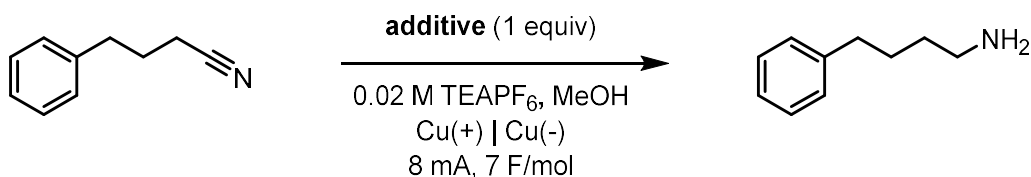
Aromatic Nitrile:

Reaction length was reduced to deliver 5 F/mol because reducing aromatic nitriles is an easier reduction than aliphatic nitriles.



6.7.4. Glorius Screen

Substrates were chosen as additives that have one functional group of interest. A standard nitrile reduction reaction was run with one of the additives added to it. Each additive was studied in an independent reaction.

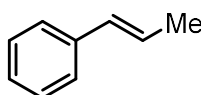


General Procedure:

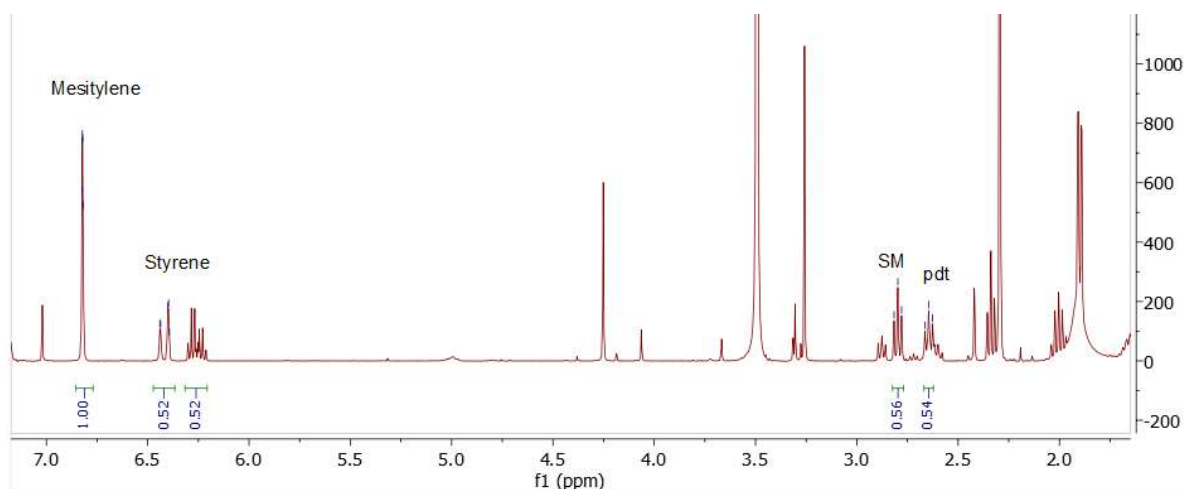
To a 16x100 mm test tube was added tetraethylammonium hexafluorophosphate (22 mg, 0.08 mmol, 0.4 equiv), a stir bar, 4-phenyl-1-butyronitrile (29.8 μL , 0.2 mmol, 1 equiv), an additive (0.2 mmol, 1 equiv) and methanol (4 mL) with no attempts to exclude air or exogenous water. A 14/24 setpa equipped with copper wire electrodes was affixed to the reaction vessel and the electrodes were connected to a galvanostat set to deliver 8 mA. The reaction was electrolyzed at constant current for 4.7 hours (to deliver 7 F/mol).

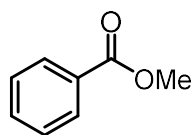
Workup: To the reaction solution was added mesitylene (18 μL , 0.13 mmol) as an internal standard. A 0.2 mL aliquot of the reaction solution was transferred to a vial and diluted with 2 mL of a 25% EDTA aqueous solution. The mixture was stirred for 1 hour and deuterated chloroform was added to the solution, mixed and extracted for NMR analysis.

Trans- β -methylstyrene (**3**)

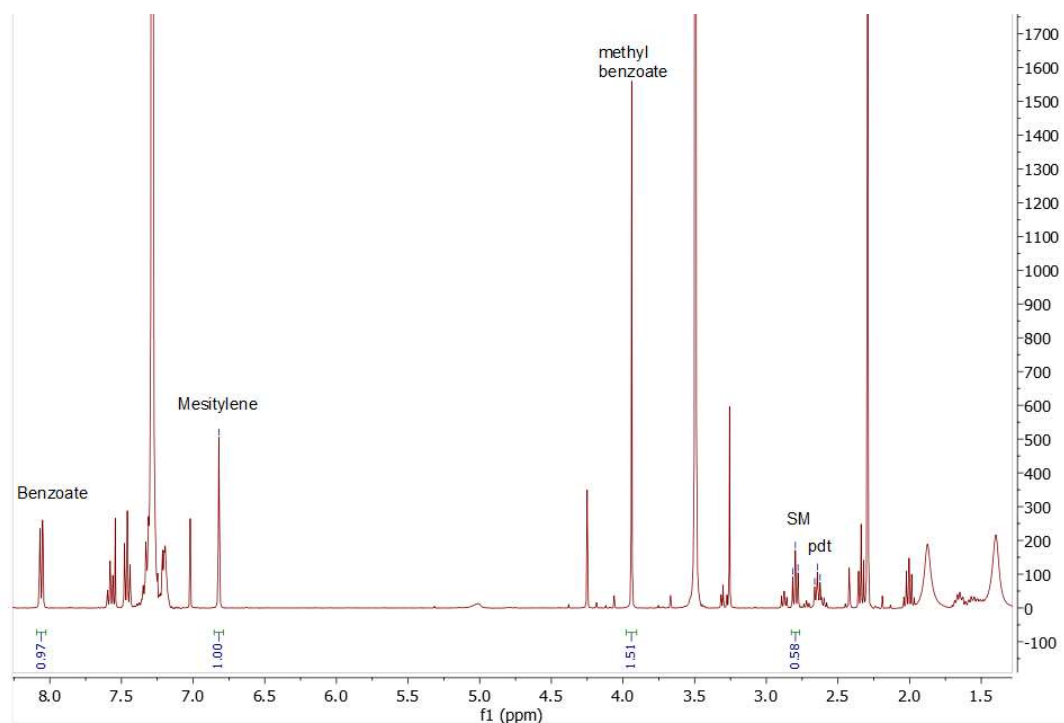
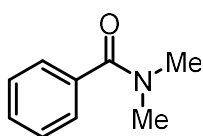


Trans- β -methylstyrene was studied in a nitrile reduction reaction according to the general procedure and was retained in 100%, analyzed by crude reaction ^1H NMR analysis of distinctive signals.

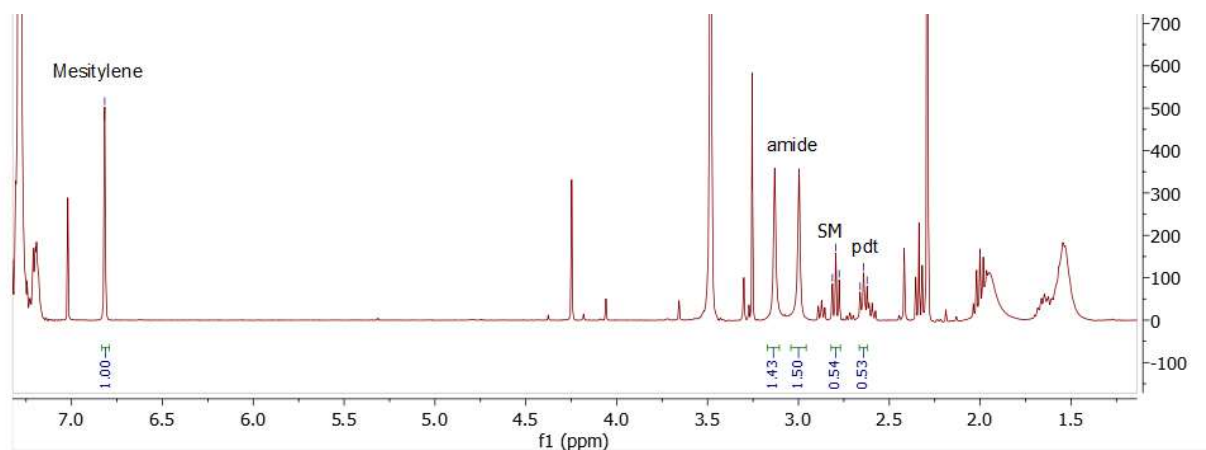


Methyl benzoate (**4**)

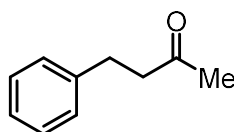
Methyl benzoate was studied in a nitrile reduction reaction according to the general procedure and was retained in 98%, analyzed by crude reaction ^1H NMR analysis of distinctive signals.

N,N-dimethylbenzamide (**5**)

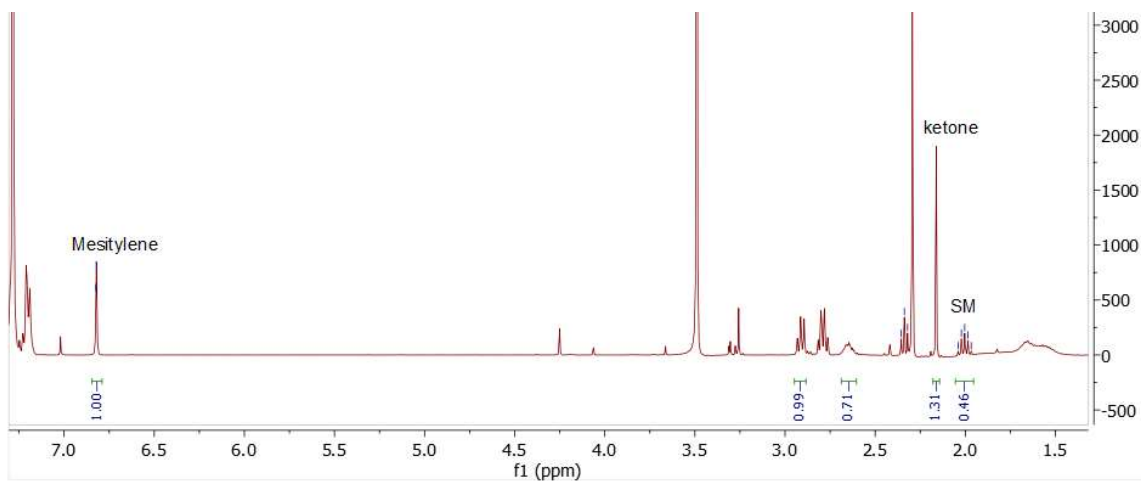
N,N-dimethylbenzamide was studied in a nitrile reduction reaction according to the general procedure and was retained in 98%, analyzed by crude reaction ^1H NMR analysis of distinctive signals.



4-phenyl-2-butanone (6)



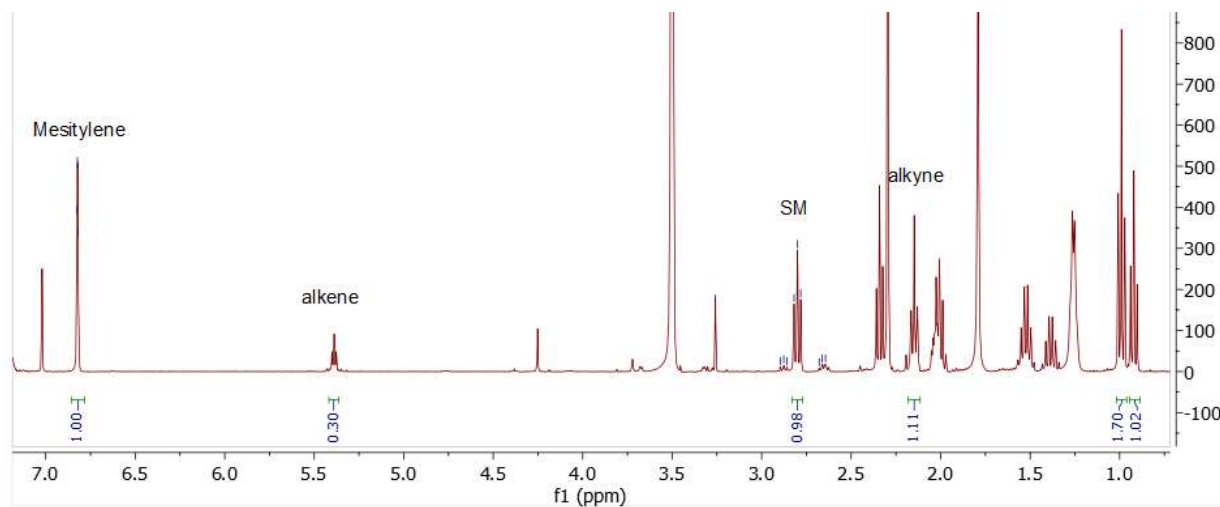
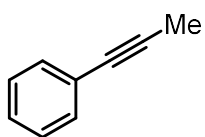
4-phenyl-2-butanone was studied in a nitrile reduction reaction according to the general procedure and was retained in 85%, analyzed by crude reaction ^1H NMR analysis of distinctive signals.



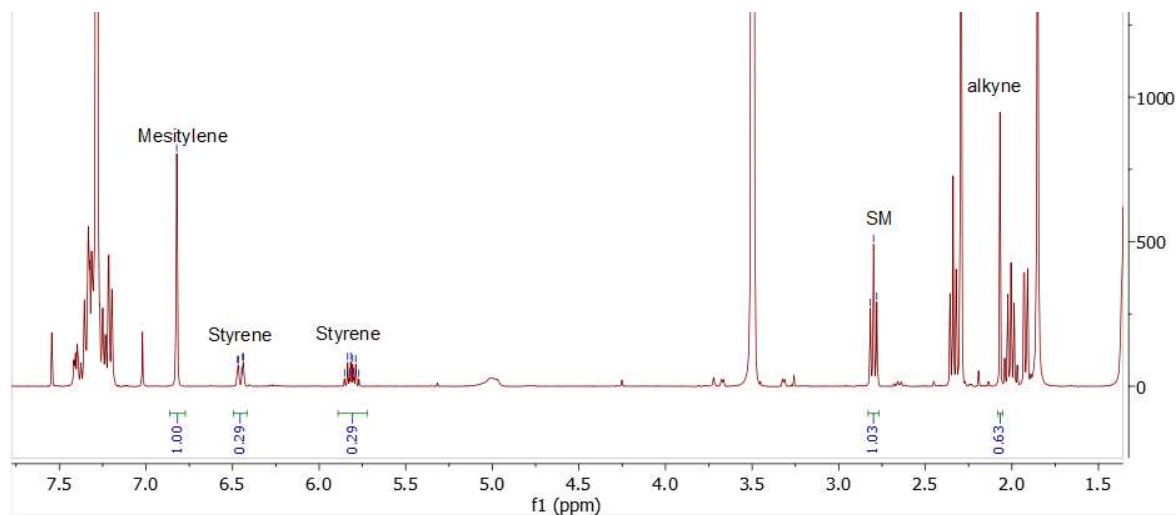
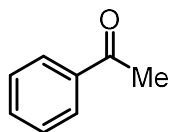
4-octyne (7)



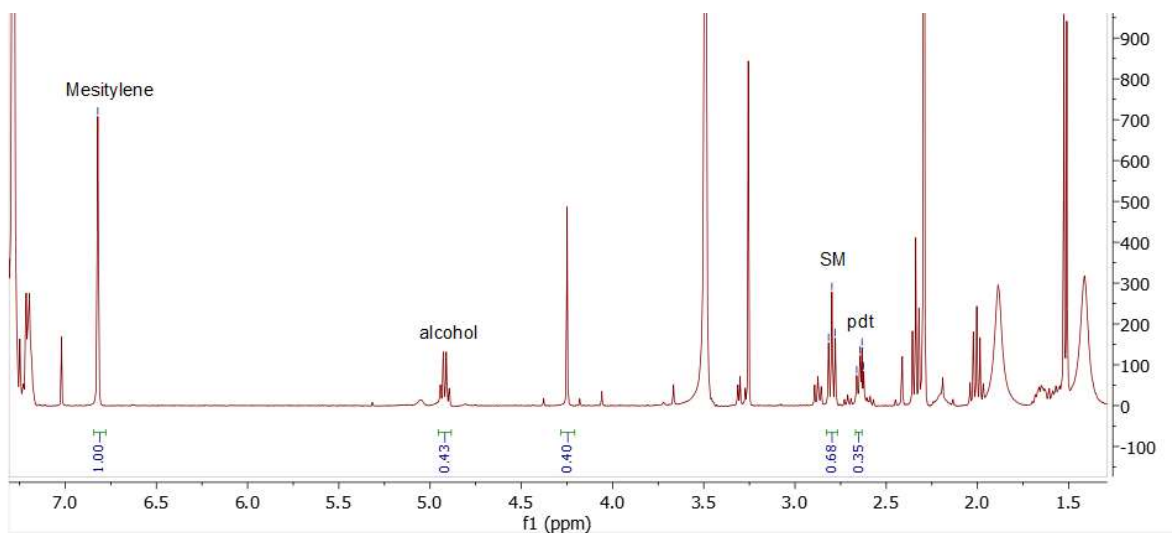
4-octyne was studied in a nitrile reduction reaction according to the general procedure and was retained in 55%, analyzed by crude reaction ^1H NMR analysis of distinctive signals.

1-phenyl-1-propyne (**8**)

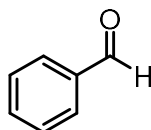
1-phenyl-1-propyne was studied in a nitrile reduction reaction according to the general procedure and was retained in 41%, analyzed by crude reaction ¹H NMR analysis of distinctive signals.

Acetophenone (**9**)

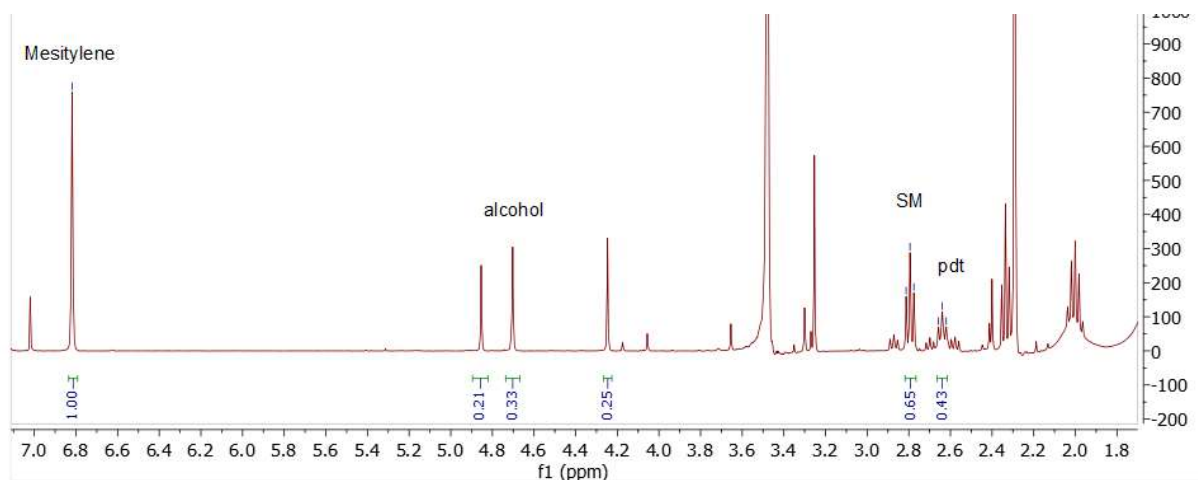
Acetophenone was studied in a nitrile reduction reaction according to the general procedure and was reduced to the alcohol in 84%, the ketone was retained in 5%, analyzed by crude reaction ^1H NMR analysis of distinctive signals.



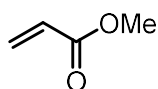
Benzaldehyde (10)



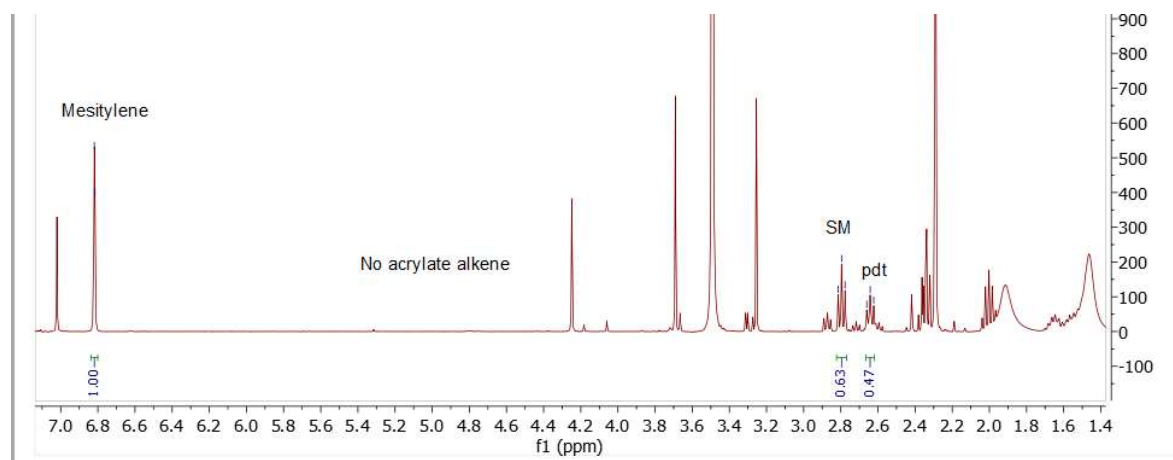
Benzaldehyde was studied in a nitrile reduction reaction according to the general procedure and was reduced to the alcohol in 32%, the aldehyde was not retained, analyzed by crude reaction ^1H NMR analysis of distinctive signals.



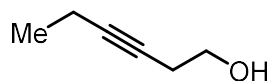
Methyl acrylate (11)



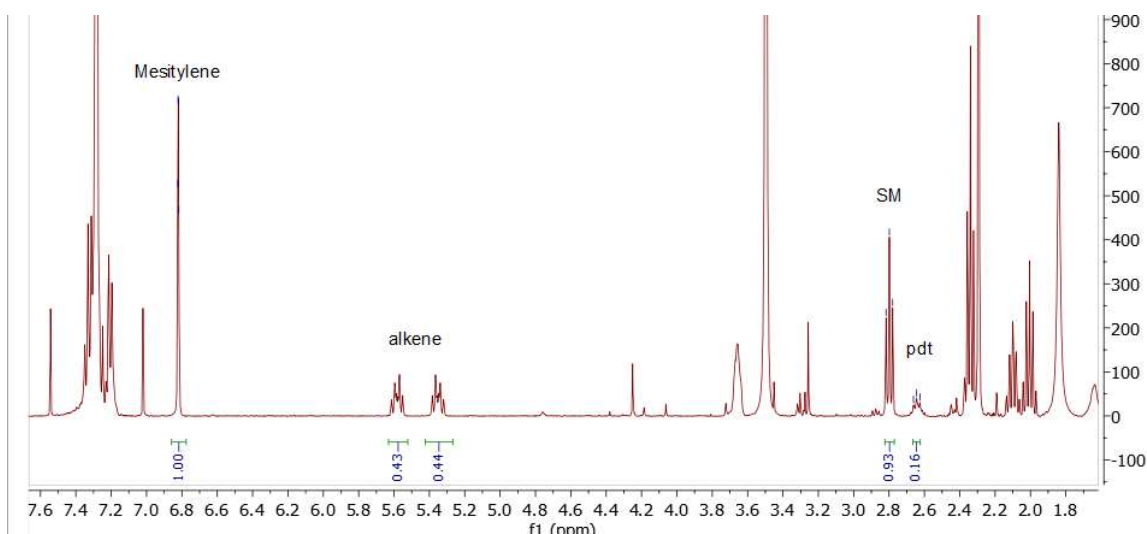
Methyl acrylate was studied in a nitrile reduction reaction according to the general procedure and was hydrogenated in 100% yield, the acrylate was not retained, analyzed by crude reaction ^1H NMR analysis of distinctive signals.



3-hexynol (12)



3-hexynol was studied in a nitrile reduction reaction according to the general procedure and was hydrogenated to the alkene in 100% yield, the alkyne was not retained, analyzed by crude reaction ^1H NMR analysis of distinctive signals.

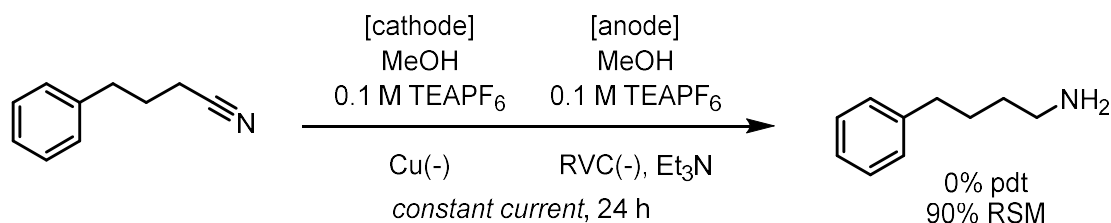


6.7.5. Control Experiments

Divided cell experiments

Divided cell reactions were run to determine if nitrile reduction is purely a cathodic reaction or if the oxidation half reaction of an undivided cell is important.

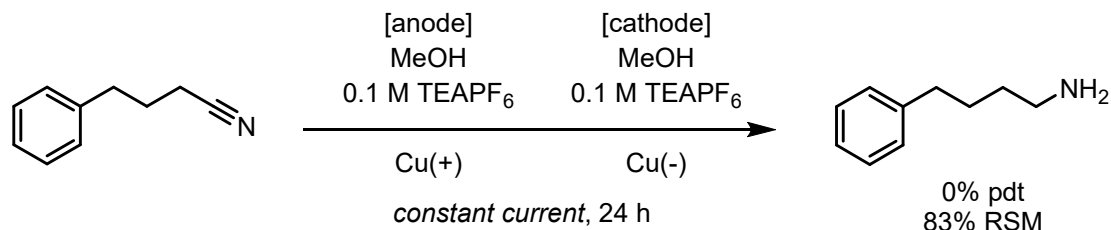
Cathode divided cell:



An oven dried, H-type divided cell with a glass frit was equipped with stir bars and 4-phenylbutyronitrile (28.9 μ L, 0.2 mmol, 1 equiv), and Et₄NPF₆ (150 mg, 0.5 mmol, 2.7 equiv) were added to the cathodic chamber while Et₄NPF₆ (150 mg, 0.5 mmol, 2.7 equiv) was added to the anodic chamber. To the anode and then the cathode was added methanol (4 mL) and triethylamine (220 μ L, 1.6 mmol, 4 equiv) was added to the anode. An electrode setup was assembled with a copper wire cathode and an RVC anode. The divided cell was equipped with the electrode assembly, sealed with septa. Electrodes were connected to a galvanostat and electrolyzed at 8 mA for 24 hours.

Workup and analysis: To the reaction solution was added mesitylene (18 μ L, 0.13 mmol) as an internal standard. A 0.2 mL aliquot of the reaction solution was transferred to a vial and diluted with 2 mL of a 25% EDTA aqueous solution. The mixture was stirred for 1 hour and deuterated chloroform was added to the solution, mixed and extracted for NMR analysis.

Anode divided cell:



An oven dried, H-type divided cell with a glass frit was equipped with stir bars and 4-phenylbutyronitrile (28.9 μ L, 0.2 mmol, 1 equiv), and Et₄NPF₆ (150 mg, 0.5 mmol, 2.7 equiv) were added to the anodic chamber while Et₄NPF₆ (150 mg, 0.5 mmol, 2.7 equiv) was added to the cathodic chamber. To the cathode and then the anode was added methanol (4 mL). An electrode setup was assembled with a copper wire cathode and anode. The divided cell was equipped with the electrode assembly, sealed with septa. Electrodes were connected to a galvanostat and electrolyzed at 8 mA for 24 hours.

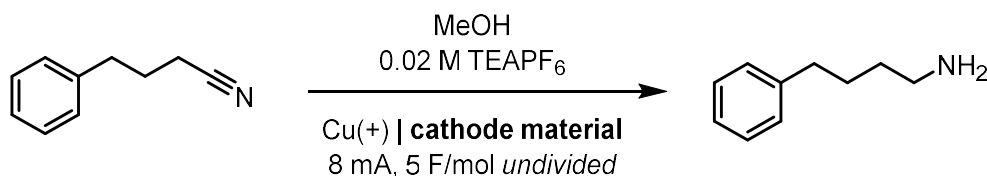
Workup and analysis: To the reaction solution was added mesitylene (18 μ L, 0.13 mmol) as an internal standard. A 0.2 mL aliquot of the reaction solution was transferred to a vial and diluted

with 2 mL of a 25% EDTA aqueous solution. The mixture was stirred for 1 hour and deuterated chloroform was added to the solution, mixed and extracted for NMR analysis.

Undivided Cell Experiments

Undivided cell experiments where the anode and cathode electrode materials were altered to determine what copper components are necessary for the reaction.

Cathode material:



Reactions were setup according to the general procedure except the cathode material was systematically changed to other established electrode materials.

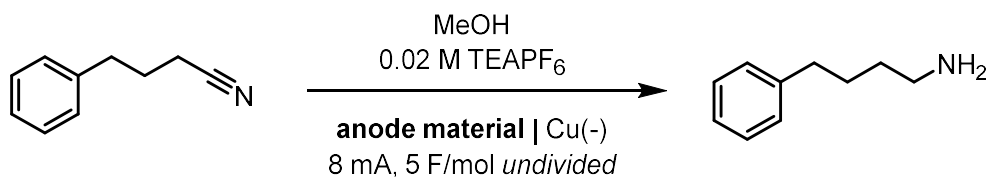
- Nickel Foam
- RVC on stainless steel
- Platinum

Standard reaction conditions under these electrolysis conditions using a copper cathode yields 46% amine product.

cathode	pdt (%)
Cu	46
Ni foam	47
RVC	43
Pt	14

These results reveal that the cathode does not need to be copper for the reaction to proceed.

Anode material:



Reactions were setup according to the general procedure except the anode material was systematically changed to other established sacrificial electrode materials.

- Zinc
- Magnesium

Standard reaction conditions under these electrolysis conditions using a copper cathode yields 46% amine product.

anode	pdt (%)
Cu	46
Zn	0
Mg	0

These results reveal that the reaction requires copper as an anode material and simply exchanging for a different sacrificial anode material prevents the reaction from occurring